Northumbria University at Newcastle upon Tyne

HIGH TEMPERATURE CORROSION STUDIES AND INTERDIFFUSION MODELLING IN TiAl BASED ALLOYS COATED WITH HIGH PERFORMANCE SURFACE LAYERS

TOMASZ DUDZIAK

PhD

October 2009

Northumbria University at Newcastle upon Tyne

HIGH TEMPERATURE CORROSION STUDIES AND INTERDIFFUSION MODELLING IN TiAl BASED ALLOYS COATED WITH HIGH PERFORMANCE SURFACE LAYERS

TOMASZ DUDZIAK

A thesis submitted in partial fulfilment

Of the requirements of the

University of Northumbria at Newcastle

For the degree of

Doctor of Philosophy

Research Undertaking In the School of Computing, Engineering and Information Sciences

October 2009

Declaration

During the period I have been registered for the degree of PhD, for which the thesis is submitted, I have been not registered candidate for any other award of a University.

Furthermore I have attended relevant seminars within the University of Northumbria at Newcastle upon Tyne, and presented papers and posters on several conferences and relevant meetings on the subject of high temperature corrosion.

Name: Tomasz, Pawel Dudziak

Signature:

Date:

Acknowledgements

I would like to thank Dr Hailiang Du, Dr Robert Miles, and Dr Ken Leung my supervisors for their help, advice, and encouragement with this thesis.

Very special thanks to Prof. Santu Datta for being an excellent adviser, a partner in discussion and a good friend. Every meeting was an inspiration.

I also wish to take an opportunity to thank for all other staff and research students within the Northumbria University and Advanced Material Research Institute for all assistance.

In particular I would like to thank Bob Best for assistance and help with Scanning Electron Microscopy and Energy Dispersive Spectroscopy analysis.

In the end I would like to thank my family for the opportunity to be here for all goodness, care which I have received from their. I know that each single day during my PhD all of you were with me.

Abstract

This work forms a part of a large EU project (InnovaTiAl) designed to increase the service temperature (up to 1273 K) of TiAl based intermetallics (Ti45Al8Nb) coated with high performance surface layers for applications in power generation and also in aerospace components.

In this thesis the high temperature corrosion behaviour of some of these newly developed high performance coatings deposited on Ti45Al8Nb alloys using UBM and HIPIMS/UBM has been studied. The coatings studied included intermetallic coatings: TiAlCr, TiAlCrY, Al_2Au, and ceramic coatings: CrAl2%YN, TiAlYN/CrN+Al_2O_3, TiAlN+Al_2O_3, CrAlYN/CrN+CrAlYON coated Ti45Al8Nb etched by Cr, CrAlYN/CrN+CrAlYON coated Ti45Al8Nb etched by CrAl, CrAlYN/CrN+CrAlYON coated Ti45Al8Nb etched by Y, CrAlYN/CrN coating Y etch, CrAl (thin), CrAlYN/CrN coating Cr etch, CrAl (thin), CrAlYN/CrN coating, Y etch, CrAlY (thick) coated Ti45Al8Nb.

High temperature corrosion investigations were carried out by the exposing the coated materials in oxidising (static air, pO_2 = 21278.25 Pa), sulphidising ($pS_2 = 10^{-1}$ Pa, and $pO_2 = 10^{-18}$ Pa) and hot corrosion (20%NaCl/80%Na_2SO_4) environments at temperatures range 1023 – 1223 K. The long term oxidation studies have been performed up to 5000 hours at 1023 K.

Weight change data have been used to determine the corrosion kinetics. SEM studies have provided information on morphology; EDS analyses have given the information on concentration profiles and phase contents have been obtained by XRD analyses.

The excellent high temperature oxidation resistance has been achieved for the CrAl2%YN coating at temperature rage 1023 – 1123 K for 500 hours. Also TiAlCr and TiAlCrY have shown moderate degree of corrosion resistance in oxidising environment after 500 hours of exposure at temperature range 1023 – 1223 K.

The sulphidation experiments for 1000 and 675 hours at 1023 K and 1123 K respectively showed that the uncoated material developed a multilayered thick scale with poor resistance to sulphidation. The ceramic coatings developed a good protective Al_2O_3/Cr_2O_3 on places where the coatings remained intact and did not undergo cracking. However due to the cracks in the top coat, the development of non protective TiO_2 occurred at 1023 and 1123 K. Hot corrosion studies performed at 1023 K for 150 hours under this thesis showed that all exposed materials (CrAl2%YN, TiAlN+Al_2O_3, and TiAlYN/CrN+Al_2O_3) suffered uneven attacks (crack formation, spallation, and the lack of Al_2O_3 formation).

Interdiffusion studies of mass transport have been performed by GDM on TiAlCrY coated alloy after 500 hours oxidation at 1023 and 1123 K. A reasonable degree of agreement between the experimental and the simulated profiles has been achieved.

Copyrights

List of publications arising from this thesis

1) Sulphidation/Oxidation Behaviour of TiAlCr and Al_2Au Coated Ti45Al8Nb Alloy at 750^oC, Corrosion Science
2) Studies of the Effectiveness of Certain High Performance Coatings in Preventing Hot Corrosion Degradation of Ti - Aluminide Alloys, Defect and Diffusion Forum
3) Defects of SiC nanowires studied by STM and STS, Applied Surface Science Journal (In Press)
4) The influence of nanocrystalline coatings on the sulphide corrosion of Ti-45Al-8Nb alloy at 750^oC, Materials and Corrosion Journal (In Press)

List of Contents

List of Figures

List of Tables

Chapter I - Introduction

Introduction to PhD Thesis

In recent years there have been significant interests in the use of intermetallics as structural materials.

Intermetallics are the compounds with a strong metallic bonding between two atoms. From bonding comes crystal structure, ordering, high strength at low and at high temperature and low ductility at low temperature. The major concern to use intermetallic compounds are their poor ductility and low toughness (K_{Ic}). However in recent years the knowledge of mechanical properties of intermetallics has significantly increased adding improved understanding of their high lattice stress, complex crystal structure, large Burgers vectors, inability to develop cross slip and lack of grain boundary cohesion responsible for low fracture strain and K_{Ic}. This improved understanding and better knowledge of the mechanical properties have allowed development of different types of interesting intermetallic compounds however low K_{Ic} and low ductility are still the main concern.

Recent research has shown that TiAl intermetallics compounds are potential candidates for automotive, aerospace applications. Intermetallic materials with improved mechanical properties, which are much better than conventional Ti – based alloys in the intermediate range of temperature 873 – 1073 K, are now available with higher specific stiffness, strength (800 MPa), creep resistance (1% strain after 500 hours), fatigue resistance (480 MPa). The main advantage in the use of TiAl intermetallic material is weight savings, the density of TiAl intermetallic is equivalent to 50% of Ni-base superalloy density (~3, 6 g/cm^3, ~7, 8 g/cm^3 respectively).

The maximum service temperature for TiAl intermetallic alloys is around 1073 K, however further demand on the efficiency of the energy systems, requires higher operating temperatures >1073 K. The current project has been designed in order to employ the TiAl alloys at higher service temperatures. This also brings benefits in terms of reduced emission and conservation of world resources (reduced use of Cr and other expensive elements).

At higher service temperature (> 1023 K) TiAl intermetallic compounds suffer environmental attack (oxidation, sulphidation, hot corrosion). Clearly to achieve the higher efficiency and avoid or inhibit corrosion degradation at high temperature, TiAl intermetallic alloys need to be protected by the specially designed coatings to promote the development of highly protective Al_2O_3 outer scale. However the available protective coatings for TiAl intermetallic alloys provide only short-term protection. Clearly there is a need to develop new generation of coatings capable of resisting high temperature corrosion damage over a prolonged period of exposure to corrosion environments.

InnovaTiAl project has been established to design such new types of coatings on Ti45Al8Nb alloy (γ-TiAl) to withstand exposure to high temperature (up to 1273 K and corrosive gases simultaneously. The new type of coatings designed cover: superlattice coatings, intermetallic coatings with top coats. Thus the technical objectives of this InnovaTiAl project were to synthesize ultra-performance nanoscale-structured PVD thin films, capable of providing environmental protection at high temperatures in the range from 923 – 1273 K; this will greatly increase the applications of γ-TiAl to high service temperatures and improve lifetime. The InnovaTiAl project employed a novel PVD method – High Power Impulse Magnetron Sputtering (HIPIMS) replacing the old arc discharge in ABS (Arc Bond Sputtering). This new process allowed deposition of protective nanostructured coatings with the highest adhesion and full density, which improved protection against high temperature atmospheres (oxidation/ sulphidation/ hot corrosion) and preserved the mechanical properties of the substrate material (Ti45Al8Nb). The HIPIMS technology allowed the development of a new generation of Ti free nanoscale multilayer coatings with trace additions (~1%) of group III rare earth element Y, to enable self- healing, self- adapting mechanisms, and ultra-performance at high temperatures up to 1273 K; new, CrAlYN/CrN+CrAlYON and CrAlYN/CrN superlattice systems.

This work in the thesis is concerned with studies of the corrosion behavior – oxidation, oxidation/sulphidation, hot corrosion – of these new types of coatings at temperature 1023 – 1223 K. The coatings studied included: TiAlCr (Ti42Al15Cr wt%),

TiAlCrY (Ti55Al14Cr0.3Y), Al_2Au, CrAl2%YN, TiAlYN/CrN+Al_2O_3, TiAlN+Al_2O_3, CrAlYN/CrN+CrAlYON coated Ti45Al8Nb etched by Cr, CrAlYN/CrN+CrAlYON coated Ti45Al8Nb etched by CrAl, CrAlYN/CrN+CrAlYON coated Ti45Al8Nb etched by Y,) CrAlYN/CrN coating Y etch, CrAl (thin), CrAlYN/CrN coating Cr etch, CrAl (thin), CrAlYN/CrN coating, Y etch, CrAlY (thick).

A significant part of this project involved modelling of interdiffusion processes in the systems promoted by oxidation treatments (open system). Generalised Darken's Method (GDM) has been used to model interdiffusion in the multicomponent systems studied under this project. The thesis has been structured in eight main chapters with relevant sections:

Chapter I – Introduction

Chapter II, Section 1 – Critical Literature Review – Oxidation of γ - TiAl

Chapter II, Section 2 – Critical Literature Review – Sulphidation/Oxidation of γ - TiAl

Chapter II, Section 3 – Hot Corrosion/oxidation of TiAl Alloys – Critical review

Chapter II, Section 4 – Interdiffusion Modelling – Short Literature Review

Chapter III – Deposition Techniques and Coatings

Chapter IV – Methodology and Current Work to Date

Chapter V - Introduction to Current Work Undertaken in This Project

Chapter VI, Section 1 – High Temperature Oxidation of γ - TiAl – Results

Chapter VI, Section 2 – High Temperature Sulphidation/Oxidation of γ - TiAl – Results

Chapter VI, Section 3 – High Temperature Hot Corrosion of γ - TiAl – Results

Chapter VI, Section 4 – Interdiffusion Modelling – Results

Chapter VII – Discussion of the Results

Chapter VIII – Conclusions and Future Work

Chapter II – Literature Review

Chapter II – Section 1 - Critical Literature Review – Oxidation of γ - TiAl alloys

Ch.II.Sec.1.1 Introduction to literature review

This section of PhD thesis presents a review of the available literature relating to the main themes of the oxidation at the high temperature. The corrosion behaviour of Ni – Cr, Fe – Cr, Ni – Al, Co – base alloys and an intermetallic TiAl alloys in oxidising environment will be reviewed.

Ch.II.Sec.1.2 Background of oxidation and thermodynamical data

High temperature oxidation is one of the most common mode of degradation for all materials. Much progress has been achieved in understanding the mechanisms of oxidation [1].

When a clean metal surface is exposed to an oxidation environment, the initial step involves adsorption of the gas molecules on the metal surface; some of the oxygen ions (O^{2-}) may dissolve in the metal matrix. Then the reaction between a metal and the oxygen particles produces a thin film, which starts to separate the material from ambient environment. Both the adsorption and film formation is a function of surface orientation, crystal defects at the surface, surface preparation and impurities in both, metals and environments.

In the case of formation of a continuous film covering the surface the reaction can proceed by solid state diffusion within the scales formed on the metals exposed to high temperatures; the scale growth is determined by the chemical gradients across the scale. A schematic which illustrates the formation of oxide scale is presented in **figure 1**.

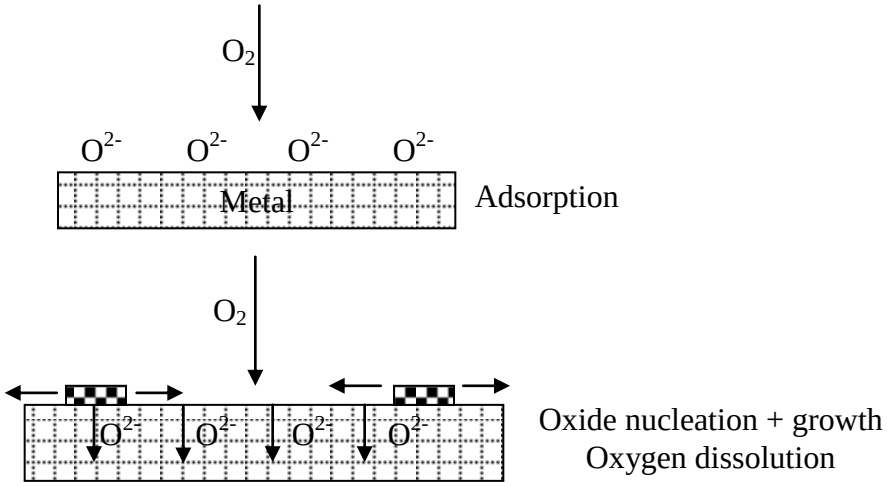

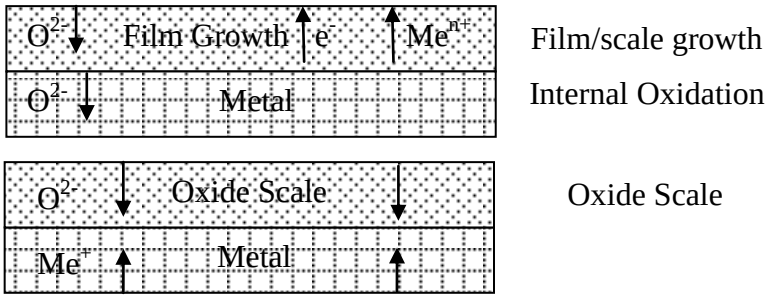

Figure 1 Oxidation mechanism at high temperature [1]

It needs to be noted that if the oxide scale exceeds a critical volume, then cracks start to initiate in the oxide scale which undermine the protectivity of the scale what schematically is described in **figure 2**.

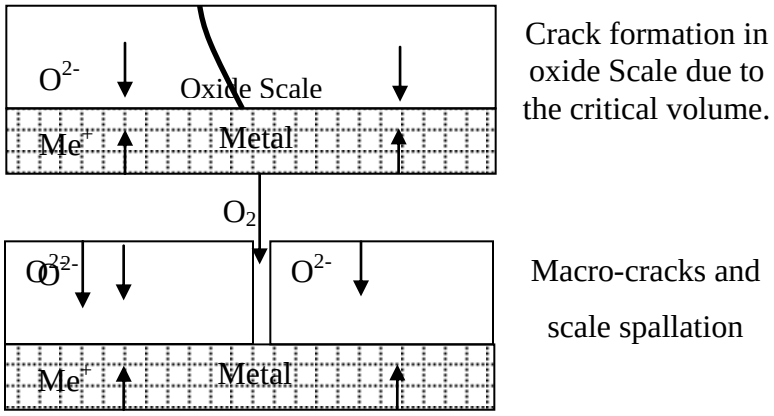

Figure 2 Degradation of oxide scale due to the thick oxide scale [1]

The metal oxidizes at the metal-oxide interface and produces metallic ions which diffuse towards the external part of the film. At the external surface (oxide-gas interface) gaseous oxygen is reduced to form O^{2-} ions, these ions diffuse towards the metal-oxide interface. The electrons released at the metal-oxide interface diffuse trough the oxide scale.

The chemical reaction which takes place can be considered as follows:

Reaction 1 $$Me + \frac{1}{2} X_2 \rightarrow MeX$$

where Me is a metal, X_2 is a oxygen, and MeX is a oxide (reaction product).

Due to the oxidation processes the change in thermodynamic potential ΔG is given by:

Equation I
$$\Delta G = \mu MeX - \mu Me - \frac{1}{2}\mu X_2$$

where μ = chemical potential

The following reaction relates chemical potential and activity:

Equation II
$$\mu_i = \mu_i^0 + RT \ln a_i$$

where R is a gas constant equal to 8,314 [$\frac{J}{mol * K}$], T is temperature in K scale, a_i is a activity of the reagent in the system, and μ_i^0 is chemical potential in standard conditions (T = 298 K, p = 101325 Pa) when activity is equal 1 (a_i = 1). The activities of solid state pure reagents are always equal to 1 thus if $\mu_{Me} = \mu_{Me}^0$ and $\mu_{MeX} = \mu_{MeX}^0$. If X in the reaction is in gaseous (N_2, O_2, S_2) state then the **equation (III)** becomes:

Equation III
$$\mu X_2 = \mu_{X2}^0 + RT \ln px_2$$

Thus **equation II** can be defined according to the relation where:

Equation IV
$$\Delta G = \mu_{MeX}^0 - \mu_{Me}^0 - \frac{1}{2}\mu_{X_2}^0 - \frac{1}{2}RT \ln pX_2$$

The algebraic sum of the standard chemical potentials is equal to change of thermodynamic potential of the reaction in standard conditions (ΔG^o). Then the above **equation (IV)** can be re-written as:

Equation V
$$\Delta G = \Delta G_T^0 - \frac{1}{2}RT \ln pX_2$$

In equilibrium state, when metal does not form an oxide or when oxide (MeX) formed does not decompose $\Delta G_T^0 = 0$, then **equation V** can be expressed as follow:

Equation VI

$$\Delta G_T^0 = \frac{1}{2} RT \ln p_{X_2}^r$$

where $p_{X_2}^r$ denotes the decomposition vapour pressure of MeX phase. The overall equation finally can be described as follows:

Equation VII

$$\Delta G_T^0 = \frac{1}{2} RT \ln p_{X_2}^r - \frac{1}{2} RT \ln p_{X2}$$

Where: $p_{X2} > p_{X_2}^r$, $\Delta G_T^0 < 0$ then reaction is spontaneous, when $p_{X2} < p_{X_2}^r$, $\Delta G_T^0 > 0$ then MeX cannot be formed, and starts to decompose for free Me and free X.

Thus the thermodynamic basis allows predict the formation of oxides, or other phases during exposure of metals in oxidising environment at high temperature. Furthermore it is also possible to predict which metal can react with the atmosphere, or which won't react with reactive atmosphere and will act as a noble metal. To know this phenomenon it is essential to calculate ΔG^o from temperature for particular metal. It needs to be pointed out that the metals with higher oxidant state have a higher decomposition vapour pressure.

Figure 3 shows the Ellingham – Richards diagram, the diagram shows the decomposition vapour pressure at any temperature, and also knows the ΔG^o of formation particular oxide phases.

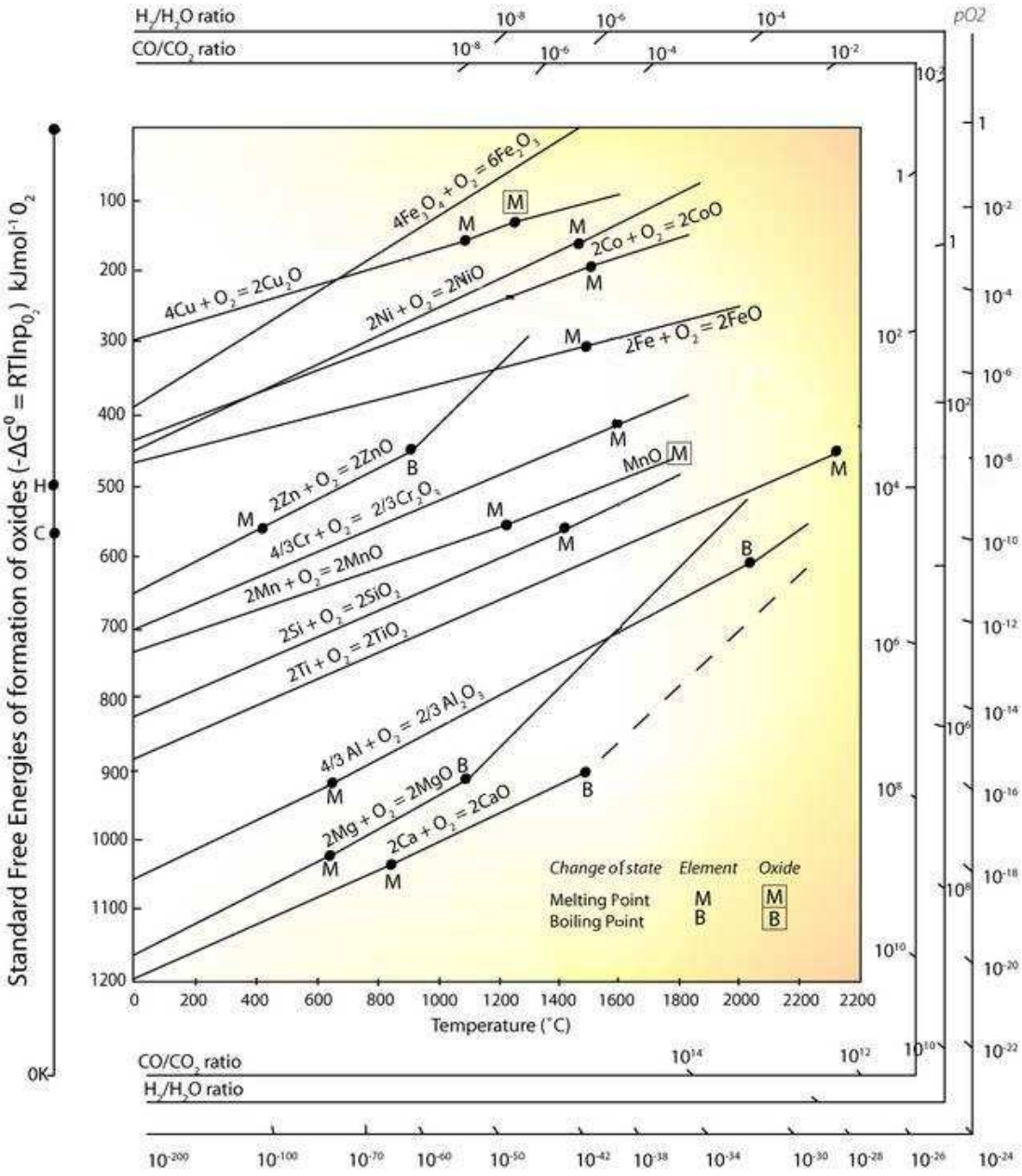

Figure 3 Ellingham – Richards diagram of the oxides formation [2]

Ch.II.Sec.1.3 Wagner Theory

Wagner theory derived from classical diffusion theory and theory of the defects in ionic crystals is based on the following assumptions [3]:

1) The scale formed on the metal substrate is compact and very adherent to the substrate.

2) The diffusion of reagents in the scale can be considered only by mass transport provided by movements ions and electrons controlled by the defect structures of the scale.

3) The chemical reactions on each interface are faster than diffusion mass transport in the scale. Thus the diffusion processes determine the velocity of the scale growth.

4) The diffusion processes are controlled by the concentration gradients of the defects within the scale; the gradients are generated by chemical potentials of the oxidants.

5) At the interfaces (substrate/scale and scale/atmosphere) the lattice defects concentration is constant in stationary state, due to the constant concentration of the lattice defects the oxidation process occurs by a parabolic rate.

6) The thermodynamic stability occurs in both interfaces; substrate/scale and scale/atmosphere.

Figure 4 shows the schematic models of the scale which develop according to the Wagner theory.

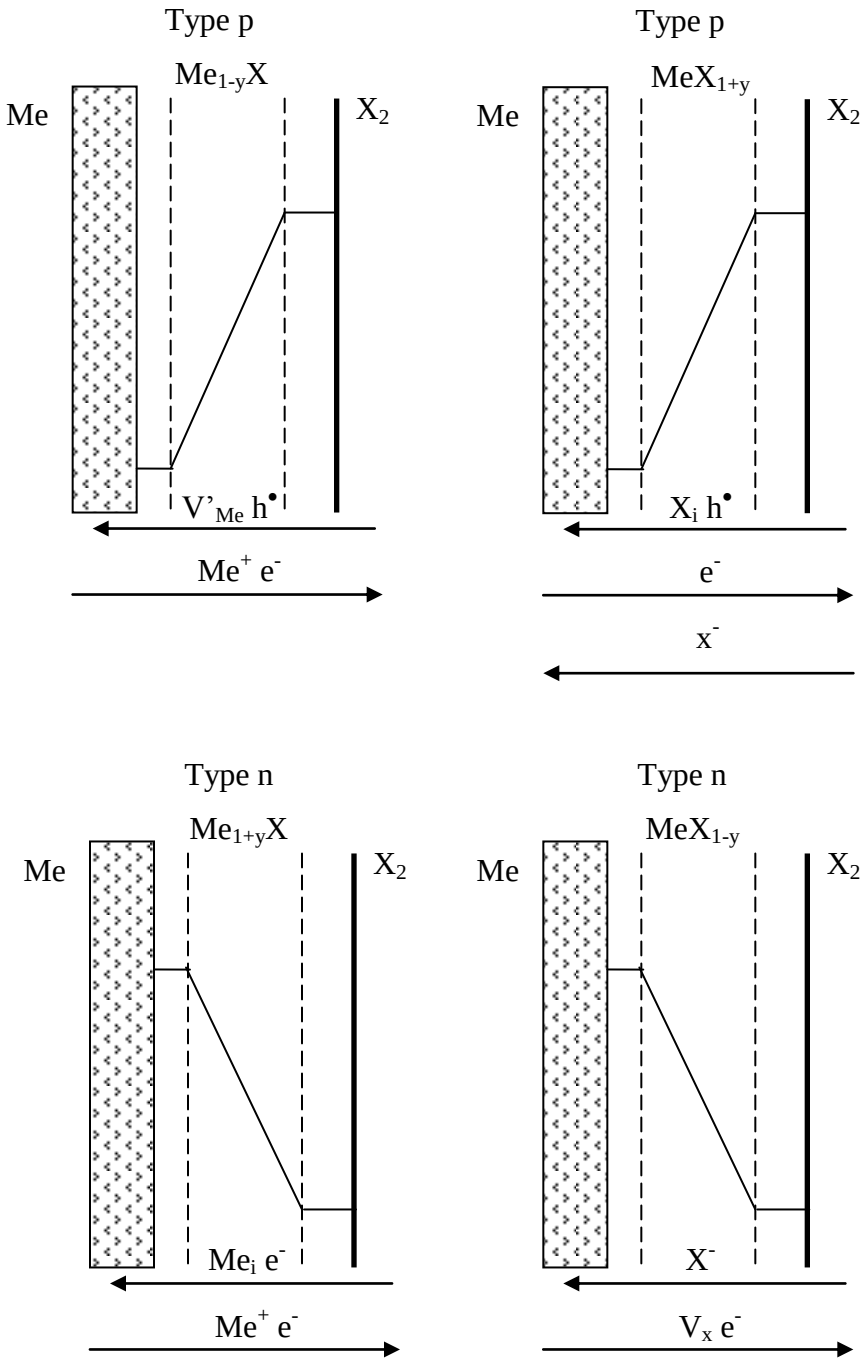

Figure 4 Concentration profiles for diffusion processes during the oxide scale growth. Arrows indicate direction of ionic and electronic diffusion defects and fluxes of diffusion ions [3].

As was postulated by Wagner, the scale growth is related to diffusion of both reagents (Me, X). The mass transport within the scale is determined only by the number of defects in the structure. Thus if the corrosion product is defected only in cationic side, then the scale growth is due to the outward diffusion of Me; in $Ni_{1-y}O$ oxide Me diffusion occurs through the cation gaps and electron holes. Furthermore in $Zn_{1+y}O$, the diffusion processes are related to interstitial region. Moreover the scale formation in materials with MeX_{1-y} is related to the inward diffusion of oxidant.

Based on Wagner theory the overall expression for parabolic rate of the scale growth is given by **equation VIII**:

Equation VIII

$$\frac{dN}{dt} = [A\int_{\mu_X'}^{\mu_X''} \frac{1}{|z^2|}(l_1 + l_2)l_3\sigma d\mu_X]\frac{1}{\chi}$$

Where:

dN – velocity of oxide process

χ - thickness of the scale in time [t]

μ_x – chemical potential

μ_x and μ_x' – chemical potentials of the oxidant in the scale/substrate and oxide/atmosphere interfaces

l_1, l_2, l_3 - passing numbers, for anions, cations, and electrons

σ - electric conductivity [Ω^{-1}*cm^{-1}]

z – oxidation state on oxidant

A – constant equal to $A = \frac{300}{FNe}$ where: F- Faraday constant (96485,339 C/mol), N – Avogadro number ($6.023x10^{23}$ mol), and e – elementary charge ($1.602x10^{-19}$ C)

Ch.II.Sec.1.4 Kinetic laws

Reaction rates are dependent on many factors – temperature, time, oxygen partial pressure, surface preparation, and pre-treatment of metal. In reality three main reaction rates have been recognized when the product/s of the oxidation reaction is/are solid/solids:

Ch.II.Sec.1.4.1 Linear Rate

Linear rate of oxidation can be described by **equation X**:

Equation IX

$$\frac{dx_{Me}}{dt} = k_l$$

where:

x_{Me} – is mass gain of the metal [g]

t – time of reaction [s]

k_l – linear oxidation constant

Ch.II.Sec.1.4.2 Parabolic rate

If the corrosion product is in solid state, then the nature of the scale formed and the temperature determines the rate of reaction. When the formed scale is porous and the ingress of oxygen is sufficiently high, then the slowest process which can determine the scale growth is the chemical reaction at the scale/metal interface. The rate of this reaction is constant in time, and linear rate of scale growth can be estimated. However if the scale is non porous (compact structure) then the rate of the oxidation becomes slower than during the chemical reaction. Moreover during exposure the surface of the substrate becomes separate from the ambient atmosphere and the growth rate is controlled by diffusion processes within the oxide scale.

It was observed that within the large temperature range, the rate of oxidation of many metals and alloys is disproportionate to the thickness of the formed scale. This phenomenon can be described as a parabolic rate law discovered by Tamman [4]:

Equation X

$$\frac{dx}{dt} = \frac{k'_p}{x}$$

where:

x – thickness of the corrosion product in time t

k'_p – parabolic rate constant

Equation X denotes that the slowest process which determines the scale development in adherent scale is a diffusion of reagents which takes place under a constant gradient.

Ch.II.Sec.1.4.3 Cubic rate

It was observed [5] that at high temperatures the oxidation rate can be described by cubic rate constant where:

Equation XI

$$x^3 = 3k'_c\, t + C$$

where:

k'_c – cubic rate constant

The measurement of the kinetic rate includes the measurement of mass gain per unit area of exposed sample. The thickness of the corrosion product is proportional to the mass of oxidant which reacts with the area of the sample. The overall equation permits to calculate the kinetic rate is presented below:

Equation XII

$$(\frac{\Delta m}{q})^n = k''\, pt + C$$

where:

Δm – mass of reacted oxidant [g], q – area of the exposed sample [cm^2]

Ch.II.Sec.1.5 Oxidation of specific alloys

Ch.II.Sec.1.5.1 Oxidation of Ni – Cr and Fe – Cr alloys

Ni – Cr and Fe – Cr alloys are the basis of many materials for high temperature applications (jet engines, combustion chambers, pistons, etc.). **Table 1** and **2** are presenting a chemical compositions of Ni and Fe alloys which are in use in the different corrosion atmospheres [6].

The overall, microstructure of Fe – base alloys, Ni – base alloys can be described by the austenitic FCC (Face Centered Cubic) matrix and carbides phases: M_6C, $M_{23}C_6$, and M_7C_3.

Family	Common name	UNS No.	Form	Composition, wt%												
				Ni	Co	Mo	Cr	Fe	W	Mn	Si	C	Al	Ti	Other
Ni-Cr	80A	N07080	Wrought (age hardenable)	bal	2(a)	...	19.5	3(a)	...	1(a)	1(a)	0.1(a)	1.4	2.3	Cu 0.2(a)
	FM 72	N06072	Filler metal	bal	...	...	44	0.5(a)	...	0.2(a)	0.2(a)	0.1(a)	...	0.7	Cu 0.5(a)
	600	N06600	Wrought	76	...	...	15.5	8	...	0.5	0.2	0.08	...	...	Cu 0.2
	602 CA	N06025	Wrought	bal	...	...	25	9.5	...	0.1(a)	0.5(a)	0.2	2.1	0.15	Cu 0.1(a)
															Y 0.09
															Zr 0.06
	625	N06625	Wrought	61	...	9	21.5	2.5	...	0.2	0.2	0.05	0.2	0.2	Nb + Ta 3.6
	625 LCF	N06626	Wrought	58(b)	1(a)	9	21.5	2.5	...	0.2	0.15(a)	0.03(a)	0.2	0.2	Nb + Ta 3.6
	671	...	Cast, powder metallurgy	bal	...	...	48	...	...	...	...	0.05	...	0.35	...
	690	N06690	Wrought	58(b)	...	...	29	9	...	0.5(a)	0.5(a)	0.05(a)	...	...	Cu 0.5(a)
	693 (53 MD)	N06693	Wrought	bal	...	...	29	4.25	...	...	0.5(a)	0.15(a)	3.25	...	Nb 1.5
	X-750	N07750	Wrought (age hardenable)	73	...	...	15.5	7	...	0.5	0.2	0.04	0.7	2.5	Cu 0.2
															Nb + Ta 1
	214	N07214	Wrought	75	2(a)	0.5(a)	16	3	0.5(a)	...	0.2(a)	0.04	4.5	...	Y 0.01
Ni-Cr-Mo	S	N06635	Wrought	67	2(a)	15	16	3(a)	1(a)	0.5	0.4	0.2(a)	0.25	...	Cu 0.35(a)
															La 0.02
															B 0.015(a)
Ni-Cr-W	230	N06230	Wrought	57	5(a)	2	22	3(a)	14	0.5	0.4	0.1	0.3	...	La 0.02
Ni-Co-Cr	HR-160	N12160	Wrought	37	29	1(a)	28	2(a)	1(a)	0.5	2.75	0.05	0.4(a)	0.5	...
	263	N07263	Wrought (age hardenable)	52	20	6	20	0.7(a)	...	0.4	0.2	0.06	0.6(a)	2.4(a)	Cu 0.2(a)
	617	N06617	Wrought	52	12.5	9	22	1	...	...	0.5	0.07	1.2	0.3	...
Ni-Cr-Fe	X	N06002	Wrought	47	1.5	9	22	18	0.6	...	1(a)	0.1	0.5(a)	...	...
	718	N07718	Wrought (age hardenable)	52.5	...	3	19	18.5	...	0.2	0.2	0.04	0.5	0.9	Cu 0.2
															Nb + Ta 5.1
	45 TM	N06045	Wrought	45(b)	...	...	27.5	23	...	1(a)	2.75	0.09	0.2(a)	...	Cu 0.3(a)
															Rare earths 0.1
	RA 333	N06333	Wrought	45.5	3.3	3.3	25.5	bal	3.3	2(a)	1.2	0.08(a)	...	...	Cu 0.5(a)
	601	N06601	Wrought	60.5	...	...	23	15	...	...	0.5(a)	0.1(a)	1.4	...	...
Ni-Fe-Cr	706	N09706	Wrought (age hardenable)	41.5	...	...	16	40	...	0.2	0.2	0.03	0.2	1.8	Cu 0.2
															Nb + Ta 2.9
	HR-120	N08120	Wrought	37	3(a)	1(a)	25	33	...	...	0.6	0.05	0.5(a)	...	Nb 0.7
															N 0.2
Ni-Mo	242	N10242	Wrought (age hardenable)	65	1(a)	25	8	2(a)	...	0.8(a)	0.8(a)	0.03(a)	0.5(a)	...	Cu 0.5(a)

(a) Maximum. (b) Minimum

Table 1 Chemical composition in wt% of Ni – alloys which are in use in different corrosion atmospheres [7]

UNS designation	Type	Composition(a); wt% C	Mn	P	S	Si	Cr	Ni	Mo	Others
Austenitic grades										
S20100	201	0.15	5.5–7.5	0.060	0.030	1.00	16.0–18.0	3.5–5.5	...	0.25N
S20200	202	0.15	7.5–10.0	0.060	0.030	1.00	17.0–19.0	4.0–6.0	...	0.25N
S30100	301	0.15	2.00	0.045	0.030	1.00	16.0–18.0	6.0–8.0	...	0.10N
S30200	302	0.15	2.00	0.045	0.030	0.75	17.0–19.0	8.0–10.0	...	0.10N
S30215	302B	0.15	2.00	0.045	0.030	2.00–3.00	17.0–19.0	8.0–10.0	...	0.10N
S30300	303	0.15	2.00	0.20	0.15 min	1.00	17.0–19.0	8.0–10.0	0.60	...
S30323	303Se	0.15	2.00	0.20	0.06	1.00	17.0–19.0	8.0–10.0	...	0.15Se min
S30400	304	0.08	2.00	0.045	0.030	0.75	18.0–20.0	8.0–10.5	...	0.10N
S30403	304L	0.030	2.00	0.045	0.030	0.75	18.0–20.0	8.0–12.0	...	0.10N
S30409	304H	0.04–0.10	2.00	0.045	0.030	0.75	18.0–20.0	8.0–10.5	...	...
S30451	304N	0.08	2.00	0.045	0.030	0.75	18.0–20.0	8.0–10.5	...	0.10–0.16N
S30500	305	0.12	2.00	0.045	0.030	0.75	17.0–19.0	10.5–13.0	...	...
S30800	308	0.08	2.00	0.045	0.030	0.75	19.0–21.0	10.0–12.0	...	...
S30900	309	0.20	2.00	0.045	0.030	1.00	22.0–24.0	12.0–15.0	...	...
S30908	309S	0.08	2.00	0.045	0.030	0.75	22.0–24.0	12.0–15.0	...	...
S31000	310	0.25	2.00	0.045	0.03	1.50	24.00–26.00	19.00–22.00	...	...
S31008	310S	0.08	2.00	0.045	0.030	1.50	24.0–26.0	19.0–22.0	...	...
S31400	314	0.25	2.00	0.045	0.030	1.50–3.00	23.0–26.0	19.0–22.0	...	...
S31600	316	0.08	2.00	0.045	0.030	0.75	16.0–18.0	10.0–14.0	2.00–3.00	0.10N
S31603	316L	0.030	2.00	0.045	0.030	0.75	16.0–18.0	10.0–14.0	2.00–3.00	0.10N
S31651	316N	0.08	2.00	0.045	0.030	0.75	16.0–18.0	10.0–14.0	2.00–3.00	0.10–0.16N
S31700	317	0.08	2.00	0.045	0.030	0.75	18.0–20.0	11.0–15.0	3.0–4.0	0.10N
S31703	317L	0.030	2.00	0.045	0.030	0.75	18.0–20.0	11.0–15.0	3.0–4.0	0.10N
S32100	321	0.08	2.00	0.045	0.030	0.75	17.0–19.0	9.0–12.0	...	TC: 5(C + N) min
N08330	330	0.08	2.00	0.030	0.030	0.75–1.50	17.0–20.0	34.0–37.0	...	...
S34700	347	0.08	2.00	0.045	0.030	0.75	17.0–19.0	9.0–13.0	...	Nb: 10 × C min
S34800	348	0.08	2.00	0.045	0.030	0.75	17.0–19.0	9.0–13.0	...	Nb: 10 × C min
S38400	384	0.08	2.00	0.045	0.030	1.00	15.0–17.0	17.0–19.0	...	...
Ferritic grades										
S40500	405	0.08	1.00	0.040	0.030	1.00	11.5–14.5	0.60	...	0.10–0.30Al
S41008	410S	0.08	1.00	0.040	0.030	1.00	11.5–13.5	0.60	...	...
S42900	429	0.12	1.00	0.040	0.030	1.00	14.0–16.0	...	...	...
S43000	430	0.12	1.00	0.040	0.030	1.00	16.0–18.0	0.75	...	...
S43020	430F	0.12	1.25	0.06	0.15 min	1.00	16.0–18.0	0.75	0.60	...
S43023	430FSe	0.12	1.25	0.06	0.06	1.00	16.0–18.0	0.75	...	0.15Se min
S43400	434	0.12	1.00	0.040	0.030	1.00	16.0–18.0	...	0.75–1.25	...
S43600	436	0.12	1.00	0.040	0.030	1.00	16.0–18.0	...	0.75–1.25	Nb: 5×C–0.80
S43035	439	0.030	1.00	0.040	0.030	1.00	17.0–19.0	0.50	...	4(C + N) + 0.20 ≤Ti ≤1.10
S44200	442	0.20	1.00	0.040	0.040	1.00	18.0–23.0	0.60	...	...
S44400	444	0.025	1.00	0.040	0.030	1.00	17.5–19.5	1.00	1.75–2.50	4(C + N) + 0.20 ≤Ti + Nb≤0.80
S44600	446	0.20	1.50	0.040	0.030	1.00	23.0–27.0	0.75	...	0.25N
Martensitic grades										
S40300	403	0.15	1.00	0.040	0.030	0.50	11.5–13.0	0.60	...	...
S41000	410	0.08–0.15	1.00	0.040	0.030	1.00	11.5–13.5	0.75	...	...
S41400	414	0.15	1.00	0.040	0.030	1.00	11.5–13.5	1.25–2.50	...	...
S41600	416	0.15	1.25	0.060	0.15 min	1.00	12.0–14.0	...	0.60	...
S41623	416Se	0.15	1.25	0.060	0.060	1.00	12.0–14.0	...	...	0.15Se min
S42000	420	0.15 min	1.00	0.040	0.030	1.00	12.0–14.0	0.75	0.50	...
S42020	420F	0.15 min	1.25	0.060	0.15 min	1.00	12.0–14.0	0.50	0.60	0.60Cu
S42200	422	0.20–0.25	1.00	0.025	0.025	0.50	11.0–12.5	0.50–1.00	0.90–1.25	0.20–0.30V, 0.90–1.25W
S43100	431	0.20	1.00	0.040	0.030	1.00	15.0–17.0	1.25–2.50	...	...
S44002	440A	0.60–0.75	1.00	0.040	0.030	1.00	16.0–18.0	...	0.75	...
S44003	440B	0.75–0.95	1.00	0.040	0.030	1.00	16.0–18.0	...	0.75	...
S44004	440C	0.95–1.20	1.00	0.040	0.030	1.00	16.0–18.0	...	0.75	...
Precipitation-hardening grades										
S17400	630	0.07	1.00	0.040	0.030	1.00	15.0–17.5	3.00–5.00	...	3.00–5.00Cu, 0.15–0.45Nb
S17700	631	0.09	1.00	0.040	0.030	1.00	16.0–18.0	6.50–7.75	...	0.75–1.50Al
S15700	632	0.09	1.00	0.040	0.030	1.00	14.0–16.0	6.5–7.7	2.00–3.00	0.75–1.50Al
S35000	633	0.07–0.11	0.50–1.25	0.040	0.030	0.50	16.0–17.0	4.00–5.00	2.50–3.25	0.07–0.13N
S35500	634	0.10–0.15	0.50–1.25	0.040	0.030	0.50	15.0–16.0	4.00–5.00	2.50–3.25	0.07–0.13N
S66286	660	0.08	2.00	0.040	0.030	1.00	13.5–16.0	24.0–27.0	1.00–1.50	1.90–2.35Ti, 0.35Al, 0.10–0.50V, 0.001–0.010B

(a) Maximum unless otherwise indicated; all compositions include balance of iron

Table 2 Chemical composition in wt% of Fe – alloys which are in use in different corrosion atmospheres [7]

The good corrosion resistance of Ni – Cr and Fe – Cr alloys is derived from the ability of these alloys to form a protective scale (Cr_2O_3) with low porosity and good adherence, high thermodynamic stability and to grow at a slow rate of protective scale. It was observed that 20 wt% is the minimum content of Cr to develop a protective scale (Cr_2O_3) in Fe – Cr base alloys [8].

The Fe – Cr steels which contain less than 20 wt% of Cr, develop in oxidising environment a multilayer structure consisting of (from top): Fe_2O_3 (hematite), Fe_3O_4 (magnetite), spinel ($FeCr_2O_4$), wustite (FeO), and chromia oxide (Cr_2O_3). It was suggested [9,10] that in low Cr, Fe – Cr steels, the oxides grow by the outward diffusion (from metal matrix) of Fe ions, due to the very small lattice diffusion of O^{2-} anions in iron oxides. Another studies [11,12] reported, that the inward oxide growth in temperature range 773 – 873 K is favourable due to the fast diffusion of oxygen anions (O^{2-}) along oxides grain boundaries.

The formation of protective Cr_2O_3 oxide scale is the key point for corrosion resistance of high Cr content Fe – Cr and Ni – Cr alloys. A number of investigations have been carried out, to understand the mechanism of Cr_2O_3 growth at the temperature up to 1273 K [13,14,15,16].

Confirming the previous observation [8] Wasilewski, Robb, Giggins, and Pettit [17,18] indicated that the minimum content of Cr (wt %) which promotes, the formation of Cr_2O_3 oxide scale is equivalent to 20 – 25 wt%.

Another study performed by Birks and Rickret [19] reported that if Cr content is around 10 wt% then spinel $(Cr,M)_3O_4$ develops, authors suggested that for the formation of protective Cr_2O_3 thin scale 20 wt% of Cr is required or more.

Sims [20] studies showed that in Fe and Ni base alloys a Cr content of 15 wt% offer a reasonable degree of protection against high temperature oxidation. However for the formation of a continuous scale the Cr content needs to be between 18 – 19 wt%.

Wood [21] proposed a mechanism of oxidation of Ni – Cr alloys with high content of Cr (25 – 30 wt %). It was suggested that in the beginning of oxidation process Ni and Cr oxides are formed due to the outward diffusion of Ni and Cr from the matrix (Ni – Cr alloy) **(Fig 5a)**.

Due to the lower ΔG° (ΔG° of Cr_2O_3 = - 544284 J/mole) of the formation of Cr_2O_3, the chromium oxide will form first, then NiO (ΔG° = -125604 J/mole).

However the NiO growth is faster than the growth rate of Cr_2O_3, the whole surface of the alloy is covered by a thin NiO oxide **(Fig 5B)**. The mechanism proposed is shown in **figure 5**.

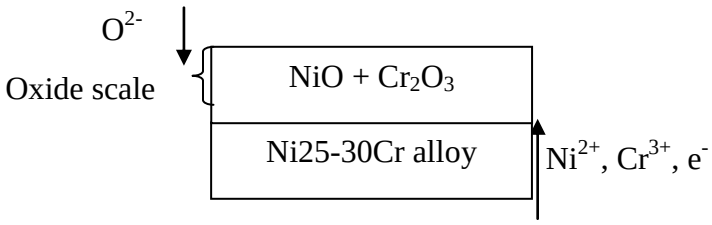

A) Initial stage of oxidation of Ni 25 – 30 wt% alloy in oxidation atmosphere [21]

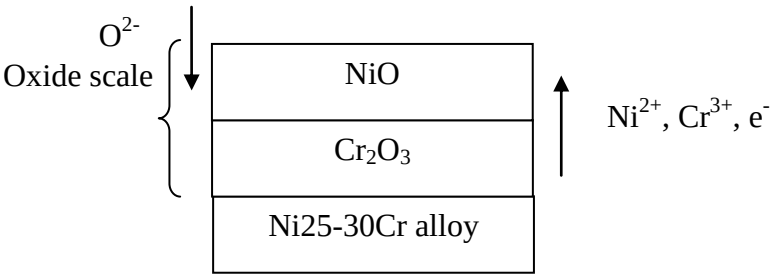

B) NiO development during oxidation of Ni 25 – 30 wt% alloy in oxidation atmosphere [21]

The further mass transport of Ni ions from the bulk material to outer scale produces a solid solution of $NiO + Cr_2O_3$, underneath this outer scale of solid solution of $NiO + Cr_2O_3$, a solid solution of $Cr_2O_3 + NiO$ formed. The solid solution of $Cr_2O_3 + NiO$ formed due to the outward diffusion of Ni ions to the outer scale (solid solution of $NiO + Cr_2O_3$).

Between the substrate (Ni25-30Cr alloy) and innermost layer (a solid solution of $Cr_2O_3 + NiO$) a Ni-Cr + Cr_2O_3 band appeared. This band formed due to the inward diffusion of O^{2-} ions and formation of an internal oxidation region. The final scale of exposed Ni-25-30Cr alloy in oxidation atmosphere is shown in **figure C.**

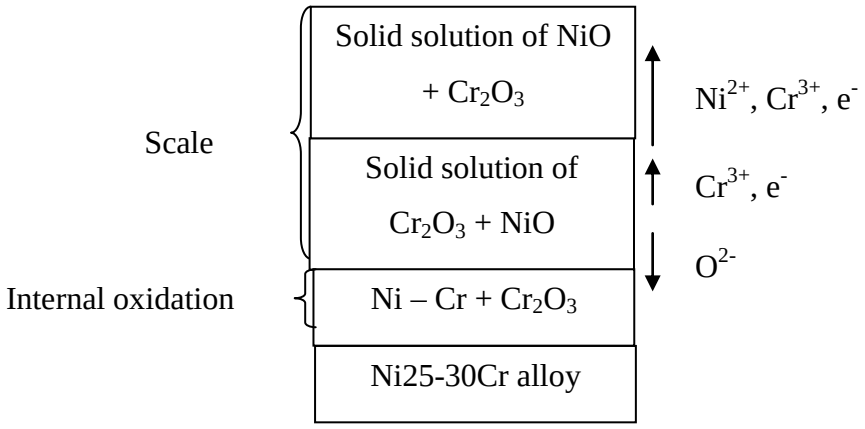

C) Final scale structure of exposed material [21]

Figure 5 Oxidation mechanism on rich in Cr, Ni – Cr alloys [21]

During exposure the thickness of the layers are constant because due to the following **reaction 2** which takes place within the formed scale:

Reaction 2 $$2Cr^{3+} + 3NiO \rightarrow 3Ni^{2+} + Cr_2O_3$$

Such scale may lose the protective properties due to the crack formation but re-healing of scale formed in Ni – Cr alloys is faster than on Fe – Cr alloys. Fe – Cr – alloys are unable to re – heal its scales. The re-healing process is Ni-Cr alloys are due to the faster diffusion of Cr in Ni-Cr alloys than in Fe-Cr alloys.

Ignatow and Szamugunowa [22] observed that in the temperature range between 773 – 973 K in Ni – alloys the Cr_2O_3 formed when Cr content was equivalent to 20 wt%, the scale morphology at higher temperature 1073 – 1273 K consisting of: the outer scale $NiCr_2O_4$ and the inner scale consisting of Cr_2O_3 oxide. When temperature is rising (1273 K) a Cr_2O_3 phase content in the outer scale decreases and forming very thin layer in the scale/alloy interface.

Giggins and Petit [18] observed that protective oxide scale (Cr_2O_3) may be formed at 1073 – 1273 K, when Cr content in the Ni – alloy is equivalent to 10 – 12 wt%, moreover at 1473 K more than 15 wt% of Cr is required to develop a protective

scale. Due to evaporate process of Cr_2O_3 oxide at the temperature higher than 1473 K the Cr content should be higher than 15 wt% in the exposed Ni – alloys.

General statement was postulated by Wasilewski and Rapp [17], the authors classified Ni – base alloys with different addition of Al and Cr into three different groups, according to their ability to develop scales of the constituted elements.

1. Type I –Ni base alloys with very low Al and Cr content, scale morphology consisting of: NiO the outer scale with internal Cr_2O_3 and Al_2O_3 oxides.

2. Type II – Ni base alloys with low content of Al (1 – 3 wt %), high Cr content (>15 wt %), the scale morphology consisting of: Cr_2O_3 outer scale with the internal Al_2O_3 oxide

3. Type III – Ni base alloys with high Al content (>3 wt %) and high Cr content (>15 wt %), scale morphology consisting of: Al_2O_3 oxide scale.

The authors [17] observed that the oxidation kinetic rate is decreases more than one order of magnitude when Fe - or Ni base alloys are moved from Type I to Type II chemical composition. Similar the kinetic rate was observed to decrease when the chemical composition of Fe – Ni alloys is shifted from Type II to Type III. The elimination of NiO formation is essential to improve the corrosion resistance of Fe – Ni – base alloys. Furthermore the development of internal Cr_2O_3 oxide reduces the inward diffusion of O^{2-} ions and reduces the activity of oxygen. In needs to be noted that 3 wt% of Al is a critical concentration of Al in order to develop protective Al_2O_3 scales.

Trindade and Krupp [23] investigated three ferritic steels, at high temperatures (**Table 3,** in wt %). The three low alloy steels (A, B, and C) were subjected to oxidation at 823 K for 72 hours, while the austenitic Fe – alloy (TP 347) was exposed to 1023 K for 120 hours.

Alloy	C	Cr	Si	Mn	Al	Mo	Ti	Fe	Ni
A	0.076	0.55	0.36	1.01	0.04	-	-	Bal.	0.21
B	0.06	1.43	0.22	0.59	0.04	-	-	Bal.	0.04
C	0.09	2.29	0.23	0.59	0.01	1.0	-	Bal.	0.44
TP 347	0.04	17.50	0.29	1.84	-	-	-	Bal.	10.7

Table 3 Chemical composition (wt %) of Fe – based alloys used in oxidation experiment at high temperature [23]

The three low Fe – alloy steels (alloy A, B, and C) developed during the oxidation test at 550^{o}C (823 K) a multilayered scale consisting of Fe_2O_3 (outer layer) followed by Fe_3O_4 second layer. Below this second layer the inner scale was formed with: Fe_2O_3, Fe_3O_4, $FeCr_2O_4$ spinel, and Cr_2O_3 in sequence. The scale morphology developed during oxidation at 823 K is presented in **figure 6**:

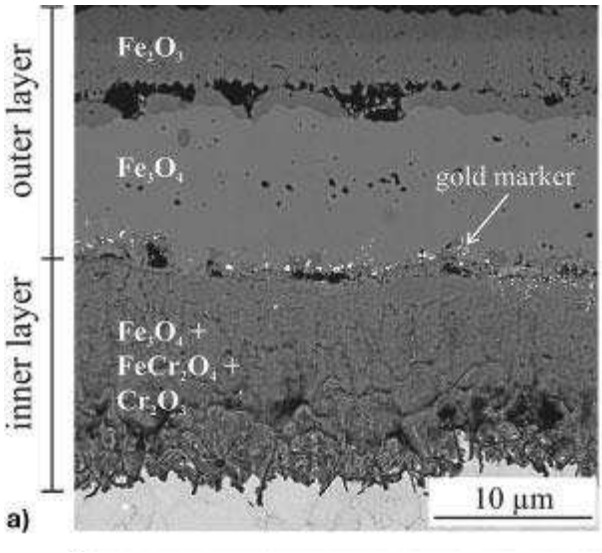

Figure 6 Scale morphology of steel B - low Fe alloy steel exposed to oxidation atmosphere at 823 K for 72 hours test [23]

The kinetic growth of exposed samples (low alloying Fe steels) is presented in **figure 7**.

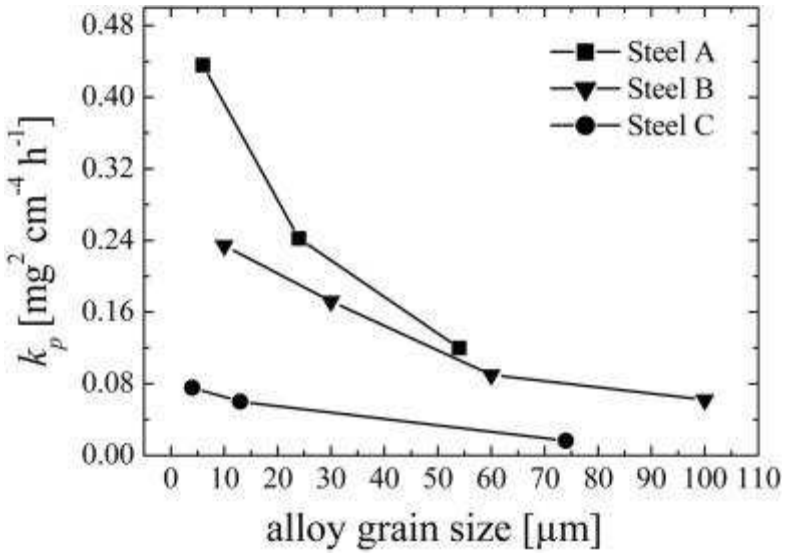

Figure 7 Kinetic data of low alloy steels in laboratory air at 823 K for 72 hours [23]

Trindade [23] in his work deposited a gold marker on the low alloy steels (A, B, and C) sample surface in order to investigate the growth mechanism in oxidizing environment at 823 K. It was observed that after oxidation period of 72 hours the marker was found within the developed scale. The position of the marker revealed that the mechanism of oxidation involved outward transport of Fe^{3+} or Fe^{2+} ions from the bulk material, and inward diffusion of O^{2-}.

The austenitic Fe - alloy steel (TP 347) formed an outer scale consisted of a thin but not a continuous protective oxide scale of Cr_2O_3 and a non protective FeO (high amount of cation defects) oxide after 120 hours of exposure at 1023 K in air atmosphere. The scale morphology is presented in **figure 8**.

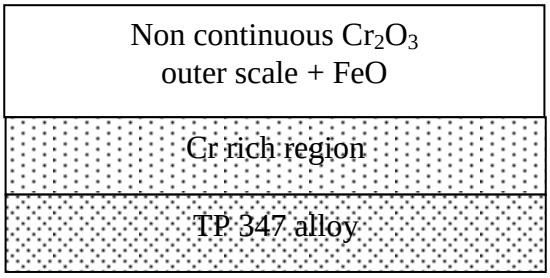

Figure 8 TP 347 scale morphology after exposure for 120 hours at 1023 K [23]

The author [23] suggested that the formation of Cr_2O_3 strongly depends on the grain size. In sample with small grain size allowed high Cr flux from the bulk promoted by grain boundary diffusion leading to the formation of Cr_2O_3.

The samples with bigger grains, the scale morphology consisted of: an outer layer of Fe_2O_3 + Cr_2O_3, and an inner layer consisting of mixed oxides of Fe, Cr, Mn, and Ni.

Figure 9 shows the kinetic data for TP 347 austenitic Fe – alloy with various of grains size after air oxidation at 823 K for 120 hours.

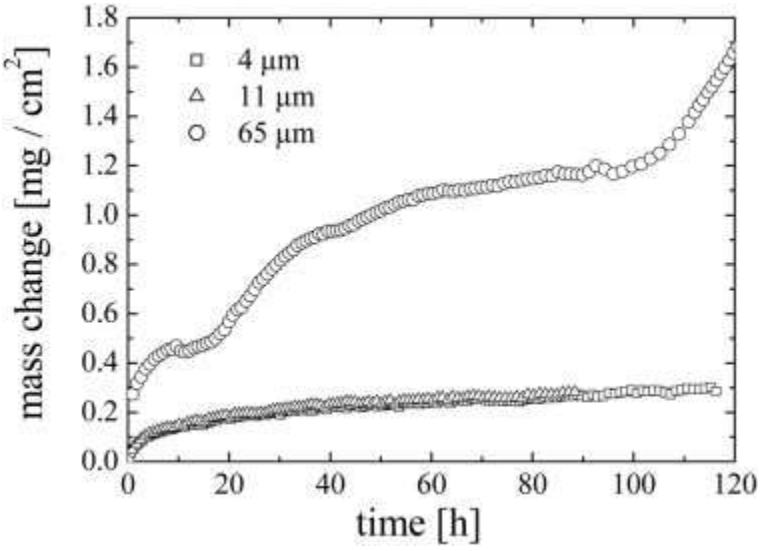

Figure 9 Kinetic data for TP 347 austenitic alloy with different grain sizes after exposure at 1023 K for 120 hours in air atmosphere [23]

The author [23] concluded a low concentration of Cr (17,5 wt%) is required to develop a Cr_2O_3 oxide scale when Fe – Cr alloys possess a fine grains in the microstructure.

In the case of samples with coarse grains (65 µm), higher amount of Cr (over 17,5 wt%) is required to develop a slow growing Cr_2O_3 scale as the influence of the grain boundary, diffusion is minimised in these materials.

The oxidation of Fe3Cr alloy at 1073 K for 6 hours 40 minutes in dry air was investigated by Kahveci and Welsch [24].

The Cr was introduced to Fe – base alloy in order to suppress the formation of multilayer scale consisted of: FeO (wustite), Fe_3O_4 (magnetite) and Fe_2O_3 (hematite). The Kahveci [24] shows that after heat treatment in dry air at 1073 K for

6 hours and 40 minutes of Fe3Cr alloy, a multilayered scale formed, however the scale did not consist FeO (wustite). The scale morphology is presented in **figure 10**.

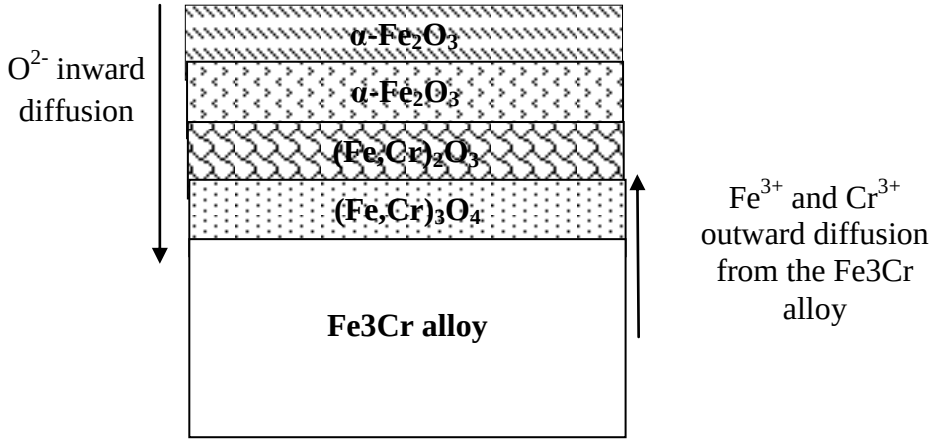

Figure 10 Scale morphology developed after 6 hours and 40 minutes oxidation in dry air at 1073 K on Fe3Cr alloy [24]

The mechanism of the scale development in Fe3Cr alloy has been proposed by Kahveci and Welsch [24]. It was observed that inward diffusion of O^{2-} ions and outward diffusion of Fe^{3+} and Cr^{3+} ions occurred in order to produce a multilayered scale structure. Oxygen ions diffuses through all layers and causes the internal oxidation near to the scale/alloy interface where $(Fe,Cr)_3O_4$ and $(Fe,Cr)_2O_3$ formed. Due to the higher diffusion coefficient of Fe, the outer scale consisted Fe_2O_3 scale. The doubled Fe_2O_3 scale developed with different microstructure; the outer Fe_2O_3 possessed small grains whereas the inner Fe_2O_3 layer had a bigger grains. Moreover the authors observed that the enrichment zone of Cr in the spinel layers ($(Fe,Cr)_2O_3$ and $(Fe,Cr)_3O_4$ in **Fig. 10)**, led to decrease in oxidation kinetic law. The lower kinetics was due to reduction of the diffusion paths (grain boundaries) for Fe^{3+} ions within the spinel layers.

The similar mechanism was postulated by Atkinson [25] for the oxidation of nickel. The kinetics data obtained for oxidised Fe3Cr alloy at 800^{o}C (1073 K) for 6 hours and 40 minutes, show, that the alloy was consumed in the first stage (50 minutes of the test) of experiment according to the parabolic rate, whereas the next stage (from 50 minutes to 6 hours and 40 minutes) alloy was consumed following to a less than parabolic law.

The high temperature behaviour of Fe-Cr alloys in wet oxygen was investigated by Jianian [26]. The author oxidised two different alloys in air with different amounts of the water vapour (10vol. % of H_2O and 25vol. % of H_2O) at two

temperatures 1173 and 1273 K. The chemical composition (wt %) of the alloys used in the test is presented in **table 4**:

Alloy	Cr	Mn	Si	C	S	P	Fe
Fe15Cr	17.73	<0.01	<0.005	0.007	0.008	<0.005	Balance
Fe20Cr	19.65	<0.01	<0.005	0.009	0.008	<0.005	Balance

Table 4 The chemical composition of the alloys used in the experiment with different amount of water vapour [26]

When a Fe20Cr alloy was exposed to 1273 K with 10vol. % of H_2O a protective Cr_2O_3 developed in the outer part of the scale in the first hours of exposure.

However iron-rich nodules developed on the edges and corners of oxidised sample, the sample Fe20Cr showed the formation of a thin scale in the central part (Cr_2O_3) of the scale and a thick scale at the edges (Fe_2O_3). In the next period of experiment (over 10 hours), a thin scale (Cr_2O_3) disappeared and the whole sample Fe20Cr was covered by a thick scale (Fe_2O_3). The thick scale revealed that the outer part of the multilayered scale consisted of Fe_2O_3; the innermost part was occupied by the spinel $FeCr_2O_4$, the middle layer was formed from Cr- rich band. This Cr-rich band derived from the Cr_2O_3 formed in the initial period of the experiment. The schematic of the scale degradation is presented in **figure 11**. First hours of exposure of Fe20Cr alloy to 10vol. % H_2O at 1273 K.

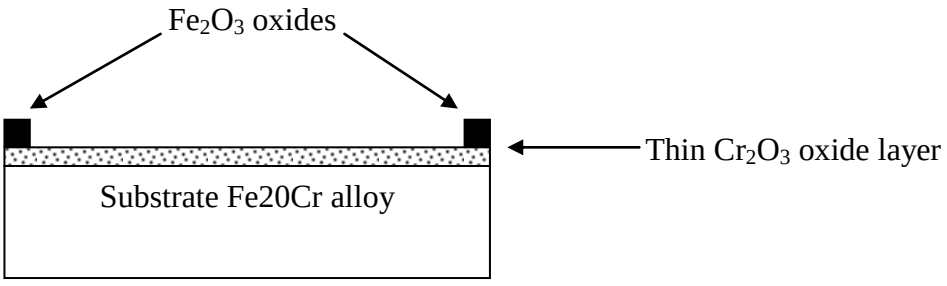

Scale development after 10 hours of exposure of Fe20Cr alloy to 10vol. % H_2O at 1273 K [26]

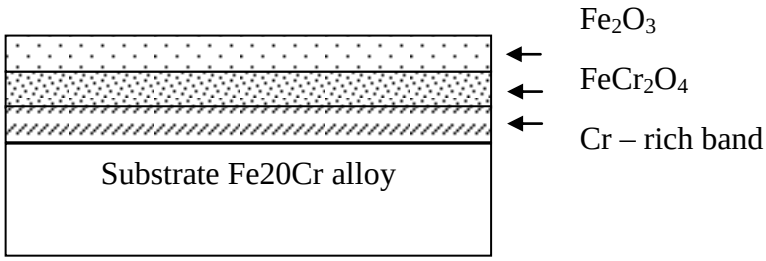

Figure 11 Scale development of oxidized sample in 10%vol. % H_2O at 1000 hours for 20 hours [26]

The influence of water vapour was concluded [26] to the effect of the transformation from protective Cr_2O_3 scale to non-protective Fe_2O_3 scale, this conclusion is in good agreement with other studies [27, 28]. Moreover the water vapour effect is associated with the incubation period; the incubation period is related to the amount of water vapour in the ambient atmosphere, temperature, and the Cr content in the exposed alloy.

If temperature of exposure is high or if high amount of water vapour is in the oxidised atmosphere and low Cr content in the alloy, the incubation time becomes shorter. It was also suggested that the transformation from protective to non-protective scale was related to the formation of iron-rich nodules. When iron-rich nodules were formed, the incubation period was finished and the breakaway oxidation starts to ensure.

Based on observations from experiments (Fe20Cr alloy exposed to water vapour (10% vol. of H_2O) oxidation atmosphere, Jianian [26] proposed the mechanism of the scale degradation is related to the water vapour effect.

Due to the outward diffusion of Cr from the bulk material voids and micro-cracks probably formed in the oxide scale in initial period of exposure, the pits, voids, micro-cracks start to appear, more often in the corners than in central part of the sample (**Figure 12a**). The micro-crack formations are related to the stresses and strains, which are developed particularly in the non-flat areas.

When the micro-cracks are developed, the oxygen from the ambient atmosphere (O^{2-}) starts the inward diffusion through these micro-cracks and then reaches the scale/substrate interface (**Figure 12b**). Moreover at the high temperature the H_2O become unstable and transform into gaseous state according to the reactions which occurred in the top scale of oxidised sample (Fe20Cr):

Reaction 3 $$H_2O \rightarrow 2H^+(g) + \frac{1}{2}O^{2-}(g)$$

The released H^+ and O^{2-} react in the depleted region of Cr^{3+} on the surface of the alloy (Cr^{3+} ions formed a thin oxide layer in the initial period of the experiment) with Fe^{3+} ions which are in the bulk material and forms Fe_2O_3 according to the **reaction 4** (**Figure 12c**):

Reaction 4 $$2H^+(g) + 3O^{2-}(g) + 2Fe^{3+} \rightarrow Fe_2O_3(s) + 2H^+(g)$$

The released H^+ ions reduce the protectiveness of the Cr_2O_3 by following **reaction 5**:

Reaction 5 $$6H^+(g) + Cr_2O_3 \rightarrow 2Cr^{3+} + 3H_2O$$

At this moment, the concentration of H^+ and O^{2-} ions (in the atmosphere due to the decompose of H_2O according to the **reaction 3** is very high, then Fe_2O_3 reacts with H^+ and O^{2-} ions to produce a thicker scale and also Fe_2O_3 reacts with Cr to produce Fe-Cr spinel ($FeCr_2O_4$) according to the following reaction (**Figure 12d**):

Reaction 6 $$Fe_2O_3 + 4Cr^{3+} + H^+ + O^{2-} \rightarrow 2FeCr_2O_4 + H^+$$

Thus, when the micro-cracks appeared in the Cr_2O_3 scale in the initial period of oxidation in wet atmosphere (with some content of H_2O vapour), the breakaway oxidation will accelerate the degradation of Fe-Cr alloy. The schematic breakaway oxidation of Fe-Cr alloys is presented in **figure 12a - 12d.**

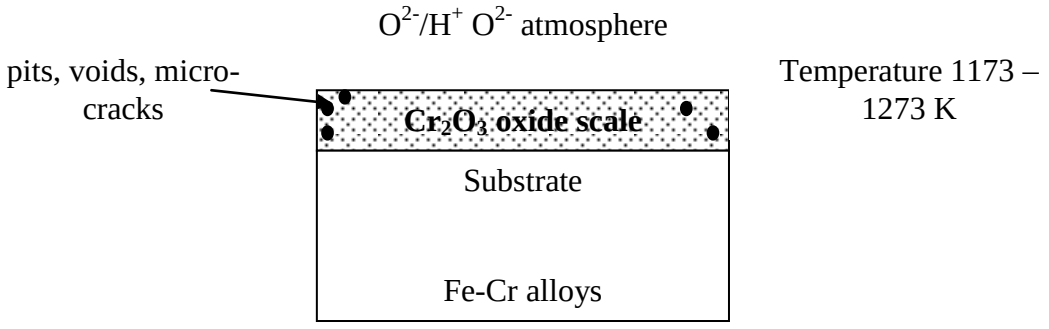

Figure 12a Initial period of oxidation in the wet atmosphere at temperature 1173 – 1273 K of Fe20Cr alloys [26]

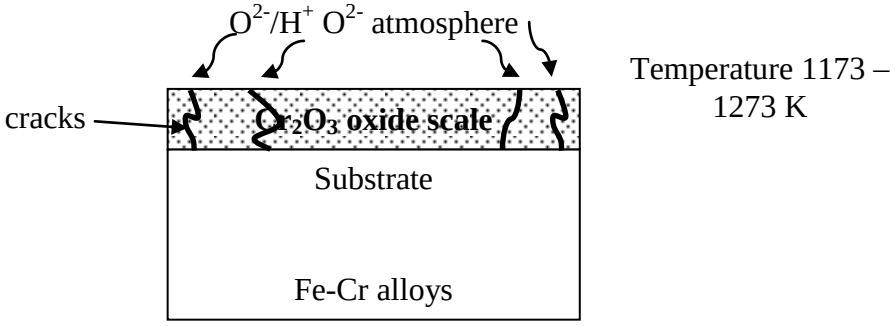

Figure 12b Crack initiation during the oxidation in the wet atmosphere at temperature 1173 – 1273 K of Fe20Cr alloys [26]

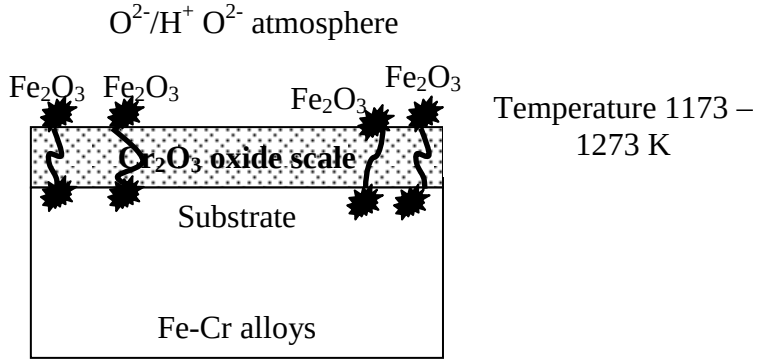

Figure 12c Breakaway stage in wet atmosphere at temperature 1173 – 1273 K of Fe20Cr alloys [26]

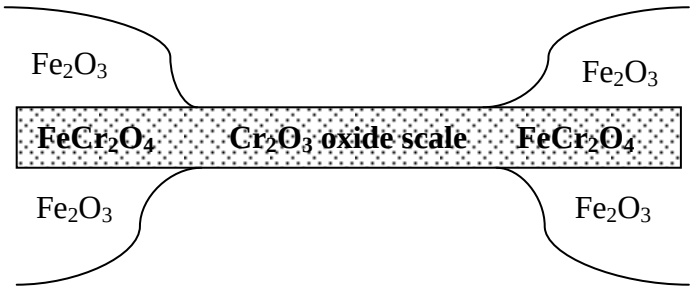

Figure 12d Final stage of the degradation of Fe20Cr alloys at temperature 1173 – 1273 K in wet atmosphere [26]

Figure 12 Breakaway mechanism of Fe-Cr alloys at temperature range 1173 – 1273 K in wet atmosphere (with water vapour content) [26]

The effect of addition of a thin CeO_2 deposit on the surface of Fe20Cr alloy was also investigated in this work [26]. It was concluded that the addition of a small deposit on the surface of F20Cr alloy reduces the risk of breakaway oxidation due to the improved adhesion between scale and the substrate. According to the work performed by Nicholls and Hancock [29] who suggested, that a small addition of

reactive element reduces the number of voids and inhibits the initiation of the scale degradation.

The kinetics data obtained from Jianian [26] experiment show, that at the two different temperatures 1173 and 1273 K with different amount of water vapour all samples (Fe15Cr and Fe20Cr) except sample with CeO_2 deposit (Fe20Cr coated with CeO_2 deposit) suffered the breakaway oxidation degradation.

Trinidade and Krupp [23] investigated the oxidation of Ni – base alloys (Inconel 625 Si and Inconel 718) exposed at 1273 K for 100 hours. The chemical composition (wt %) of the alloys is given in **table 5**.

	C	Cr	Si	Mn	Al	Mo	Ti	Fe	Ni
Alloy									
Inconel 625 Si	0.01	19.00	1.20	0.07	0.24	8.9	0.28	2.80	Bal.
Inconel 718	0.04	18.20	0.40	0.06	0.50	3.0	1.00	18.70	Bal.

Table 5 Chemical composition of the alloys used in oxidation experiment at 1273 K for 100 hours [23]

Both exposed alloys (Inconel 625 Si and Inconel 718) developed a continuous Cr_2O_3 outer scale. Furthermore, in the case of Inconel 625Si, underneath the Cr_2O_3 a SiO_2 layer formed. Also it is important to note that in both alloys internal oxidation took place; due to the fast inward diffusion ox O^{2-} ions via grain boundaries, as a result Al_2O_3 oxide formed at the grain boundaries.

Figure 13 presents the scale morphology of cross – sectioned samples (a) Inconel 625 Si and b) Inconel 718 after 90 and 100 hours respectively. The experiment was carried out at 1273 K for 100 hours.

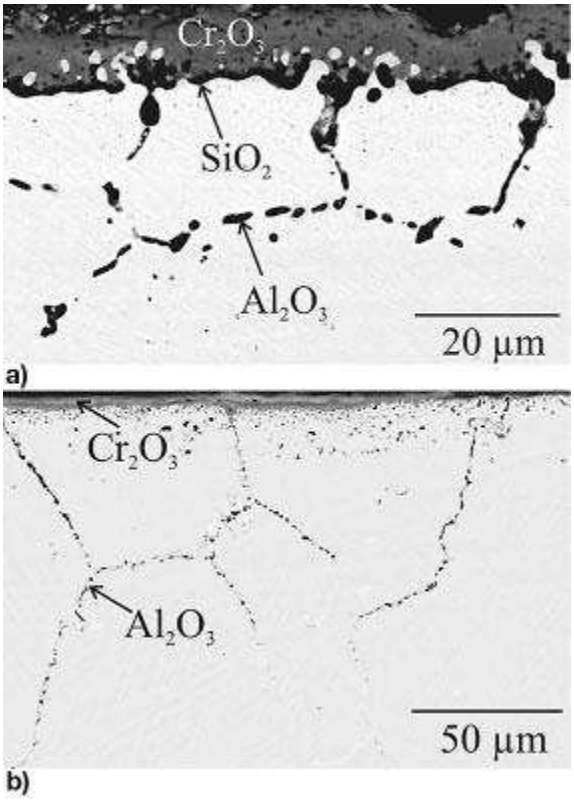

Figure 13 Scale morphology of; a) Inconel 625Si and b) Inconel 718 after 90 and 100 hours respectively at 1273 K in air atmosphere [23]

The formation of SiO_2 underneath the outer Cr_2O_3 scale, clearly had a beneficial effect on kinetic growth; the mass gain of Inconel 625 Si was smaller than Inconel 718 after exposure to air atmosphere at 1000^{o}C (1273 K) for 100 hours.

Figure 14 shows the kinetic data of exposed Inconel samples with parabolic rate constant values.

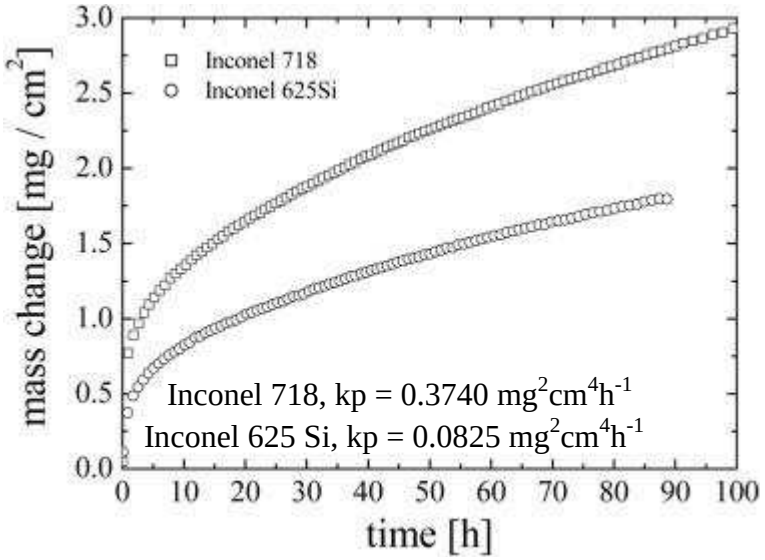

Figure 14 Kinetic data form a) Inconel 625Si and b) Inconel 718 after 90 and 100 hours respectively at 1273 K in air atmosphere [23]

Hong, Hwang, Han, and Kang [30] investigated the cyclic oxidation (500 cycles of 40 min + 20 min of cooling) of Pt/Pd modified aluminide coating on Ni – base super-alloy (Inconel 738LC) at 1423 K, the chemical composition of exposed alloy is given in **table 6**.

Alloy	C	Cr	Ni	Co	Mo	W	Ti	Al	B	Zr	Ta
IN 738LC	0.11	16.00	Bal.	8.5	1.75	2.6	3.4	3.4	0.01	0.06	1.75

Table 6 Chemical composition (in wt %) in oxidized atmosphere at 1423 K [30]

The Pt/Pd coating was deposited by electroplating two separate layers of Pt and Pd. The Al pack cementation was carried out at 1323 K for 5 hours in pack mixture consisting of: Inconel 738LC with pre-deposited Pt, Pd, Pt/Pd coatings, 15wt% Al powder, 2wt% of NH_4Cl and 83 wt% of Al_2O_3 as a filler. The deposited coatings after annealing and aluministation consisted of a Pt modified coating containing three layers: β-NiAl, $PtAl_2$, and β-NiAl and an interdiffusion zone. Both Pd and Pt/Pd modified aluminide coatings contained two layers: β-NiAl and an interdiffusion zone.

Figures 15 and **16** show the microstructure formed on Inconel 738LC with Pt and Pt/Pd modified aluminide coatings after 250 and 500 hours of cyclic oxidation at 1423 K respectively.

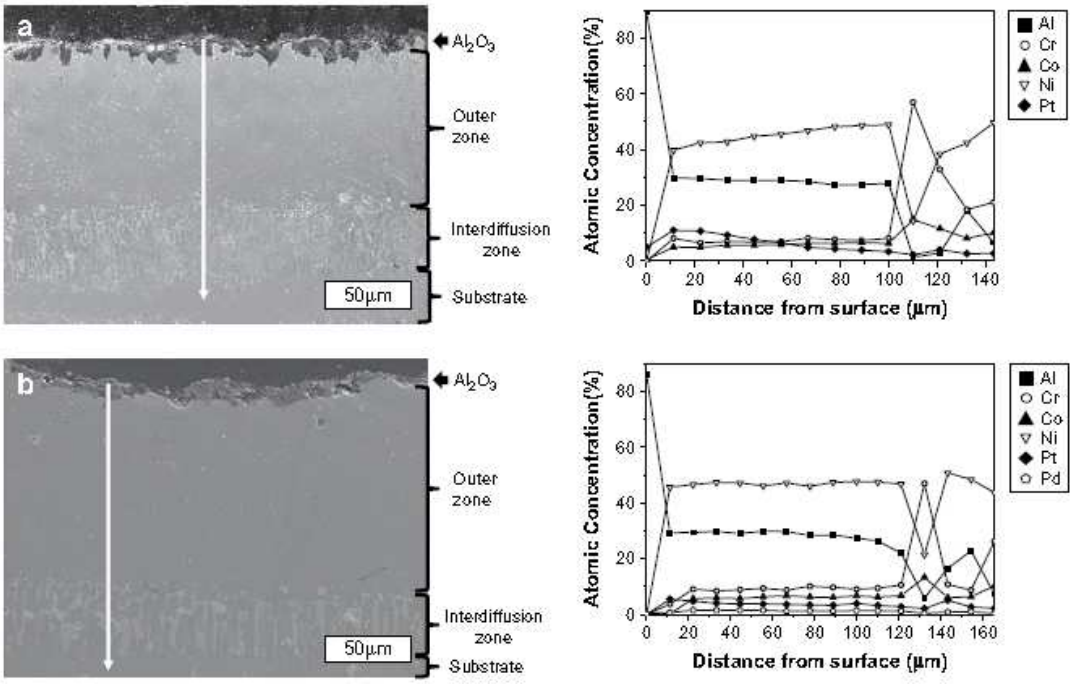

Figure 15 Cross – sectional images with EDS concentration profiles of Inconel 738LC after 250 hours of cyclic oxidation in air at 1423 K, a) Pt modified aluminide coating, B) Pt/Pd modified aluminide coating [30]

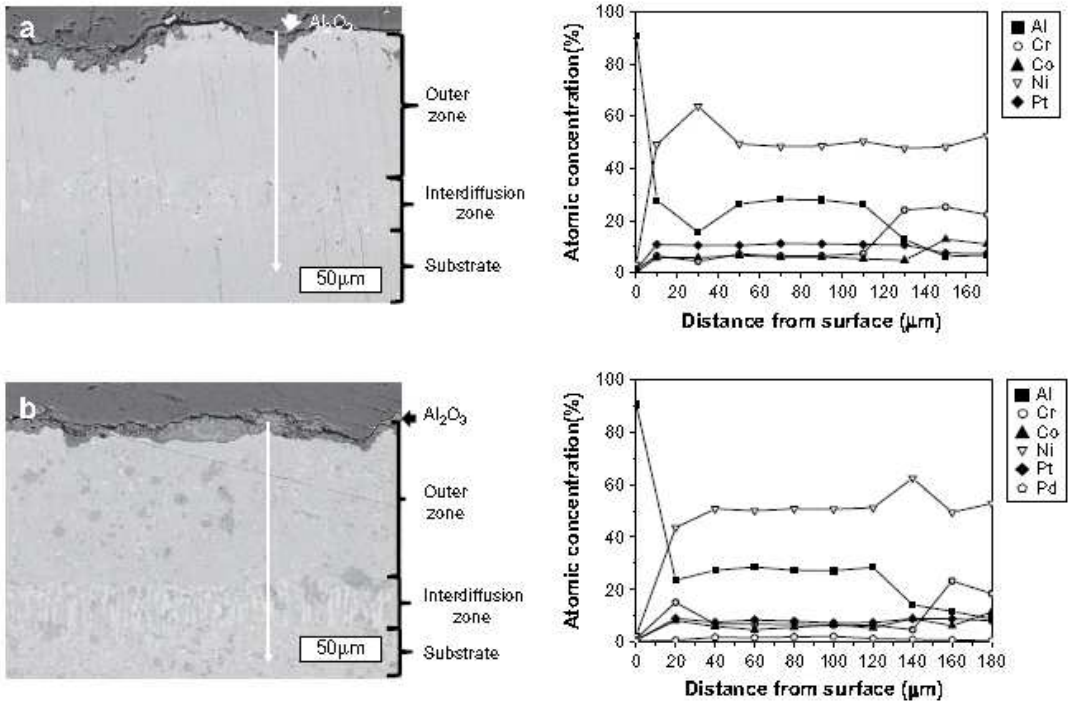

Figure 16 Cross – sectional images with EDS concentration profiles of Inconel 738LC after 500 hours of cyclic oxidation in air at 1423 K, a) Pt modified aluminide coating, B) Pt/Pd modified aluminide coating [30]

Figure 17 presents the damaged Pd modified coating deposited on Inconel 738LC, the deposited coating failed (due to the crakes propagation and scale spallation) and was not investigated after 200 hours of cyclic oxidation at 1423 K.

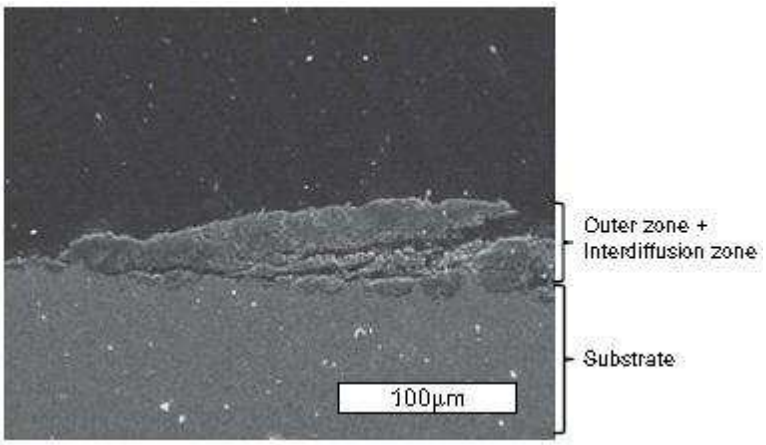

Figure 17 Pd modified aluminide coating on Inconel 738LC after 200 hours of cyclic oxidation at 1423 K [30]

After 500 hours of cyclic oxidation, in both coatings β-NiAl transformed into γ' – Ni_3Al phase, γ - Ni phase was observed only in Pt/Pd modified coating, but not in Pt modified after 500 hours of cyclic oxidation at 1423 K. Furthermore, in Pt/Pd modified coating γ - Ni phase contained a large amount of Cr, a region with high Cr content in γ - Ni developed beneath the Al_2O_3 outer scale. The high content of Cr increased the adhesion and stability of Al_2O_3 oxide scale. The kinetic data for Pt, Pd and Pt/Pd modified aluminide coating is presented in **figure 18**.

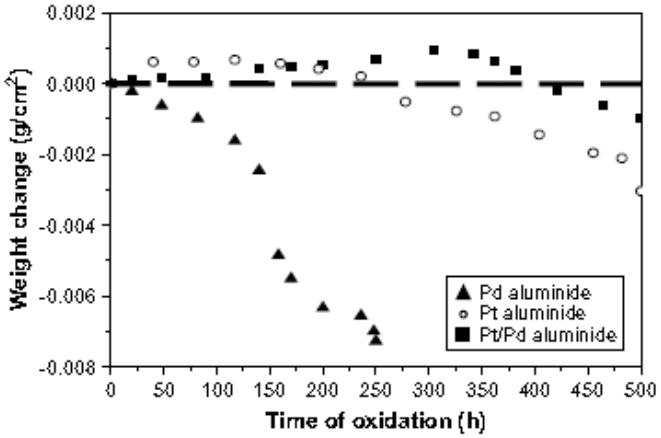

Figure 18 Cyclic oxidation data, obtained for Pt, Pd, and Pt/Pd modified aluminide coating after 500 hours of heat treatment at 1423 K [30]

The Pd modified aluminide coating, showed a large mass loss during the short period of cyclic oxidation at 1423 K. The highest mass gain was reached by

Pt/Pd modified coating after 250 hours cycles of oxidation at 1423 K. The Pt modified coating shown the mass gain after 125 hours of cyclic oxidation, then weight losses after 230 hours of cyclic oxidation, thus spallation and loss of mass occurred in Pt modified coating. The mass losses of Pt and Pd modified coating were equivalent to 3,5 mg/cm^3 and 2,5 mg/cm^3 respectively after 500 hours of cyclic oxidation.

Ch.II.Sec.1.5.2 Oxidation of γ - TiAl alloys

The current information on the high temperature oxidation behaviour of TiAl and TiAl base materials displays a complex pattern [31] [32] [33] [34]. The formation of slow-growing adherent and protective Al_2O_3 scale is much more difficult in TiAl intermetallics than in disordered titanium-aluminium alloys and in NiAl [35] [36].

The difficulty in the development of Al_2O_3 scale in TiAl intermetallics is associated with the requirement for the higher activity of Al in order materials. The thermodynamic imperative predicts the formation of both titanium and aluminium oxides [37].

Legzdina and Robertson [38] have found in that in the temperature range (823-1173 K) in low partial pressure of oxygen the oxidation of TiAl (Ti52.1Al2Ta at %) resulted in the formation of a multi-layered surface oxide structure with outer layer being Al_2O_3 followed by a layer of TiO_2. It was shown [18] that the dopant element as Nb can improve the oxidation resistance of TiAl.

Despite of many attractive properties (high temperature strength, reasonable K_1C) however the poor oxidation resistant of these alloys is a major concern. To improve its oxidation resistance at high temperature (1173 K), niobium is considered an excellent dopant.

Yoshihara and Miura [39] investigated addition of 2 to 15 at% of Nb to Ti50Al alloy in oxidation environment at temperature range 1173 1273 K for 25 hours. The authors found that small addition of Nb (up to 10 wt % of Nb) is an effective in decreasing the oxidation rate. More than 15 at% of Nb causes increasing oxidation rate due to the formation of $TiNb_2O_7$ phase. The following mechanism of the improved oxidation resistance of Ti50Al doped by Nb ions was postulated; rutile is known as a non stechiometric phase as $Ti_{1+x}O_{2-y}$. According to Kofstad [40] the

defect structure involves: oxygen vacancies and interstitials Ti^{3+} and Ti^{4+} ions. Moreover oxygen vacancies dominate at low temperatures and high oxygen partial pressures, however interstitial defects (Ti^{3+} and Ti^{4+} ions) dominates at high temperatures and low partial pressures of oxygen. Therefore the defects structure of TiO_2 mainly appears at temperature range between 1173 – 1273 K. Marker experiment shows that the rutile (TiO_2) growth via inward oxygen diffusion.

The effect of impurities on the concentration of defects in TiO_2 was studied [40] the defects in TiO_2 are double charged oxygen vacancies and interstitial Ti ions (Ti^{3+} and Ti^{4+} ions). When addition of metal with higher valence than Ti is introduced, then occupy normal Ti – sites. The substitution of two Nb^{5+} cations with valence 5 reduces one oxygen vacancy and inhibits the kinetics of TiAl alloy. Thus addition of Nb reduces oxygen concentration in TiO_2 phase.

Jiang, Hirohasi and Imanari [41] also found that the niobium can improve the oxidation resistance of TiAl alloys. The tested Ti(0-50 at%)Al alloy with different addition of Nb (0-30 at%) was exposed at 1173 K in dry air at a flow of 100 ml/min for 24 hours. The kinetic data presented by the authors [41] indicates that when Nb concentration increased in the alloy up to 15 – 20 at% the oxidation rate decrease, beyond 15 – 20 at% of Nb the oxidation rate starts to increased. The relationship between Al content and Kp value, shows that increases of Al content leads to decreased of Kp value in all samples (Ti(0-50at%)Al.

The morphologies of exposed samples (Ti10Nb, Ti_3Al15Nb, TiAl20Nb, TiAl15Nb, Ti_3Al20Nb, and TiAl30Nb) shows that when $C_{Nb} >> 15$ at% developed scale consisted of TiO_2 and $TiNb_2O_7$, in Ti_3AlNb when $C_{Nb} << 15$ at% the scale consisted of TiO_2 and Al_2O_3, when $C_{Nb} >> 20$ at% the scale formed TiO_2, Al_2O_3 and $AlNbO_4$ phases. For the TiAl-Nb alloy when $C_{Nb} << 20$ at% scale consisted o TiO_2 and Al_2O_3, when $C_{Nb} = 30$ at%, then TiO_2, Al_2O_3, and $AlNbO_4$ oxides formed.

The authors concluded that Nb improved the oxidation rate; however the development of $TiNb_2O_7$ and $AlNbO_4$ phases may increase the oxidation rate. Zhang and Li [42] investigated three Ti48Al alloys with different implanted Nb ions ($3x10^{15}$, $3x10^{16}$, and $3x10^{17}$ [ions/cm^2]) at 1173 K and 1223 K in oxidation environmental (static air) for 100 hours. The kinetic results show that oxidation rate decrease with increase implanted dose of Nb ions. The investigation performed by EDS analysis indicates that non-implanted sample (Ti48Al) at both temperatures 1173 K and 1223 K developed multilayered structure consisted of TiO_2 and Al_2O_3,

however, the top scale consisted Al_2O_3 oxide scale, however this scale was discontinuous with islands of TiO_2. In implanted alloy (Ti48Al implanted by $3x10^{17}$ Nb ions/cm^2), the outer scale consisted only continuous Al_2O_3 oxide scale. The authors [42] concluded that beneficial effect of Nb ions incorporation is related to the reduction of Ti outward diffusion. Moreover their conclusions are based on postulated theory stated by Yoshihara and Miura [39].

Another study performed with ion implantation of Nb ions was performed by Li and Taniguchi et al [43]. The researchers implanted Al and Nb ions to Ti48Al1.3Fe1.1V0.3B alloy, which was exposed to 1173 K for 349.2 ks to atmospheric air. In this study the researchers found that implantation of Al and Nb ions are beneficial, reducing the oxidation rate at 1173 K. The low oxidation rate of exposed sample (Ti48Al1.3Fe1.1V0.3B) occurred due to the development of a thin and continuous Al_2O_3 scale. Inhibiting the inward diffusion of O_{2-} ions from ambient atmosphere; additionally Nb ions promotes the formation of Al_2O_3 scale, prohibits the outward diffusion of Ti from the bulk material.

Schmutzler and Zheng [44] also investigated the oxidation behaviour of implanted (10^{17}Nb ions/cm^2) and non implanted Ti48Al2Cr and Ti482Cr2Nb intermetallic alloys under cyclic oxidation (800 - 1h cycles) and isothermal oxidation for 800 and 100 hours respectively at 1073 K. It was observed that the implanted Ti48Al2Cr alloy by Nb ions enhanced the cyclic oxidation resistance at 1073 K in static air for 100 hours. The observed higher mass gain of non implanted alloy (Ti48Al2Cr) compared to the implanted alloy (Ti48Al2Cr (after 100 hours of cyclic oxidation at 1073 K was related to the formation of TiO_2 outer scale. The TiO_2 non protective outer scale formed on the non implanted alloy (Ti48Al2Cr). The implanted Ti48Al2Cr alloy by Nb ions shows the formation a thin Al_2O_3 and protective oxide scale. After 800 hours of 1 hour cycles, the implanted (by Nb ions) Ti48Al2Cr alloy was covered with TiO_2 oxide scale but no spallation was observed, non implanted alloy (Ti48Al2Cr) was covered by TiO_2 oxide but spallation occurred. The authors observed that Nb does not change drastically the scale growth mechanism, but the kinetic growth is reduced significantly.

The authors proposed a few mechanisms where Nb ions are beneficial for oxidation of γ-TiAl and α_2-Ti_3Al intermetallic alloys at high temperatures.

1. The Nb implantation reduces oxygen solubility in TiAl alloy, moreover Nb stabilize β phase in which mass transport of Al is much faster than for Ti in Ti_3Al phase.
2. The Nb increased of Al activity in the alloy, favouring the formation of alumina rich scale
3. The implantation of Nb, changing the diffusion process, causing reduced metal/oxygen transport
4. The Nb ions decreasing the oxygen vacancies and titanium interstitial defects in TiO_2 lattice
5. The formed Nb_2O_5 phase within the scale act as "glue", and allows the formation of coherent scales depressing the fast diffusion paths within the scale.

In other study [45] Schmitz – Niederau and Schutze investigated the thermogravimetric oxidation behaviour of three alloys (compositions given in **table 7)** at 1173 K for 1130 hours.

Element [at. %]	Al	Ti	Nb	Fe	C	O
Alloy						
Ti50Al	50.7	49.2	0.004	0.007	0.019	0.12
Ti50Al2Nb	50.2	47.5	1.99	0.016	0.026	0.24
Ti23Al	23	77	-	-	-	-

Table 7 Chemical composition of alloys used in oxidation test at 1173 K for 1130 hours [45]

The scale morphology of Ti50Al alloy oxidised at 1173 K for 1130 hours in static air is shown in **figure 19.**

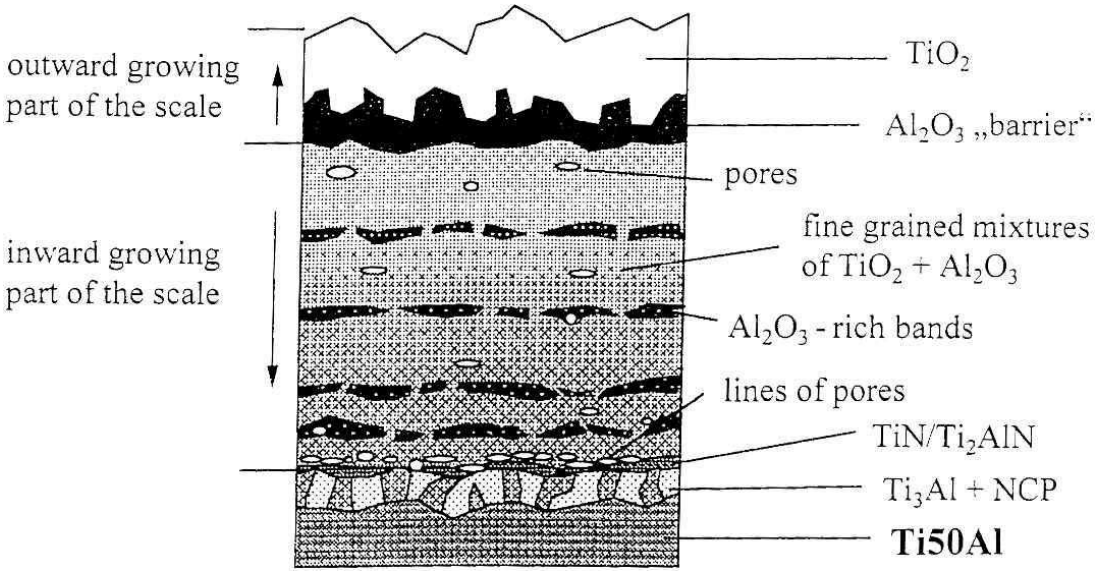

Figure 19 Scale morphology developed during oxidation at 1173 K for 1130 hours on Ti50Al alloy [45]

The multilayered scale developed on Ti50Al alloy after oxidation at 1173 K for 1130 hours as shown in **figure 19**. The outer layer consisted of a thick TiO_2 scale. Beneath the outer TiO_2 layer, a diffusion barrier of Al_2O_3 formed, the third layer consisting of mix TiO_2 and Al_2O_3 developed under the Al_2O_3 diffusion barrier The Al_2O_3 rich bands developed over the TiN and Ti_2AlN region. The innermost Ti_3Al layer developed due to the outward diffusion of Al from bulk material (Ti50Al). The NCP (New Cubic Phase) often called Z – phase ($Ti_{50}Al_{30}O_{20}$) also was detected.

The author [45] suggested that multilayer scale **(Fig. 19)** was formed before breakaway of the scale.

Breakaway of the scale was also observed by Du and Datta et. al [46], the authors investigated Ti6Al4V alloy in oxidation atmosphere at 923 – 1123 K, they found that sandwich like scale (TiO_2 – Al_2O_3) developed, the number of layers increasing with increasing temperature and time.

The cracks between layers indicate, the poor adhesion between layers, the cracks caused the detachment of the oxide scale from the substrate. Thus the crack formation reduced the corrosion resistance of the Ti6Al4V alloy in oxidation atmosphere.

Figure 20 shows a scale development on Ti50Al2Nb alloys after oxidation at 900^{o}C (1173 K) for 1130 hours [45]

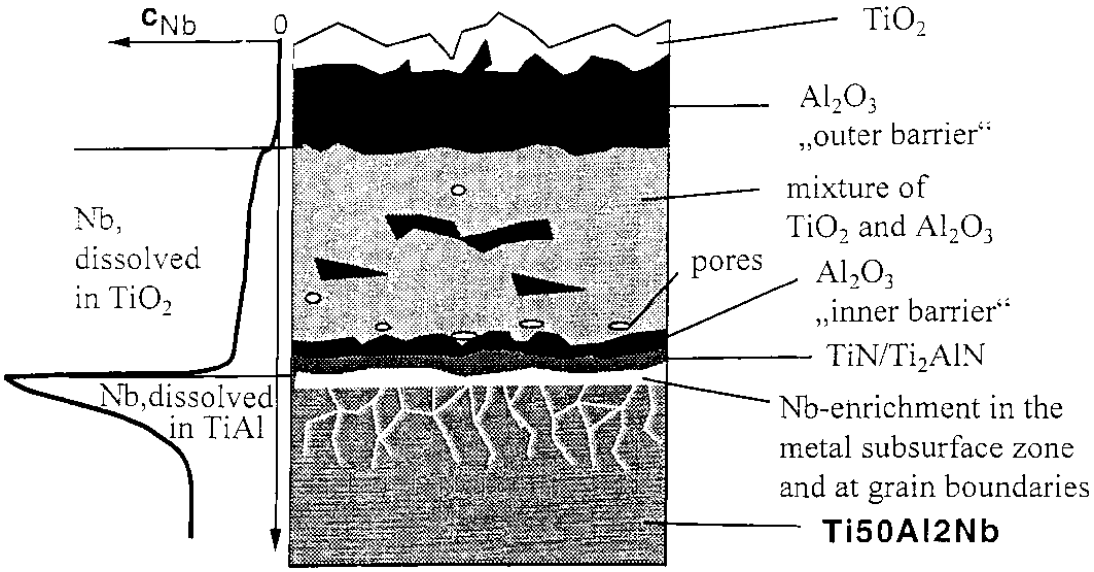

Figure 20 The cross – section diagram of scale development on Ti50Al2Nb alloy after oxidation at 1173 K for 1130 hours [45]

Similar to the oxidation behaviour of Ti50Al alloy, the Ti50Al2Nb alloy developed a multilayer scale with the outer scale consisting of TiO_2. The outer layer of TiO_2 was thinner that in Ti50Al alloy, also the diffusion barrier of Al_2O_3 which developed beneath TiO_2 during exposure was much thicker than that in Ti50Al alloy. Thus Nb had a beneficial influence for oxidation resistance of TiAl alloys (Nb reduces the number of oxygen vacancies in the TiO_2 matrix). Furthermore, the thick band of TiO_2, where Nb is dissolved prohibited the fast outward diffusion of Ti from the bulk material and decreased the oxidation rate. **Figure 21** presents a scale morphology of Ti23Al alloys exposed to the same atmosphere in the same conditions 1173 K for 1130 hours [45].

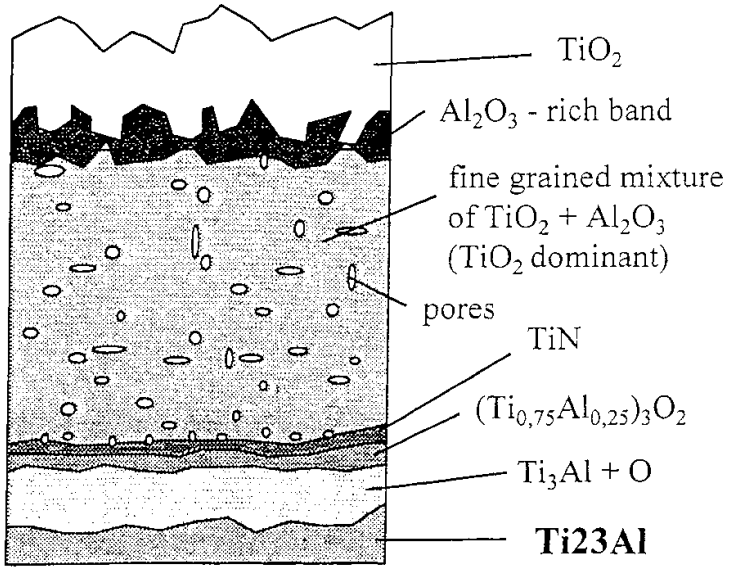

Figure 21 Scale development of Ti23Al after oxidation at 1173 K for 1130 hours [45]

Again a multilayer scale developed on Ti23Ti alloy after oxidation at 1173 K for 1130 hours **(Fig. 21)**. An outer thick TiO_2 scale was formed, the top and beneath the outer an on Al_2O_3 thin layer also formed. The innermost a very thick layer consisted mixture of TiO_2 and Al_2O_3 oxides with large TiO_2 content formed underneath Al_2O_3 band. The very thin layer of TiN developed under a thick region of oxide mixture (TiO_2 and Al_2O_3). Underneath this layer a thin $(Ti0.75Al0.25)_3O_2$ layer also was detected. At the scale/substrate interface a thick Ti_3Al layer with inclusion of O^{2-} formed.

The marker experiment [45] showed that the outer layer of TiO_2 growth occurred via outward diffusion of Ti from the bulk material, whereas, the complex structures containing Al_2O_3 growth via inward diffusion of O^{2-}.

The kinetic data for Ti23Al (α_2 - Ti_3Al), Ti50Al2Nb, and Ti50Al alloy after exposure at 1173 K for 1130 hours and 110 hours for Ti23Al alloy are presented in **figures 22, 23**, **and 24** respectively. The numbers in the kinetic figures **(22, 23, and 24)** indicate the temporary parabolic rate constants.

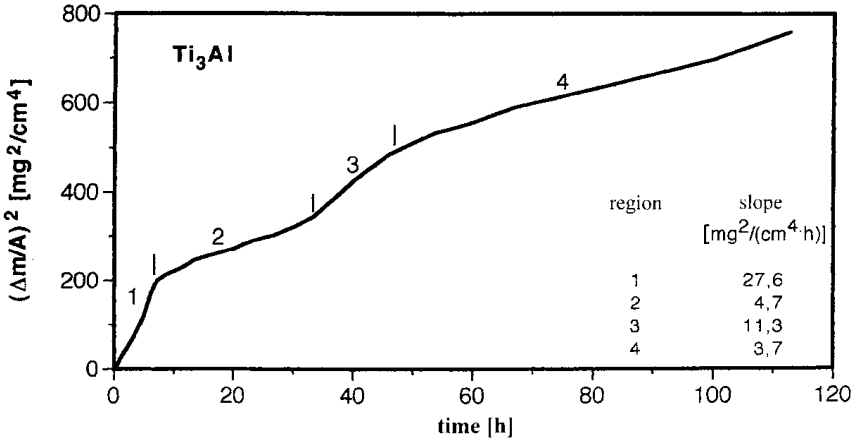

Figure 22 Thermogravimetric measurement of kinetic data for Ti23Al alloy after 120 hours of oxidation at 1173 K [45]

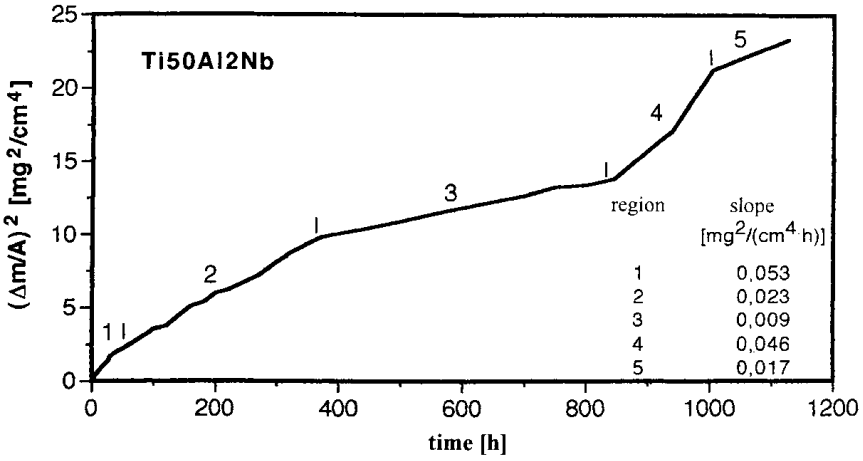

Figure 23 Thermogravimetric measurement of kinetic data for Ti50Al2Nb alloy after 1130 hours of oxidation at 1173 K [45]

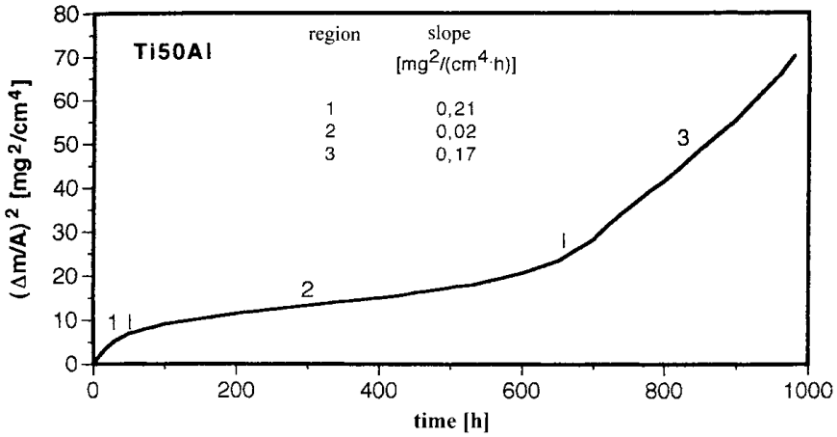

Figure 24 Thermogravimetric measurement of kinetic data for Ti50Al alloy after 110 hours of oxidation at 1173 K [45]

The kinetic rates in **figures 22, 23, and 24** shows that the highest mass gain occurred to Ti23Al alloy, the poor oxidation was caused by the lack of required level of Al in the alloy.

The required level of Al according to McKee [47] needs to be around 50 at% of Al to developed a protective Al_2O_3 oxide scale on TiAl ordered intermetallic alloys. Approximately 60 ~ 70 at% of aluminium is needed for binary TiAl alloys to form continuous Al_2O_3 layer, 47 ~ 49 at% of Al is needed to of Al_2O_3 in pure oxygen. However a larger amount of Al may cause lack of ductility and formation of brittle $TiAl_3$. Welsh et al [48] pointed out that between 0 and 25 at% there is impossible to developed a protective Al_2O_3 scale on TiAl ordered intermetallic alloy.

The kinetic data for Ti50Al and Ti50Al2Nb shows that the higher amount of Al decreases the oxidation rate; furthermore also small addition of Nb is also beneficial for oxidation resistance of Ti50Al alloys. As mentioned before the positive role of Nb addition is associated with decrease in oxygen vacancy and Ti interstitial defects in TiO_2 and increase Al activity. McKee [47] has showed (by thermodynamic calculation) in TiAl base intermetallic the required level of Al is a 50 at% to develop Al_2O_3 scale. The isothermal and cyclic oxidation investigated by Haanappel, Sunderkotter [49] on Ti48Al2Mn2Nb, Ti48Al2Cr2Nb, and Ti48Al2Cr at high temperatures; 1073 and 1173 K was performed in synthetic air (80% N_2, 20% O_2) for 150 hours and 1500 1 h cycles in the static laboratory air. The chemical composition in at % of the alloy subjected to the oxidation experiment is given in **table 8.**

Alloy	Ti	Al	Cr	Mn	Nb	O (ppm)	N (ppm)	C (ppm)	H (ppm)
Ti48Al2Mn2Nb	Bal.	47	-	2	2	570	< 5		< 10
Ti48Al2Cr2Nb	Bal.	48	2	-	2	850	60		< 10
Ti48Al2Cr	Bal.	48	2	-	-	750	220	55	< 10

Table 8 Chemical compositions of the alloys subjected to oxidation experiments at 1073 and 1173 K respectively [49]

The kinetic data for oxidation experiment in synthetic air (80%N_2 and 20% O_2) at 1073 and 1173 K is presented in **figure 25a and 25b**.

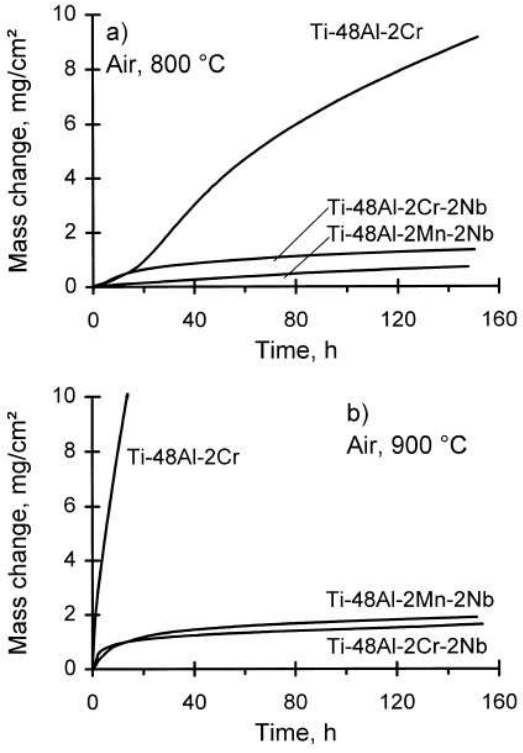

Figure 25 The kinetic data of exposed samples in isothermal oxidation at 1073 and 1173 K [49]

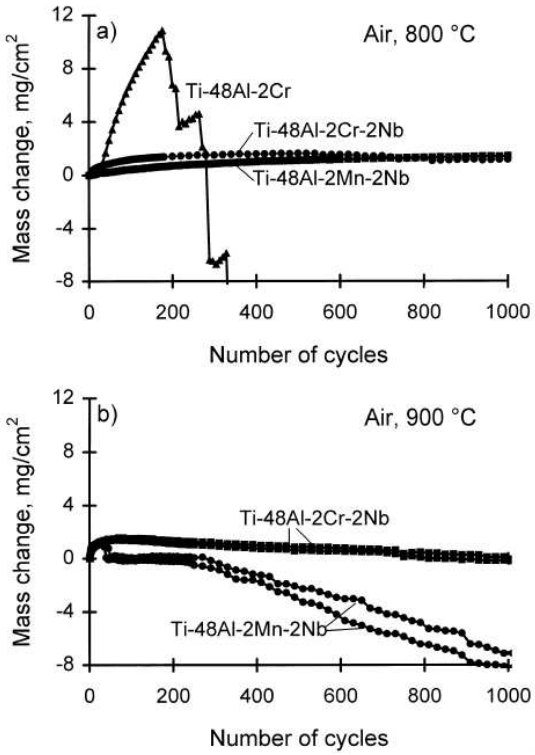

Figure 26 The cyclic oxidation kinetic data obtained at 1073 and 1173 K after 1000 cycles of Ti48Al2Cr, Ti48Al2Mn2Nb, and Ti48Al2Cr2Nb alloys [49]

Figures 26a and 26b show the kinetic data from cyclic oxidation after 1000 cycles at 1073 and 1173 K for exposed samples (Ti48Al2Cr, Ti48Al2Mn2Nb, and Ti48Al2Cr2Nb). **Figure 26a** shows the cyclic oxidation behaviour of Ti48Al2Cr, Ti48Al2Cr2Nb, and Ti48Al2Mn2Nb alloys at 1073 K. It was observed that Ti48Al2Cr2Nb, and Ti48Al2Mn2Nb have a similar kinetic rate, whereas Ti48Al2Cr alloy shows a large mass gain up to 200 hours at 1073 K of cycling oxidation, and then the scale spalled off from the alloy.

Cyclic oxidation behaviour at higher temperature 1173 K is given in **figure 26b**, the Ti48Al2Cr alloy was not subjected to cyclic oxidation, due to the poor oxidation resistance against cyclic oxidation at lower temperature 1073 K.

However the Ti48Al2Cr2Nb and Ti48Al2Mn2Nb show the similar behaviour under cyclic conditions at 1173 K; from both samples the scale spalled off, therefore Ti482Cr2Nb showed better oxidation resistance (mass loss was smaller than Ti48Al2Mn2Nb alloy). The authors [49] concluded that the spallation which occurred at higher temperature (1173 K) during cycling oxidation was due to mismatch in the thermal coefficient. The scale morphology developed on both alloys (Ti48Al2Mn2Nb, Ti48Al2Cr2Nb) after 150 hours of oxidation at 1073 K is shown in **figures 27a** and **27b**.

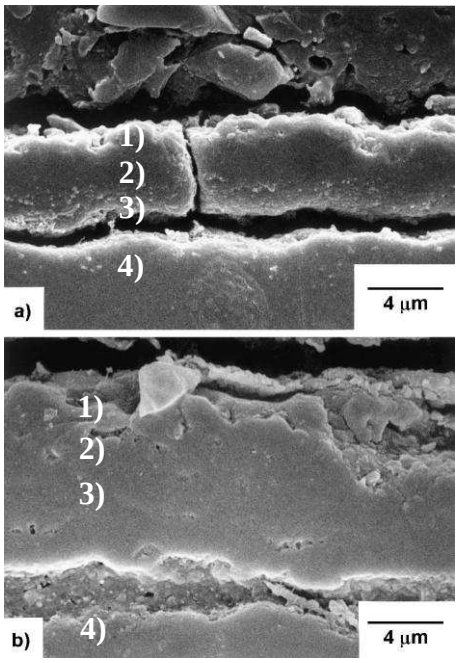

1) TiO_2 outer scale
2) Al rich band beneath this TiO_2 oxide
3) Enrichment region of Nb, Cr, and Mn with Al and Ti oxides layer
4) Substrate (Ti48Al2Mn2Nb)

1) TiO_2 outer scale
2) Al rich band beneath this TiO_2 oxide
3) Enrichment region of Nb, Cr, and Mn with Al and Ti oxides layer
4) Substrate (Ti48Al2Cr2Nb)

Figure 27 Scale morphology of oxidized samples (Ti48Al2Mn2Nb, Ti48Al2Cr2Nb) after 150 hours at 1073 K [49]

The outer layer of the specimens (Ti48Al2Mn2Nb, Ti48Al2Cr2Nb) is covered by TiO_2, below the outer layer, the rich Al region formed. Between the Al rich region and the substrate, a region of mixed Ti, Al oxides with some enrichment of Nb, Mn, and Cr also developed. At higher temperature (1173 K) the oxide scale was thicker than formed at 1073 K with similar structure and composition (TiO_2 developed as an outer oxide). The investigated Ti48Al2Cr alloy [49] developed at 1073 K a TiO_2 oxide scale (TiO_2) with larger crystals and porous structure, below the oxide scale (TiO_2), an Al depleted region developed at 1073 K after 150 hours of isothermal oxidation. The isothermal oxidation at 1173 K for 150 hours reveals that Ti48Al2Cr alloy develop very thick TiO_2 oxide scale (200 – 250 µm). Furthermore, the scale of Ti48Al2Cr alloy after 1173 K isothermal oxidation was similar as found after 1500 cycles at 1073 K.

The cyclic oxidation performed on Ti48Al2Mn2Nb alloy at 1073 K in produced an adherent TiO_2 oxide top scale, below which a region rich in Al formed. The Al rich region formed due to the outward diffusion of Ti from bulk material, the concentration of Ti decreased and Al content increase.

Between this Al rich region and the substrate, a zone of mixed TiO_2 and Al_2O_3 oxides developed. At the scale/substrate interface Nb rich zone was detected.

After oxidation at 800^{o}C (1073 K) the concentration of Mn decreased to 0 in the outer part of the oxide scale and Mn did not form any phases. At higher temperature (1173 K), the scale was similar structure and composition with thicker (35 µm) outer oxides scale (TiO_2), however a significant spallation occurred from the outer part of the scale formed by TiO_2 oxide. Moreover the rich Mn and Nb regions were detected underneath the top oxide scale (TiO_2). The subjected Ti48Al2Cr alloy after exposure to cyclic oxidation at 1073 K the scale structure developed in Ti48Al2Cr alloy contained multiple layers as shown in **figure 28**.

Layer 1 – a thick outer scale of TiO_2 oxide with rich in Al particles

Layer 2 – Al rich layer

Layer 3 – consisted region of Al (dark areas) and Ti (bright areas), moreover it was found that Cr content in Al rich region was higher than in Ti rich region

Layer 4 – it was observed from EDX analysis that ratio Al:Ti was similar to bulk material

Layer 5 – Al depleted zone

Layer 6 – bulk material (Ti48Al2Cr)

The total thickness of the scale formed during cyclic oxidation at 1073 K was equivalent to 300 µm.

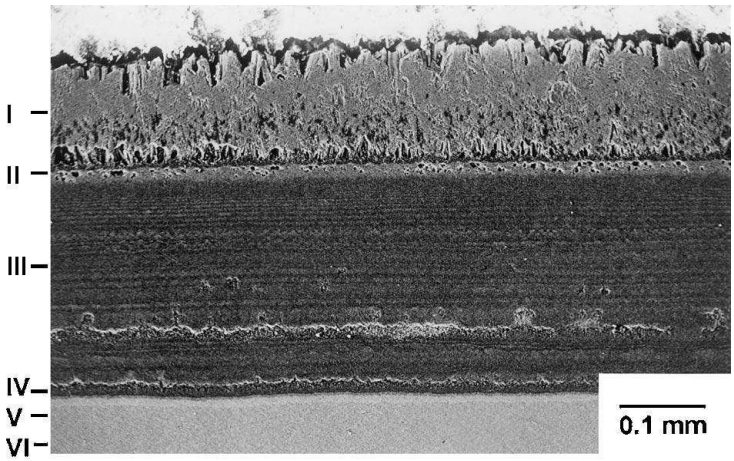

Figure 28 The scale development of Ti48Al2Cr2Nb after 1h 1500 cycles at 1073 K in the static atmospheric air [49]

The Ti48Al2Cr2Nb after exposure to the cyclic oxidation in 1h 1500 cycles at 1173 K showed no spallation. **Figure 29a** and **29b** shows the adherent, scale in Ti48Al2Cr2Nb and, spallation of the scale in Ti48Al2Mn2Nb alloy after 1500 cycles at 1173 K. The spallation in Ti48Al2Mn2Nb alloy according to Herbelin and Mantel [50] who discovered that Mn in TiAl alloys mainly occupied the outer part of the oxide scale due to the fast outward diffusion of Mn from the bulk material. Also it was suggested that spallation is due to the formation of Mn – oxides in the outer part of the scale, the formed Mn – oxides cause a cracks and spallation of the oxide layer, however the mechanism is not known yet.

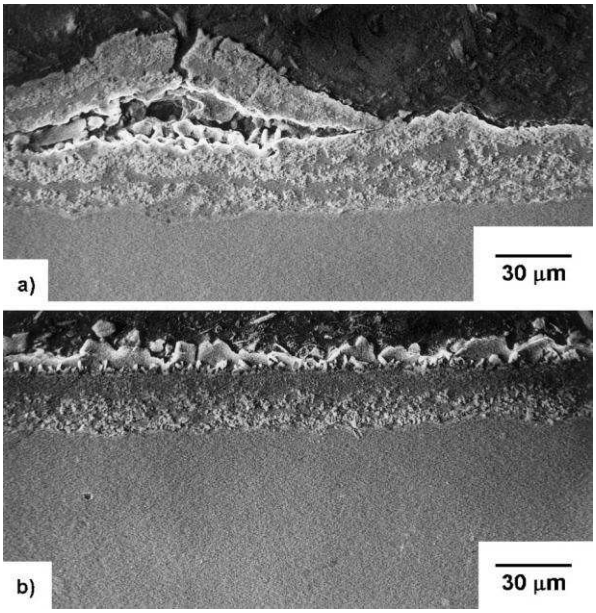

Figure 29 The cross – sectional SEM images of a) Ti48Al2Mn2Nb and b) Ti48Al2Cr2Nb alloys after 1500 cycles at 1173 K in static air [49]

The cyclic and isothermal oxidation behaviour of TiAl based intermetallic alloy with 10 at% addition of Cr was investigated at temperature range 1073 – 1373 K by Wang and Tang [51]. The cyclic and isothermal oxidation was performed on three alloys: Ti50Al, Ti45Al10Cr, and Ti50Al10Cr. The isothermal oxidation tests were carried out at 1073 – 1373 K for 100 hours, while cyclic oxidation tests (100 1h test with 10 minutes cooling down period) were conducted at 1173 – 1373K.

The kinetic results present that in isothermal oxidation regime the best resistance was achieved by Ti50Al10Cr alloy at 1373 K. **Table 9** presents results achieved by researches [51]:

T [^{o}C]	Cyclic oxidation		Isothermal oxidation	
	Alloy	Mass gain [mg/cm^2]	Alloy	Mass gain [mg/cm^2]
800	Ti50Al	Not performed	Ti50Al	1
800	Ti45Al10Cr	Not performed	Ti45Al10Cr	1
800	Ti50Al10Cr	Not performed	Ti50Al10Cr	0.2
900	Ti50Al	Large spallation	Ti50Al	4
900	Ti45Al10Cr	3.0	Ti45Al10Cr	7.5
900	Ti50Al10Cr	1.5	Ti50Al10Cr	0.45
1000	Ti50Al	Large spallation	Ti50Al	>20
1000	Ti45Al10Cr	-2.5	Ti45Al10Cr	16
1000	Ti50Al10Cr	0.5	Ti50Al10Cr	0.4
1100	Ti50Al	Large spallation	Ti50Al	>>20
1100	Ti45Al10Cr	0.2	Ti45Al10Cr	1.2
1100	Ti50Al10Cr	0.5	Ti50Al10Cr	0.8

Table 9 Kinetic results from cyclic and isothermal oxidation of Ti50Al, Ti45Al10Cr, and Ti50Al10Cr alloys [51]

The scale morphology of Ti45Al10Cr oxidised for 100 hours of at 1173 K shows the similar scale development as in Ti50Al alloy. The outer layer consisted of TiO_2 crystals, in the middle layer Al_2O_3 formed, and the third layer consisted of mixture TiO_2 with Al_2O_3. Moreover in the outer scale some of Cr particles were detected. However the mass gain of Ti45Al10Cr alloy was higher than Ti50Al alloy. The higher mass gain after 100 hours at 1173 K of Ti45AlCr10 alloy was related to the increase in defected structure of TiO_2 and also to formation of highly unstable CrO_3 oxide, it needs to be pointed out that the 45 at% of Al was insufficient amount to develop thin protective layer of Al_2O_3, however the addition of Cr was appreciable (10 at%) to support the development of Al_2O_3 thin oxide scale.

When temperature was raised to 1373 K Ti45Al10Cr was covered by thin Al_2O_3 layer in the outer part of the oxide scale, and mass gain was smaller than at 1173 K after 100 hours of isothermal oxidation. The alloy with higher Al concentration (Ti50Al10Cr) developed after 100 hours oxidation at temperature range 1073 – 1373 K a continuous Al_2O_3 scale, however there is no data about TiO_2 formation in the scale.

Wang and Tang [51] did not present the scale morphology of exposed sample to the cyclic oxidation at temperature range 1173 – 1373 K. The authors suggested

only that Ti50Al alloy suffered the major scale spallation in whole range of temperature 1173 K – 1373 K during cycling oxidation.

Other alloys (Ti4510Cr and Ti50Al10Cr) developed an Al_2O_3 scale with good adherence, which suppressed the scale degradation during 100 hours cyclic oxidation. Moreover, it was suggested that addition of 10%Cr improved the adherence of the scale and promoted the development of Al_2O_3 phase. The improved adherence is related to the low thermal coefficient for Ti50Al10Cr alloy.

Sunderkotter [52] investigated the influence of Cr addition on Ti48Al2Cr, Ti482Cr2Nb, and Ti47Al2Cr0.2Si behaviour in cyclic and isothermal oxidation at high temperature at 700 and 800^{o}C (973 and 1073 K). The alloys were subjected to isothermal oxidation in synthetic air (80% N_2 and 20% O_2) for 150 hours and cyclic oxidation for 3000 1 hour cycles.

The kinetic data of Ti48Al2Cr, Ti482Cr2Nb, and Ti47Al2Cr0.2Si obtained after isothermal oxidation for 150 hours at 1073 K indicated that the Ti48Al2Cr alloy had a higher mass gain, where Ti48Al2Cr2Nb shows the lowest mass gain. The results of the oxidation at 973 K were not provided. The kinetics of cyclic oxidation at 973 K revealed, the Ti48Al2Cr alloy shows the highest mass gain, but without spallation, Ti47Al2Cr0.2Si and Ti48Al2Cr2Nb alloys also shows lack of spallation, however the lowest mass gin was attributed to Ti48Al2Cr2Nb alloy. At higher temperature (1073 K) of the cyclic oxidation, the best corrosion resistant shows Ti48Al2Cr2Nb alloy, moreover Ti48Al2Cr alloy shows the highest mass gain but without spallation, whereas the scale from Ti47Al2Cr0.2Si alloy spalled off due to the low amount of Si in bulk material.

The author [52] concluded that the isothermal and cyclic oxidation corrosion resistance for Ti48Al2Cr, Ti482Cr2Nb, and Ti47Al2Cr0.2Si was excellent.

The corrosion products on Ti48Al2Cr2Nb alloy after 1 hour of isothermal oxidation at 1073 K measured by GAXRD (Glanced Angle X-Ray Diffraction Analyser) revealed, that TiO_2, TiN and Ti_2AlN phases were observed in the outer part of the formed scale. However after longer exposure (26 hours) at the same temperature (1073 K) the peaks of TiN and Ti_2AlN were not detected, only peaks of TiO_2 and Al_2O_3 were detected. Moreover the similar behaviour was observed in Ti47Al2Cr0.2Si, where mainly TiO_2 and Al_2O_3 peaks were discovered. Upon longer exposure (150 hours of isothermal oxidation) the whole surface was covered by TiO_2 oxide scale.

In general, the scale morphology developed during 150 hours of isothermal oxidation at 1073 K on Ti47Al2Cr0.2Si was similar to Ti48Al2Cr2Nb alloy and consisting of multilayered structure; TiO_2 was an outer layer, beneath the outer layer the, Al_2O_3 rich layer develop, mixed TiO_2 – Al_2O_3 layer was observed upon subsurface metal layer. As mentioned previously, the scale morphology developed on Ti48Al2Cr2Nb was similar to those obtained on Ti47Al2Cr0.2Si but much thinner.

During the cyclic oxidation of Ti48Al2Cr2Nb alloy (3000 1 hour cycle) at 1073 K a multilayered scale developed; TiO_2 was detected as an outer part of the scale, underneath the mixed Ti and Al rich oxide layer existed, the rich Nb layer on the scale/metal interface was detected. The scale shows good adherence against cyclic oxidation. The Ti48Al2Cr alloy consisted mainly mixed oxide scale consisted TiO_2 and Al_2O_3 with small amounts of Cr.

Sunderkotter [52] concluded that addition of silicon improved the isothermal oxidation, and improved the scale adherence in cyclic oxidation, the beneficial effect of Si is attributed to the formation of non – continuous SiO_2 layer in the scale/metal interface [53]. Author suggested that it was impossible to detected the Si oxide, however the lack of SiO_2 in the scale, is associated with the low concentration of Si in the bulk material (0.2 at %).

Du and Datta [54] investigated Ti6Al4V alloy in oxidation environment at temperature range 923 – 1123 K for 100 hours. The morphology of exposed samples consisted mainly Al_2O_3 and TiO_2 layer, the number of layers and the thickness of the scales depended on the exposure time and temperature; if temperature was increased the number of the layer also increased. **Figure 30** shows scale development of Ti6Al4V alloy after 100 hours of the oxidation at 1123 K.

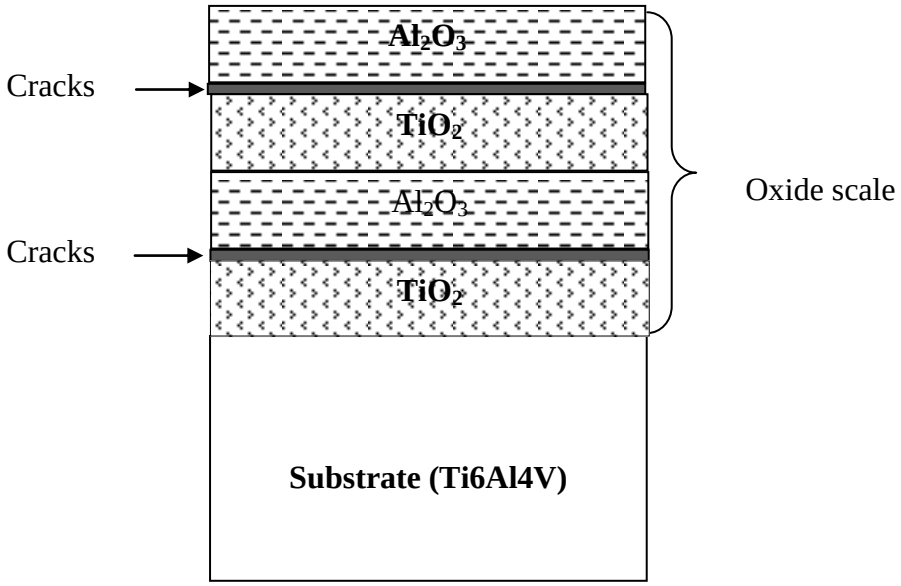

Figure 30 Scale development on Ti6Al4V alloy after 100 hours oxidation at 1023 K [54]

The mechanism of the scale development proposed by Du and Datta [54] based on the thermodynamical calculations which are presented in **table 10**. The proposed mechanism of the scale development is presented in **figures 31a, b, c**, and **d**. The activation energy values in **table 10** indicate that once Ti6Al4V alloy is exposed to oxidation atmosphere, TiO_2 starts to develop.

Activity	T = 923 K	T = 973 K	T = 1023 K	T = 1073 K	T = 1023 K
a_{Al}	$2.8x10^{-39}$	$7.6x10^{-37}$	$1.2x10^{-35}$	$1.2x10^{-32}$	$7.7x10^{-31}$
a_{Ti}	$1.6x10^{-42}$	$7.3x10^{-40}$	$3.8x10^{-37}$	$2.6x10^{-35}$	$2.4x10^{-33}$

Table 10 Activation energy of Ti and Al for different temperatures [54]

When the Ti6Al4V alloy was exposed to oxidation atmosphere (static air) a thin oxide layer of TiO_2 layer is developed (**Fig. 31a**).

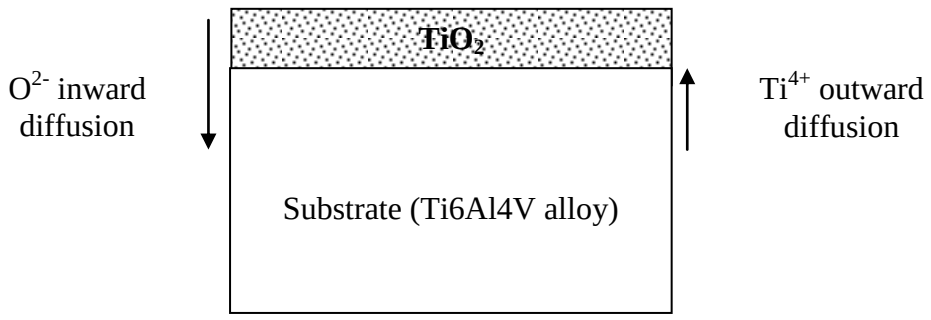

Figure 31a Formation of TiO_2 layer [54]

When TiO_2 thin scale is formed, than the partial pressure of O_2 decreased at the scale/metal interface, the decreased pressure of O_2 approaching to dissociation partial pressure of TiO_2. In this moment with such low pO_2, the minimum activity of Al required for the formation of Al_2O_3 is reached (**Fig. 31b**). It needs to be pointed out that not only TiO_2 developed on the outer scale, but also other types of the titanium oxides (TiO and Ti_2O_3), where Al_2O_3 may be dissolved and activity of Al is reduced at the interface (oxide/substrate interface.

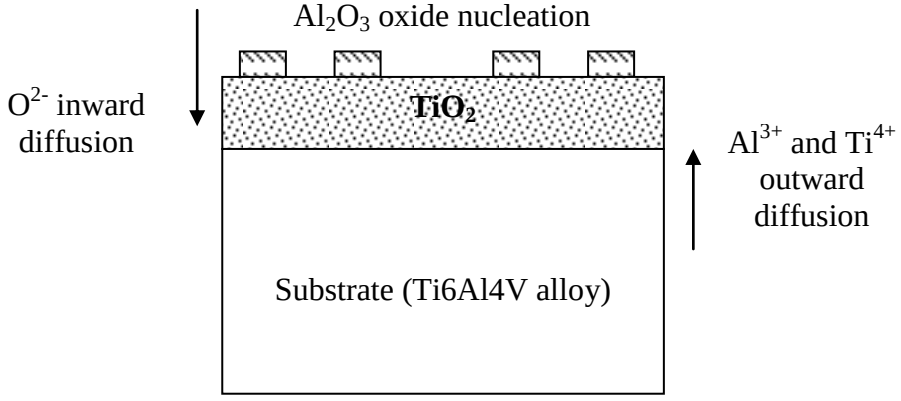

Figure 31b Nucleation of Al_2O_3 oxide and thickening of TiO_2 [54]

It was suggested that Al and Ti may diffuse outward from the substrate; also O^{2-} diffuses inward, and react with titanium in the formed oxide scale (TiO_2) and form a TiO_2 and increase the thickness of TiO_2 layer. As result titanium is trapped between outer Al_2O_3 scale and the inner oxide scale/substrate where due to the outward diffusion of Ti and inward diffusion oxygen, the TiO_2 layer is developed. The trapped titanium allowed to outward diffusion of Al and formation of Al_2O_3 scale.

During exposure, the thickness of inner layer and also outer increased, the plasticity of the scale is lower when experiment is longer and thickness of the scale is higher. Thus when oxide scale exceeded, the crack formation may initiated, also the different thermal coefficient between substrate and the oxide scale, form the cracks (**Fig. 31c**). The formation of crack/s cause a detachment between oxide scale and the substrate (Ti6Al4V), thus the mass transport from the substrate is more difficult and is likely to decrease.

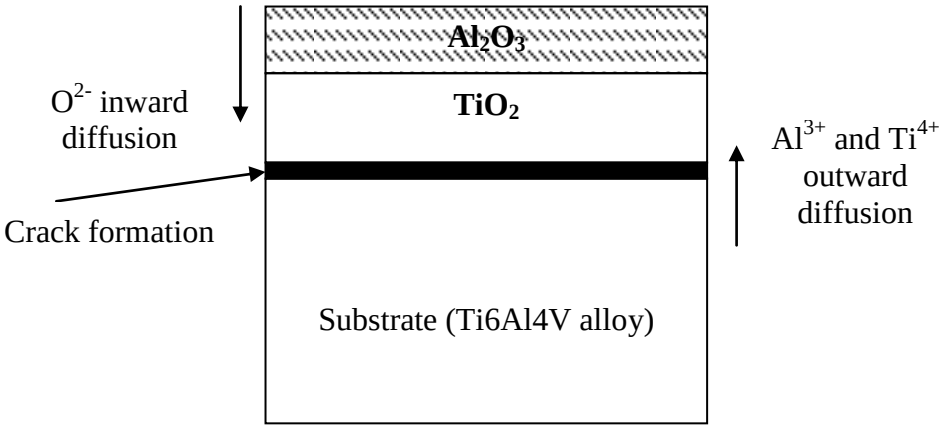

Figure 31c Al_2O_3 and the crack formation [54]

The crack formation allows the formation of new TiO_2 layer on the substrate surface, due to the high partial pressure of oxygen in the crack. The formed TiO_2 layer again separates the substrate form the high partial pressure of oxygen. Moreover aluminium from the substrate (Ti6Al4V) diffuse outward through TiO_2 layer and forms second layer of Al_2O_3 on upon second layer of TiO_2 after some time a new crack propagation is appeared (**Fig. 31d**).

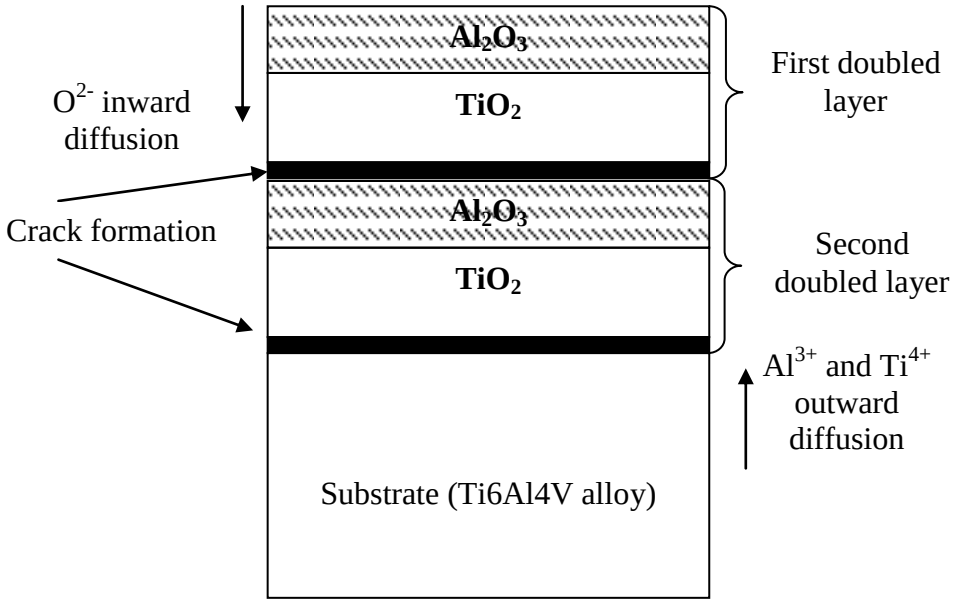

Figure 31d Subsequent Al_2O_3 and TiO_2 layers on Ti6Al4V alloy after oxidation in the temperature range 923 – 1123 K [54]

Figure 31 Formation of the scale on exposed material [54]

The mechanism of the scale development is again reproduced and the next layer of $Al_2O_3 – TiO_2$ is formed. The **reactions 7 and 8** present the formation of the scale during exposure of Ti6Al4Al at temperature range 923 – 1123 K.

Reaction 7 $$Ti(s) + O_2(g) \rightarrow TiO_2(s)$$

Reaction 8 $$2Al(l) + \frac{3}{2}O_2(g) \rightarrow Al_2O_3(s)$$

For **reactions 7 and 8**, the ΔG_T^o, [J/mole] can be calculated from following equations:

Equation XIII $$\Delta G^o_{TiO2,T} = -910.000 + 173T$$

Equation XIV $$\Delta G^o_{Al2O3,T} = -1676.000 + 320T$$

The calculated values are in **table 11**.

ΔG_T^o [J/mole]	T = 923 K	T = 973 K	T = 1023 K	T = 1073 K	T = 1123 K
TiO_2	-750321	-741671	-733021	-724371	-715721
Al_2O_3	-1380640	-1364640	-1348640	-1332640	-1316640

Table 11 Calculated ΔG_T^o values for TiO_2 and Al_2O_3 formation [54]

Also:

Equation XV $$\Delta G^O_{TiO2} = -RT \ln K = -RT \ln \frac{aTiO_2}{aTi * pO_2}$$

Equation XVI $$\Delta G^O_{Al2O3} = -RT \ln K = -RT \ln \frac{aAl_2O_3}{aAl * (pO_2)^{3/2}}$$

Equations XV and **XVI** are the equilibrium constants for reaction of the formation TiO_2 and Al_2O_3 oxides. **Equations XV** and **XVI** can be transformed into another form:

Equation XVII $$\Delta G^O_{TiO2} = -RT \ln(a_{Ti})^{-1} = 2RT \ln a_{Ti}$$

Equation XVIII $$\Delta G^O_{Al2O3} = -RT \ln(a_{Al})^{-2} = 2RT \ln a_{Al}$$

The kinetic data obtained from the oxidation experiment at 923 and 973 K followed by logarithmic law in initial period, after 2 hours the kinetics followed by

parabolic rate law. With increase a temperature (1023, 1073, 1123 K) the Ti6Al4V alloy followed by linear – parabolic rate low.

The mechanism of phase development in Ti6Al4V alloy presented in this study [54] is in contradiction with the results presented by the same authors in other study [55]. Du and Datta exposed to atmospheric air Ti46.7Al1.9W0.5Si alloy at temperature range between 1023 – 1223 K. Researchers suggested that formation of TiO_2 is more favourable than Al_2O_3 due to the following calculations:

Equation XIX $$\Delta G^{o}_{TiO2,T} = -910.000 + 173T$$

Equation XX $$\Delta G^{o}_{Al2O3,T} = -1676.000 + 320T$$

Du and Datta observed that in high partial pressure of oxygen (pO_2 = 21278.25 atm in atmospheric air) in oxidation environment the scale has a multilayer structure as shown in **figure 32**:

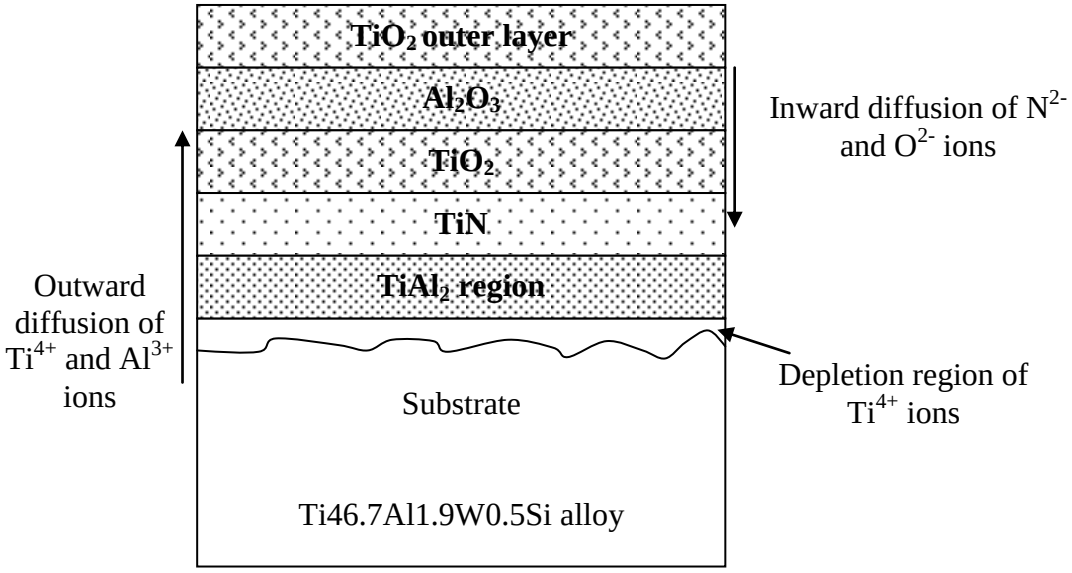

Figure 32 The scale development after oxidation at temperature range 1023 – 1223 K for Ti46.7Al1.9W0.5Si alloy in static air [55]

In this study Du and Datta et al. [55] investigated the oxidation process of Ti46.7Al1.9W0.5Si alloy at temperature range between 1023 – 1223 K. The formation of the oxide scale can be described as follows: TiO_2 (outer scale) the inner Al_2O_3, TiO_2 beneath Al_2O_3 layer, underneath TiO_2 a TiN ceramic layer was detected. The nitrogen from external atmosphere with higher partial pressure than oxygen (pO_2

= 21278.25 Pa, pN_2 = 79033.5) diffuses inwards through the TiO_2 outer scale and Al_2O_3 inner region to Ti enrich region where following reaction appears:

Reaction 9 $$\mathrm{Ti(s)} + \frac{1}{2}\mathrm{N_2(g)} \rightarrow \mathrm{TiN(s)}$$

Thus TiN creates beneath the Al_2O_3 layer, meantime O_2 diffuses inward to the interface between Al_2O_3 and TiN layer. In this moment the partial pressure of oxygen reaches the certain level, where TiN becomes unstable and released N_2 from TiN phase according to the following reaction:

Reaction 10 $$\mathrm{TiN(s)} + \mathrm{O_2(g)} \rightarrow \mathrm{TiO_2(s)} + \mathrm{N_2(g)}$$

The released N_2 from **reaction 10** migrates inward, the partial pressure of N_2 increased, in the same moment the outward diffuses Ti^{4+} ions from the substrate (Ti46.7Al1.9W0.5Si alloy) produce a TiN phase again according to the **reaction 10**:

Reaction 11 $$\mathrm{Ti(s)} + \frac{1}{2}\mathrm{N_2(g)} \rightarrow \mathrm{TiN(s)}$$

In the result of TiN formation **(reaction 11)** the concentration of Ti in the material, near to the scale/substrate interface, is depleted. The depleted region of Ti is used for the formation of the new phase $TiAl_2$ as shown in **figure 32**.

Thus Du and Datta [55] suggested in atmospheric air the formation of TiN and $TiAl_2$ whereas in the paper [54] researcher forgot to mention about the formation of these two phases (TiN and $TiAl_2$). Furthermore the total concentration of Ti in Ti6Al4V alloy is higher than in Ti46.7Al1.9W0.5Si alloy, and authors should expect the formation TiN phase. Moreover the temperature range was almost the same in both studies [54, 55]. It needs to be added that similar result with TiN formation was also suggested by another authors [56,57,58], where researchers found, that beneath mixed TiO_2+Al_2O_3 oxide scale, a thin TiN layer formed.

It is important to note that the Ti46.7Al1.9W0.5Si alloy is an ordered and Ti6Al4V alloy is a disordered intermetallic material. However in the in both alloys (Ti46.7Al1.9W0.5Si, Ti6Al4V) are sufficient amount of Ti to develop a thin TiN layer in the inner part of the oxide scale.

Chapter II – Section 2 - Critical Literature Review – Sulphidation/Oxidation of γ - TiAl alloys

Ch.II.Sec.2.1 Introduction to literature review

This chapter of PhD thesis will review some of the results obtained in the field of the sulphidation/oxidation of the different alloys at high temperature (above 873 K).

Ch.II.Sec.2.2 Background of sulphidation and thermodynamical data

The degradation of the metallic alloys in highly sulphidized environments (pure S_2 or experiments at high partial pressure of S_2 and low partial pressure of O_2) is a major concern of many industries – power generation, aerospace, processing.

At temperature above 973 K the S_2 is an important reactive species; at lower temperatures the species are S_6, S_7, and S_8.

Sulphur environment is more aggressive for metals than oxygen [59]. Silver in atmosphere of oxygen is a noble metal, but at temperature above 423 K Ag reacts very violently in sulphur environment, also copper react very rapidly with sulphur according to the following reaction:

Reaction 12 $Cu + S_2 \rightarrow Cu_2S$

Common structured metals; Iron, Nickel, Cobalt and their alloys with the addition of aluminium or chromium react also with sulphur faster, and reaction rates are several orders of magnitude higher than in oxygen atmosphere. **Table 12** compares the oxidation and sulphidation rates.

Reacting gases	Parabolic rate constant kp [$g^2/(cm^4s)$]			
	Ni	Co	Fe	Cr
O_2	$9.1x10^{-11}$	1.610^{-9}	$5.510x10^{-8}$	$4.5x10^{-12}$
Temperature	1273 K	1223 K	1073 K	1273 K
S_2	$8.5x10^{-4}$	$6.7x10^{-6}$	$8.1x10^{-6}$	$8.1x10^{-7}$
Temperature	923 K	993 K	1073 K	1273 K

Table 12 Parabolic rate constants kp for oxidation and sulphidation of some metals in O_2 and S_2 respectively at 101325 Pa [60]

The higher sulphidation rate is related to the higher deviation of the stoichiometry in sulphides (product of reactions) and higher concentration of lattice defects. **Table 13** shows the defect concentration in $Cu_{2-y}S$ and $Cu_{2-y}O$:

Compound	Defect concentration	Atmosphere	Temperature [K]
$Cu_{2-y}S$	17%	101325 Pa S_2	973 - 1223
$Cu_{2-y}O$	$2x10^{-3}$	10132.5 Pa O_2	1298

Table 13 Defects concentration in copper oxide and copper sulphide [61]

It is be noted that in the sulphides the defects are in cationic site of atomic lattice (sulphides of silver, copper, cobalt, iron, chromium) and consequently the scales on these metals develop via outward diffusion of metal cations For example: $Cu_{2-y}S$, $Co_{2-y}S$, $Fe_{2-y}S$, $Cr_{2-y}S_3$, $Ag_{2-y}S$, $Ni_{3-y}S_3$, $Ni_{1-y}S$.

In these sulphides, self diffusion is much larger than in oxides Al_2O_3, SiO_2, Cr_2O_3, NiO, and FeO. On other hand in manganese sulphide (MnS), the deviation of stoichiometry is lower by one order of magnitude than in MnO [62]. Sulphides of refractory elements also possess smaller number of defects in the structure; WS_2 and MoS_2 [59].

The large amount of lattice defects in growing sulphide scales (M_xS_y) show that the scale grows due to the lattice diffusion. This fact probably explains that the curves frequently show parabolic behaviour. Thus grain boundary diffusion is less important for sulphides kinetics.

Also lower melting points of sulphides in contrast to those of oxides promote faster rate of reaction during the exposure of metals to high temperature above (600^oC (873 K)) at the liquid phase/scale interface.

This behaviour is related to the commonly used alloy: Ni, Co and Fe; Ni and Ni_3S_2 create Ni-S liquid solution at 908 K, Co and Co_4S_3 form Co – S liquid solution at 1073 K, and in case of Fe, iron with Fe – S generates liquid solution at 1258 K.

The formation of sulphides are harder than the formation of oxides; from thermodynamic point of view – the free energies of formation for sulphides are higher than those for oxides [62]. **Table 14** presents $\Delta G^o(kJ/mol)$ values of oxides and sulphides:

Sulphides		Oxides	
Compound	$\Delta G^o(kJ/mol)$	Compound	$\Delta G^o(kJ/mol)$
Al_2S_3	- 219	Al_2O_3	- 429
Cr_2S_3	- 135	Cr_2O_3	- 261
FeS	- 86	FeO	- 176
CoS	- 80	CoO	- 136
NiS	- 88	NiO	- 127
MnS	- 190	MnO	- 294

Table 14 Standard free energies of formation calculated for sulphides and oxides at 1273 K [62]

In order to estimate phase formation in sulphidized and oxidised environments Du and Datta at el. [60] assumed that in the environment containing

oxygen or sulphur the following reactions need to be considered for a divalent metal, M:

Equation XXI

$$M + \frac{1}{2}O_2 = MO$$

Equation XXII

$$M + \frac{1}{2}S_2 = MS$$

The equilibrium oxygen and sulphur partial pressure are defined by the following relations:

Equation XXIII

$$pO_2^{1/2} = \exp(\frac{\Delta G^o_{MO}}{RT})$$

Equation XXIV

$$pS_2^{1/2} = \exp(\frac{\Delta G^o_{MS}}{RT})$$

Equations XXIV and XXV allow the establishment of conditions necessary for oxidation and sulphidation; however a further reaction must be considered:

Equation XXV

$$MS + \frac{1}{2}O_2 = MO + \frac{1}{2}S_2$$

With the equilibrium condition:

Equation XXVI

$$\frac{pS_2^{1/2}}{pO_2^{1/2}} = \exp(\frac{\Delta G^o_{MS}}{RT} - \frac{\Delta G^o_{MO}}{RT})\frac{a_{MS}}{a_{MO}}$$

If unit activities are assumed for the phases MO and MS, **Eq.XXVI** can be reduced to:

Equation XXVII

$$\frac{pS_2^{1/2}}{pO_2^{1/2}} = \exp(\frac{\Delta G^o_{MS}}{RT} - \frac{\Delta G^o_{MO}}{RT})$$

From equations presented above (**equations: XXII – XXVII**) it is possible to predict the formation of possible products during oxidation and sulphidation experiments. Furthermore an examination of **equations; XXIII, XXIV, and XXVII** allows to predict the formation of various corrosion product as follows:

1. If $(pO_2)_{gas} > (pO_2)_{eq}$ and $(pS_2)_{gas} < (pS_2)_{eq}$, then MO is the only stable surface phase
2. If $(pO_2)_{gas} < (pO_2)_{eq}$ and $(pS_2)_{gas} > (pS_2)_{eq}$, then MS is the only stable surface phase
3. If $(pO_2)_{gas} > (pO_2)_{eq}$ and $(pS_2)_{gas} > (pS_2)_{eq}$, then both MO and MS are stable surface

Equation XXVII indicates that the formation of only one phase depending on which of the following conditions prevail:

$(pS_2 / pO_2)_{gas} > (pS_2 / pO_2)_{eq}$ - such conditions are favoured for sulphide (MS) formation **(equation XXV)** and sulphide will be the stable phase, where the metal is in contact with gas.

$(pS_2 / pO_2)_{gas} < (pS_2 / pO_2)_{eq}$ - such conditions are favoured for oxide formation and MO phase will be the stable phase, and **equation XXV** will move to the right.

Moreover it is very important to mention, that the formation of sulphides can be presented in form of graph; Ellingham – Richardson diagram. Ellingham – Richardson diagram showing a standard free energy of formation of sulphides [ΔG^o] as a function of temperature [K] is presented in **figure 33**:

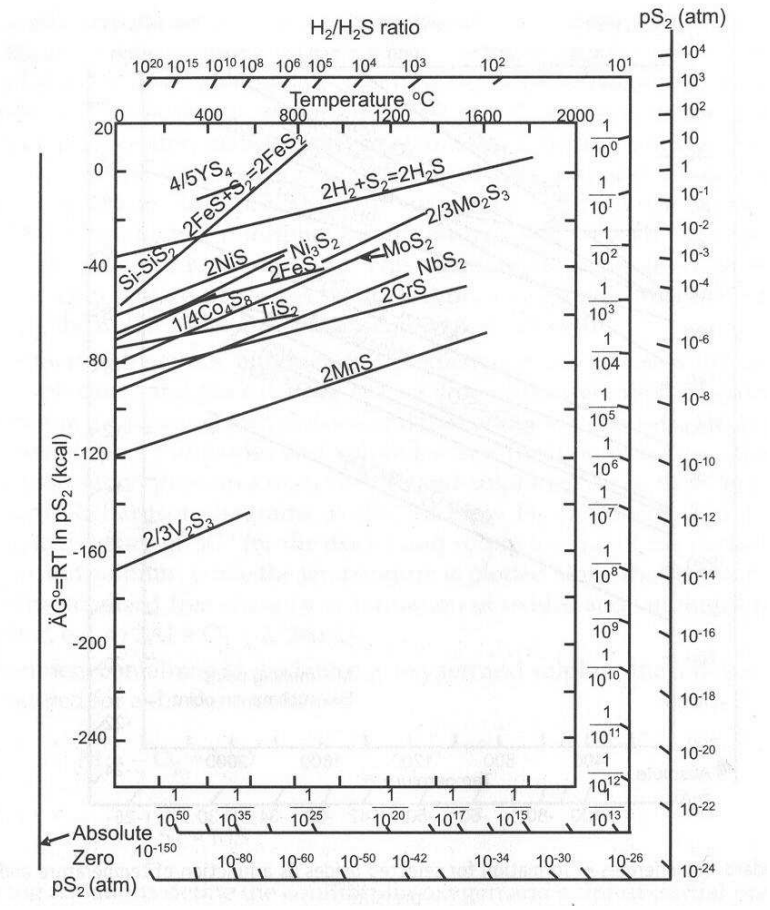

Figure 33 Ellingham – Richards diagram for sulphides formation as a function of standard free energy, temperature and sulphur partial pressure [60]

If equilibrium partial pressure is known, it is possible to form a thermodynamic stability diagram, as presented on **figure 34**. This type of diagram gives the stability of all relevant phases; metal, oxide, and sulphide at a given temperature.

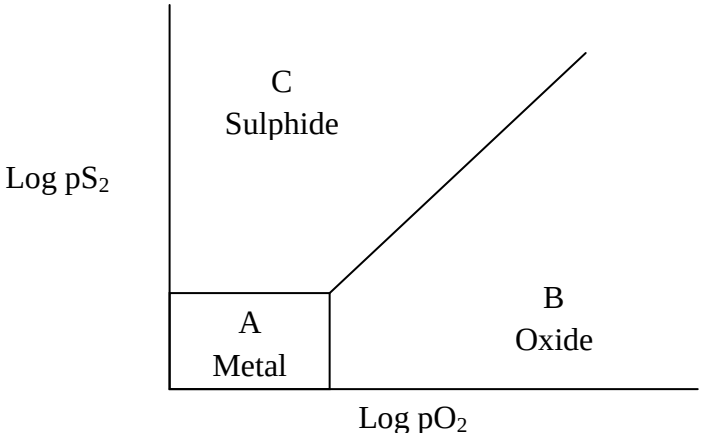

Figure 34 Phase stability diagram for sulphides and oxides as a function of log of pS_2 and pO_2 [60]

Two dimensional diagram for metal (M) exposed to oxidizing – sulphidising atmosphere can be determined by reactions presented below:

Reaction 13 $$M + \frac{1}{2}O_2 \leftrightarrow MO$$

Reaction 14 $$M + \frac{1}{2}S_2 \leftrightarrow MS$$

Reaction 15 $$MO + \frac{1}{2}S_2 \leftrightarrow MS + \frac{1}{2}O_2$$

The equilibrium from **reactions 13 and 14** define a critical pressure of pO_2 and pS_2 (dissociation pressure) for M/MO and M/MS equilibrium; **reaction 15** denotes the critical pO_2/ pS_2 ratios for MS/MO [63]. **Figure 34** shows the stability diagram, which present the stability range for oxides and sulphides products. Diagram shows that:

A) Metal is only stable phase

B) Oxide is only stable phase

C) Sulphide is only stable phase

It should be noted that the gas equilibrium can be determined for many mixtures of gases at different temperatures and pressures. However as the surface of the substrate exposed to corrosive environments (oxidation, sulphidation, hot corrosion) is covered with corrosion products (oxides, sulphides, carbides), thermodynamics cannot be employed in order to predict the progress in corrosion development. In such condition, kinetics, and diffusion processes play the most important role in the degradation of the metallic materials.

Ch.II.Sec.2.3 Sulphidation of specific alloys

Ch.II.Sec.2.3.1 Ni – Cr and Fe – Cr binary alloys

Ni – Cr and Fe – Cr alloys exhibit similar behaviour in sulphidising environments. The sulphidation resistance depends on the chromium content in the bulk material.

Mrowec and Webber [59] investigated a series of alloys Ni – Cr with chromium content (up to 20 at %) in highly sulphidized environments (pS_2 = 101325 Pa) in the temperature range 773 – 1223 K. They distinguished three different periods of corrosion which depending on chromium content. When the content of chromium was 0.1wt %, the scale morphology consisted of one phase; solid solution of chromium sulphide (Cr_2S_3) in nickel sulphide (NiS). The scale development was due to the outward diffusion of metal. The corrosion resistant of this type of Ni alloys (with 2 wt% of Cr) in sulphidising atmosphere was lower than for pure Ni. The faster corrosion was due to the presents of Cr^{3+} ions introduced into the crystal lattice of NiS. Furthermore the NiS compound is a p type semiconductor with insufficient cations in the NiS lattice. When Cr^{3+} is introduced to the NiS lattice, then concentration of cation vacancies will increase.

When the Cr content was between 0.1 and 20 wt% the scale had a two phase structure; the outer layer consisting of NiS and the inner layer consisting of Cr_2S_3.

The scale morphology for these conditions was similar to that of the first condition and consisted of solid solution of NiS in Cr_2S_3. The improvement in corrosion resistance was due to the introduction of Ni^{2+} ions to the Cr_2S_3 lattice. It was observed by Mrowec and Weber [59] that the Cr_2S_3 is also a semiconductor of type p with an insufficient amount of cations in Cr_2S_3 lattice. Thus when Ni^{2+} ions are introduced the defects concentration in Cr_2S_3 lattice is decreased.

The mechanism of the development Fe – Cr scale morphology was similar to that of Ni – Cr alloys. Weber and Mrowec [59] observed that high content Fe-Cr alloys formed Cr_2S_3 scale with some of inclusions of Fe^{2+} ions.

In another study by Romeo [64] a low corrosion resistance of low Cr content in Ni and Fe base alloys was observed at high temperature (above 873 K).

The low corrosion resistance occurred, due to the formation of a liquid Ni - Ni_3S_2 solution at 908 K with inclusions of Cr. The low content of Cr was insufficient to develop a protective Cr_2O_3 oxide scale, the higher concentration of Ni^{2+} in the Ni – Cr alloy matrix and high sulphur pressure (pS_2 = 1 Pa) was sufficient to developed a liquid phase of Ni – Ni_3S_2.

The study carried out by Vineberg and Douglass [65], Ni10Cr5Al, Ni10Cr-5Al, and Ni50Cr5Al with and without addition of 1wt% of Y were investigated in the sulphidation atmosphere (10132.5 Pa of S_2) at 973 K.

Table 15 shows the chemical composition of alloys, partial pressure of sulphur, experiment temperature, and duration of the test.

Alloy [wt%]	Sulphur pressure [Pa]	Temperature [K]	Time [hours]
Ni10Cr5Al	10132.5	973	15
Ni20Cr5Al	10132.5	973	12
Ni50Cr5Al	10132.5	973	24
Ni10Cr5Al-1Y	10132.5	973	24
Ni20Cr5Al-1Y	10132.5	973	24
Ni50Cr5Al-1Y	10132.5	973	24

Table 15 Experimental details of exposed Ni-Cr-Al alloys to sulphidation environments at 973 K [65]

This study [65] showed the development of two types of morphology on three different Ni – Cr alloys (Ni10Cr5Al, Ni20Cr5Al, and Ni50Cr5Al).

In details the alloys with the lowest content of chromium (Ni10Cr5Al, Ni10Cr5Al) produced a lamellar scale with two forms of structure; the bright layer in the scale of Ni10Cr5Al, was occupied by $NiS_{1.03}$, the dark areas of the scale developed on Ni10Cr5Al consisted of mixed sulphides (Cr_2S_3 and Al_2S_3).

The sample with higher amount of chromium (Ni20Cr5Al) after 12 hours of sulphidation at 973 K developed similar structure of the scale as in (Ni10Cr5Al), scale consisted an outer layer $NiS_{1.03}$, and inner lamellar layer built from lamellae of Cr_2S_3 and Al_2S_3 in $NiS_{1.03}$ matrix.

The scale developed on the alloy with the highest contents of Cr (Ni50Cr5Al) was thin and brittle; this scale spalled off from the substrate (Ni50Cr5Al) during the cooling down period. Scale mainly consisted chromium sulphide (Cr_2S_3).

Alloys Ni10Cr5Al with/without small addition of Y (1 wt %) exposed to the same environment (10132.5 Pa sulphur pressure at 973 K) developed a similar scale morphologies. Furthermore the addition of 1 wt% yttrium did not change scale morphology in Ni10Cr5Al-1Y alloy. The developed scale on Ni10Cr5Al-1Y alloy consisted of an outer layer of $NiS_{1.03}$ and inner layer of Cr_2S_3 and Al_2O_3 lamellae in a $NiS_{1.03}$ matrix. Yttrium in Ni10Cr5Al-1Y alloy was detected on the grain boundaries at the scale/alloy interface.

The alloy (Ni20Cr5Al-1Y) investigated for 24 hours at 973 K developed also $NiS_{1.03}$ as an outer layer and an inner layer of lamellae of mixed Cr_2S_3 and Al_2S_3 in a $NiS_{1.03}$ matrix. The outer $NiS_{1.03}$ was relatively massive, accounting for the half of the

overall scale thickness developed during 24 hours of sulphidation at 973 K). This scale was adherent and uniformly covered the whole Ni20Cr5Al-1Y exposed alloy. For the same alloy without 1 wt % of yttrium (Ni20Cr5Al), the scale also consisted of an outer $NiS_{1.03}$ layer but the scale was thinner and less uniform.

Sample with highest amount of chromium (Ni50Cr5Al-1Y) and with addition of 1 wt % of yttrium, showed the development of very thin Cr_2S_3 scale. The Cr_2S_3 scale was non adherent, and easily spalled off from the surface of the alloy (Ni50Cr5Al-1Y) during cooling from the sulphidation temperature 973 K.

Vineberg and Douglass [65] also observed that mass gain for samples with low content of Cr (Ni10Cr5Al, Ni20Cr5Al, Ni10Cr5Al-1Y, and Ni20Cr5Al-1Y) followed a linear rate law, whereas the alloys with the highest amount of Cr (Ni50Cr5Al, Ni50Cr5Al-1Y) followed by parabolic rate law when exposed to 10132.5 Pa sulphidation environment at 973 K. The role of yttrium to improve the sulphidation resistance of Ni – Cr – Al alloys at 973 K acted to reduce the rate of reactions at high temperature 973 K. Yttrium dissolves in $Cr_{2+y}S_3$ sulphide as a donor. The dissolved Y^{5+} ions decrease the concentration of interstitial Cr^{3+} and reduce the rate law. Authors [65] suggested also that different mechanism may occur; yttrium has a large ionic size, thus adsorption is possible in the grain boundaries in order to minimize the strains energy. Moreover the yttrium ions fit better in the grain boundaries than in the lattice structure due to their size.

Morphologies of exposed samples are almost the same, but thickness of the scale is different.

Similar results were obtained by Zurek [66], who exposed Ni22Cr10Al-1Y alloy to H_2/H_2S gas mixture with 10^{-3} Pa and 1 Pa at 1173, 1273 K.

The same alloy (Ni22Cr10Al-1Y) also was exposed to SO_2 atmosphere at the same temperatures (1173 and 1273 K). The alloy Ni22Cr10Al-1Y during sulphidation at 1 Pa of S_2 in H_2/H_2S gas mixture showed a linear rate law. The fast rate of the corrosion of the exposed sample (Ni22Cr10Al-1Y) at 1 Pa sulphur pressure at 1173 K an 1273 K was due to the formation of liquid eutectic (Ni – Ni_3S_2) which forms at 908 K [67]. At lower pressure ($pS_2 = 10^{-3}$ Pa) NiS was unstable and the sulphidation rate was lower, following to a parabolic rate law.

In case of SO_2 exposure at high temperatures (1173 and 1273 K respectively), the corrosion rate were lower than that in a H_2/H_2S gas mixture. The corrosion rate at 1173 and 1273 K respectively, in SO_2 atmosphere was lower due to

the formation of Al_2O_3, NiO, and Cr_2O_3 oxide. The formation of Al_2O_3, NiO, and Cr_2O_3 reduced the ingress of S_2 from atmosphere to the bulk material and blocked the formation of liquid eutectics (Ni – Ni_3S_2) which forms at 908 K.

The scale formed during sulphidation in H_2/H_2S gas mixture consisted of $NiCr_2S_3$, Ni_3S_2, and Cr_xS_y at 1173 K. The chromium rich – sulphide phases (Cr_xS_y) were developed when partial pressure of S_2 was decreased (from 1 Pa to 10^{-3} Pa) and the temperature was increased from 1173 K to 1123 K. When Ni22Cr10Al-1Y alloy was exposed to SO_2 atmosphere in the temperature range; 1173 K to 1123 K then various oxides were developed (Al_2O_3, NiO, Cr_2O_3).

Douglass and Wu [68] investigated the sulphidation behaviour of Ni-Cr-Mo alloys with various Cr and Mo contents **(Table 16)** at 973 K for 11 hours. The effect of molybdenum additions (5, 10, 15, and 20 wt %) to Ni – Cr alloy was investigated in pure sulphur vapour at 973 K, along with the effect of chromium addition (5, 10, 15, and 20 wt %). The results obtained by Douglas and Wu [68] are similar to those observed by Vineberg [65] and Zurek [66]. Douglas and Wu [68] observed that NiCr alloys with the addition of Mo (5, 10, 15, and 20 wt% of Mo) in pure sulphur vapour at 973 K showed a linear or near linear rate law.

The sulphidation kinetics of Ni20Mo alloy was slightly lower than that of Ni20Cr. Alloys with the smallest addition of ternary element (Ni20Cr-5Mo and Ni20Mo-5Cr) showed the highest reaction rate. It is interesting to note that the highest alloying addition of Mo (20 wt %) in Ni20Cr alloy had no significant benefit for the sulphidation rate. All exposed alloys **(Table 16)** developed multilayered scales. The outer layer of the scale of exposed alloys in sulphidation at pure sulphur vapour at 973 K for 11 hours always consisted of $NiS_{1.03}$ scale, underneath $NiS_{1.03}$ scale, Cr_3S_4 with inclusion of dissolved Mo appeared.

The Cr_2S_3 phase developed between of the Cr_3S_4 layer and the outer $NiS_{1.03}$ layer was generally observed in the Cr containing alloys, expect Ni20Mo5Cr alloy. The innermost MoS_2 phase developed on the all alloys which content more than 10 wt% of Mo at pure sulphur vapour at 973 K. **Table 16** presents the scale structures on exposed samples:

Alloy	Scale structure				Pure Sulphur Vapour
Ni20Cr	Cr_3S_4	Cr_2S_3	$Ni_3S_2/NiS_{1.03}$		
Ni20Cr-5Mo	$(Cr/Mo)_3S_4$	Cr_2S_3	$NiS_{1.03}$		
Ni20Cr-10Mo	MoS_2	$(Cr/Mo)_3S_4$	Cr_2S_3	$NiS_{1.03}$	
Ni20Cr-15Mo	MoS_2	$(Cr/Mo)_3S_4$	Cr_2S_3	$NiS_{1.03}$	
Ni20Cr-20Mo	MoS_2	$(Cr/Mo)_3S_4$	Cr_2S_3	$NiS_{1.03}$	
Ni20Mo	MoS_2/Mo_2S_3		$Ni_3S_2/NiS_{1.03}$		
Ni20Mo-5Cr	$(Mo, Cr)S_2$	MoS_2	Cr_3S_4	$NiS_{1.03}$	
Ni20Mo-10Cr	MoS_2	$(Cr/Mo)_3S_4$	Cr_2S_3	$NiS_{1.03}$	
Ni20Mo-15Cr	MoS_2	$MoS_2/(Cr/Mo)_3S_4$		Cr_2S_3	$NiS_{1.03}$

Table 16 Scale structures developed during sulphidation in pure sulphur vapour at 973 K for 11 hours [68]

Douglass and Wu [68] concluded, that the formation of phases with high number of defects: (Cr_3S_4 and $NiS_{1.03}$) in all exposed samples **(Table 16)** at 973 K is a one of the main concerns.

Furthermore the addition of various content of Mo (5, 10, 15, and 20 wt% of Mo) to exposed alloy (Ni20Cr) did not prohibit the formation of these scales (Cr_3S_4 and $NiS_{1.03}$), the authors suggested that the lack of formation Mo_2S_3 in the outer layer of corrosion product is due to the lack of required Mo content or due to the lack of elements which can stabilize the Mo_2S_3 phase.

The results presented by Douglass and Wu [68], reported no benefits have due to the addition of Mo; these results are in contradiction with work reported by Young [71].

Young's [69] results showed that the sulphidation of Ni20Mo alloy at 973 K in H_2/H_2S mixture at low partial pressure of sulphur ($pS_2 = 5x10^{-6}$ Pa) led to the formation of Mo_2S_3 phase; also this phase was very protective (due to the low defects amount in the atomic lattice). The same author [69] observed that in the pressure range ($pS_2 = 2x10^{-3}$ Pa – $pS_2 = 10^3$ Pa) a duplex structure developed on Ni20Mo alloy consisting of; an outer layer of solid nickel sulphide, underneath the outer solid nickel layer a liquid Ni-Mo sulphide phase existed and an inner layer with a two phase structure: MoS_2 and nickel sulphide. Schematic diagram in **figure 35** shows the phase structure on sulphidized Ni20Mo alloy at 973 K in $pS_2 = 2x10^{-3}$ Pa – $pS_2 = 10^3$ Pa.

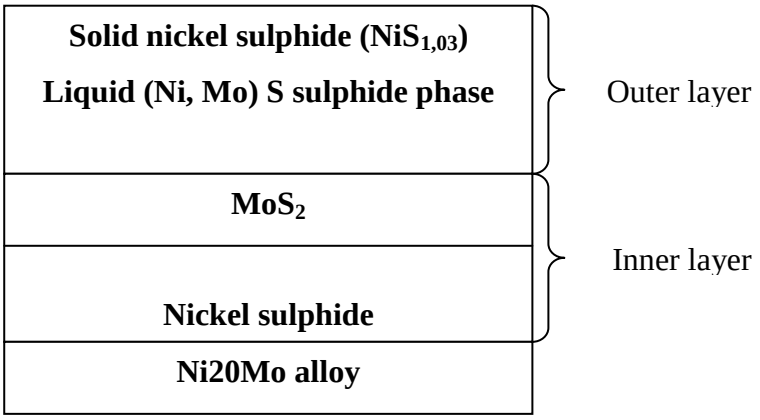

Figure 35 Schematic diagram presents a phase formation on Ni20Mo alloy after sulphidation at 973 K at ($pS_2 = 2x10^{-3}$ Pa – $pS_2 = 10^3$ Pa) [69]

The same author [70] investigated the behaviour of ternary alloys of NiCrMo; Ni20Cr5Mo exposed to H_2/H_2S gas mixture, where $pS_2 = 6.07x10^{-1}$ Pa at 700°C (973 K).

The lower kinetic growth of ternary alloy (Ni20Cr5Mo) compared to the binary Ni20Cr alloy was associated to the destabilization pressure of Cr_3S_4 upon the addition of Mo, and raising the dissociation pressure of Cr_3S_4.

Southwell and Young [71] investigated the sulphidation behaviour of the binary alloys: Fe25Cr, FeMn and ternary alloys: Fe10Mn10Cr, Fe20Mn25Cr and Fe25Mn10Cr at temperature range 973 – 1073 K in H_2/H_2S mixture corresponding to equilibrium sulphur partial pressures of 10^{-3} Pa and 8 Pa.

The authors concluded that even the binary alloy FeMn develops a duplex scale consisting of: $Fe(Mn)_{1-x}S$ layer above a α-Mn(Fe)S layer under $pS_2 = 10^{-3}$ Pa and 8 Pa at 973 and 1073 K. Fe25Cr binary alloy developed two different scales. At higher temperature 1073 K at $pS_2 = 10^{-3}$ Pa and 8 Pa Fe25Cr alloy developed a scale consisting an outer layer $Cr(Fe)_{1-x}S$ and inner $Cr(Fe)S_x$. Furthermore at 973 K with $pS_2 = 8$ Pa, Fe25Cr alloy developed a third intermediate layer of $(Cr,Fe)_3S_4$.

Similar to Fe25Cr binary alloy, the ternary Fe25Cr10Mn and Fe10Mn10Cr alloys developed Cr_3S_4 layers at 973 K and $pS_2 = 8$ Pa, this scale (Cr_3S_4) was not observed when $pS_2 = 10^{-3}$ Pa at 973 K and also at 1073 K in both atmospheres where pS_2 (10^{-3} and 8 Pa). The phase formation observed on the binary Fe25Cr alloy is in

good agreement with results obtained by Narita and Smeltzer [72] where Fe5Cr to Fe60Cr alloys were investigated.

The high content of Cr (25 wt %) in ternary alloy Fe10Mn25Cr formed Cr_3S_4 layer in both sulphur pressures (10^{-3} and 8 Pa) at 973 K, in other hand at 1073 K high content Cr alloy (Fe10Mn25Cr) was not formed Cr_3S_4 layer in both partial pressures (10^{-3} and 8 Pa).

The lack of formation of Cr_3S_4 when $pS_2 = 10^{-3}$ Pa at 973 K and at 1073 K in both atmospheres where $pS_2 = 10^{-3}$ and 8 Pa was suggested to be associated with the low activity of Cr at 973 K in 10^{-3} Pa sulphur partial pressure. Furthermore a low concentration (10 wt %) of Cr in ternary alloys (Fe25Mn10Cr and Fe10Mn10Cr) was insufficient amount to develops the Cr_3S_4 scale at 1073 K in both atmospheres where pS_2 (10^{-3} and 8 Pa).

It was observed by the authors [71] that Mn improves the sulphidation resistance because Mn – S system is much more refractory with eutectic temperature equivalent to 1515 K. Furthermore the sulphidation of Mn leads to the formation of α-MnS phase. α-MnS phase has unusually small diffusion coefficient, due to the small deviation from stoichiometry [61]. In order to estimate which phase should form before other, authors [71] present a table **(Table 17)** with free energy of formation of different sulphide at 973 and 1073 K.

Compound	T = 973 K	T = 1073 K
FeS	-198	-188
$FeCr_2S_4$	-226	-214
Cr_3S_4	-271	-258
CrS	-296	-285
MnS	-410	-398

Table 17 Standard free energy in of formation [kJ] for selected sulphides at 973 and 1073 K [71]

Diagrams below **(Figs. 36 - 39)** show the scale morphology of exposed alloys ternary Fe10Mn10Cr, Fe20Mn25Cr and Fe25Mn10Cr alloys at temperature range 973 – 1073 K in H_2/H_2S mixture corresponding to equilibrium sulphur partial pressures of 10^{-3} Pa and 8 Pa.

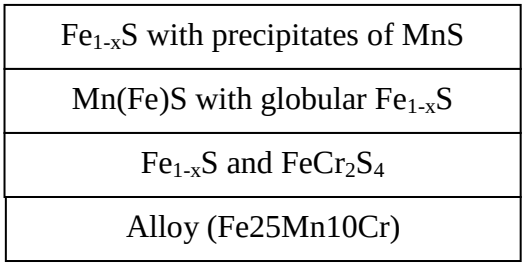

Figure 36 Diagram of scale morphology of Fe25Mn10Cr at 1073 K in pS_2 = 8 Pa [71]

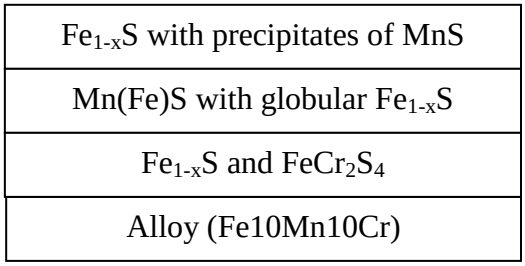

Figure 37 Diagram of scale morphology of Fe10Mn10Cr at 973 K in pS_2 = 8 Pa [71]

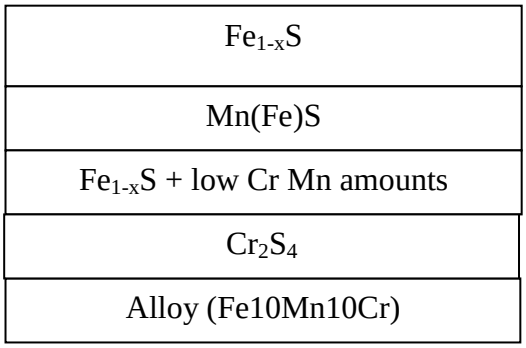

Figure 38 Diagram of scale morphology of Fe10Mn10Cr at 973 K in pS_2 = 8 Pa [71]

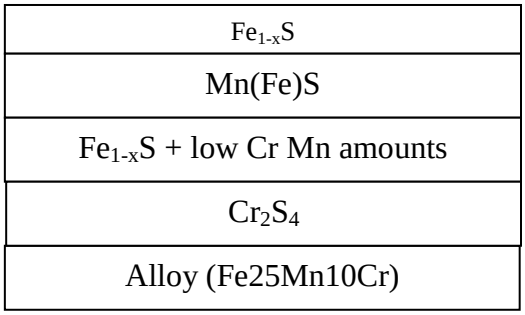

Figure 39 Diagram of scale morphology of Fe25Mn10Cr at 973 K in pS_2 = 8 Pa

The high Cr alloy Fe10Mn25Cr formed a four layers of morphology in both values of pS_2 (10^{-3} and 8 Pa) at 973 K. The developed scale was similar to those

formed on low chromium alloys (Fe10Mn10Cr, Fe25Mn10Cr). At higher temperature (1073 K) and in pS_2 = 8 Pa an additional layer ($FeCr_2S_4$ + Cr_3S_4 + Fe) is formed at the scale base.

Figure 40 presents a diagram of the scale morphology of exposed to (1073 K) and pS_2 = 8 Pa Fe10Mn25Cr alloy.

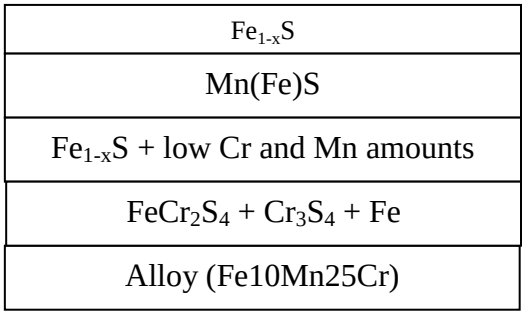

Figure 40 Diagram of scale morphology of Fe10Mn25Cr at 973 K in pS_2 = 8 Pa

Fe10Mn25Cr alloy in $pS_2 = 10^{-3}$ Pa at 1073 K consisted of three layers; the type of layers was the same as in the low content chromium alloys (Fe10Mn10Cr, Fe25Mn10Cr); a thin outer layer of $Fe_{1-x}S$ and a thick innermost $Fe_{1-x}S$ + $FeCr_2S_4$.

All exposed alloys (Fe10Mn10Cr, Fe20Mn25Cr, and Fe25Mn10Cr) reacted according to the parabolic rate law. The Fe25Mn alloy showed the highest sulphidation rate at 973 K in sulphur pressure pS_2 = 8 Pa. The best performance was observed for Fe10Mn25Cr alloy at 973 K but not at 1073 K. The addition 10% of Cr to Fe10Mn alloy decreased the sulphidation resistance under the most reaction conditions due to the substitutional dissolution of Cr^{3+} in MnS lattice postulated by Papaiacovou [73]. Substitutional dissolution increases the cation vacancy concentration in MnS matrix, and then MnS become more defected.

Ch.II.Sec.2.3.2 M-CrAlYX alloys

The sulphidation/oxidation behaviour of M-CrAlYX alloys was studied in details by Du and Datta [74,75] (where M is Co or Fe and X is V, Nb, Mo or W added in combination and in different amounts) at temperature 1023 K at $pS_2 = 10^{-1}$ and $pO_2 = 10^{-18}$ Pa for 240 hours. For each exposed alloy a parabolic rate law was achieved at prolongated time of exposure (240 hours). It is important to note that the inclusion of Mo in the alloy which contains V and Nb and of combined mixture of Mo and W led to improved sulphidation/oxidation resistance at 1023 K.

The authors [74, 75] also observed superior degradation resistance when Co element was partly replaced by Fe. The scale formed on exposed samples in (CoCrAlYX) in (sulphidation/oxidation environment at $pS_2 = 10^{-1}$ and $pO_2 = 10^{-18}$ Pa at 1023 K at $pS_2 = 10^{-1}$ and $pO_2 = 10^{-18}$ Pa for 240 hours) showed the development of a multilayer structures as presented in **figure 41**.

The outer layer was occupied by Co_9S_8 and Co_3S_4 phases, inner layer consisted of Cr_3S_4, and an innermost layer contained of chromium and refractory metal sulphide. A schematic diagram presented on **figure 41** shows that at the initial period of exposure the high affinity of Co to S_2 in CoCrAlYX favours the formation of Co_9S_8 or Co_3S_4; these phases start to form in the beginning on the surface of exposed material (CoCrAlYX alloy) to 1023 K in $pS_2 = 10^{-1}$ and $pO_2 = 10^{-18}$ Pa atmosphere. At the same time a thin layer of α - Al_2O_3 starts to develop underneath sulphide outer layer **(Fig. 41a)**.

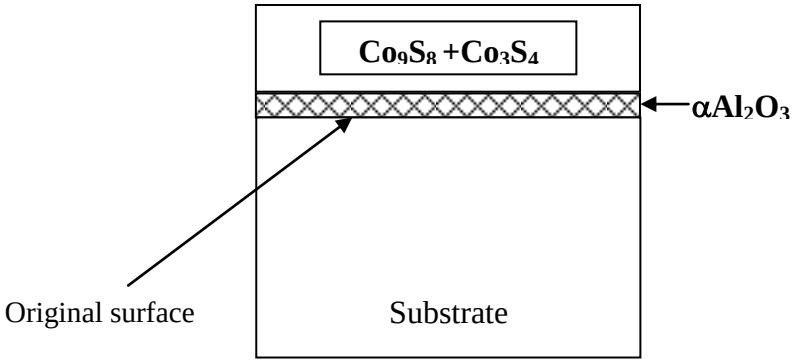

41a) Formation of cobalt sulphide [74 75]

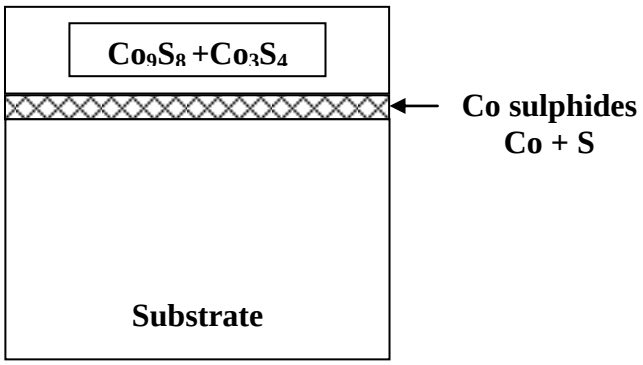

41b) Dissociation of cobalt sulphides [74 75]

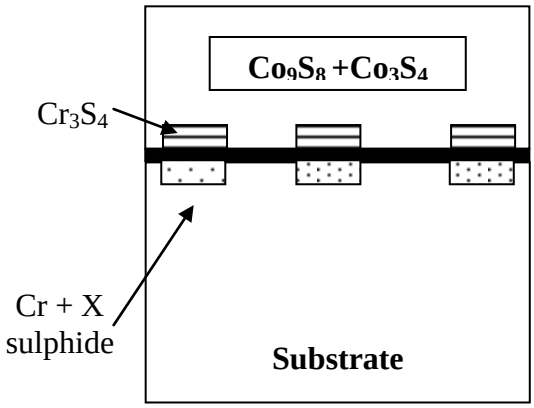

41c) Formation of Cr and refractory metal sulphides [74 75]

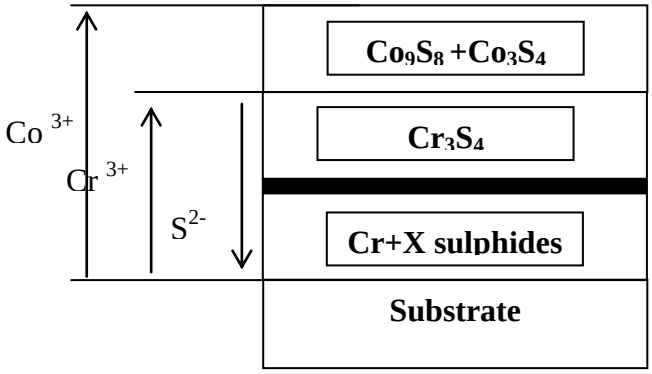

41d) Final stage [74 75]

Figure 41 Scale development of exposed CoCrAlYX alloy at 1023 K at $pS_2 = 10^{-1}$ and $pO_2 = 10^{-18}$ Pa for 240 hours [74, 75]

After initial period the pS_2 decreases below the level of dissociation pressure of cobalt sulphide. At this moment when dissociation pressure of cobalt sulphide drops down, cobalt sulphide starts to decompose to Co^{3+} cations and sulphur anions S^{2-} (**Fig 41a**), according to the **reaction 16**:

Reaction 16 $$Co_3S_4 \rightarrow Co^{3+} + 2S^{2-}$$

This type of mechanism when cations of metal (cobalt) are released is called "dissociation mechanism" and was described in details by Mrowec [76].

Released cobalt cations from decomposed cobalt sulphides, diffuse outward and starts to react with sulphur on the top of the scale, where partial pressure of sulphur is enough high enough to develop Co_9S_8 and Co_3S_4 **(Fig. 41b)**.

Reaction 17 $Co^{3+} + 2S^{2-} \rightarrow Co_3S_4$

Furthermore sulphur anions diffuse inward, where chromium cations with high activity start to form a chromium sulphide (Cr_3S_4) as reaction below presents:

Reaction 18 $Cr^{3+} + 2S^{2-} \rightarrow Cr_3S_4$

Sulphur anions (S^{2-}) also react with refractory metal (Mo) to develop refractory sulphides:

Reaction 19 $Mo^{2+} + S^{2-} \rightarrow MoS$

Reaction 20 $Mo^{4+} + S^{2-} \rightarrow MoS_2$

The development of an inner layer decreases the partial pressure of sulphur and decreases the inward diffusion of sulphur **(Fig. 41c)**. It needs to be stated that the dissociation of cobalt sulphides (Co_3S_4 and Co_9S_8) does not increase the thickness of the scale, but only shift the outer/mid layer interface in the outward direction. The formation of duplex scale also was observed in FeCrAlYX alloy after sulphidation at temperature 1023 K in $pS_2 = 10^{-1}$ and $pO_2 = 10^{-18}$ Pa for 240 hours. The outer layer was occupied by Fe_3S_4, Co_9S_8, and Cr_3S_4, the inner layer with sulphides of chromium and refractory metals (W, Mo, and Nb). Furthermore both types of alloys (FeCrAlYX and CoCrAlYX) developed a thin alumina oxide layer, between the substrate and the inner scale, the formation of Al_2O_3 thin layer was suggested to decrease an outward diffusion of the base elements. In the case of Fe, Co alloys, a thin layer of Cr_3S_4, Fe_3S_4 and Co_9S_8 develops in the beginning of the sulphidation process at 1023 K in $pS_2 = 10^{-1}$ and $pO_2 = 10^{-18}$ Pa. The depletion of Co, Fe, and Cr decreases the activity of these elements in the alloys (Co, Fe alloys). Thus the activity values of refractory elements beneath the outer layer formed by Cr_3S_4, Fe_3S_4, and Co_9S_8, start to increase and the formation of refractory sulphides of Nb and V is initiated. During the formation of duplex (Cr_3S_4, Fe_3S_4, and Co_9S_8) scale Fe, Co, Cr ions diffuse outwards and form an outer layer, at the same time sulphur ions diffuse inward and develop an inner layer congaing vanadium sulphide and niobium sulphide. It was suggested that the adherent inner scale of V and Nb as well as Cr sulphide as an outer layer improves the sulphidation/oxidation behaviour of these types of alloys (Co, Fe alloys). Schematic diagram is illustrated on **figure 42**.

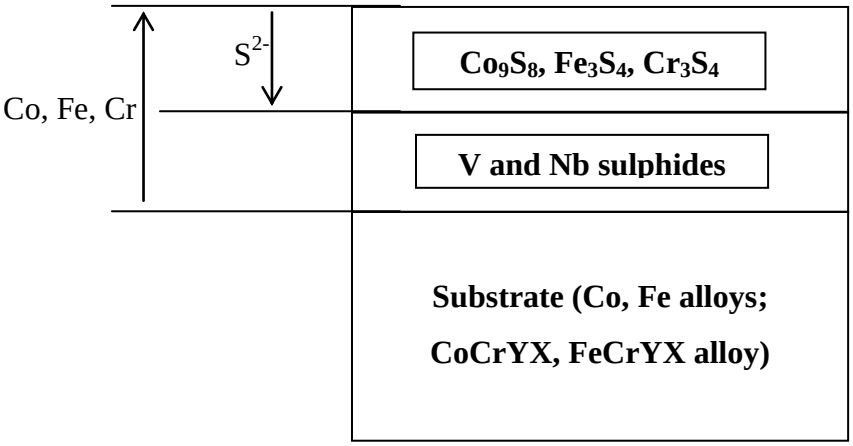

Figure 42 Schematic of diffusion direction during exposure to sulphidation environment $pS_2 = 10^{-1}$ and $pO_2 = 10^{-18}$ Pa at 1023 K [74 75]

Ch.II.Sec.2.4 Sulphidation/Oxidation of TiAl alloys – Critical review

Until recently the high temperature sulphidation behaviour of TiAl and TiAl based intermetallics has not been studied extensively.

Extensive work was carried out by Du and Datta with co partners [77], which investigated the sulphidation/oxidation behaviour of AlTiN coated Ti46.7Al1.9W0.5Si intermetallic alloy with and without the addition of NbN and CrN diffusion barriers at 1123 K in $H_2/H_2S/H_2O$ in $pO_2 = 10^{-18}$ Pa, $pS_2 = 10^{-1}$ Pa) for 240 hours.

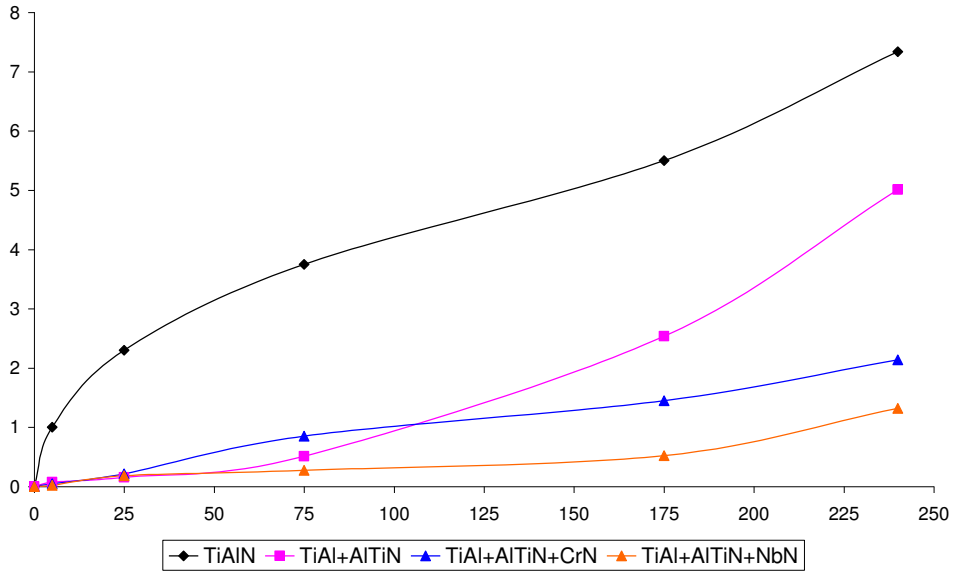

Figure 43 Oxidation/Sulphidation kinetic data for AlTiN, AlTiN+CrN, AlTiN+NbN coated and uncoated Ti46.7Al1.5W0.9Si alloy at 1123 K in $H_2/H_2S/H_2O$ atmosphere [77]

Figure 43 shows the kinetic data obtained from sulphidation/oxidation test at 1123 K for 240 hours in $H_2/H_2S/H_2O$ atmosphere. The sulphidation/oxidation test showed that mass gain of subjected materials showed the parabolic rate of the scale growth. The parabolic rate constant for the uncoated material (Ti46.7Al1.9W0.5Si) was equivalent to kp = $6x10^{-11}$ [$g^2/cm^4/s$]. **Figure 43** shows kinetic data from sulphidized materials.

The mass gain of coated samples reveals that the diffusional barrier coatings; NbN and CrN showed good protection against high sulphidized environment (pS_2 = 10^{-1} Pa). The mass gain of coated samples had a tendency to increase after 240 hours of exposure. AlTiN, AlTiN+CrN, AlTiN+NbN coated Ti46.7Al1.9W0.5Si base material showed enhanced the corrosion resistance with reduced mass gain. TiAlN coating employed on substrate material (Ti46.7Al1.9W0.5Si) did not improve the sulphidation/ oxidation corrosion resistance; the mass gain of coated sample (TiAlN coated Ti46.7Al1.9W0.5Si) was similar to that of uncoated material Ti46.7Al1.9W0.5Si and has the same tendency (appreciable increases in the mass gain after 75 hours of exposure) what is presented on **Fig 43**. The multi – layered scale formed on uncoated material Ti46.7Al1.9W0.5Si consisted of: TiO_2 (outer layer) Al_2O_3 beneath this layer and TiS layer (with scattered W particles) developed

as an inner layer. The authors found that the fast outward diffusion of Ti from the substrate led to the formation of $TiAl_2$ and $TiAl_3$ layer between scale and substrate (due to reduce of Ti concentration in the substrate). Schematic diagram of scale development observed is presented in **figure 44**:

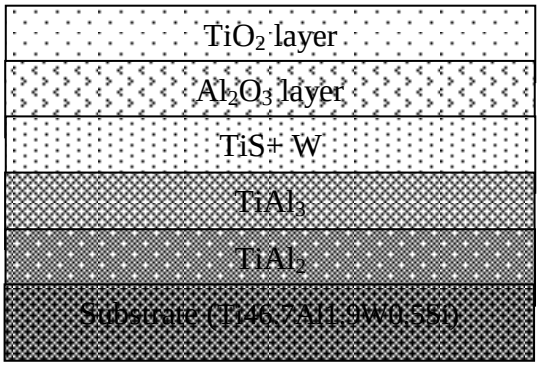

Figure 44 Uncoated Ti46.7Al1.9W0.5Si after oxidation/sulphidation exposure at 1123 K for 240 hours in $H_2/H_2S/H_2O$ atmosphere [77]

The TiAlN coated Ti46.7Al1.9W0.5Si alloy developed a multilayered structure which consisted of: (TiO_2/Al_2O_3/TiS with W scattered/$TiAl_3/TiAl_2$/substrate). This structure was similar to those formed on uncoated alloy Ti46.7Al1.9W0.5Si after sulphidation/oxidation at 1123 K in $H_2/H_2S/H_2O$ in $pO_2 = 10^{-18}$ Pa, $pS_2 = 10^{-1}$ Pa) for 240 hours. **Figure 45** presents an EDS X-Ray mapping performed on TiAlN coated Ti46.7Al1.5W0.9Si alloy. The outer scale consist the TiO_2 oxide, whereas Al_2O_3 developed under the outer oxide (TiO_2), moreover S_2 developed with Ti ions, TiS compound within the outer scale TiO_2. The $TiAl_3$ and $TiAl_2$ developed underneath the TiS layer due to the outward diffusion of titanium from bulk material to outer part of the scale, to form non protective TiO_2. Depletion of Ti caused increase of Al activity and concentration in the alloy (Ti46.7Al1.5W0.9Si). On other hand the $TiAl_3$ is very brittle phase, and such phase may causes spallation or cracks in the material during cooling periods.

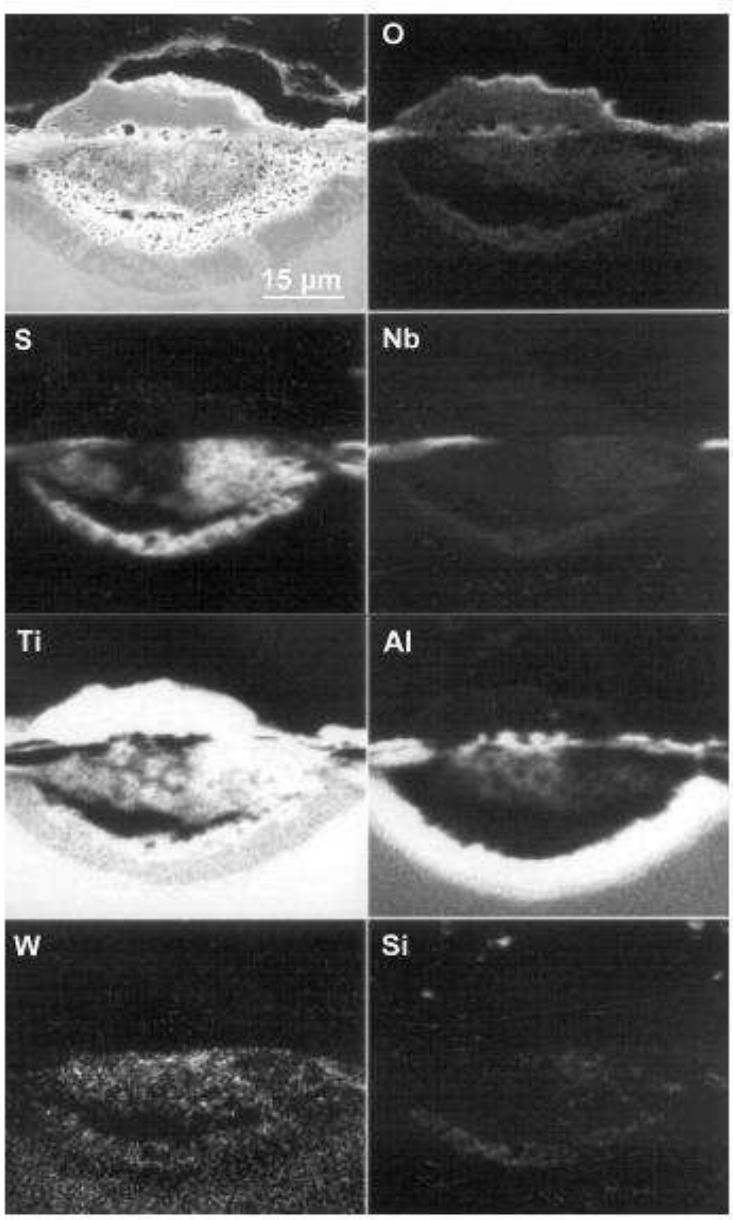

Figure 45 Digimaps performed on sulphidized TiAlN coated Ti46.7Al1.5W0.9Si alloy at 1123 K in $H_2/H_2S/H_2O$ atmosphere [77]

In case of TiAlN coated Ti46.7Al1.9W0.5Si with diffusion barrier of NbN and CrN, the enhanced corrosion resistance was due to the decreased outward diffusion of titanium from the substrate (Ti46.7Al1.9W0.5Si) through the ceramic coatings NbN and CrN.

It was observed [77] that during exposure at 1123 K in $H_2/H_2S/H_2O$ in $pO_2 = 10^{-18}$ Pa, $pS_2 = 10^{-1}$ Pa) for 240 hours the transformation occurred from NbN to Nb_2N and CrN to Cr_2N. The transformation occurred due to the outward diffusion of nitrogen from CrN and NbN ceramic phases during exposure at 1123 K in sulphidation/oxidation atmosphere.

The high temperature (1123 K) exposure to sulphidation/oxidation environment shows that the non protective TiO_2 developed regardless of the presence of NbN and CrN diffusion barrier coatings on the top of the oxide scale.

Du and Datta [78] prepared a model, to explain phase formation during 240 hours of sulphidation test at 1123 K. The model predicts phase formation on the basis of thermodynamic calculations:

Reaction 21 $2Al(l) + 3/2O_2(g) \rightarrow Al_2O_3(s)$

Reaction 22 $Ti(s) + O_2(g) \rightarrow TiO_2(s)$

For these reactions standard free energies (ΔG_T^o J/mole) with temperature (T in Kelvin) has been estimated from equations **XXVIII and XXIX** [79]:

Equation XXVIII $\Delta G^o_{Al2O3,T} = -1676.000 + 320T$

Equation XXIX $\Delta G^o_{TiO2,T} = -910.000 + 173T$

The **equations XXVIII and XXIX** show that preferentially titanium oxide will form first, because ΔG_T^o has a smaller value compare to that of Al_2O_3.

Thus, when Ti46.7Al1.9W0.5Si material is exposed to the sulphidation environment at high temperature (above 923 K) it is more favourable for TiO_2 to form as Ti diffused faster than aluminium.

During the investigation on oxidation/sulphidation environment at high temperature, the high affinity titanium and aluminium for oxygen leads to formation of an outer layer of TiO_2 beneath which Al_2O_3 layer forms [80]. The development of TiO_2 layer leads to the depletion of Ti increasing aluminium activity beneath the TiO_2 layer which promotes the formation of Al_2O_3 layer by the ingress of oxygen species through the TiO_2. The sulphur and oxygen ions diffuse through both oxides (TiO_2 and Al_2O_3) and reach the interface between the scale and the substrate.

The oxygen partial pressure in the scale is lower than that in the external environment. In this case sulphur ingresses inward to reach the scale/substrate interface, high activity of Ti and high affinity Ti to S forms TiS compound. It is very important to note that the thermodynamic conditions do not allow developing tungsten sulphide, silicide, or oxide. When W reacts with oxygen and sulphur, some reactions take place:

Reaction 23 $W + O_2 \rightarrow WO_2$

Reaction 24 $W + S_2 \rightarrow WS_2$

The value of standard free energies (ΔG_T^o, J/mole) with temperature in K, can be calculated from equations below [79]:

Equation XXX $\Delta G_{WO2}^{O} = -260{,}900 + 96T$ **(Oxide)**

Reaction XXXI $\Delta G_{WS2}^{O} = -579.484 + 153T$ **(Sulphide)**

Equation XXXII $$\Delta G_{WO2}^{O} = -RT \ln K = -RT \ln \frac{aWO_2}{aW * pO_2}$$

Reaction XXXIII $$\Delta G_{WS2}^{O} = -RT \ln K = -RT \ln \frac{aWS_2}{aW * pS_2}$$

Assuming unity activities of WS_2 and WO_2, the minimum activities to form WS_2 and WO_2 at 1123 K are 10^{-2} and 7.3 respectively. The formation of WO_2 can be excluded from phase formation because minimum W activity to formation WO_2 is greater than unity. In case of WS_2, the partial pressure of S_2 in the scale formed during exposure is even lower that $6.8x10^{-1}$ Pa, so the minimum activity of W required developing WS_2 will be higher than 10^{-2}. Furthermore, W content was only equivalent to 1,9 at%, development of WSi can only decrease the activity of W further in the material, so WS_2 cannot be formed due to the and low concentration, low activity and of this element in this condition of exposure.

Another studies carried out by Du and Datta [78], was performed on Ti46Al8Nb1B, Ti-44Al8Nb1B, and Ti48Al2Cr2Nb1B (at %) in $H_2/H_2S/H_2O$ ($pS_2 \approx 6.8x10^{-1}$ Pa and $pO_2 \approx 10^{-15}$ Pa) environment at 1123 K. **Figure 46** shows a kinetic data for exposed samples.

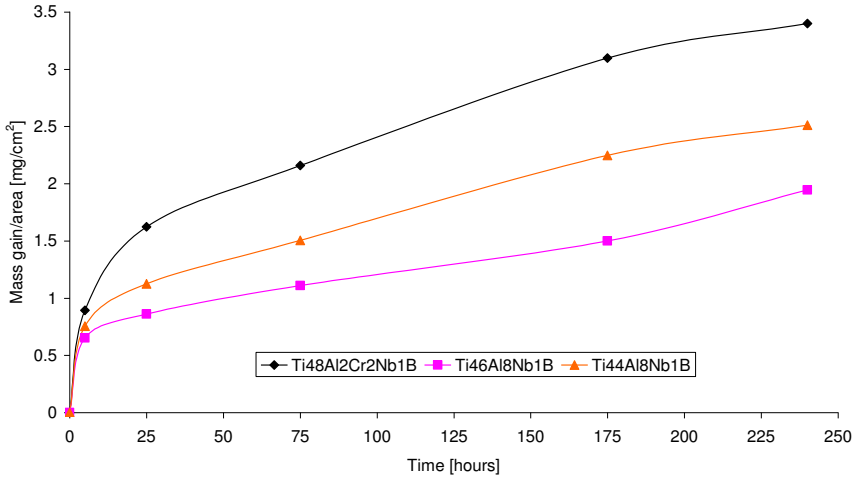

Figure 46 Mass gain of exposed samples to $H_2/H_2S/H_2O$ environments at 1123 K in sulphidation/oxidation test [78]

All exposed samples show quasi – parabolic or parabolic character. The mass gain of the exposed samples (Ti46Al8Nb1B, Ti-44Al8Nb1B, and Ti48Al2Cr2Nb1B) shows that increasing the Nb content enhanced corrosion resistance of the materials (Ti46Al8Nb1B, Ti-44Al8Nb1B). When the concentration of Nb decreased (Ti48Al2Cr2Nb1b) the highest mass gain of the exposed material occurred.

All exposed materials (Ti46Al8Nb1B, Ti-44Al8Nb1B, and Ti48Al2Cr2Nb1B) developed a multi-layered scale.

The TiO_2 developed as an outer layer and beneath this TiO_2, Al_2O_3 formed, and then TiO_2 formed again. TiS and $NbAl_3$ was observed below TiO_2 layer where Al – rich zone appeared. Al – rich zone developed due to the formation of TiS and depletion of Ti from bulk material (outward diffusion of Ti). Decreases in Ti concentration in the materials (Ti46Al8Nb1B, Ti-44Al8Nb1B, and Ti48Al2Cr2Nb1B) leads to lower activity of Ti.

Figure 47 shows a cross – sectional SEM image of Ti48Al2Cr2Nb1B where multilayered scale developed. **Figure 48** presents the EDS concentration profiles from the same sample.

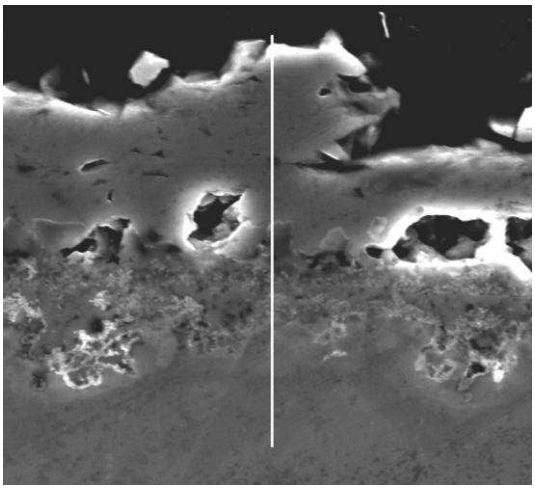

Figure 47 Cross – sectioned SEM of Ti48Al2Cr2Nb1B after 240 hours of sulphidation/oxidation test at 1123 K [78]

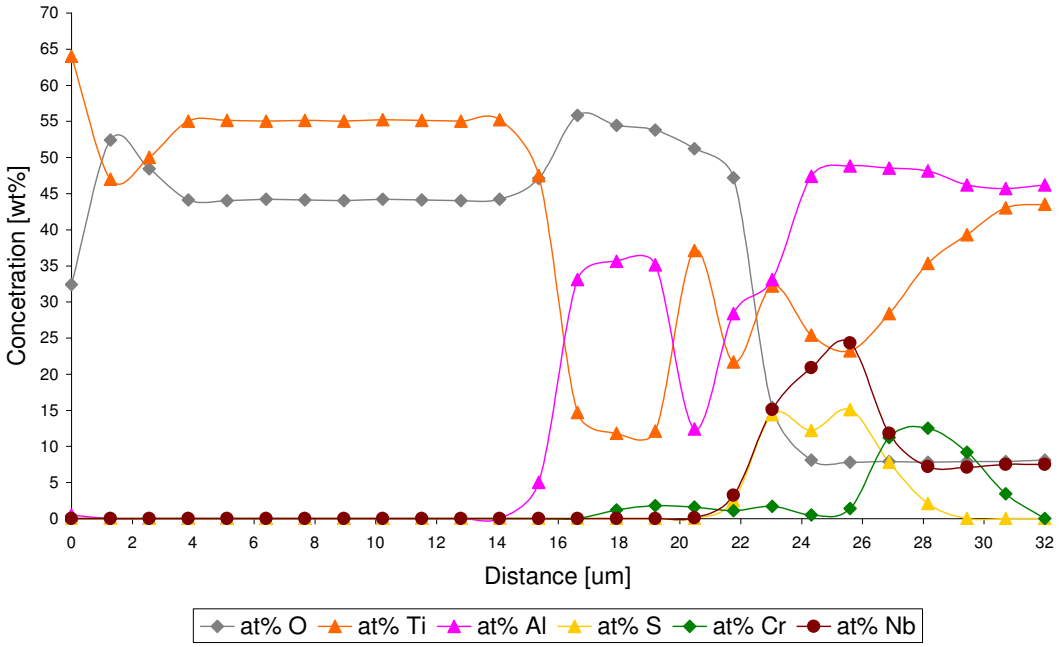

Figure 48 EDS concentration profiles of Ti48Al2Cr2Nb1B after 240 hours of sulphidation/oxidation test at 1123 K [78]

Figure 48 shows the EDS concentration profiles of Ti48Al2Cr2Nb1b alloy after sulphidation at $H_2/H_2S/H_2O$ ($pS_2 \approx 6.8x10^{-1}$ Pa and $pO_2 \approx 10^{-15}$ Pa) environment at 1123 K for 240 hours. The alloy developed a thick (15 μm) outer layer consisting of TiO_2. Underneath this TiO_2 layer, Al_2O_3 formed (5 μm); this Al_2O_3 was partly

mixed with TiO_2 phase which is demonstrated in the EDS concentration profiles **(Fig. 48).**

On the scale/substrate interface the high concentration of sulphur developed TiS, underneath this TiS phase an $NbAl_3$ phase also formed. The multilayer scale contained: $TiO_2/Al_2O_3/TiO_2/TiS/NbAl_3$ respectively.

Furthermore it is important to note that instead of $TiAl_2$ and $TiAl_3$ $NbAl_3$ phase formed due to outward diffusion of Ti from bulk material. Ti diffused outward and developed an outer layer which consisted of TiO_2. The depletion of Ti due to the outward diffusion from bulk material caused higher concentration of Al in the substrate near to the substrate/scale interface where development of $NbAl_3$ occurred.

This situation means that affinity of titanium to oxygen is much greater than affinity of titanium to aluminium, or activity of titanium decreases below the required level which allows the formation of $TiAl_2$ or $TiAl_3$.

Chromium was not detected in the outer scale due to the low diffusion coefficient compare to Ti ($D_{Cr} = 8.21E^{-13}$ cm^2/s, $D_{Ti} = 3.37E^{-10}$ cm^2/s), chromium only developed rich Cr zone underneath of $NbAl_3$ phase.

In case of Ti44Al8Nb1B alloy exposed to the same atmosphere ($pO_2 \approx 1.2x10^{-15}$ Pa, $pS_2 \approx 6.8x10^{-1}$ Pa) at 1123 K, multilayer scale was also formed (SEM image **(Fig. 49)**).

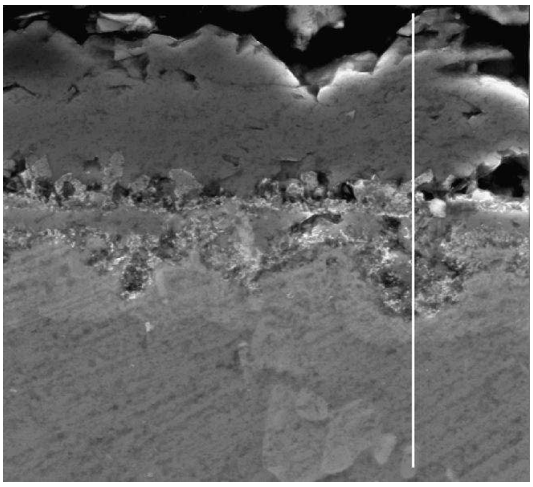

Figure 49 Cross – sectioned SEM image of Ti44Al8Nb1B after 240 hours of sulphidation/oxidation test at 1123 K [78]

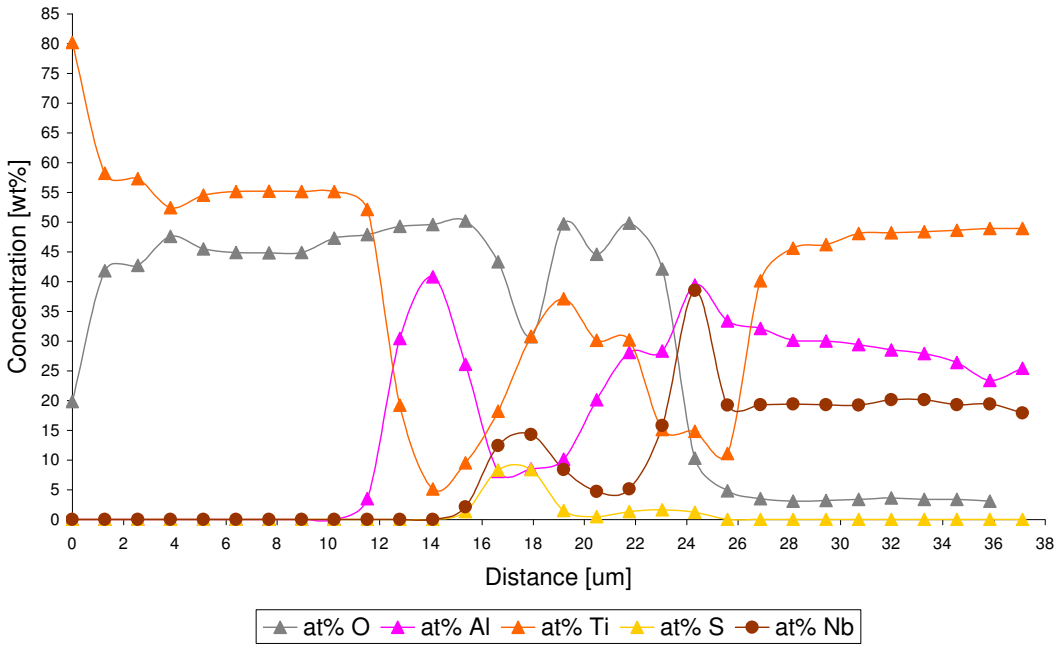

Figure 50 EDS concentration profiles of Ti44Al8Nb1B after 240 hours of sulphidation/oxidation test at 1123 K [78]

Figure 50 shows and EDS concentration profiles where a thick TiO_2 formed as a top layer (10 μm), underneath this thick TiO_2 layer, a mixed layer of Al_2O_3 and TiO_2 formed. The scale/substrate interface was occupied by $NbAl_3$ thin layer (2 μm).

The activity of sulphur in this alloy is smaller than in Ti48Al2Cr2Nb1b one, EDS investigation presented in **figure 50** does not show TiS layer.

Authors of this study [78] proposed mechanism of degradation of exposed alloys: Ti46AlNb1B, Ti-44Al8Nb1B, and Ti48Al2Cr2Nb1B to $H_2/H_2S/H_2O$ ($pS_2 \approx 6.8x10^{-1}$ Pa and $pO_2 \approx 10^{-15}$ Pa) environment at 1123 K:

Reaction 25 $$2\,Al(l) + \frac{3}{2}O_2(g) \rightarrow Al_2O_3(s)$$

Reaction 26 $$Ti(s) + O_2(g) \rightarrow TiO_2(s)$$

Reaction 27 $$2\,Nb(s) + \frac{5}{2}O_2(g) \rightarrow Nb_2O_5(s)$$

Standard free energies of formation (ΔG_T^o , [J/mole]) with temperature in K, can be calculated from equations (**equations** XX**XIV – XXXVI**) [79]:

Equation XXXIV $$\Delta G^o_{Al2O3,T} = -1676.000 + 320T$$

Equation XXXV $\Delta G^{o}_{TiO2,T} = -910.000 + 173T$

Equation XXXVI $\Delta G^{o}_{Nb2O5,T} = -1920,00 - 12.4T\log T + 800T$

Equilibrium constants also in case of these reactions were calculated:

Equation XXXVII $\Delta G^{O}_{Al2O3,T} = -1316.64\,[kJ/mole]$

Equation XXXVIII $\Delta G^{O}_{TiO2,T} = -715.721\,[kJ/mole]$

Equation XXXIX $\Delta G^{O}_{Nb2O5,T} = -1434.039\,[kJ/mole]$

This mechanism is not very clear; the authors suggested the formation of Nb_2O_5, in the scale. In fact the EDS concentration profiles (**Fig. 48, 50**) performed on sulphidized/oxidised samples (Ti48Al2Cr2Nb1b, Ti-44Al8Nb1B respectively) does not show the Nb_2O_5. Furthermore, the formation of NbS or NbS_2 is more likely to form that of Nb_2O_5; the activity of oxygen within the scale is smaller than sulphur (pS_2 >> pO_2 [Pa]) as oxygen was consumed to produce an outer layers (TiO_2 and Al_2O_3).

It is well known from thermodynamic point of view that the formation of sulphides is faster than oxides (lower standard free energy of formation for sulphides than oxides). **Table 18** presents values of free energy of the formation.

Sulphides		Oxides	
Compound	ΔG^{o} (kJ / mol)	Compound	ΔG^{o} (kJ / mol)
Al_2S_3	-219	Al_2O_3	-429
Cr_2S_3	-135	Cr_2O_3	-261

Table 18 Standard free energies of formation calculated for sulphides and oxides at 1273 K

Du and Datta [78] also show a schematic diagram on **Figure 51** for degradation of Ti46Al8Nb1B, Ti-44Al8Nb1B, and Ti48Al2Cr2Nb1B (at %) in $H_2/H_2S/H_2O$ ($pS_2 \approx 6.8x10^{-1}$ Pa and $pO_2 \approx 10^{-15}$ Pa) environment at 1123 K, diagram does not present relevant information for the formation of Nb_2O_5.

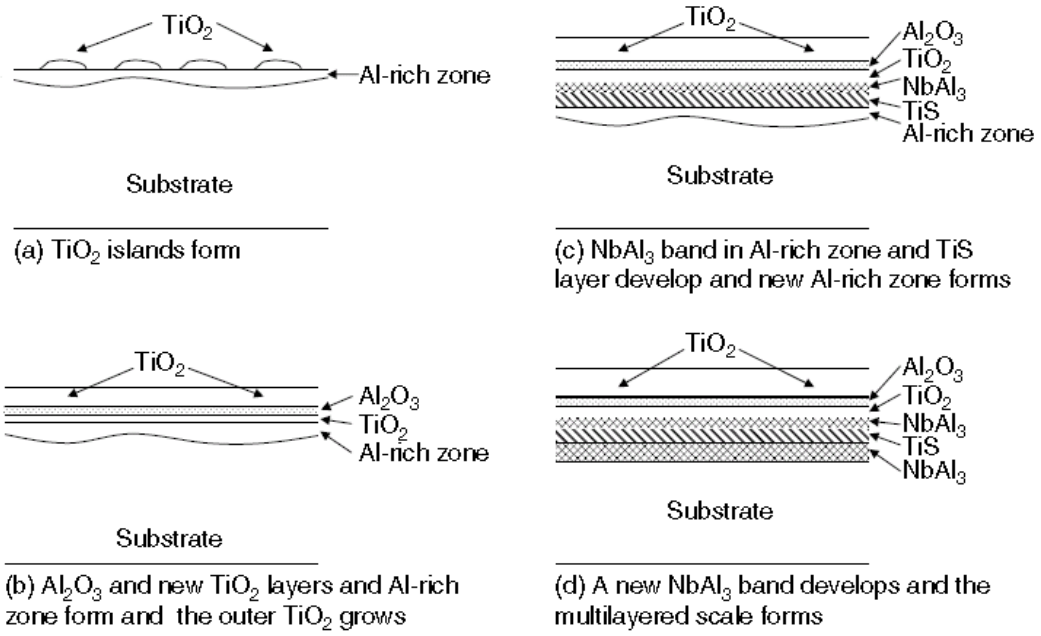

Figure 51 Degradation mechanism for TiAl based intermetallics in $H_2/H_2S/H_2O$ environment at 1123 K [78]

It can be suggested that the small addition of Cr (Cr has a smaller oxidation grade (3^+) compare to Ti (4^+)) may change the electron structure in the atomic lattice of TiO_2. Alloy (Ti48Al2Cr2Nb1b) with small addition of Cr^{3+}, produce the larger amount of defects in the atomic lattice of TiO_2; scale is growing due to outward diffusion which increases amount of cations vacancies in the atomic lattice of TiO_2. Addition of Nb with higher than 4^+ oxidation grade (as in Ti), reduce the amount of defects in TiO_2 structure. This process leads to decrease in mass gain of exposed samples (Ti46Al8Nb1B, Ti-44Al8Nb1B). TiO_2 is semiconductor n-type and contains the interstitial ions based on Ti^{3+} and Ti^{4+} existing together with doubly ionized oxygen vacancies [81]. Karake et al. indicated that the doubly ionised oxygen vacancies are responsible for kinetic rate of growth TiO_2 scale over Ti, thus, any dopant element in the titanium oxide scale (TiO_2) which is able to minimize the concentration of these vacancies will reduce the oxidation rate [82]. The Nb atoms substitute the Ti site in the TiO_2 lattice due to the higher number of oxidation state (5^+) and can reduce the number of interstitial oxygen ion vacancies in the oxide [83]. Chromium with 3^+ oxygen state increases an amount of oxygen vacancies due to the lower than 4^+ oxygen state of Ti in TiO_2 and increases mass gain of the material

(Ti48Al2Cr2Nb1b). The addition of boron to TiAl alloys is to refine the grain size, thus improving the processibility of the alloys. The addition of Nb is well known to improve high temperature oxidation [84], strength and creep resistance. Thus the degradation resistance of exposed materials decreased in order from: Ti46Al8Nb1B, Ti-44Al8Nb1B, and Ti48Al2Cr2Nb1B. Du and Datta [85] investigated duplex (D – alloy) and laminar (L – alloy) TiAl alloy (Ti46.6Al1.4Mn2Mo) at 1023 and 1173 K respectively for 168 hours at low potential of oxygen ($pO_2 \sim 10^{-15}$ Pa) and high potential of sulphur ($pS_2 \sim 10^{-1}$ Pa).It was shown [85] that the degradation of duplex and laminar alloy is more severe in lower temperature (1023 K) than at higher (1173 K). The mass gain of exposed samples obtained is presented on **Figures 52 and 53**.

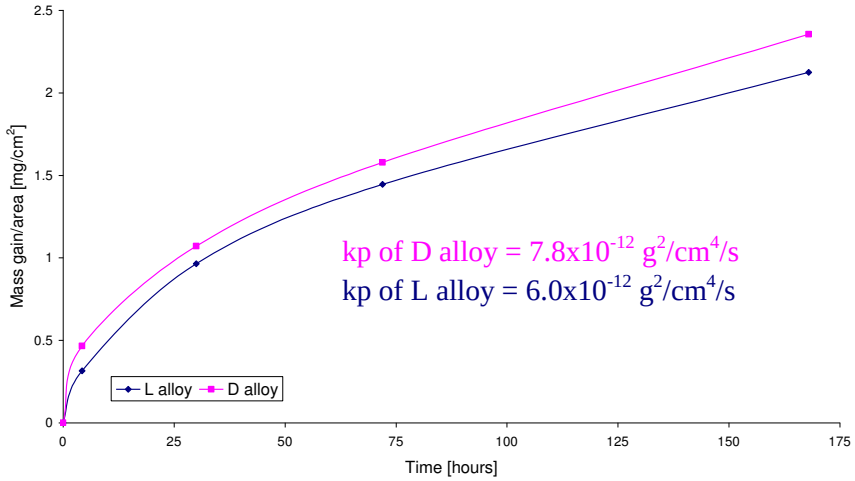

Figure 52 Mass gain of exposed samples (D – alloy and L - alloy) with kp values (Ti46.6Al1.4Mn2Mo) to sulphidized/oxidised atmosphere at 1023 K [85]

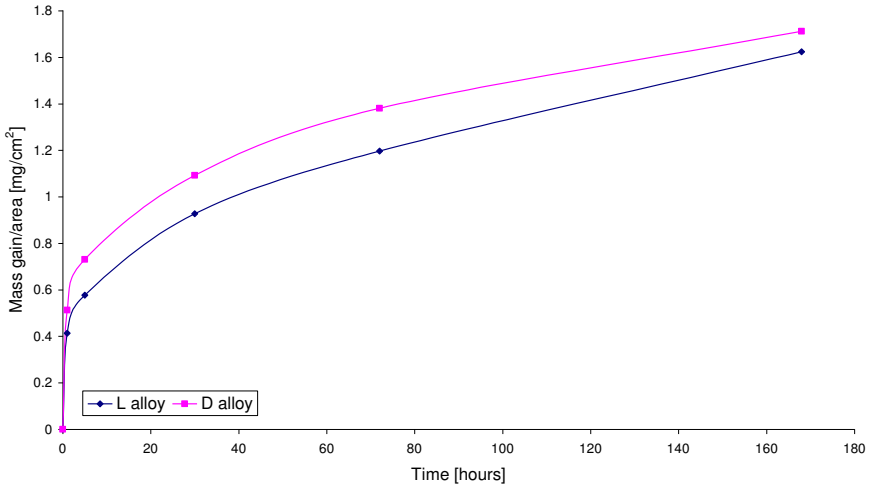

Figure 53 Mass gain of exposed samples (D and L) (Ti46.6Al1.4Mn2Mo) to sulphidized/oxidised atmosphere at 1173 K [85]

Figure 52 presents a kinetic data of exposed samples; duplex (D – alloy) and laminar (L – alloy) TiAl alloy (Ti46.6Al1.4Mn2Mo) at 1023 and 1173 K respectively) for 168 hours at low potential of oxygen ($pO_2 \sim 10^{-15}$ Pa) and high potential of sulphur ($pS_2 \sim 10^{-1}$ Pa) samples investigated at 1023 K showed a parabolic rate at that temperature. **Figure 53** shows mass gain of exposed samples at 1173 K in the same environmental, the samples (D – alloy and L alloy) showed a cubic rate of scale growth.

The outer scale formed at both temperatures (1023 and 1173 K respectively) was covered by TiO_2 crystals and underneath of this TiO_2 crystals the Al_2O_3 layer developed. Du and Datta [85] also suggested that beneath the Al_2O_3 layer, Al_2S_3 and MnS formation occurred, **figure 54** shows a EDS X-Ray digimaps of D – alloy and L – alloy exposed to $H_2/H_2S/H_2O$ at 900^oC (1173 K) after 168 hours.

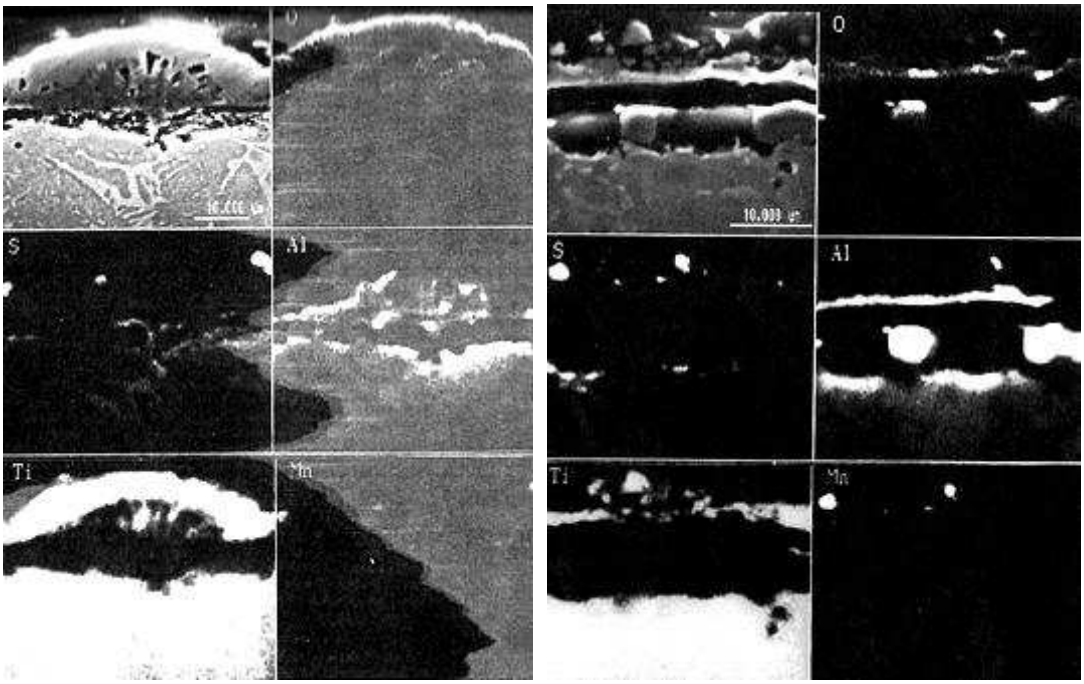

Figure 54 Digimaps performed on L - alloy (left) and D - alloy (right) exposed to $H_2/H_2S/H_2O$ at 1173 K after 168 hours [85]

In this study Du and Datta [85] observed and suggested general statement that the oxygen vacancies and interstitial Ti ions are important defects in TiO_2 phase. The interstitial Ti ions are predominating at low oxygen partial pressure and at high temperature. Oxygen vacancies are important at high partial pressure and at low temperature.

Furthermore at low pO_2 the high concentration of Ti ions is present in the TiO_2 oxide. As mentioned previously the high partial pressure of oxygen would result in decrease the interstitial amount of Ti ions. It is beneficial that reduced amount of interstitial Ti ions improved the corrosion resistance of the TiAl alloy (reducing transport of Ti ions through the TiO_2 oxide scale).

In this study the pO_2 at 1173 K was four order of magnitude higher than at 1023 K but Du and Datta [85] indicated, that the increase in temperature may not significantly change the diffusion nature of Ti and O_2 in these specific alloys (D – alloy and L – alloy of Ti46.6Al1.4Mn2Mo.

This statement is based on observation carried out also by Du and Datta [86] that after exposure of Ti46.6Al1.4Mn2Nb alloy to the air atmosphere at 973 and 1173 K respectively, the mass gain was only slightly higher at 1173 K than 973 K.

The results proposed by Du and Datta [85] conclude, that the increase of oxygen partial pressure at 1173 K will increase the oxygen vacancies in TiO_2 oxide and thereby enhanced the inward diffusion of oxygen and promote the formation of more protective Al_2O_3 oxide scale on Ti46.6Al1.4Mn2Mo alloy in low potential of oxygen ($pO_2 \sim 10^{-15}$ Pa) and high potential of sulphur ($pS_2 \sim 10^{-1}$ Pa). The suggestion that the higher partial pressure can promote the formation of Al_2O_3 is correct but the authors did not to mention about sulphide formation. Moreover the high pressure of oxygen indeed increases the oxygen vacancies at 1173 K and more oxygen vacancies in the alloy (duplex or laminar) is formed. Thus, the scale should be more porous, less resistant and more aggressive agents (O^{2-} ions, S^{2-}) can diffuse in to the scale. Due to the higher partial pressure ($pS_2 \sim 10^{-1}$ Pa) than ($pO_2 = 10^{-18}$ Pa) and slightly higher $\Delta G^{o}(kJ/mol)$ for the formation of MnS = - 190 kJ/mol **(Table 14)**, and MoS = - 209 kJ/mol (according to the Ellingham – Richardson Diagram) than of TiO_2 = - 715 kJ/mol also it is necessary take into consideration, the formation of MnS phase.

Gill [87] investigated the high temperature corrosion behaviour of ternary alloys Ti50Al2Ag and Ti48Al2Cr and quaternary alloys Ti50Al2Ag1Mo, Ti50Al2Ag1Nb, and Ti50Al2Ag1Mn. The kinetics of alloys was studied in the air and in SO_2 atmosphere at 1073 K for 100 and 10 hours respectively. Gil postulated that in oxidising environment, the mass gain of Ti50Al2Ag was smaller than the mass gain obtained for Ti48Al2Cr **(Fig. 55).** The smaller mass gain of Ti50Al2Ag alloy at 1073 K in air was due to the stabilizing of Al_2O_3 oxide by Ag.

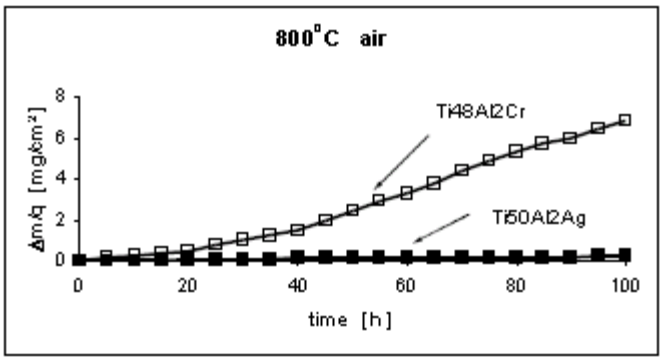

Figure 55 Oxidation studies performed on Ti50Al2Ag and Ti48Al2Cr at 800°C (1073 K) [87]

The investigation in SO_2 atmosphere at 1073 K for 10 hours carried out by Gil [87] shows that Ti50Al2Ag was consumed by catastrophic corrosion, but Ti48Al2Cr alloy showed a good corrosion resistance. The good corrosion resistance of Ti48Al2Cr alloy is due to the formation of stable and protective Cr_3S_2 chromium sulphide, instead of the formation of liquid eutectic with melting point equivalent to 840 K.

The kinetic data for sulphidation tests in SO_2 atmosphere for 10 hours is presented in **figure 56**.

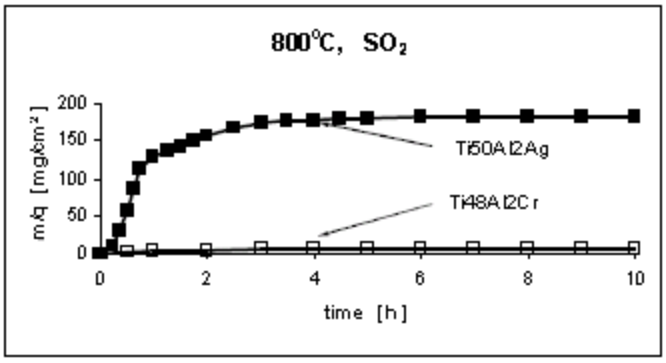

Figure 56 Sulphidation/oxidation studies performed on Ti50Al2Ag and Ti48Al2Cr at 1073 K for 10 hours test

It can be derived from the Al-Ag phase diagram, that liquid eutectic formed at 840 K. In the presence case due to the liquid eutectic formation catastrophic corrosion took place in Ti50Al2Ag alloy (faster reaction in the liquid/oxide scale interface). The SEM/EDS investigations performed on exposed Ti50Al2Ag sample after 10 hours of exposure in SO_2 environment at 1073 K reveals that the outer layer

formed by TiO_2+Al_2O_3 oxides and Al – Ag phase developed with inclusions of $TiAl_3$ underneath **(Fig. 57).**

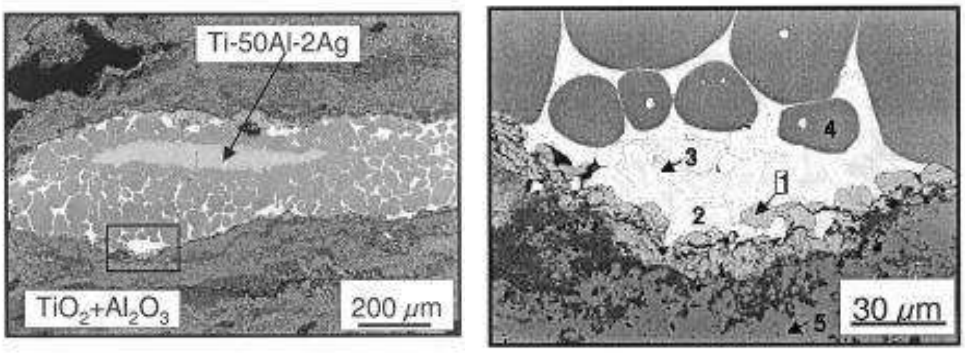

Figure 57 SEM investigation performed on exposed Ti50Al2Ag sample in SO_2 environment after 10 hours at 1073 K [87]

Phase development is confirmed by the EDS analysis and showed in **table 19**.

	1	2	3	4	5
Ti	50.9	-	-	24.8	31.9
Al	-	81.8	48.3	75.2	-
Ag	-	18.2	51.7	-	-
S	49.1	-	-	-	-
O	-	-	-	-	68.1

Table 19 EDS investigation in at% performed on exposed Ti50Al2Ag sample in SO_2 environment after 10 hours at 800°C 1073 K [87]

The EDS X-Ray mapping performed on Ti50Al2Ag sample (**Fig.58)** shows also that underneath of Al-Ag liquid phase, the TiS also was formed.

The TiS phase was formed due to the high activity of S^{2-} ions in the inner part of formed scale, the ingress of S^{2-} shows that the outer scale was porous and sulphur ions were easily diffused inwards.

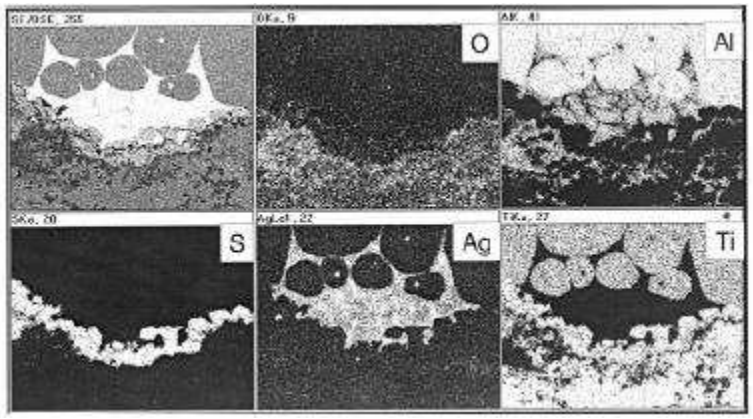

Figure 58 Cross – section mapping performed of Ti50Al2Ag sample after exposed to SO_2 environment at 1073 K for 10 hours [87]

The author of this study [87] did not clarify the positive effect of Cr in sulphidized atmosphere. It can be suggested that the positive effect of Cr [88], is related to the melting temperature of Al-Cr system; Al-Cr phase melts at 1523 K, Al-Ag phase melts at 840 K, additionally the stabilization of Al_2O_3 by Cr plays an important role in the corrosion resistance of Ti48Al2Cr alloy in SO_2 atmosphere at 1073 K.

Takeshi [89] investigated Ti50Al and TiAlX alloys with 2 at% of different additions (X = V, Fe, Co, Cu, Nb, Mo, Ag, and W) at 1173 K at 1,3 Pa sulphur pressure in H_2S/H_2 atmosphere for 86.4 ks. Samples with 2 at% addition of Ag and Cu sulphidized faster than pure TiAl alloy.

The faster sulphidation rate observed for these samples is due to the larger amount of lattice defects in $Cu_{2-y}S$ in agreement with previous study carried out by Kofstad [62].

Furthermore, the author suggested also that the large mass gain of TiAl2Cu is due to the formation of liquid phase of Al – Cu, according to the Al – Cu system at 821 K [90].

In the case of the alloy with Ag addition, the result is in good agreement with work performed by Gil [87]. The addition of Ag in TiAl alloy in sulphur environment, produce a liquid eutectic at 840 K. The thickness of the scale

developed on the exposed alloys (TiAlX alloys with 2 at %) decreased in order of addition of V, Co, Fe, W, Mo, and Nb.

Exposed samples (TiAlX (X = V, Fe, Co, Cu, Nb, Mo, Ag, and W) in 1, 3 Pa sulphur pressure in H_2S/H_2 atmosphere for 86.4 ks at 1173 K developed at least two phases, white and gray, the white phase was Ti – sulphide (TiS and Ti_3S_4) the grey Al – sulphide (Al_2S_3). Sulphidized alloys were divided into two groups. Group A contains: TiAlX where X = V, Fe, Co, and Cu), group B of TiAl2X where X = Nb, Mo, and W alloys.

Within the first group (A) the external scales were divided into four layers, these layers are indicated as: 1) Ti sulphides with alloying elements as inclusions 2) an layer of Ti sulphide and inclusions of Al_2S_3, 3) inner layer rich in Ti – sulphide in duplex phases, 4) innermost (mainly Ti – sulphide), 5) denotes based alloy (Ti50Al)

Within second group (B) the external scale consisted 3 layers: 1) Mainly Ti – sulphide, 2) layer of Ti sulphide and inclusions of Al_2S_3, 3) inner layer rich in Ti – sulphide in duplex phases, 4) innermost layer in group B was missing. (instead of this missing layer, 4 denotes based alloy (Ti50Al).

Figure 59 shows the cross sectional SEM images of all sulphidized samples at 1173 K and 1.3 Pa sulphur pressure for 86.4 ks

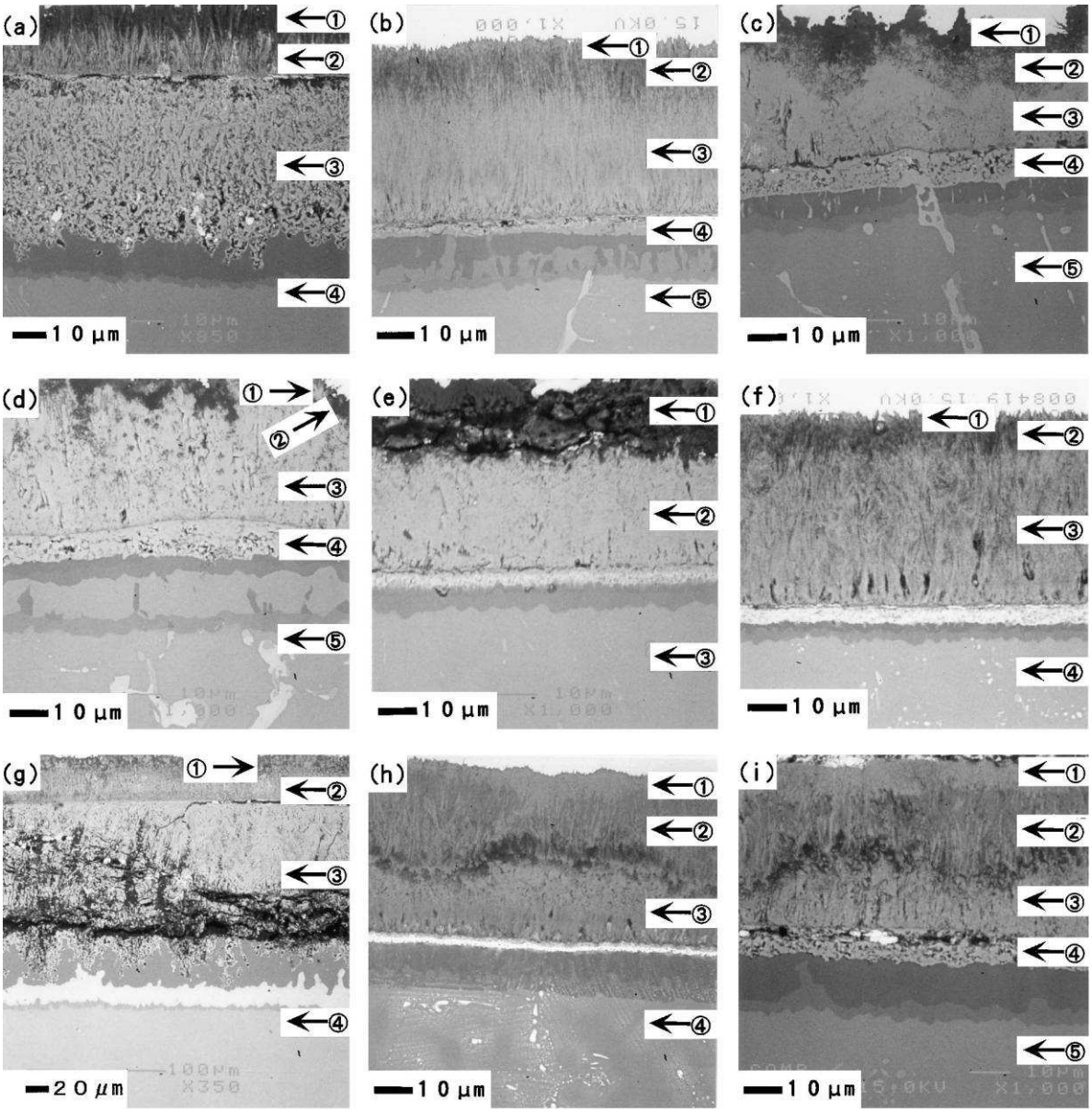

Figure 59 Cross-sectional structures of $TiAl_2$ at% X alloys sulphidized at 1173 K for 86.4 ks at 1.3 Pa sulphur pressure in an H_2S/H_2 gas mixture. Alloying elements are (a) V; (b) Fe; (c) Co; (d) Cu; (e) Nb; (f) Mo; (g) Ag; (h) W and (i) TiAl binary alloy [89]

Concentration profiles of all exposed samples are shown on **Figure 60**, and **61**.

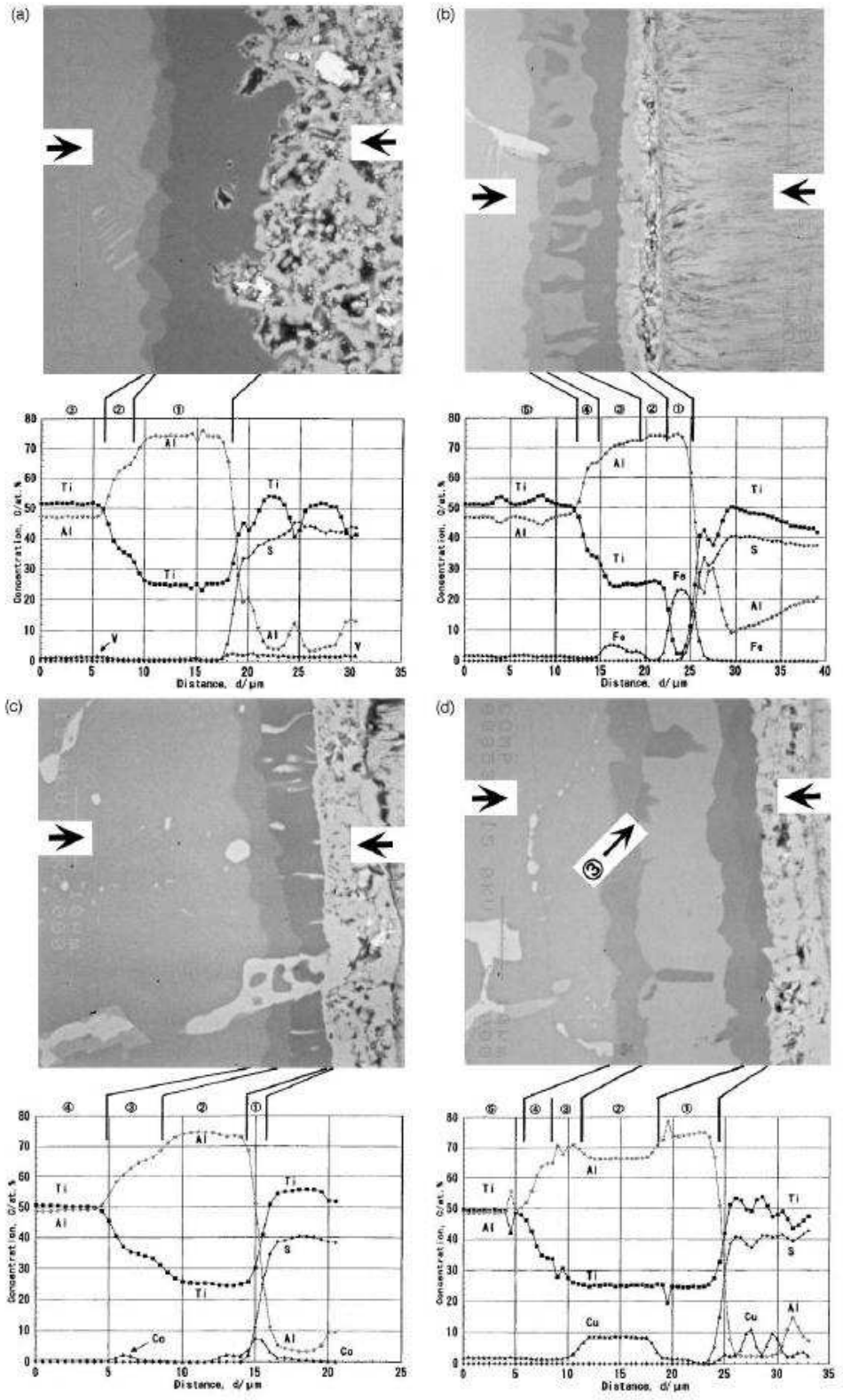

Figure 60 Cross-sectional microstructure of the alloy surface layer and concentration profiles of Ti, Al, S and alloying elements for TiAl2X alloys. (a) TiAl2V; (b) TiAl2Fe; (c) TiAl2Co; (d) TiAl2Cu [89]

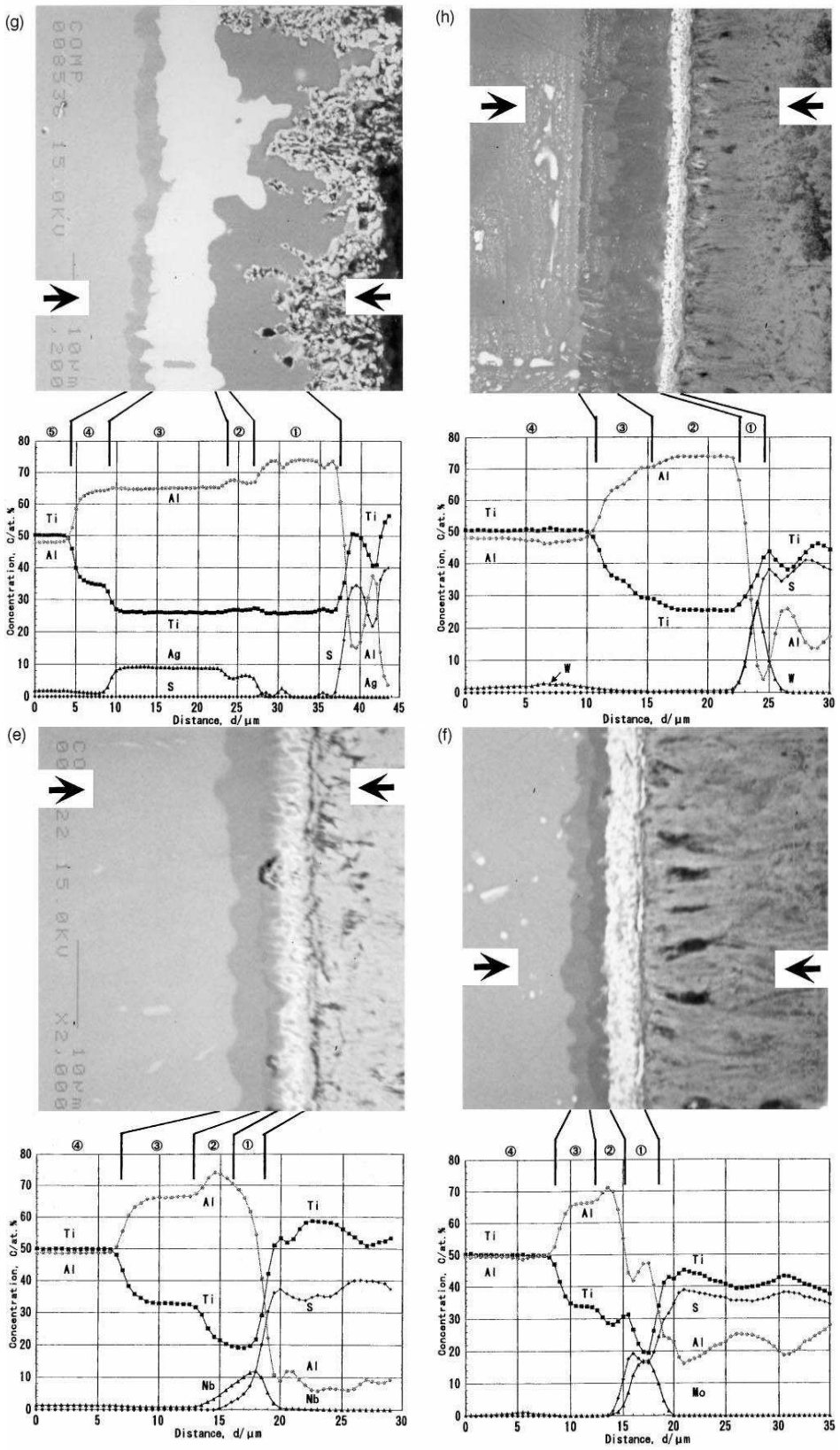

Figure 61 Cross-sectional microstructure of the alloy surface layer and concentration profiles of Ti, Al, S and alloying elements for TiAl2X alloys: TiAl2Nb; (f) TiAl2Mo; (g) TiAl±2Ag; (h) TiAl2W [89]

The kinetic data obtained for alloys: TiAl2Fe, TiAl2V, TiAl2Mo, TiAl2Co, and TiAl2Nb) were almost the same, while the thickness of the scale decreased in order: V>Co>Fe>Mo>W>Nb. All samples formed; outer layer consists: Ti_3S_4 and TiS layer, beneath this TiS layer, Al_2S_3 layer developed. All alloying element were detected (in little amounts) on the surface (TiS) of the material (V, Fe, Co and Cu).

The author [89] concluded that all samples can be divided into 4 groups:

1. with V and Co: alloy/$TiAl_2$/$TiAl_3$/sulphides (V and Co included)
2. with Nb, Mo and W: alloy/$TiAl_2$/$TiAl_3$ (Nb, Mo or W)-Al alloys/sulphides
3. with Ag and Cu: alloy/$TiAl_2$/Ti(Al, Ag or Cu)$_3$ with $L1_2$ structure/$TiAl_3$/sulphides
4. with Fe: alloy/$TiAl_2$/Ti(Al, Fe)$_3$ with an $L1_2$ structure/$TiAl_3$/$FeAl_3$/sulphides

It needs to be considered that author of this work [89] does not mention about formation of oxides. It is well known that by the high affinity titanium to oxygen TiO_2 is likely to form (or other Ti oxides).

Du and Datta at el [91] studied the sulphidation and oxidation behaviour of pure Ti and Ti6Al4V alloy in $H_2/H_2O/H_2S$ ($pO_2 = 10^{-18}$ Pa, $pS_2 = 10^{-1}$ Pa) H_2/H_2O ($pO_2 = 10^{-18}$ Pa) and air environments for up to 240 hours.

The kinetic results (not shown here) of sulphidation/oxidation ($H_2/H_2O/H_2S$ ($pO_2 = 10^{-18}$ Pa, $pS_2 = 10^{-1}$ Pa)), oxidation in H_2/H_2O with low oxygen partial pressure ($pO_2 = 10^{-18}$ Pa) and in atmospheric air of pure Ti and Ti6Al4V alloy indicate linear kinetic law for pure Ti and quassi - parabolic kinetic law for Ti6Al4V alloy at the sulphidation oxidation regime ($H_2/H_2O/H_2S$ ($pO_2 = 10^{-18}$ Pa, $pS_2 = 10^{-1}$ Pa) at 1023 K. Parabolic rate law was observed for both materials (pure Ti and Ti6Al4V alloy) in H_2/H_2O atmosphere at 1023 K. Oxidation in air atmosphere shows that the oxidation resistance of Ti6Al4V was superior in low O_2 content ($pO_2 = 10^{-18}$ Pa), whilst in the air oxidation the mass gain of Ti6Al4V was higher than for a pure material (pure Ti). It is important to note that addition of Al and V has a more detrimental effect on corrosion resistance of Ti6Al4V at 1023 K. The corrosion products developed on the surfaces of the exposed materials (pure Ti and Ti6Al4V) during sulphidation/oxidation ($H_2/H_2O/H_2S$), low oxygen atmosphere (H_2/H_2O) and air oxidation experiments after 72 hours at 1023 K are shown in **figure 62, a, b, c, d, e** and **f**. However pictures **62 b, d f** are higher magnifications of pictures **62 a, c, e**

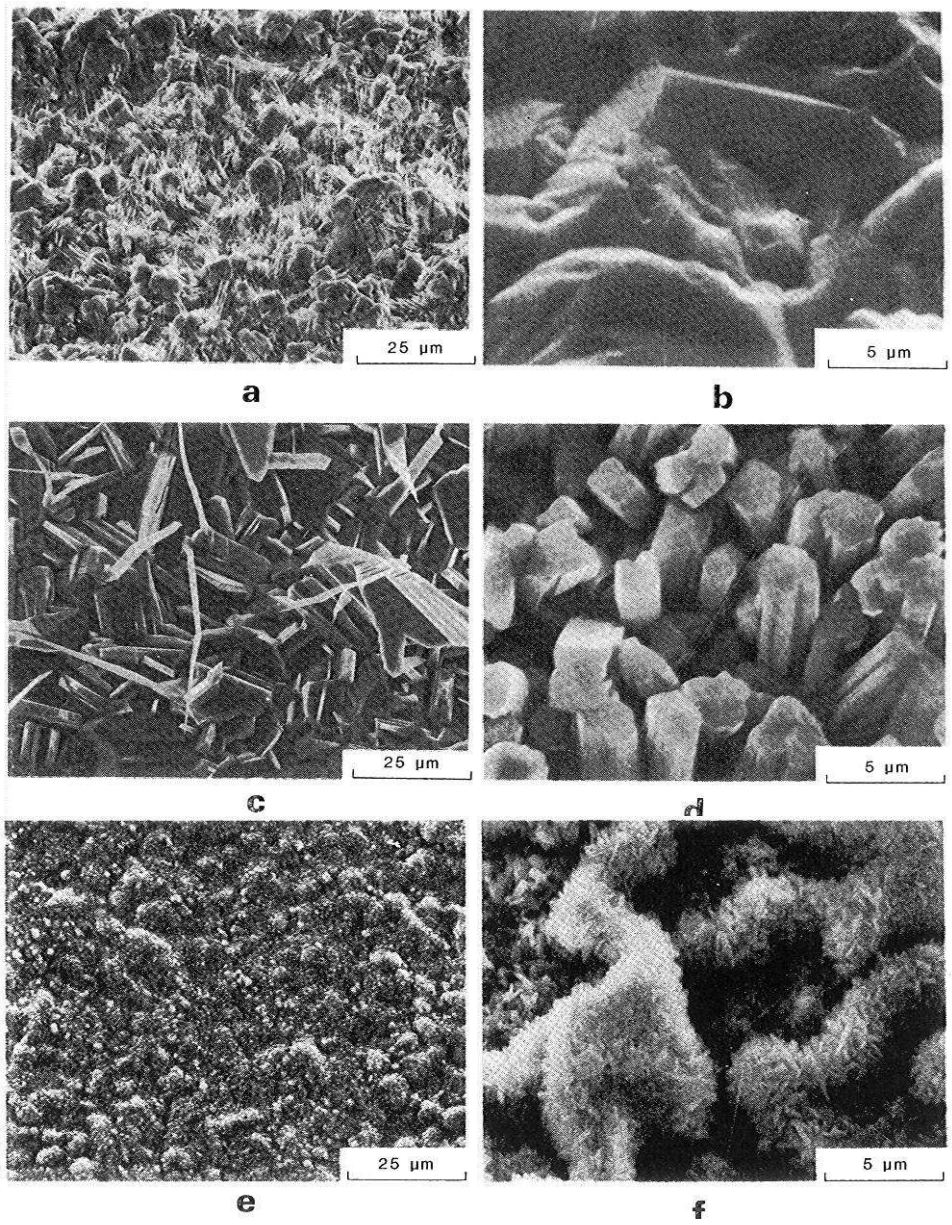

Figure 62 Scanning electron micrographs showing surface morphology of Ti and Ti6Al4V after exposure for 72 hours at 1023 K; **a)** Ti and **b)** Ti6Al4V in $H_2/H_2O/H_2S$; **c)** Ti and **d)** Ti6Al4V in H_2/H_2O; **e)** Ti and **f)** Ti6Al4V in air [91]

Figure 62a and **62b** show corrosion products after 72 hours of sulphidation – oxidation experiment (sulphidation/oxidation ($H_2/H_2O/H_2S$), low oxygen atmosphere (H_2/H_2O) and air oxidation experiment for 72 hours at 1023 K of pure Ti and Ti6Al4V alloy respectively. The dense and compact scale of TiO_2 developed on pure Ti material, in the case of Ti6Al4V alloy, a rough scale formed consisting of TiO_2 and Al_2O_3 phases.

Figures 62c and **62d** present surface morphology of pure Ti and Ti6Al4V alloy after oxidation at low oxygen partial pressure ($pO_2 = 10^{-18}$ Pa) in H_2/H_2O

mixture at 1023 K. Pure Ti developed after 72 hours at 1023 K a TiO_2 scale (**Fig. 62c**), for Ti6Al4V TiO_2 and Al_2O_3 scale was observed only at the initial stage of experiment and after 72 hours of exposure in H_2/H_2O mixture with $pO_2 = 10^{-18}$ Pa, all Al_2O_3 phase was buried by TiO_2 (**Fig, 62d**).

Air oxidation for 72 hours at 1023 K of pure Ti and Ti6Al4V alloy showed that the TiO_2 developed for pure Ti (**Fig. 62e**) and TiO_2 with Al_2O_3 phase formed on the surface of Ti6Al4V alloy (**Fig. 62f**). **Figure 63** present scale morphology on pure Ti after 72 hours at sulphidation oxidation environment ($H_2/H_2O/H_2S$) at 1073 K:

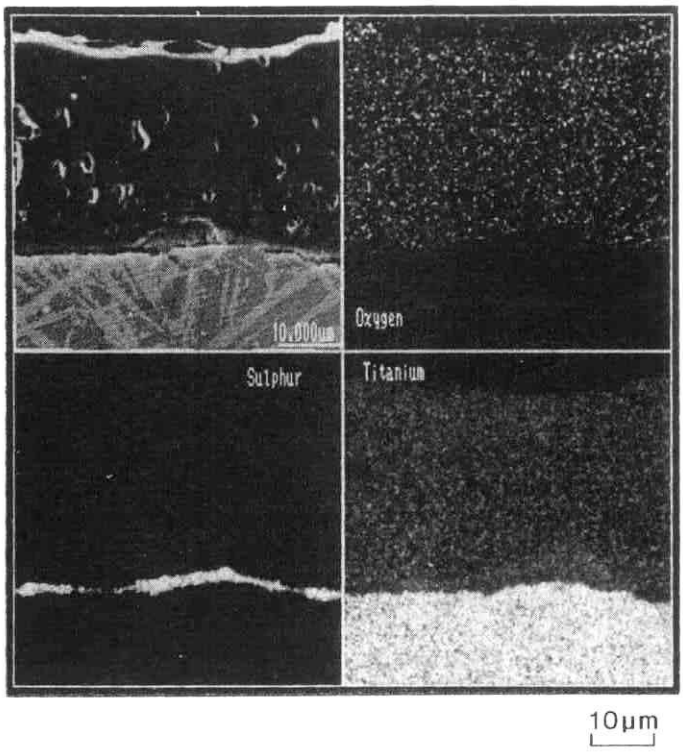

Figure 63 Digimaps of scale morphology on pure Ti after 72 hours at sulphidation oxidation environment ($H_2/H_2O/H_2S$) at 1023 K [91]

Pure Ti exposed to the $H_2/H_2O/H_2S$ environment at 1073 K for 72 hours developed a thick scale of TiO_2 with a thin TiS_2 film at the scale/substrate interface.

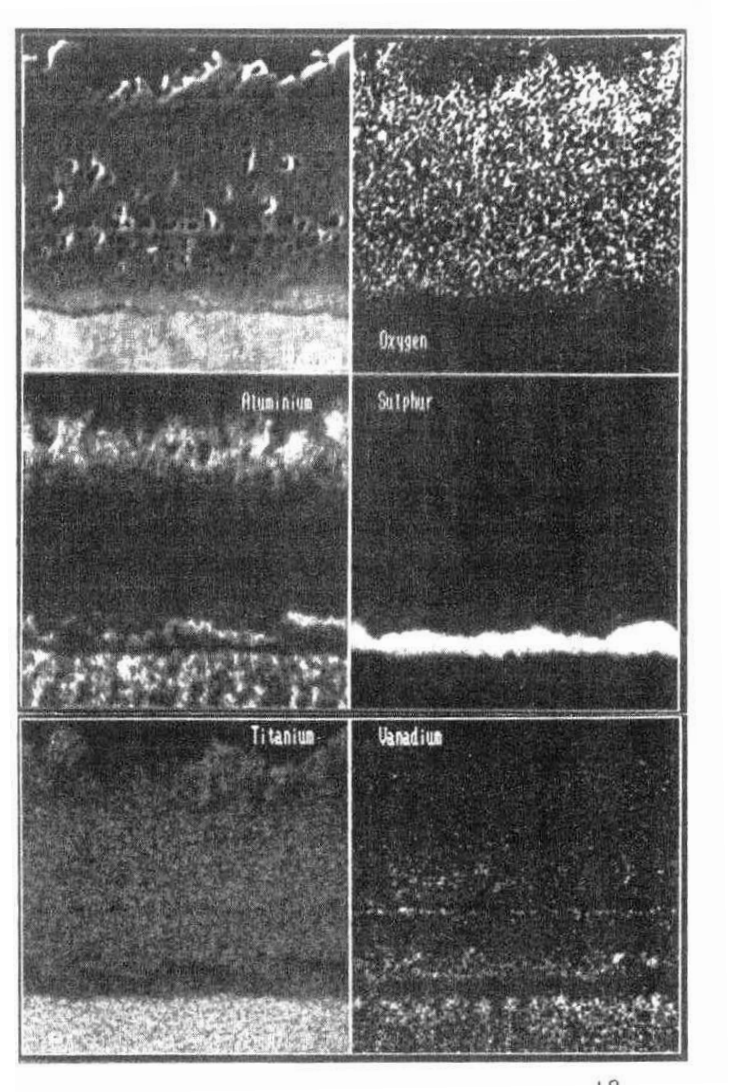

Figure 64 Digimaps of scale morphology of Ti6Al4V alloy after 72 hours at sulphidation oxidation environment ($H_2/H_2O/H_2S$) at 1023 K [91]

In the case of Ti6A4V alloy **(Fig. 64)** exposed to ($H_2/H_2O/H_2S$ ($pO_2 = 10^{-18}$ Pa, $pS_2 = 10^{-1}$ Pa) at 1023 K for 72 hours, a double TiO_2 layer formed together with Al_2S_3, TiS_2, and vanadium sulphide after sulphidation/oxidation experiment at 1023 K. Vanadium sulphide developed in the inner layer of TiO_2.

Following the oxidation in low oxygen partial pressure ($pO_2 = 10^{-18}$ Pa) atmosphere at 1073 K for 72 hours, also a doubled layer of TiO_2 scale formed on both materials; pure Ti and Ti6Al4V alloy at 1023 K. Furthermore, the scale developed on Ti6Al4V alloy consist an α-Al_2O_3 film situated between outer and the inner part of the scale (TiO_2).

In case of air oxidation the multilayer structure developed on both materials (pure Ti and Ti6Al4V) after exposure to air atmosphere at 1073 K for 240 hours. Pure Ti formed TiO_2 while Ti6Al4V developed TiO_2/Al_2O_3 multilayer scale at 1023 K. Digimaps of oxidised pure Ti and Ti6Al4V after 240 hours are presented in **figures 65** and **66** respectively.

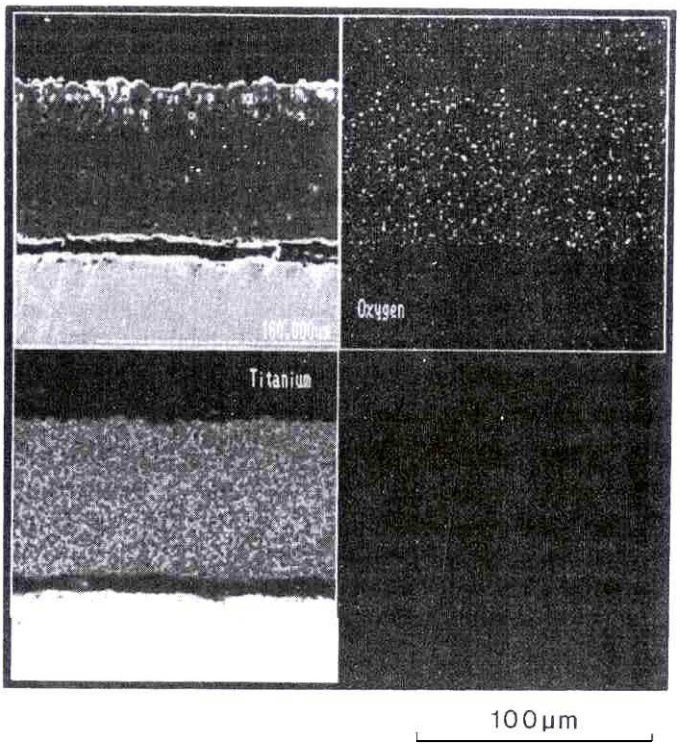

Figure 65 EDS digimaps after air oxidation of pure Ti for 240 hours at 1023 K [91]

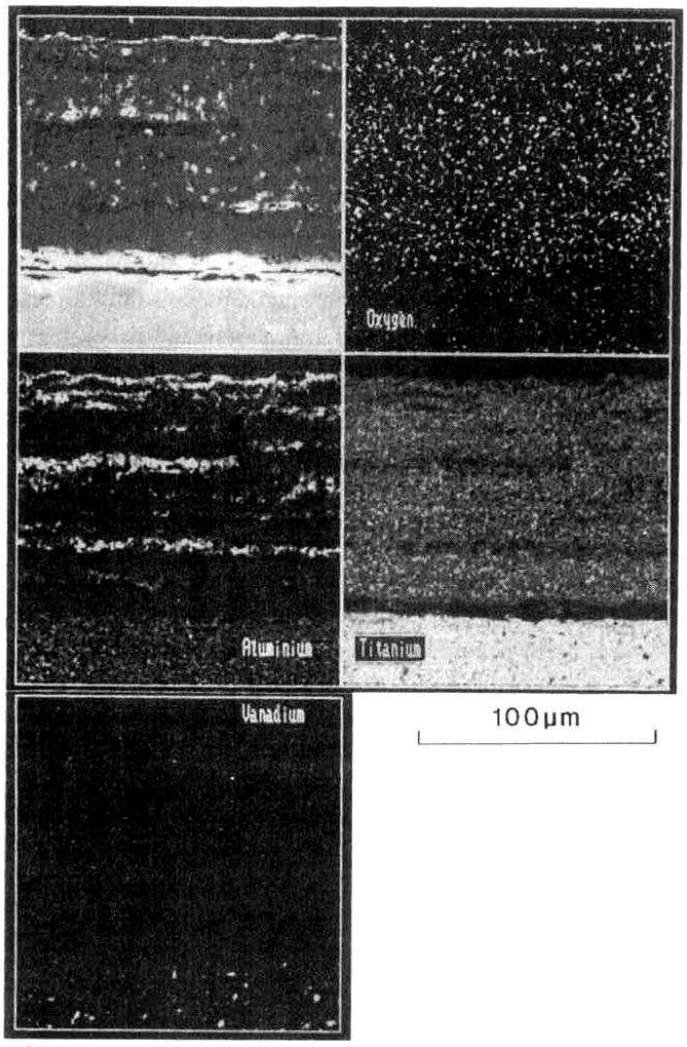

Figure 66 EDS digimaps after air oxidation of Ti6Al4V alloy for 240 hours at 1023 K [91]

Du and Datta [91] suggested the mechanism of degradation of pure Ti and Ti6AlV4 alloy at corrosion environments (sulphidation/ oxidation ($H_2/H_2O/H_2S$ where $pS_2 = 10^{-1}$ Pa and $pO_2 = 10^{-18}$ Pa), oxidation at low partial pressure of oxygen (H_2/H_2O, where $pO_2 = 10^{-18}$ Pa), air oxidation) at 1023 K for 240 hours.

The scale formation of exposed samples (pure Ti and Ti6Al4V alloy) where two layers of TiO_2 developed was due to the outward diffusion of Ti from the material (pure Ti and Ti6Al4V alloy) at 1023 K.

The formation of inner layer of TiO_2 was explained by; ingress of oxygen spices, molecular or anionic, directly from the gaseous phase, or by ingress of oxygen species derived from the dissociation of the outer layer of TiO_2.

Overall the inner layer developed due to the ingress of oxygen from external environment. The authors [91] also suggested that the outward flux of Ti was greater than inner flux of oxygen since the growth of the outer layer of TiO_2 was much thicker than inner one.

The influence of pS_2, pO_2, a_{Al} and a_{Ti} (where a_{Al} and a_{Ti} denotes activity of Al and Ti respectively) are very important for this results and these values are essential for corrosion products development at 1023 K at three different atmospheres; (sulphidation/ oxidation ($H_2/H_2O/H_2S$ where $pS_2 = 10^{-1}$ Pa and $pO_2 = 10^{-18}$ Pa), oxidation at low partial pressure of oxygen (H_2/H_2O, where $pO_2 = 10^{-18}$ Pa), and air oxidation.

The formation of scale development at sulphidation/oxidation environment can be described as follows:

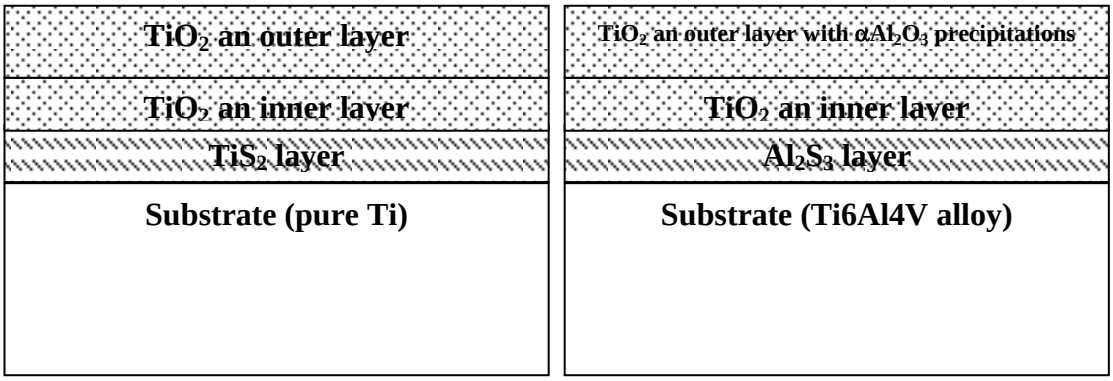

Figure 67 Scale formation on pure Ti and Ti6Al4V alloy after exposure to sulphidation/oxidation ($H_2/H_2O/H_2S$ where $pS_2 = 10^{-1}$ Pa and $pO_2 = 10^{-18}$ Pa) environment at 1023 K [91]

It is well known from the open literature that when pO_2 and pS_2 decreased in the same time a_{Al} and a_{Ti} increased toward the substrate. Thus the reactions at the oxide/sulphide – substrate interface can be considered as:

Reaction 28 $Ti_{(s)} + O_{2(g)} \rightarrow TiO_{2(s)}$

Reaction 29 $Ti_{(s)} + S_{2(g)} \rightarrow TiS_{2(s)}$

} For pure Ti

Reaction 30 $Ti_{(s)} + O_{2(g)} \rightarrow TiO_{2(s)}$

Reaction 31 $Al_{(s)} + S_{2(g)} \rightarrow Al_2S_{3(s)}$

} For pure Ti6Al4V alloy

Equilibrium constants for these four reactions can be written as:

Equation XL $K_{17} = K_{TiO_2} = a_{Ti}^{-1} * pO_2^{-1}$

Equation XLI $K_{18} = K_{TiS_2} = a_{Ti}^{-1} * pS_2^{-1}$

Equation XLII $K_{19} = K_{TiO_2} = a_{Ti}^{-1} * pO_2^{-1}$

Equation XLIII $K_{20} = K_{Al_2S_3} = a_{Al}^{-2} * pS_2^{-3/2}$

At the interface TiO_2/Al_2S_3 in Ti6Al4V alloy insufficient sulphur species diffuse through a thick TiO_2, in this moment the sulphur pressure is not high enough, and the equilibrium of reaction between Al and S_2 is shifted to the left side, and Al_2S_3 sulphide starts to decompose. The released Al^{3+} ions diffuse towards the outer part of the scale (TiO_2) and forms Al_2O_3 where oxygen partial pressure is enough high to promote the formation of Al_2O_3:

Reaction 32 $Al_{(s)} + O_{2(g)} \rightarrow Al_2O_{3(s)}$

An equilibrium constant for reaction 36 is described as follows:

Equation XLIV $K_{21} = K_{Al_2O_3} = a_{Al}^{-2} * pO_2^{-3/2}$

Meanwhile sulphur species (S^{2-}) from the decomposed Al_2S_3 diffused inward developed TiS_2 sulphide. It is suggested that the same types of reaction are likely to form in pure Ti exposed to sulphidation/ oxidation ($H_2/H_2O/H_2S$ where $pS_2 = 10^{-1}$ Pa and $pO_2 = 10^{-18}$ Pa at 1023 K.

The exposure of pure Ti and Ti6AlV4 alloy at oxidation at low partial pressure of oxygen (H_2/H_2O, where $pO_2 = 10^{-18}$ Pa at 1023 K reveals that a double TiO_2 layer formed on Ti6Al4V alloy as well as on pure Ti.

Du and Datta [91] suggested that similar reaction are likely to occur at low partial pressure of oxygen ($pO_2 = 10^{-18}$ Pa). The activities of the reaction products

(a_{TiO2} and a_{Al2O3}) can be considered as equal to 1, and then the equilibrium reaction can be estimated by the reactions below:

Equation XLV $$K_{TiO_2} = a_{Ti}^{-1} * pO_2^{-1}$$

Equation XLVI $$K_{Al_2O_3} = a_{Al}^{-2} * pO_2^{-3/2}$$

The formation of Al_2O_3 reduces the partial pressure of oxygen underneath the Al_2O_3 scale. At this moment if insufficient amount of Ti will diffuse to the outer part of the scale, the **equation XLV** will move in the left. If it is assumed that the partial pressure of oxygen at the interface (Al_2O_3/TiO_2) is equal to $pO_2 = 10^{-18}$ Pa, (highest possible value) which is equal to the experimental value in H_2/H_2O mixture used in this test, or lower $pO_2 = 10^{-41}$ Pa which is equal to decomposition pressure of Al_2O_3 oxide, then the minimum activity of Al is equal to $6.6x10^{-18}$ or 1, and minimum activity of Ti to form Ti is equal to $3.7x10^{-15}$ or $3x10^{8}$. These activity results show that the minimum activity to form an Al_2O_3 oxide is smaller than this for TiO_2. The actual value of oxygen partial pressure was estimated above 10^{-41} Pa (dissociation partial pressure of Al_2O_3) and lower than 10^{-18} Pa (highest value of partial pressure of oxygen used in this test (H_2/H_2O mixture)). In this experiment the conditions were more favourable for the promotion and formation of Al_2O_3 than TiO_2. On other hand, the released Ti from dissociation reaction of TiO_2 which is presented below will diffuse outward through Al_2O_3 scale.

Reaction 33 $$TiO_2 \rightarrow Ti + O_2$$

The diffused species of Ti will form a TiO_2 compound above the Al_2O_3 oxide scale, meanwhile released oxygen from **reaction 33** is consumed in the formation of the Al_2O_3. It is important to note that the outer and inner TiO_2 scale formation is enhanced by ingress of oxygen form ambient atmosphere where $pO_2 = 10^{-18}$ Pa.

The air oxidation developed a multilayer scale consisting of TiO_2 and Al_2O_3 on the surface of Ti6Al4V alloy, TiO_2 developed on pure Ti surface. In case of Ti6Al4V alloy the number of layer TiO_2/Al_2O_3 depend from temperature and exposure time.

Chapter II – Section 3 – Critical Literature Review – Hot Corrosion /Oxidation of γ-TiAl alloys

Ch.II.Sec.3.1 Introduction to literature review

In this section a review of hot corrosion behaviour of selected materials is presented.

Ch.II.Sec.3.2 High Temperature Hot Corrosion/Oxidation

Hot corrosion/oxidation may be defined as an accelerated corrosion attack, supported by the presence of aggressive agents (salts): Na_2SO_4, KCl, NaCl, and V_2O_5. The presence of salts at high temperature above 923 K may form molten deposits, mainly of Na_2SO_4. The primary source of sodium sulphate in marine or in aircraft engines is due to the reactions of sodium chloride and sulphur (from fuel) with atmospheric air and water vapour during combustion process. The reactions in combustion process are presented below:

Reaction 34 $\frac{1}{2}S_2 + O_2 \rightarrow SO_2$ **(Sulphur reacts with oxygen to produce SO_2)**

Reaction 35 $S_2 + \frac{3}{2}O_2 \rightarrow 2SO_3$ **(Sulphur reacts with oxygen to produce SO_3)**

Then SO_2 and SO_3 react **(reactions 34 and 35)** with NaCl, air and water vapour, according to the reactions:

Reaction 36 $2NaCl + SO_2 + \frac{1}{2}O_2 + H_2O \rightarrow Na_2SO_4 + 2H^+ \uparrow + 2Cl^- \uparrow$

Reaction 37 $2NaCl + SO_3 + H_2O \rightarrow Na_2SO_4 + 2H^+ \uparrow + 2Cl^- \uparrow$

It is considered that the sulphidation of sodium chloride **(reactions 36 and 37)** takes place in hot zones of engine or turbine where temperature is higher than the melting point of pure NaCl (1074 K).

The faster rate of hot corrosion/oxidation degradation of metallic materials (alloys, alloys with coatings) leads to decreased effectiveness and appreciable abridge of the lifetime of the components. The formation of hot corrosion/oxidation aggressive products on aerospace, automotive engines causes a main concern. With increasing hot working temperature there is the possibility to reach a critical temperature, where catastrophic corrosion takes place. Rapid deterioration of the components due to hot corrosion/oxidation depends on the chemical concentration of the aggressive elements (S_2, Cl_2, and Na) in combustion gases or ashes.

From a chemical point of view it is possible to divide the sources of aggressive agents in three categories:

1. fuels without salts and ashes
2. fuels with salts but without ashes
3. fuels with salts and ashes
4. environment containing Na_2SO_4, NaCl, and other salts (oceans, seas)

The hot corrosion/oxidation of metallic compounds is very complex in nature; many chemical reactions take place in parallel. The hot corrosion attack, unlike oxidation, consumes the materials in unpredictable rate. Here are two different kinds of hot corrosion/oxidation behaviour: [92].

- Low Temperature Hot Corrosion/Oxidation (LTHC – Type II) (923 – 1123 K)
- High Temperature Hot Corrosion/Oxidation (HTHC – Type I) (1123 – 1223 K)

The presented mechanisms of degradation due to hot corrosion attack are related to both types of hot corrosion/oxidation, it is important to note that the border between type I and type II of hot corrosion/oxidation is no clearly defined.

Ch.II.Sec.3.3 Types of Hot Corrosion/Oxidation

Ch.II.Sec.3.3.1 Low Temperature Hot Corrosion/Oxidation (LTHC – Type II)

Type II hot corrosion/oxidation is observed mainly in the temperature range 923 K and 1123 K. LTHC can be characterised by the formation of pitting in the scale due to the development of low melting eutectics e.g. $Na_2SO_4 + CoSO_4$ (melting point 813 K. $CoSO_4$ is a corrosion product of a reaction between the surfaces of blades components made of cobalt base alloys (WI-52, FSX 414) [93] and SO_3 (SO_3 forms due to the reaction $1/2S_2+3/2O_2 \rightarrow SO_3$) from the combustion gases, according to the following reaction:

Reaction 38 $Na_2SO_4 \rightarrow 2Na^+ + SO_4^{2-}$

Reaction 39 $Co^{2+} + SO4^{2-} \rightarrow CoSO_4$ **(Melting point 813 K)**

It is suggested [94], that the high partial pressure of SO_3 is required for the LTHC reactions to occur.

With high partial pressure of SO_3 the activity of S_2 is enough high to start reaction with elements (Co, Ni) to form liquid products **(reaction 39)**. In contrast, HTHC does not require a high partial pressure of SO_3. Due to the presence of high temperature of reaction (higher than in LTHC), the activity of S_2 is high and S_2 starts to react with Co and Ni. Furthermore LTHC involves an incubation period (incubation period is related to formation of protective oxide scale) [95].

Ch.II.Sec.3.3.2 High Temperature Hot Corrosion/Oxidation (HTHC – Type I)

The type I hot corrosion/oxidation named as a High Temperature Hot Corrosion/Oxidation (HTHC), takes place at temperatures between 1123 K and 1223 K [96] and starts from the condensation of fused alkali metals salts on the surface of materials.

The type I of hot corrosion/oxidation is mainly generated by Na_2SO_4 (melting point 1157 K, but impurities or additional amounts of others salts (NaCl) or elements (phosphorus, chlorine) drastically decrease the melting point of Na_2SO_4 to 893K [97]. Sodium sulphate forms aqueous solutions with a pH equal to 7 (neutral factor), this value of pH is derived from strong acid H_2SO_4 and strong base sodium hydroxide NaOH [98]. The significant sources of sodium sulphate are: oceans, fuel, and industrial pollutants (combustion gases).

Ch.II.Sec.3.4 Historical Aspects of Hot Corrosion Investigations

The first contact with hot corrosion/oxidation degradation was illustrated in aircraft engines installed on patrol boat in 1959 [99]; turbine manufacturers were also aware of hot corrosion/oxidation attack during war in Vietnam in late 1960's. The first attempt to characterise mechanism of hot corrosion/oxidation behaviour was prepared by Simons et al in early 1960 [100]. It was considered that the reaction

mechanism between metal (Ni) at Na_2SO_4 salt, was related to the accelerated oxidation rate of a sulphide eutectic (Ni – Ni_3S_2). Luthra [105] emphasized that the formation of chromium sulphide (Cr_2S_3) in Na_2SO_4 is very important; depletion in chromium due to formation of chromium sulphide, accelerates the degradation of the alloy. Bronstein and Decresente [101] demonstrated that the degradation of alloy does not depend on sulphidation/oxidation mechanism. They proposed that the degradation of alloys may be related to dissolution of protective scales (Cr_2O_3/Al_2O_3), based on the evidence that the pre – sulphidized alloys at 1173 K did not accelerate the attack during subsequent oxidation.

Rapp [102] measured the oxide solubilities in molten Na_2SO_4 as a function of acidity of the salt. Author's conclusions involved the occurrence of the dissolution of protective oxide layer followed by the re-precipitation of the oxide as non – protective particles within the salt film. Thereby, the oxide at the oxide scale - salt interface exhibits a higher (acidic or basic) solubility than farther out in the slat film (partial pressure of O_2 decreases).

Geobel and Petit [103] investigated hot corrosion/oxidation behaviour of Ni base alloys with fused Na_2SO_4 film at 1273 K; the authors showed that the NiO formation increases the sulphur activity due to the formation NiO and consumption oxygen from the melt. This mechanism allows creating nickel sulphide (Ni_3S_2).

The mechanism of inward diffusion of sulphur has not been explained; the authors suggested a salt fluxing mechanism; where the protective role of the oxide scale may be lost due to fluxing of this layer in the molten salt. Two types of fluxing mechanism were proposed:

Ch.II.Sec.3.5 Fluxing mechanisms

Ch.II.Sec.3.5.1 Acidic Fluxing Mechanism of Hot Corrosion

Acidic dissolution occurs when the activity of O^{2-} is very low, and leads to much more severe oxidation than basic fluxing.

Reaction 40 $NiO \rightarrow Ni^{2+} + O^{2-}$

The acidic condition occurs when partial pressure of sulphate SO_3 gas in ambient atmosphere reaches a required level and then the SO_3 gas and salt (Na_2SO_4) start to react, with a protective scale such as Al_2O_3 by following reaction:

Reaction 41 $$Na_2O + SO_3 \rightarrow Na_2SO_4$$

Reaction 42 $$Al_2O_3 + 3Na_2SO_4 \rightarrow Al_2(SO_4)_3 + 3Na_2O$$

Reaction 42 can be written as:

Reaction 43 $$Al_2O_3 + Na_2O + SO_3 + \frac{3}{2}O_2 \rightarrow Al_2(SO_4)_3 + Na_2O$$

This type of acidic fluxing takes a place in HTHC Type I; below the melting point of Na_2SO_4 (1157 K). The melting point of pure sodium sulphate is higher than the regime of HTHC Type I. In fact other sulphates or contaminants (other slats NaCl) may decrease the melting temperature of Na_2SO_4.

Ch.II.Sec.3.5.2 Basic Fluxing Mechanism of Hot Corrosion

- Ni metal reacts with fused Na_2SO_4 to form NiO

Reaction 44 $$Ni + Na_2SO_4 \rightarrow NiO + SO_3 + 2Na$$

- The oxygen activity decreases and sulphur activity increases

- Formation of liquid nickel sulphide **(reactions 45 and 46)** causes an increase in local salt basicity (sodium oxide activity).

Reaction 45 $$Na_2SO_4 \rightarrow 2Na^+ + SO_4^{2-}$$

Reaction 46 $$Ni + SO_4^{2-} \rightarrow NiS + 2O_2$$

- Normally protective NiO scale is dissolved/fluxed to form basic solute + nickel ions. ($Na_2O + Ni^+$)
- With a negative solubility gradient, non-protective NiO particles are precipitated within the salt film.

- The reactions above support a basic fluxing reaction, i.e. corrosive attack by forming a basic solute of the protective scale.

Reaction 47 $4Ni + Na_2SO_4 \rightarrow Na_2O + 3\,NiO + NiS$

The basic condition takes place in temperature where melt of Na_2SO_4 is richer in Na_2O. The molten sulphate may react with aluminium oxide to form aluminate, chromate with chromium oxide or titminate when melts are react with aluminium, chromium, and titanium oxide by following reactions:

Reaction 48 **(Basic fluxing)** $2Al_2O_3 + 2Na_2O + O_2(gas) \rightarrow 4NaAlO_2$

Reaction 49 **(Basic fluxing)** $2Cr_2O_3 + 2Na_2O + O_2(gas) \rightarrow 4CrAlO_2$

Reaction 50 **(Basic fluxing)** $4TiO_2 + 2Na_2O + O_2(gas) \rightarrow 4NaTiO_2$

Ch.II.Sec.3.6 Hot corrosion of Some Specific Alloys

Ch.II.Sec.3.6.1 Ni – Cr Alloys

Ni – Cr and Co – Cr alloys are more resistant for hot corrosion than pure Ni and Co. Higher resistivity occurs due to development of protective oxide scale (Cr_2O_3) instead of less protective NiO and Co_3O_4. This however is true at temperature above 1073 K where chromia scale forms easier due to higher activity of Cr^{3+} ions.

This is a reason why Ni – Cr and Co – Cr are more resistible above 1073 K than at lower temperature. At lower than 1073 K the chromia scale fails to form and Ni_3S_2 develops (as a top layer) instead of protective oxide. Moreover the Ni^{2+} ions diffuse outward from the alloy (via fast diffusion paths in defected Ni_3S_2) and react with melted $NiSO_4$ to form the sulphide with low melting point (908 K) [104]. The reaction presenting this mechanism:

Reaction 51 $Na_2SO_4 \rightarrow 2Na^+ + SO_4^{2-}$

Sodium reacts with oxygen from combustion air according to the following reaction:

Reaction 52 $2Na^+ + O^{2-} \rightarrow Na_2O$

Reaction 53 $Ni^{2+} + SO_4^{2-} \rightarrow NiSO_4$

Reaction 54 $9Ni + 2NiSO_4 \rightarrow Ni_3S_2 + 8NiO$

Above 1073 K Ni_3S_2 is no longer stable and decomposes to Ni – S liquid solution. This liquid solution dissolves chromium from the alloy (NiCr alloy) and transported Cr outwards to the reaction interface to form a protective scale. Thus for chromia forming alloys hot corrosion rate falls rapidly above 1073 K.

Ch.II.Sec.3.6.2 Co – Cr Alloys

The behaviour of Co – Cr alloys is different from that of Ni – Cr alloys. Under the same conditions, Co – Cr alloys are less resistant to hot corrosion attack. The main reasons for that are:

- Higher stability of $CoSO_4$ than CoO/Co_3O_4 as compared to $NiSO_4$ with respect to NiO. This means that it is much easier to form mixture of Na_2SO_4 and $CoSO_4$
- Co is a better catalyst for the reaction:

Reaction 55 $SO_2 + \frac{1}{2}O_2 \rightarrow SO_3$

This reaction increase pressure of SO_3 to the required level to form cobalt sulphate

- Lower temperature of eutectic $CoSO_4$ + Na_2SO_4 (838 K) than $NiSO_4$ + Na_2SO_4 (944 K).

Reaction 56 $Na_2SO_4 \rightarrow 2Na^+ + SO_4^{2-}$

Reaction 57 $Co^{2+} + SO_4^{2-} \rightarrow CoSO_4$ **(Melting point (838 K)**

Thus Co – Cr alloys are more susceptible to hot corrosion than Ni – Cr alloys.

Luthra [105] investigated Co base alloy exposed to temperature range 873 – 1023 K with thin salt deposit (Na_2SO_4) in O_2-SO_2-SO_3 mixture to stabilize a Na_2SO_4-Co_SO_4 liquid on Co_3O_4 oxide. It was concludes that Co – Cr alloy suffered hot corrosion attack in the forms of pits and sulphur rich band (on the bottom of the pits), this band was filled by Cr_xS_y sulphide. The other morphologies were depended on partial pressure of SO_3 and temperature. At experimental temperature (1023 K) the

outer scale of exposed alloy (Co – base alloy) was built from Co_3O_4 (external part of the scale) and $CoSO_4$ inner part of the scale).

When pSO_3 was not enough high then Cr_2O_3 and $CoCr_2O_4$ formed in the alloy/scale interface.

At lower temperature and higher pSO_3 where $CoSO_4$ was stable, large needles were observed of Cr_2O_3 and $CoCr_2O_4$.

Ch.II.Sec.3.6.3 Co – Al Alloys

The same author [105] exposed Co – Al alloys in the same conditions (873 – 1023 K, thin deposit Na_2SO_4 in O_2-SO_2-SO_3 atmosphere). Generally Co – Al alloy suffered frontal attack rather than pits. The morphologies formed during exposure to aggressive environment were similar to those obtained for Co – Cr alloy. Instead of chromium sulphide, aluminium sulphide developed in the alloy/scale interface with greater thickness as in Co – Cr alloys. The outer layer of the scale contained Co_3O_4 and $CoSO_4$.

It has been found [106,107] that the alumina forming alloys are not very interesting materials for hot corrosion applications, especially at temperature range 873 – 1073 K; because

- γ-alumina is formed in this condition instead of more protective α-alumina
- Al_2S_3 is less stable than Cr_2S_3 thus Cr from Ni – Cr alloy will tend to react with S_2 on the metal/scale interface.
- The stable sulphide Cr_2S_3 changes to a protective oxide Cr_2O_3 more easily than less stable Al_2S_3
- Chromia and alumina, both show difference in solubility in sulphate melts. Both of these oxides are amphoteric; both may be dissolved by acidic and basic flux mechanism. Appropriate reactions are:

Reaction 58 $Na_2SO_4 \rightarrow 2Na_2O + SO_3$

Reaction 59 $Na_2O \rightarrow 2Na^+ + O^{2-}$

Reaction 60 $Cr_2O_3 + 2Na^+ + O^{2-} \rightarrow \frac{3}{2}O_2 + 2Na^+ + 2CrO_4^{2-}$ **(Basic mechanism)**

SO_3 is a product of decomposition of Na_2SO_4 via following reactions:

Reaction 61 $Na_2SO_4 \rightarrow Na_2O + SO_3$

Reaction 62 $Cr_2O_3 + SO_3 \rightarrow 2Cr^{3+} + +2SO_4^{2-}$ **(Acidic mechanism)**

If equilibrium partial pressure is known, it is possible to form a thermodynamic stability diagram, such as presented on **figures 68 and 69**.

This type of diagram gives the stability of all relevant phases (salts, oxides, sulphides) at a given temperature. **Figure 68** shows phase stability diagram of Cr_2O_3 at 1173 K in the stability region Na_2SO_4, **reactions 59 to 62** are related to this diagram.

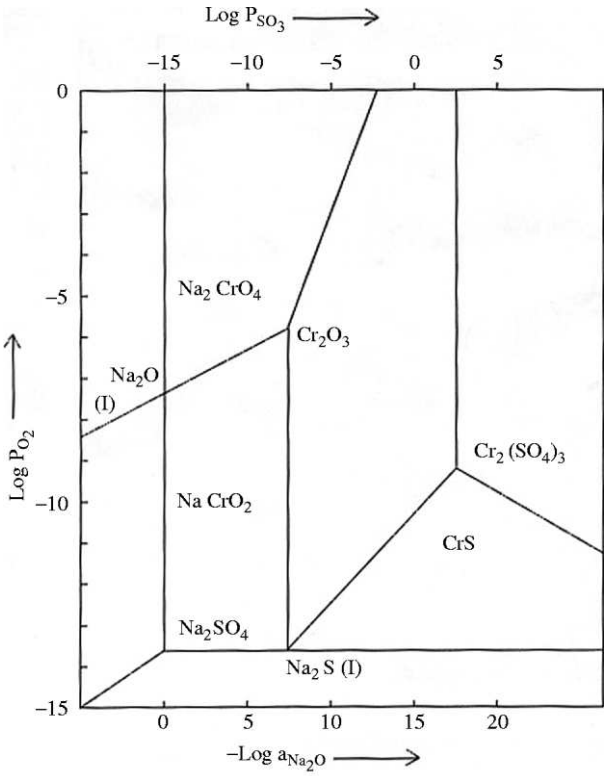

Figure 68 Phase stability diagram Cr_2O_3 at 1173 K in the stability region Na_2SO_4 [107]

In similar way an alumina is dissolve as AlO^{2-} and Al^{3+} ions due to basic and acidic mechanism respectively.

Reaction 63 $Na_2SO_4 \rightarrow 2Na_2O + SO_3$

Reaction 64 $Na_2O \rightarrow 2Na^+ + O^{2-}$

Reaction 65 $Al_2O_3 + O^{2-} \rightarrow 2AlO^{2-}$ **(Basic mechanism)**

Reaction 66 $Na_2SO_4 \rightarrow Na_2O + SO_3$

Reaction 67 $Al_2O_3 + SO_3 \rightarrow 2Al^{3+} + 3SO_4^{2-}$ **(Acidic mechanism)**

Reactions 63 to **67** are related to phase stability diagram Al_2O_3 at 1173 K in the stability region Na_2SO_4 which is given in **figure 69:**

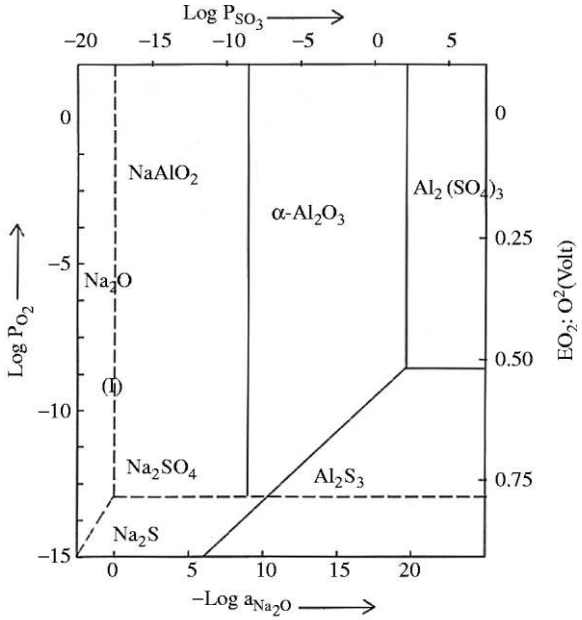

Figure 69 Phase stability diagram Al_2O_3 at 1173 K in the stability region Na_2SO_4 [107]

It is important to note that the surface of the substrate exposed to corrosive environment (hot corrosion) is covered with corrosion products (oxides, sulphides); thermodynamics cannot be employed in order to predict a progress in corrosion development. In such condition, kinetics, and diffusion processes play the most important role in the degradation of the metallic materials.

Ch.II.Sec.3.7 Hot Corrosion/oxidation of TiAl Alloys – Critical review

Extensive research have been carried out by the authors [108, 111, 113, 114] which used the mixture of NaCl and Na_2SO_4 to indicate hot corrosion and to determine the mechanism of degradation and the hot corrosion/oxidation behaviour

of TiAl base alloys. The NaCl and Na_2SO_4 are the commonly used mixtures in the hot corrosion/oxidation literature. The addition of NaCl to Na_2SO_4 scientifically depresses melting point form 1157 K for pure Na_2SO_4 to 893 K [97].

It has been reported [108] that at 1173 K Ti50Al alloy does not possesses hot corrosion/oxidation resistance due to the formation of non protective mixed Al_2O_3 and TiO_2 instead of pure Al_2O_3 scale. It was demonstrated that the Ti50Al alloy during exposure to hot corrosion/oxidation environment may react via the following reactions:

Reaction 68 $$Na_2SO_4 \rightarrow Na_2O + SO_3$$

Reaction 69 $$Na_2O \rightarrow 2Na + \frac{1}{2}O_2$$

Reaction 70 $$SO_3 \rightarrow \frac{1}{2}S_2 + \frac{3}{2}O_2$$

The non protective mixed TiO_2 and Al_2O_3 scale on surface allows S_2 to diffuse through the scale to the scale/alloy interface. The affinity of Ti to S_2 is much greater than that of Al to S_2, the following reaction may occur:

Reaction 71 $$3TiAl + S_2 \rightarrow 2TiS + TiAl_3$$

Thus TiS and Al rich $TiAl_3$ develops near to the scale/alloy interface. Zhaolin Tang, Wang, and Wu [108] investigated the hot corrosion/oxidation behaviour of Ti50Al, Ti48Al2Cr2Nb, and Ti50Al10Cr alloys at (Na, K)$_2$ SO_4 at 1173 K and Na_2SO_4 + NaCl at 1123 K melts for 100 hours. The author discovered that in the (Na, K) SO_4 at 1173 K Ti50Al was covered by two types of morphology: partly by TiO_2 and Al_2O_3 and a continuous Al_2O_3. TiS developed in the scale/alloy interface (S_2 derived from decomposition of Na_2SO_4).

The Ti48Al2Cr2Nb alloy was covered only by mixed TiO_2 and Al_2O_3 oxides, no sulphide (TiS) was observed in this sample (Ti48Al2Cr2Nb). An adherent, protective scale of Al_2O_3 developed only on Ti50Al10Cr alloy, and provided excellent corrosion resistance.

Generally, Al_2O_3 and TiO_2 developed during exposure of Ti50Al, Ti48Al2Cr2Nb, and Ti50Al10Cr to molten salts (Na_2SO_4 + NaCl) at 1123 K. The author [108] proposed a chemical model for hot corrosion behaviour at Na_2SO_4 +

NaCl at 1123 K where at the beginning the oxides of Al and Ti react with NaCl as given below:

Reaction 72 $$2NaCl + Al_2O_3 + \frac{1}{2}O_2 \rightarrow 2NaAlO_2 + Cl_2$$

Reaction 73 $$NaCl + TiO_2 + O_2 \rightarrow 2NaTiO_4 + \frac{1}{2}Cl_2$$

The chlorine gases produced in reactions **72 and 73** ingress through the scale via pores and cracks and reach the scale/substrate interface and react with Ti and Al according to the reactions:

Reaction 74 $$Ti + Cl_2 \rightarrow TiCl_{2(g)}$$

Reaction 75 $$Al + \frac{3}{2}Cl_2 \rightarrow AlCl_{3(g)}$$

The chlorides form **reactions 74, 75** diffuse outwards through the scale to the outer surface (Ti50Al, Ti48Al2Cr2Nb, and Ti50Al10Cr). The oxygen partial pressure is higher at the surface where $TiCl_2$ and $AlCl_3$ **(reactions 76 and 77)** re-oxidise:

Reaction 76 $$TiCl_2 + O_2 \rightarrow TiO_2 + Cl_{2(g)}$$

Reaction 77 $$AlCl_3 + \frac{3}{2}O_2 \rightarrow Al_2O_3 + 3Cl_{2(g)}$$

The regenerated chlorine **(reactions 75, 76)** re-diffuses into the scale (TiO_2 and Al_2O_3) and reacts with TiO_2 and Al_2O_3 according to the reactions:

Reaction 78 $$Cl_2 + TiO_2 \rightarrow TiCl_2 + O_2$$

Reaction 79 $$Al_2O_3 + \frac{3}{2}Cl_2 \rightarrow 2AlCl_3 + \frac{3}{2}O_2$$

At the scale (TiO_2 and Al_2O_3), aluminium and titanium are consumed by chemical reaction with chlorine **(reactions 75, 76, 77, and 78),** and in the meantime pits may initiate on the surface. This mechanism shows that the only small amount of chloride phase needs to be present and the chlorides phase acts as a catalyst.

Similar results where chlorides played important role in degradation of TiAl based intermetallics were reported by Zhang, Li, and Gao [109]. The TiAl based

intermetallics alloys were exposed to three types of hot corrosion/oxidation tests (presented in **figure 70**; specimens were suspended in salt vapour; immersed in salts mixture and samples were deposited with salt films.

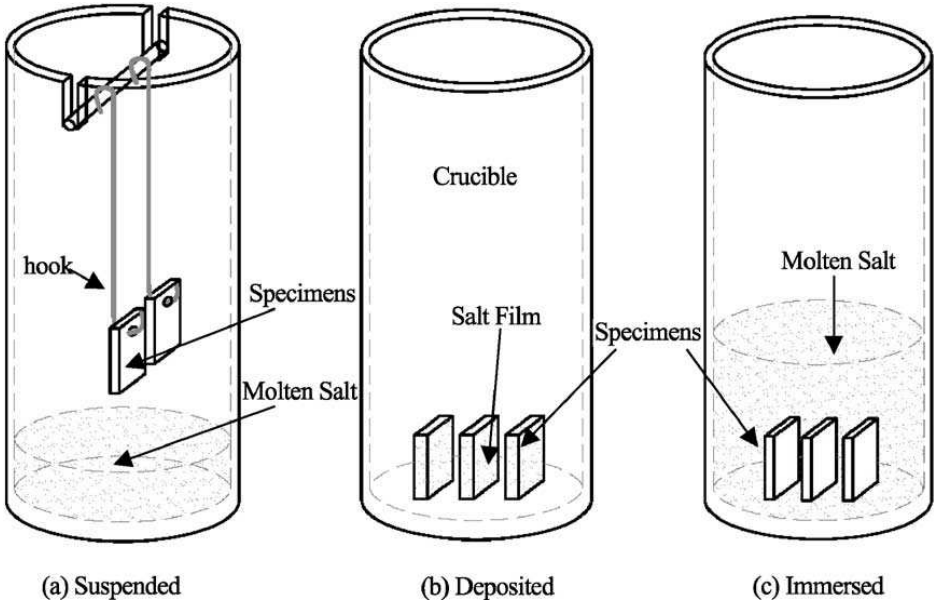

Figure 70 Hot corrosion test performed on TiAl alloys at 20%NaCl80%Na_2SO_4 (wt %) at 1073 K [109]

Three different alloys were used in this experiment: Ti48Al, Ti52Al, and Ti48Al2Cr (all in at %). The investigations were performed in 20%NaCl80%Na_2SO_4 (wt %) at 1073 K. The authors [109] observed that all the samples suspended in salt vapour suffered corrosion attack; the kinetics of corrosion attack for Ti52Al and Ti48Al2Cr followed parabolic character (parabolic rate law). Moreover Ti48Al showed scale spallation during cooling and heating cycles.

Figure 71 shows kinetic data obtained from the specimens suspended in salt vapours of 20%NaCl80%Na_2SO_4.

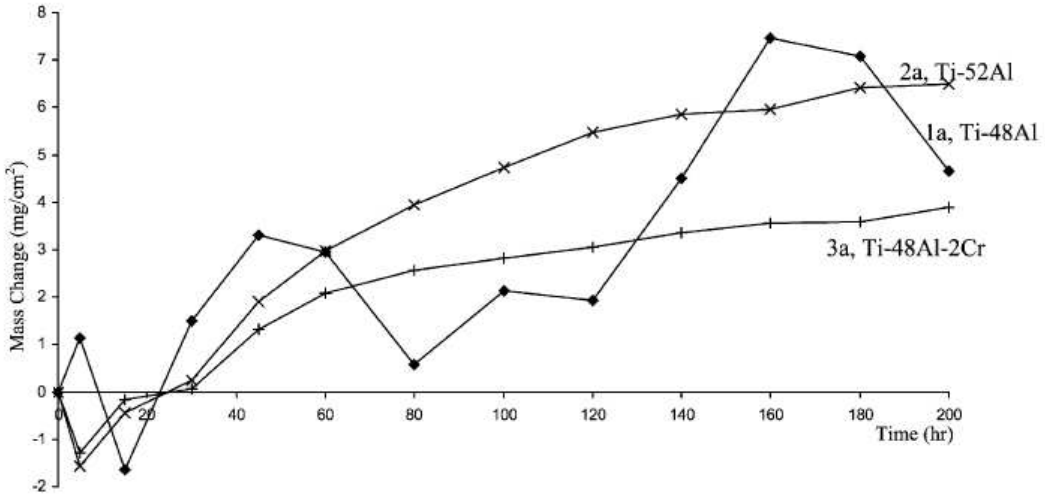

Figure 71 Hot corrosion/oxidation kinetic data for the specimens suspended in salt vapour at 1073 K [109]

The results obtained here are in good agreement with previous work [108]. The decomposition of volatile chlorides is a main concern regarding the degradation of the protective scale. The decomposed volatile chlorides ($TiCl_2$, $TiCl_4$, and $AlCl_3$) on the top of the $Al_2O_3 + TiO_2$ scale, released chlorine according to the reactions:

Reaction 80 $$TiCl_2 \rightarrow Ti^{4+} + Cl_{2(g)}$$

Reaction 81 $$TiCl_4 \rightarrow Ti^{4+} + 2Cl_{2(g)}$$

Reaction 82 $$AlCl_3 \rightarrow Al^{3+} + \frac{3}{2}Cl_{2(g)}$$

Released chlorine migrates inward to the TiO_2 and Al_2O_3 top oxide scale and reacts with Al and Ti oxides by following reactions:

Reaction 83 $$Cl_2 + TiO_2 \rightarrow TiCl_2 + O_{2(g)}$$

Reaction 84 $$3Cl_2 + Al_2O_3 \rightarrow 2AlCl_3 + \frac{3}{2}O_{2(g)}$$

The released free oxygen **(reactions 83 and 84)** react with Al and Ti (product of decomposition of volatile chlorides **(reactions 80, 81, and 82)** to enlarge the top oxide scale of TiO_2 and Al_2O_3.

It is suggested that the poor corrosion resistance Ti48Al alloy is due to the fact that Ti48Al alloy does not contain sufficient high amounts of Al to develop a

protective Al_2O_3 scale. The activity of Al in Ti48Al is not enough high to promote formation of Al_2O_3.

Furthermore the sample with 48 at% of aluminium possesses a multi-phase structure (γ and α_2 phases), whereas Ti52Al and Ti48Al2Cr consist of a near γ-phase structure. Kai Zhang [109] suggested a mechanism of degradation of TiAl based alloy suffering hot corrosion in salts mixture (80%$Na_2SO_4$20%NaCl). This mechanism is based on the theory that the degradation of TiAl alloys are due to the released chlorine form the decomposition of NaCl at 1073 K:

Reaction 85 $$NaCl \rightarrow Na^{+} + Cl^{-}$$

The released chlorine reacts with Al and Ti from the oxide scales formed in initial stage of exposure (when temperature increased from 293 to 1073 K respectively, according to the reactions:

Reaction 86 $$TiCl_2 \rightarrow Ti^{4+} + Cl_{2(g)}$$

Reaction 87 $$TiCl_4 \rightarrow Ti^{4+} + 2Cl_{2(g)}$$

Reaction 88 $$AlCl_3 \rightarrow Al^{3+} + \frac{3}{2}Cl_{2(g)}$$

Due to these reactions, the strains and cracks may occur in the oxide scale (TiO_2 and Al_2O_3) at 1073 K. The released chlorine (Cl_2) migrates through the porous scale or cracks in the scale, and reaches the scale/substrate interface; it is postulated that chlorine acts in the same way as postulated by Zhaolin Tang, Wang, and Wu [108].

Kai Zhang performed investigations with salts deposited on the surfaces of the material at 1073 K. Salt mixture with composition 20%NaCl80%Na_2SO_4 (wt %) was deposited both sides of the sample surface. When the specimens were cooled down, the salt film with deposited salt (20%NaCl-80%Na_2SO_4) spalled off. It was difficult to analyse this kinetics because of the mixed salt – oxide layers and since the salt film was spalled away after two first cycles (15 hours).

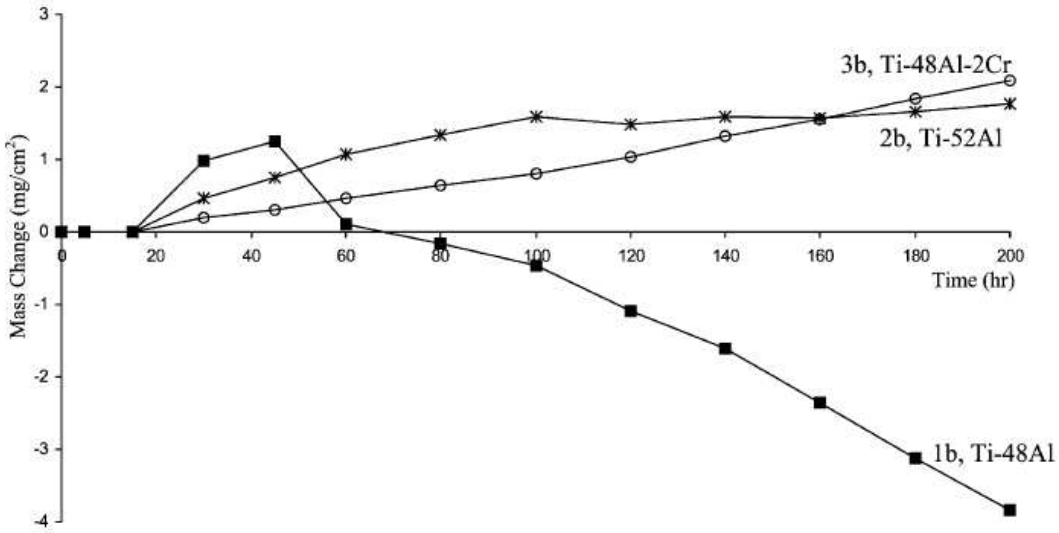

Figure 72 Kinetic data obtained from hot corrosion/oxidation test with salt (20%NaCl80%Na_2SO_4) deposited samples at 1073 K [109]

This spallation in initial period of experiment occurred due to the lack of adherence of a deposited salt (20%NaCl80%Na_2SO_4)

Figure 72 reveals larger mass gain for Ti48Al2Cr sample, the lowest for Ti52Al, Ti48Al showing the most significant mass spallation. These results show that the high aluminium content has beneficial effect for hot corrosion/oxidation resistance. Higher aluminium is likely to allow easy development of an adherent alumina scale (Al_2O_3) and reduce hot corrosion/oxidation degradation. In salt deposited experiment. The addition of Cr 2 wt % to TiAl alloy (Ti48Al2Cr) did not improve hot corrosion/oxidation resistance; the mass gain was higher showing a linear growth rate of the scale.

These results do not fully explain the mechanism of porous scale growth during hot corrosion/oxidation experiment at 1073 K. It can be suggested that the small addition of Cr (Cr has a smaller oxidation grade (3^+) compared to Ti addition (4^+)) may change the electron structure in the atomic lattice of TiO_2. Titanium with small addition of Cr develops a thick and porous scale; this porous scale is growing due to the outward diffusion of Ti^{4+} ions which increases amount of cations vacancies in the atomic lattice of TiO_2:

Reaction 89 $Ti_{1+y}O_{2-y}$

Where: Ti^{****} and $V_O^{\bullet\bullet}$ four titanium atoms in the interstitial positions and doubled ionic vacancies of oxygen. Cr addition causes increasing amount of cations vacancies in the atomic lattice of TiO_2 and promotes faster kinetic due to mass transport via point defects:

Reaction 90 $$Cr_2O_3 \rightarrow Ti_{1+y}O_{2-y}$$

Reaction 91 $$2Cr_2O_3 + Ti_{Ti} \rightarrow 4Cr_{Ti}^{\bullet} + Ti_i^{****} + 6O_O$$

Reaction 92 $$Cr_2O_3 + O_O \rightarrow 2Cr_{Ti}^{'} + V_O^{\bullet\bullet} + 4O_O \rightarrow V_O^{\bullet\bullet}$$

Kai Zhang [109] also investigated hot corrosion/oxidation of immersed samples (Ti48Al, Ti52Al, and Ti48Al2Cr) in salt mixture (20%NaCl80%Na_2SO_4) at 800^{o}C (1073 K). Samples suffered the worst corrosion attack due to continuous reactions with aggressive salts. Large mass spallation occurred in all tested samples as shown in **figure 73**.

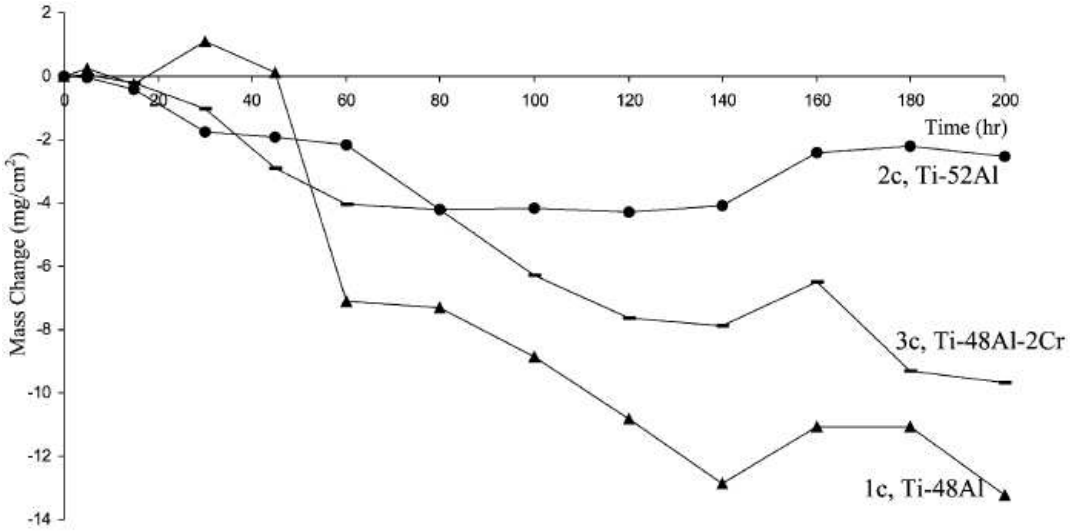

Figure 73 Kinetic values obtained for immersed samples after 200 hours of hot corrosion/oxidation test at 1073 K [109]

Immersion tests are not very reliable for industrial applications; in fact such tests are applicable for test of the large components. These results are in good agreement with those obtained Tang, Wang, and Wu [110] who investigated the influence of magnetron sputtering TiAlCr coating with 10 at% of Cr on hot

corrosion/oxidation behaviour. Experiments were performed in slat mixture containing $(Na, K)_2 SO_4$ at 1173 K, and in 25%NaCl75%Na_2SO_4 at 1123 K for 100 hours test.

Tang, Wang and Wu [110] suggested that the improvement of hot corrosion/oxidation of Ti50Al is due to the employment of Ti50Al10Cr coating at 1173 K allowing the formation of a continuous Al_2O_3 scale

On other hand the Ti50Al10Cr coating does not improve corrosion resistance at 1123 K in 25%NaCl75%Na_2SO_4 salt mixture. Poor corrosion resistance was achieved at lower temperature due to the formation of mixed layer of TiO_2 and Al_2O_3. This scale has a tendency to spall off from the material during test. The kinetics data from this experiment are shown in **Fig. 74 and Fig. 75**:

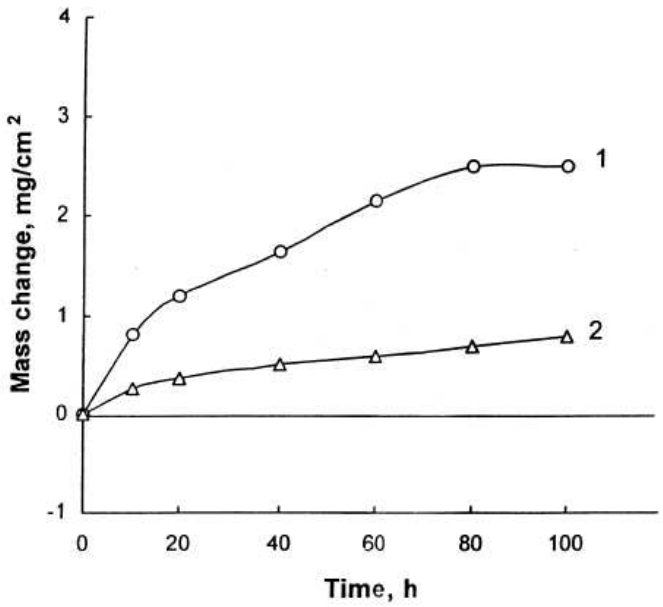

Figure 74 Hot corrosion kinetics of specimens in 25%NaCl75%Na_2SO_4 at 1123 K; 1) Ti50Al alloy, Ti50Al10Cr coated Ti50Al [110]

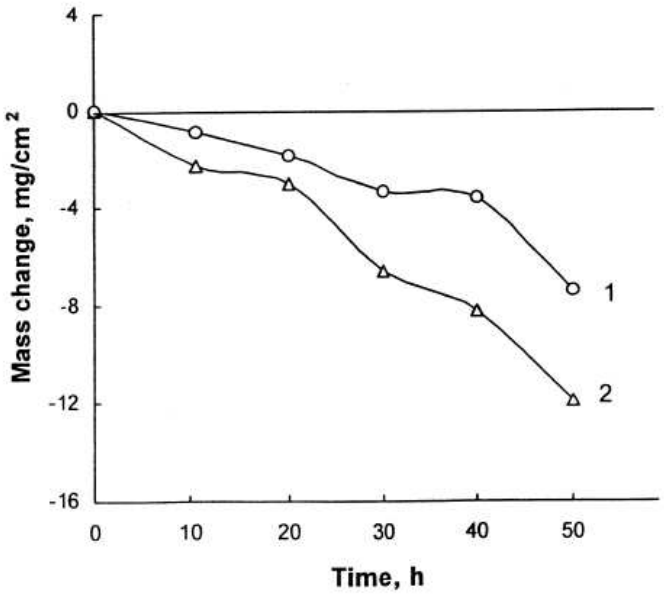

Figure 75 Corrosion kinetics of specimens (1) Ti50Al alloy, Ti50Al10Cr coated Ti50Al) after exposed to salt melts $(K, Na)_2SO_4$ at 1173 K [110]

Here it is important to note that the salt mixture $(Na, K)_2 SO_4$) with small addition of potassium at higher temperature is less aggressive that the mixture of salt which contains: 25%NaCl/75%Na_2SO_4 at lower temperature.

The improvement role of Cr also was achieved by Fuhui Wang [111], where the addition of Cr increased the corrosion resistance at the higher temperature (1373 K) and decreases at lower temperature (1073 – 1173 K respectively). The decreased corrosion resistance at 1073 – 1173 K is due to the fact that the Cr_2O_3 in this range of temperature is volatile [112], and decompose as:

Reaction 93 $$Cr_2O_3 \rightarrow 2Cr^{3+} + 3O^{2-}$$

The released Cr^{3+} may diffuse to the oxide scale (TiO_2 + Al_2O_3). Diffusion of Cr^{3+} into TiO_2 scale does change the electron chemistry in the TiO_2 in atomic lattice; Cr addition causes increasing amount of cations vacancies in the atomic lattice of TiO_2 and promote faster kinetic due to mass transport via point defects **(reactions 90, 91, and 92)**. Chromium ions do not diffuse into Al_2O_3 due to the low defect content in the aluminium oxide.

The oxidation and hot corrosion/oxidation behaviour of Al_2O_3 (magnetron sputtered coating) and enamel **(Table 20)** coated Ti50Al [at%] alloy was investigated

by Tang, Wang and Wu [113] at 1173 K. Enamel frit was sprayed on the surface of the alloy (Ti50Al), and then heated up for 1 hour at 1273 K.

SiO_2	Al_2O_3	ZrO_2	ZnO	B_2O_3	CaO	Na_2O	Balance
58.26	7.98	5.29	9.00	4.66	3.66	3.40	7.75

Table 20 The nominal composition (wt %) of enamel frit [113]

Tang, Wang, and Wu determined that coatings (enamel coating and sputtered Al_2O_3) decreased the oxidation rate, but due to cyclic oxidation sputtered Al_2O_3 coating spalled off from the substrate caused by the mismatch of thermal coefficient between the coating and the substrate.

Enamel coating showed excellent behaviour; no cracks and spallation were occurred during the oxidation test. Furthermore these coatings were exposed to aggressive (Na, $K)_2SO_4$ environment at 1173 K. The enamel coating exhibited adherent structure giving very good hot corrosion/ oxidation resistance. The excellent hot corrosion/oxidation resistance of enamel coating is due to the presence of high amount of SiO_2 (58.26 wt %) in deposited layer of the enamel coating. **Figures 76A and 76B** show cross sectional images of exposed samples to hot corrosion/ oxidation environment at 1173 K.

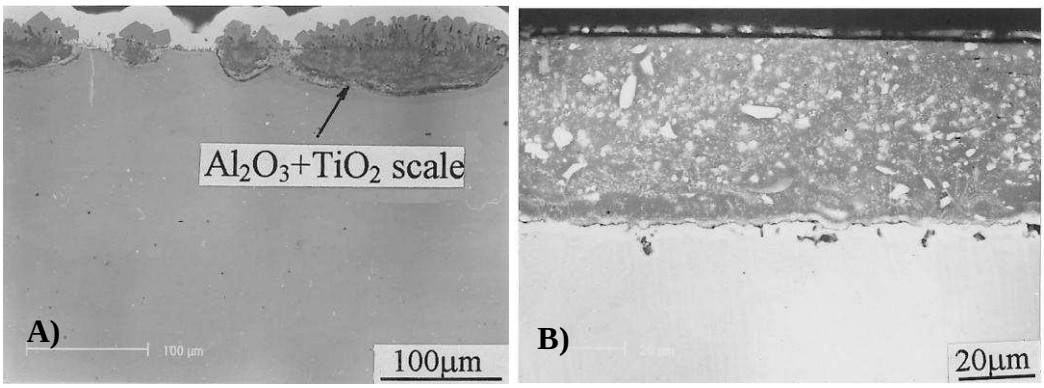

Figure 76 Cross sectional images: A) TiAl uncoated alloy after 100 hours hot corrosion test at $Na_2SO_4+K_2SO_4$, B) TiAl alloy with enamel coating after 100 hours hot corrosion test at $Na_2SO_4+K_2SO_4$ [113]

Further investigations are necessary to examine the effectiveness of the enamel coating, particularly for longer time of exposure and with different salt mixture compositions.

Zhang, Liang, and Gao [114] investigated the hot corrosion/oxidation behaviour of Ti48Al with 1, 2, and 3 at% addition of Ag with a view to understand the role of Ag. The experiments involved suspension of the specimens (Ti48Al1Ag, Ti48Al2Ag, and Ti48Al3Ag) in 20%NaCl80%Na_2SO_4 at 1073 K for 200 hours [114] as presented on **figure 77**.

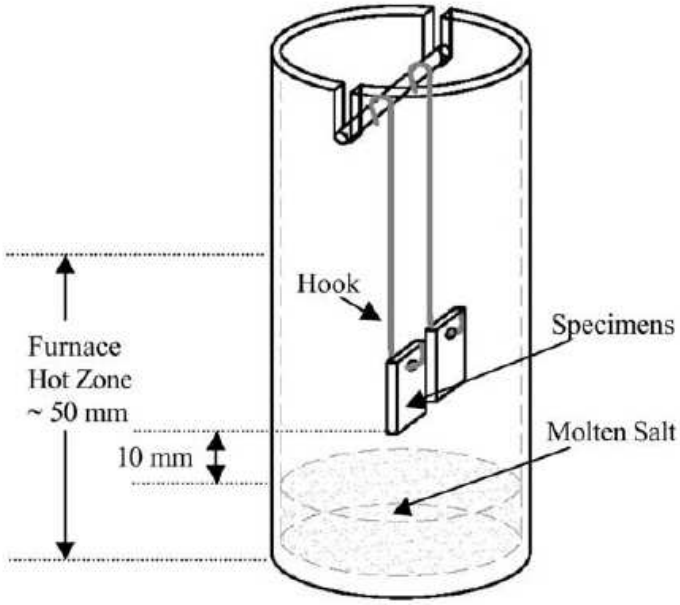

Figure 77 Schematic of hot corrosion test setting by Zhang [114]

The cross - sectional SEM images of treated samples are presented on **figure 78**. **Figure 79** shows the EDS concentration profiles of the specimens (Ti48Al1Ag, Ti48Al2Ag, and Ti48Al3Ag) after exposure to 20%NaCl80%Na_2SO_4 at 1073 K for 200 hours.

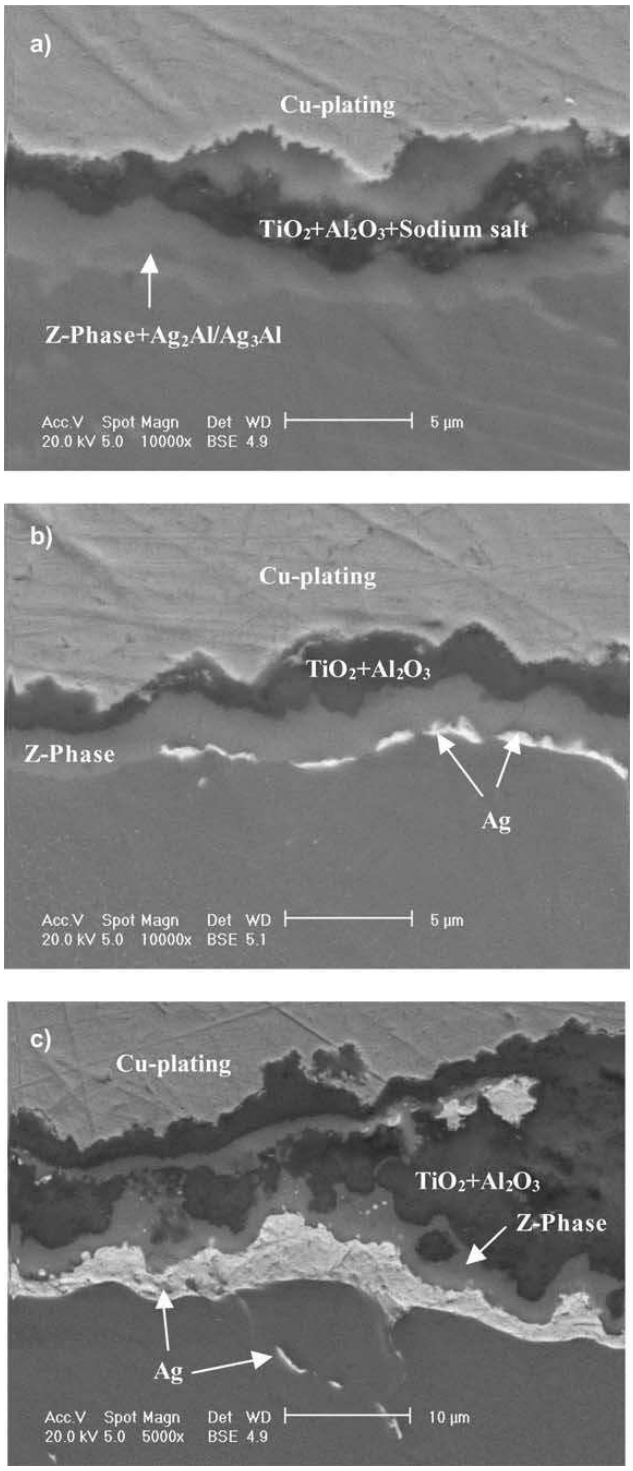

Figure 78 SEM cross – section images of samples exposed to hot corrosion/oxidation treatment at 20%NaCl80%Na_2SO_4 at 1073 K for 200 hours. A) Ti48Al1Ag, B) Ti48Al2Ag, and C) Ti48Al3Ag [114]

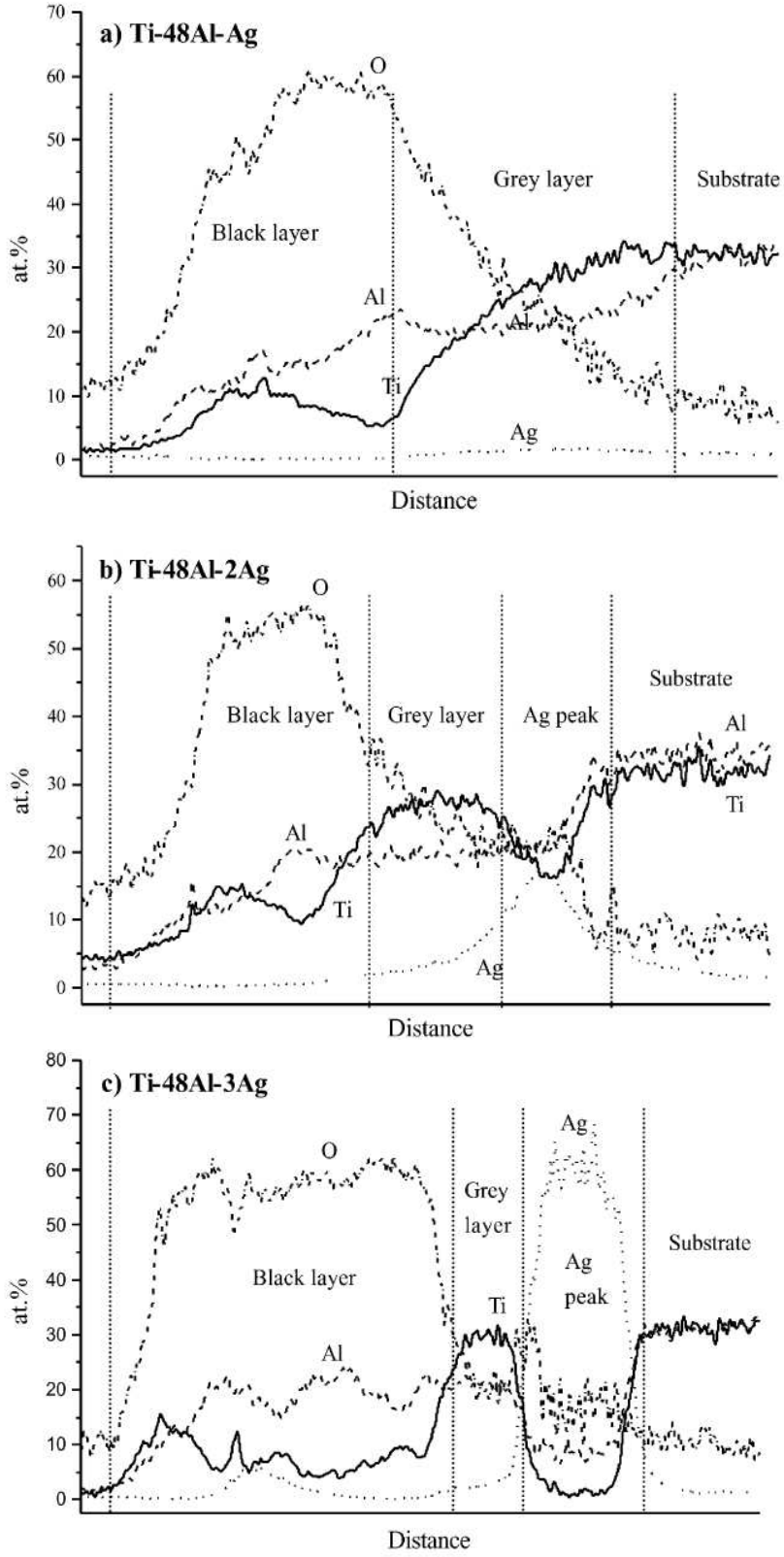

Figure 79 EDS investigations of exposed to hot corrosion/oxidation treatment at 20%NaCl80%Na_2SO_4 at 1073 K for 200 hours: A) Ti48Al1Ag, B) Ti48Al2Ag, and C) Ti48Al3Ag [114]

The best corrosion resistance was achieved for Ti48Al2Ag alloy, due to suppression of formation of α_2-Ti_3Al by stabilizing the Z-phase ($Ti_{50}Al_{30}O_{20}$) beneath the oxide scale. The mechanism of formation Z-phase was discussed previously [115]:

Reaction 94 $\gamma - Ti_{50}Al_{48} + 20O \rightarrow Z - Ti_{50}Al_{30}O_{20} + 18Al$

The stoichiometry of this reaction is approximate, it was suggested that the transformation from γ to Z phase requires a little amount of titanium.

On other hand the addition of 1 at% of silver is not enough to stabilize Z-phase formation in contrast to 3 at% of silver which produce a thick silver enriched layer that decreases the stability of Z-phase. The addition 2 at% of Ag to Ti48Al alloy stabilizes the Z-phase and provides the best corrosion resistance for Ti48Al alloy. The mass gain results show, that the addition of 2 and 3 at% has a similar effect for kinetic data obtained for exposed samples **(Fig 80).**

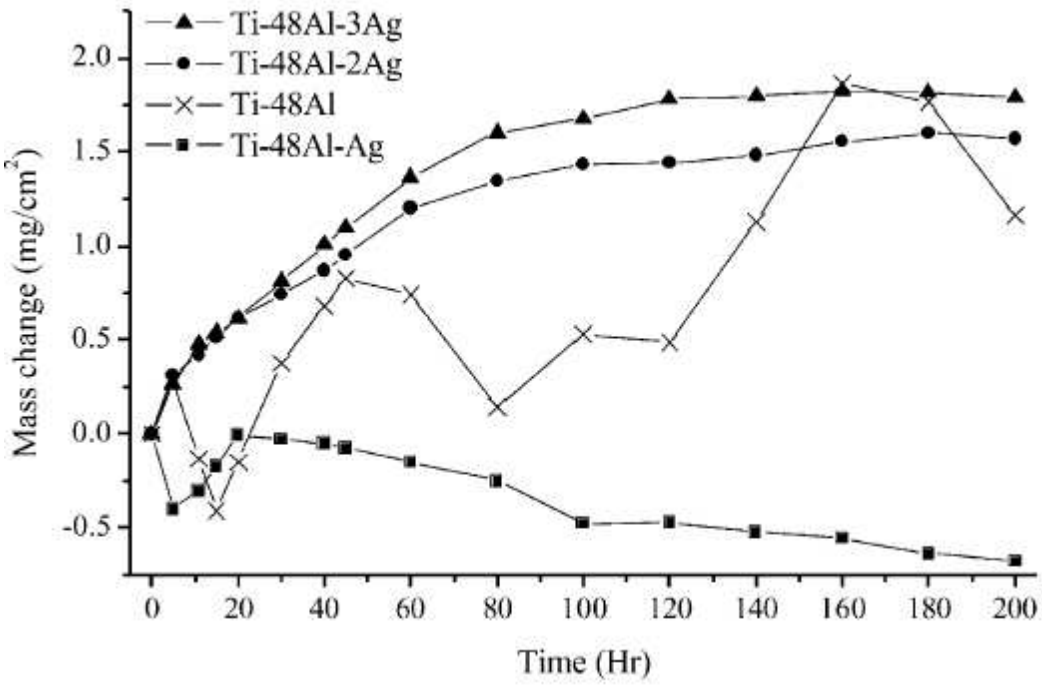

Figure 80 Hot corrosion mass change of TiAl alloy with Ag addition in 20%NaCl80%Na_2SO_4 salt vapour at 1073 K [114]

However the results of hot corrosion/oxidation of Ti48Al1Ag, Ti48Al2Ag, and Ti48Al3Ag in 20%NaCl80%Na_2SO_4 at 1073 K for 200 hours reported by Zhang [114] are not very clear. It has been reported that the addition of 2 at% of silver has a

beneficial effect for the hot corrosion/oxidation of Ti48Al alloy, but mass gain obtained for both alloys (Ti48Al2Ag and Ti48Al3Ag) are very similar. Clarify further work is necessary involving prolonged exposure to high temperature/oxidation agents.

Gurrappa [116] proposed a mechanisms of the scale degradation induced by hot corrosion of Ti alloys (IMI 834, the composition given below).

Ti	Al	Sn	Zr	Nb	Mo	Si	C	Fe	O	N
Balance	5.8	4.06	3.61	0.60	0.54	0.32	0.05	0.009	0.105	0.002

Table 21 Chemical composition of α - Ti alloy IMI 834 (wt %) [116]

In this work the alloy was exposed to different salt mixture including: pure Na_2SO_4, 10%NaCl90%Na_2SO_4, 5%NaCl5%$V_2O_5$90%Na_2SO_4 at 873 and 973 K respectively. It was observed that the IMI834 alloy undergoes by pitting – type corrosion in the presence of NaCl. Degradation of IMI834 alloy takes place due to the reactions between oxide scale (Al_2O_3 and TiO_2) with chlorine and sulphur at 873 K in 10%NaCl90%Na_2SO_4 **(reactions 95 – 109).**

The author suggested a degradation mechanism which is similar to those presented earlier [108 - 111]. In the initial period of the experiment, the alloy developed mainly TiO_2 oxide with some of islands of Al_2O_3. Titanium oxide started to react with chlorine derived from the decomposition of NaCl salt;

Reaction 95 $NaCl \rightarrow Na^{+} + Cl^{-}$

Reaction 96 $TiO_2 + 2Cl^{-} \rightarrow TiCl_2 + O_2$

Reaction 97 $Al_2O_3 + 3Cl^{-} \rightarrow AlCl_3 + \frac{3}{2}O_2$

The generated chlorides ($TiCl_2$ and $AlCl_3$) developed during reactions between the oxide scales (TiO_2 and Al_2O_3) of IMI 834 alloy and aggressive environment starts to decompose via following reaction:

Reaction 98 $TiCl_4 \rightarrow Ti^{4+} + 4Cl^{-}$

Reaction 99 $AlCl_3 \rightarrow Al^{3+} + 3Cl^{-}$

The released titanium and aluminium ions start to react with oxygen on the top of the scale where partial pressure of oxygen is high. Through these reactions new layers of the non protective scale (TiO_2 + Al_2O_3) are formed:

Reaction 100 $Ti^{4+} + 2O^{2-} \rightarrow TiO_2$

Reaction 101 $2Al^{3+} + 3O^{2-} \rightarrow Al_2O_3$

Furthermore oxygen ions (O^{2-}) were consumed in the formation of oxides and hence due to the lack of oxygen in the atmosphere Na_2SO_4 starts to decompose, according to the following reactions:

Reaction 102 $Na_2SO_4 \rightarrow Na_2O + SO_3$

Reaction 103 $SO_3 \rightarrow SO_2 + \frac{1}{2}O_2$

Reaction 104 $SO_2 \rightarrow \frac{1}{2}S_2 + O_2$

The released sulphur **(reaction 104)** may migrate to the oxide scale (TiO_2+Al_2O_3) and forms TiS due to the higher affinity to Ti than Al.

Reaction 105 $Ti + S_2 \rightarrow TiS$

Furthermore TiO_2 and Al_2O_3 (oxide scale) react with Na_2O released from decomposition of Na_2SO_4 according to the following reactions:

Reaction 106 $TiO_2 + Na_2O \rightarrow Na_2TiO_3$

Reaction 107 $Al_2O_3 + Na_2O \rightarrow NaAlO_2$

Titanium and aluminium oxides from the top of the scale developed on IMI 834 are non adherent and non protective and spall very easily from the substrate. Chlorine released from the decomposition of NaCl and from volatile chlorides ($TiCl_2$ and $AlCl_3$) reacts with TiO_2 to produce again volatile chlorides:

Reaction 108 $TiO_2 + 2Cl^- \rightarrow TiCl_2 + O_2$

Reaction 109 $Al_2O_3 + 3Cl^- \rightarrow AlCl_3 + \frac{3}{2}O_2$

Subsequently titanium diffuses outward from deeper region of the material and causes depletion of titanium in the substrate (IMI834). When titanium diffuses outward, oxygen diffuses inward to penetrate the alloy and form an oxygen dissolution region due to high oxygen solubility in titanium alloys [117].

The author suggested a similar reactions for aluminium, these postulated reactions are not very correct; in fact aluminium was in the alloy, but alloy contains only 5, 8 wt% of Al, some of this amount was consumed for reactions with chlorine **(reactions from 95 to 109)** and reactions with Na_2O **(reaction 107)**, what is not sufficient amount to develop a continuous Al_2O_3 scale and enough resist oxide layer (instead of γ-Al_2O_3 other form of Al_2O_3 could develops: κ- Al_2O_3, β-Al_2O_3, θ-Al_2O_3 which are not as resist as γ-Al_2O_3).

Furthermore author does not mention about the role of vanadium oxide (V_2O_5) from salt mixture (5%NaCl5%$V_2O_5$90%Na_2SO_4) in degradation mechanism at high temperature.

Vanadium oxide is often present, in a low quality fuel or in ashes from combustion processes. As reported by Samuel [118] the most resistant alloys for vanadium contaminations are cobalt and nickel base alloy; and the chromium and nickel – containing chromium steels are the least resistant, even less than Fe – base alloys. Linblad [119] determined the aggressivity of the ashes with vanadium content; it was suggested that the higher aggressive character of vanadium oxide (V_2O_5) increases with increasing of oxygen content, at the reacting atmosphere; with a low content of oxygen, vanadium oxide does not react with alloys, or produce only a thin film.

Moreover V_2O_5 is more aggressive in the presence of sulphides or sulphur oxides (SO_2, SO_3). The alloys subjected to vanadium corrosion produce porous and thick scales, which are likely to spall off from the material. The aggressiveness of V_2O_5 sufficiently increased in the presence of Na_2SO_4 was reported by Reidler [120]. This effect is due to the presence of liquid eutectics (sodium vanadates phase) with low melting point, produced by the following reactions:

Reaction 110 $V_2O_5 + Na_2SO_4 \rightarrow 2NaVO_3 + SO_3$ **(Melting point 903 K)**

Reaction 111 $V_2O_5 + 2Na_2SO_4 \rightarrow 2Na_4V_2O_7 + 2SO_3$ **(Melting point 908 K)**

Reaction 112 $V_2O_5 + 3Na_2SO_4 \rightarrow 2Na_3VO_4 + 3SO_3$ **(Melting point 1123 K)**

The vanadates are highly aggressive and attack oxide scales by a fluxing process **(reactions 110, 111, and 112).** The acceleration of degradation reaction depends on oxygen diffusion in liquid phase (product of reaction).

Another mechanism of degradation of the hot corrosion was proposed by Bartlett [121]. Bartlett suggested that V_2O_5 considerably decreases the decomposition temperature of Na_2SO_4.

The decomposition of sodium sulphate produces SO_3; this gaseous phase is subject to further decomposition via reaction:

Reaction 113 $$SO_3 \rightarrow SO_2 + \frac{1}{2}O_2 \uparrow$$

The released oxygen has a high reactivity (O^{2-} is free ion and needs to react to form a compound) and can migrate into the material and causes catastrophic corrosion. At the beginning of the corrosion process of the oxide scale developed in vanadium environment is adherent to the substrate, afterward a liquid eutectics (metal – vanadium eutectic; $NaVO_3$) formation causes a catastrophic corrosion [120]. The catastrophic corrosion mechanism is presented in **figure 81**:

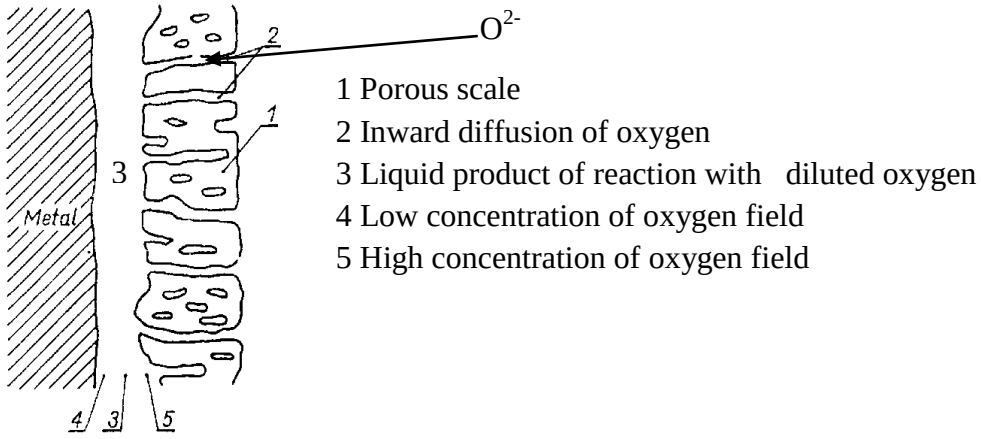

Figure 81 Mechanism of catastrophic corrosion induced by V_2O_5 phase [3]

Mechanism of degradation TiAl alloys induced by a mixture of Na_2SO_4 and V_2O_5 has not been established. The mechanisms of degradation of nickel base alloy or FeAl intermetallic can be considered as a preliminary pointer to TiAl alloy degradation.

Hot corrosion at 1223 K for 10 hours of Ni base alloy (INCONEL 601) coated with zircona 8wt% ytria (YSZ) ceramic coating with/without Al_2O_3 top coat was investigated by Wu [122].

The studies were carried out in salt mixtures Na_2SO_4 + (0 – 15%V_2O_5). The mechanism of degradation of Ni base alloy was estimated for different scenarios; in pure Na_2SO_4 and with V_2O_5 addition.

When Na_2SO_4 is exposed to 1223 K it starts to react with V_2O_5 (from salt mixture) according to the reactions:

Reaction 114 $Na_2SO_4 + V_2O_5 \rightarrow 2NaVO_3 + SO_3$

Furthermore, the formation of oxides (Cr_2O_3, Al_2O_3, or SiO_2) decreased amount of oxygen in atmosphere and causes decomposition of Na_2SO_4

Reaction 115 $Na_2SO_4 \rightarrow Na_2O + SO_3$

Reaction 116 $SO_3 \rightarrow SO_2 + \frac{1}{2}O_2$

Reaction 117 $SO_2 \rightarrow \frac{1}{2}S_2 + O_2$

The released sulphur **(reaction 117)** may diffuse inward (through cracks in oxide scale (Cr_2O_3, Al_2O_3, or SiO_2) and creates sulphides (Cr_2S_3, Al_2S_3) beneath the oxide scale.

Molten salt exhibits acid/base chemistry with the basic component Na_2O and the acid component SO_3. As the activity of Na_2O increases the activity of SO_3 decreases and vice versa; thus hot corrosion may induce fluxing mechanism – basic or acidic; when the activity of Na_2O is high, alumina can react with Na_2O and dissolve in molten sulphate by basic fluxing:

Reaction 118 $Na_2SO_4 + Al_2O_3 \rightarrow NaAlO_2 + SO_3 \uparrow$

Basic fluxing consumes oxide ions in the melt and releases complex ions
For low activity of Na_2O (acidic fluxing):

Reaction 119 $Na_2SO_4 + Al_2O_3 \rightarrow Al_2(SO_4)_3 + SO_3 \uparrow$

In the case when Na_2O and SO_3 are in the intermediate range, alumina is stable. The addition of V_2O_5 forms a liquid eutectic (melting point (903 K) with Na_2SO_4, via following reaction:

Reaction 120 $V_2O_5 + Na_2SO_4 \rightarrow 2NaVO_3 + SO_3$

When YSZ/Al_2O_3 system is exposed to high temperature 1223 K [122], the system becomes covered by the liquid phase ($NaVO_3$). Aluminium oxide and $NaVO_3$ due to exposure to high temperature form a liquid phase at 610^oC (883K), according to phase diagram published by Klinkova [123].

In this situation the metal oxides: Al_2O_3, Y_2O_3 react with the liquid phase of $NaVO_3$ via following reactions:

Reaction 121 $$Al_2O_3 + 2NaVO_3 \rightarrow 2AlVO_4 + Na_2O$$

Reaction 122 $$Y_2O_3 + 2NaVO_3 \rightarrow 2YVO_4 + Na_2O$$

Due to the formation of a liquid phase degradation of aluminium oxide top coat and Y_2O_3 layer occurs. It was suggested in this study [122] that Al_2O_3 protects material against hot corrosion when concentration of V_2O_5 is less than 5wt%.

Similar results were obtained by Rodriguez and Haro [124], the author investigated 25Cr35Ni0.45C, Fe35Cr45Ni with 0.12 and 0.45C addition at V_2O_5 + Na_2SO_4 melts at temperatures above 1073 K. The mechanism of degradation of heat resistant alloy in aggressive environment starts from oxidation of the alloy.

During the oxidation process, oxides develop (Al_2O_3, Cr_2O_3, and Fe_2O_3) and then these oxides start dissolution in molten salts (80%V_2O_5 and 20%Na_2SO_4 (wt %))

At the beginning, the mixture of salts (80%V_2O_5 and 20%Na_2SO_4 (wt %)) starts to melt when reach the melting point temperature (903 K). Possible reactions of molten mixture are shown:

Reaction 123 $$Na_2SO_4 + V_2O_5 \rightarrow 2NaVO_3 + SO_3$$

Reaction 124 $$Na_2SO_4 \rightarrow Na_2O + SO_3$$

Reaction 125 $$Na_3VO_4 \rightarrow V_2O_5 + 3NaVO_3$$

The formation of suitable oxides (Cr_2O_3, NiO, and Fe_2O_3) cause a depletion of oxygen in the salt melts. The depletion of oxygen causes decomposition of Na_2SO_4 according to the following reaction:

Reaction 126 $$Na_2SO_4 \rightarrow Na_2O + SO_3 \rightarrow SO_3 \rightarrow SO_2 + \frac{1}{2}O_2 \uparrow$$

Reaction 127 $$SO_2 \rightarrow \frac{1}{2}S_2 + O_2$$

The released oxygen and sulphur **(reaction 127)** penetrate the cracks and the pores in the oxide scale and reach the scale/alloy interface.

It was suggested that sulphides (Cr_2S_3, NiS, and Fe_2S_3) were detected in an inner part of the scale.

In the case of pure Na_2SO_4 J.G Gonzalez – Rodriguez, Haro [124] considered other mechanisms; they suggested that the formed oxides (Cr_2O_3, NiO, and Fe_2O_3) are dissolved according to:

Reaction 128 $NiO + Na_2SO_4 \rightarrow NiSO_4 + Na_2O$ (acid dissolution)

Reaction 129 $\frac{1}{2}Cr_2O_3 + \frac{3}{2}Na_2SO_4 \rightarrow Cr_2(SO_4)_3 + \frac{3}{2}Na_2O$ (acid dissolution)

Reaction 130

$$\frac{1}{2}Fe_2O_3 + \frac{3}{2}Na_2SO_4 \rightarrow Fe_2(SO_4)_3 + \frac{3}{2}Na_2O \text{ (acid dissolution)}$$

In pure V_2O_5, degradation of alloys at high temperature is according to general reaction which takes place:

Reaction 131 $M_2O_3 + V_2O_5 \rightarrow 2MVO_4$

Work generated by Rodriguez [124] can be used as a basis for TiAl intermetallic degradation mechanism induced by hot corrosion.

In fact not much work or even any work has been carried out to generate degradation mechanism induced by Na_2SO_4 and V_2O_5 on TiAl alloys.

Furthermore if these alloys need to be used in future it is essential to establish a model for degradation of TiAl in Na_2SO_4 + V_2O_5. It can be suggested that TiAl mainly develop TiO_2 and Al_2O_3 (α or β) oxides at temperature above 873 K. As a result of the reactions between oxides and salts, probably the products of reactions are generated by following reactions:

Reaction 132 $2TiO_2 + 4Na_2SO_4 \rightarrow Ti_2(SO_4)_4 + 4Na_2O$ (acid dissolution)

Reaction 133 $\frac{1}{2}Al_2O_3 + \frac{3}{2}Na_2SO_4 \rightarrow Al_2(SO_4)_3 + \frac{3}{2}Na_2O$ (acid dissolution)

It is important to note that it needs to be considered that Na_2SO_4 will decompose according to the reactions:

Reaction 134 $Na_2SO_4 \rightarrow Na_2O + SO_3 \rightarrow SO_3 \rightarrow SO_2 + \frac{1}{2}O_2 \uparrow$

Sulphur oxide and free oxygen may oxidise and sulphidize the inner part of the scale to promote the development of sulphides or oxides.

Chapter II – Section 4 – Interdiffusion modelling – Short Literature Review

Ch.II.Sec.4.1 Introduction

Darken [125] proposed method to describe interdiffusion process observed in materials. In his model he assumed that the total mass flux is a sum of the diffusion flux and the drift flux. The drift velocity is a physical (real) velocity of an "ideal" marker placed in the diffusion zone. This velocity called Kirkendall effect [126]. In this paper Darken's method for multi-component non-ideal open systems will be presented. The equations of mass conservation, the postulate of constant molar volume of the system and the appropriate initial and boundary conditions allow computation of the concentration profiles of the components and the drift velocity in the interdiffusion zone. The main advantages of this method are the generalized initial and boundary conditions, which allow the quantitative analysis of the interdiffusion process for the arbitrary initial concentration profiles of the components in the open as well as in the closed systems.

Advanced materials are very often multi-component and have complex structure (gradient materials, coatings, etc.) and from the thermodynamic point of view are non-ideal. Interdiffusion and interfacial reactions play important role during processing of many functional materials and limit their long-term exploitation. Understanding of these processes has fundamental practical importance. There are different approaches to reach this goal. These are Onsager phenomenology [127] and Darken method [125], they differ in form of the constitutive flux formula. From Darken point of view flux formula can be described as following:

Equation XLVII

$$J_i = J_{i,d} + \rho_i \upsilon$$

Where:

J_i - flux of i-th element, $J_{i,d}$ - diffusion flux, $\rho_i \upsilon$ - drift flux. Differ approach is presented by Onsager, he say that flux can be written as following:

Equation XLVIII

Where:

$$Ji = \rho i \upsilon i - u$$

Equation XLIX

$$u = \sum_{i=1}^{r} \frac{\rho_i \upsilon_i}{\rho}$$

Where: u is denote as velocity of the local centre of mass, J_i - flux of i-th element, ρ_i - density of i-th element and υ_i - velocity of i-th element.

Investigations of multi-component diffusion based on the Onsager concept are usually restricted to the determination of interdiffusion coefficients and fluxes in ternary systems. The use of Onsager phenomenology for more than four-component systems is unattainable due to the serious theoretical and experimental obstacles.

The Onsager phenomenological scheme is useful in describing the diffusion in a closed system. In the open system the translation velocity usually does not vanish [128] and consequently interdiffusion in the multi-component open system cannot be described by a simple extension of the methods currently in use.

The description of interdiffusion phenomenon let us consider an isothermal and isobaric multi-component single-phase region in which diffusion occurs in one direction only. The two alloys of different composition and/or components are joined together to form a diffusion couple. Now on the components start to diffuse from high concentration to low concentration regions. When any compound interacts with a field, resulting in a gradient of chemical potential, the different elements respond in different ways. In the case of multi-component solutions the force, being a result of chemical potential gradient, causes the atoms of a particular component move with a velocity υ_i, which may differ from the velocity of the atoms of the other elements. Because the system is common for the components, all the fluxes are coupled and their local changes may affect the common system drift velocity υ. This phenomenon is called interdiffusion. Because of interdiffusion the concentration profiles of all components are affected. At the end of the process all elements become homogeneous and interdiffusion ends.

Ch.II.Sec.4.2 Generalized Darken Method for Multi-component Alloys

Ch.II.Sec.4.2.1 Formulation of the Model

In this section formulation of the model, i.e., the initial boundary-value problem for the interdiffusion in multi-component non-ideal oxidized alloy is presented in a classical way, i.e., presenting data, physical laws, initial and boundary conditions and finally the unknowns to be calculated.

Ch.II.Sec.4.2.2 Data

1. $M_1,...,M_r$ - molar masses of the elements, where r - is the number of components in the alloy;
2. Λ - a position of the alloy/scale interface ;
3. $\overset{o}{c}_1 = \overset{o}{c}_1(x),...,\overset{o}{c}_r = \overset{o}{c}_r(x)$ - the initial distributions of the components, such that:

Equation L $$c_{alloy} = \overset{o}{c}_i = \text{const.}$$

where c_{alloy} is the molar concentration of the system;

4. $D_1^* = D_1^*(N),...,D_r^* = D_r^*(N)$ - self diffusion coefficients of the components, which may depend on components' molar fractions, $N = (N_1,...N_r)$;
5. $\mu_1 = \mu_1(N),...,\mu_r = \mu_r(N)$ - the chemical potentials of the components as functions of components' concentration;
6. $\hat{t}$ - the time of the process duration;

$j_{i\Lambda}(t),\ i = 1,...,r$ - Evolution of mass flow of the i-th component through the alloy/scale interface.

Ch.II.Sec.4.2.3 Physical Laws

7. **Law of the mass conservation of an i-th element**. That law tells that a local change of density of an i-th element is a result of its net in- or outflow only:

Equation LI
$$\frac{\partial c_i}{\partial t} + \frac{\partial J_i}{\partial x} = 0 \quad i = 1,\ldots,r.$$

Following Darken's drift flow idea, it is postulated that the flux of an i-th element, J_i, is a sum of its diffusion flux, J_i^d, and the drift flux, $(c_i \upsilon)$:

Equation LII
$$J_i := J_i^d + c_i \upsilon.$$

The effective solution of Darken's model for non-ideal multi-component systems can be obtained when the diffusion flux is expressed by [129]:

Equation LIII
$$J_i^d = B_i c_i \sum_j F_j,$$

where B_i is the mobility of an i-th element and $\sum_j F_j$ - the sum of the internal or external forces which act on a system. It is generally accepted, that the diffusion force in the **equation LII** can be described as the spatial gradient of the chemical potential, μ_i, and the corresponding flux can be expressed by the following expression:

Equation LIV
$$J_i^d = -B_i c_i \frac{\partial \mu_i}{\partial x}.$$

The gradient of the chemical potential can be calculated as follows:

Equation LV
$$\frac{\partial \mu_i}{\partial x}(c) = \sum_{j=1}^{r} \frac{\partial \mu_i}{\partial N_j}(c) \frac{\partial N_j}{\partial x}.$$

where $c = (c_1,\ldots, c_r)$.

Using **equations LIV and LV** the diffusion flux can be expressed in the form

Equation LVI
$$J_i^d = -B_i c_i \sum_{j=1}^{r} \frac{\partial \mu_i}{\partial N_j} \frac{\partial N_j}{\partial x}.$$

Substituting the Nernst-Einstein relation $(D_i^* = B_i kT)$ into **Eq. LVI**, we get

Equation LVII
$$J_i^d = -\left(D_i^* / kT\right) c_i \sum_{j=1}^{r} \frac{\partial \mu_i}{\partial N_j} \frac{\partial N_j}{\partial x}.$$

Above diffusion flux formula can be rearranged to the final form

Equation LVIII
$$J_i^d = -\sum_{j=1}^{r} D_{ij} \frac{\partial N_j}{\partial x},$$

Where the partial intrinsic diffusivities, D_{ij}, are defined as follows:

Equation LIX
$$D_{ij}(c) := \left(D_i^*(c) / kT\right) N_i \sum_{j=1}^{r} \frac{\partial \mu_i}{\partial N_j}(N).$$

8. **A postulate of the constant molar volume of the alloy**. Consequently the molar concentration of the alloy being a sum of the concentrations of all elements at any position for every time is constant:

Equation LX
$$c_1 + ... + c_r = c_{alloy} = \text{const}.$$

Ch.II.Sec.4.2.4 Initial and boundary conditions

9. The initial concentration distributions of the components in the alloy:

Equation LXI
$$\overset{o}{c}_i(x) = c_i(0, x) \quad i = 1, ..., r.$$

10. The following boundary conditions are postulated:

Equation LXII
$$J_i\left(t, \Lambda\right) = j_{i\Lambda}(t), \; i = 1, ..., r.$$

For the oxidation process (the open system) the functions, $j_{i\Lambda}(t)$, can be calculated e.g. from the known rate of reactions at the boundary or from the experimental data. The flux of component at the alloy/scale interface, ($x = \Lambda$), which is oxidised (forms a scale) can be expressed as follows:

Equation LXIII
$$J_i(t, \Lambda) = J_i^{diff}(t, \Lambda) + c_i(t, \Lambda) \frac{d\Delta X}{dt}(t),$$

Where $d\Delta X / dt$ is the rate of the alloy consumption due to oxidation.
The fluxes of the elements in the alloy which do not form a scale equal zero

Equation LXIV
$$J_i(t, \Lambda) = 0$$

And consequently:

Equation LXV

$$J_i^{diff}(t,\Lambda) = -c_i(t,\Lambda)\frac{d\Delta X}{dt}(t).$$

If the scale (oxide) is compact and adheres to the alloy, the rate of the alloy consumption is inversely proportional to instantaneous thickness of the oxide layer, which in turn is proportional to the displacement of the alloy surface ΔX. Thus the rate of the alloy consumption can be expressed as follows:

Equation LXVI

$$\frac{d\Delta X}{dt} = \frac{k_p}{\Delta X}$$

Where k_p is a parabolic rate constant of an alloy consumption. The displacement of the alloy surface due to oxidation can be obtained solving the **equation LXVI:**

Equation LXVII

$$\Delta X = \sqrt{2k_p t}$$

And consequently:

Equation LXVIII

$$\frac{d\Delta X}{dt} = \sqrt{\frac{k_p}{2t}}.$$

Expressions, LXIII, LXIV, **and LXVIII** introduced into equation **LXII** describe boundary conditions for the selective oxidation.

Ch.II.Sec.4.2.5 The unknowns

11. Concentrations of the components in the alloy as functions of time and position, $c_i(t,x),\ i=1,\ldots,r$.

12. A drift velocity as a function of time and position, $\upsilon(t,x)$.

Ch.II.Sec.4.3 Inverse method calculations

Diffusion coefficients by Inverse Method can be calculated in several steps:

1) Perform oxidation or sulphidation (opened system) or diffusion annealing (closed system) experiments,
2) Creates the EDS profiles from the exposed material,

3) In appropriate software (Origin, Excel) it is necessary to build the graph; distance [µm] vs. concentration [at%],

4) The difference between each point (by inverse method) in the concentration profile of several elements (Al, Au, Ti, Nb, or Cr). This calculation can be performed using following equations:

Equation LXIX

$$\frac{c(x)-c_s}{c_0-c_s}=\operatorname{erf}\left(\frac{x}{2\sqrt{Dt}}\right)$$

Equation LXX

$$\operatorname{inverf}\frac{c(x)-c_s}{c_0-c_s}=\left(\frac{x}{2\sqrt{Dt}}\right)$$

$$\underbrace{\operatorname{inverf}\frac{c(x)-c_s}{c_0-c_s}}_{y}=x\cdot\underbrace{\frac{1}{2\sqrt{Dt}}}_{A}$$

$$y=Ax$$

Where: $C_{(x)}$ – is a concentration of the element

$C_{(s)}$ – concentration of the element before diffusion process (initial concentration of the element)

C_0 – concentration of the element in X_0

Above equations is solution of the 2nd Fick's law for constant surface concentration. According to the slope and intercept of linear relationship between $\frac{c(x)-c_s}{c_0-c_s}$ versus x, the interdiffusion coefficients were calculated.

5) The least squares method has been used to compare between the experimental and numerical concentration value for each component.

Equation LXXI

$$\text{Error}=\sum_{i=1}^{N}(Y_i-y_i)^2$$

Yi – Experimental calculations

yi – Modelling calculations

N – Represents the number of points in the concentration profiles

Ch.II.Sec.4.4 Short literature review

It is important to point out, interdiffusion modelling in multicomponent systems have not been studied extensively. Two important pieces of work have been reviewed.

Significant progress has been achieved in the field of interdiffusion modelling in multicomponent systems by Datta, Filipek, and Danielewski [130,131,132,133,134]. The chemical composition of the alloy used in the experiment is shown in **table 22**.

Cr	Al	Ti	Co	W	Ta	Mo	Hf	Fe	Zr	B	C	Ni
9	5.5	1.5	10	10	2.5	0.5	1.25	<0.5	0.1	0	0	Bal.

Table 22 Chemical composition of MAR M002 substrate (wt%) [132]

Calculations were performed of the interdiffusion processes in Pt modified β-NiAl – MAR M002 diffusion couple after diffusion annealing in the temperature range 1073 - 1373 K for 100 hours. **Table 23** shows intrinsic diffusivities used in computed interdiffusion modelling.

Temperature [K]	Intrinsic diffusivities [cm^2/s]				
	D_{Al}	D_{Cr}	D_{Co}	D_{Ni}	D_{Pt}
1073	$2.73x10^{-12}$	$8.59x10^{-13}$	$9.42x10^{-13}$	$2.50x10^{-13}$	$8.30x10^{-13}$
1173	$9.28x10^{-12}$	$4.17x10^{-12}$	$4.17x10^{-12}$	$1.39x10^{-11}$	$6.28x10^{-13}$
1273	$2.49x10^{-11}$	$1.43x10^{-11}$	$1.05x10^{-11}$	$1.68x10^{-11}$	$2.17x10^{-11}$
1373	$5.08x10^{-11}$	$2.77x10^{-11}$	$2.27x10^{-11}$	$1.06x10^{-10}$	$4.22x10^{-11}$

Table 23 Computed diffusion coefficients in the substrate/coating system (Pt modified β-NiAl coating on MAR M002 [133]

The good agreement has been achieved between experimental and simulated concentration profiles for Ni and Al; the simulated results are shown in **figure 82**.

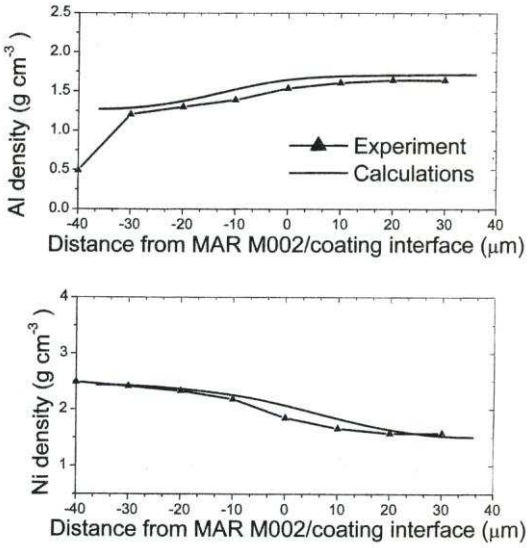

Figure 82 Experimental and simulated Ni and Al profiles [133]

However the disagreement between experimental and simulated results in Pt concentration profiles derived from underestimation of the values of intrinsic diffusivities. This mismatch of Pt concentration profiles is shown in **figure 83**.

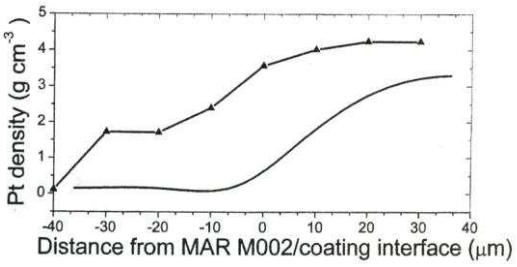

Figure 83 Experimental and simulated Pt concentration profile [133]

The interdiffusion studies by Generalized Darken Method (GDM) of CoFeNi alloys (with different composition) have been performed by Filipek and Danielewski [135]. In this work several diffusion couples were used, the details of experiments are shown in **table 24**.

Diffusion couple	Temperature [K]	Time [hours]
P1	1273	68
P2	1323	50
P3	1373	140
P4	1423	85
P5	1473	59
P6	1523	24
P7	1588	17
P8	1588	131

Table 24 Examined diffusion couples [135]

The intrinsic diffusion coefficients after diffusion annealing treatment (from concentration profiles) have been calculated using the inverse method. The calculated values are shown in **table 25**:

Temperature [K]	Intrinsic diffusion coefficients [cm^2/s]		
	Fe	Co	Ni
1273	$4.97x10^{-12}$	$1.53x10^{-12}$	$7.86x10^{-13}$
1323	$1.78x10^{-11}$	$3.83x10^{-12}$	$3.42x10^{-12}$
1373	$5.78x10^{-11}$	$1.53x10^{-11}$	$1.14x10^{-11}$
1423	$1.21x10^{-10}$	$3.44x10^{-11}$	$2.67x10^{-11}$
1473	$3.22x10^{-10}$	$1.06x10^{-10}$	$5.14x10^{-11}$
1523	$4.86x10^{-10}$	$1.43x10^{-10}$	$1.23x10^{-10}$
1588	$1.20x10^{-9}$	$4.28x10^{-10}$	$2.35x10^{-10}$

Table 25 Calculated intrinsic diffusivities by inverse method [135]

The computed results are shown in **figures 84 and 85.**

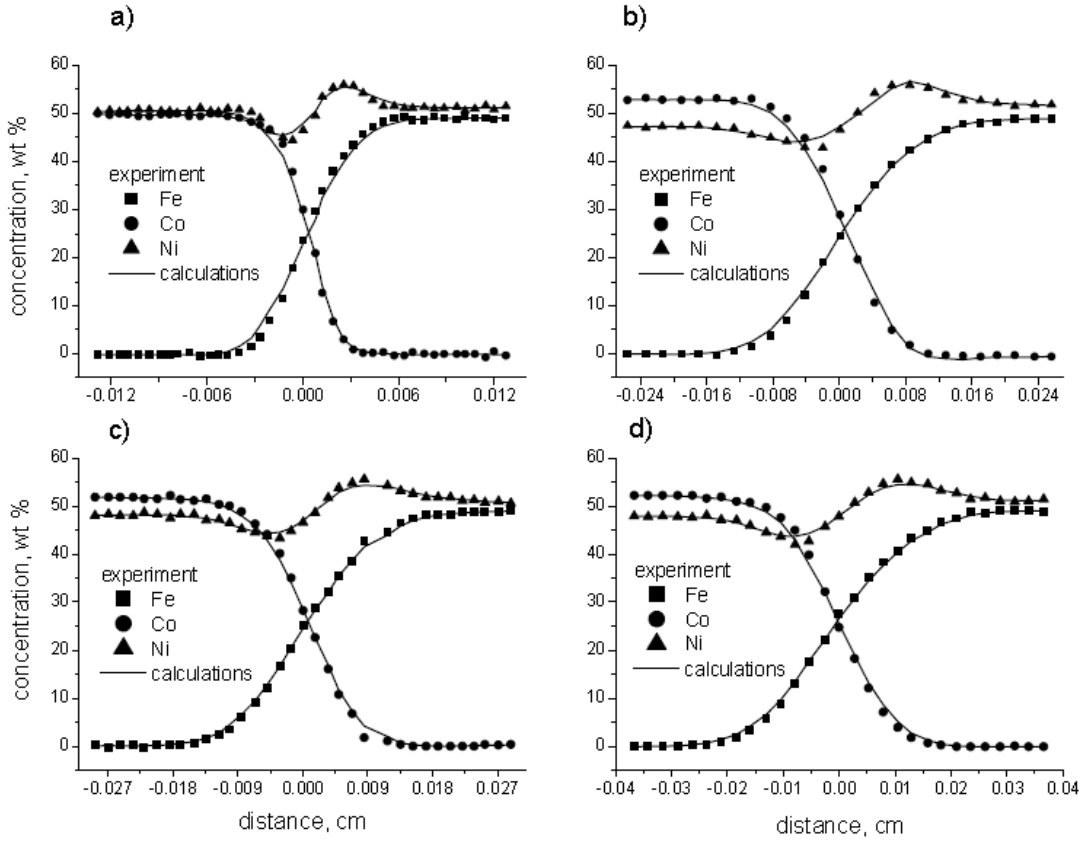

Figure 84 Computed and experimental concentration profiles of diffusion couples; a) P2, b) P3, c) P4, and d) P5 [135]

The excellent agreement between predicted and experimental results derived from intrinsic diffusivities calculated by the inverse method. Additionally authors [135] found that D_{Fe} has a higher value than D_{Ni} and D_{Co} ($D_{Fe} > D_{Ni} > D_{Co}$), what is in good agreement with other studies [136, 137].

Figure 85 shows interdiffusion modelling on CoFeNi diffusion couples (P6, and P7).

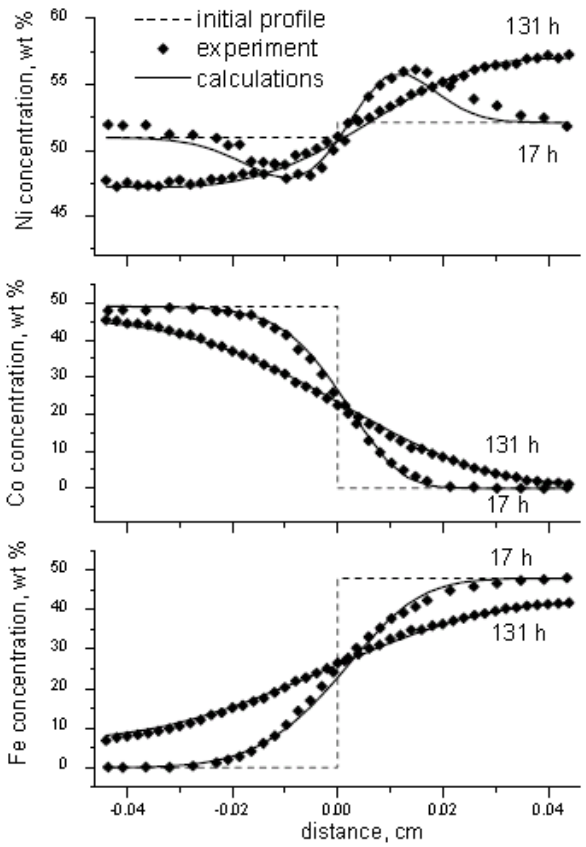

Figure 85 Computed and experimental concentration profiles of diffusion couples; a) P6 and P7 [135]

Chapter III – Deposition Techniques and Coatings

Ch.III.1 Introduction

This chapter of PhD thesis reviews relevant information about deposition techniques and coatings used in this study. The short description of the deposition techniques covers: Unbalanced Closed-Field Magnetron Sputtering System (UBM), High Power Impulse Magnetron Sputtering System/Unbalanced Closed-Field Magnetron Sputtering System (HIPIMS/UBM).

Ch.III.2 Coating Deposition Techniques

Ch.III.2.1 HIPIMS (TiAlYN/CrN + CrAlYON TiAlYN/CrN+Al_2O_3 and TiAlN+ Al_2O_3 coatings)

High Power Impulse Magnetron Sputtering (HIPIMS) is the latest innovation in physical vapour deposition (PVD) technologies. At the present moment the technique is operated on commercial grade industrial size equipment and research is concentrated on the development of novel material systems. HIPIMS is based on conventional magnetron sputtering and shares a similar flexibility in the choice of target materials.

The deposition vapour is generated by sputtering of the cathode due to its interaction with a plasma discharge. The discharge is extremely bright and is homogeneously distributed over the whole area of the cathode providing uniform erosion and a high utilization of the target. As in conventional magnetron sputtering, the discharge is confined by a magnetic field. One of the main differences from the conventional magnetron sputtering is that HIPIMS utilizes extremely high power densities applied in pulses. The power densities required are two orders of magnitude (100 times) greater than in conventional techniques. In order to avoid overheating of the cathode in these extreme conditions, the power is applied in very short repetitive pulses.

Typically, the power density on the cathode reaches values >1 $kWcm^{-2}$ PP equivalent to > 0.5 megawatts on a target of size 500 cm^2. The usual repetition rate is 100 Hz with on-times (duration of power pulse) of ~100 microseconds and off-times (time between pulses) of ~10 000 microseconds. The on-time is only ~1% of the off-time. This ensures that the average power is equivalent to the levels of operation of conventional sputtering. The advantage of HIPIMS over conventional techniques lies just in the utilization of such extreme powers on the target. In these conditions, HIPIMS produces a highly ionized flux containing gas and metal ions.

The plasma produced has an extremely high density (10^{13} per cm^3compared to only 10^{10} ions per cm^3 for conventional sputtering). This in turn allows high fractions of the sputtered metal vapour to be ionized - 30% ionization has been

measured for Cr. In comparison, conventional magnetron sputtering incorporates only 1% of ionized metal ions.

Ch.III.2.2 Deposition strategy of nanocomposite coatings

The deposition used strategy included: Substrate Pre-Treatment, Base Layer Deposition, Superlattice Coating Deposition, and Topcoat Deposition.

Ch.III.2.2.1 Substrate pre-treatment

All TiAl intermetallic substrates were polished with 1 μm diamond paste in the final stage, to obtain surface roughness Ra ≤ 0.01 μm. The substrates were cleaned in heated ultrasonic baths including aqueous based alkali detergents and de-ionized water for cleaning. After cleaning the samples were dried in vacuum by radiation heating shortly before being loaded into the vacuum chamber to minimize the effect of water vapour condensation on the substrate surface. Cleaned substrate of Ti45Al8Nb alloy was firstly treated by chromium ions generated by a HIPIMS discharge to promote high adhesion. High bias voltage in the range of Ub= -1200V was applied to the substrate to produce a low energy Cr ion implantation and achieve high adhesion of the coating.

Ch.III.2.2.2 Base Layer Deposition

Two sources furnished with TiAl targets were operated in unbalanced magnetron sputtering mode in a mixed N^{2+} Ar^{+} atmosphere to deposit TiAlN base layer. This layer provided smooth transition in hardness and residual stress and therefore contributed to further adhesion enhancement.

Ch.III.2.2.3 Superlattice Coating Deposition

All sources operated at preselected high power in a mixed N^{2+} and Ar^{+} atmosphere. The substrate table was rotated with a defined rotation speed. The

TiAlYN/CrN and TiAlYN/CrN + CrAlYON nanoscale multilayer formed due to the sequential exposure of the sample surface to the material fluxes from the four sources. The bi-layer thickness, (superlattice period), a parameter which defines the performance characteristics of the coating was controlled by the power dissipated on the targets, the rotation speed, the applied bias voltage and reactive gas partial pressure.

Ch.III.2.2.4 Top coat deposition

The Al_2O_3 process was made from sputtering of an Al target in an O_2 and Ar atmosphere. The deposition was made by using one source in sputtering mode either by pulsed DC or by HIPIMS discharge. To control the amount of oxygen during the Al_2O_3 deposition, a feedback control loop to regulate the oxygen flow was used. This will ensure that the correct stoichiometry in the Al_2O_3 coatings was achieved.

Ch.III.2.3 UBM – Unbalanced Magnetron Sputtering System

The magnetron discharges are cold cathode discharges within a magnetic field the operating pressures is around $p < 7.5x10^{-6}$ Pa with current densities equal to 0.01-0.1 Acm^{-2} for the cathode and negative discharge voltages Ud of 700-1000 V [138]. Electrons in the plasma travel on helical trajectories along the magnetic field lines and are confined near the target surface. This confinement acts as trap for the plasma. This confinement provides high density plasma with a high collision probability between electrons and sputtered metal atoms. The metal ionization is then initiated by electron impact which is the main ionization and excitation mechanism in magnetron discharges [139]. The ionization degrees for metal species in the basic magnetron operation are typically less than 1% and therefore in a similar range to the basic sputtering process described earlier [140].

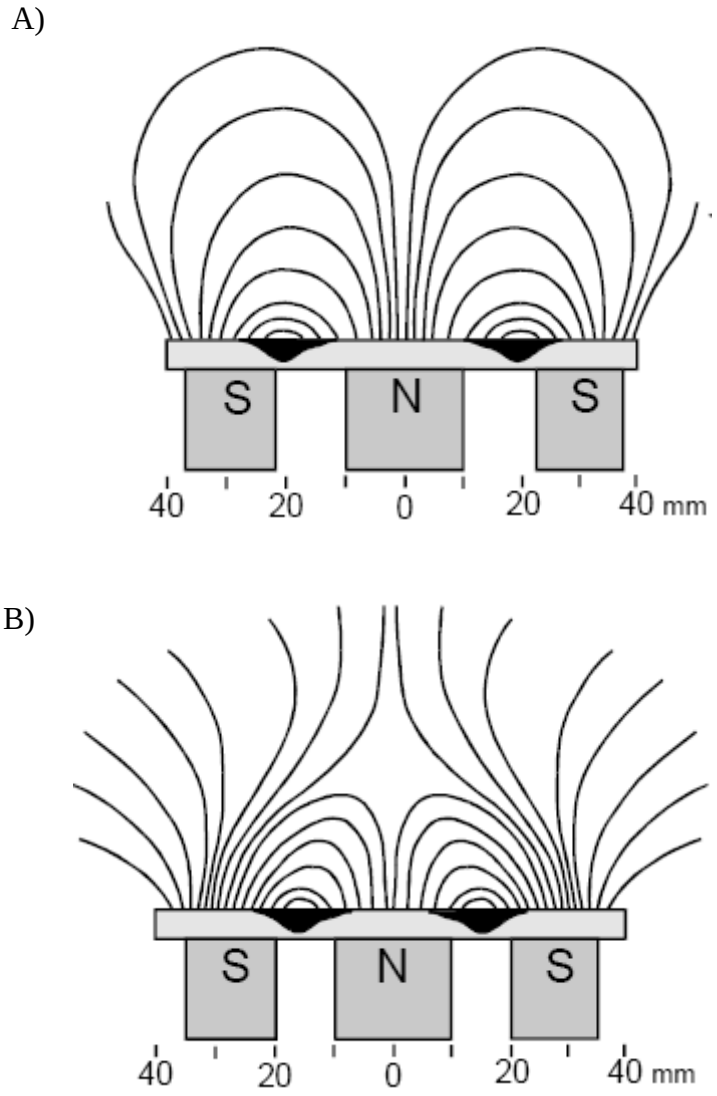

Figure 86 Magnetic field lines in (a) a conventional, balanced magnetron and (b) and unbalanced magnetron [142]

A method to enhance the ionization and ion flux to the substrate was introduced by unbalancing the magnetron magnetic field [141,142]. Here, the magnetic field lines are changed by strengthening the outer poles of the magnets as shown in **figure 86** resulting in some magnetic lines proceeding perpendicular to the cathode surface, while the lines close to the target surface were still arched **(Fig.86A)**. Unbalancing the magnetron significantly improves degree of ionisation with maximum metal ionization degrees of 5% [139]. The ion flux to the substrate increases strongly at the same time. Some electrons no longer remained confined to the near-target region, but are able to follow the magnetic field lines towards the substrates **(Fig.86B)**. The ions are forced to follow the electron movement due to the

ambipolarity of the plasma medium and, as a consequence, the ion bombardment at the substrate is increased. This ion bombardment during coating growth, in turn, enhances the density of deposited coatings. A further increase in ionization levels can be achieved by using multiple- magnetron systems in a closed field assembly also referred to as closed field-UBM.

Ch.III.2.3.1 UBM Coatings

Ch.III.2.3.1.1 CrAl2%YN coating

The CrAl2%YN and TiAlN + Al_2O_3 topcoat coatings were produced by Unbalanced Closed-Field Magnetron Sputtering System and deposited on polished samples of uncoated alloy (Ti45Al8Nb). The 3 – 4 µm thick coatings were produced under Ar + N_2 glow discharged TiAl and CrAl compound targets with different Y contents. The polished uncoated alloy (Ti45Al8Nb) was placed above a target in distance equal to 50 mm. Placed sample (Ti45Al8Nb) was then coated from both sides. The fresh CrAlYN coatings with Al/Cr ratio of 1.2 and YN mole fraction equal of 0, 2 exhibited the NaCl phase structure [143,144].

Ch.III.2.3.1.2 TiAlCr and TiAlCrY intermetallic coatings

The Ti42Al15Cr [at%] and Ti55Al14Cr0.3Y [at%] (Y as a dopant element was introduced in order to improve a selective oxidation of Al [145]) coating with the composition of TiAlCr were produced by unbalanced close field magnetron sputtering system. The TiAlCr coatings consist of γ-TiAl and TiAlCr Laves phase. The high content of Cr was introduced in order to enhance the selective oxidation of Al [146]. The sputtering parameters were as follows: argon pressure 0.2 Pa, power density ca. 4.2 W/cm^2, and substrate temperature 250^{o}C. Several authors noted [147] that TiAlCr alloys containing a minimum of 8-10% Cr exhibited excellent oxidation resistance due to the formation of continuous Al_2O_3 scale. Recently TiAlCr alloys were successfully tested as a coating material for the protection of TiAl. Low-pressure plasma spray Ti-51Al-12Cr coatings and magnetron sputtered Ti-50Al-10Cr

coatings, not only provided an excellent protection for TiAl against oxidation at 1073 – 1223 K, but also exhibited a much better coating/substrate compatibility than conventional aluminide and MCrAlY coatings.

Ch.III.2.3.1.3 Al_2Au intermetallic coating

Al_2Au phase representing Zintl phase with the cubic CaF_2 structure, Al_2Au shows a distinct reflectivity minimum at 545 nm, resulting in a purple-red colour. Being relatively hard and brittle at room temperature, it shows plastic deformation and possibility self-lubrication at high temperatures. With a melting point 1333 K, Al_2Au is the thermally most stable intermetallic phase within Al-Au phase diagram, whereas the other phases $AlAu_2$, Al_2Au_5 and $AlAu_4$ show meting temperatures between 798 and 898 K. Coating used in this study was deposited using unbalanced D.C (direct current) magnetron sputtering system. The coatings (Al_2Au) were deposited onto Ti45Al8Nb material in Ar atmosphere at 0.2 Pa. The substrate temperature, bias voltage and sputter power was 300^{o}C, -50V and 380W. Prior to deposition, all substrates used were metallographically grounded, polished, and ultrasonically cleaned with ethylene and acetone. After target (Al, Au) pre-cleaning and ion etching of the substrates within the deposition chamber, coatings in the thickness range between 0, 1 and 7 μm were deposited [148].

Chapter IV – Methodology and Current Work to Date

Ch.IV.1 Introduction

This chapter of PhD thesis provides the relevant information relating to the base material used in this study (Ti45Al8Nb), experimental work performed in this study on coated and uncoated material, and analytical procedure of exposed samples is also consider.

Ch.IV.2 Experimental

This chapter describes the experimental methodology used to investigate the high temperature degradation behaviour of materials/coatings selected for study in this project.

Ch.IV.3 Materials used

The base material used in this study was TiAl alloy – Ti45Al8Nb. The Ti45Al8Nb consists of mainly γ-TiAl phase with small amount of α_2 – phase Ti_3Al. The specimen with dimensions around 15 x 2 mm were machined from cast alloys and ground with SiC papers up to 1200 grit finish. Prepared alloy specimens were then used as substrates for the deposition of various coatings by different techniques. The types of coatings and the technology of deposition were discussed in **chapter V**.

Ch.IV.3.1 The base material (Ti45Al8Nb)

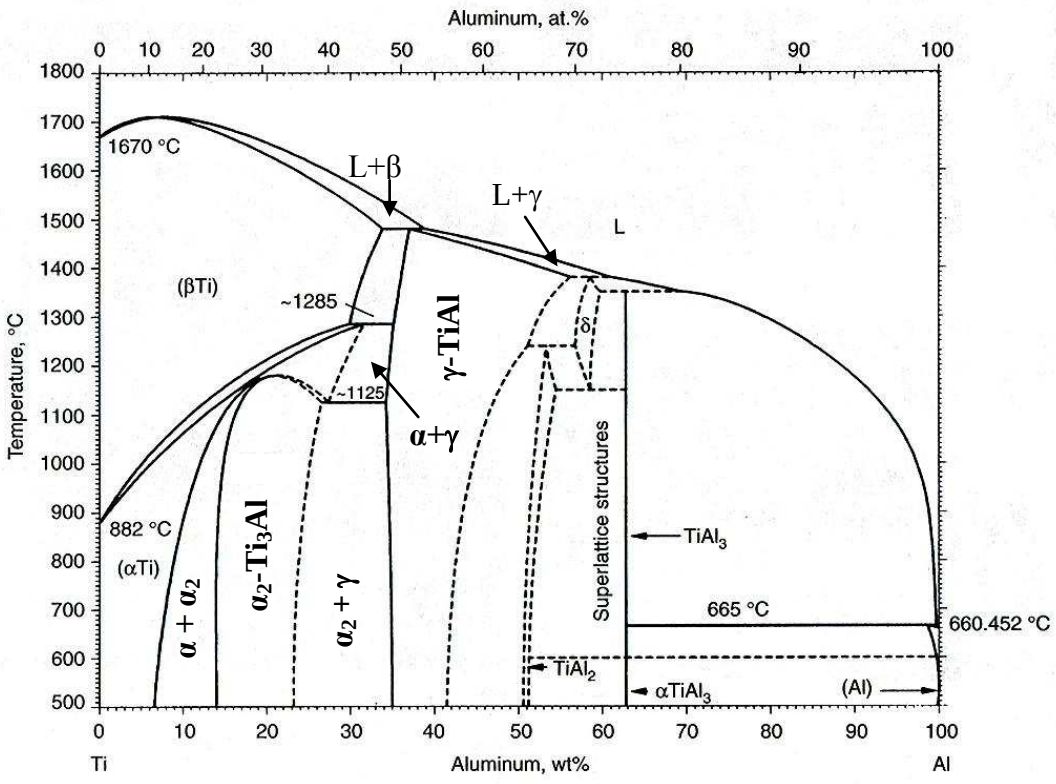

Figure 87 The binary titanium-aluminium phase diagram [149]

Figure 87 shows the binary titanium-aluminium phase diagram. There are four binary intermetallic compounds of interest in the Ti-Al system; Ti_3Al (α_2), TiAl (γ), $TiAl_2$ and $TiAl_3$.

The γ - TiAl phase has a $L1_0$ ordered face cantered tetragonal structure. The crystal structure of the hexagonal α_2 – Ti_3Al is DO_{19}. At the equiatomic TiAl composition the c/a ratio is 1.02 and the tetragonality increases up to c/a = 1.03 with increasing aluminium concentration. The γ-TiAl phase remains ordered up to it is melting point of about 1723 K.

Ch.IV.3.2 The Ti-Al-O phase stability diagram

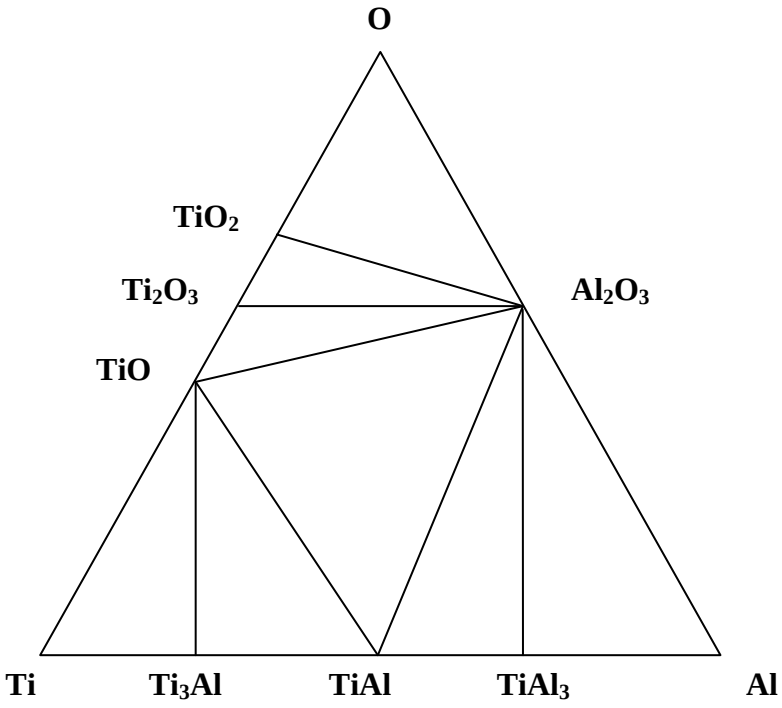

Figure 88 The phase diagram of Al-Ti-O according to Rahmel [150]

Figure 88 presents the phase stability diagram of Al-Ti-O designed by Rahmel and Spencer [150]. Researchers assumed that only Al_2O_3 and TiO oxides are in equilibrium with metal phase. Moreover Luthra [151] found the same conclusions that the change in the oxide stability occurs in the homogeneity range of TiAl. Becker et al. [152] shows that such diagram as presented by [150] does not occur in reality. Becker presented different phase diagram, based on the experimental results

conducted at 1173 K for 1000 hours and analysed by EPMA (Electron Probe Micro-Analysis). Phase diagram prepared by Becker is shown in **figure 89**.

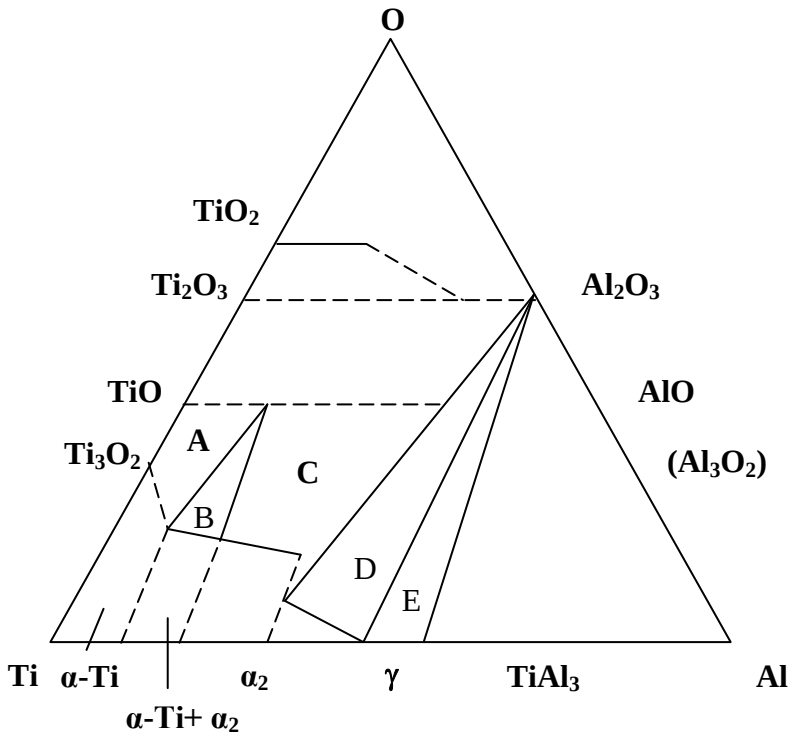

Figure 89 The phase diagram of Al-Ti-O according to Becker [152]

The phase diagram includes:

A) α-(Ti,Al) + oxide

B) α-(Ti,Al) + α_2-Ti_3Al + oxide

C) α_2-Ti_3Al + oxide

D) α_2-Ti_3Al + oxide + γ-TiAl + oxide

E) γ-TiAl + oxide

It is important to note that the α-(Ti,Al) = solid solution of Al in α-Ti. The most important differences between both diagrams are:

1) The α-Ti_3Al phase dissolve 19 – 20at% of oxygen according to [152], and 12 at% of oxygen following the results obtained by Zhang [153]. Gil [154] postulated that Ti_3Al phase can dissolve approximately 20 at% of oxygen, and Gauer [155] found 10 – 12 at% of oxygen within α-Ti_3Al phase

2) A change in the oxide phase in equilibrium with metal phase from Al_2O_3 to $(Ti,Al)_3O_2$ or (Ti,Al)O occurs only in α-Ti_3Al phase; this conclusion is in agreement with results obtained by Becker [152], Zhang [153], and Gil [154].
3) Significant solid solubility exists between the different oxide phases of Al and Ti in the particularly in low valency oxide.
4) Becker [152] suggested that the rich Ti alloy (binary alloy) at 1173 K is not in equilibrium with TiO oxide but with $(Al,Ti)_3O_2$ phase.

The high solubility of oxygen in α_2-Ti_3Al is easy to understand, because the lattice parameter in α_2-Ti_3Al is very similar to the α-Ti phase. At temperature equal to 1173 K α-Ti phase is able to dissolve up to 32 at% of oxygen.

Ch.IV.3.3 The microstructure of TiAl alloys

Most of TiAl alloys include two phases; γ-TiAl as a main phase and additional 3 – 15vol% of α_2-Ti_3Al phase. The α_2-Ti_3Al phase is introduced in γ-TiAl in order to improve the mechanical properties of the bulk material. In general two phases alloy shows a lamellar γ/α_2 structure. It depends on the phase diagram which is shown in **figures 87, 88,** and **89**. During the preparation of the alloy, the material is heated up to 1523 K and then cooled down to room temperature. In this period of heat treatment, the γ-phase remains stable, however α-phase transforms according to the following reaction at 1393 K:

Equation LXXII $$\alpha \rightarrow \gamma \rightarrow \alpha_2$$

The reaction above leads to the formation of a lamellar γ/α_2 structure. Gil [154] observed that when phase with low concentration of Al (α_2-Ti_3Al) which tends to form the non-protective scales, is distributed as fine lamellas, then Al_2O_3 is favourable. Recent results [156] indicates that in the coarse grained microstructure of single phase alloy (γ-TiAl), Al_2O_3 or a mixture of Al_2O_3 and TiO_2 develops in the initial period of oxidation. It is important to note, that during high temperature treatment the transformation from α_2-γ to α-γ at 1393 K develops only non-protective scale, for a correct interpretation of the results the chemical composition needs to be considered.

The base alloy used was Ti45Al8Nb; Nb has been included in the alloy for the following reasons:

The mechanical properties (ductility and toughness) can be improved by addition of Nb to α_2 and γ - Titanium aluminides [157]. It was reported previously [158,159,160] that 2 – 30 wt% addition of Nb decreases the oxidation rate. The scale adherence to the matrix is improved by the addition of Nb ions to TiAl alloy for thermal cyclic oxidation at 1173 K. Addition of Nb also can favour the formation of Al_2O_3 scale in the initial stage of oxidation and suppress further oxidation of the alloy [161]. It was also observed by Tetsui and Ono [158] that the addition of Nb improves the erosion resistance in turbochargers.

Ch.IV.4 Experimental

It is important to say that reproducibility of every point of kinetic measurements (oxidation experiments) was average of three measurements. However in some cases (sulphidation, hot corrosion) due to the difficulty in coating development, the limited number of measurements was carried out.

Ch.IV.4.1 Oxidation, Hot Corrosion and Sulphidation Studies

First each sample was ultrasonically cleaned in acetone for 10 minutes and then weighted using a digital balance (accuracy 10^{-6} g). Having completed this procedure, the samples were then suspended in a high purity alumina ceramic boat before loading into the test furnace at room temperature.

Ch.IV.5 Experiments procedure

Ch.IV.5.1 Oxidation in Static Air Experiment

Oxidation tests were carried out discontinuously. The furnace was loaded with number of samples at the test temperature. After exposure for a predetermined time individual sample/samples was/were withdraw from the furnace, weighted and examined using OM (Optical Microscope), SEM (Scanning Electron Microscope), EDS (Energy Dispersive Spectroscopy), and XRD (X-Ray Diffraction) analysis. This procedure was continued until the end of the test. **Table 26** shows oxidation experiments conducted in this project. Flow chart below shows the oxidation rig used in this project.

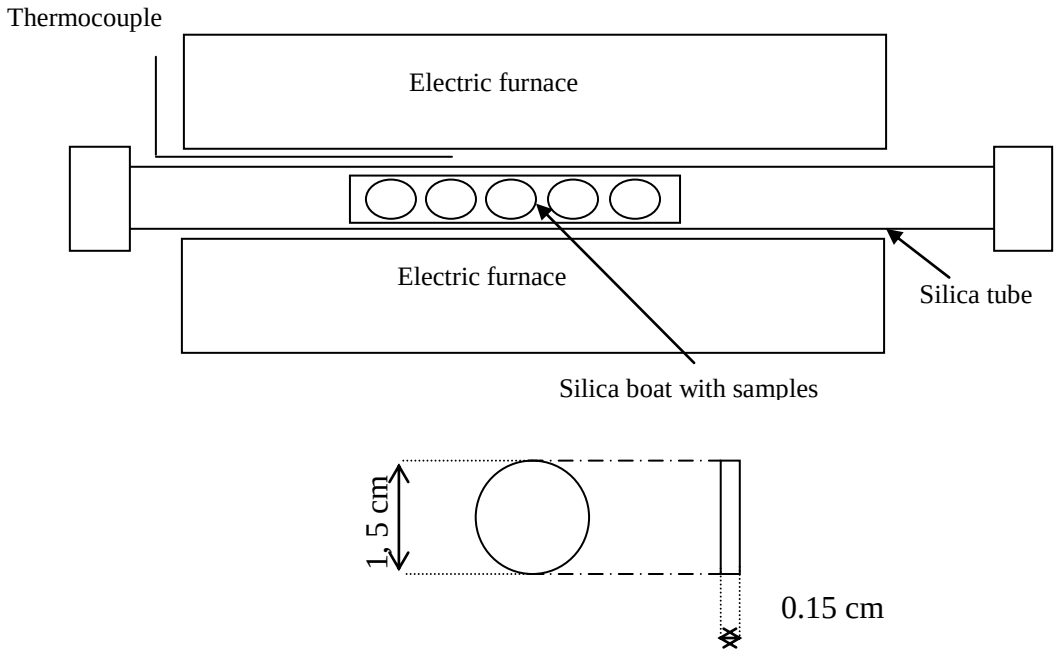

Specimen geometry used in this project for oxidation tests

Oxidation experiments in this projects			
Alloy	Coating	Temperature K	Time [hrs]
Ti45Al8Nb	TiAlCrY	1023	500
Ti45Al8Nb	TiAlCrY	1123	500
Ti45Al8Nb	TiAlCrY	1223	500
Ti45Al8Nb	CrAl2%YN	1023	500
Ti45Al8Nb	CrAl2%YN	1123	500
Ti45Al8Nb	CrAl2%YN	1223	500
Ti45Al8Nb	uncoated	1023	1000
Ti45Al8Nb	Al_2Au	1023	1000
Ti45Al8Nb	Ti43Al13Cr	1023	1000
Ti45Al8Nb	CrAlYN/CrN+CrAlYON etched by Cr	1023	1000
Ti45Al8Nb	CrAlYN/CrN+CrAlYON etched by CrAl	1023	1000
Ti45Al8Nb	CrAlYN/CrN+CrAlYON etched by Y	1023	1000
Ti45Al8Nb	TiAlCr (Ti42Al15Cr)	1023	5000
Ti45Al8Nb	TiAlYN/CrN	1023	5000
Ti45Al8Nb	TiAlN + Al_2O_3	1023	5000

Table 26 High temperature oxidation experiments performed in this project

Ch.IV.5.2 Sulphidation/Oxidation Experiment

The sulphidation experiments were carried out discontinuously in $H_2/H_2S/H_2O$ gas mixture.

The furnace was loaded with number of samples at the test temperature. The argon flow was used to purge the system form oxygen and other impurities. After 1 hour of argon flow, a predetermined mixture of aggressive gasses was turned on to the system, when the furnace reached the required temperature, and the gas flow was adjusted to the required level. Water bath was used to suitable level of humidity in the system. The system allowed an atmosphere of $pS_2 = 10^{-1}$ Pa and $pO_2 = 10^{-18}$ Pa. The sulphidation testes were carried out at 1023 and 1123 K for 1000 and 675 hours respectively.

After exposure for a predetermined time individual sample/samples was/were withdraw from the furnace, weighted and examined using OM (Optical Microscope), SEM (Scanning Electron Microscope), EDS (Energy Dispersive Spectroscopy), and XRD (X-Ray Diffraction) analysis. This procedure was continued until the end of the test. **Table 27** shows sulphidation/oxidation experiments conducted in this project.

A schematic diagram of sulphidation/oxidation test rig is presented below:

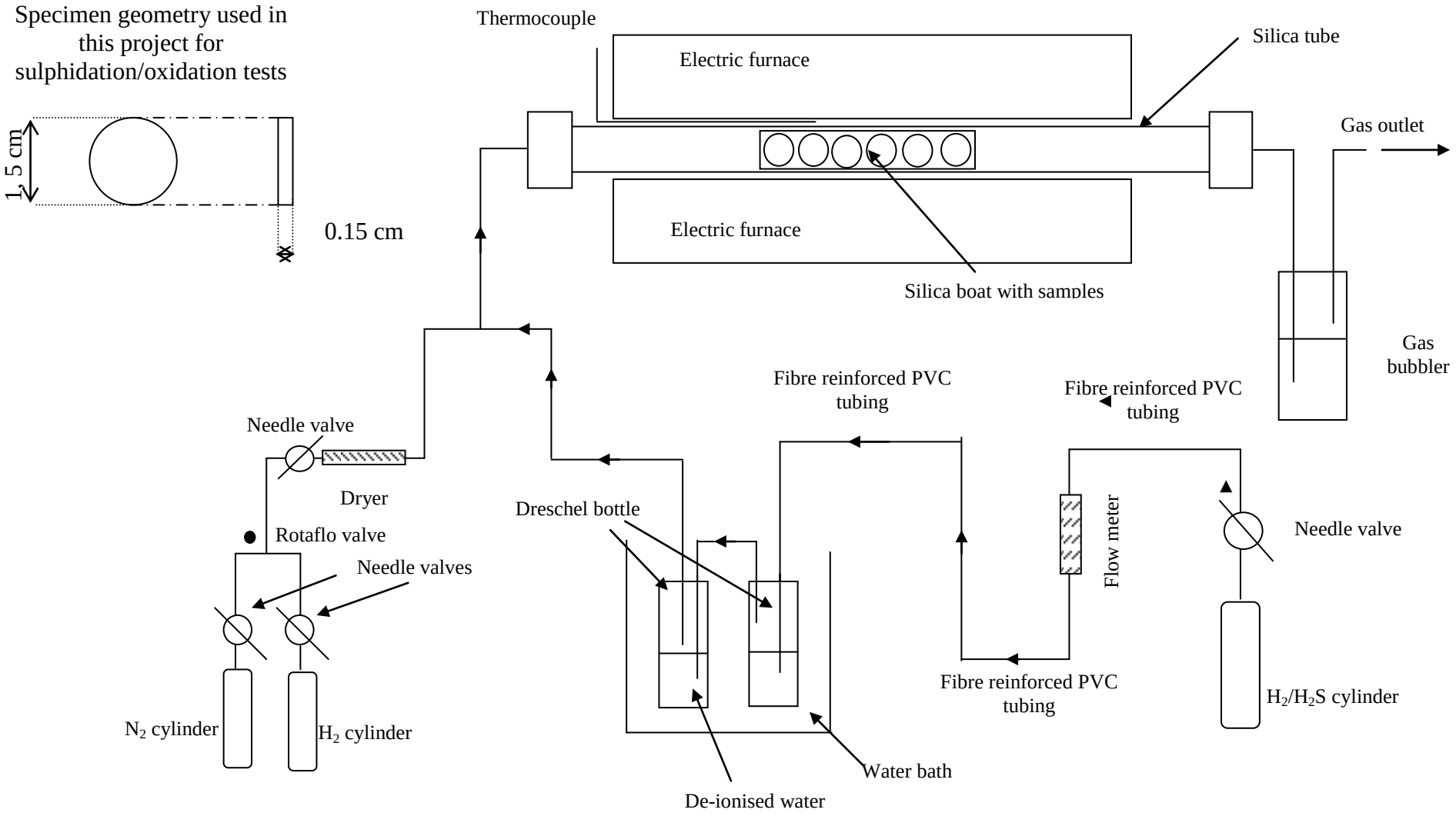
Specimen geometry used in this project for sulphidation/oxidation tests
1, 5 cm
0.15 cm
Thermocouple
Electric furnace
Silica tube
Gas outlet
Electric furnace
Silica boat with samples
Gas bubbler
Fibre reinforced PVC tubing
Fibre reinforced PVC tubing
Needle valve
Dryer
Dreschel bottle
Rotaflo valve
Needle valves
Flow meter
Needle valve
Fibre reinforced PVC tubing
H_2/H_2S cylinder
N_2 cylinder
H_2 cylinder
Water bath
De-ionised water

Sulphidation/oxidation experiments in this project				
Alloy	Coating	Sulphidation mixture	Temperature K	Time [hours]
Ti45Al8Nb	Uncoated alloy	$H_2S/H_2O/H_2$ ($pS_2 = 10^{-1}$ Pa, $pO_2 = 10^{-18}$ Pa)	1023	1000
Ti45Al8Nb	Al_2Au	$H_2S/H_2O/H_2$ ($pS_2 = 10^{-1}$ Pa, $pO_2 = 10^{-18}$ Pa)	1023	1000
Ti45Al8Nb	TiAlCr (Ti42Al15Cr)	$H_2S/H_2O/H_2$ ($pS_2 = 10^{-1}$ Pa, $pO_2 = 10^{-18}$ Pa)	1023	1000
Ti45Al8Nb	CrAlYN/CrN+CrAlYON etched by Cr	$H_2S/H_2O/H_2$ ($pS_2 = 10^{-1}$ Pa, $pO_2 = 10^{-18}$ Pa)	1023	1000
Ti45Al8Nb	CrAlYN/CrN+CrAlYON etched by CrAl	$H_2S/H_2O/H_2$ ($pS_2 = 10^{-1}$ Pa, $pO_2 = 10^{-18}$ Pa)	1023	1000
Ti45Al8Nb	CrAlYN/CrN+CrAlYON etched by Y	$H_2S/H_2O/H_2$ ($pS_2 = 10^{-1}$ Pa, $pO_2 = 10^{-18}$ Pa)	1023	1000
Ti45Al8Nb	Uncoated alloy	$H_2S/H_2O/H_2$ ($pS_2 = 10^{-1}$ Pa, $pO_2 = 10^{-18}$ Pa)	1123	675
Ti45Al8Nb	CrAlYN/CrN coating Y etch, CrAl (thin)	$H_2S/H_2O/H_2$ ($pS_2 = 10^{-1}$ Pa, $pO_2 = 10^{-18}$ Pa)	1123	675
Ti45Al8Nb	CrAlYN/CrN coating Cr etch, CrAl (thin)	$H_2S/H_2O/H_2$ ($pS_2 = 10^{-1}$ Pa, $pO_2 = 10^{-18}$ Pa)	1123	675
Ti45Al8Nb	CrAlYN/CrN coating, Y etch, CrAlY (thick)	$H_2S/H_2O/H_2$ ($pS_2 = 10^{-1}$ Pa, $pO_2 = 10^{-18}$ Pa)	1123	675

Table 27 High temperature sulphidation/oxidation experiments performed in this project

Ch.IV.5.3 Hot Corrosion Experiment

Hot corrosion was induced by salt spray method. After measuring and weighing each 15mm diameter disc sample a fine platinum wire was fitted to allow suspension of the sample from a pre-drilled hole. The sample was cleaned using isopropanol and then reweighed after drying. A hot air gun was then used to heat the sample, which was suspended from a stiff wire, to a temperature of over 373 K. A close to saturated solution of the salt mixture (20%NaCl/80%Na_2SO_4) was sprayed onto both sides of the hot sample so that the salt crystallized almost instantly on the surface. This procedure was repeated for each side several times until a uniform coverage was achieved with a loading of around 8 to 12 mg per sample, corresponding to 2 to 3 mg/cm^2. Hot corrosion investigation was carried out at 1023 K (schematic diagram is presented below) . The coated samples together with an uncoated Ti45Al8Nb control sample were suspended from alumina rods, using the platinum wire loops, held in an alumina boat with slotted sides. The furnace was then switched on to ramp up to the test temperature to 1023 K, at 278 K/min where it was held for the chosen period of hours (150 hours). Below, schematic diagram shows hot corrosion experiment

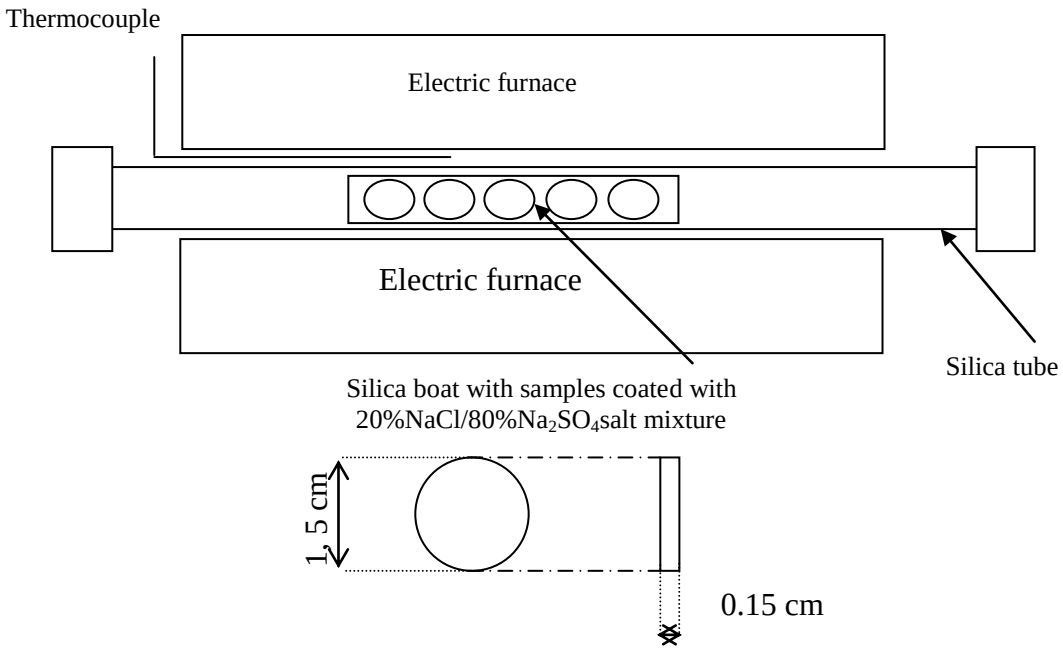

Specimen geometry used in this project for hot corrosion tests

All exposed samples were studied using OM (Optical Microscope), SEM (Scanning Electron Microscope), EDS (Energy Dispersive Spectroscopy), and XRD (X-Ray Diffraction) analysis. **Table 28** shows hot corrosion experiment conducted in this project.

Hot corrosion experiment in this projects				
Alloy	Coating	Salt mixture	Temperature K	Time [hrs]
Ti45Al8Nb	CrAl2%YN	20%NaCl80%Na_2SO_4	1023	150
Ti45Al8Nb	TiAlYN/CrN	20%NaCl80%Na_2SO_4	1023	150
Ti45Al8Nb	TiAlN + Al_2O_3	20%NaCl80%Na_2SO_4	1023	150

Table 28 High temperature hot corrosion experiment performed in this project

Ch.IV.6 Analytical Procedures

Ch.IV.6.1 X-Ray Diffraction (XRD) Analysis/Scanning Electron Microscopy (SEM)/Energy Dispersive X-Ray Analysis (EDS)

Phase identification of exposed samples was performed using a Siemens 5000 X-Ray Diffractometer (XRD). The samples were fixed into machine to a sample holder and bombarded by Cu-Kα radiation. XRD patterns showing the phases presents were obtained.

Scanning Electron Microscope (SEM) produced by FEI (Quanta 200) was used to observe the morphology of the exposed samples, to different environments (oxidation, hot corrosion, and sulphidation).

Surface analysis and composition profiles from exposed samples were obtained by Energy Dispersive X-Ray Analyzer (EDS) produced by Inca – Oxford instruments.

Qualitative (not quantitative), X-Ray distribution maps of the required elements, present in the samples were recorded photographically. Chemical compositions of the exposed and unexposed materials were examined by the EDS analysis.

Chapter V – Introduction to Current Work Undertaken in This Project

Ch.V.1 Introduction

The literature review presented in **chapter II (sections 1, 2, 3, and 4)** shows that extensive amount of work has been done on high temperature corrosion behaviour of TiAl and Ti-Al based intermetallics [162, 163, 164, 165] and interdiffusion modelling of multicomponent systems [166, 167, 168, 169, 170, 171]. Improved understanding of the fracture behaviour of such materials has led to material modifications to produce TiAl base materials with improved K_{1C}. High temperature corrosion behaviour of such materials has also been studied to some extent [172].

Disagreement still exists on the effect of N_2 and oxygen and rare earth elements addition on the high temperature corrosion behaviour of such materials [173]. The most important problems relating to the use of TiAl and TiAl based materials are their poor corrosion behaviour – oxidation, sulphidation. For these materials, exposed to oxidising environment at elevated temperature, the thermodynamic imperative, detects the formation of both non-protective TiO_2 and protective Al_2O_3; the TiO_2 formation is also kinetically favoured due to the higher D_{Ti} compared to D_{Al} ($D_{Ti} = 5.10E^{-11}$ cm^2/s, $D_{Al} = 4.71E^{-12}$ cm^2/s). An additional complication arise from the fact that TiAl materials require higher Al activity to form continuous, protective Al_2O_3 scale, than what is needed in TiAl disordered alloys. Many attempts have been made to overcome such problems by alloy composition adjustment and/or by depositioning a protective layer/layers on the surface. This area has been reviewed by Datta et. al [174, 175].

However the existing coatings which are available do not confer the oxidation resistance above 1073 K for prolonged period of exposure. With this in mind a large EU project (InnovaTiAl) was designed to produce a new generation of coatings aimed to increase the temperature capability of TiAl based materials beyond 1073 K exposed to oxidising environment over longer duration while maintaining their fatigue and creep resistance. The rationale for this InnovaTiAl project has been described elsewhere [174]. Briefly the objective has been to increase the application of TiAl and TiAl based materials in power generation, aerospace and other processing industries by increasing their resistance to high temperature corrosion, so that the service temperature of the plants and engines can be increased to above 1073 K.

The work in this thesis has been specifically designed to investigate the oxidation, sulphidation, and hot corrosion behaviour of TiAl base materials (Ti45Al8Nb alloy) coated with the new generation of coatings produced under InnovaTiAl project. In initiating this work note has been taken of the existing information relating to this work. Literature review indicates the existence of a wealth of information of TiAl and TiAl based intermetallics – compositions, chemical and mechanical properties [162,172,174]. It is also important to note that a significant amount of research has been carried out in this laboratory and elsewhere in the general area of oxidation, sulphidation, and hot corrosion of materials [174, 175, 176, 177] substantially improving our understanding of high temperature degradation processes.

In spite of this progress much work remains to be done particularly on the response of the new generation coatings, produced under this programme, to the exposure at high temperature in oxidising (static air), sulphidising (low $pO_2 = 10^{-18}$ Pa, high $pS_2 = 10^{-1}$ Pa), and hot corrosion 20%NaCl/80%Na_2SO_4 environments. The degree of protectivity to be conferred by these new coatings against high temperature corrosion of TiAl materials is not known. Neither it is not known the mechanisms of degradation. Long term protectivity to be obtained by using these coatings has not been determined. The temperature capabilities of such coatings have remained uncertain.

This work was undertaken to address these gaps in knowledge regarding the high temperature corrosion behaviour of such coatings. The work has been designed to establish the scale growth and scale failure processes in these coatings and ascertain the mechanisms of degradation – occurring under oxidising, sulphidising (low $pO_2 = 10^{-18}$ Pa, high $pS_2 = 10^{-1}$ Pa), and hot corrosion 20%NaCl/80%Na_2SO_4 environments at temperatures 1023 – 1223 K. Significant emphasis has been placed on gathering extensive amount of microstructural information through analyses using SEM, EDS, and XRD.

Glaring gaps have been found to exist in the area of interdiffusion studies. Interdiffusion is known to play a critical role in determining the protectivity of high temperature coatings. Until recently not much work has been done in the area of interdiffusion. Datta et. al [172] was the first of the group of the researchers who

attempted to model the interdiffusion processes after oxidation/diffusion annealing treatment [178].

To increase further the knowledge on the role of interdiffusion in the consideration of the degree of the protectivity to be achieved from newly developed coatings, this research has been planned to study the processes of interdiffusion in such coating/substrate systems. Thus interdiffusion modelling both in close and open systems has formed a significant part of this project. Darkens method has been used to model interdiffusion in the multicomponent systems. A novel aspect of this modelling work has been the use of inverse method to determine the diffusion coefficients of constituent coating/substrate elements.

In summary, the work in this thesis has been concerned to address the issues highlighted in the above discussion. Research in this thesis has involved studies of the high temperature corrosion behaviour of some new generation of coatings **(Table 29),** produced to protect the TiAl based intermetallic alloy (Ti45Al8Nb) against oxidation, sulphidation, and hot corrosion environments at 1023 – 1223 K – **Table 29**. Extensive structural information has been gathered from the analyses of the exposed samples using SEM, EDS, and XRD. The kinetic data together with microstructural information have been used to produce a mechanistic framework of the degradation of the coated materials underpinned by thermodynamic modelling and interdiffusion modelling.

Coating	Environment exposed	Temperature [K]	Time [hours]
Ti55Al14Cr0.3Y (TiAlCrY)	Oxidation (pO_2 = 21278.25 Pa)	1023 – 1223	500
CrAl2%YN	Oxidation (pO_2 = 21278.25 Pa)	1023 – 1223	500
Ti42Al15Cr (TiAlCr)	Oxidation (pO_2 = 21278.25 Pa)	1023	5000
25Ti25Al50N+Al_2O_3	Oxidation (pO_2 = 21278.25 Pa)	1023	5000
TiAlYN/CrN+Al_2O_3	Oxidation (pO_2 = 21278.25 Pa)	1023	5000
Ti42Al15Cr (TiAlCr)	Sulphidation (pO_2 =10^{-18} Pa, pS_2 = 10^{-1} Pa)	1023	1000
Al_2Au	Sulphidation (pO_2 =10^{-18} Pa, pS_2 = 10^{-1} Pa)	1023	1000
CrAlYN/CrN+CrAlYON etched by Cr	Sulphidation (pO_2 =10^{-18} Pa, pS_2 = 10^{-1} Pa)	1023	1000
CrAlYN/CrN+CrAlYON etched by CrAl	Sulphidation (pO_2 =10^{-18} Pa, pS_2 = 10^{-1} Pa)	1023	1000
CrAlYN/CrN+CrAlYON etched by Y	Sulphidation (pO_2 =10^{-18} Pa, pS_2 = 10^{-1} Pa)	1023	1000
CrAlYN/CrN coating Y etch, CrAl (thin)	Sulphidation (pO_2 =10^{-18} Pa, pS_2 = 10^{-1} Pa)	1123	675
CrAlYN/CrN coating, Y etch, CrAlY (thick)	Sulphidation (pO_2 =10^{-18} Pa, pS_2 = 10^{-1} Pa)	1123	675
CrAlYN/CrN coating Cr etch, CrAl (thin)	Sulphidation (pO_2 =10^{-18} Pa, pS_2 = 10^{-1} Pa)	1123	675
CrAl2%YN	Hot corrosion (20%NaCl/ 80%Na_2SO_4)	1023	150
TiAlN+Al_2O_3 (Ti25Al50N)	Hot corrosion (20%NaCl/ 80%Na_2SO_4)	1023	150
TiAlYN/CrN+Al_2O_3	Hot corrosion (20%NaCl/ 80%Na_2SO_4)	1023	150

Table 29 Coating used in this thesis

Chapter VI - Results

Chapter VI – Section 1 – Oxidation of γ-TiAl alloy - Results

Ch.VI.Sec.1.1 Introduction to high temperature oxidation results

Part one presents the results of oxidation at 1023, 1123, and 1223 K for 500 hours.

Long term oxidation results (5000 hours at 1023 K) are described in part two.

Part One – Oxidation studies at 1023 – 1223 K for 500 hours

Ch.VI.Sec.1.2 Oxidation kinetics for two coatings at 1023 – 1223 K

Figures 90, **91,** and **92** show the kinetic data of exposed samples (TiAlCrY coated Ti45Al8Nb and CrAl2%YN coated Ti45Al8Nb) after oxidation at 1023, 1123, and 1223 K for 500 hours respectively.

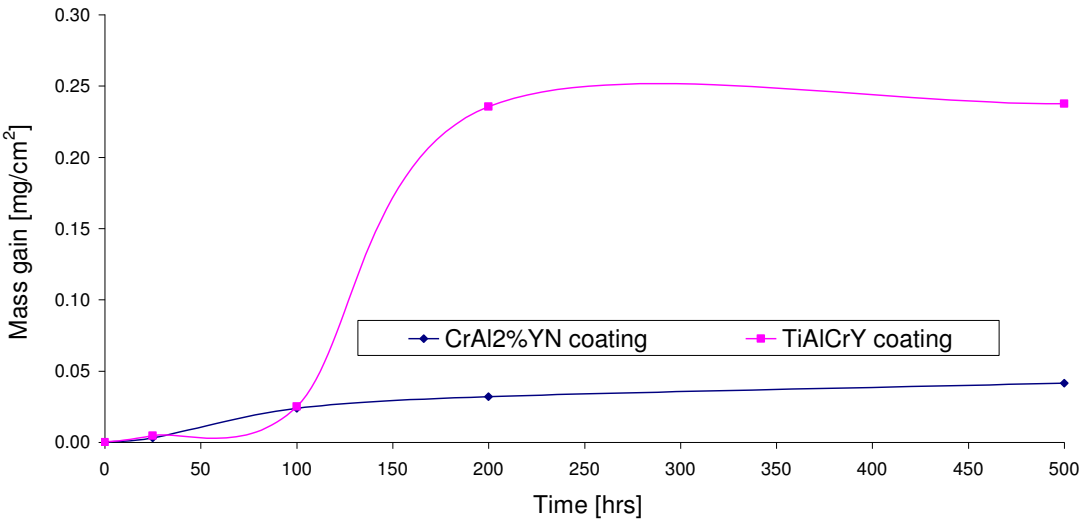

Figure 90 Kinetic data obtained for exposed samples to static air at 1023 K for 500 hours

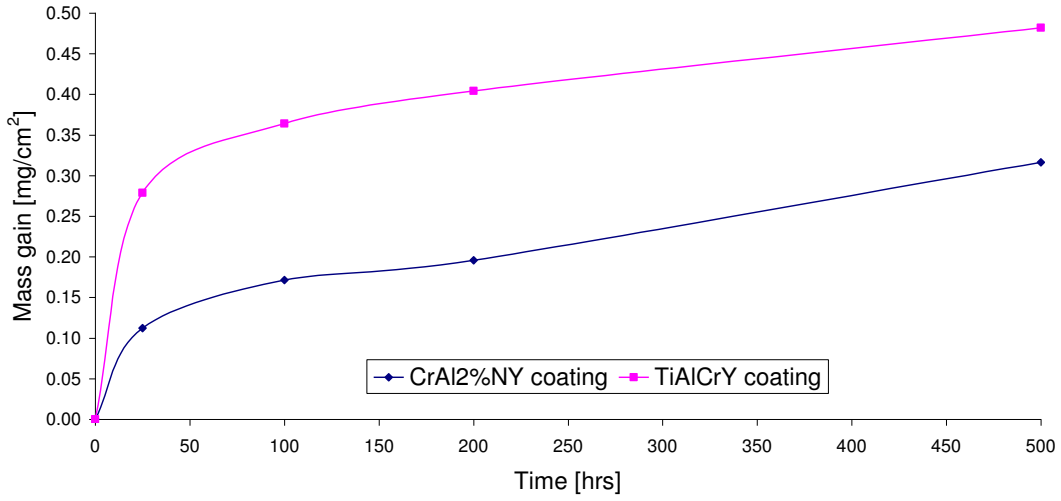

Figure 91 Kinetic data obtained for exposed samples to static air at 1123 K for 500 hours

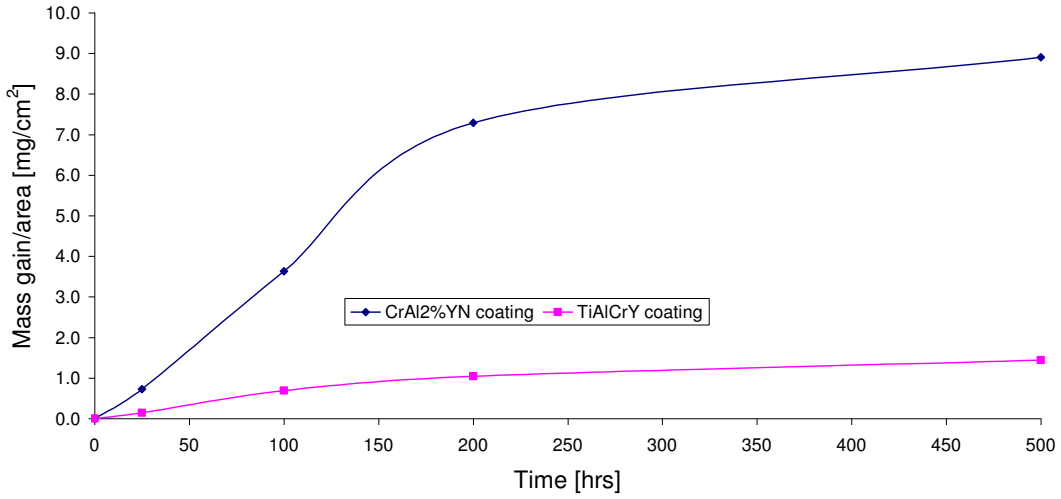

Figure 92 Kinetic data obtained for exposed samples to static air at 1223 K for 500 hours

Table 30 shows the parabolic rate constant for exposed samples at 1023, 1123, and 1223 K for 500 hours.

Temperature [K]	TiAlCrY	CrAl2%YN
1023	$3.51304E^{-10}$	$9.71493E^{-12}$
1123	$1.08145E^{-09}$	$5.88475E^{-10}$
1223	$1.18304E^{-08}$	$4.64201E^{-07}$
Unit	$[mg^2/cm^4/s]$	$[mg^2/cm^4/s]$

Table 30 Parabolic rate constant values obtained from oxidation experiment performed at 1023, 1123, 1223 K for 500 hours

The kinetics data shown in **figures 90**, **91**, and **92** indicates that both samples (TiAlCrY (Ti55Al14Cr0.3Y [at%]) coated Ti45Al8Nb and CrAl2%YN coated Ti45Al8Nb) followed parabolic rate, or nearly parabolic rate growth. The obtained data suggest that the both materials displayed good oxidation behaviour at 1023 and 1123 K. However at 1223 K TiAlCrY coated alloy showed better oxidation behaviour than that shown by CrAl2%YN coated alloy.

Ch.VI.Sec.1.3 TiAlCrY coated Ti45Al8Nb alloy 1023 K

The surface morphologies of TiAlCrY (Ti55Al14Cr0.3Y) presented in **figure 93** show the presence of small crystals while corrosion products were absent from some areas.

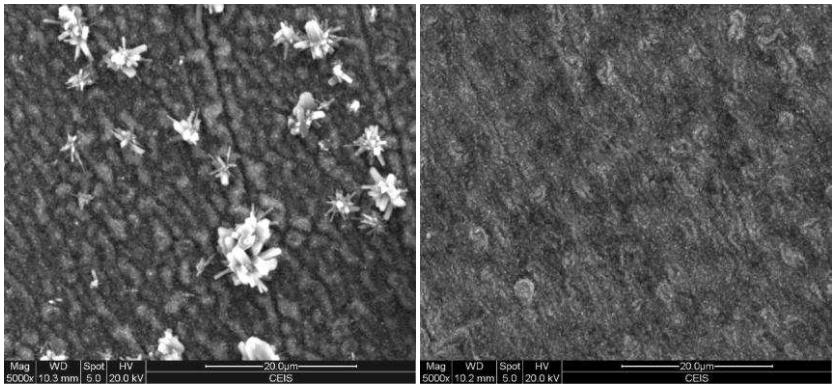

A: 5000x B: 5000x

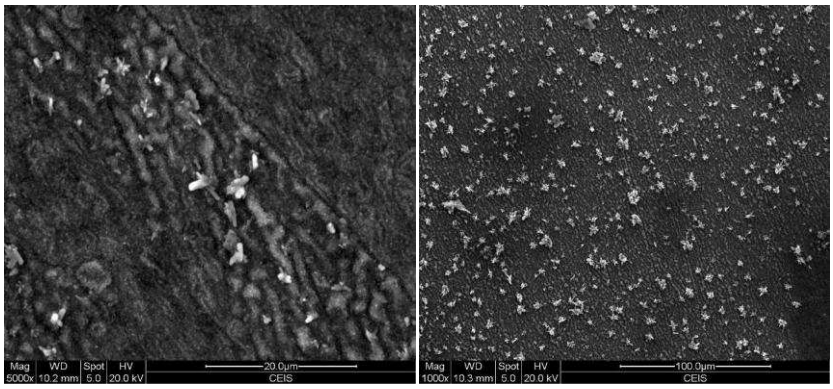

C: 5000x D: 2500x

Figure 93 SEM images from surface of TiAlCrY coated Ti45Al8Nb after 500 hours oxidation at 1023 K (magnification under images)

The surface analysis performed on TiAlCrY coated Ti45Al8Nb alloy after 500 hours oxidation at 1023 K shows the presence of Al_2O_3 with some inclusion of Ti and Cr ions. **Table 31** shows EDS analysis from different areas of the exposed sample.

Image	at% O	at% Al	at% Ti	at% Cr	at% Y
A	62.613	22.312	12.022	3.007	0.046
B	63.922	21.713	11.446	2.612	0.308
C	67.175	5.062	27.762		
D	78.978	3.292	17.730		

Table 31 Surface analysis performed by EDS investigation of TiAlCrY coated Ti45Al8Nb after 500 hours of oxidation at 1023 K

Figure 94 presents cross – sectioned SEM images of TiAlCrY coated Ti45Al8Nb alloy after 500 hours oxidation at 1023 K in static air. The scale shows good protection against high temperature in oxidised environmental, furthermore, lack of spallation or cracks was observed. The different areas with different magnifications show that the whole sample corroded with similar rate.

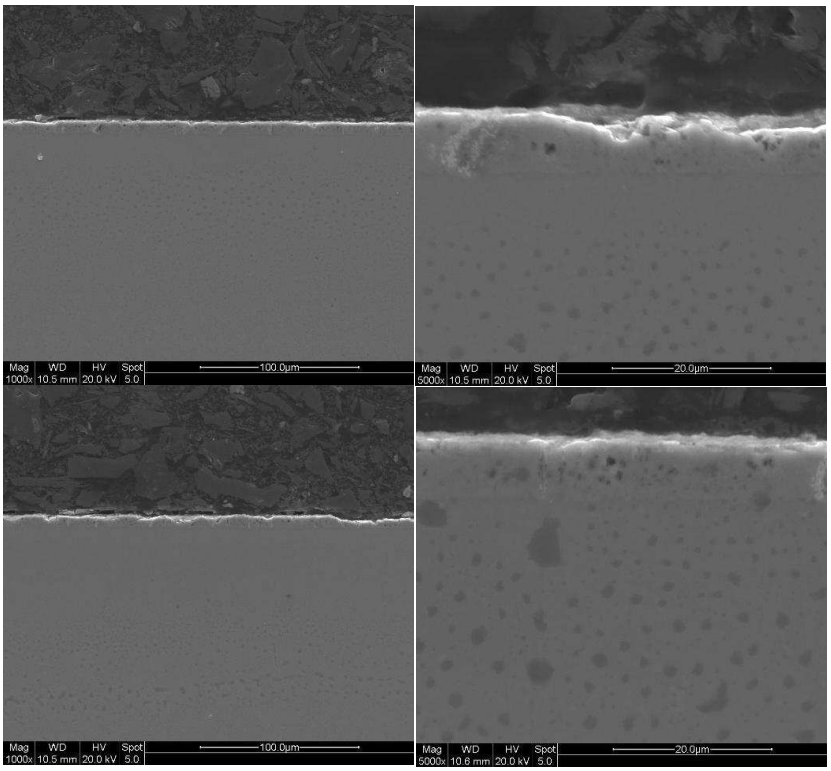

TiAlCrY coated Ti45Al8Nb alloy after 500 hours of oxidation at 1023 K Mag.1000 (left) and 5000 (right) – near to the edge of the sample

Figure 94 Cross – sectional images of TiAlCrY coated Ti45Al8Nb after 500 hours of oxidation at 1023 K

The cross – sectioned SEM image in **figure 95** showed good adherence between the oxide scale and the modified coating; however some areas showing crack formation.

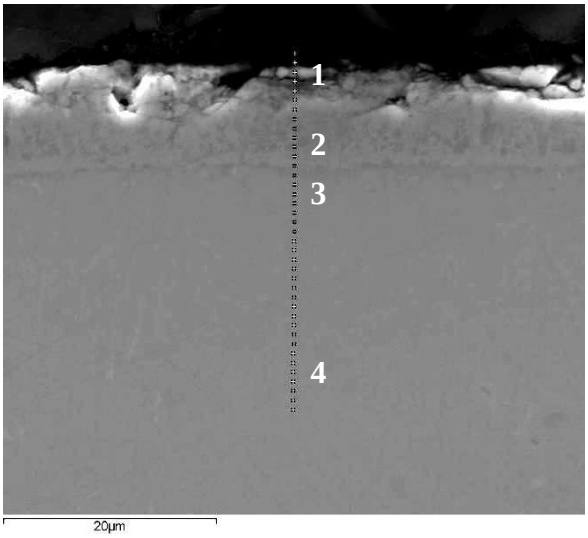

1) Al/Ti/Cr oxide scale

2) Modified coating (TiAlCrY) and depletion zone of Ti and Al

3) Pre-depletion zone of Ti and Al

4) Substrate (Ti45Al8Nb alloy)

Figure 95 Cross – section SEM image of TiAlCrY coated Ti45Al8Nb alloy after 500 hours of oxidation at 1023 K

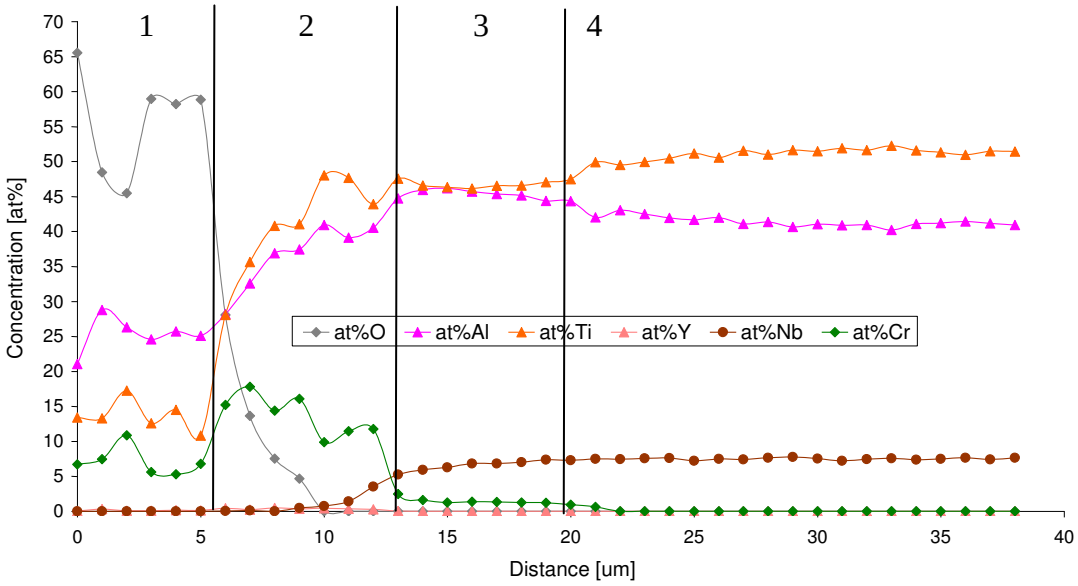

Figure 96 EDS concentration profiles obtained from TiAlCrY coated Ti45Al8Nb alloy after 500 hours of oxidation at 1023 K

Figure 96 shows the cross – sectional EDS concentration profiles of the exposed to oxidation TiAlCrY coated alloy for 500 hours at 1023 K. A thick (5 µm) oxide scale

consisting of Al, Cr, and Ti oxides is seen to form at the top. Underneath the top scale exists the modified coating (TiAlCrY). The modified coating/substrate interface shows a depletion zone of Al and Ti. Beneath the depletion zone is a zone depleted in Ti (pre-depletion zone); where Al concentration increased due to the faster outward diffusion of Ti ions from the bulk material. Nb remains in the substrate (Ti45Al8Nb). The EDS analysis shows in **figure 96** shows, the scale structure which formed during oxidation at 1023 K for 500 hours. The straight line in the EDS concentration profiles indicate the different regions formed after exposure. The numbers in the EDS profiles correlate with the SEM image showed in **figure 95**. The EDS X-Ray mapping in **figure 97** shows good agreement with analytical data obtained from the EDS concentration profiles **(Fig. 96)**. An oxide scale of Al, Cr, and Ti is seen to as on outer scale and Nb remains in the substrate (TiAl45Al8Nb). The EDS X-ray mapping detects the increased concentration of Al in area where depletion zone of Ti formed.

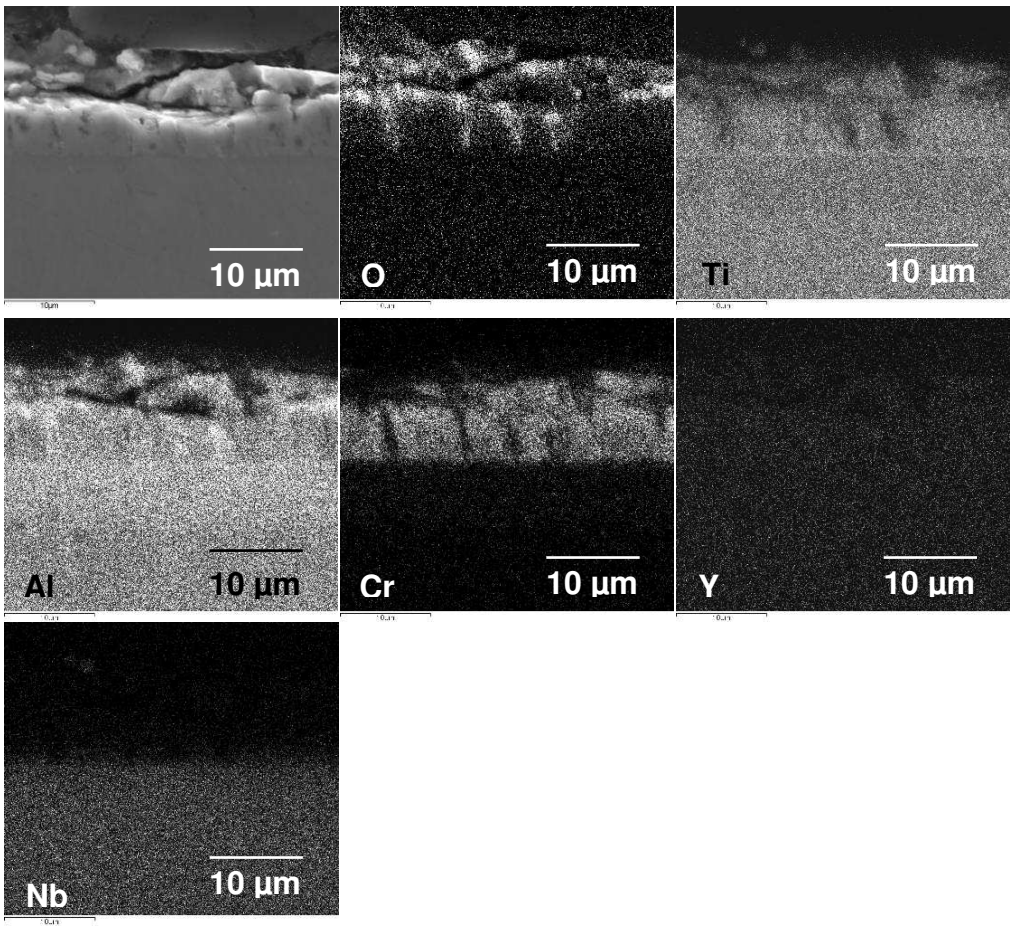

Figure 97 Digimaps of TiAlCrY coated Ti45Al8Nb after 500 hours oxidation at 1023 K

The XRD analysis shown in **figure 98** performed on exposed TiAlCrY coated Ti45Al8Nb sample confirm, the development of Al_2O_3 and TiO_2 oxides, the analysis detected also phases from the substrate ($TiAl_3$, $TiAl_2$) and also formation of Cr_2O_3 oxide.

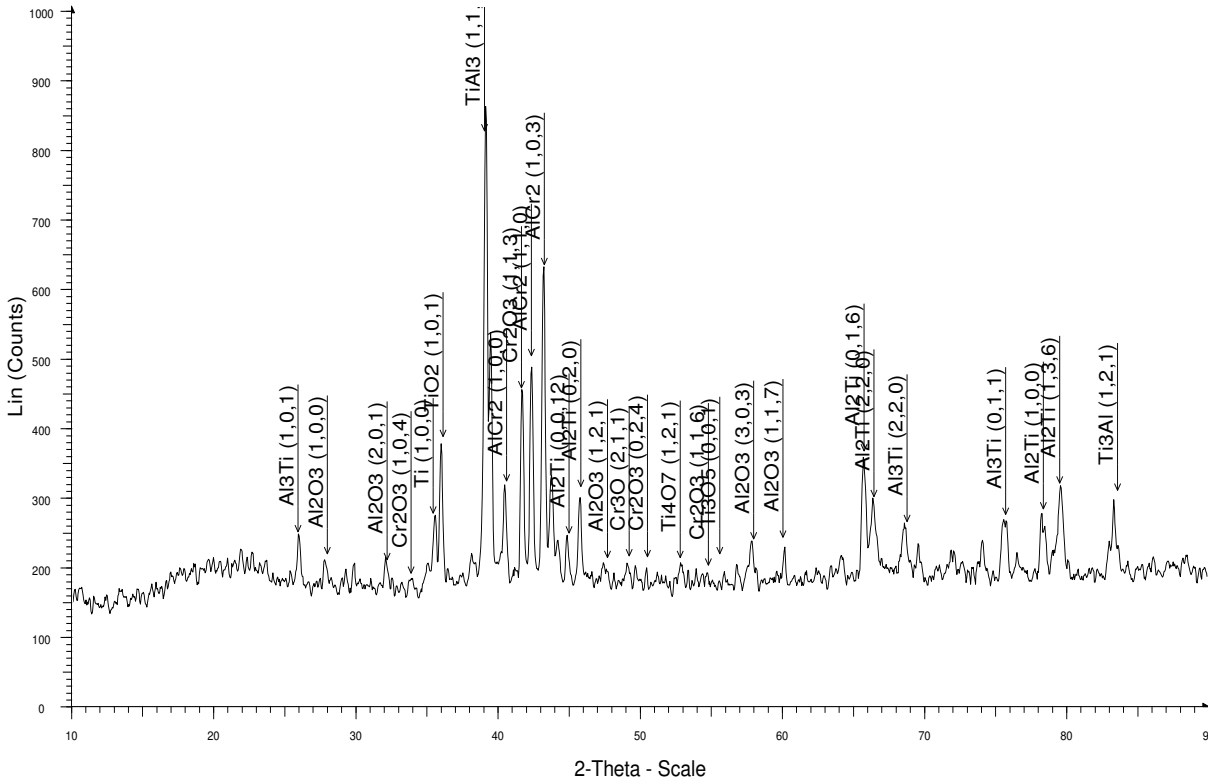

Figure 98 XRD pattern obtained from TiAlCrY coated Ti45Al8Nb after 500 hours oxidation at 1023 K

Ch.VI.Sec.1.4 CrAl2%YN coated alloy oxidised at 1023 K

Figure 99 shows the exposed surface of CrAl2%YN coated Ti45Al8Nb alloy after 500 hours oxidation at 1023 K. The surface is observed to be covered partly by TiO_2 and Al_2O_3 oxides. These oxides developed when micro-cracks formed allowing Ti

with Al diffusion outward to produce the oxides (**Figure 99a, b**). In other areas (**Figure**s **99c, d**) where coating was more resistant to cracking by thermal shock, mainly Al_2O_3 developed with high concentration of Cr, TiO_2 was not detected as a main surface phase.

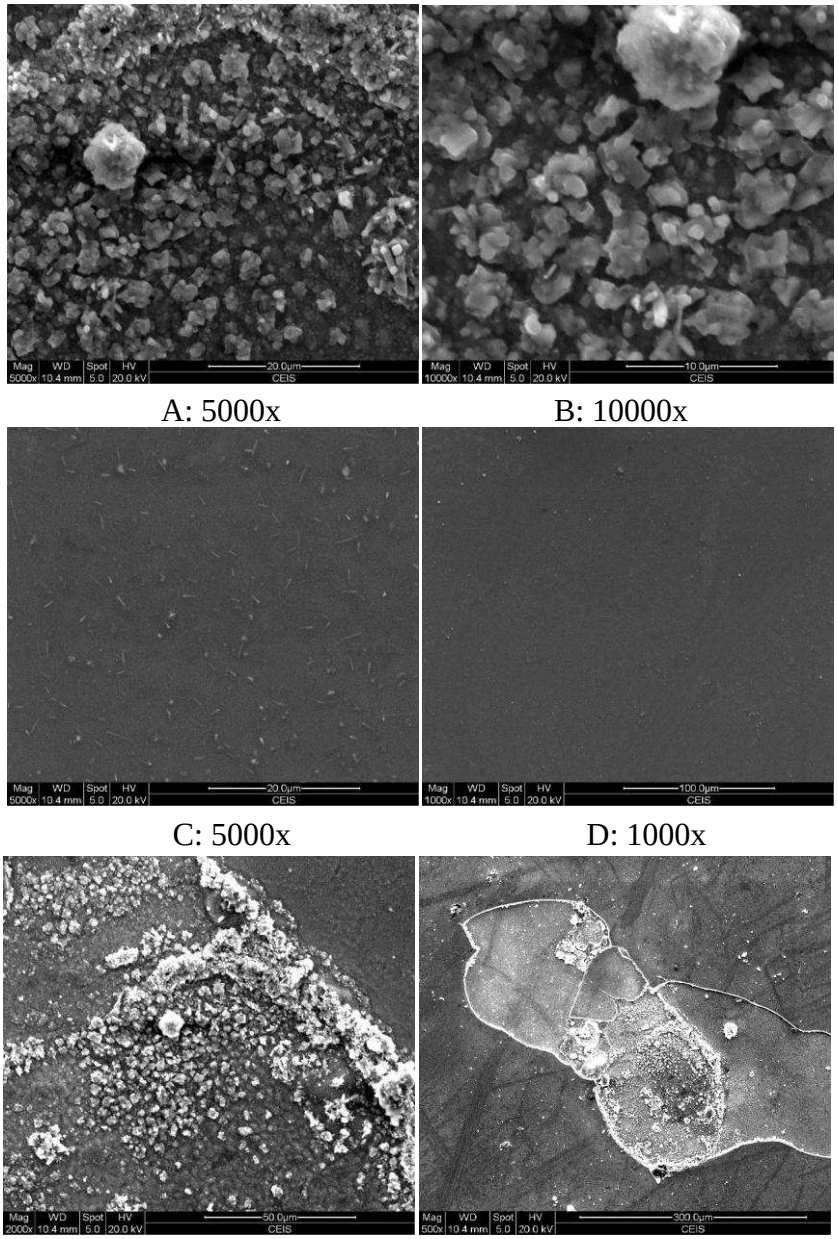

Figure 99 SEM images from surface of CrAl2%YN coated Ti45Al8Nb after 500 hours oxidation at 1023 K (magnification under images)

Table 32 clearly shows that the coating consisting of two regions; one region covered by less protective TiO_2 oxide, and the second region with more protective Al_2O_3 oxide. Nb is not present on the surface of the exposed sample.

Image	at%N	at%O	at%Al	at%Ti	at% Cr	at%Y	at%Nb
A		70.611	14.210	14.508	0.670		
B		68.935	18.978	11.520	0.567		
C	27.409	20.529	28.513	0.491	22.309	0.749	
D	25.521	23.077	28.553	0.575	21.442	0.833	
E	4.927	56.677	15.961	19.663	0.701		2.071

Table 32 Surface analysis performed by EDS investigation of CrAl2%YN coated Ti45Al8Nb after 500 hours of oxidation at 1023 K

Figure 100 shows several cross – sectioned SEM pictures of CrAl2%YN coated Ti45Al8Nb sample exposed to 1023 K for 500 hours. The thin and mixed oxides of Al_2O_3 and Cr_2O_3 developed on outer scale. The cross – sectioned SEM images reveals that the coating in some areas is compact and adherent, while in other places the coating has a less adherent character (indicated by arrows). Moreover the coating on the edge of the sample appears very brittle and spalled off from the material (indicated).

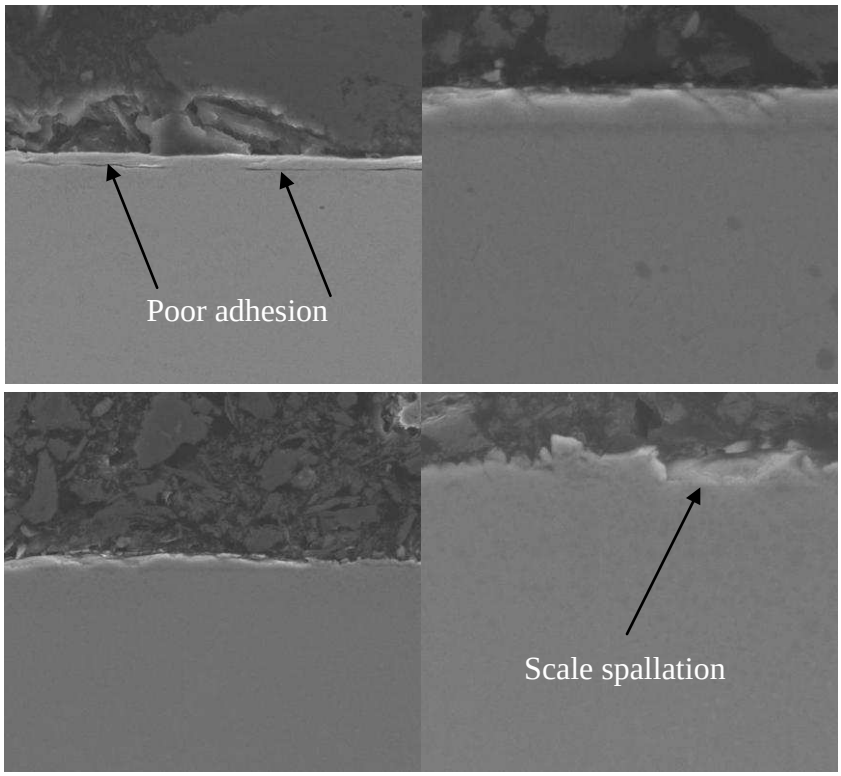

Figure 100 Cross – sectional images of CrAl2%YN coated Ti45Al8Nb after 500 hours of oxidation at 1023 K. Mag.1000 (left) and 5000 (right) – near to the edge of the sample

The CrAl2%YN coated Ti45Al8Nb material is presented in cross – sectioned SEM image in **figure 101**. The top layer is seen to consist of highly protective Al_2O_3 and Cr_2O_3 oxide scales. Moreover at the coating/substrate interface a thin TiN layer developed. This layer consumed Ti ions from the bulk material and formed a ceramic TiN bond. The EDS concentration profiles in **figure 102** reveal that the outer scale is protective due to the formation of thin and continuous Al_2O_3 and Cr_2O_3 oxides.

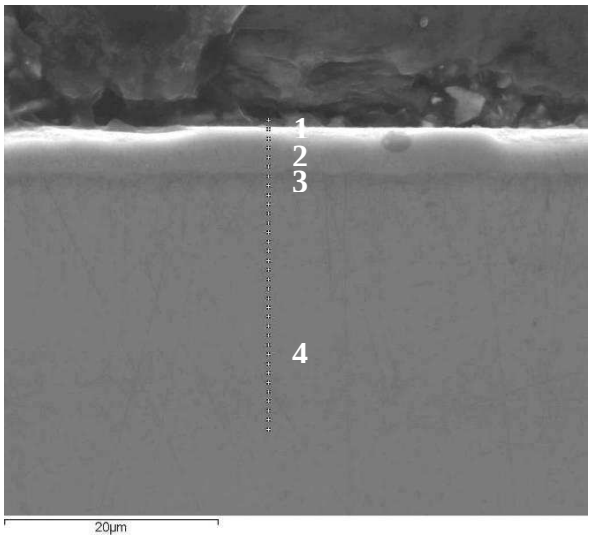

1) Al and Cr oxide scale
2) Modified coating (CrAl2%YN)
3) Ceramic layers (TiN, AlN) and depletion zone of Ti and Al
4) Substrate (Ti45Al8Nb alloy)

Figure 101 Cross – section SEM image (mag. 5000x) of CrAl2%YN coated Ti45Al8Nb alloy after 500 hours of oxidation at 1023 K

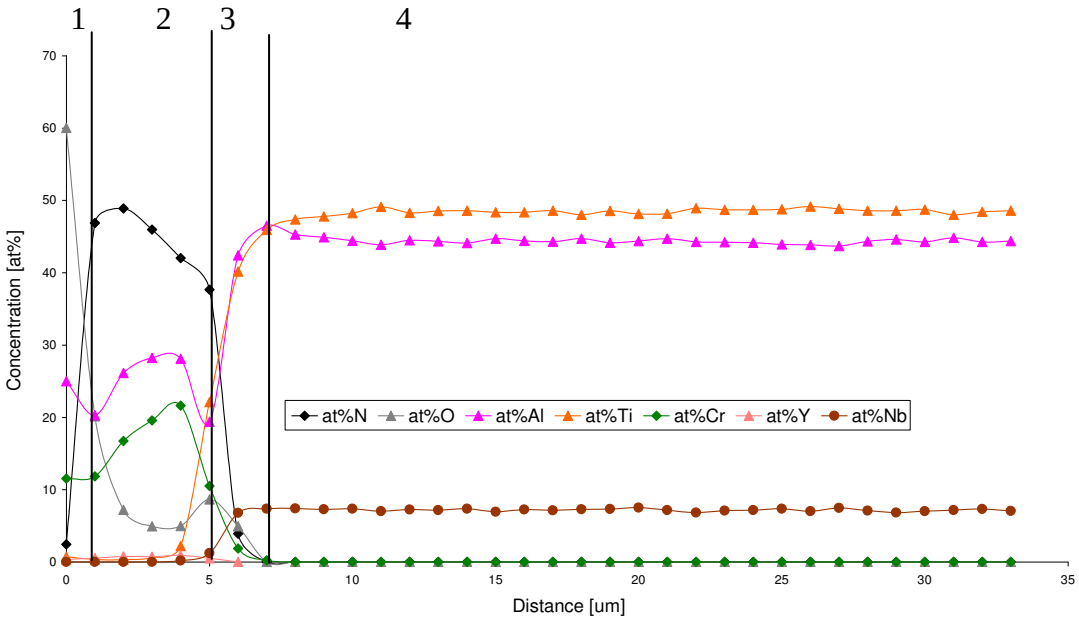

Figure 102 The EDS concentration profiles obtained from CrAl2%YN coated Ti45Al8Nb alloy after 500 hours of oxidation at 1023 K

The EDS concentration profiles (**figure 102**) taken form oxidised CrAl2%YN coated material (1023 K, 500 hours) shows the presence of a thin (1 µm) mixed Al_2O_3/Cr_2O_3 top scale oxide scale, a second layer of modified coating. Beneath this layer of modified coating a TiN/AlN is seen to be formed. The nitride layer inhibited Ti outward diffusion from the bulk material allowing the development of protective oxide scale of Al_2O_3/Cr_2O_3.

The EDS X-Ray mappings presented in **figure 103** and performed on exposed sample confirm the formation of Al and Cr oxides. Moreover TiN phase also was detected (Ti and N map are overlapped).

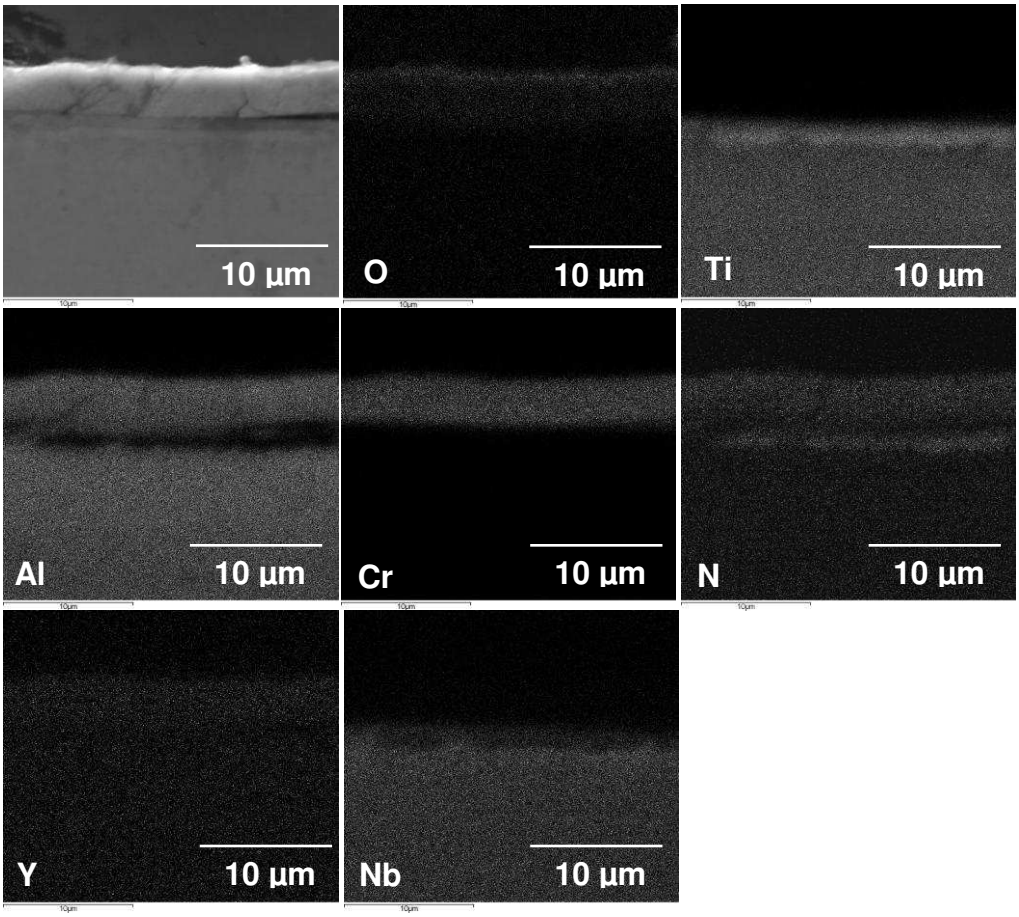

Figure 103 Digimaps of CrAl2%YN coated Ti45Al8Nb after 500 hours oxidation at 1023 K

The XRD analysis performed on the exposed CrAl2%YN coated Ti45Al8Nb sample, shows that EDS analysis is well confirmed in the XRD pattern in **figure 104**.

The XRD pattern presented in **figure 104** shows the peaks from the deposited coating (Cr_2N, CrN) but also peaks of TiN were detected. It is needs to be pointed out. The thin scale of Al_2O_3 and Cr_2O_3 detected by the EDS and the EDS X-Ray mapping was too thin for the XRD to analyse.

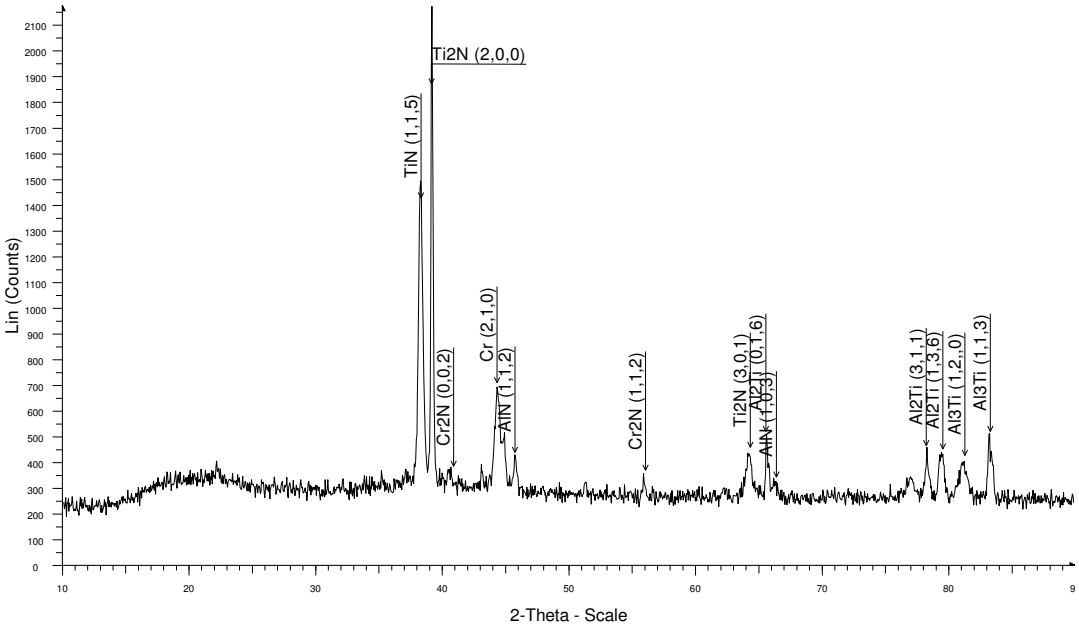

Figure 104 XRD pattern obtained from CrAl2%YN coated Ti45Al8Nb after 500 hours oxidation at 1023 K

Ch.VI.Sec.1.5 TiAlCrY coated Ti45Al8Nb alloy 1123 K

The surface images of the morphology developed on TiAlCrY (Ti55Al14Cr0.3Y) coated Ti45Al8Nb alloy performed by SEM investigation is shown in **figure 105**. The scale formed during oxidation process 1123 K consisted of a small crystals of TiO_2 and Al_2O_3 oxides (as shown in **table 33**).

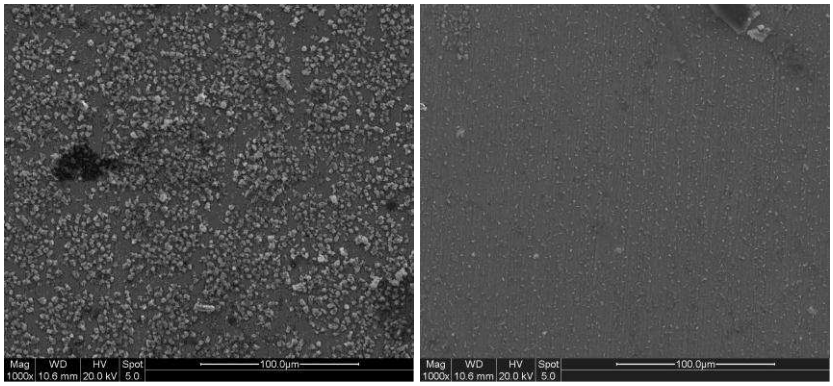

A: 1000x B: 1000x

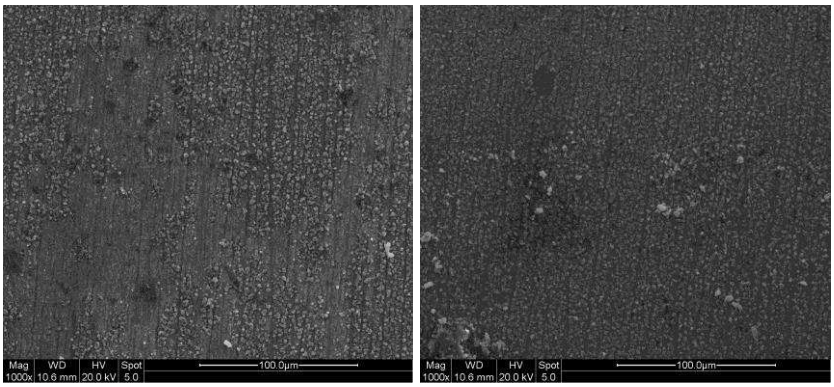

C: 1000x D: 1000x

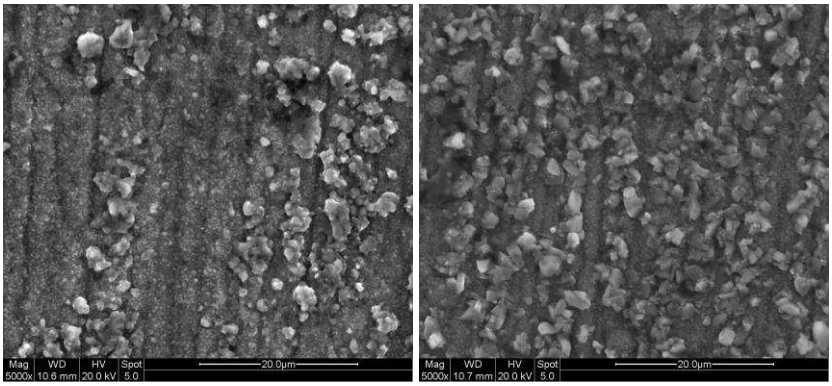

E: 5000x F: 5000x

Figure 105 SEM images from surface of TiAlCrY coated Ti45Al8Nb after 500 hours oxidation at 1123 K (magnification under images)

The oxide formation is well confirmed by the EDS analysis in **table 33**.

Image	at% O	at% Al	at% Ti	at% Cr
A	69.076	19.957	10.230	0.737
B	62.451	24.936	11.842	0.771
C	65.098	21.754	12.238	0.910
D	65.297	20.082	13.642	0.979

Table 33 Surface analysis performed by EDS investigation of TiAlCrY coated Ti45Al8Nb after 500 hours of oxidation at 1123 K

The cross – sectioned SEM images from different regions of the TiAlCrY coated Ti45Al8Nb alloy after 500 hours of oxidation at 1123 K are presented in **figure 106**. Figure shows the formation of a brittle scale containing voids and pits, showing poor adhesion.

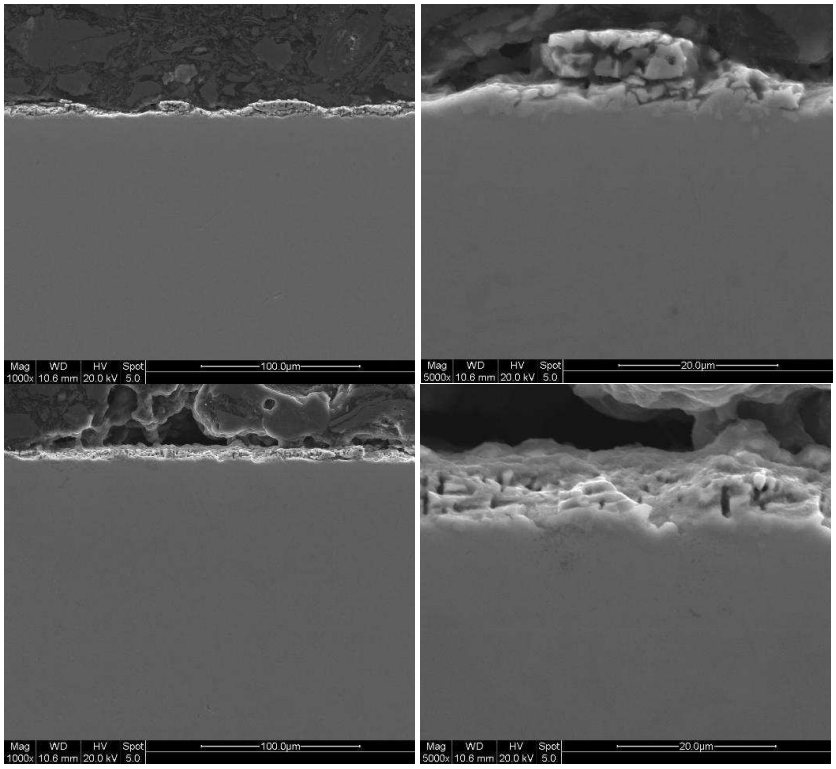

TiAlCrY coated Ti45Al8Nb alloy after 500 hours of oxidation at 1123 K Mag.1000 (left) and 5000 (right) – near to the edge of the sample

Figure 106 Cross – sectional images of TiAlCrY coated Ti45Al8Nb after 500 hours of oxidation at 1123 K

The SEM cross – sectioned image of TiAlCrY exposed sample at 1123 K in **figure 107** the development of a porous and brittle scale; the holes in the scale are

indicated by arrows. The EDS concentration profiles of exposed sample are presented in **figure 108**.

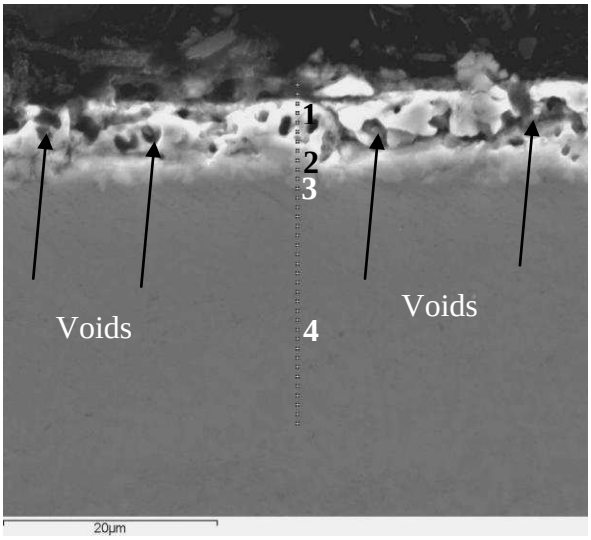

1) TiO_2 and Al_2O_3 oxide top scale

2) Ti/Al/Cr oxide region

3) Coating (TiAlCrY) and depletion zone of Ti and Al

4) Substrate (Ti45Al8Nb)

Figure 107 Cross – section SEM image (mag. 5000x) of TiAlCrY coated Ti45Al8Nb alloy after 500 hours of oxidation at 1123 K

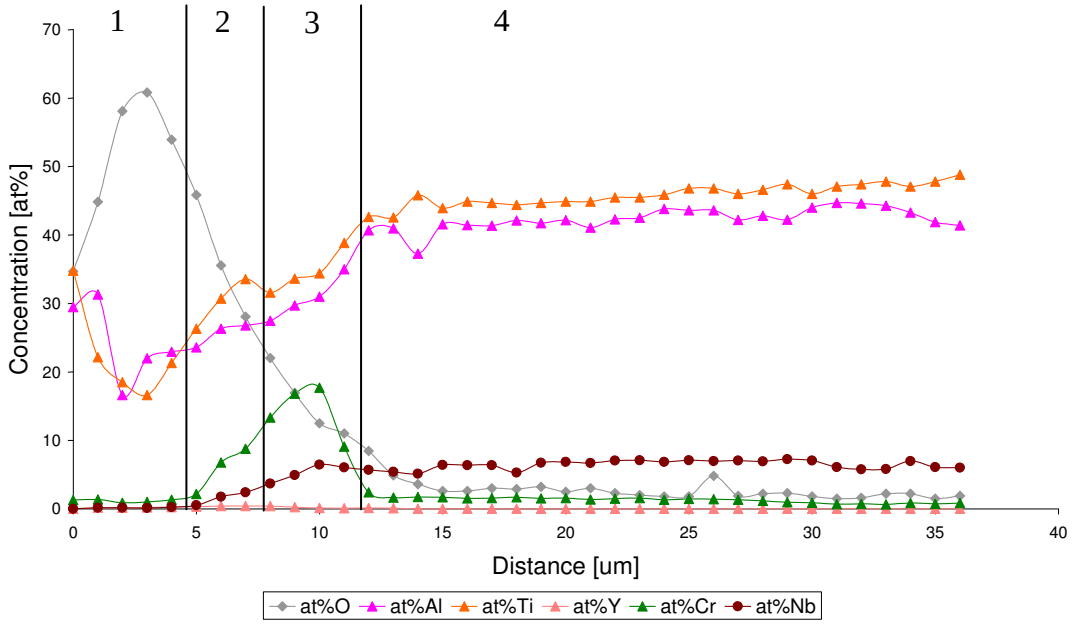

Figure 108 EDS concentration profiles obtained from TiAlCrY coated Ti45Al8Nb alloy after 500 hours of oxidation at 1123 K

The EDS profiles (**Fig. 108**) do not confirm the formation of Cr-oxide, Cr remaining in the modified coating (TiAlCrY). It was suggested that the higher affinity of

Ti and Al to oxygen than Cr causes the formation of Al and Ti oxides during exposure, whereas the lack of Cr oxide formation in the top part of oxide scale, however in the deeper region of the top scale some Cr_2O_3 oxide was observed **(region 2 Fig. 108)**. The EDS concentration profiles in **figure 108** reveals also a thin coating (TiAlCrY) remained in the system **(region 3 Fig. 108)** after 500 hours exposure at 1123 K. Furthermore the presence of a large diffusion zone of Al and Ti ions is indicated by the EDS profiles. The EDS concentration profiles consist of following regions:1) TiO_2 and Al_2O_3 oxide top scale, 2) Ti/Al/Cr oxide region, 3) Coating (TiAlCrY) and depletion zone of Ti and Al, 4) Substrate (Ti45Al8Nb). The EDX X-Ray mappings presented in **figure 109** are in good agreement with the EDS concentration profiles. The formation of the main phases (Al, Ti oxides) is confirmed also is confirmed the higher concentration of Cr at the scale/substrate interface. Nb remained in the substrate.

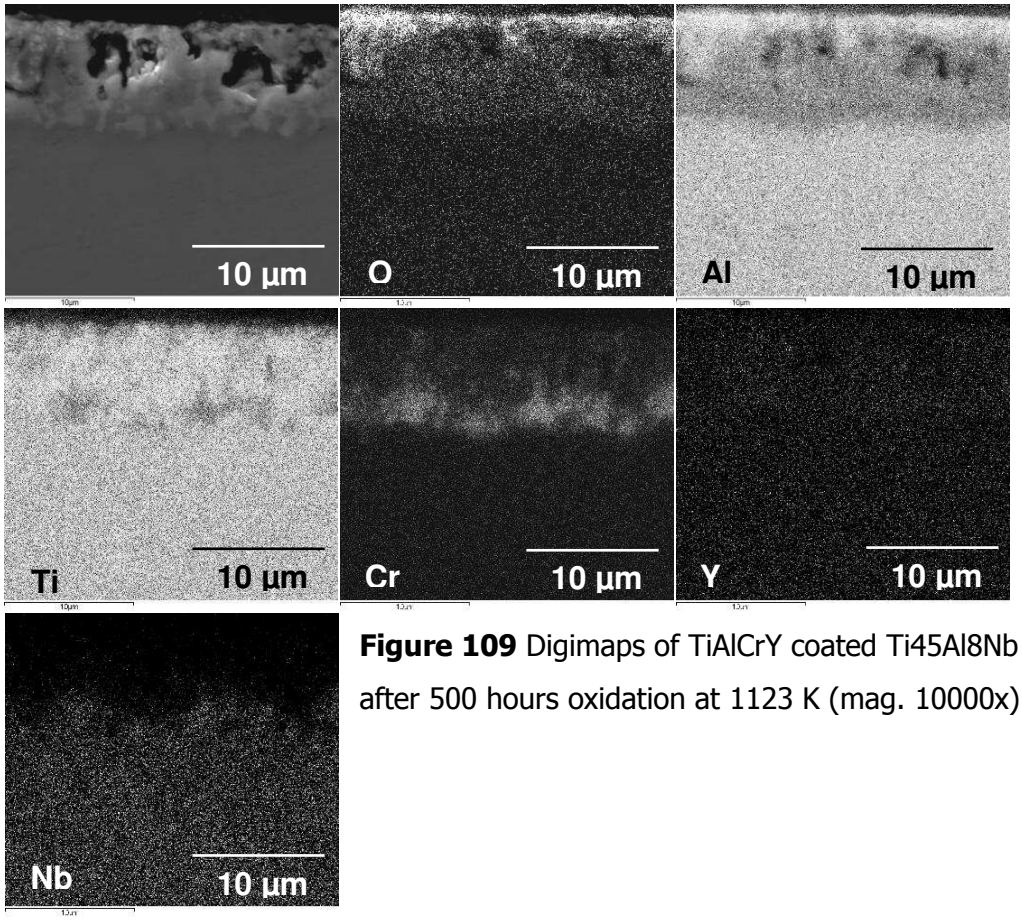

Figure 109 Digimaps of TiAlCrY coated Ti45Al8Nb after 500 hours oxidation at 1123 K (mag. 10000x)

The XRD analysis (not shown here) confirmed, the formation of Al_2O_3 and TiO_2 oxides, moreover $TiAl_2$, $TiAl_3$, and Cr_2O_3 oxide also were detected.

Ch.VI.Sec.1.6 CrAl2%YN coated Ti45Al8Nb alloy 1123 K

The surface of CrAl2%YN coated Ti45Al8Nb alloy presented in **figure 110** shows the lack of corrosion products after oxidation for 500 hours at 1123 K.

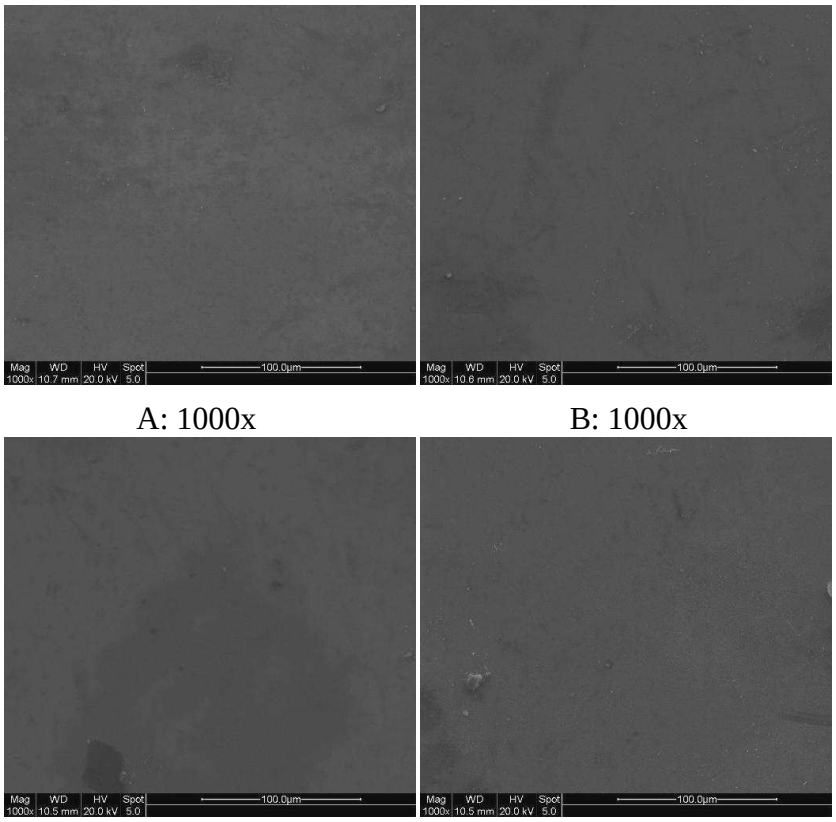

A: 1000x B: 1000x

C: 1000x D: 1000x

Figure 110 SEM images from surface of CrAl2%YN coated Ti45Al8Nb after 500 hours oxidation at 1123 K (magnification under images)

The EDS surface analysis is given in **table 34** and performed in different areas of the specimen indicates that mainly Al_2O_3 and Cr_2O_3 oxides developed with the minor amounts of Ti and Y.

Image	at% O	at% Al	at% Ti	at% Cr	at% Y
A	58.773	29.175	0.399	11.068	0.585
B	57.888	28.771	0.456	12.195	0.690
C	56.845	29.517	0.440	12.506	0.693
D	58.760	28.155	0.460	12.009	0.616

Table 34 Surface analysis performed by EDS investigation of CrAl2%YN coated Ti45Al8Nb after 500 hours of oxidation at 1123 K

Figure 111 presents cross – sectioned SEM images of CrAl2%YN coated Ti45Al8Nb alloy after oxidation at 1123 K for 500 hours. The scale morphology of CrAl2%YN coated Ti45Al8Nb alloy is similar to those obtained at lower temperature (1023 K). The coating shows good corrosion resistance at 1123 K due to the development Al_2O_3 and Cr_2O_3 oxide scale.

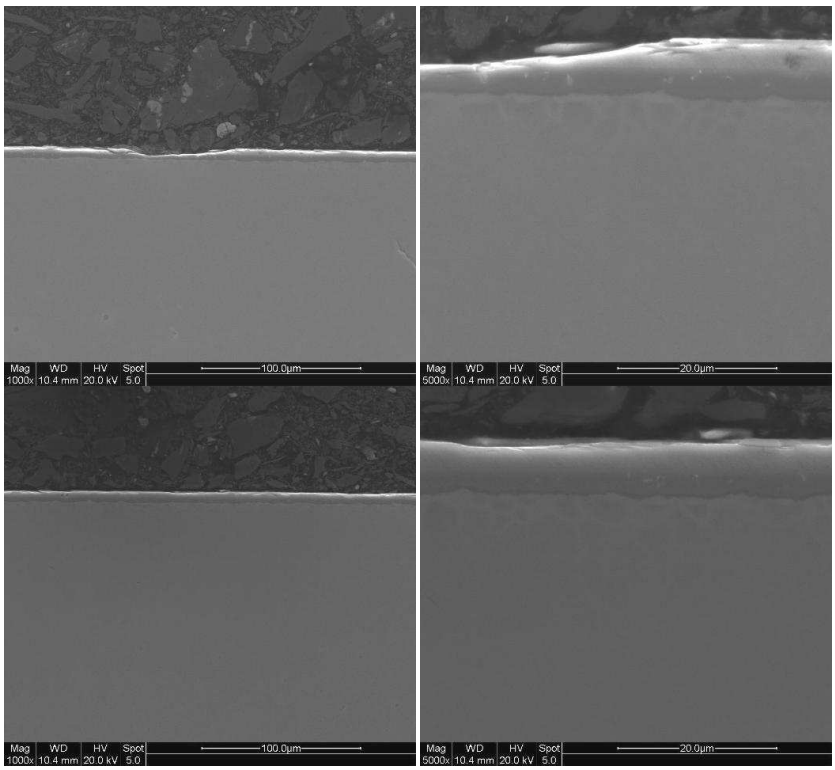

CrAl2%YN coated Ti45Al8Nb alloy after 500 hours of oxidation at 1123 K. Mag.1000 (left) and 5000 (right) – near to the edge of the sample

Figure 111 Cross – sectional images of CrAl2%YN coated Ti45Al8Nb after 500 hours of oxidation at 1123 K

Figure 112 shows CrAl2%YN coated Ti45Al8Nb alloy after exposure at 1123 K in oxidation atmosphere for 500 hours. The thicker scale of Al_2O_3 and Cr_2O_3 developed than at 1023 K was confirmed by the EDS concentration profiles in **figure 113**. However the scale shows brittleness (arrows in **figure 112**).

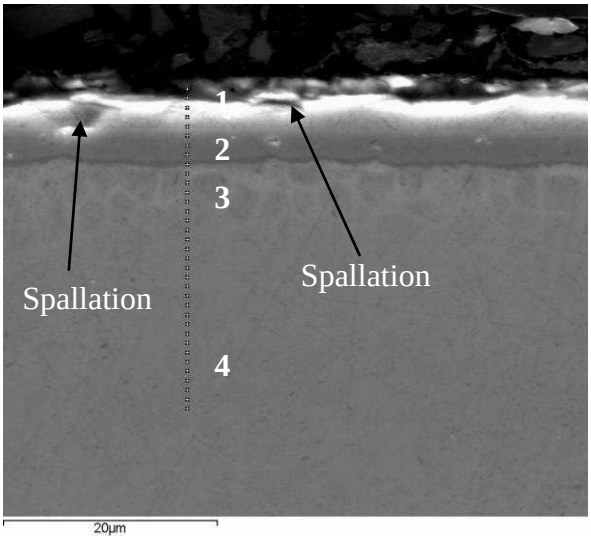

1) Cr_2O_3 and Al_2O_3 oxides scale
2) Modified coating (CrAl2%YN)
3) TiN layer

4) Substrate (Ti45Al8Nb alloy)

Figure 112 SEM cross – section image of CrAl2%YN coated Ti45Al8Nb alloy after 500 hours of oxidation at 1123 K (mag. 5000x)

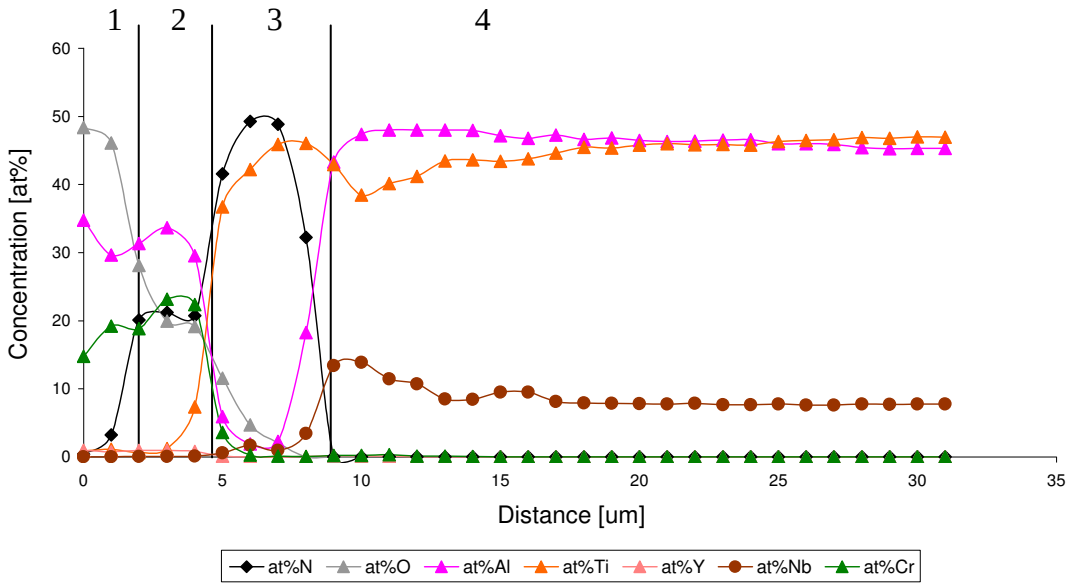

Figure 113 EDS concentration profiles obtained from CrAl2%YN coated Ti45Al8Nb alloy after 500 hours of oxidation at 1123 K

Figure 113 shows concentration profiles of CrAl2%YN coated Ti45Al8Nb alloy after exposure at 1123 K in oxidation atmosphere for 500 hours. A thicker (than that at 1023 K) scale of Al_2O_3 and Cr_2O_3 developed. Moreover, underneath the modified coating a thicker TiN layer also formed. This thicker TiN layer is an excellent diffusion barrier for Ti mass transport through the coating preventing the formation of a non protective scale (TiO_2). At the TiN/substrate interface a depletion zone of Ti occurred, this depletion zone was related to the outward diffusion of Ti ions in order to form TiN layer. The straight lines in the concentration profiles indicate the different regions with different phase formation. More details of scale formation is observed from EDS X-Ray mapping performed on exposed CrAl2%YN coating in **figure 114**. The outer scale is covered by Al and Cr oxides (Al_2O_3 and Cr_2O_3), and Nb ions reaming in the substrate (Ti45Al8Nb). The EDS X-Ray mapping detected TiN thick layer formed under modified coating.

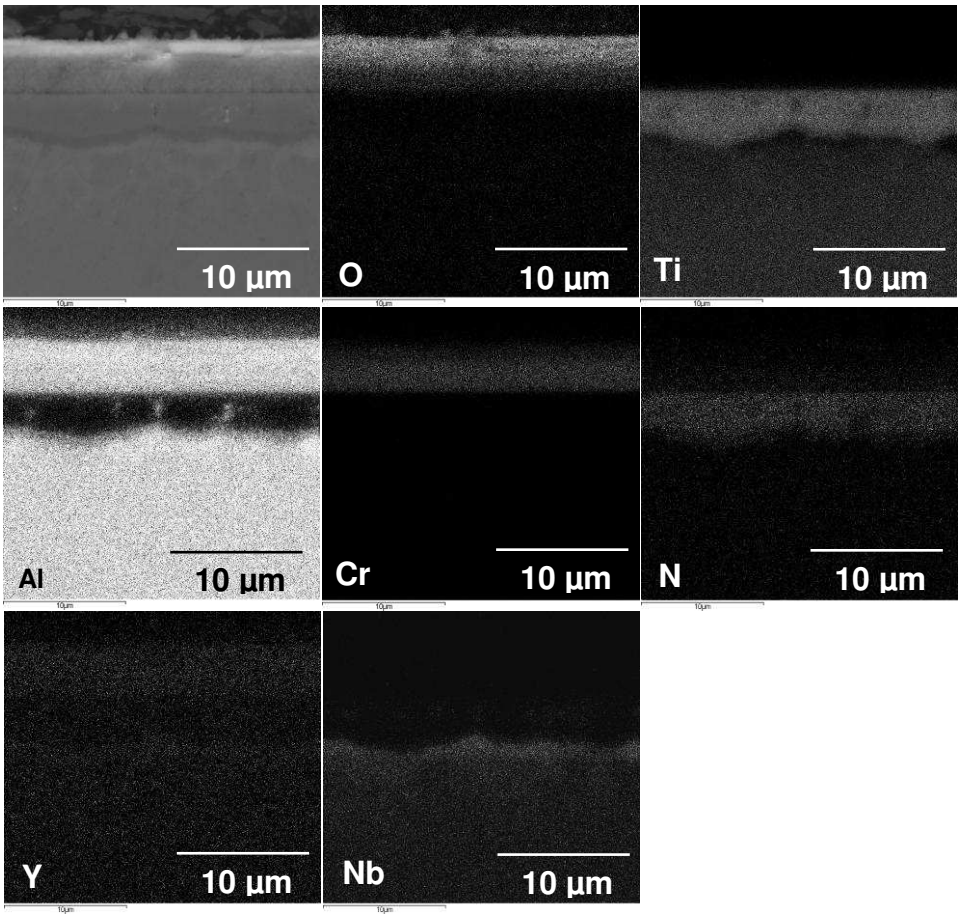

Figure 114 Digimaps of CrAl2%YN coated Ti45Al8Nb after 500 hours oxidation at 1123 K (mag. 10000x)

The XRD pattern (not presented here) was in is in good agreement with the EDS concentration profiles and EDS X-Ray mapping analysis. The XRD detected Al_2O_3, Cr_2O_3, and the substrate phases: $TiAl_3$, $TiAl_2$. However the XRD did not detect TiN layer although the TiN layer was thicker than at 1023 K.

Ch.VI.Sec.1.7 TiAlCrY coated Ti45Al8Nb alloy 1223 K)

Figure 115 presents SEM micrographs of the surface of the TiAlCrY (Ti55Al14Cr0.3Y) coated Ti45Al8Nb alloy after 500 hours oxidation at 1223 K. The SEM images show, the formation of large and thick crystals of mixed TiO_2 and Al_2O_3. The scale developed at 1223 K was similar to that at 1123 K however; the crystal size was much bigger.

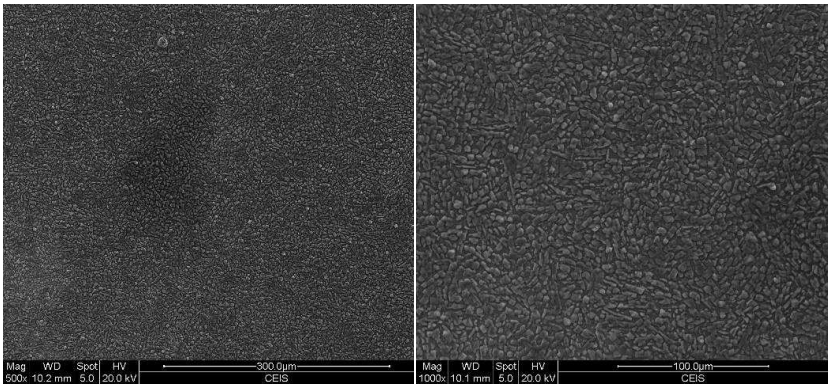

A: 500x B: 1000x

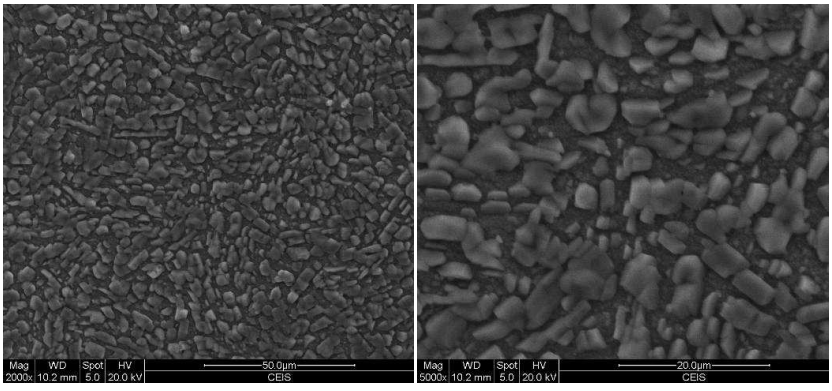

C: 2000x C: 5000x

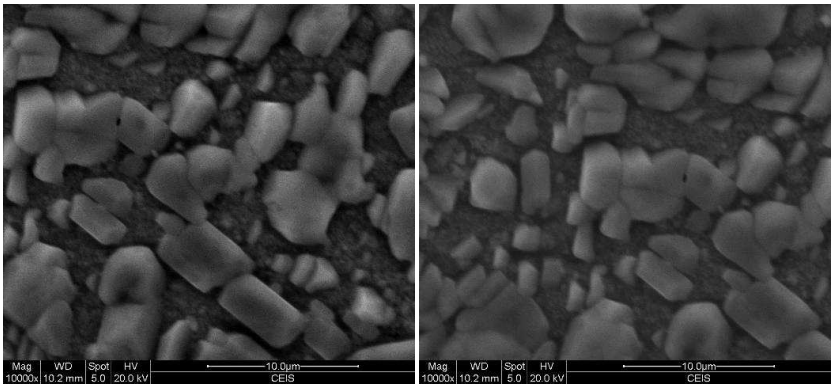

E: 10000x F: 10000x

Figure 115 SEM images from surface of TiAlCrY coated Ti45Al8Nb after 500 hours oxidation at 1223 K (magnification under images)

The EDS surface analysis is presented in **table 35** performed on exposed sample indicates the development of mainly Ti and Al oxide. It is important to note that the trace amounts of Y and Cr also were detected.

Image	at%O	at%Al	at%Ti	at%Cr	at%Y
A	70.221	9.407	19.413	0.917	0.041
B	66.735	18.486	13.939	0.775	0.064
C	66.516	18.325	14.012	0.796	0.350
D	65.969	18.951	14.084	0.723	0.274

Table 35 Surface analysis performed by EDS investigation of TiAlCrY coated Ti45Al8Nb after 500 hours of oxidation at 1223 K

Figure 116 shows the cross – sectioned SEM images of the scale developed on TiAlCrY coated Ti45Al8Nb alloy after 500 hours oxidation at 1223 K. The scale formed during oxidation was brittle but did not spall off from the material; the mass gain of the sample had a constant character without spallation region. The spallation of the brittle oxide scale occurred during cutting cycle where sample was prepared for cross – section investigation. The cross – section investigation in details is presented by SEM image in **figure 116** and the EDS concentration profiles in **figure 118**.

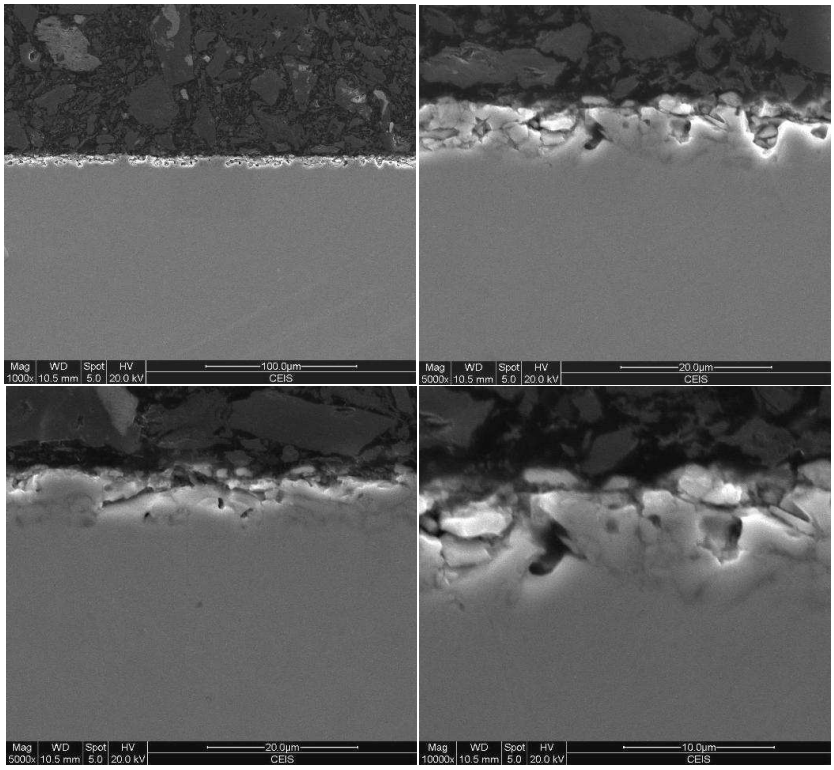

5000 (left) and 10000 (right) images of TiAlCr coated Ti45Al8Nb after 500 hours oxidation at 1223 K

Figure 116 Cross – sectional images of sample TiAlCrY coated Ti45Al8Nb after 500 hours oxidation at 1223 K

The cross section SEM micrograph of the exposed TiAlCrY coated alloy in **figure 117** shows that the scale morphology after exposure is similar to those obtained at 1123 K. Voids and brittle scale formed consisting of Al and Ti oxides. Moreover the outer scale of the exposed material (TiAlCrY coated Ti45Al8Nb alloy) was very porous and large concentration of oxygen was detected by the EDS analysis shown in **figure 118.**

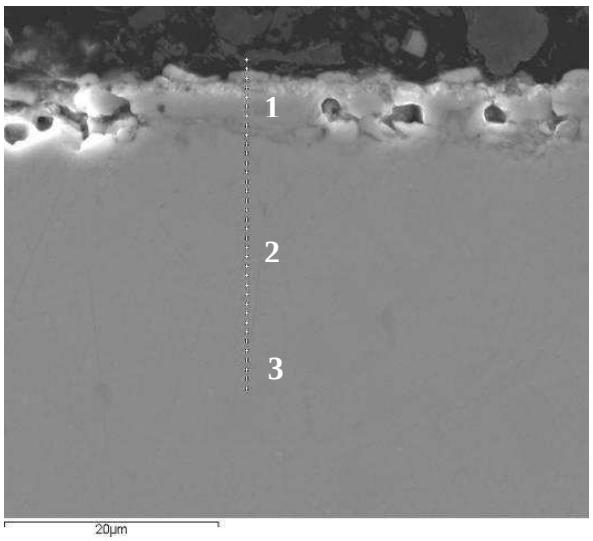

1) Less dense TiO_2, Al_2O_3 oxide layer
2) More denser TiO_2, Al_2O_3 oxide layer
3) Substrate (Ti45Al8Nb alloy)

Figure 117 Cross – section SEM image (mag. 5000x) of TiAlCrY coated Ti45Al8Nb alloy after 500 hours of oxidation at 1223 K

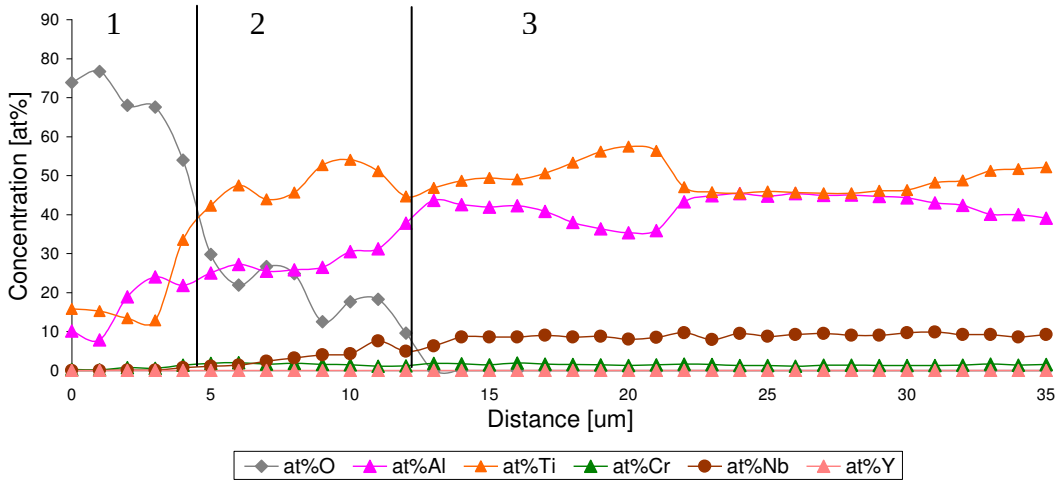

Figure 118 EDS concentration profiles obtained from TiAlCrY coated Ti45Al8Nb alloy after 500 hours of oxidation at 1223 K

The EDS concentration profiles in **figure 118** show the outer scale consisting mixed Al_2O_3 and TiO_2 oxides. Underneath the outer porous scale consisted of Al and Ti oxides the inner layer also consisting of Al and Ti oxides however the structure was denser. The concentration of Cr is equivalent to zero. It appears that the original TiAlCrY coating was transformed into the scale. The outward diffusion of Al and Ti

from the bulk material and high partial pressure of oxygen caused the formation of Al and Ti oxides showing a porous and brittle structure.

EDS X-Ray mapping presented in **figure 119** confirms the formation of phases (Al and Ti oxides) developed after exposure at 1223 K. Additionally the Ti and Al maps indicate significant interdiffusion within the alloy and oxide scales. These diffusion regions are associated with the phase transformation from nearly γ-TiAl (Ti45Al8Nb alloy) to α_2 – Ti_3Al and α-$TiAl_3$. Based on this observation it can be suggested that these regions are source of Al and Ti ions for the formation of Al and Ti oxides.

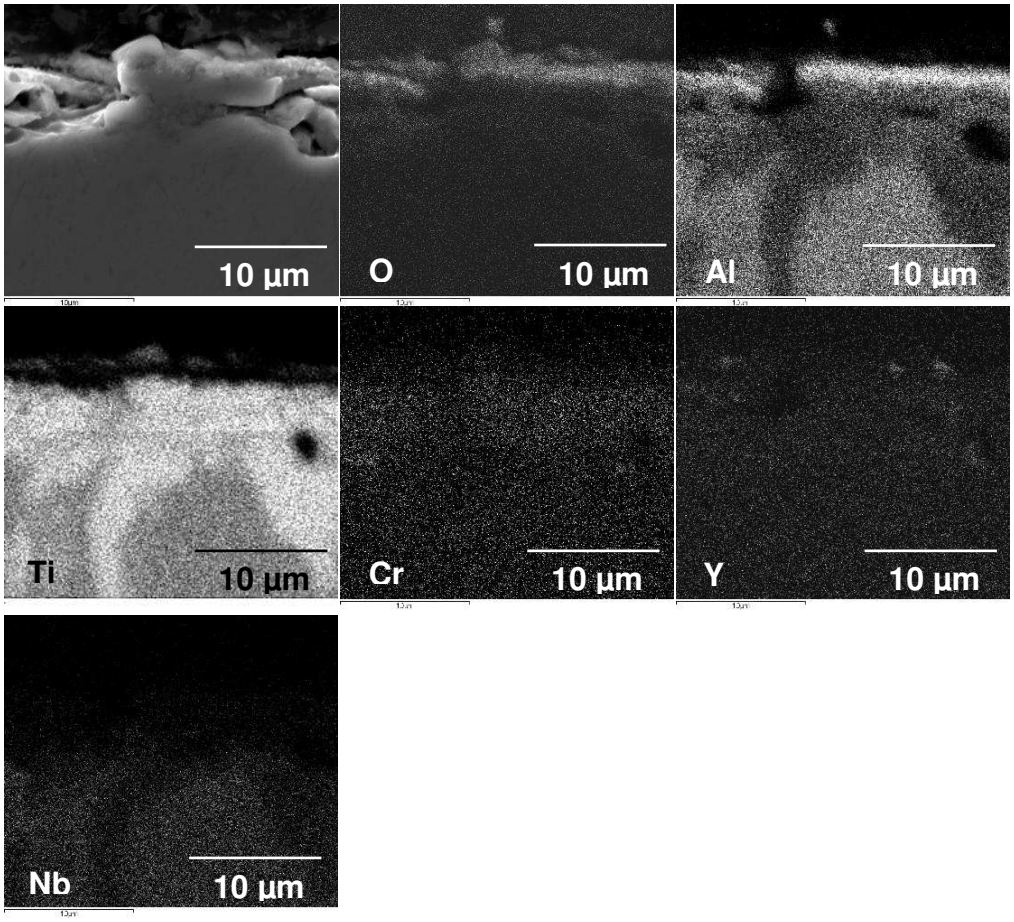

Figure 119 Digimaps of TiAlCrY coated Ti45Al8Nb after 500 hours oxidation at 1223 K (mag. 5000x)

The XRD analysis (not presented here) indicates that Al_2O_3 and TiO_2 oxides formed after 500 hours oxidation at 1223 K. However some small peaks of Cr oxides were detected (Cr_3O_4, Cr_2O_3), also peaks from the substrate were observed, mainly $TiAl_2$ and $TiAl_3$, however, these peaks, were probably detected due to the porous scale, formed at 1223 K.

Ch.VI.Sec.1.8 CrAl2%YN coated Ti45Al8Nb alloy at 1223 K

Figure 120 shows micrographs form CrAl2%YN coated Ti45Al8Nb alloy surface after 500 hours oxidation at 1223 K. The rough surface was developed due to the fast outward diffusion of Ti ions from the bulk material.

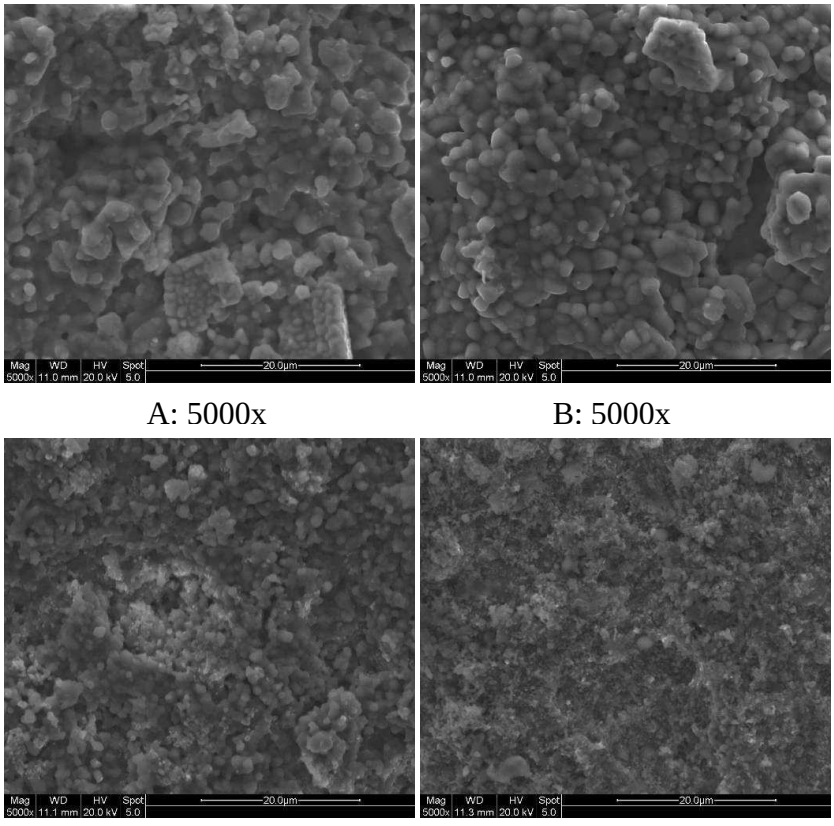

A: 5000x B: 5000x

C: 5000x D: 5000x

Figure 120 SEM images from surface of CrAl2%YN coated Ti45Al8Nb after 500 hours oxidation at 1223 K (magnification under images)

The development of the TiO_2 oxide was confirmed by the EDS analysis in **table 36** performed in particular places and indicates that apart from TiO_2 small amounts of Al, Cr, and Nb were detected due to the outward diffusion from the substrate.

Image	at% O	at% Al	at% Ti	at% Cr	at% Y	at% Nb
A	76.196	3.245	18.696	0.283	1.246	0.334
B	75.205	3.332	21.083	0.379		
C	79.512		15.580	0.325		4.583
D	72.280	11.015	13.953			2.751

Table 36 Surface analysis performed by EDS investigation of CrAl2%YN coated Ti45Al8Nb after 500 hours of oxidation at 1223 K

Figure 121 shows a several pictures of the scale formed (at various magnifications) on CrAl2%YN coated Ti45Al8Nb alloy after exposure in oxidation atmosphere in static laboratory air at 1223 K. The thick scale formed due to the coating failure in the initial stage of oxidation. During heating or cooling period, the stresses generated due to the mismatch of thermal coefficient between CrAl2%YN coat and Ti45Al8Nb alloy destroyed the coating. The damaged coating was not spalled off (kinetic data **Fig. 92**) but the cracks in the coating provided the fast diffusion paths for oxygen and for diffusion metallic ions from the bulk material.

The more details are shown in the EDS concentration profiles presented in **figure 122**.

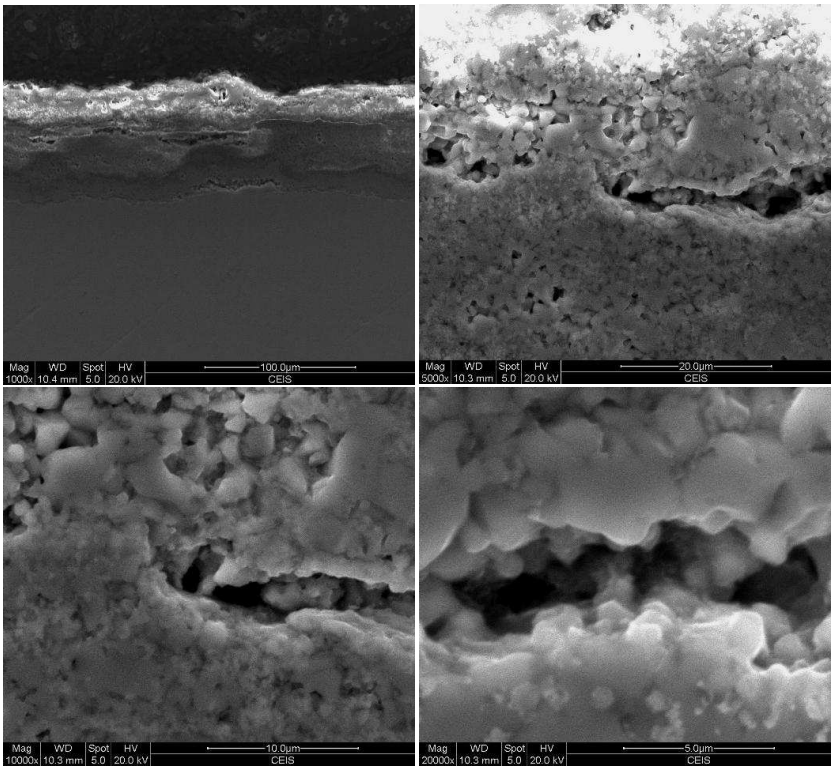

CrAl2%YN coated Ti45Al8Nb alloy after 500 hours of oxidation at 1223 K. Mag.10000 (left) and 20000 (right) – near to the edge of the sample

Figure 121 Cross – sectional images of sample CrAl2%YN coated Ti45Al8Nb after 500 hours oxidation at 1223 K

Figure 122 shows SEM image of cross – sectioned CrAl2%YN coated Ti45Al8Nb alloy after 500 hours oxidation at 1223 K. The large and thick scale formed on the substrate mainly consisted of TiO_2 and Al_2O_3 oxides. The sandwich like structure (of alternative layers of TiO_2/Al_2O_3) developed a 90 µm thick scale and this scale is shown on the EDS concentration profiles in **figure 123**. The oxidation resistance of this coating was limited only to 1123 K because at higher temperature the breakdown oxidation occurred causing a catastrophic corrosion.

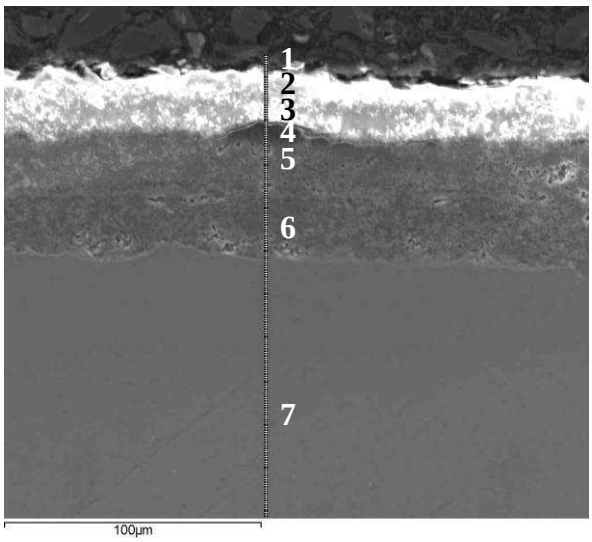

1) TiO_2 oxide layer
2) TiO_2/Al_2O_3 oxides layer
3) Al_2O_3 oxide layer
4) TiO_2 oxide layer
5) Al_2O_3 oxide layer
6) TiO_2 oxide layer
7) Substrate (Ti45Al8Nb)

Figure 122 Cross – section SEM image (mag. 5000x) of CrAl2%YN coated Ti45Al8Nb alloy after 500 hours of oxidation at 1223 K

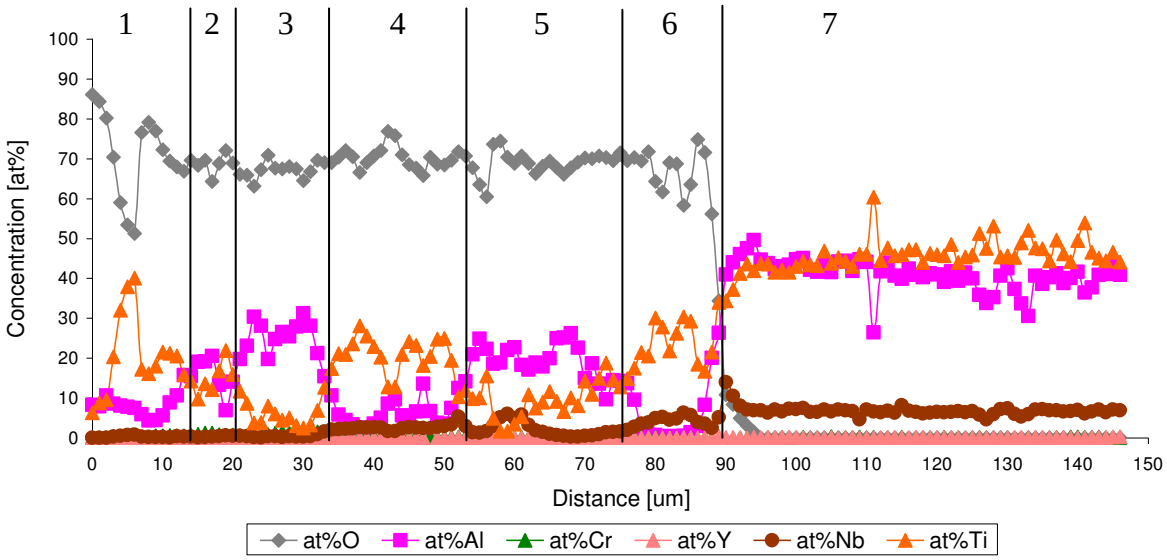

Figure 123 EDS concentration profiles obtained from CrAl2%YN coated Ti45Al8Nb alloy after 500 hours of oxidation at 1223 K

The EDS concentration profiles in **figure 123** show the formation a thick TiO_2 and Al_2O_3 scale. It is suggested that the scale was initiated at the beginning of the experiment, when impact of high temperature (1223 K) decomposes the TiN layer.

The EDS X-Ray mapping performed on CrAl2%YN Ti45Al8Nb alloy is presented in **figure 124** and confirms, that a thick TiO_2 and Al_2O_3 scale was formed at 1223 K other elements: Cr, N, and Y were not detected by EDS X-Ray mapping presented in **figure 124**. However EDS X-Ray mapping shows that Nb ions formed two very thin layers (EDS X-Ray mapping) within the thick TiO_2 and Al_2O_3 scale. It can be suggested that formation of Nb_2O_5 was likely to occur, however, the XRD pattern did not detected this phase during investigation.

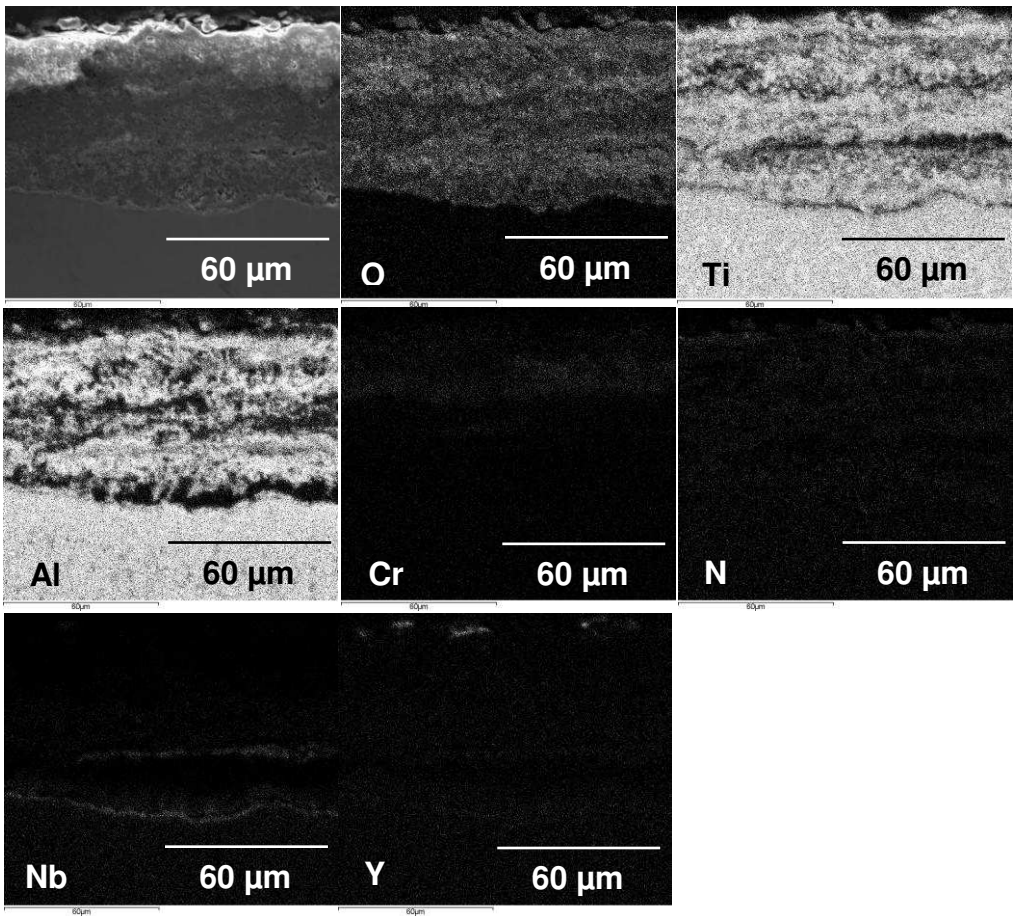

Figure 124 Digimaps of CrAl2%YN coated Ti45Al8Nb after 500 hours oxidation at 1223 K (mag. 5000x)

The XRD pattern (not shown here) confirmed the presence of only al and Ti oxides – no other phases were detected.

Part Two – Oxidation studies at 1023 K for 5000 hours

The long term oxidation tests at 1023 K for 5000 hours were carried out on three coatings:

1) TiAlCr (Ti42Al15Cr) [at%]

2) TiAlYN/CrN+Al_2O_3

3) TiAlN + Al_2O_3 (25Ti25Al50N+Al_2O_3) [at%]

Ch.VI.Sec.1.9 Oxidation kinetics for three coatings

Figure 125 presents kinetic data obtained for the samples after 5000 hours at 1023 K.

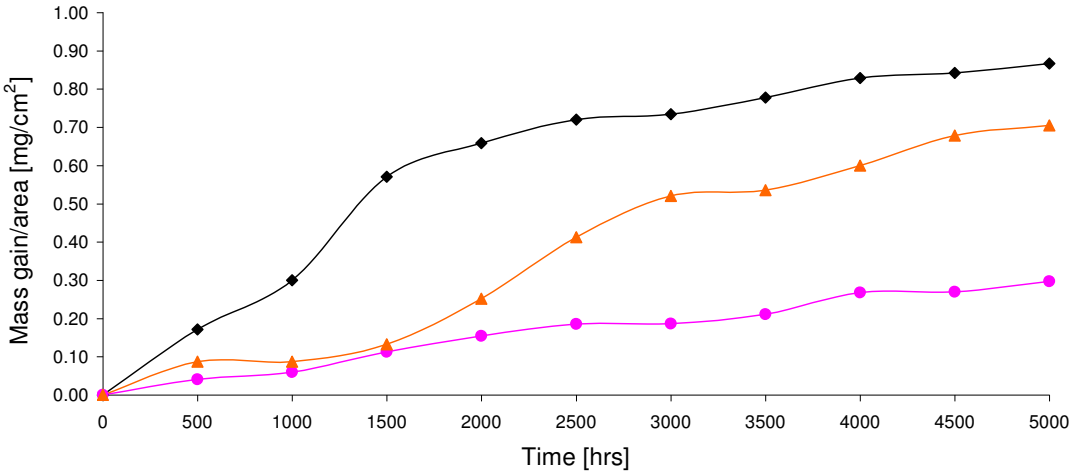

♦ TiAlCr coating, ● TiAlYN/CrN+Al_2O_3 coating, ▲ TiAlN+Al_2O_3 coating

Figure 125 Kinetic data obtained for exposed samples to static air at 1023 K for 5000 hours

The kinetic data shown in **figure 125** reveals highest mass gain for TiAlCr coating and lowest mass gain was obtained for the TiAlYN/CrN+Al_2O_3 coating. The exposed samples did not suffer spallation, however an increase in the mass gain of

TiAlN + Al_2O_3 coating was visible between 2000, and 3000 hours of exposure. Similar to TiAlN+Al_2O_3 coating, TiAlCr coating showed the acceleration in the mass gain between 500 and 1500 hours of exposure. The calculated kp values are presented in **table 37**.

The calculated values of the parabolic rate constant **(Table 37)**, indicates that TiAlYN/CrN+Al_2O_3 showed the best corrosion resistance during very long oxidation test, whereas TiAlCr coating the poorest corrosion resistance.

Sample	TiAlCr	TiAlYN/CrN+Al_2O_3	TiAlN+Al_2O_3	Unit
kp	$4.508E^{-08}$	$5.068E^{-09}$	$3.079E^{-08}$	$[mg^2/cm^4/s]$

Table 37 Parabolic rate constant values obtained from oxidation experiment performed at 1023 K for 5000 hours

Ch.VI.Sec.1.10 TiAlCr coated Ti45Al8Nb alloy

The surface morphologies of oxidised TiAlCr (Ti42Al15Cr) coated Ti45Al8Nb sample are given in **figure 126**. The surfaces show the formation of the development of different morphologies in different areas. The SEM images of the edge of the sample (**Figs. 126C, 126E**) show the development of a thick rough oxide and whisker structure (**Fig 126D**); however the middle part of the sample formed tinny crystals. The details of the corrosion product which covered the surface of exposed sample performed by the EDS investigation are presented in **table 38**.

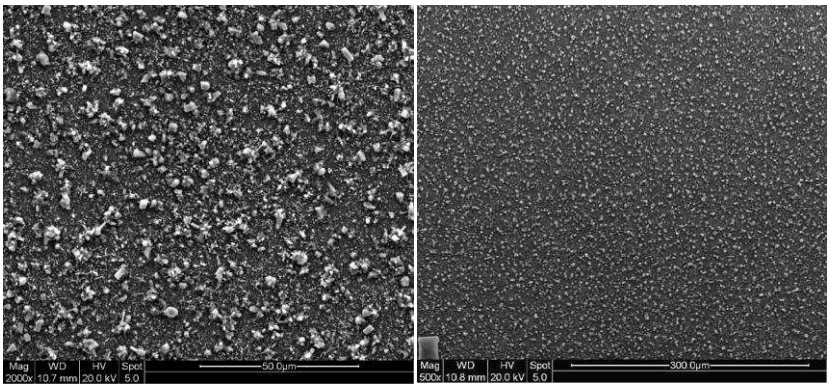

A: 1000x B: 500x

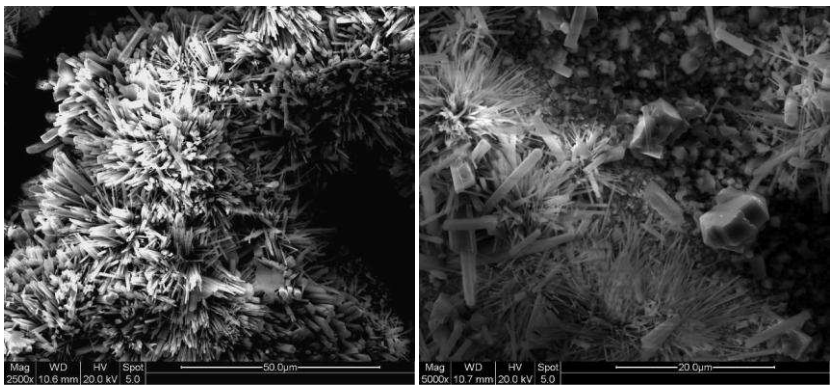

C: 2500 x D: 5000x

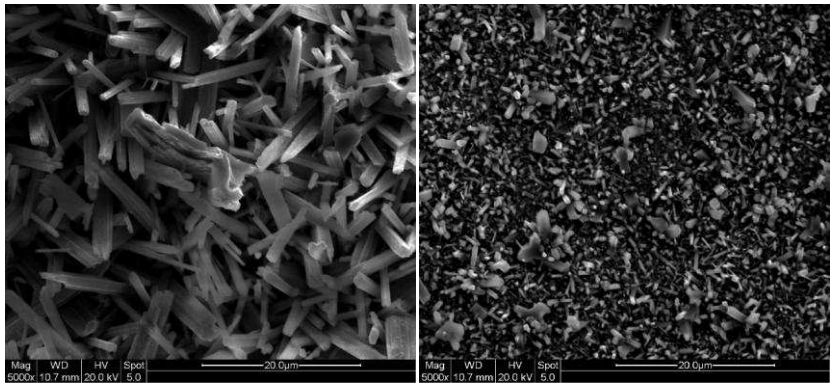

E: 5000x F: 5000x

Figure 126 SEM images from surface of TiAlCr coated Ti45Al8Nb after 5000 hours of oxidation at 1023 K (magnification under images)

The middle part of the sample was covered by the TiO_2 and Al_2O_3 mixed oxides with trace amount of Cr, however edge of the oxidised sample was covered mainly by TiO_2 with very small addition of Al_2O_3 oxide, and trace amount of Cr. Nb was not detected in on the surface of oxidised sample and remained in the alloy (Ti45Al8Nb).

Image	at% O	at% Al	at% Ti	at% Cr
A	65.708	17.532	15.250	1.510
B	66.107	18.423	14.460	1.048
C	69.056	4.135	26.491	0.318
D	69.486	10.823	18.531	1.160
E	70.112	1.713	28.175	
F	64.529	18.443	15.646	1.383

Table 38 Surface analysis performed by EDS investigation of TiAlCr coated Ti45Al8Nb after 5000 hours of oxidation at 1023 K

The SEM cross – section investigation performed on oxidised TiAlCr coated Ti45Al8Nb sample given in **figure 127** reveals that the coating suffered corrosion forming a thick, brittle, and non protective scale, which spalled off from the substrate. Moreover the scale formed after oxidation at 1023 K consisted of a multilayered structure with high porosity. Figures on the left hand side present scale structure from the middle part of the sample, whereas images on the right hand side show the scale developed at the edges of the sample. More details related to the scale structure are presented in **figure 128 and 129**, where SEM and the EDS analysis with concentration profiles are given.

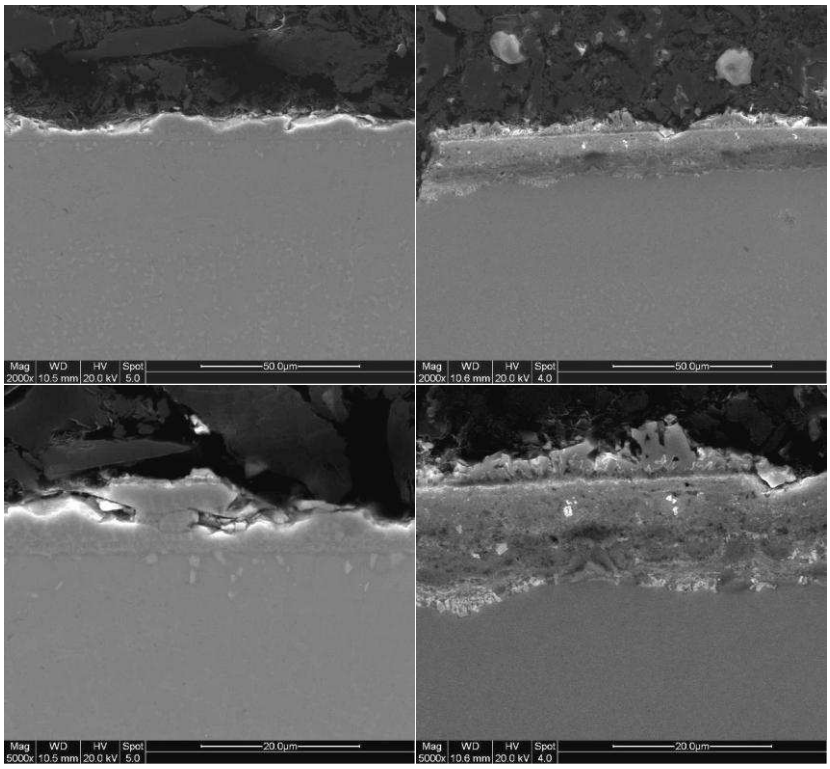

Figure 127 Cross – sectional images of sample (TiAlCr coated Ti45Al8Nb) after 5000 hours of oxidation at 1023 K. Scale formed on edges (right) scale formed in the middle of the sample (left)

The SEM image of the edge of TiAlCr coated Ti45Al8Nb alloy subjected to oxidation at 1023 K for 5000 hours is presented in **figure 128**.

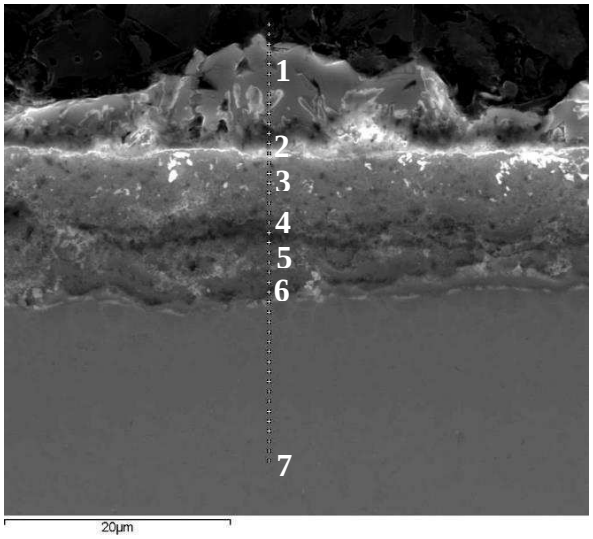

1) TiO_2 oxide layer
2) TiO_2/Al_2O_3 oxides layer
3) Al_2O_3 oxide layer
4) TiO_2 oxide layer + small amount of Cr_2O_3
5) Al_2O_3 oxide layer + small amount of Cr_2O_3
6) TiO_2 oxide layer/diffusion zone of Al and Ti
7) Substrate (Ti45Al8Nb alloy)

Figure 128 SEM cross section image (mag. 5000x) of the sample (TiAlCr coated Ti45Al8Nb after 5000 hours of oxidation at 1023 K) – edge of the sample

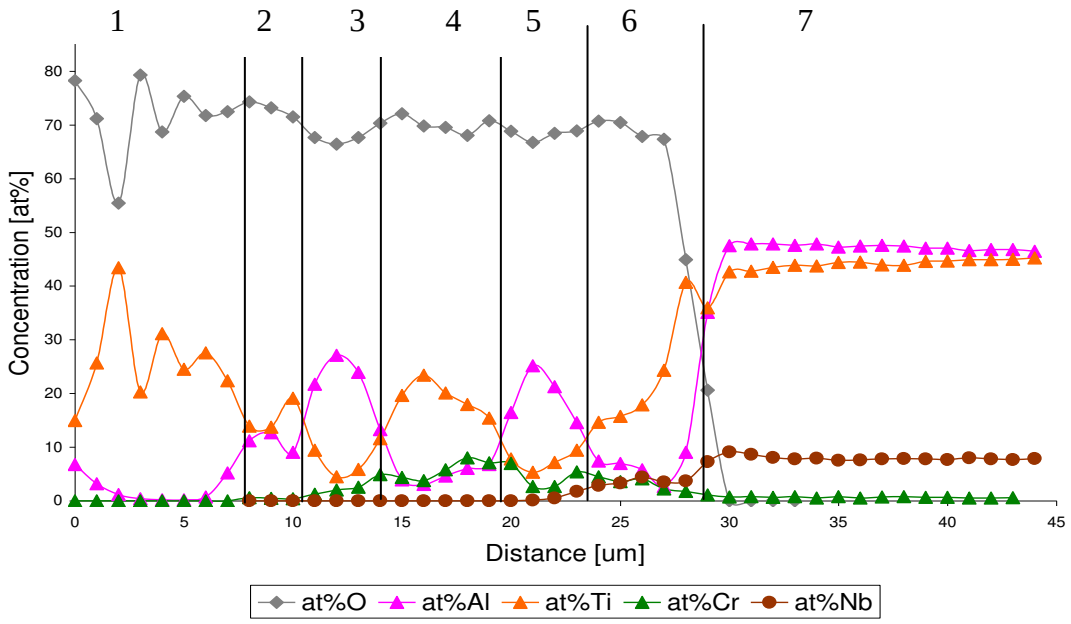

Figure 129 The EDS concentration profiles obtained from TiAlCr coated Ti45Al8Nb alloy after 5000 hours of oxidation at 1023 K (profiles obtained from edges of the sample)

The concentration profiles of exposed sample performed by the EDS analysis shown in **figure 129** display that the outer scale was occupied by a thick (7 µm) TiO_2 oxide scale, below that scale a thin (2 µm) mixed TiO_2 and Al_2O_3 layer developed, underneath mixed oxides layer Al_2O_3 oxide formed.

An alternate layer of TiO_2/Al_2O_3 developed. Between substrate and Al_2O_3 layer a large depletion zone of TiO_2 formed where content of Al, Cr and Nb was very low. However, the observed a higher concentration of Cr in the middle of the formed oxide scale indicates that modified coating existed in the middle of the scale. It is suggested that the mass transport occurred from the coating and from the substrate simultaneously, this means that the diffusion of Ti ions and Al ions to formed a mixed $TiO_2 – Al_2O_3$ oxide scale came from two sources; the coating and the substrate. **Figure 130** shows the SEM micrograph of the scale structure developed in the middle part of the sample. A relatively thin (2 µm) oxide scale developed on oxidised sample. The scale was brittle and non protective and spalled off from material. The spallation occurred during cutting cycle not during experiment. The mass gain of exposed sample does not show spallation behaviour (**Fig. 125**). The more details about scale development are presented in **figure 131** where the EDS concentration profiles are given.

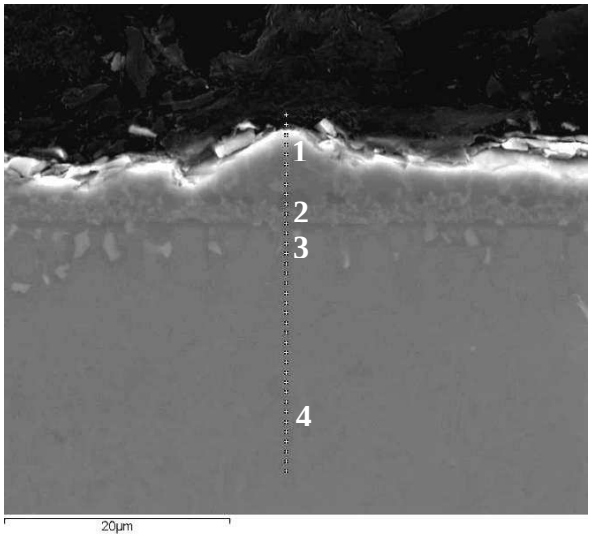

1) TiO_2/Al_2O_3 oxides layer
2) Modified coating (TiAlCr)
3) Diffusion zone

4) Substrate (Ti45Al8Nb alloy)

Figure 130 SEM cross section image (mag. 5000x) of the sample (TiAlCr coated Ti45Al8Nb after 5000 hours of oxidation at 1023 K) – middle of the sample

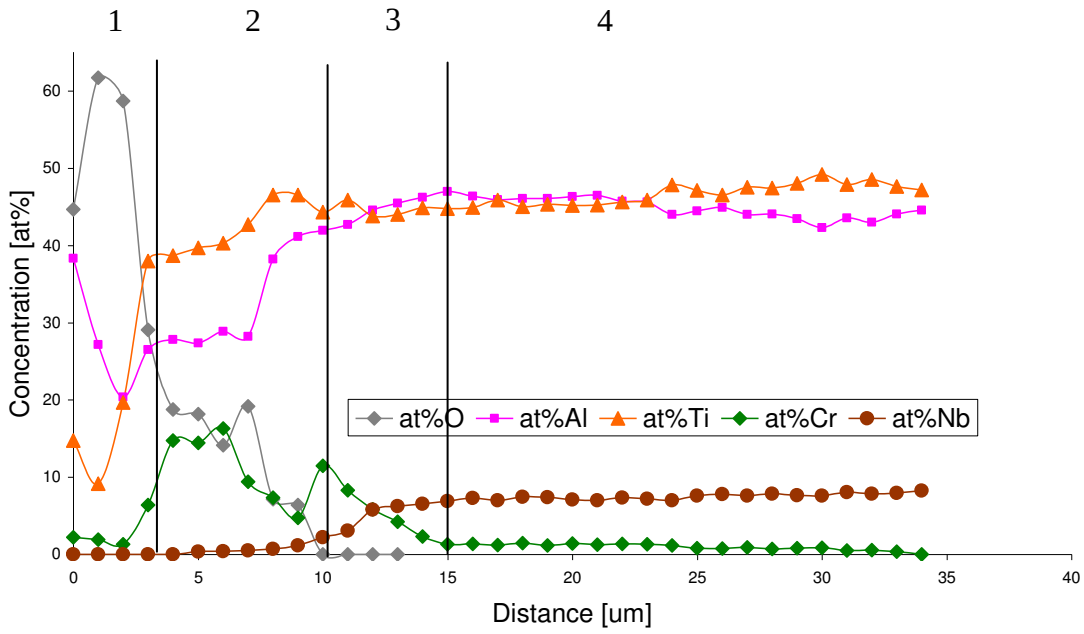

Figure 131 EDS concentration profiles obtained from TiAlCr coated Ti45Al8Nb alloy after 5000 hours at 1023 K (profiles obtained from middle of the sample)

The concentration profiles of exposed sample (TiAlCr coated Ti45Al8Nb) (**Fig. 131**) show that the outer scale is occupied by mixed TiO_2 and Al_2O_3 oxides, underneath this mixed oxide scale there was the modified coating with relatively high Cr content (around 20 at %). Within the modified coating the depletion zone of Ti and Al ions existed. It is interesting to note that Cr content increased in the modified coating/substrate interface. As **figure 131** shows the Nb remained in the substrate, and did not form an oxide in the outer part of the scale. The EDS X-Ray mapping from edge of the sample is shown in **figure 132**, the good agreement between the EDS concentration profiles (**Fig. 131**) and the EDS X-Ray mapping, confirms that during heat treatment at 1023 K for 5000 hours, a multilayered oxide scale developed consisting of TiO_2 and Al_2O_3 oxides. Moreover EDS X-Ray mapping shows that Cr remained in the modified coating, and was not detected in the outer part of the scale, Nb also remained in the substrate.

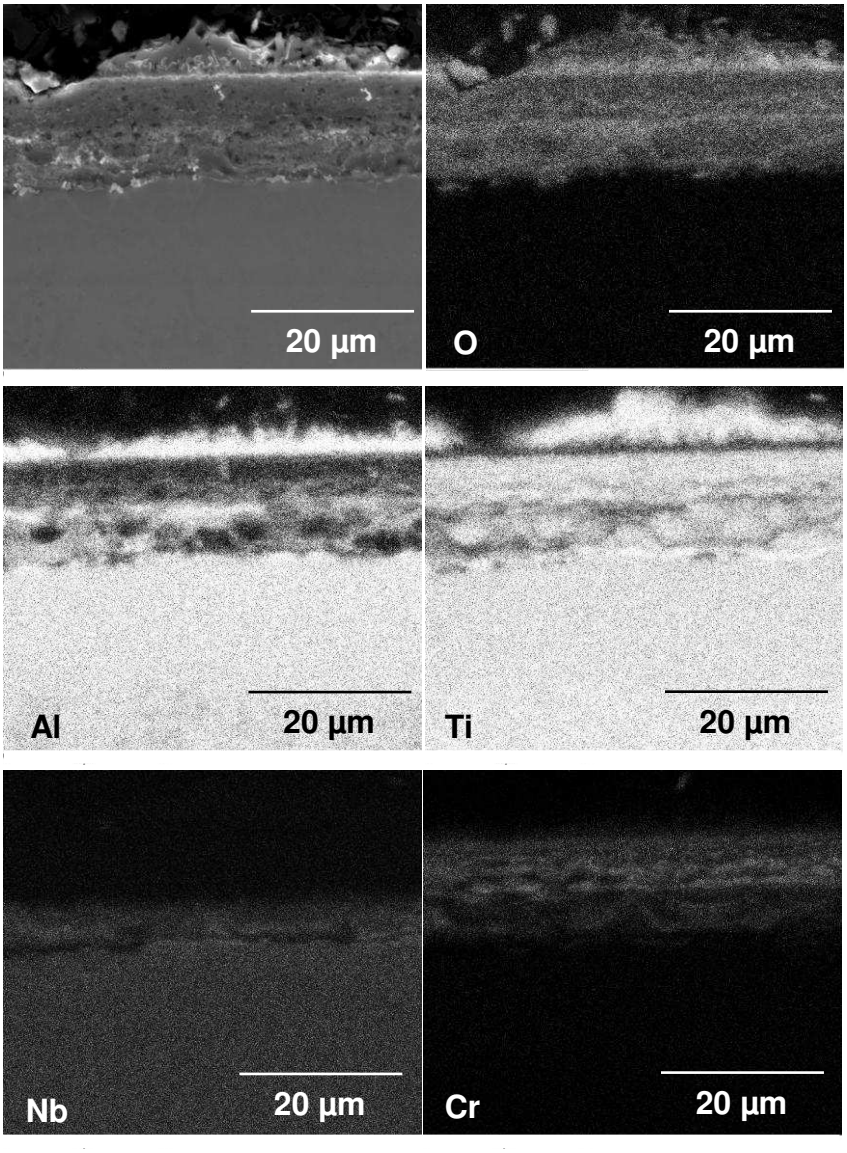

Figure 132 EDS cross section mapping of TiAlCr coated Ti45Al8Nb after 5000 hours of oxidation at 1023 K – mappings taken from the edge of the sample (mag. 5000x)

The EDS X-Ray mapping of the middle part of the oxidised sample (TiAlCr coated Ti45Al8Nb) is given in **figure 133.** The EDS X-Ray mapping in **figure 132** shows good agreement between the EDS concentration profiles (**Fig 131**).

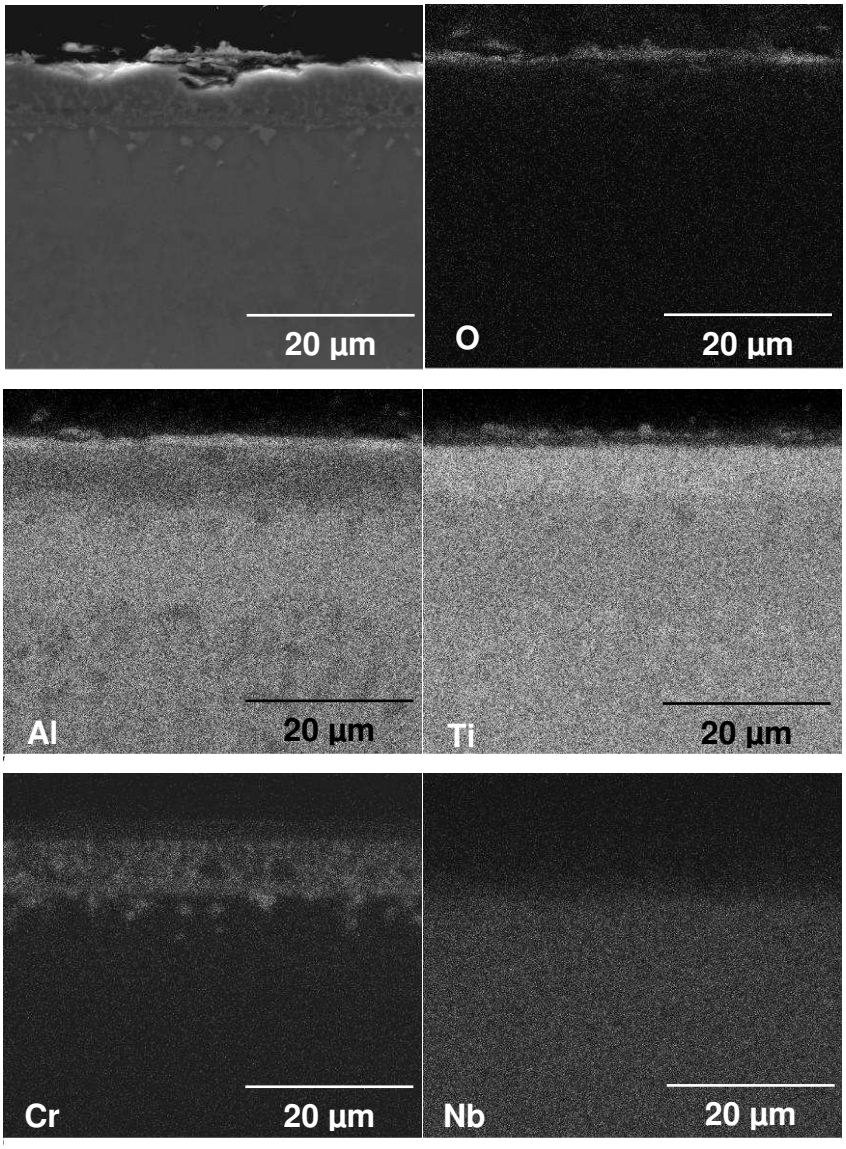

Figure 133 EDS cross section mapping of TiAlCr coated Ti45Al8Nb after 5000 hours at 1023 K – mappings taken from middle of the sample (mag. 5000x)

The XRD analysis (not shown here) confirmed the information given by the EDS concentration profiles and EDS X-Ray mapping (edge of the sample, middle part of the sample).

Ch.VI.Sec.1.11 TiAlYN/CrN+Al_2O_3 coated Ti45Al8Nb alloy

The surface morphologies of TiAlYN/CrN+Al_2O_3 coated Ti45Al8Nb alloy after 5000 hours oxidation at 1023 K presented in **figure 134** shows that the surface of the exposed sample suffered oxidation damage mainly at the edges, where oxide scales

developed **(Figs. 134B, D, and E)**. However, the middle part of the surface shows good oxidation resistance and some small singular crystals developed. **Figure 134G** reveals pit formation on the surface. The EDS analysis performed on particular places **(Table 39)** shows the nature of the oxides formed on exposed sample.

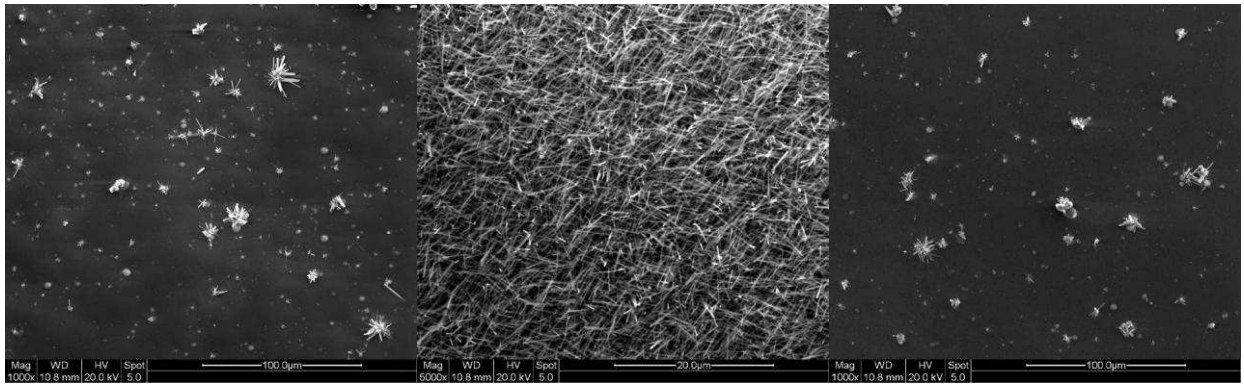

A: 1000x B: 5000x C: 1000x

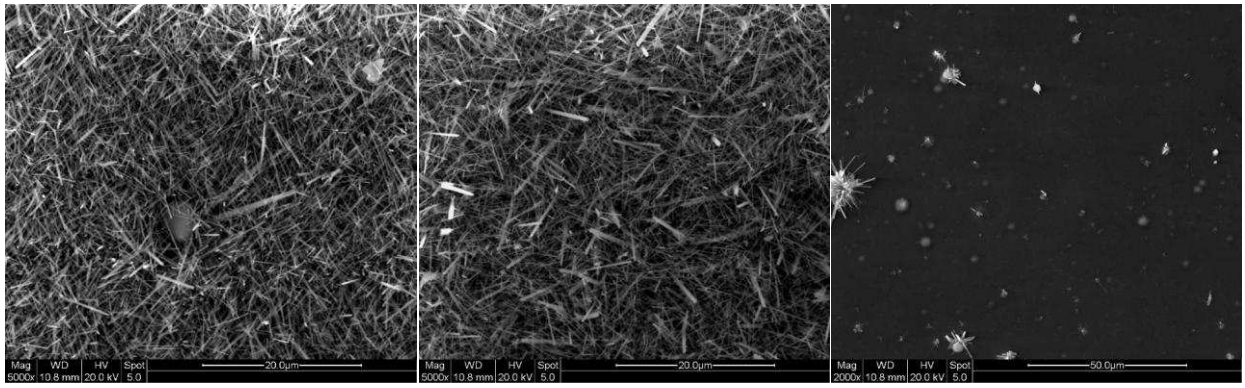

D: 5000x E: 5000x F: 5000x

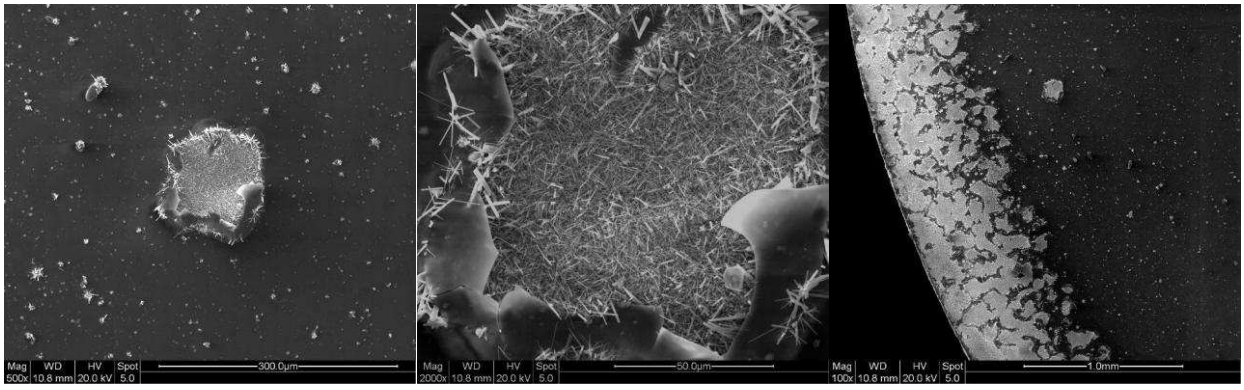

G: 5000x H: 2000x I: 100x

Figure 134 SEM images from surface of TiAlYN/CrN+Al_2O_3 coated Ti45Al8Nb after 5000 hours of oxidation at 1023 K (magnification under images)

Table 39 reveals that surface was covered by mixed TiO_2 – Al_2O_3 oxides with small amount of Cr. However some places show higher concentration of Al_2O_3 oxide (**Table 39**, image **134A**) than TiO_2, whereas some areas show higher concentration of TiO_2 than Al_2O_3. It was observed that the EDS investigations did not detect N_2; however N_2 was deposited in the exposed coating.

Image	Atomic% O	Atomic% Al	Atomic% Ti	Atomic% Cr
A	63.237	28.018	3.289	5.455
B	65.086	12.062	20.841	2.012
C	63.968	28.530	2.933	4.568
D	64.430	13.013	20.290	2.266
E	65.367	14.577	18.643	1.413
F	63.456	28.897	2.808	4.839

Table 39 Surface analysis performed by EDS investigation of TiAlYN/CrN+Al_2O_3 coated Ti45Al8Nb after 5000 hours of oxidation at 1023 K

The cross – sectioned structures of exposed sample (TiAlYN/CrN+Al_2O_3 coated Ti45Al8Nb alloy) are given in **figure 136**, the left hand side show the images taken from the middle part of exposed sample, whereas edges of the sample are shown on the right side. The middle part of the sample showed good oxidation resistance, however the edges of the sample suffered from corrosion attack 5000 hours exposure. The cracks and lack of adhesion is visible. The detailed investigations of exposed sample are presented in **figures 135** and **136** where the SEM cross – section image with different scale structures is described and the EDS concentration profiles are given.

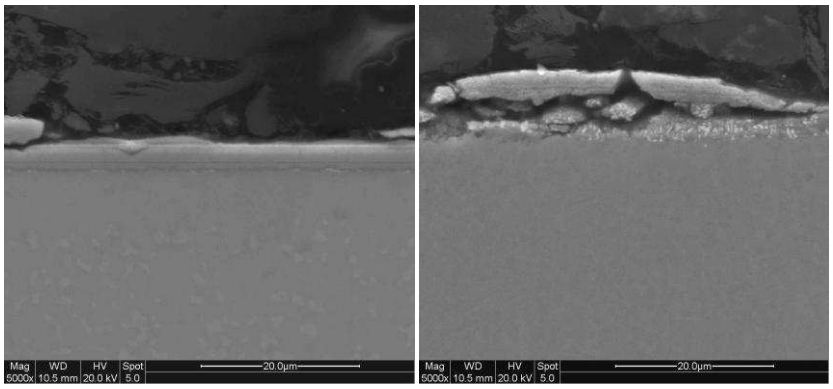

Figure 135 Cross – sectional images of sample (TiAlYN/CrN+Al_2O_3 coated Ti45Al8Nb) after 5000 hours of oxidation at 1023 K. Scale formed on the edges (right) and the scale formed in the middle of the sample (left)

The SEM cross – section micrograph taken from the edge of exposed sample given in **figure 136** shows that a multilayered structure developed, and the cracks also appeared. The poor oxidation resistance is due to the multilayer structure with poor adhesion. The EDS concentration profiles are given in **figure 137**.

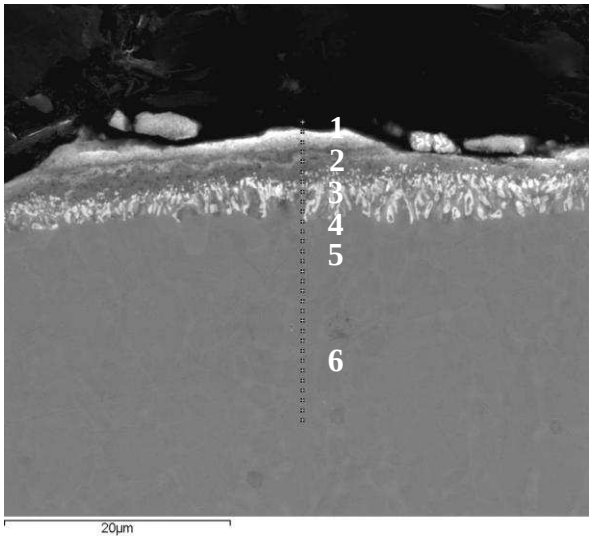

1) Al_2O_3 layer with Cr_2O_3 and TiO_2 oxide inclusions

2) TiO_2 layer with Al_2O_3 oxide inclusions

3) TiO_2/Al_2O_3 oxide layer/diffusion zone

4) TiAl layer

5) Ti_2Al layer

6) Substrate (Ti45Al8Nb alloy)

Figure 136 SEM cross section image of TiAlYN/CrN+Al_2O_3 coated alloy after 5000 hours of oxidation at 1023 K – edge of the sample

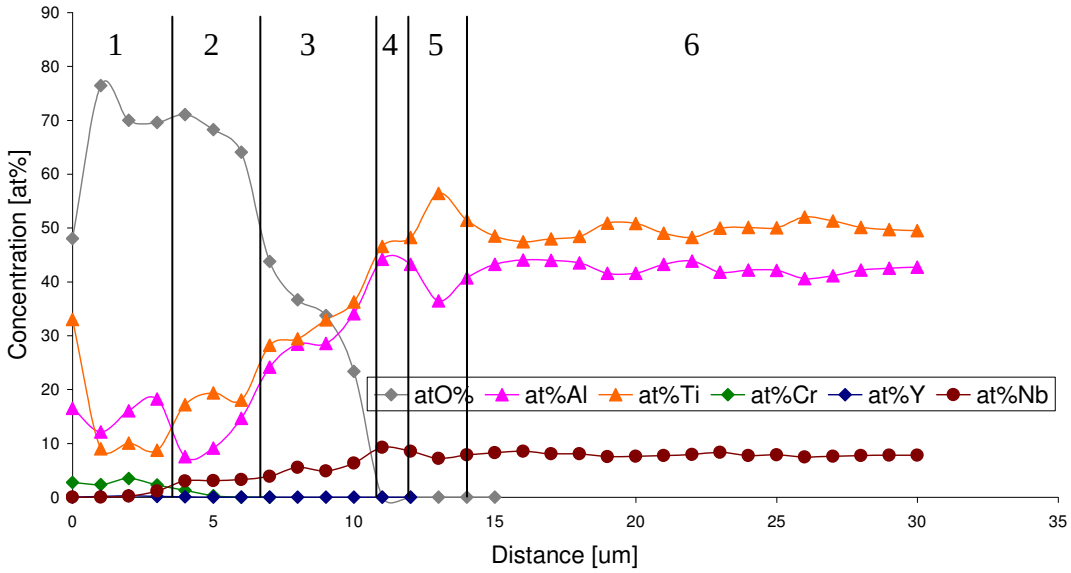

Figure 137 EDS concentration profiles obtained from TiAlYN/CrN+Al_2O_3 coated Ti45Al8Nb alloy after 5000 hours of oxidation at 1023 K (profiles obtained from edge of the sample)

The concentration profiles of exposed sample (TiAlYN/CrN+Al_2O_3 coated Ti45Al8Nb alloy) **(Fig. 137)** show that the outer oxide scale is occupied by mixed Al_2O_3 – TiO_2 oxides (with higher concentration of Al_2O_3 oxide, and very small amount of Cr_2O_3 oxide), however the high Ti content in the outer part of the oxide scale, suggest that the TiO_2 occupied the surface of the corroded material. Underneath this mixed Al_2O_3 – TiO_2 oxide scale, a next mixed TiO_2 – Al_2O_3 layer formed, however here the concentration of TiO_2 was higher than Al_2O_3. Underneath the mixed scales of TiO_2 and Al_2O_3 a large depletion zone of Ti and Al developed, where below the depletion zone a thin (1 µm) of TiAl phase region was detected. Moreover between TiAl phase and the substrate Ti_3Al phase was also found.

Figure 138 shows the scale structure which developed in the middle of the exposed sample (TiAlYN/CrN+Al_2O_3 coated Ti45Al8Nb alloy) after 5000 hours of heat treatment. The uniform scale structure in the middle of the sample indicates good oxidation resistance, however as **figure 139** show that the sample suffered corrosion

attack mainly on the edges. The EDS concentration profiles of exposed sample are presented in **figure 139**.

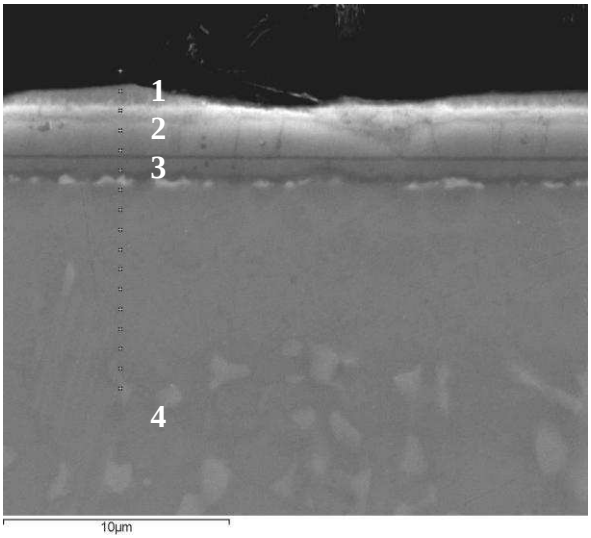

1) Al_2O_3 oxide layer
2) CrN layer
3) TiN/AlN layer
4) Substrate (Ti45Al8Nb alloy)

Figure 138 SEM cross section image (mag. 10000x) of the sample (TiAlYN/CrN+Al_2O_3 coated Ti45Al8Nb after 5000 hours of oxidation at 1023 K with EDS line – picture taken from the middle of the sample

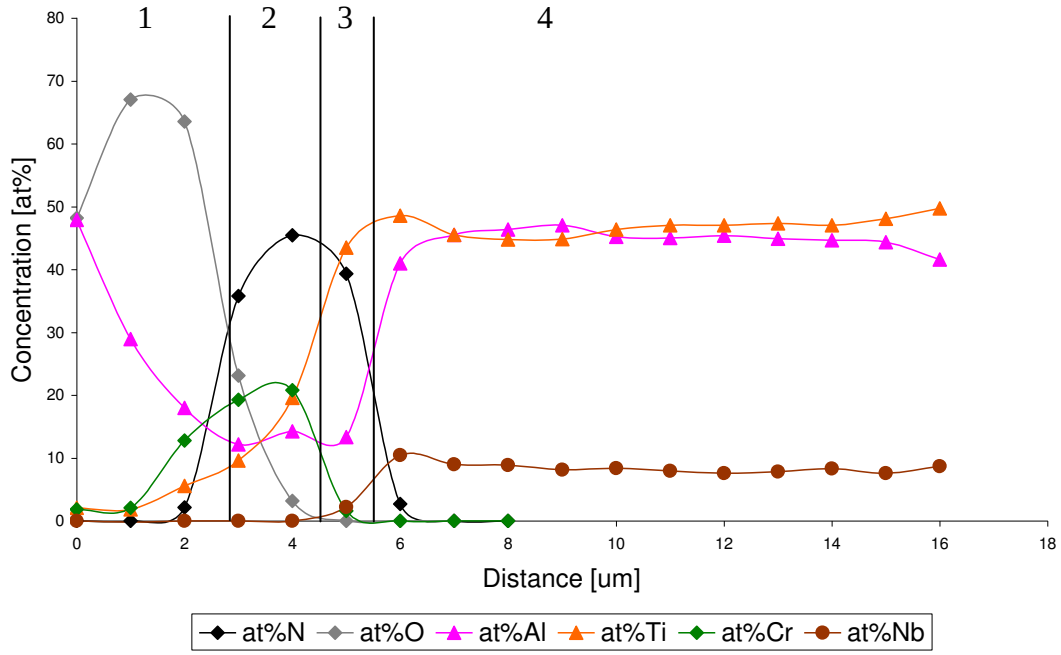

Figure 139 EDS concentration profiles obtained from TiAlYN/CrN+Al_2O_3 coated Ti45Al8Nb alloy after 5000 hours of oxidation at 1023 K (profiles obtained from the middle of the sample)

The EDS concentration profiles of TiAlYN/CrN+Al_2O_3 coated Ti45Al8Nb alloy presented in **figure 139** show that in the middle part of the sample predominantly Al_2O_3 oxide developed, with small amount of Cr_2O_3 oxide. Beneath the Al_2O_3 oxide scale a modified coating appeared and between the modified coating and the substrate a thin (1 µm) TiN layer existed. The good oxidation resistance of exposed part of the sample was due to the formation highly protective Al_2O_3, and also due to the formation of TiN underneath the TiAlYN/CrN+Al_2O_3; the TiN layer consumed a Ti ions from the substrate and inhibited the mass transport along the modified coating to the outer part of the scale. The EDS X-Ray mappings (not shown here) from the edges and middle of the exposed sample indicate good agreement with the EDS concentration profiles **(Fig. 139).** The corresponding XRD analysis (not shown here) confirms the findings of the EDS profiles and digimaps.

Ch.VI.Sec.1.12 TiAlN + Al_2O_3 coated TiAl45Al alloy

The SEM surface investigations of exposed sample TiAlN + Al_2O_3 coated TiAl45Al alloy (Ti25Al50N+Al_2O_3) after 5000 hours oxidation at 1023 K presented in **figure 140** show that different shapes of the developed oxides. Detailed analysis in **table 40** shows that mainly TiO_2 and Al_2O_3 oxides developed on the surface of oxidised sample with small amount of Cr.

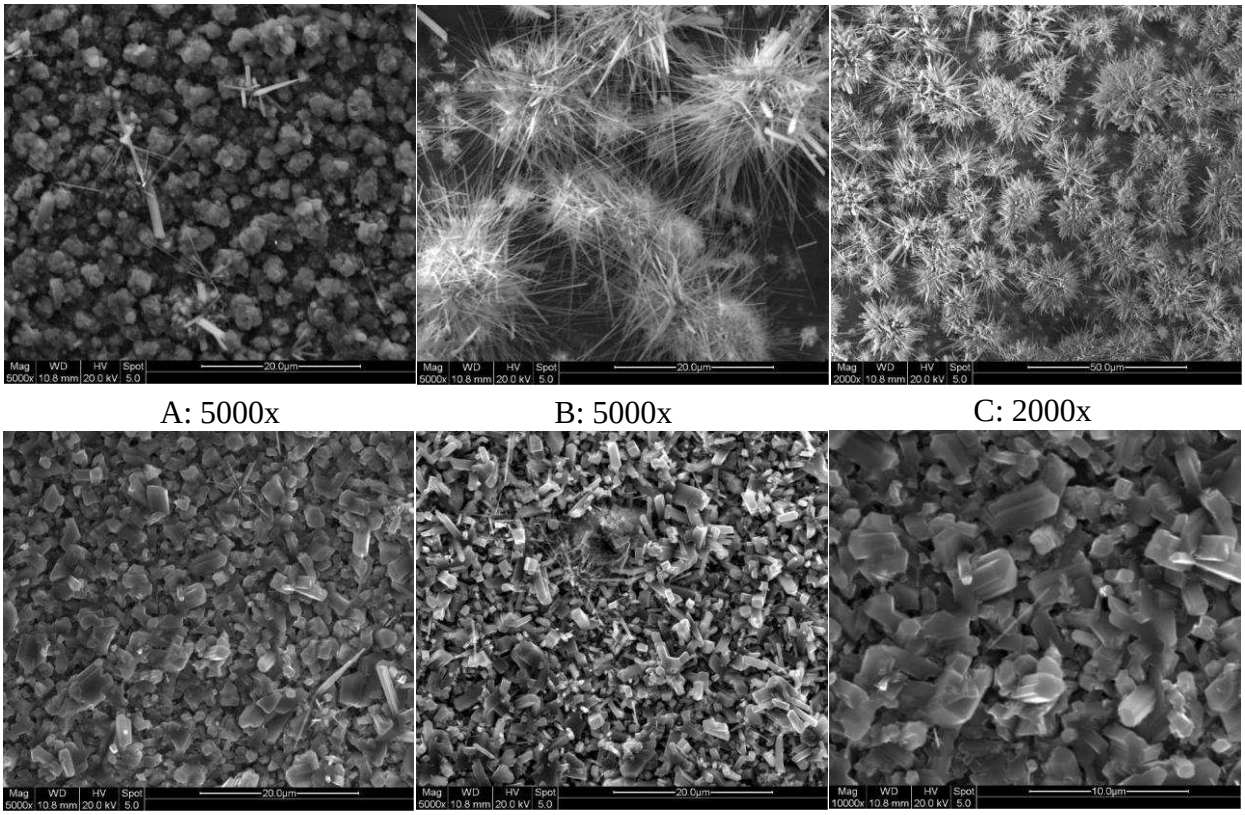

Figure 140 SEM images from surface of TiAlN + Al_2O_3 coated Ti45Al8Nb after 5000 hours oxidation of oxidation at 1023 K (magnification under images)

Image	at% O	at% Al	at% Ti	at% Cr
A	66.420	19.547	13.574	0.458
B	66.641	24.582	8.397	0.381
C	67.646	20.734	11.344	0.275
D	68.267	12.178	18.648	0.907
E	67.497	14.156	17.730	0.617

Table 40 Surface analysis performed by EDS investigation of TiAlN + Al_2O_3 coated Ti45Al8Nb after 5000 hours of oxidation at 1023 K

The SEM cross – section investigations are presented in **figure 141**, the middle part of the sample shown at the left hand side, the edge of the sample shown at the right side. The material exposed to 1023 K suffered oxidation treatment due to the formation

of a thick scale with tendency to spall off. Overall similar corrosion products developed both in the middle part and edge of the sample.

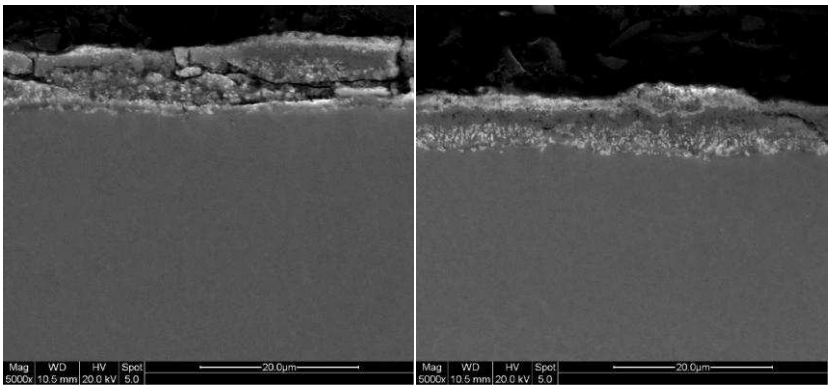

Figure 141 Cross – sectional images of sample (TiAlN + Al_2O_3 coated Ti45Al8Nb) after 5000 hours of oxidation at 1023 K. Scale formed on edges (right) scale formed in the middle of the sample (left)

The SEM cross – sectioned micrograph of the edge of the sample in **figure 142** shows a thick scale (10 µm), the EDS concentration profiles are presented in **figure 143**.

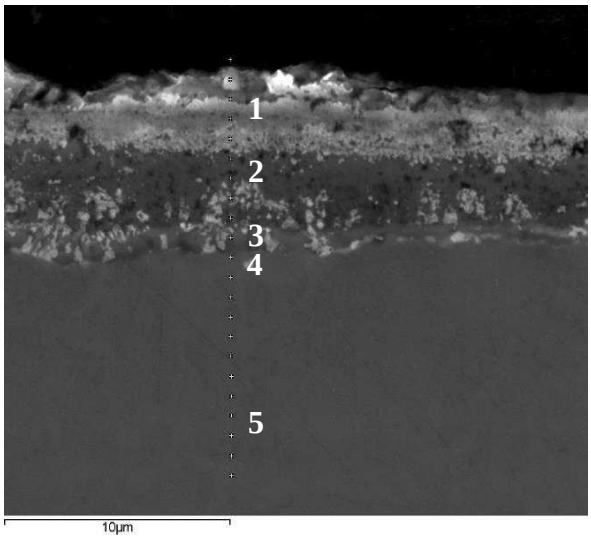

1) Al_2O_3 oxide layer with TiO_2
2) Al_2O_3/TiO_2 oxide layer
3) Modified coating (TiAlN)
4) Diffusion zone of Al and Ti
5) Substrate (Ti45Al8Nb alloy)

Figure 142 SEM cross section image (mag. 10000x) of the sample (TiAlN+Al_2O_3 coated Ti45Al8Nb after 5000 hours of oxidation at 1023 K) – edge of the sample

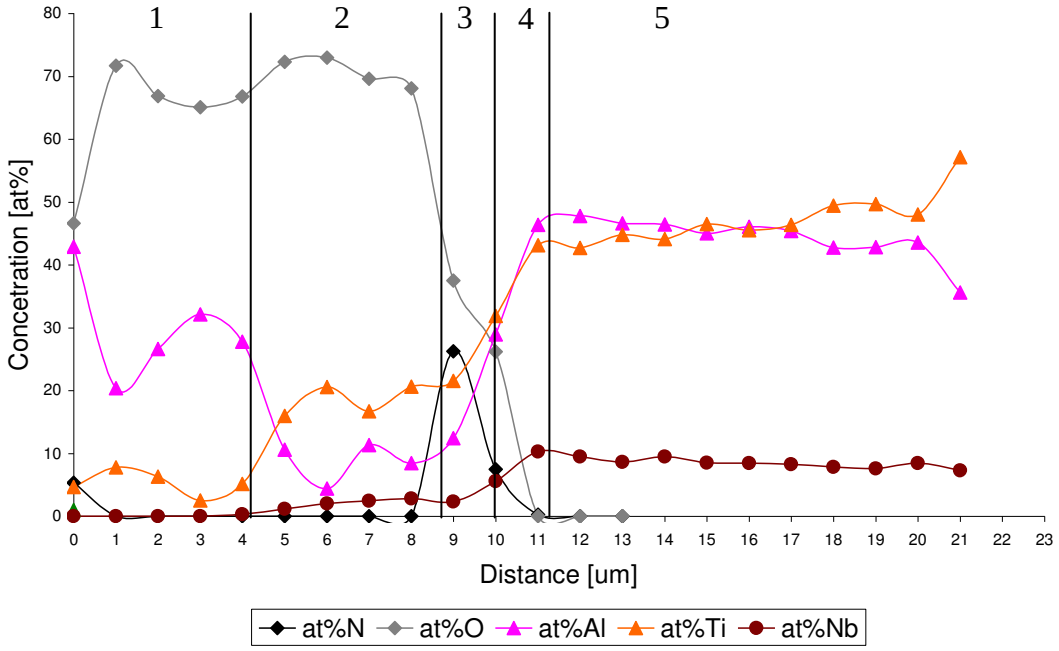

Figure 143 The EDS concentration profiles obtained from TiAlN+Al_2O_3 coated Ti45Al8Nb alloy after 5000 hours of oxidation at 1023 K – edge of the sample

The EDS concentration profiles of the sample exposed at 1023 K in **figure 143** show the following regions: 1) Al_2O_3 oxide layer, 2) Al_2O_3/TiO_2 oxide layer, 3) Modified coating (TiAlN), 4) Diffusion zone. 5) Substrate (Ti45Al8Nb alloy).

The outer layer was occupied by highly protective Al_2O_3 layer which was deposited during the coating manufacture. After exposure the deposited coating shows rather porous structure (large amount of oxygen – **Fig. 143)** however no spallation was observed. Underneath the Al_2O_3 oxide scale, a mixed layer of TiO_2 and Al_2O_3 developed, this layer developed due to the outward diffusion of Ti and Al ions from modified coating, the modified coating was localised beneath the mixed TiO_2 and Al_2O_3 layer. The thickness of the modified coating is around 1µm **(region 3 in figure 143)**. A depletion zone of Ti and Al formed between the modified coating and the substrate. A similar scale structure as in the edges of the exposed sample (TiAlN+Al_2O_3 coated alloy) was observed in the cross – sectioned micrograph given in **figure 144**. The SEM micrograph from the middle part of the sample shows that the oxide scale is thinner (7 µm) than at the edges of the exposed sample. The detailed investigation performed by the EDS is in **figure 145**.

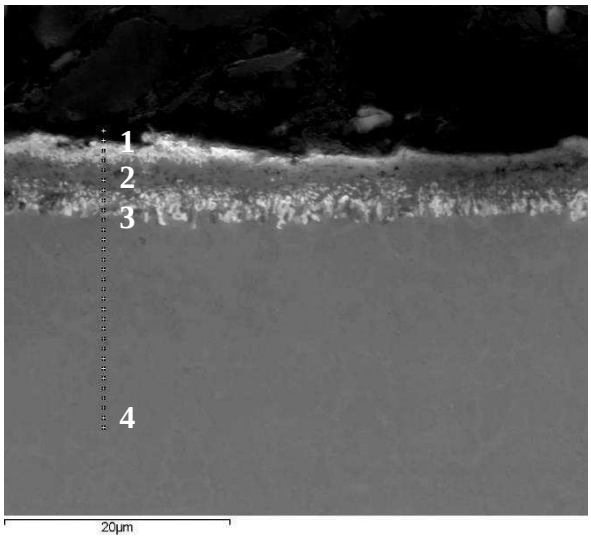

1 Al_2O_3 oxide layer with TiO_2

2) TiO_2 oxide layer

3) Diffusion zone

4) Substrate (Ti45Al8Nb alloy)

Figure 144 SEM cross section image (mag. 5000x) of the TiAlN+Al_2O_3 coated Ti45Al8Nb after 5000 hours of oxidation at 1023 K with EDS line – picture taken from middle of the sample

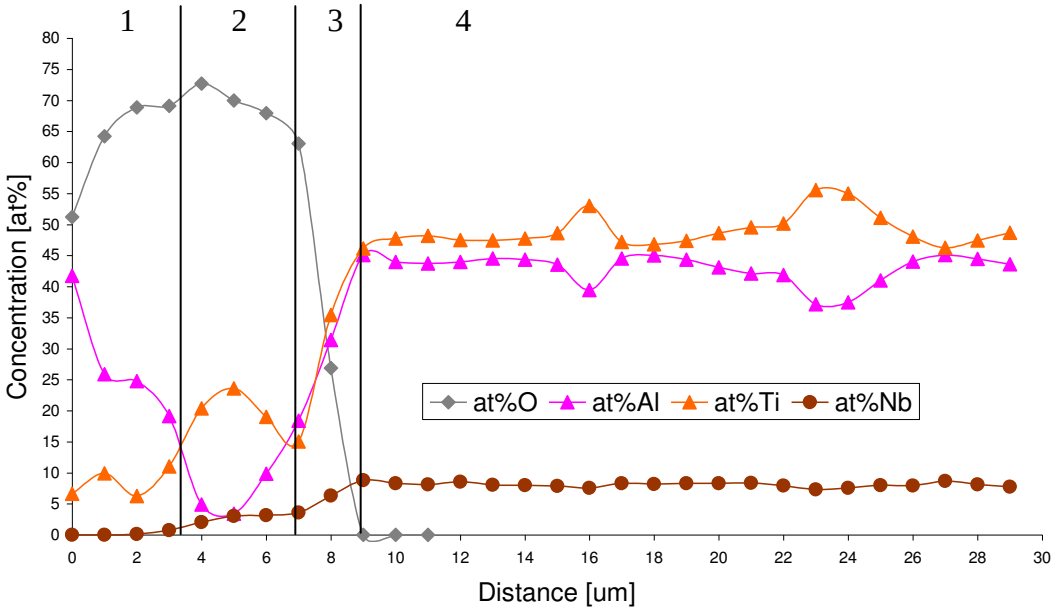

Figure 145 EDS concentration profiles obtained from TiAlN+Al_2O_3 coated Ti45Al8Nb alloy after 5000 hours of oxidation at 1023 K – middle of the sample

It was observed by the EDS concentration profiles in **figure 145** that an outer part of the scale was occupied by the Al_2O_3 oxide scale; however this oxide scale was deposited as a top coat during deposition process. Moreover the outer Al_2O_3 oxide scale in the middle part of the sample consisted of a higher amount of Ti than at the edge of the sample (10 at%, 6 at% respectively).

Underneath this Al_2O_3 oxide scale, a relatively thick (4 µm) TiO_2 oxide developed, between the substrate and TiO_2 oxide layer, a thin (2 µm) depletion zone of Al and Ti formed. However it needs to be noted that a modified coating did not exist in the middle part of the sample (the EDS concentration profiles did not show N concentration).

The EDS X-Ray mappings form the edge and from the middle of the exposed sample showed good agreements with the EDS concentration profiles (EDS X-Ray mappings are not shown here). The XRD data confirms the findings of the EDS and EDS X-Ray mappings with additional peaks of TiO_2 and Ti_2N and substrate phases being detected.

Chapter VI – Section 2 – High Temperature Sulphidation of γ-TiAl alloys – Results

Ch.VI.Sec.2.1 Introduction to sulphidation results

Chapter VI section 2 presents the sulphidation results of uncoated and coated γ-TiAl to high $pS_2 = 10^{-1}$ Pa and low $pO_2 = 10^{-18}$ Pa in $H_2/H_2S/H_2O$ gas mixture at 1023 and 1123 K for 1000 and 675 hours respectively. The results are presented in two parts.

The first part presents the results obtained from sulphidation at 1023 K for 1000 hours, while the second part gives the results gathered at 1123 K for 675 hours.

Part One – 1000 hours at 1023 K

Ch.VI.Sec.2.2 Introduction to part one

Part one presents the results of sulphidation of the following materials exposed to $pS_2 = 10^{-1}$ Pa and low $pO_2 = 10^{-18}$ Pa in $H_2/H_2S/H_2O$ gas mixture at 1023 K for 1000 hours:

1) Ti45Al8Nb uncoated alloy

2) TiAlCr (Ti42Al15Cr) coated Ti45Al8Nb alloy

3) Al_2Au coated Ti45Al8Nb alloy

4) CrAlYN/CrN+CrAlYON coated Ti45Al8Nb etched by Cr

5) CrAlYN/CrN+CrAlYON coated Ti45Al8Nb etched by CrAl

6) CrAlYN/CrN+CrAlYON coated Ti45Al8Nb etched by Y

Ch.VI.Sec.2.3 Kinetics of sulphidized samples at 1023 K

Figure 146 shows the kinetic results of Ti45Al8Nb uncoated alloy and TiAlCr and Al_2Au coated Ti45Al8Nb alloy exposed to the $pS_2 = 10^{-1}$ Pa and $pO_2 = 10^{-18}$ Pa $H_2/H_2S/H_2O$ environment at 1023 K for up to 1000 hours. During the initial period of the 50 hours, the weight gains of TiAlCr coated Ti45Al8Nb are lower than that of Al_2Au coated alloy. After prolonged exposure, the difference of weight gains between the coated materials become much closer. The coated materials had a similar mass gain at the end of experiment as the uncoated material (Ti45Al8Nb).

Etched samples (Cr, CrAl, and Y etched) showed similar behaviour in kinetics growth during exposure to sulphidation experiment at 1023 K. Calculated parabolic rate constants are presented in **Table 41.**

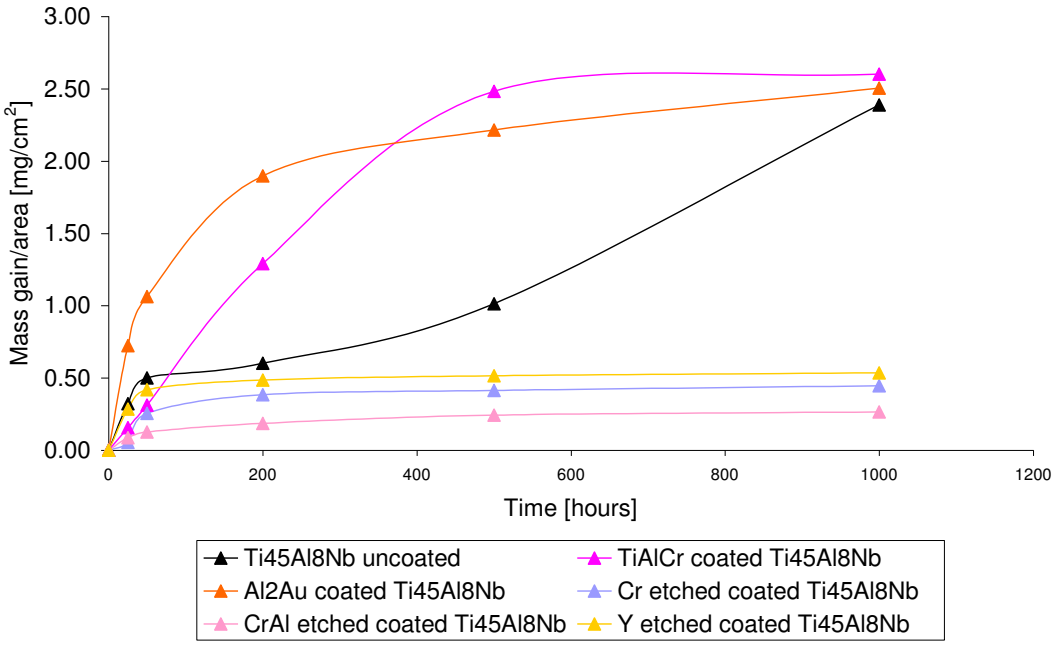

Figure 146 Mass gain obtained after sulphidation experiment at 1023 K for 1000 hours

	Ti45Al8Nb	Ti42Al15Cr	Al_2Au	Cr etched	CrAl etched	Y etched	Unit
kp value	$1.48E^{-07}$	$2.11E^{-07}$	$1.68E^{-07}$	$5.21E^{-09}$	$1.90E^{-09}$	$6.09E^{-09}$	$mg^2/cm^4/s$

Table 41 Parabolic rate constant values obtained from sulphidation experiment performed at 1023 K for 1000 hours

Ch.VI.Sec.2.4 Ti45Al8Nb uncoated alloy

The surface morphology of Ti45Al8Nb base alloy exposed to sulphidising/oxidising environment (pS_2 – 10^{-1} Pa and pO_2 – 10^{-18} Pa) in $H_2/H_2S/H_2O$ gas mixture at 1023 K for up to 1000 hours is given in **figure 147**. The whole surface of exposed sample was covered by thick crystals of TiO_2.

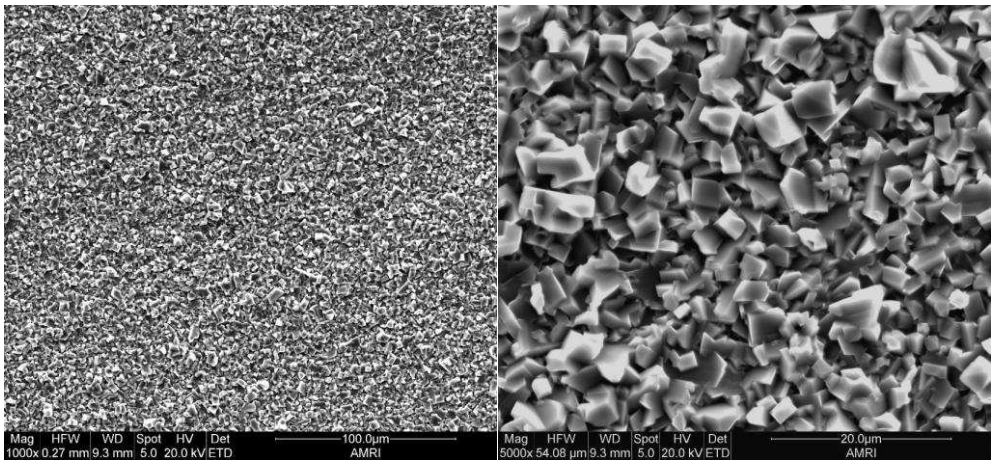

A: 1000x B: 5000x

Figure 147 Surface morphology of Ti45Al8Nb uncoated after 1000 hours of sulphidation at 1023 K (magnification under images)

Table 42 indicates that mainly TiO_2 oxide developed on the surface of exposed sample, however small amounts of Al and Nb also were detected.

Image	Atomic % O	Atomic % Al	Atomic % Ti	Atomic % Nb
A	53.851	2.493	43.388	0.266
B	53.454	2.168	43.654	0.722

Table 42 The EDS surface analysis performed on sulphidized uncoated Ti45Al8Nb alloy after exposure at 1023 K for 1000 hours

The SEM cross – section micrograph (**Fig. 147**) reveals that the outer part of the scale spalled off from the material, the lack of outer scale is visible in upper row of **figure 147**. **Figure 147** shows also that some of the outer scale of sulphidized sample remained on the surface; however the scale was very brittle, and loss of adherence occurred. The detailed analysis is shown in further **figure 148** and in **figure 149**.

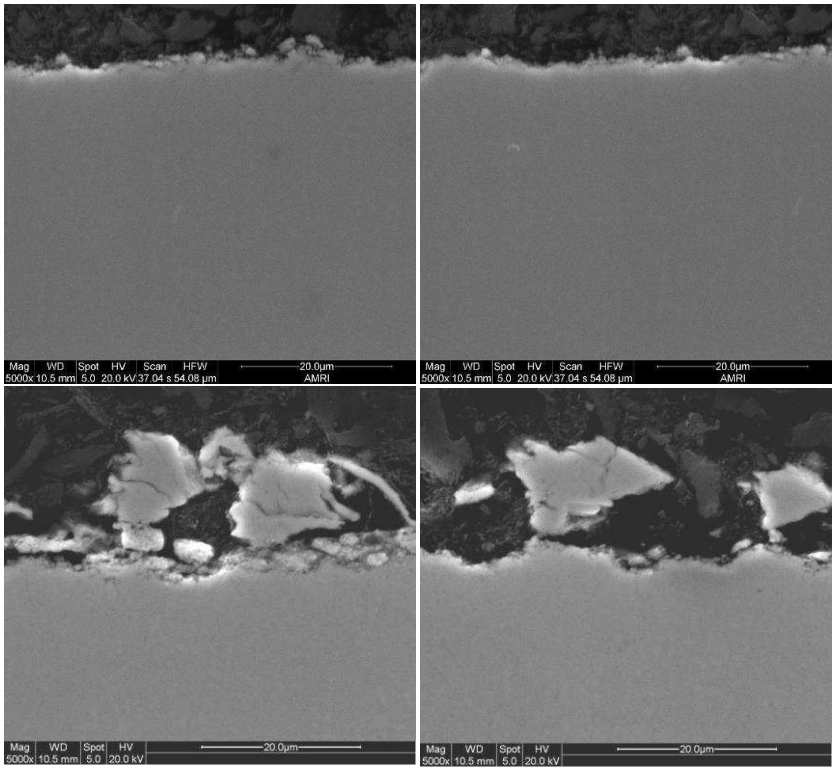

Figure 148 Cross – sectional images of Ti45Al8Nb uncoated sample after 1000 hours sulphidation at 1023 K

The SEM image in **figure 149** reveals a thick scale developed during exposure to sulphidation/oxidation atmosphere at 1023 K for 1000 hours. Moreover the scale cracked at the scale/alloy interface indicating poor mechanical properties. The detailed investigation of scale morphology and phases development is presented in **figure 150**.

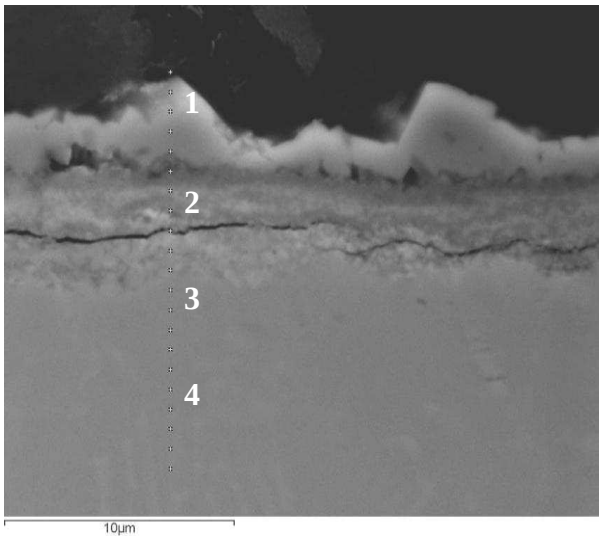

1) Titanium oxide (TiO_2)

2) Ti, Al, Nb oxide region with sulphides of Al, Ti and Nb

3) Diffusion zone of Al and Ti

4) Substrate (Ti45Al8Nb)

Figure 149 SEM image (mag. 10000x) of base material (Ti45Al8Nb) after 1000 hours of sulphidation at 1023 K

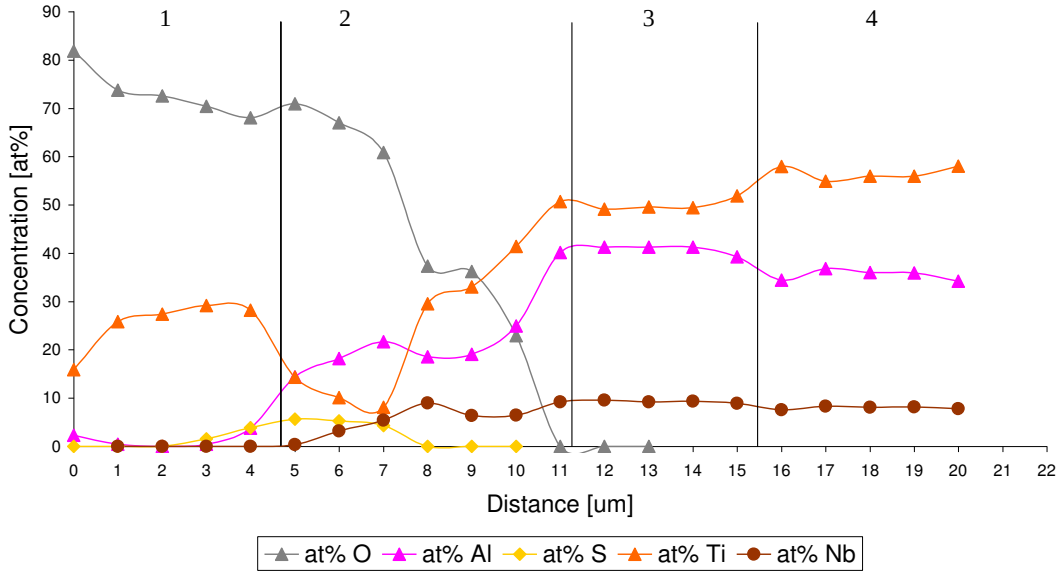

Figure 150 EDS concentration profiles obtained from Ti45Al8Nb uncoated alloy after 1000 hours of sulphidation at 1023 K

The EDS concentration profiles of sulphidized base alloy given in **figure 150** show the formation of a thick (5 µm) outer scale consisting of TiO_2. Underneath this TiO_2 outer scale also formed a relatively thick (6 µm) layer occupied by suphides Ti, Al, and Nb, and oxides of Al, Ti, and Nb. The EDS X-Ray analysis performed on the

uncoated material shown in **figure 151**, confirmed the structure detected by the EDS. The outer scale was occupied by TiO_2 thick scale, underneath this TiO_2 outer scale, the region enriched in oxygen and sulphur with Al and Nb was detected. Additionally the EDS X-Ray mapping detected regions with higher Al content (lower Ti content) and higher Ti content (lower Al content) these regions were found to be related to different phases ($TiAl_2$, $TiAl_3$, Ti_3Al, TiAl) formed in the base material.

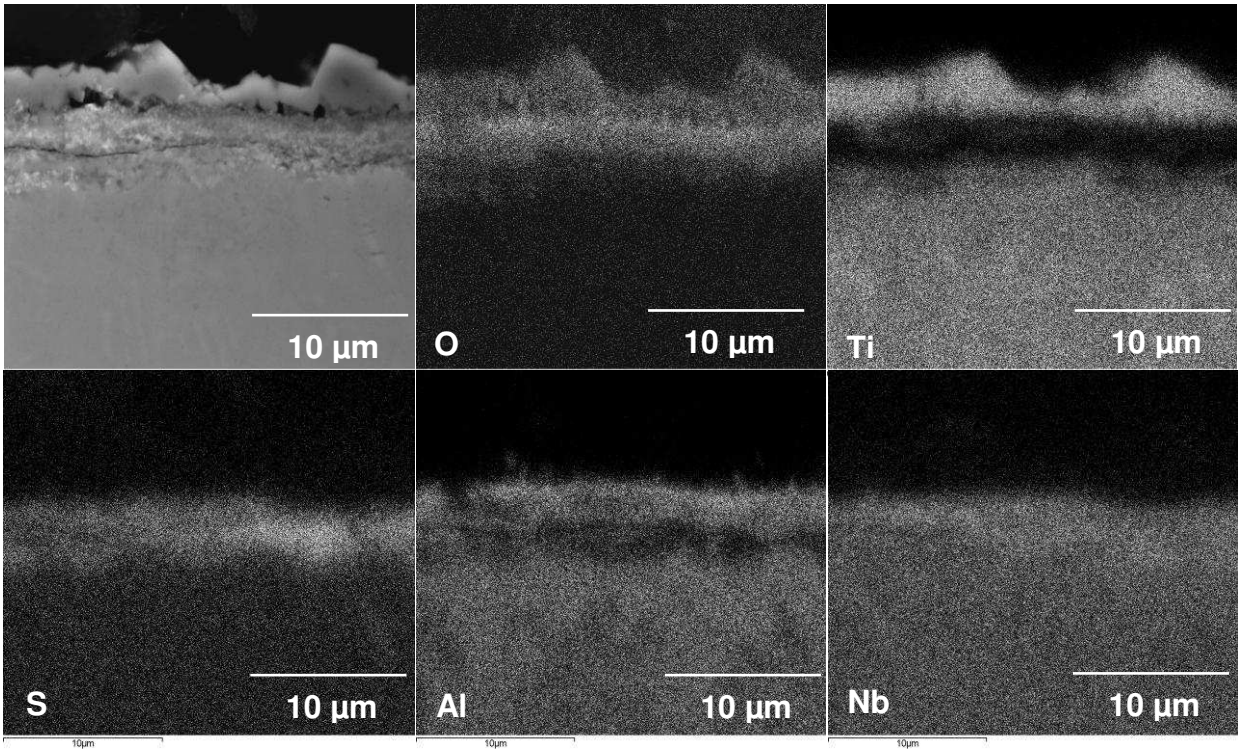

Figure 151 Digimaps of Ti45Al8Nb uncoated after 1000 hours sulphidation at 1023 K

The XRD analysis of the exposed sample given in **figure 152** shows the presence of main corrosion products (sulphides, oxides) developed after sulphidation oxidation at 1023 K. Moreover the substrate phases (TiAl, $TiAl_2$, $TiAl_3$, and Ti_3Al) were also detected. The appearance of such phases despite of a thick outer scale is related to the fact that outer scale spalled off in some areas of the exposed uncoated material (Ti45Al8Nb).

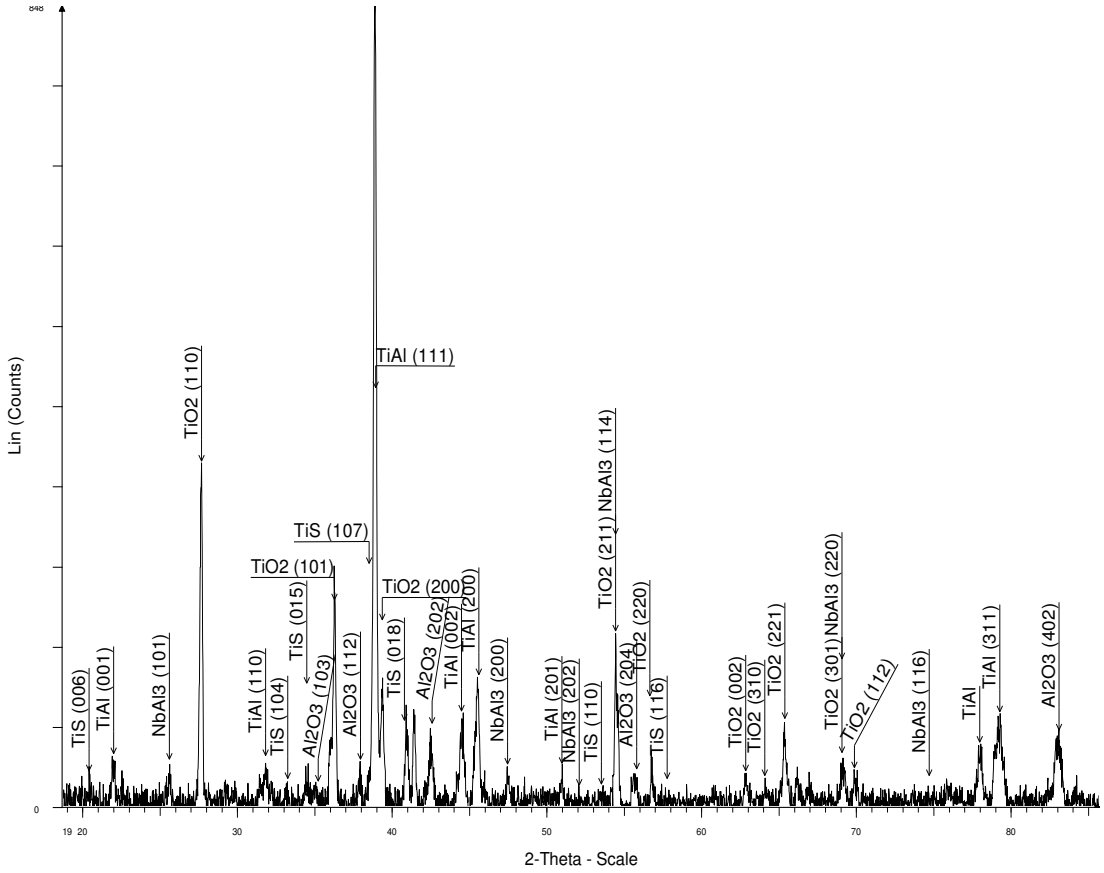

Figure 152 XRD pattern Ti45Al8Nb uncoated after 1000 hours sulphidation at 1023 K

Ch.VI.Sec.2.5 TiAlCr coated Ti45Al8Nb alloy

The surface of TiAlCr (Ti42Al15Cr) coated Ti45Al8Nb alloy exposed to sulphidation/oxidation environment is presented in **figure 153**. As observed in uncoated alloy the, coated material was also covered by a thick TiO_2 crystals. The detailed analysis performed on subjected material is given in **table 43**.

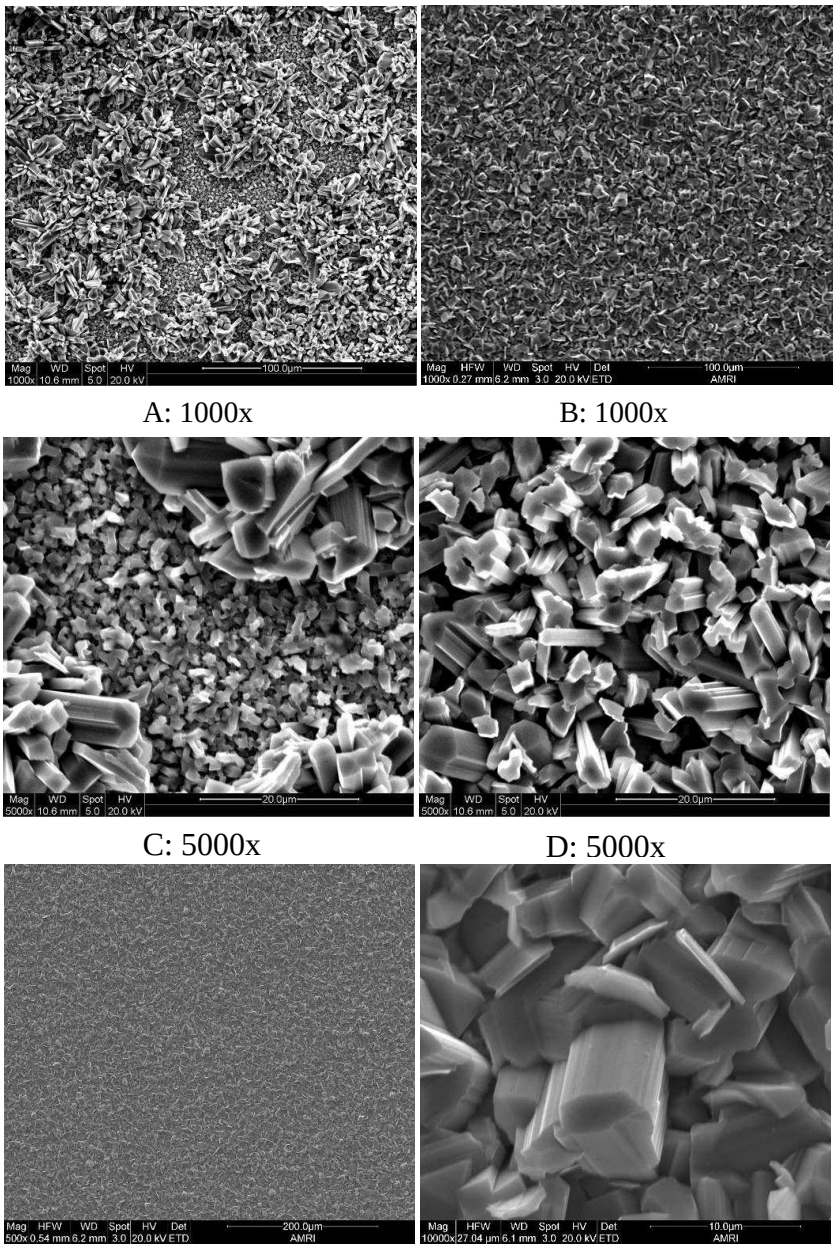

Figure 153 Surface morphology of TiAlCr coated Ti45Al8Nb after 1000 hours of sulphidation at 1023 K, (magnification under images)

The analysis shows that mainly TiO_2 oxide developed on the outer part of the material, small amounts of Cr and Al were also detected.

Image	at % O	at % Al	at % Ti	at % Cr
A	62.054	0.131	34.766	3.049
B	62.535	0.158	34.153	3.155
C	63.565	0.169	33.672	2.594
D	62.475	0.116	32.753	4.656

Table 43 Surface analysis performed by EDS investigation of TiAlCr coated Ti45Al8Nb after 1000 hours of sulphidation/oxidation at 1023 K

The cross – sectioned micrographs of exposed material (TiAlCr coated Ti45Al8Nb) alloy subjected to aggressive sulphidation atmosphere are given in **figure 154**. A thick and porous scale developed, with a different structures formed. At the scale/substrate interface a crack propagated. This crack along the material indicates a poor adhesion between the substrate and the developed scale; moreover, the bottom of the outer thick scale consisted of voids, detrimental the corrosion resistance of exposed material.

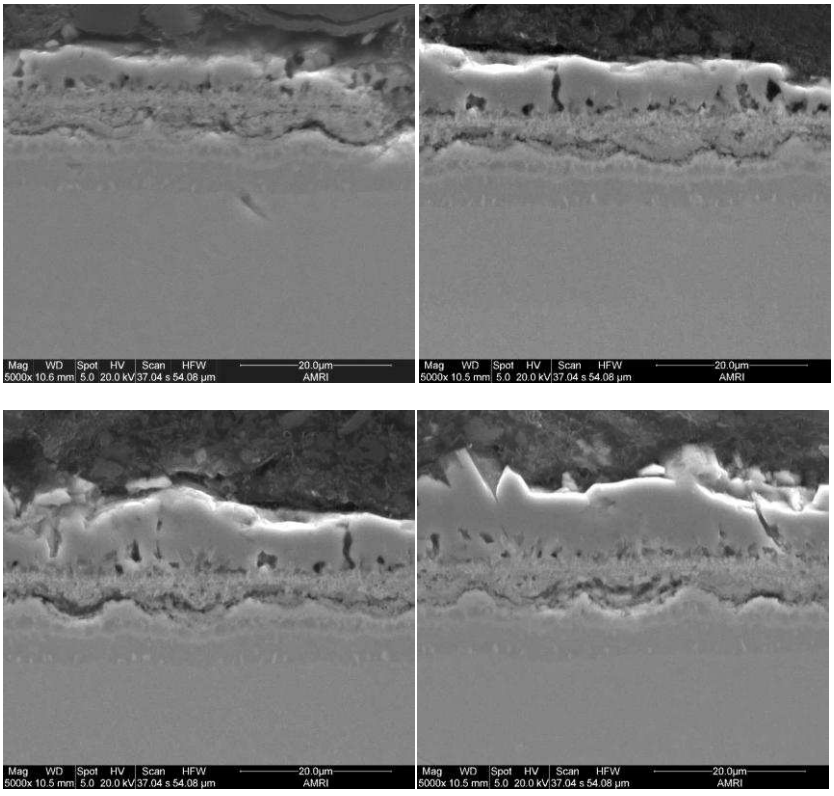

Figure 154 Cross sectional images of TiAlCr coated Ti45Al8Nb from different areas of after 1000hrs sulphidation at 1023 K; all images 5000 magnification

Figure 155 shows a cross – sectioned SEM micrograph of exposed material (TiAlCr coated Ti45Al8Nb) alloy which was used for EDS analysis given in **figure 156**.

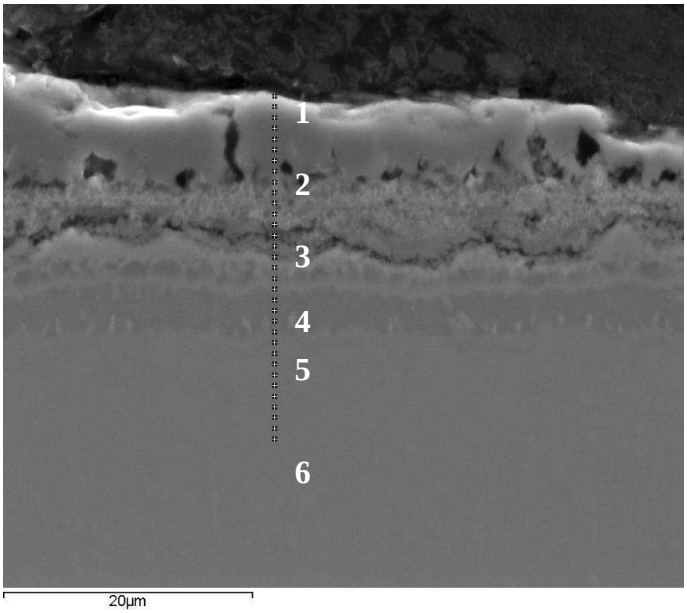

1) Titanium di-oxide (TiO_2)

2) Aluminium oxide (Al_2O_3)/ Titanium di-oxide (TiO_2)

3) Titanium Sulphur (TiS)

4) $NbAl_3$ layer

5) Diffusion zone of Ti and Al

Figure 155 SEM image (mag. 5000x) of TiAlCr coated Ti45Al8Nb after 1000hrs sulphidation at 1023 K

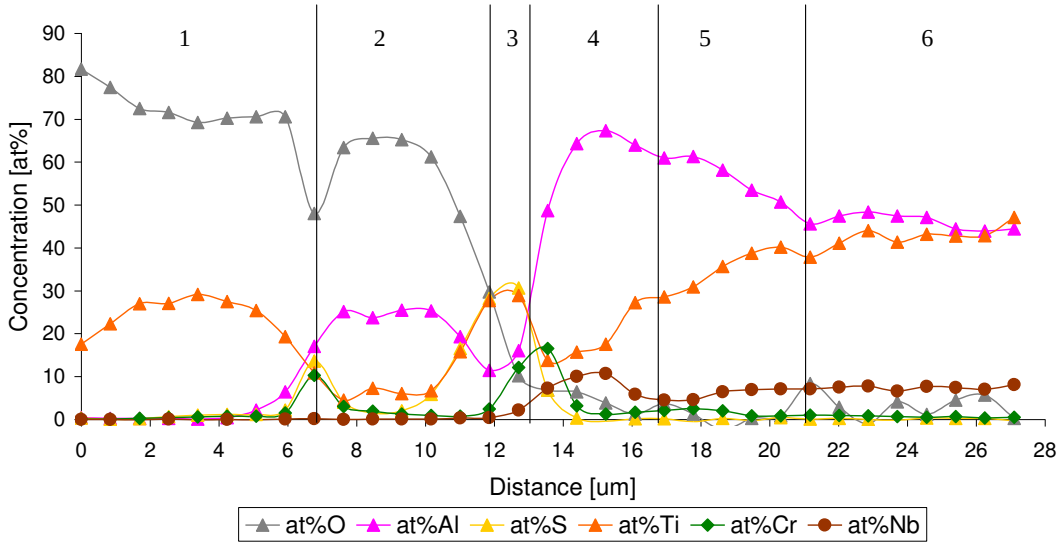

Figure 156 EDS concentration profiles obtained from TiAlCr coated Ti45Al8Nb alloy after 1000 hours of sulphidation at 1023 K

When TiAlCr coated Ti45Al8Nb was exposed to the sulphidation environment ($H_2/H_2S/H_2O$ for 1000 hours) at 1023 K, a continuous and thick (7 µm) TiO_2 layer was

formed after 1000 hours at 1023 K (**Fig. 156**). Beneath this thick outer TiO_2 scale, a mixture of TiO_2 and Al_2O_3 grew. Between this Al_2O_3 and TiO_2 mixed layer and Al rich layer, a very thin (1 µm) TiS layer developed. The development of $NbAl_3$ layer was associated with the higher content of Al near to the scale/substrate interface (**region 4 in figure 156**), where Ti ions diffused from the bulk material (Ti45Al8Nb) outward to form a TiO_2 outer scale. Moreover due to outward diffusion of Ti ions from bulk material a large depletion zone of Ti appeared in the base material (Ti45Al8Nb) (**region 4 and 5, figure 156**).

EDS X-Ray mapping is shown in **figure 157**. The EDS X-Ray mapping reveals that the outer scale partly consisted of a sulphur rich region where apart from TiO_2 the Cr - sulphide was detected. Underneath outer scale a rich band in Al_2O_3 with TiS layer was detected. A rich region of Cr was found in the scale/substrate interface, this rich in Cr content region remained after TiAlCr coating deposited on Ti45Al8Nb alloy before exposure to aggressive environment. Nb ions formed a rich region near to the scale/substrate interface and produced $NbAl_3$.

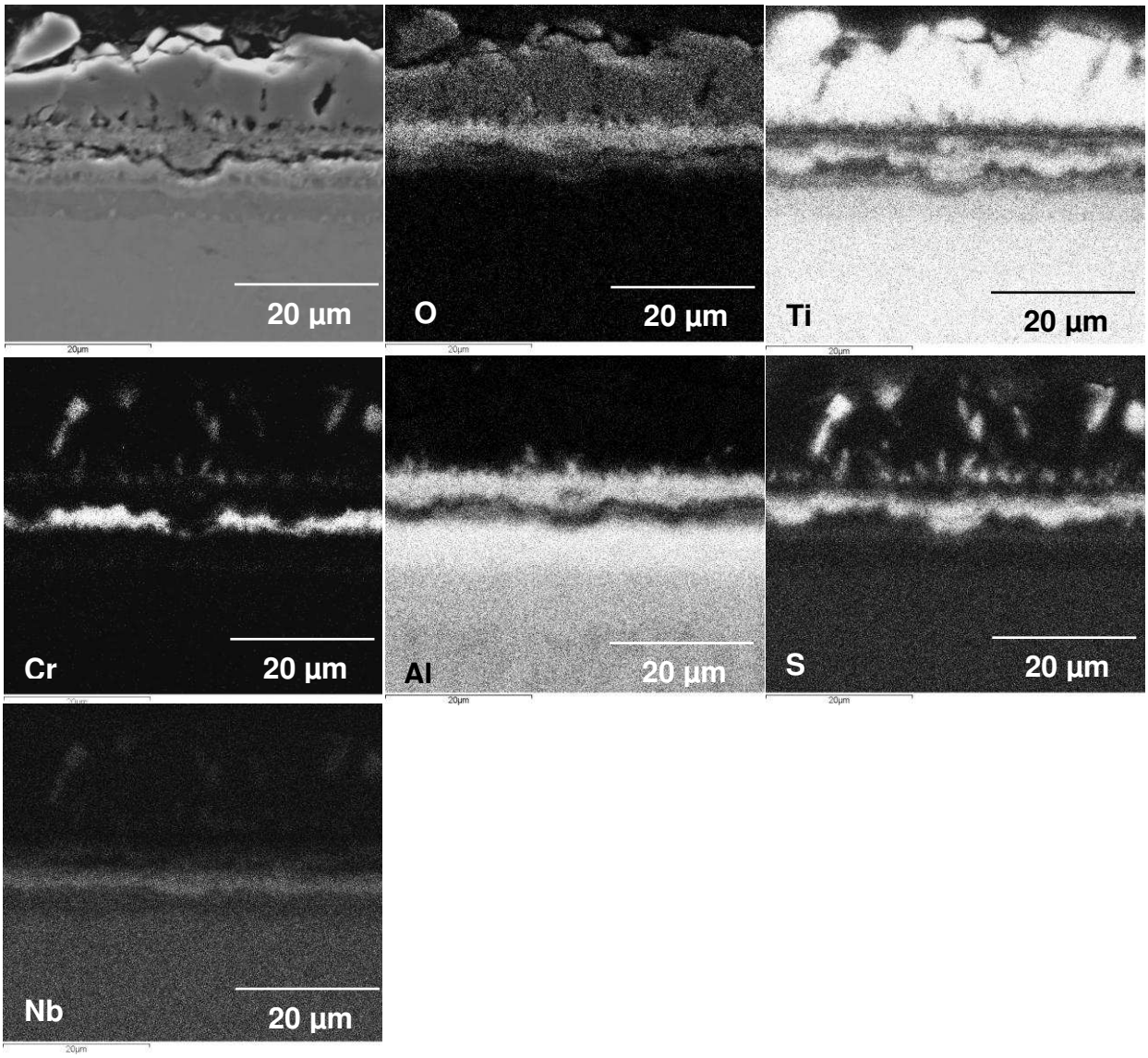

Figure 157 Digimaps of TiAlCr coated Ti45Al8Nb after 1000 hours sulphidation at 1023 K

The XRD investigation performed on sulphidised/oxidised sample (TiAlCr coated Ti45Al8Nb) alloy is given in **figure 158.** Mainly TiO_2 was detected with small amounts of Al_2O_3, Cr_2S_3. However TiS phase was not detected. It was observed also that the substarte phase $TiAl_2$ was dected despite the formation of a thick scale during exposure for 1000 hours at 1023 K.

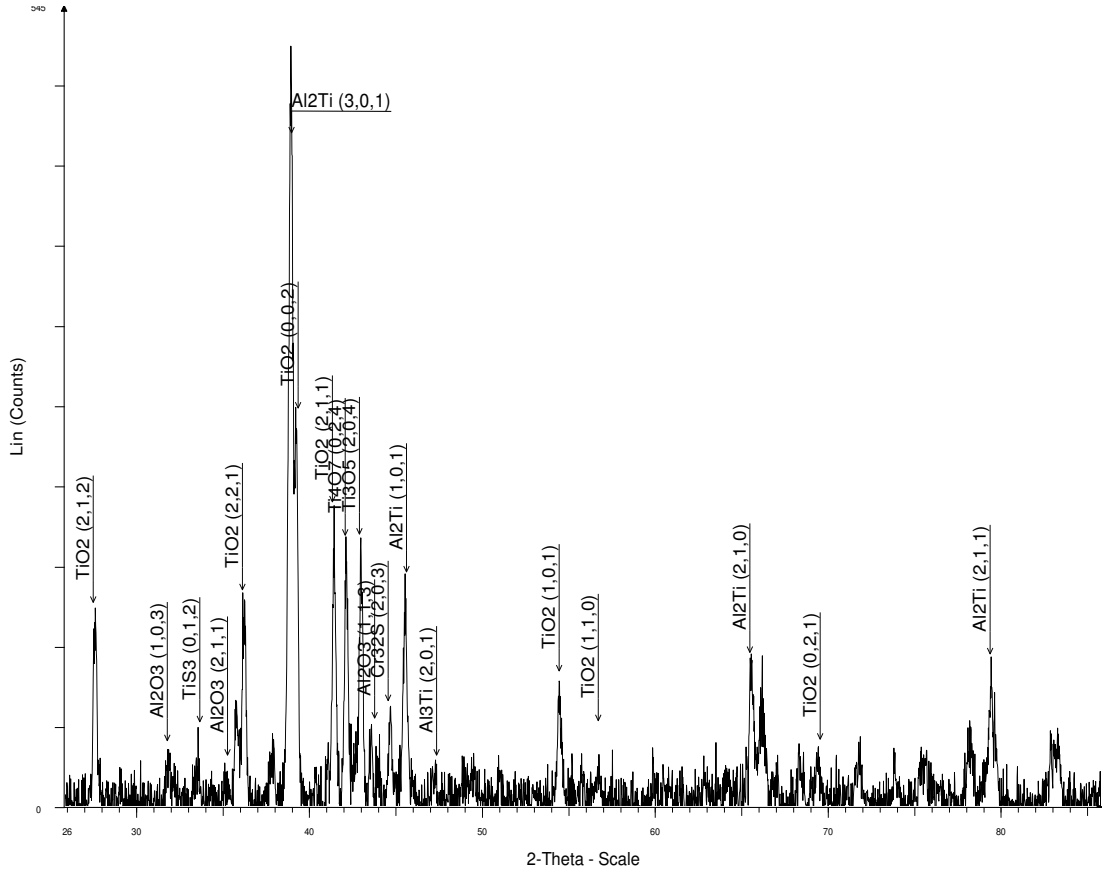

Figure 158 XRD pattern TiAlCr coated Ti45Al8Nb after 1000 hours sulphidation at 1023 K

Ch.VI.Sec.2.6 Al_2Au coated Ti48AlNb alloy

The surface morphology developed in the sulphidising sample is given in **figure 159**. The whole surface of the subjected Al_2Au coated Ti45Al8Nb alloy was covered by thick and large TiO_2 crystals. The EDS analysis of the surface which suffered corrosion attack is given **table 44**.

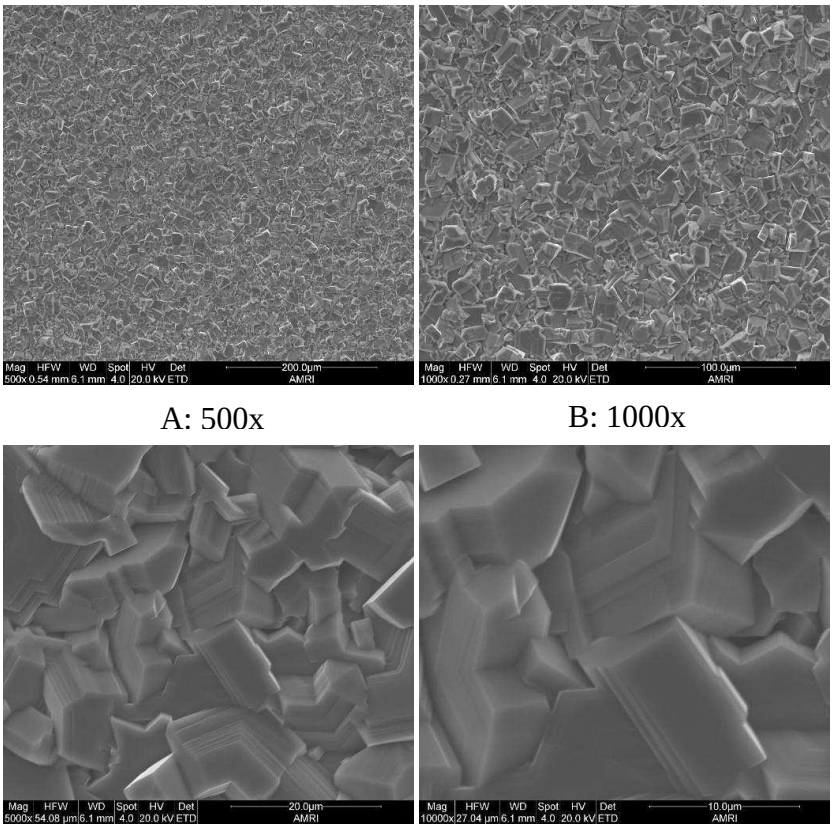

A: 500x B: 1000x

C: 1000x D: 10000x

Figure 159 Surface morphology of Al_2Au coated Ti45Al8Nb after 1000 hours of sulphidation at 1023 K, (magnification under images)

The surface EDS analysis revealed that TiO_2 phase developed as an outer scale, the trace amounts of Al and Au also were detected.

Image	at % O	at % Al	at % Ti	at% Au
A	62.159	0.317	37.261	0.264
B	60.216	0.349	38.784	0.651
C	58.186	0.349	40.620	0.845
D	61.261	0.346	38.174	0.219

Table 44 Surface analysis performed by EDS investigation of Al_2Au coated Ti45Al8Nb after 1000 hours of sulphidation/oxidation at 1023 K

The cross – section SEM image of the sulphidized at 1023 K Al_2Au sample given in **figure 160** reveals the development of the thick non-protective TiO_2 scale related to the fast outward diffusion of Ti form bulk material (Ti45Al8Nb). The different areas of the sulphidized sample shows that sample corroded in the same way – produced

a thick non protective scale. The detailed analysis of the scale structure is presented in **figure 161**.

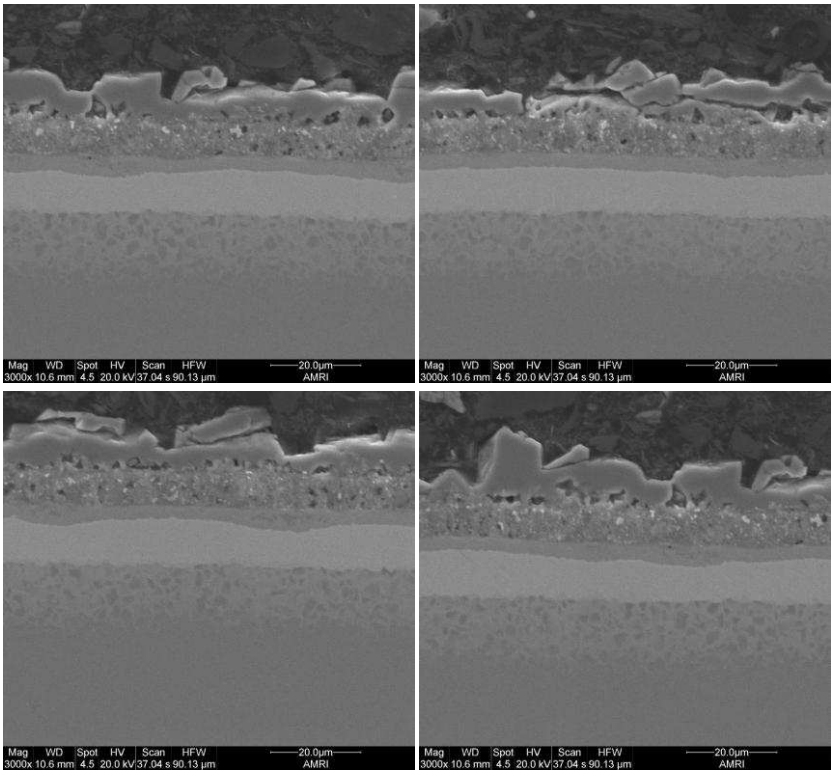

Figure 160 Cross sectional images of Al_2Au coated Ti45Al8Nb as deposited and from different areas of the sample after 1000 hours sulphidation at 1023 K

The EDS analysis taken from cross – sectional image is shown in **figure 161**.

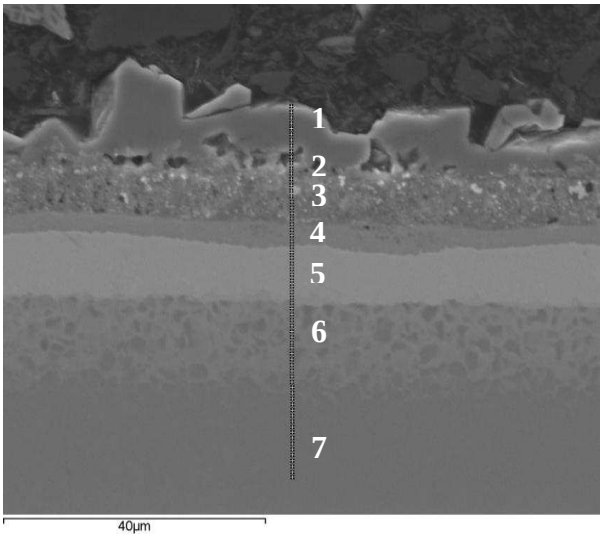

1) Titanium di-oxide (TiO_2)

2) Aluminium oxide (Al_2O_3)
3) Titanium sulphur/ oxide layer (TiS/TiO_2)
4) $NbAl_3$
5) Modified Coating (Al_2Au)

6) Diffusion zone of Ti from the alloy

7) Substrate (Ti45Al8Nb)

Figure 161 SEM image of Al_2Au coated Ti45Al8Nb after 1000hrs sulphidation at 1023 K

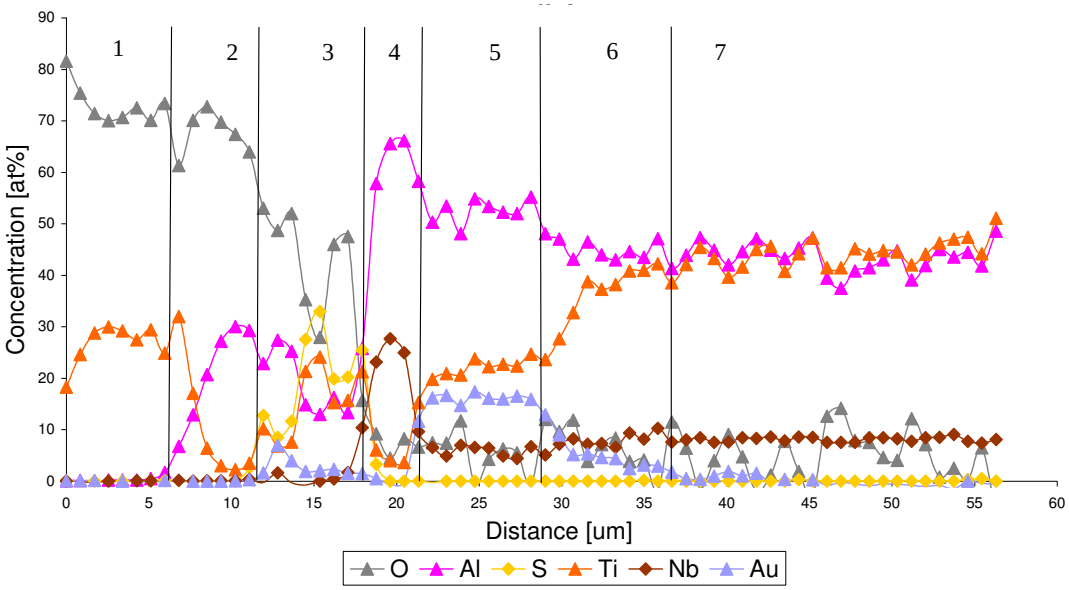

Figure 162 EDS concentration profiles obtained from Al_2Au coated Ti45Al8Nb alloy after 1000 hours of sulphidation at 1023 K

The EDS concentration profiles of exposed sample are presented in **figure 162** show the development of the following regions: 1) Titanium di-oxide (TiO_2), 2) Aluminium oxide (Al_2O_3), 3) Titanium sulphur/ oxide layer (TiS/TiO_2), 4) $NbAl_3$ 5) Modified Coating (Al_2Au), 6) Diffusion zone of Ti from the substrate, 7) Substrate

The EDS X-Ray mapping given in **figure 163** confirms, that the outer scale consisted TiO_2 thick scale, underneath this TiO_2 outer scale Al_2O_3 oxide developed. Below Al_2O_3 a region of Ti, Al oxides and sulphides also formed. Between this region and the modified coating a thin layer of $NbAl_3$ formed. It was observed that $NbAl_3$ layer formed beyond the modified coating not beneath the modified coating (TiAlCr coated alloy). This phenomena may suggest that Al from the coating (Al_2Au) was consumed for $NbAl_3$ formation, but not for the formation of a protective outer scale (Al_2O_3). The depletion zone of Ti underneath modified coating was detected by the EDS X-Ray mapping investigation.

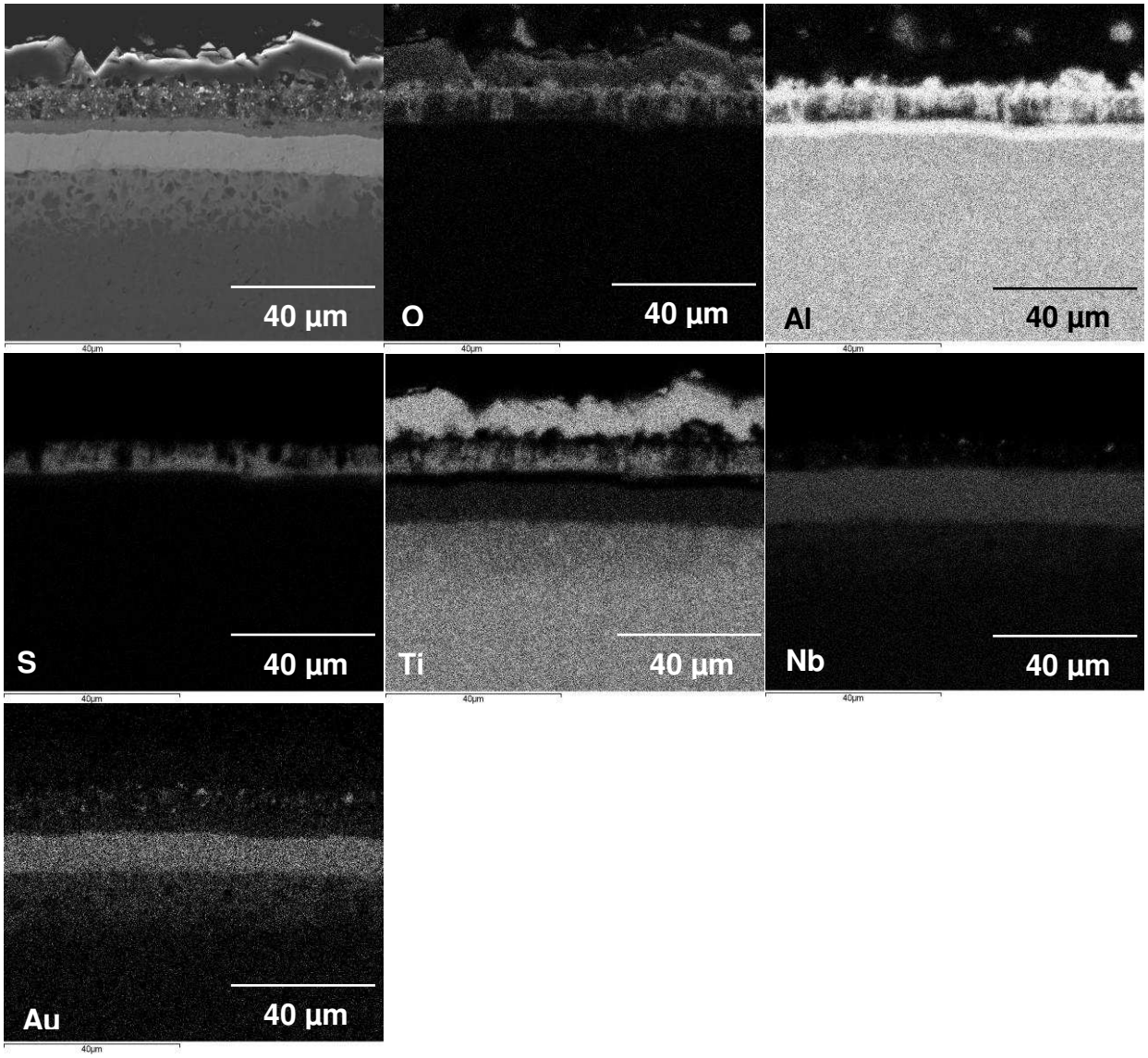

Figure 163 Digimaps of Al_2Au coated Ti45Al8Nb after 1000 hours sulphidation at 1023 K

The XRD analysis performed on the surface of the exposed sample (Al_2Au coated Ti45Al8Nb) after 1000 hours sulphidation/oxidation at 1023 K is given in **figure 164**. The XRD analysis mainly identified the TiO_2 phase with small peaks of TiS, no other phases were detected, suggesting that the scale was too thick as shown in **figures 160, 161, and 163**.

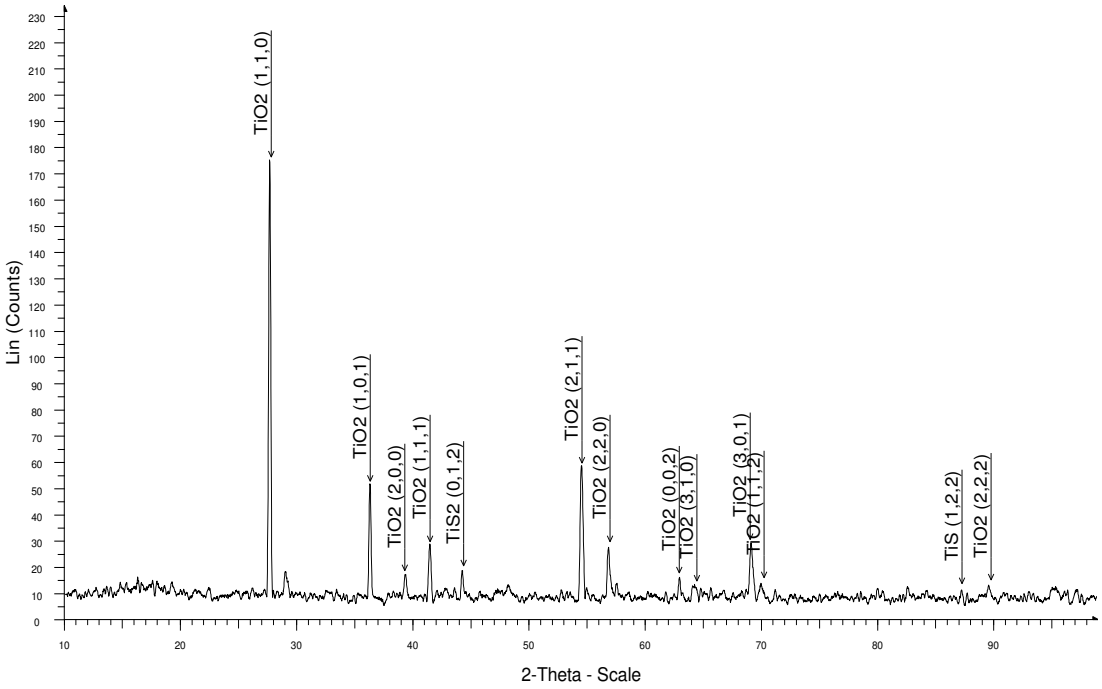

Figure 164 XRD pattern Al_2Au coated Ti45Al8Nb after 1000 hours sulphidation at 1023 K

Ch.VI.Sec.2.7 CrAlYN/CrN+CrAlYON coated Ti45Al8Nb alloy etched by Cr

The SEM surface morphology of CrAlYN/CrN+CrAlYON coated Ti45Al8Nb alloy etched by Cr given in **figure 165** shows that the surface of the exposed sample was covered partly by TiO_2 oxide. It can also be seen that however material was not covered by any corrosion products indicating that the sample suffered uneven attack.

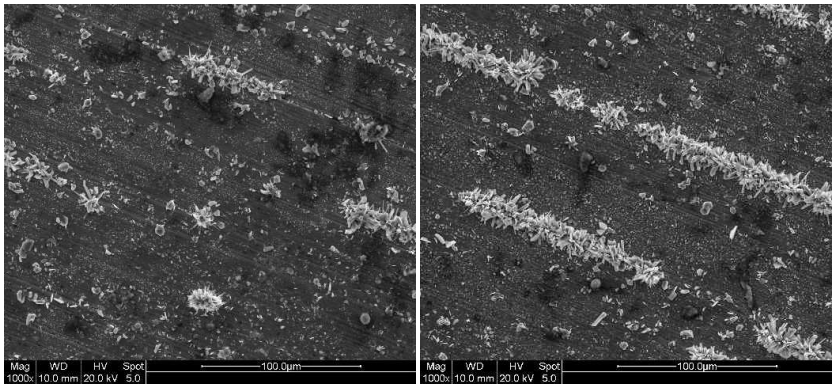

A: 1000x B: 1000x

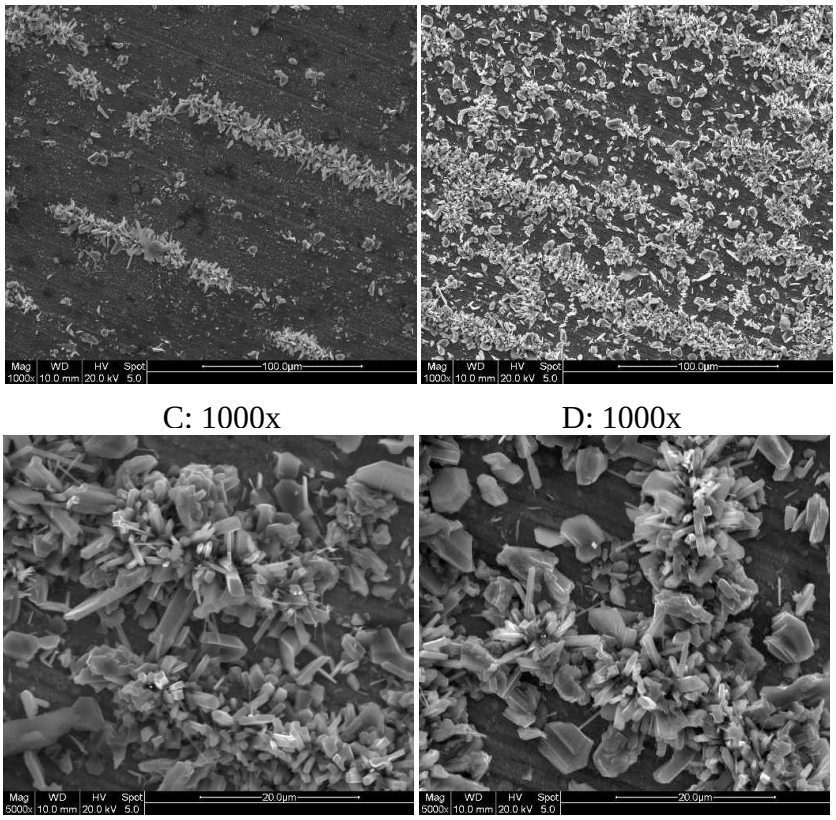

C: 1000x D: 1000x

E: 5000x F: 5000x

Figure 165 Surface morphology of CrAlYN/CrN+CrAlYON coated Ti45Al8Nb etched by Cr after 1000hrs sulphidation at 1023 K, (magnification under images)

The surface analysis performed by the EDS **(Table 45)** show, that the outer scale of the exposed sample, consisted mainly of CrN phase with Al additions, however, the TiO_2 crystals also formed. The small amount of Ti in the **table 45** is related to the fact that the surface analysis was taken from large area, but the crystals of TiO_2 were very tinny. The larger magnification of the surface covered by TiO_2 crystals is given in **figure 165E**, the analysis performed in this place show that Ti content was larger than in other places (**Figures 165A, B, C, and D**). It was observed that S_2 also was detected in the outer part of the surface, after analysis performed by the EDS.

Image	at% N	at% O	at% Al	at% S	at% Ti	at% Cr	at% Y
A	20.376	29.271	14.542	3.565	1.988	30.259	
B	14.753	31.671	14.464	4.515	4.229	30.368	
C	18.295	31.791	13.470	3.471	4.410	28.564	
D	18.372	31.914	13.302	3.821	4.273	27.968	0.350
E		51.272	5.272	8.576	18.394	16.485	

Table 45 Surface analysis performed by EDS investigation of CrAlYN/CrN+CrAlYON coated Ti45Al8Nb etched by Cr after 1000 hours of sulphidation/oxidation at 1023 K

The SEM micrographs given in **figure 166** showed that the exposed material suffered sulphidation/oxidation attack. The deposited coating developed cracks, and parts of the coating spalled off from the exposed material. It was observed that spallation occurred during cutting process when preparing sample for cross – section analysis. The kinetic data presented in **figure 146** did not indicate the spallation. More details regarding phase development during exposure to sulphidation/oxidation atmosphere is given in **figures 167** (SEM cross – section image with scan line) and **168** (EDS concentration profiles).

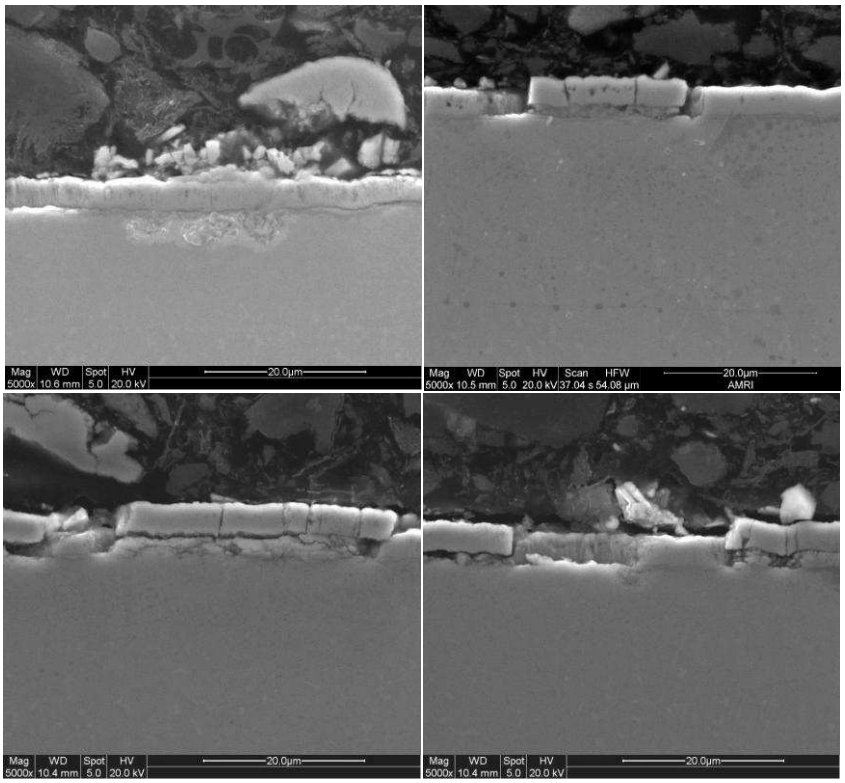

Figure 166 Cross sectional images of CrAlYN/CrN+CrAlYON coated Ti45Al8Nb etched by Cr after 1000hrs sulphidation at 1023 K

The cross – sectional SEM image in **figure 167** displays the scale structure developed. The scale was composed of Ti oxide. The details of the scale structure developed can be seen in the EDS profiles in **figure 168**.

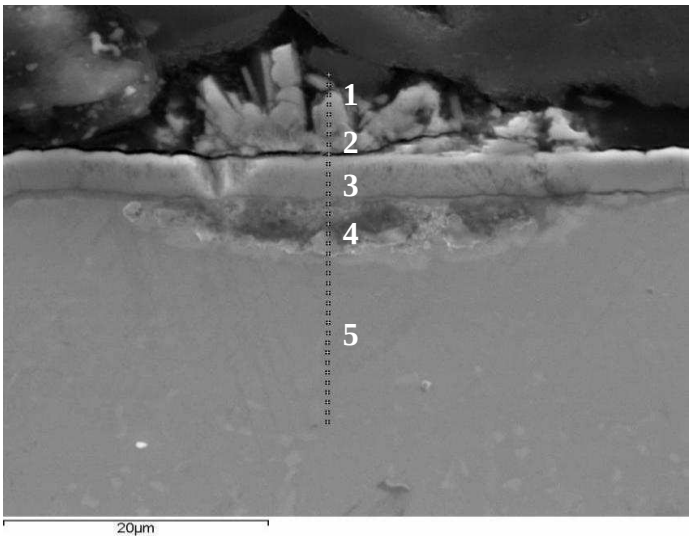

1) Titanium oxide (TiO_2)
2) Aluminium oxide (Al_2O_3)
3) Modified coating
4) Depletion zone of Al and Ti and sulphide region (TiS_2, Al_2S_3)
5) Substrate (Ti45Al8Nb)

Figure 167 SEM image (mag. 5000x) obtained from CrAlYN/CrN+CrAlYON coated Ti45Al8Nb etched by Cr after 1000 hours sulphidation at 1023 K

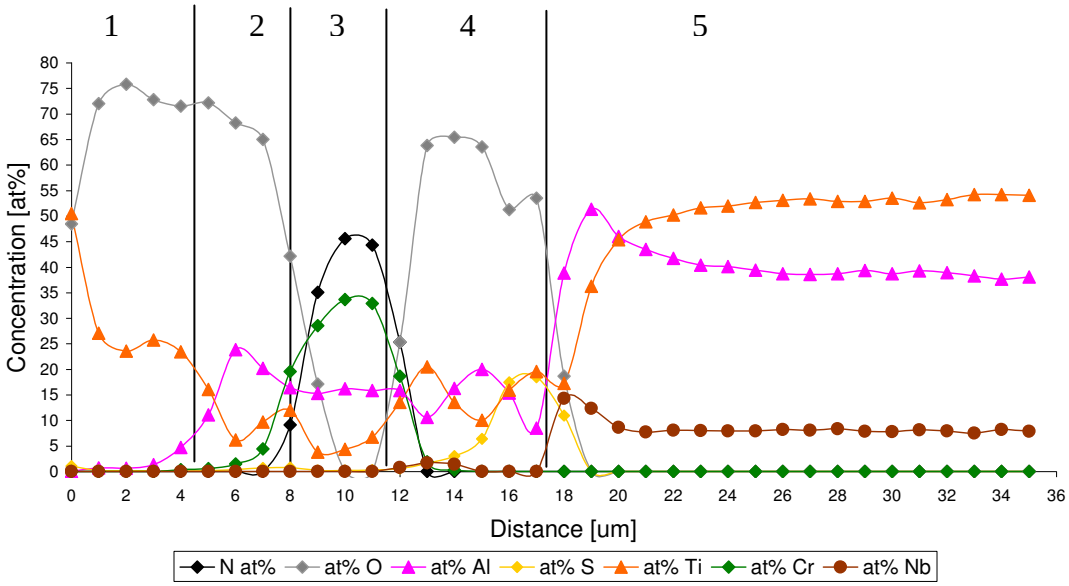

Figure 168 EDS concentration profiles obtained from CrAlYN/CrN+CrAlYON coated Ti45Al8Nb etched by Cr after 1000 hours of sulphidation at 1023 K

The EDS concentration profiles given in **figure 168** reveals that the outer part consisted of TiO_2 non protective oxide scale, underneath this non protective TiO_2 oxide scale, a thin (3 µm) layer of Al_2O_3 with some content of Ti and Cr developed. The modified coating (CrAlYN/CrN+CrAlYON) existed between Al_2O_3 oxide layer and the internal oxidation/sulphidation region with Al and Ti sulphides were detected. It was observed that at the scale/substrate NbS or NbS_2 phase formed. The EDS X-Ray mapping (**Fig. 169**) confirm the phases developed during exposure to sulphidation/oxidation region CrAlYN/CrN+CrAlYON etched by Cr coating; moreover the depletion zone of Ti **(Ti map)** formed below the deposited coating is filled by sulphur and niobium, suggesting that NbS, or NbS_2 phases were also developed. Mapping performed on exposed sample displayed also that Cr remained in the deposited coating and did not diffuse outward.

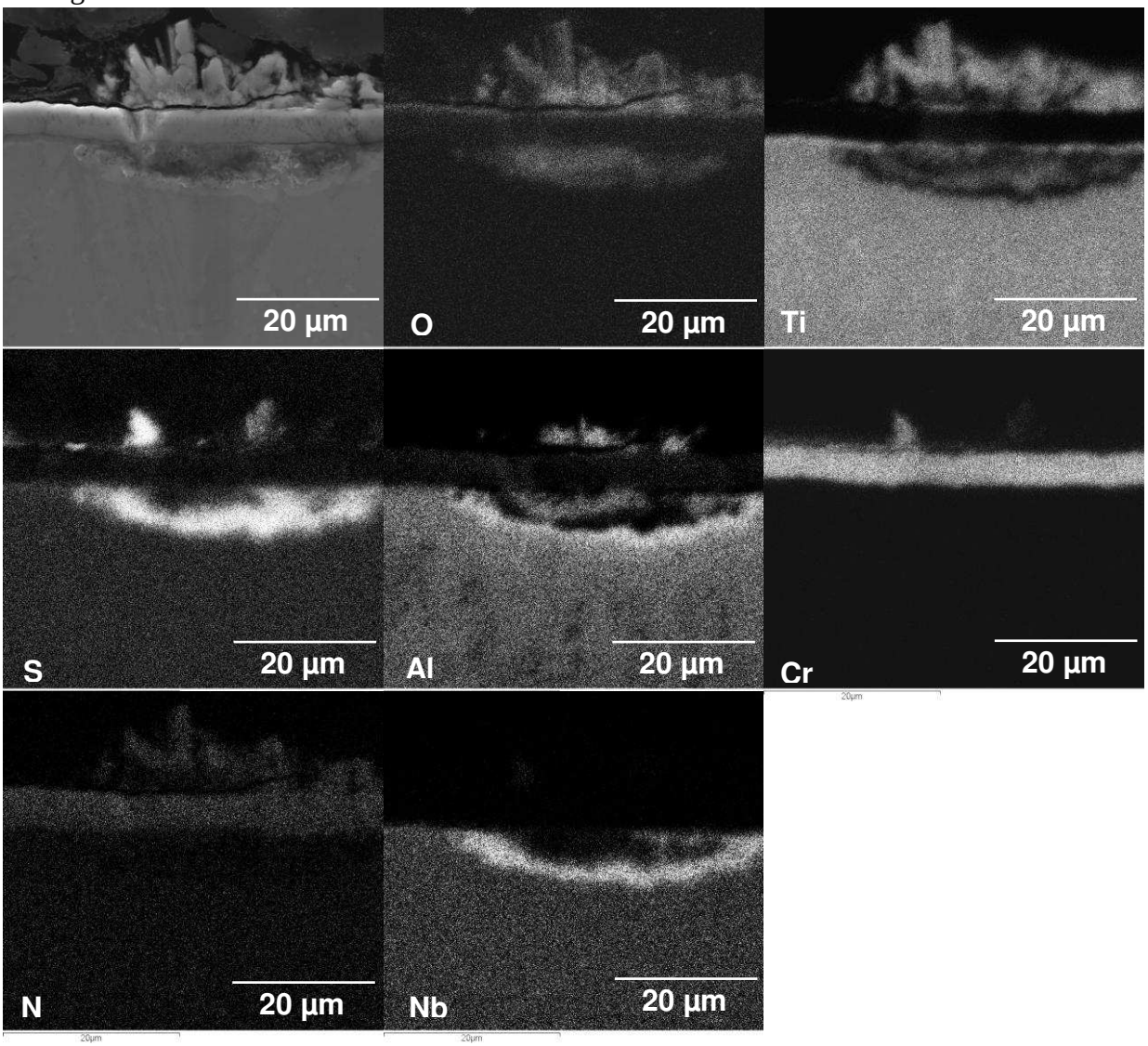

Figure 169 Digimaps of CrAlYN/CrN+CrAlYON coated Ti45Al8Nb etched by Cr after 1000 hours sulphidation at 1023 K

The XRD analysis **(Fig. 170)** indicates the presence of Ti oxides, Ti sulphides, Cr_3S_4, $NbAl_3$, $NbAl_2$, and CrN phases.

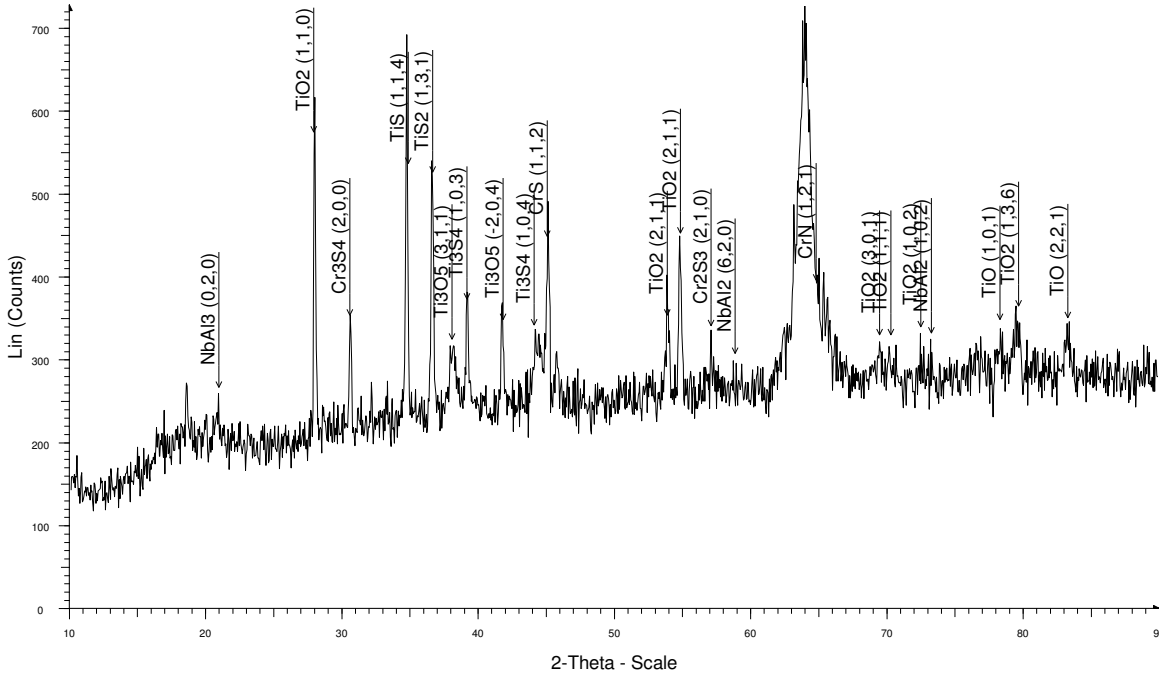

Figure 170 XRD pattern of CrAlYN/CrN+CrAlYON coated Ti45Al8Nb etched by Cr after 1000 hours sulphidation at 1023 K

Ch.VI.Sec.2.8 CrAlYN/CrN+CrAlYON coated Ti45Al8Nb alloy etched by CrAl

Morphologies **(Fig. 171)** developed on CrAlYN/CrN+CrAlYON coated Ti45Al8Nb alloy etched by CrAl were similar to these formed on CrAlYN/CrN+CrAlYON etched by Cr. As in previous case TiO_2 developed on the parts of the exposed material; however some parts of the material are not covered by any corrosion products.

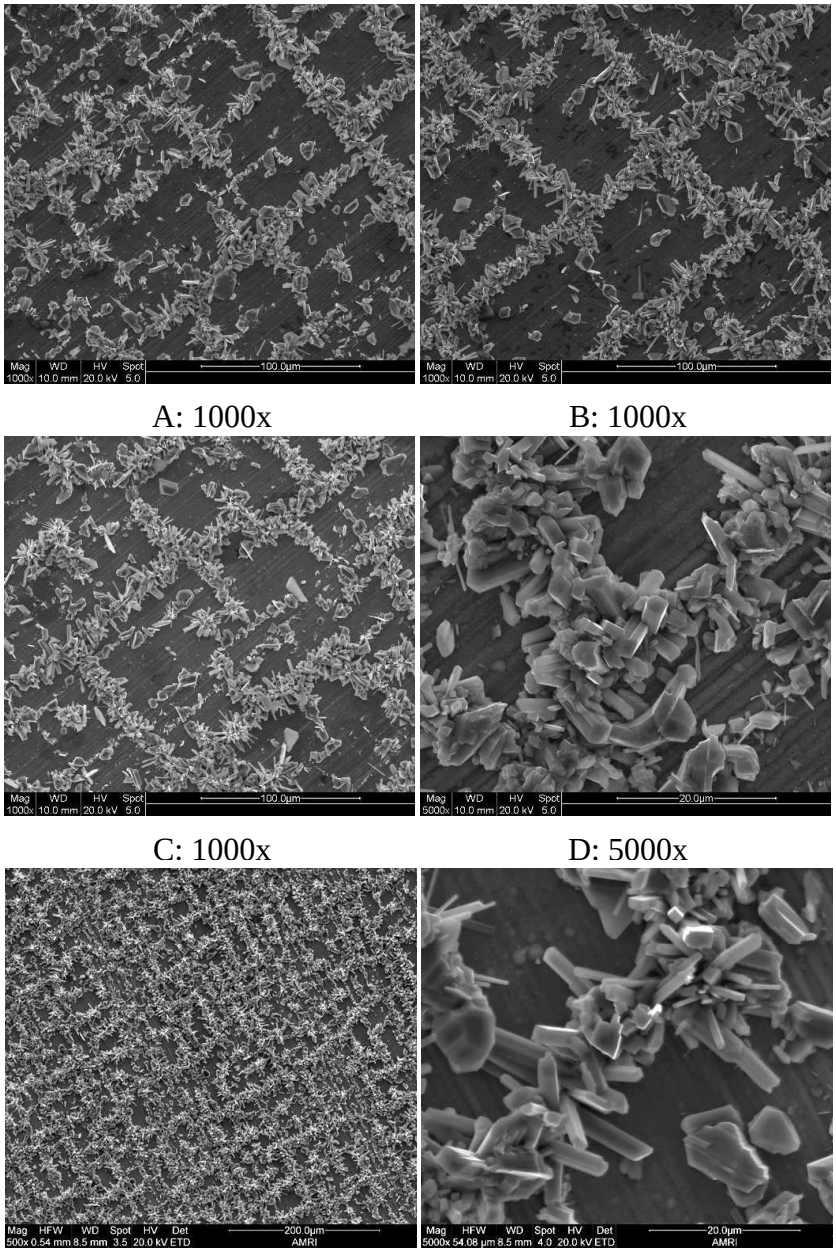

Figure 171 Surface morphology of CrAlYN/CrN+CrAlYON coated Ti45Al8Nb etched by CrAl after 1000hrs sulphidation at 1023 K, (magnification under images)

The EDS data in **table 46** shows that the surface of the exposed sample, the surface was covered by large and well developed TiO_2 crystals, however the EDS analysis also detected large amount of N and Cr. In certain parts indicating these parts did not suffer any attack. Sulphur was also detected.

Image	at % N	at% O	at% Al	at % S	at% Ti	at % Cr
A	18.496	32.259	8.378	5.572	10.050	25.244
B	18.911	28.997	9.911	6.640	8.094	27.447
C	13.877	37.499	8.585	4.462	11.357	24.220
D	6.611	41.024	5.736	9.527	15.840	21.264

Table 46 Surface analysis performed by EDS investigation of CrAlYN/CrN+CrAlYON coated Ti45Al8Nb etched by CrAl after 1000 hours of sulphidation/oxidation at 1023 K

The cross – sectioned SEM images shown in **figure 172**, demonstrates that material shows reasonably good high temperature corrosion resistance; however the micro-cracks developed (yellow circles). Additionally the CrAlYN/CrN+CrAlYON etched by Cr. The CrAlYN/CrN+CrAlYON etched by Cr showed larger amount of cracks and spallation, compared to the CrAl etched coating.

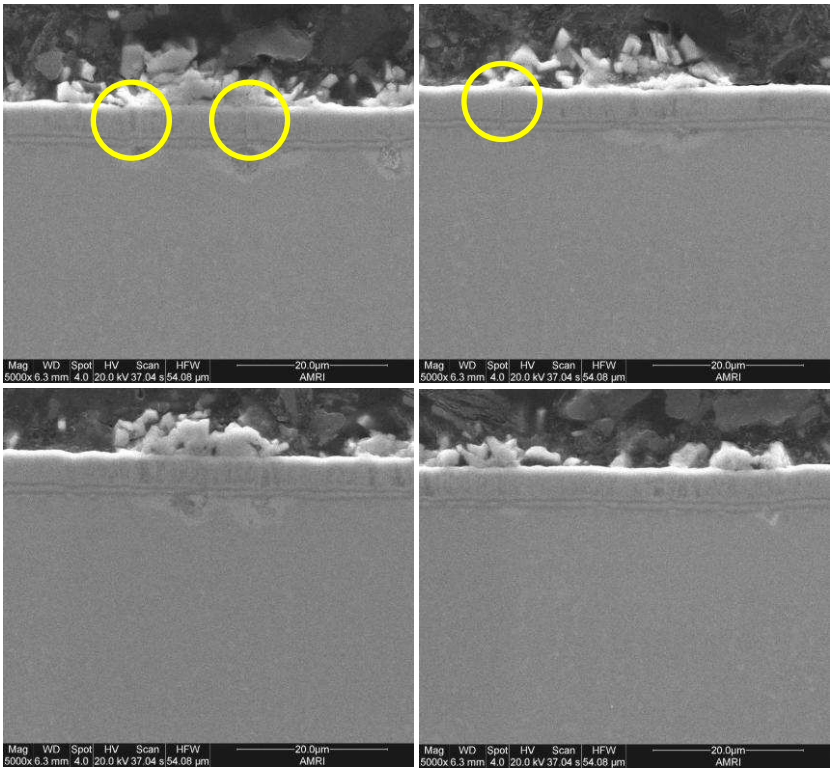

Figure 172 Cross sectional images of CrAlYN/CrN+CrAlYON coated Ti45Al8Nb etched by CrAl after 1000hrs sulphidation at 1023 K

The SEM micrograph displayed in **figure 173**, revealed that the outer scale consisted of TiO_2 oxide; the development of this non protective TiO_2 scale was related to the micro-cracks formation (indicated in yellow circles). The developed micro-cracks were paths ways for outward diffusion of Ti ions from the bulk material (Ti45Al8Nb). **Figure 174** given the EDS concentration profiles.

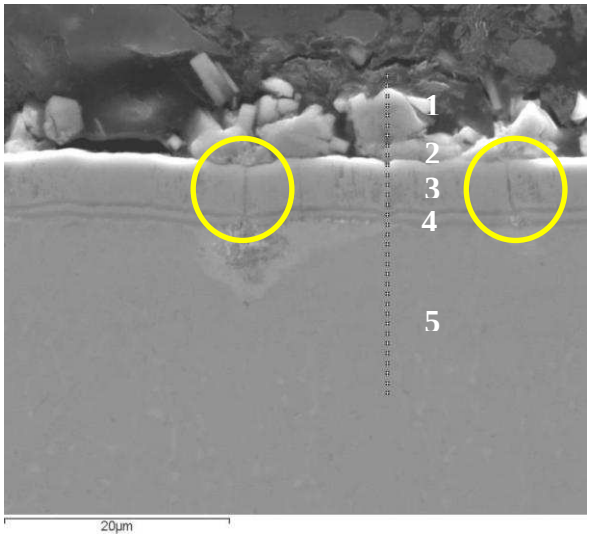

1) Titanium oxide (TiO_2)

2) Chromium sulphide (Cr_2S_3) and chromium oxide Cr_2O_3 with Ti inclusions

3) Modified coating

Figure 173 SEM image (mag. 5000x) obtained from CrAlYN/CrN+CrAlYON coated Ti45Al8Nb etched by CrAl after 1000 hours sulphidation at 1023 K

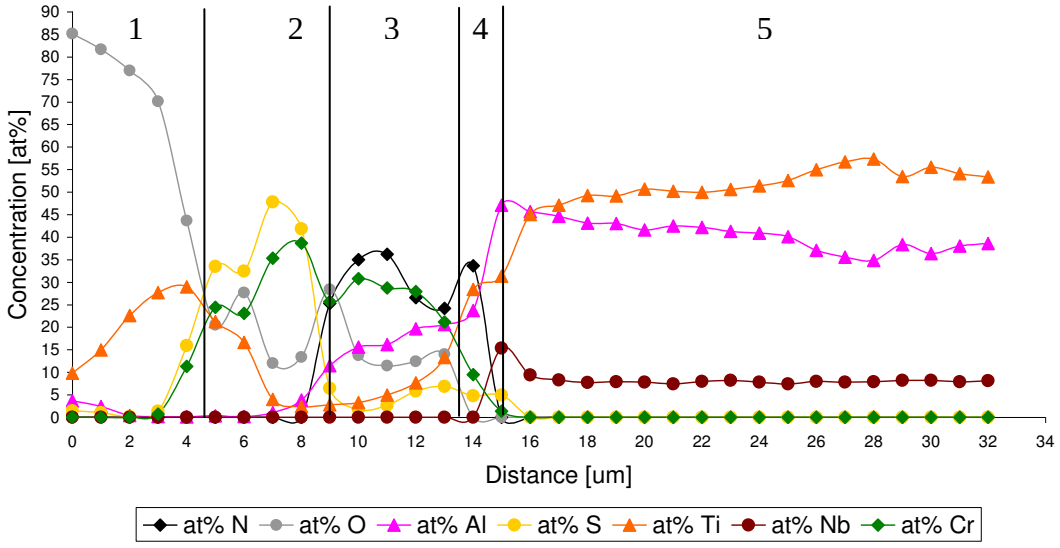

Figure 174 EDS concentration profiles obtained from CrAlYN/CrN+CrAlYON coated Ti45Al8Nb etched by CrAl after 1000 hours sulphidation at 1023 K

The EDS concentration profiles **(Fig. 174)** confirms that the outer scale consisted of TiO_2 oxide, underneath this TiO_2 oxide scale, a region consisted of Cr, Ti, O_2 and S_2 developed **(region 2, figure 174).** Between this region **(region 2, figure 174)** and a thin ceramic TiN layer **(region 4 figure. 174)** the modified coating was detected.

The presence of TiN partly inhibited Ti outward diffusion, however due to the micro-crack developed (yellow circles in **figures 172, 173**) Ti diffused outward and developed a non protective TiO_2 oxide. The EDS X-Ray mapping analysis in **figure 175** performed on exposed sample (CrAlYN/CrN+CrAlYON coated Ti45Al8Nb alloy etched by CrAl) confirmed that the outer scale was occupied by TiO_2 oxide.

However within TiO_2 oxide some amounts of S_2 was also detected. The formation of TiN layer also was confirmed, where N map and Ti map overlapped. The depletion zone of Ti **(Ti map, figure 175)** formed after outward diffusion of Ti form the bulk material was mainly filled by Nb, Al, and S_2.

It is suggested that in the depletion zone $NBAl_3$, $NbAl_2$ and Nb – sulphides formed.

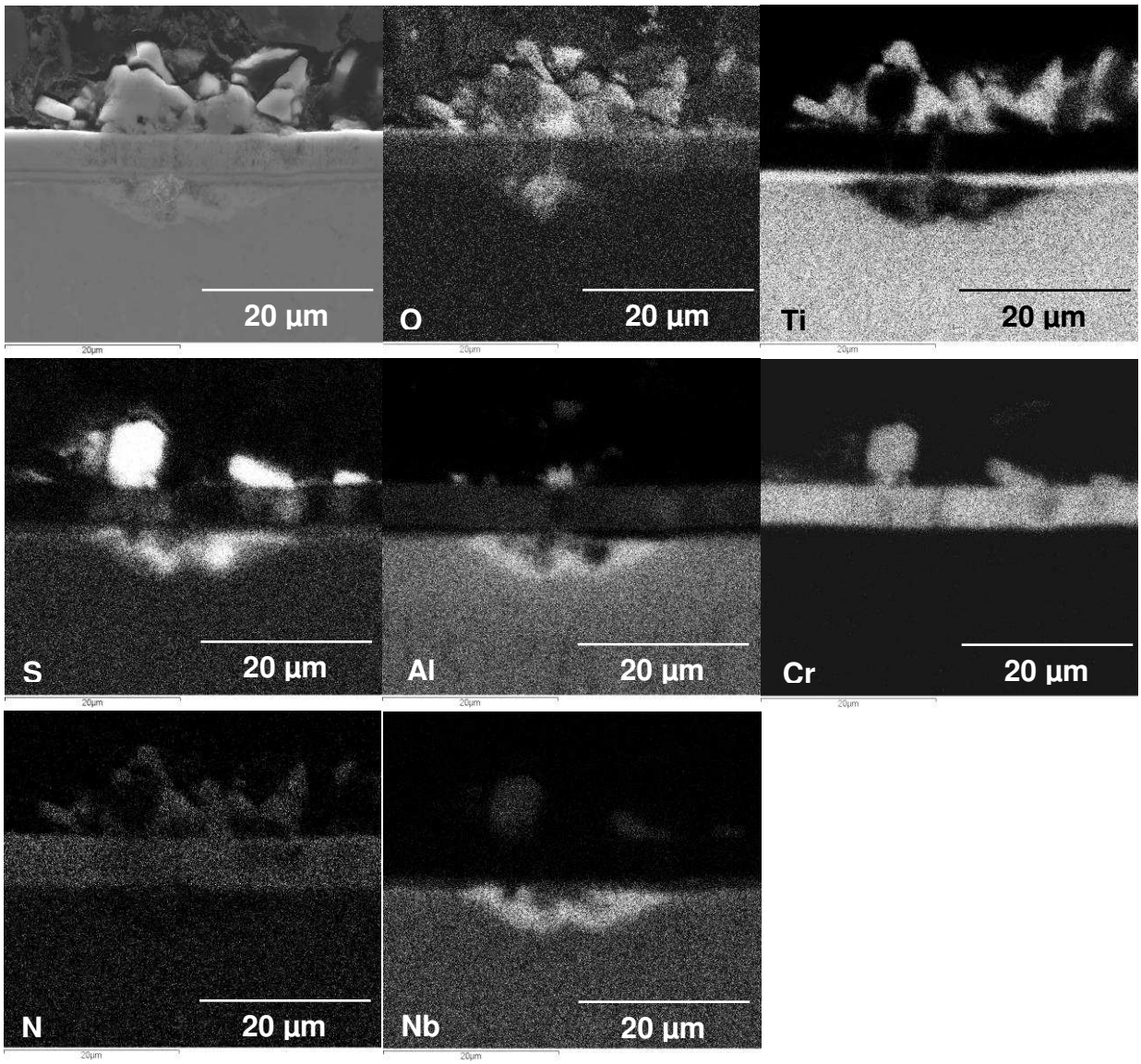

Figure 175 Digimaps of CrAlYN/CrN+CrAlYON coated Ti45Al8Nb etched by CrAl after 1000 hours sulphidation at 1023 K

The XRD analysis is given in **figure 176**, during investigation the Al, Ti, and Cr sulphides and oxides were detected, however the large CrN peak was also detected. No other peaks (substrate phases ($TiAl_2$, TiAl3, Ti3Al etc) were detected during this investigation.

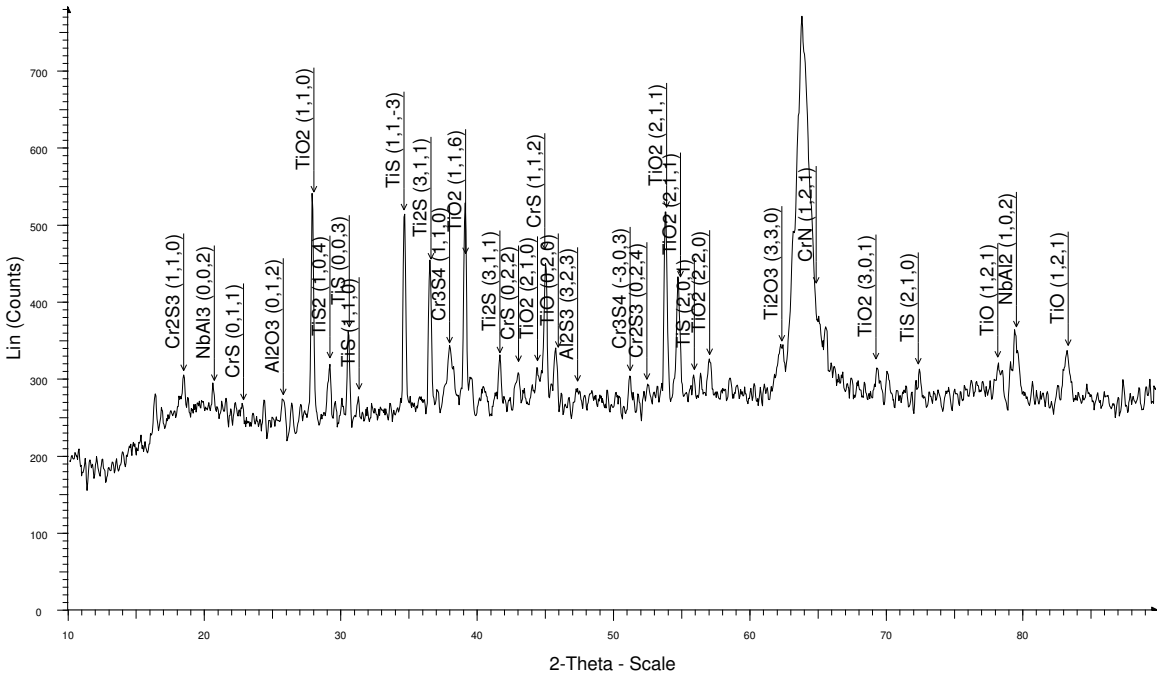

Figure 176 XRD pattern of CrAlYN/CrN+CrAlYON coated Ti45Al8Nb etched by CrAl after 1000 hours sulphidation at 1023 K

Ch.VI.Sec.2.9 CrAlYN/CrN+CrAlYON coated Ti45Al8Nb alloy etched by Y

The surface morphology of exposed CrAlYN/CrN+CrAlYON coated Ti45Al8Nb alloy etched by Y is given in **figure 177**. Similar surface morphologies as on previous samples (CrAlYN/CrN+CrAlYON etched by CrAl, CrAlYN/CrN+CrAlYON etched by Cr) were developed The detailed analysis of the corrosion products developed during exposure to sulphidation/oxidation environment at 1023 K for 1000 hours are given in **table 47**.

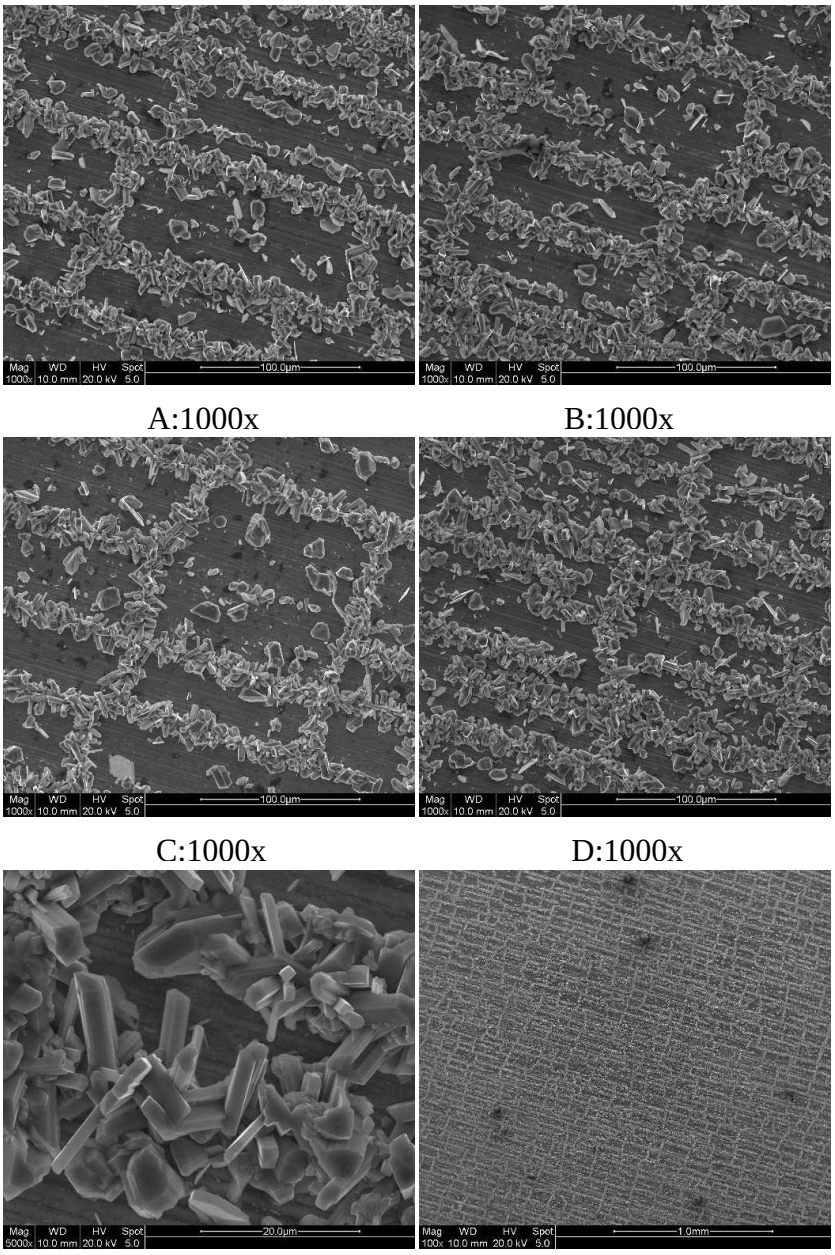

Figure 177 Surface morphology of CrAlYN/CrN+CrAlYON coated Ti45Al8Nb etched by Y after 1000hrs sulphidation at 1023 K; (magnification under images)

Table 47 reveals the presence of large amount of Cr and S_2 were detected. It is suggested that aside of TiO_2, chromium suphides also developed. However the EDS

analysis did not detected N. No other element as Nb was detected on the surface of exposed material.

Image	at% O	at% Al	at% S	at% Ti	at% Cr
A	42.245	6.547	9.866	16.639	24.703
B	37.554	10.846	7.023	13.922	30.654
C	40.139	8.307	8.921	14.741	27.893
D	42.408	7.381	7.870	16.527	25.815
E	49.922	2.091	8.947	23.338	15.702

Table 47 Surface analysis performed by EDS investigation of CrAlYN/CrN+CrAlYON coated Ti45Al8Nb etched by Y after 1000 hours of sulphidation/oxidation at 1023 K

The cross – section SEM micrographs of the scale structure developed during exposure to sulphidation /oxidation atmosphere presented in **figure 178** indicate that in some regions coating provided good adhesion to the substrate, whereas in other areas the coating developed cracks and lack of adherence was observed. The cracks and lack of adherence are indicated by the yellow circles in **figure 178**.

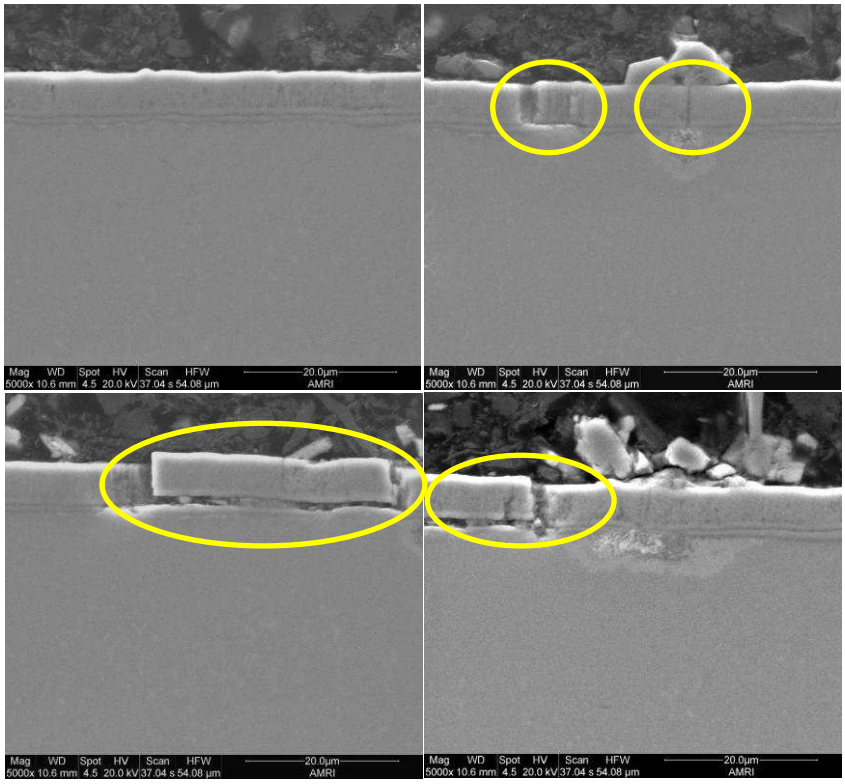

Figure 178 Cross sectional images of CrAlYN/CrN+CrAlYON coated Ti45Al8Nb etched by Y after 1000hrs sulphidation at 1023 K

The SEM micrograph with cracked coating is presented in **figure 179**. The yellow circles indicate cracks formation within the deposited coating. The detailed EDS analysis is displayed in **figure 180**.

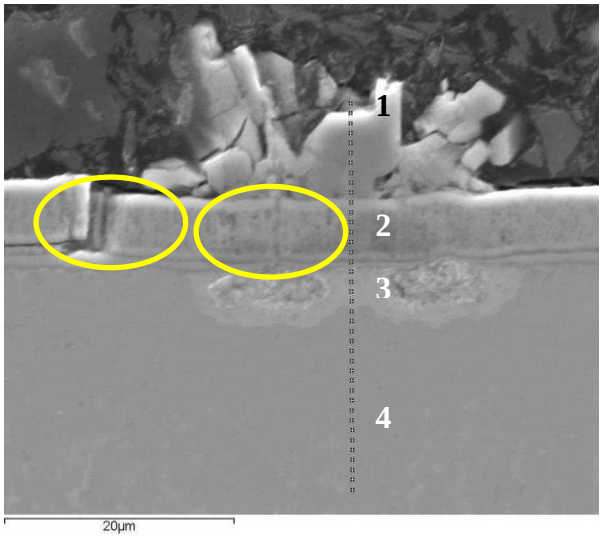

1) Titanium oxide (TiO_2) with sublayer of chromium sulphide (Cr_2S_3) and chromium oxide (Cr_2O_3)

2) Modified coating

3) Aluminium rich region

4) Substrate (Ti45Al8Nb)

Figure 179 SEM image (mag. 5000x) obtained from CrAlYN/CrN+CrAlYON coated Ti45Al8Nb etched by Y after 1000 hours sulphidation at 1023 K

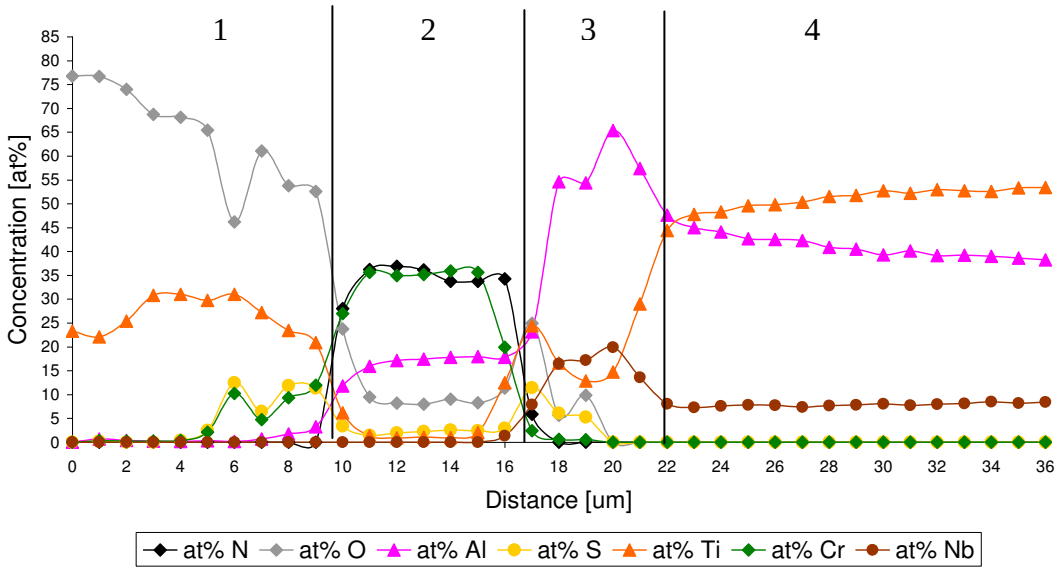

Figure 180 The EDS concentration profiles obtained from CrAlYN/CrN+CrAlYON coated Ti45Al8Nb etched by Y after 1000 hours sulphidation at 1023 K

The EDS concentration profiles given in **figure 180**, shows that a thick (10 µm) and non protective TiO_2 oxide scale was formed; at the bottom (oxide/coating interface)

a thick (5 µm) layer of chromium sulphide was detected. Beneath this thick (10 µm) TiO_2 oxide modified coating appears. The high concentration of Al was detected underneath modified coating, the higher Al concentration is related to the outward diffusion of Ti ions form the bulk material, Al replaced Ti ions and changed the structure of the material (from nearly TiAl to $TiAl_2$).

The EDS X-Ray mapping analysis performed on exposed to sulphidation/oxidation environment sample (CrAlYN/CrN+CrAlYON coated Ti45Al8Nb alloy etched by Y) is given in **figure181.** The mapping confirms that TiO_2 oxide developed as an outer scale, however EDS X-Ray mapping detected large amounts of S_2 within the developed TiO_2 oxide; moreover the Ti map revealed that Ti diffused outward **(yellow circle in figure 178**). It was observed that Al remained in the deposited coating and did not develop an oxide, whereas Cr from the coating diffused outward to the developed TiO_2 oxide scale. It is suggested that within TiO_2 oxide scale Cr_2S_3, Cr_3S_4 or other forms of chromium sulphides developed. The depleted zone of Ti **(Ti map, figure 181)** formed after Ti outward diffusion was covered by Nb, Al, and some oxygen and sulphur ions. It is appeared that in the depletion zone $NbAl_3$, $NbAl_2$, and Nb – sulphides formed. Nitrogen map shows that this element partly remained in the deposited coating and also was detected within TiO_2 oxide.

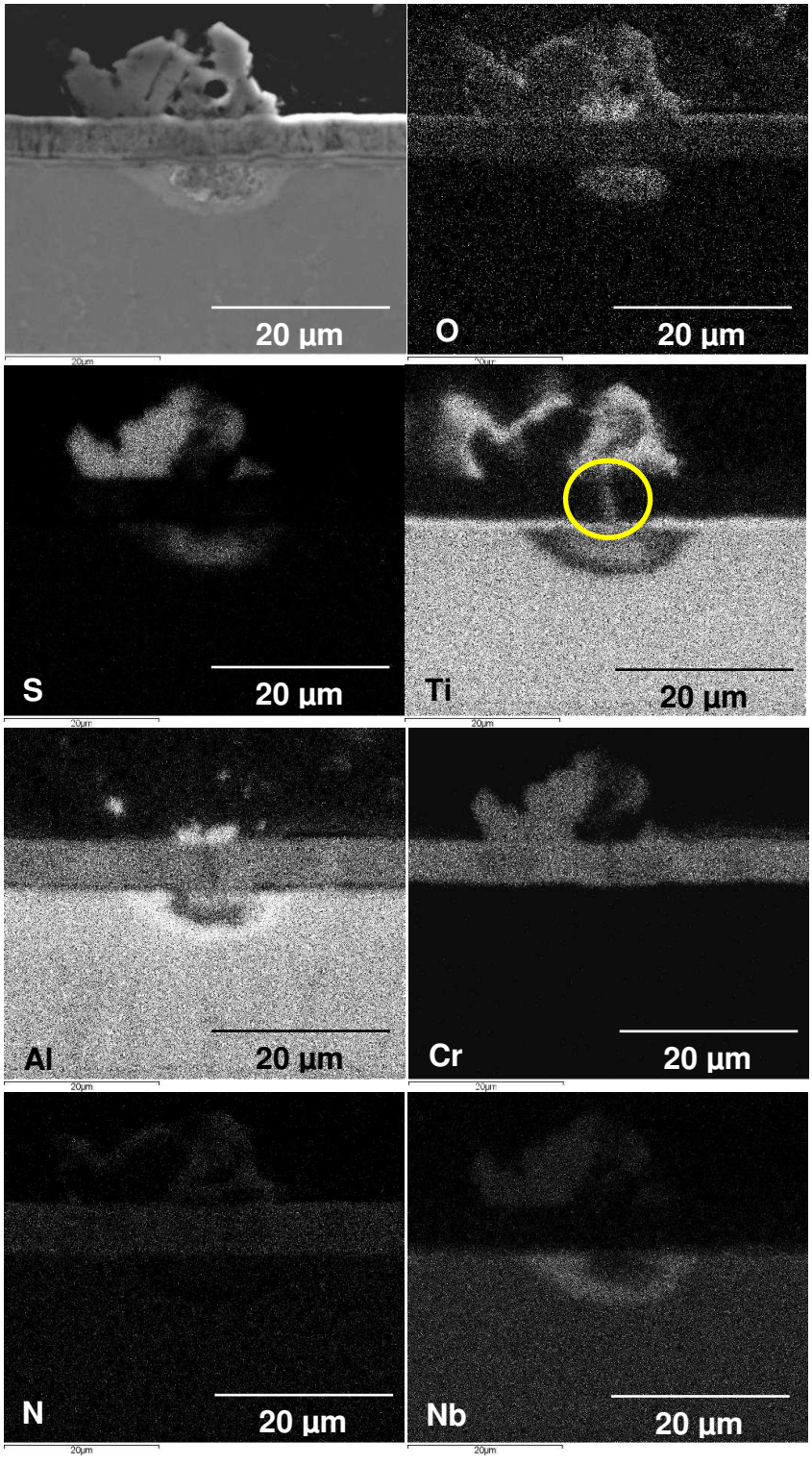

Figure 181 Digimaps of CrAlYN/CrN+CrAlYON coated Ti45Al8Nb etched by Y after 1000 hours sulphidation at 1023 K

The XRD analysis performed on sulphidized/oxidised sample (CrAlYN/CrN+CrAlYON coated Ti45Al8Nb alloy etched by Y) at 1023 K for 1000 hours is given in **figure 182**. The spectrum revealed that sulphides and oxides of Ti, Al, and Cr developed, also XRD detected peaks related to NbS_2, NbS_3 phases, and also $NbAl_3$ phase was detected.

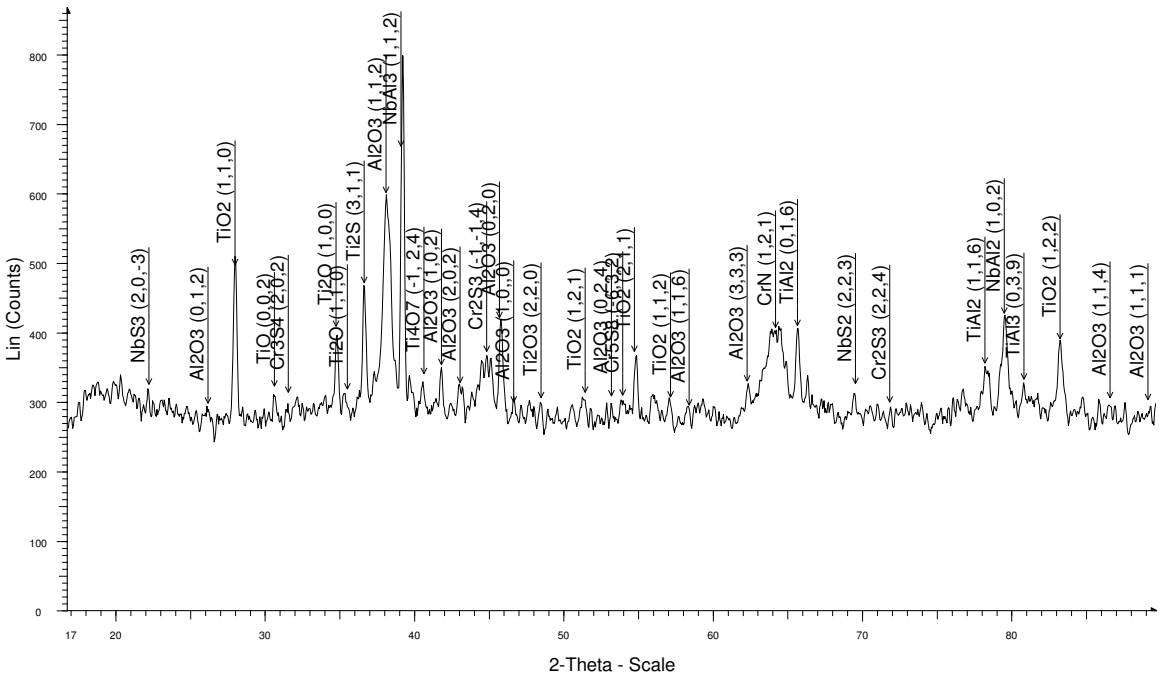

Figure 182 XRD pattern of CrAlYN/CrN+CrAlYON coated Ti45Al8Nb etched by Y after 1000 hours sulphidation at 1023 K

Part Two - 675 hours at 1123 K

Ch.VI.Sec.2.10 Introduction to part two

The high temperature sulphidation of for materials was performed in $H_2/H_2S/H_2O$ in high $pS_2 = 10^{-1}$ Pa and low $pO_2 = 10^{-18}$ Pa at 1123 K for 675 hours. The four materials involved:

1) Ti48Al8Nb uncoated alloy

2) CrAlYN/CrN coating Y etch, CrAl (thin) coated Ti45Al8Nb (2ah22)

3) CrAlYN/CrN coating Cr etch, CrAl (thin) coated Ti45Al8Nb (2ah23)

4) CrAlYN/CrN coating, Y etch, CrAlY (thick) coated Ti45Al8Nb (2ah24)

Ch.VI.Sec.2.11 Kinetics of sulphidized samples at 1123 K

Figures 183 and **184** show the kinetic data and the corresponding Kp values:

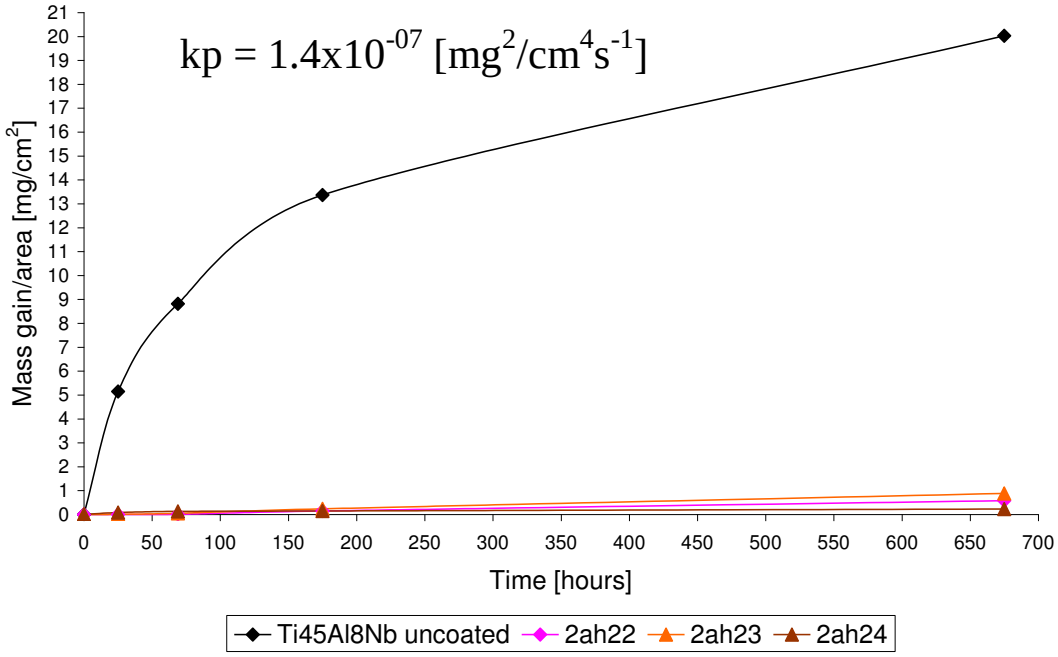

Figure 183 Sulphidation kinetic after 675 hours at 1123 K with kp value for Ti45Al8Nb alloy

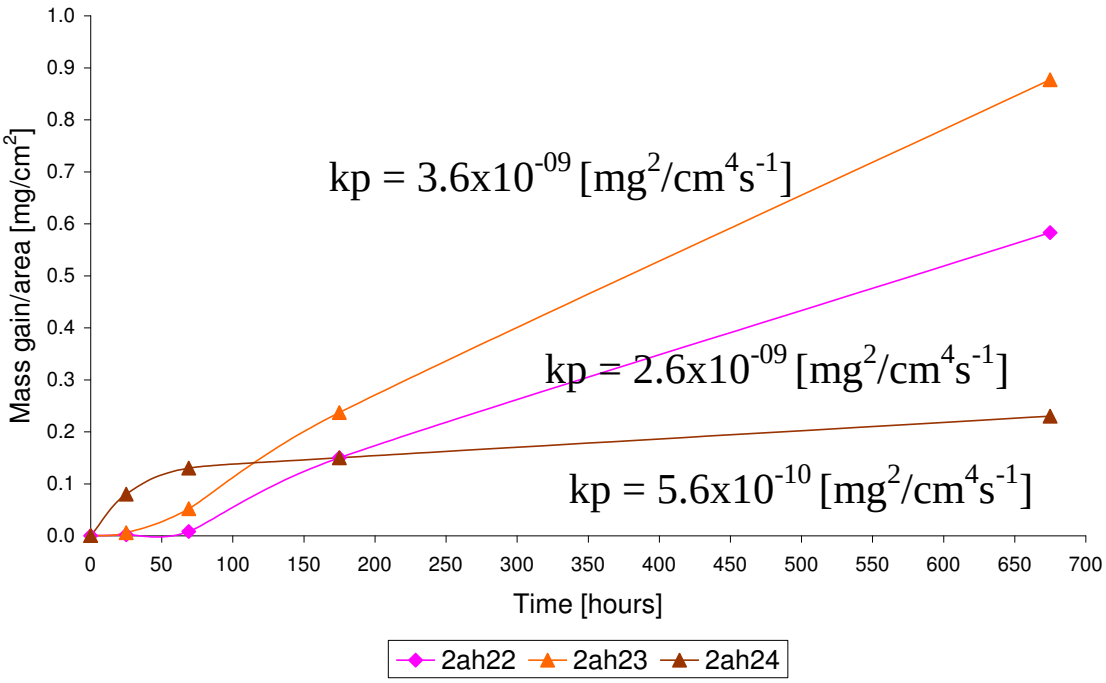

Figure 184 Sulphidation kinetic after 675 hours at 1123 K with kp value for Ti45Al8Nb alloy

The kinetic data presented in **figure 183** and **184** shows higher mass gain was for the substrate alloy (Ti45Al8Nb) alloy. All the coated materials displayed much reduced mass gain in sulphidising environment at 1123 K for 675 hours. However the data shows significant mass gains **(Fig. 184)** for two of nano-coatings (2ah22 and 2ah23) form 200 hours of exposure.

The higher mass gain of mentioned samples was related to development of fast growing TiO_2 phase due to micro-cracks formation during the cooling down period, when furnace was switched off between the intervals. The improved behaviour of 2ah24 nano-coatings in the high $pS_2 = 10^{-1}$ Pa and low $pO_2 = 10^{-18}$ Pa is related to the higher concentration of Y in etched sublayer (CrAlY - thick) in the exposed nano-coating.

Ch.VI.Sec.2.12 Ti45Al8Nb uncoated alloy

The surface morphology developed on uncoated alloy (Ti45Al8Nb) exposed to highly sulphidising ($pO_2 = 10^{-18}$ Pa, $pS_2 = 10^{-1}$ Pa) atmosphere at 1123 K is shown in **figure 185**. The surface of the exposed sample was covered with tinny TiO_2 crystals.

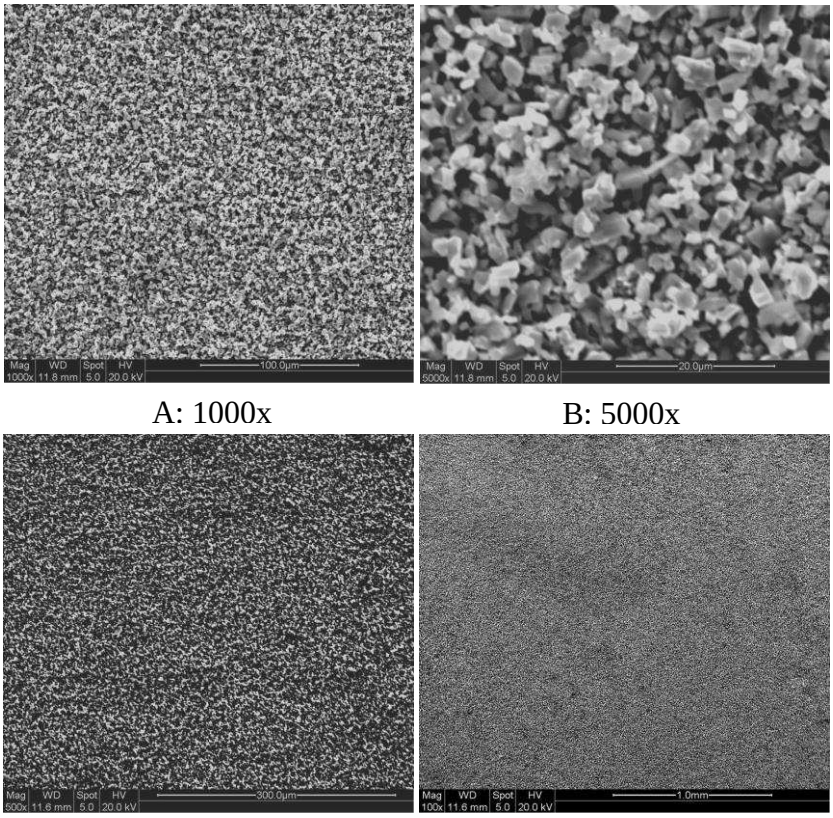

A: 1000x B: 5000x

C: 500x D: 100x

Figure 185 Surface morphology of Ti45Al8Nb uncoated after 675 hours of sulphidation at 1123 K (magnification under images)

Image	at% O	at% Ti
A	66.661	33.339
B	65.427	34.573
C	65.875	34.125
D	64.654	35.346

Table 48 Surface analysis performed by EDS investigation of Ti45Al8Nb uncoated alloy after 675 hours sulphidation at 1123 K

Table 48 presents that whole surface of uncoated material was covered by a thick TiO_2 oxide. Analysis performed in different places on the surface of exposed

samples scale indicates a similar concentration of Ti and O_2. No other elements of uncoated material (Al, Nb) were detected on the surface, indicating that the outer scale of TiO_2 was thick.

The cross – sectioned images of exposed uncoated Ti45Al8Nb alloy are presented in **figure 186** at different magnifications show, that whole of the uncoated sample was covered by the same structure of corrosion products. More details of these corrosion products are presented in cross – sectioned image of uncoated material where EDS analysis was performed.

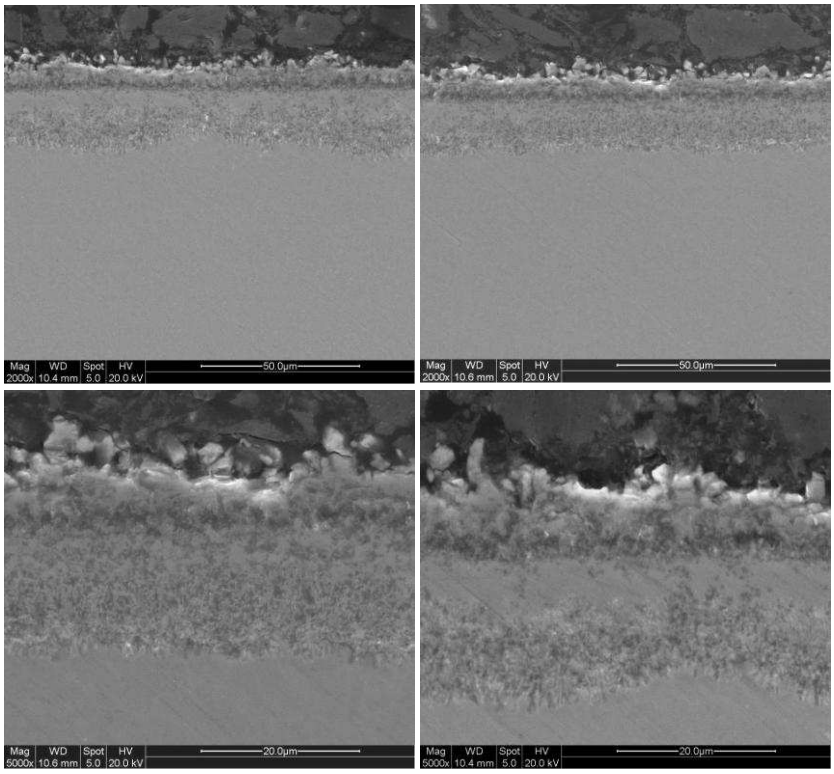

Figure 186 Cross – sectional images of Ti45Al8Nb uncoated sample after 675hours sulphidation at 1123 K

The uncoated Ti45Al8Nb alloy exposed to sulphidation environment ($H_2/H_2S/H_2O$) at 1123 K) confirms the formation of multilayer structure as given by the cross – sectioned SEM image in **figure 187**.

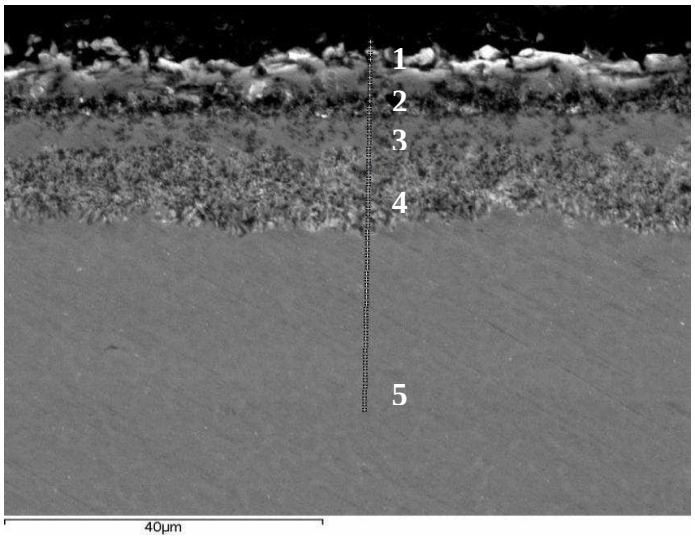

1) Titanium oxide (TiO_2)
2) Aluminium oxide (Al_2O_3)
3) Titanium oxide (TiO_2)
4) Aluminium oxide (Al_2O_3)
5) Substrate (Ti45Al8Nb)

Figure 187 SEM image (mag. 3000x) of base material (Ti45Al8Nb) after 675 hours of sulphidation at 1123 K

The EDS concentration profiles presented in **figure 188** show that the outer layer of uncoated material was occupied by a thick (8 μm) TiO_2 scale. Underneath the TiO_2 scale a thin 3 μm Al_2O_3 layer formed. Beneath the Al_2O_3 layer, again a TiO_2 developed. At the scale/substrate interface a relatively thick (10 μm) Al_2O_3 scale formed. Nb diffused outwards from the substrate to the outer part of the developed scale and reached Al_2O_3/TiO_2 interface **(figure 188, regions 3 and 4)**. Sulphur diffused inwards and reached a scale/substrate interface where Al, Nb and Ti sulphides were developed **(Fig. 188)**. The concentration profiles presented on **figure 188** also show that Nb_2O_5 is likely to develop. More detailed analysis is given in **figure 189** (EDS X-Ray mapping).

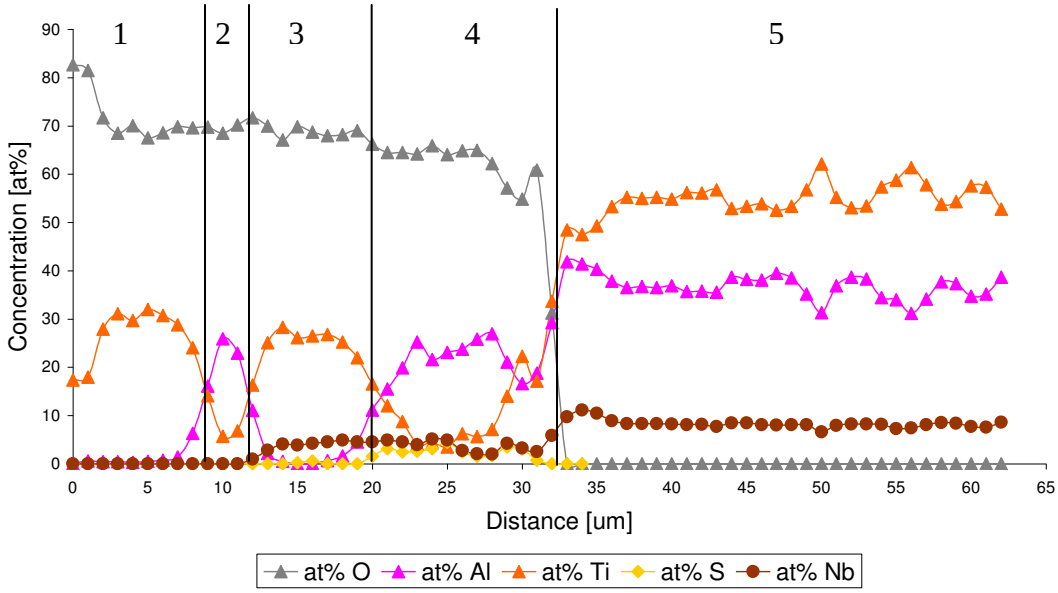

Figure 188 EDS concentration profiles of base material Ti45Al8Nb after 675 hours sulphidation at 1123 K

The EDS X-Ray mapping performed on uncoated Ti45Al8Nb alloy in **figure 189** confirms the main findings from the EDS analysis. The outer layer is occupied by a TiO_2 scale, underneath the TiO_2 outer scale, Al_2O_3 layer developed. Beneath Al_2O_3 layer again a TiO_2 layer formed. At the substrate scale interface the development of Al_2O_3 was confirmed by EDS X-Ray mapping, moreover beside Al_2O_3 at the scale/substrate interface NbS, NbS_2, TiS, and Al sulphides were detected. Furthermore the formation of Nb_2O_5 also was detected on EDS X-Ray mapping were O_2 and Nb maps overlapped.

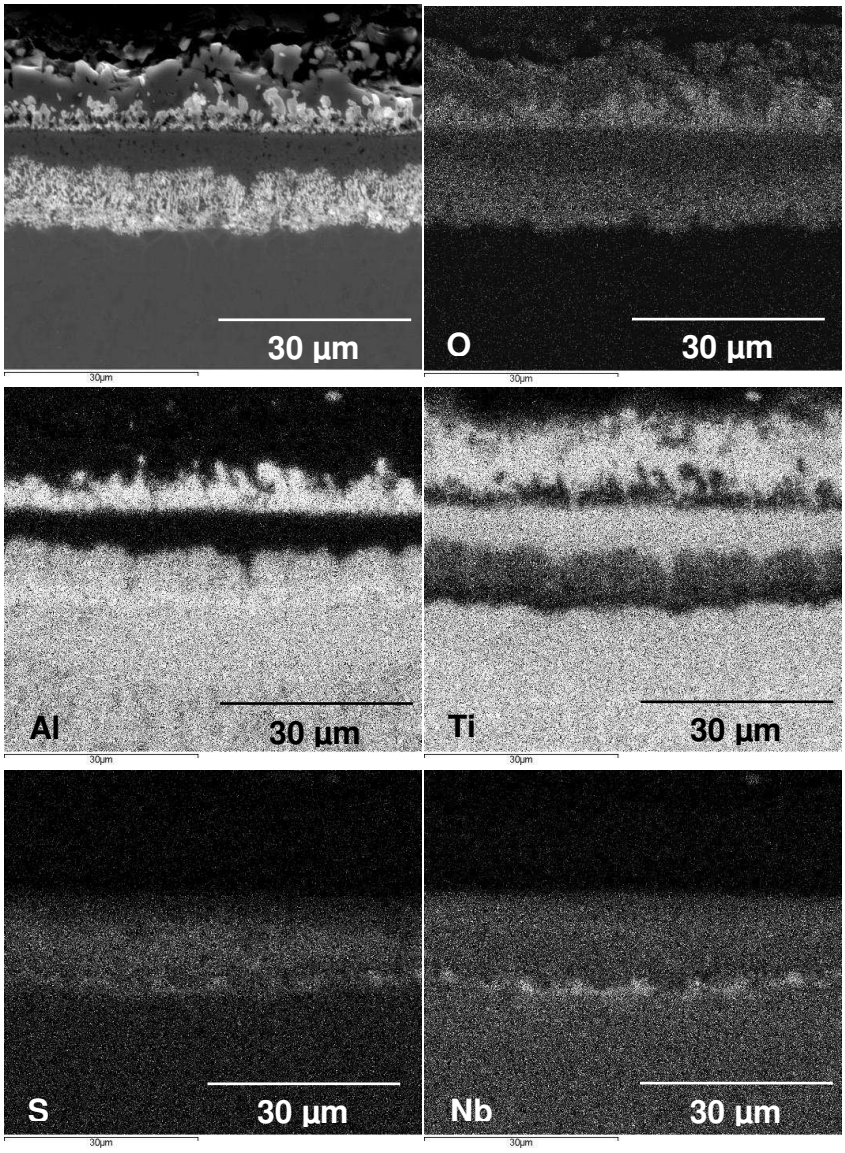

Figure 189 Digimaps of Ti45Al8Nb uncoated alloy after 675 hours sulphidation at 1123 K

The XRD pattern in **figure 190** obtained from an exposed uncoated material shows only development of TiO_2 and Al_2O_3. The XRD pattern did not detected any peaks from Nb_2O_5 and sulphides (NbS_2, NbS, TiS, Al_2S_3) probably due to the formation of a thick scale on exposed uncoated material (Ti45Al8Nb).

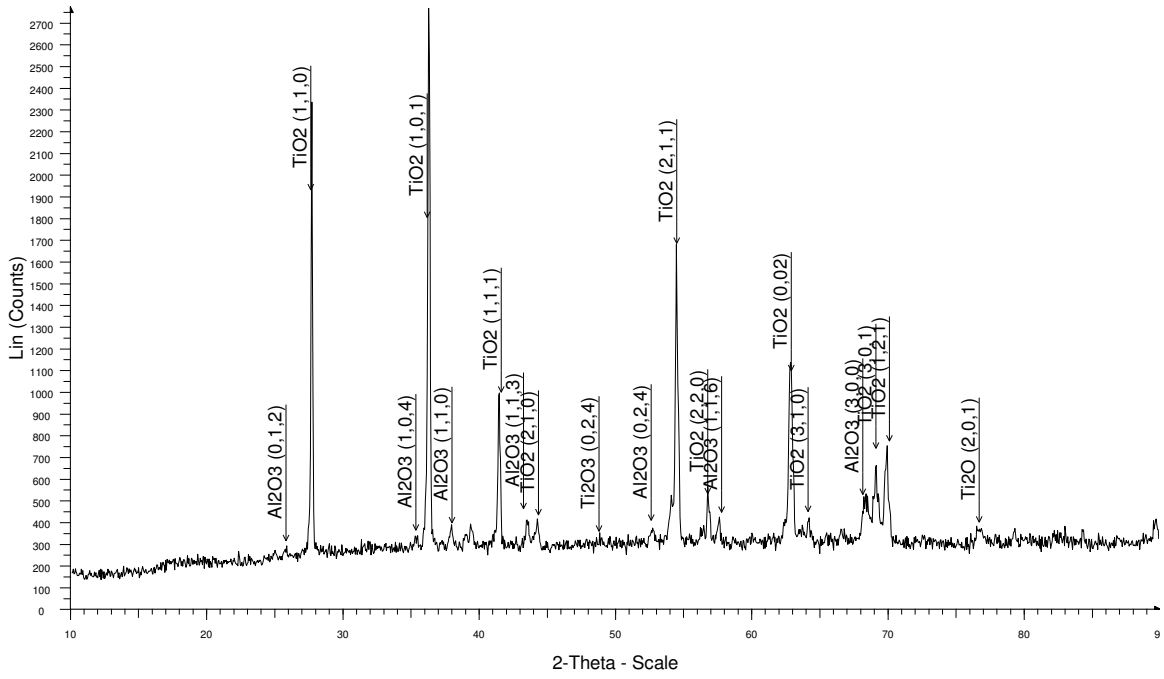

Figure 190 XRD pattern Ti45Al8Nb uncoated after 675 hours sulphidation at 1123 K

Ch.VI.Sec.2.13 CrAlYN/CrN coating Y etch, CrAl (thin) coated Ti45Al8Nb, CrAlYN/CrN coating, Y etch, CrAlY (thick), CrAlYN/CrN coating Cr etch, CrAl (thin), subjected to sulphidising environment ($pS_2 = 10^{-1}$ Pa and low $pO_2 = 10^{-18}$ Pa at 1123 K for 675 hours

The sulphidation behaviour of etched samples after 675 hours sulphidation at 1123 K is described below. All three samples suffered uneven corrosion – some parts of the sample remained virtually corrosion free (unaffected), other parts of the sample suffered damage and crack formation; these cracks accelerating further corrosion damage.

In the affected regions all three samples showed similarities and some differences in the corrosion patterns, morphologies, damage profiles, and the scale

structures developed. These features are described in **Table 49** and illustrated with appropriate and representative SEM micrographs, EDS concentration profiles, and XRD data.

Materials exposed	Observations	Atmosphere
CrAlYN/CrN coating Y etch, CrAl (thin) coated Ti45Al8Nb		$pS_2 = 10^{-1}$ Pa and low $pO_2 = 10^{-18}$ Pa, T = 1123 K for 675 hours
Regions developed		
Affected	Corrosion products (from top scale, to the substrate)	
Affected region characterised by the microcracks formation, and the development of a porous scale.	1) Titanium oxide (TiO_2) 2) Thin Al_2O_3 layer 3) Titanium oxide (TiO_2) 4) Chromium titanium thin layer 5) Modified coating 6) Low dense Al_2O_3 oxide and sulphides region 7) $NbAl_3$ region 8) Substrate (Ti45Al8Nb) **See EDS profiles in Fig. 194**	
Unaffected	Corrosion products (from top scale, to the substrate)	
Unaffected region no microcracks were found in the coating.	1) A thin Al – Cr oxide layer 2) Modified coating 3) Oxide and sulphides region 4) Substrate (Ti45Al8Nb) alloy **See EDS profiles in Fig. 197**	
CrAlYN/CrN coating, Y etch, CrAlY (thick) coated Ti45Al8Nb		$pS_2 = 10^{-1}$ Pa and low $pO_2 = 10^{-18}$ Pa, T = 1123 K for 675 hours
Regions developed		
Affected	Corrosion products (from top scale, to the substrate)	
Affected region characterised by the microcracks formation, and the development of a porous scale.	1) TiO_2 outer layer 2) Modified coating 3) Less dense mixture of phases: Al_2O_3, Cr_2O_3, TiS, TiS_2, Al_2S_3, Cr_2S_3 4) More dense mixture of phases: Al_2O_3, Cr_2O_3, TiS, TiS_2, Al_2S_3, Cr_2S_3 with high Al and Ti content 5) Substrate TiAl45Al8Nb	

	See EDS profiles in Fig. 198	
Unaffected	Corrosion products (from top scale, to the substrate)	
Unaffected region no microcracks were found in the coating.	1) A thin Cr Al oxide scale 2) Modified coating 3) Rich Ti zone 4) Cr_2O_3 thin layer 5) Diffusion zone of Cr, S, Al, Nb, O and Ti 6) Substrate (Ti45Al8Nb) **See EDS profiles in Fig. 199**	
CrAlYN/CrN coating Cr etch, CrAl (thin) coated Ti45Al8Nb		$pS_2 = 10^{-1}$ Pa and low $pO_2 = 10^{-18}$ Pa, T = 1123 K for 675 hours
Regions developed		
Affected	Corrosion products (from top scale, to the substrate)	
Affected region characterised by the microcracks formation, and the development of a porous scale.	1) Titanium oxide (TiO_2) with Cr inclusions 2) Modified coating 3) Titanium oxide/titanium sulphur layer 4) $NbAl_3$ layer 5) Substrate (Ti45Al8Nb) **See EDS profiles in Fig. 200**	
Unaffected	Corrosion products (from top scale, to the substrate)	
Unaffected region no microcracks were found in the coating.	1) A thin Al – Cr oxide layer 2) Modified coating 3) Ti, Cr, Al less dense oxide region 4) Rich Al and Ti region with Cr inclusions 5) Substrate (Ti45Al8Nb) alloy **See EDS profiles in Fig. 201**	

Table 49 Degradation rate of three etched samples exposed to sulphidation atmosphere at 1123 K for 675 hours.

The surface morphology of CrAlYN/CrN coating Y etch; CrAl (thin) coated sample exposed to sulphidising environment ($pO_2 = 10^{-18}$ Pa, $pS_2 = 10^{-1}$ Pa) at 1123 K is shown in **figure 191**. The morphologies from various locations and at different

magnifications show that the sample was partly covered by tiny TiO_2 crystals. The places not covered by the corrosion products showed the compositions of the as deposited sample **(Table 50 row B). Table 50** shows the compositions at various locations of the exposed sample.

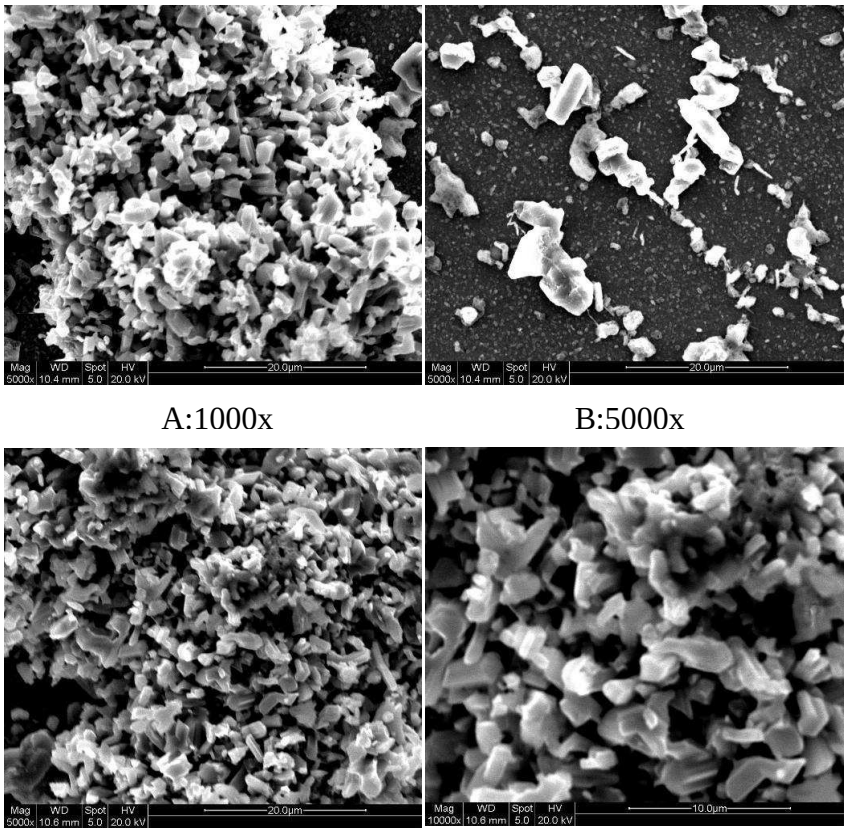

Figure 191 Surface morphology of (CrAlYN/CrN coating Y etch, CrAl (thin) coated Ti45Al8Nb) after 675 hours sulphidation at 1123 K

Image	at% N	at% O	at% Al	at% S	at% Ti	at% Cr
A		65.182	2.006	0.296	27.766	4.751
B	25.432	21.024	13.570		1.098	38.875
C		66.156	1.833	0.348	27.156	4.507
D		65.221	1.747	0.516	27.656	4.860

Table 50 Surface analysis performed by EDS investigation of CrAlYN/CrN coating Y etch, CrAl (thin) coated Ti45Al8Nb after 675 hours sulphidation at 1123 K

Table 50 confirms the formation of TiO_2 crystals; sulphur was detected in trace amount; and Y was not detected on the surface morphology.

The cross – sectioned images from Ti45Al8Nb coated with nanostructured CrAlYN/CrN coating Y etch; CrAl (thin), exposed to ($pO_2 = 10^{-18}$ Pa, $pS_2 = 10^{-1}$ Pa) atmosphere at 1123 K at different locations and different magnifications are presented in **figure 192**. Corrosion occurred only when the coating failed. The failure of the coating (indicated by yellow circles in **figure 192**), exposed to the sulphidized atmosphere was due to the mismatch of thermal expansion coefficient between deposited coating and substrate. It needs to be noticed that the coating has a ceramic structure (CrAlYN/CrN) the substrate is an intermetallic alloy (Ti45Al8Nb) alloy.

The failure locations are indicated by yellow circles; the brittle coating cracked during cooling down periods and allowed the development of non protective TiO_2 scale.

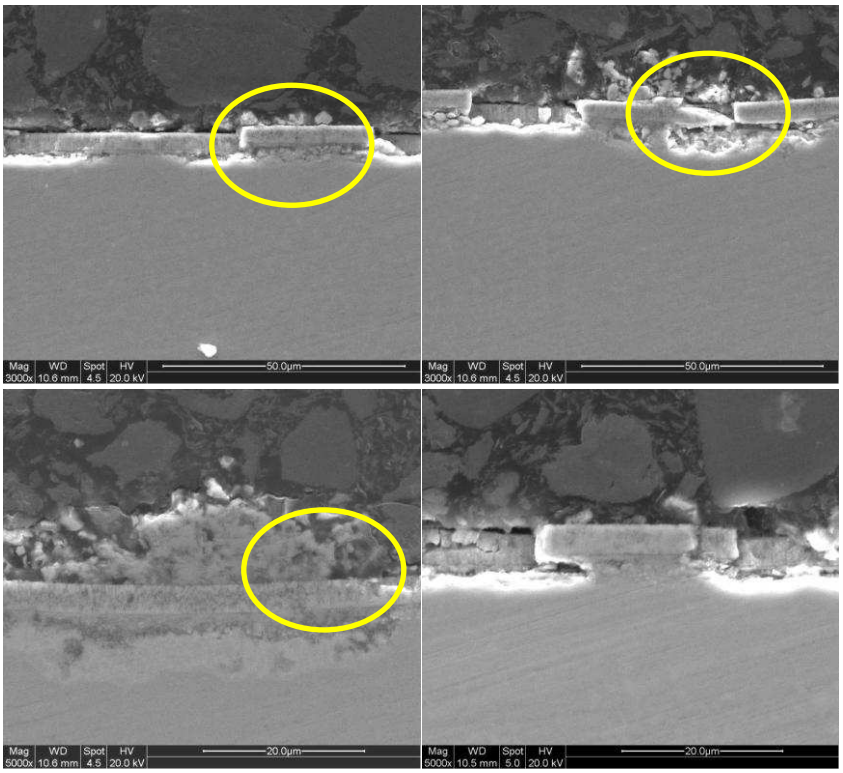

Figure 192 Cross sectional images of CrAlYN/CrN coating Y etch, CrAl (thin) coated Ti45Al8Nb after 675 hours sulphidation at 1123 K

Figure 193 shows cross – sectioned SEM image of the affected regions of crack formation. The affected region shows the formation of non –protective TiO_2. The yellow

circles indicate cracks in the coating. The multilayered scale is analysed by concentration profiles given in **figure 194**.

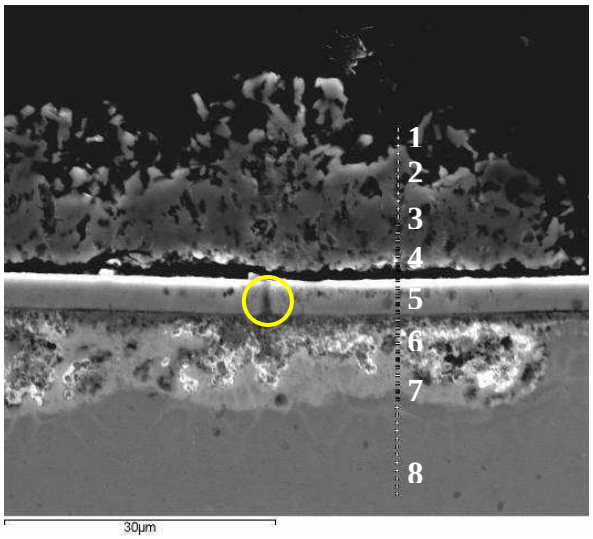

1) Titanium oxide (TiO_2)
2) Thin Al_2O_3 layer
3) Titanium oxide (TiO_2)
4) Chromium titanium thin layer
5) Modified coating
6) Low dense Al_2O_3 oxide and sulphides region (TiS_2, Al_2S_3, NbS_2)
7) $NbAl_3$ region
8) Substrate (Ti45Al8Nb)
Yellow circle – coating failure

Figure 193 SEM image (mag. 5000x) of affecter region of CrAlYN/CrN coating Y etch, CrAl (thin) coated Ti45Al8Nb after 675 hours sulphidation at 1123 K) - (affected region)

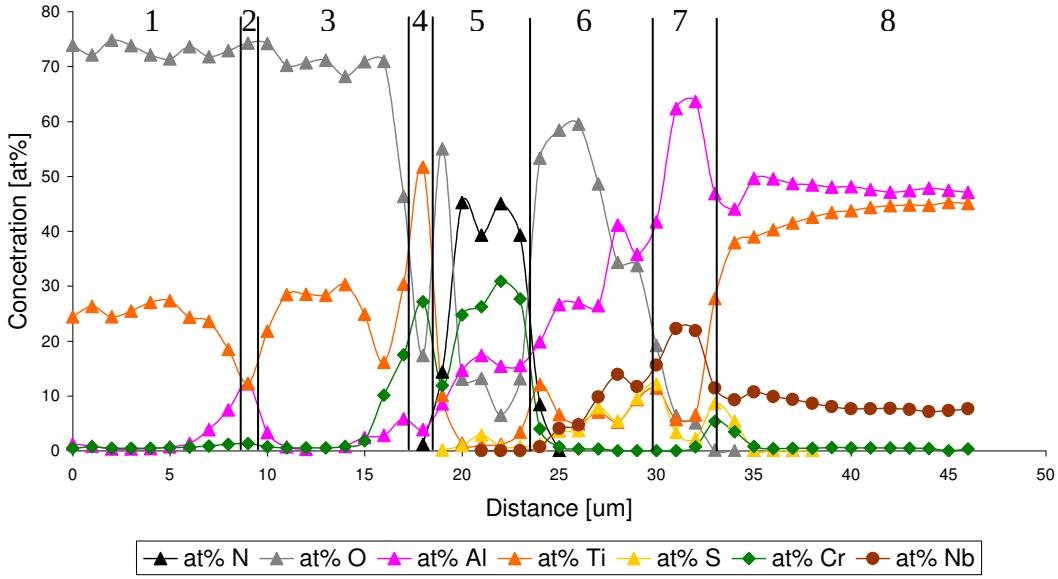

Figure 194 EDS concentration profiles of affected region of CrAlYN/CrN coating Y etch, CrAl (thin) coated Ti45Al8Nb after 675 hours sulphidation at 1123 K (affected region)

The development of TiO_2 scale is also confirmed by EDS concentration profiles performed on exposed CrAlYN/CrN coating Y etch, CrAl (thin) coated Ti45Al8Nb after

675 hours sulphidation at 1123 K are presented in **figure 194**. **Figure 195** shows EDS X-Ray mapping performed on exposed to sulphidising environment in affected region, where crack of the coating appeared (yellow circle). The cracks in the coating allowed the outward diffusion of Ti from the bulk material and development of TiO_2 outer scale; however some Ti ions also produced Ti - sulphides as revealed by the EDS X-Ray mapping investigation. The internal oxidation also is shown (white arrow on O map) in EDS X-ray mapping. Additionally within the internal oxidation region the formation of $NbAl_3$ and Al - sulphides were found. The EDS X-Ray mapping revealed that Cr and N remained in the deposited coating.

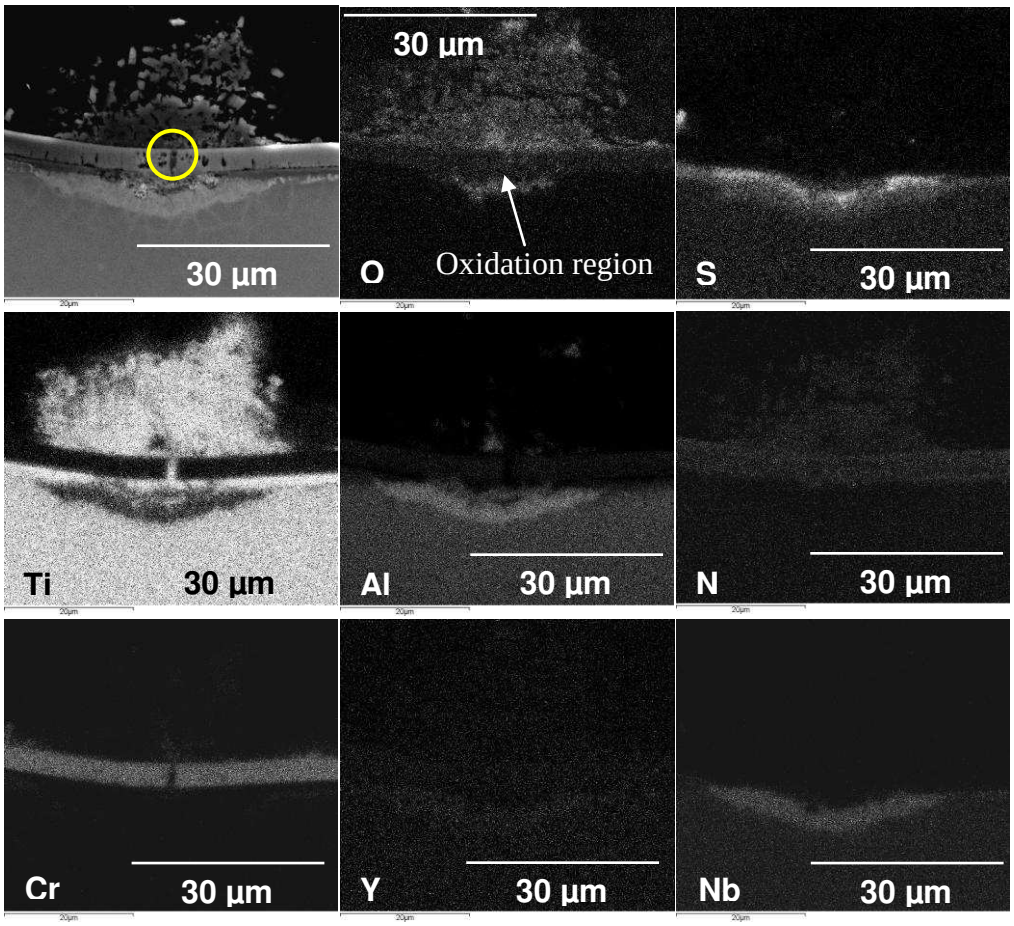

Figure 195 Digimaps of CrAlYN/CrN coating Y etch, CrAl (thin) coated Ti45Al8Nb after 675 hours sulphidation at 1123 K (affected region due to the coating failure (yellow circle))

Figure 196 shows a region of CrAlYN/CrN coating Y etch, CrAl (thin) coated Ti45Al8Nb after 675 hours of sulphidation at 1123 K which did not suffer corrosion. It

is observed that the coating protected the substrate material from the corrosion atmosphere ($pO_2 = 10^{-18}$ Pa, $pS_2 = 10^{-1}$ Pa) until the onset of coating failure.

Figure 196 shows that the TiO_2 was not developed in the outer scale, the coating decreased or even blocked the diffusion of Ti ions.

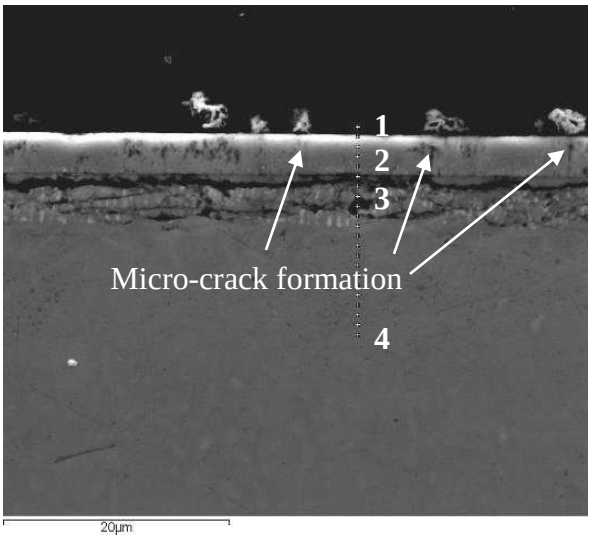

1) A thin Al – Cr oxide layer

2) Modified coating

3) Oxide and sulphides region

Figure 196 SEM image of unaffected region of CrAlYN/CrN coating Y etch, CrAl (thin) coated Ti45Al8Nb after 675 hours sulphidation at 1123 K (unaffected region)

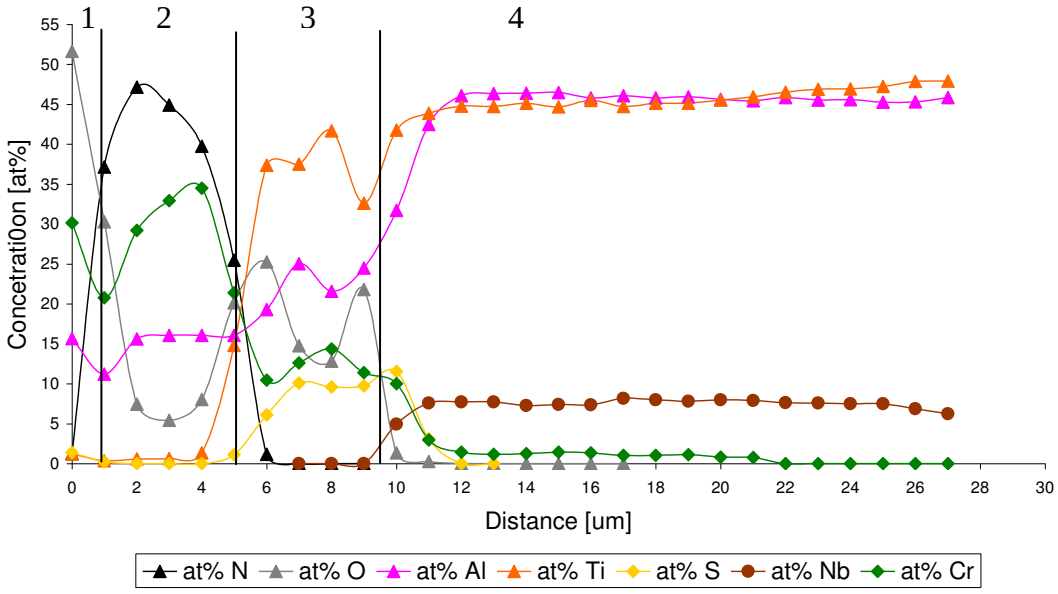

Figure 197 EDS concentration profiles of unaffected region of CrAlYN/CrN coating Y etch, CrAl (thin) coated Ti45Al8Nb after 675 hours sulphidation at 1123 K (unaffected region)

The EDS concentration profiles **(Fig. 197)** from the unaffected region show the formation of a thin (1 μm) Cr and Al oxides on the outer scale. Underneath the Cr, Al oxide scale, the deposited coating was observed. Beneath the protective coating, the region with a large amount of oxygen (25 at%) and sulphur (10 at%) with Al, Cr, and Ti ions was formed.

The XRD pattern (not shown here) detected: CrN, Cr_3S_4, TiS, NbS_3, NbS_2, TiO_2, Al_2O_3, and Cr_2N. The large numbers of the phases detected by the XRD analysis suggest that deposited coating and oxide scale which developed on the surface of the sample, was very thin. The X-Rays penetrated the regions underneath deposited coating.

Figures 198 and 199 show the EDS concentration profiles of exposed CrAlYN/CrN coating, Y etch, CrAlY (thick), form affected and unaffected region, similarly **figures 200**, **and 201** show affected and unaffected region of CrAlYN/CrN coating Cr etch, CrAl (thin) sulphidized at 1123 K for 675 hours.

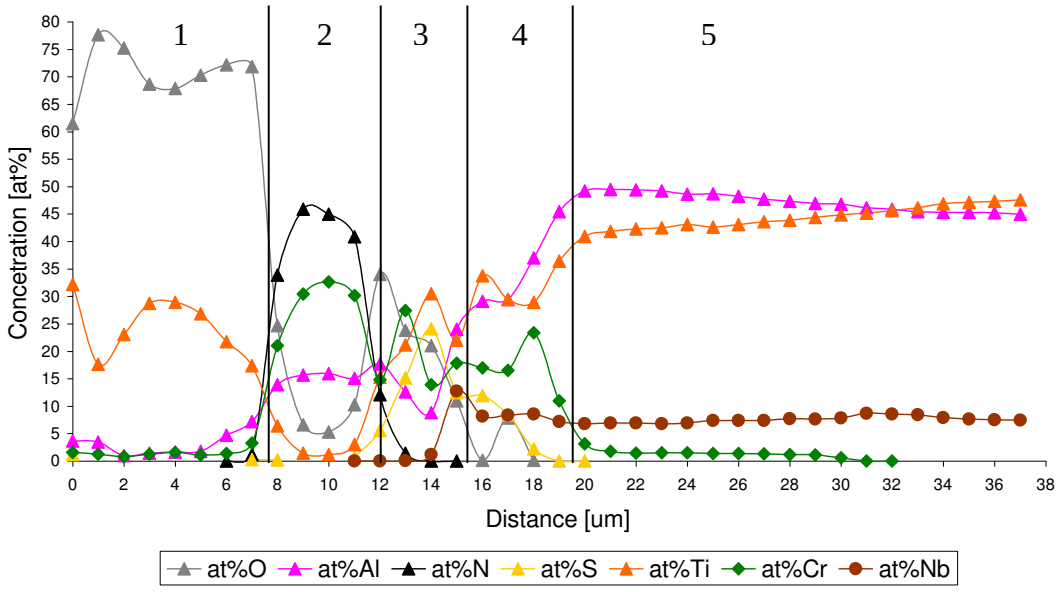

Figure 198 EDS concentration profiles of affected region of CrAlYN/CrN coating, Y etch, CrAlY (thick) coated Ti45Al8Nb after 675 hours sulphidation at 1123 K – affected region

Figure 198 gives the concentration profiles with following regions: 1) TiO_2 outer layer, 2) Modified coating, 3) Less dense mixture of phases: Al_2O_3, Cr_2O_3, TiS, TiS_2,

Al_2S_3, Cr_2S_3, 4) More dense mixture of phases: Al_2O_3, Cr_2O_3, TiS, TiS_2, Al_2S_3, Cr_2S_3 with high Al and Ti content, 5) Substrate TiAl45Al8Nb.

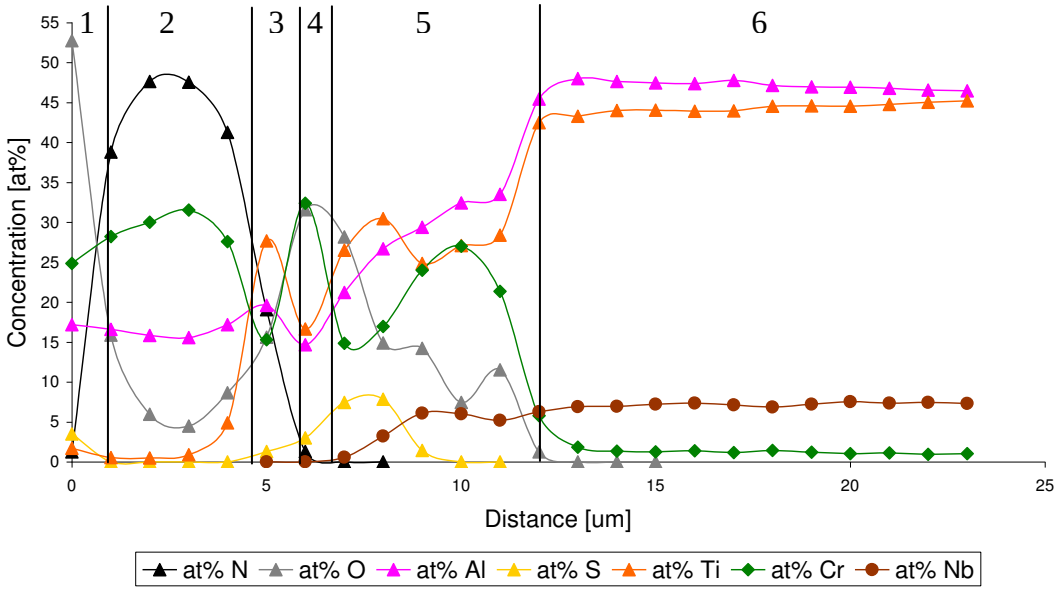

Figure 199 EDS concentration profiles of unaffected region of CrAlYN/CrN coating, Y etch, CrAlY (thick) coated Ti45Al8Nb after 675 hours sulphidation at 1123 K – unaffected region

The EDS profiles in **figure 199** give the details of the scale structure developed identifying the following regions: 1) A thin Cr Al oxide scale, 2) Modified coating, 3) Rich Ti zone, 4) Cr_2O_3 thin layer, 5) Diffusion zone of Cr, S, Al, Nb, O and Ti, 6) Substrate (Ti45Al8Nb).

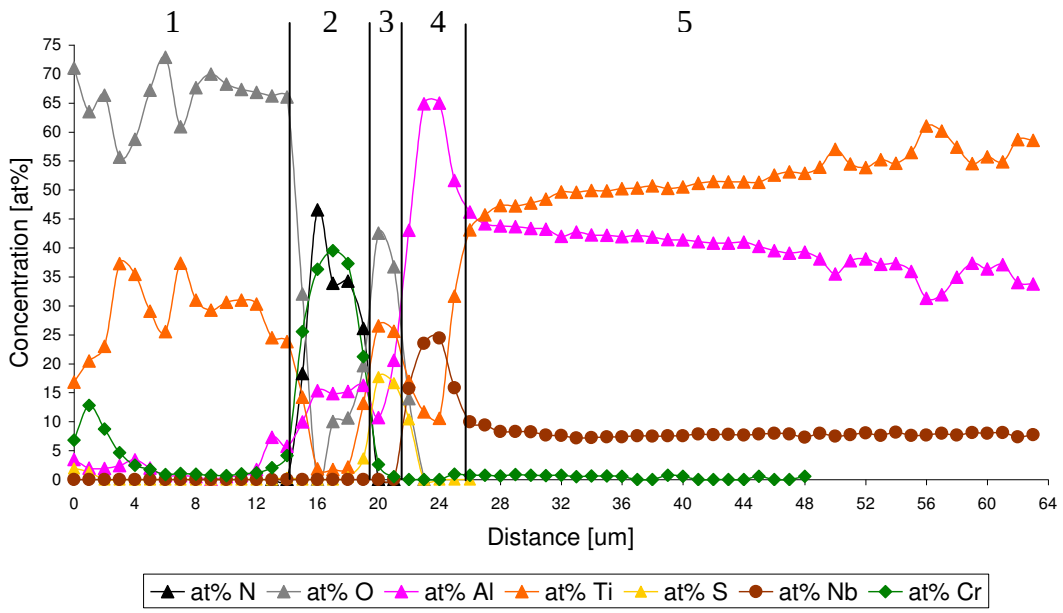

Figure 200 EDS concentration profiles of CrAlYN/CrN coating Cr etch, CrAl (thin) coated Ti45Al8Nb after 675 hours sulphidation at 1123 K – affected region

In **figure 200**, the following regions have been detected: 1) Titanium oxide (TiO_2) with Cr inclusions, 2) Modified coating, 3) Titanium oxide/titanium sulphur layer, 4) $NbAl_3$ layer, 5) Substrate (Ti45Al8Nb).

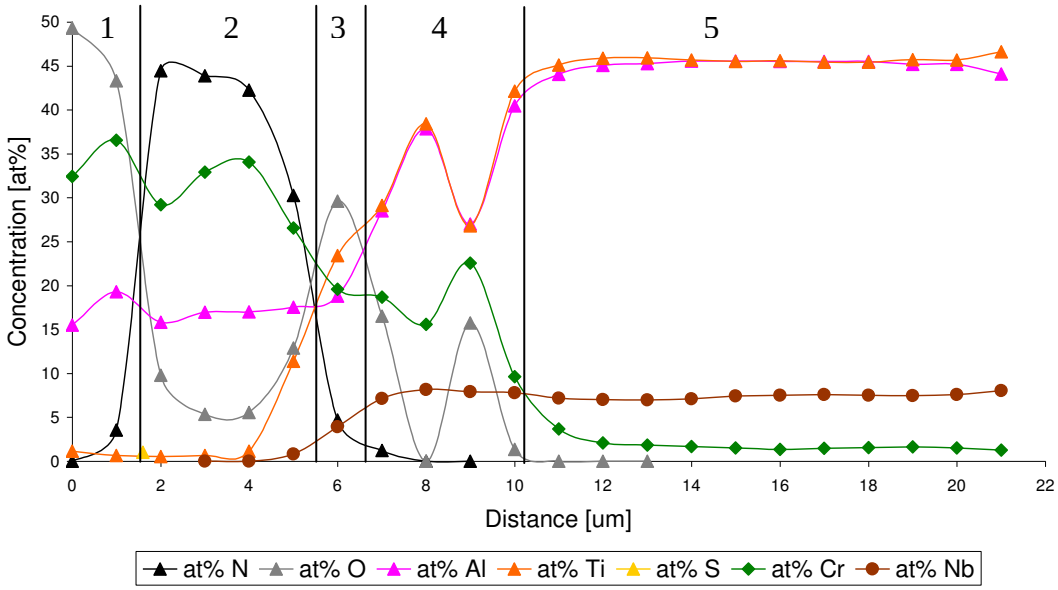

Figure 201 EDS concentration profiles of unaffected of CrAlYN/CrN coating Cr etch, CrAl (thin) coated Ti45Al8Nb after 675 hours sulphidation at 1123 K – unaffected region

Figure 201 presents EDS concentration profiles of exposed sample, the following regions developed: 1) A thin Al – Cr oxide layer, 2) Modified coating, 3) Ti, Cr, Al less dense oxide region, 4) Rich Al and Ti region with Cr inclusions, 5) Substrate (Ti45Al8Nb) alloy.

Chapter VI – Section 3 – High Temperature Hot Corrosion of γ-TiAl alloys – Results

Ch.VI.Sec.3.1 Introduction

Chapter VI section 3 shows the results of hot corrosion of γ-TiAl alloy (Ti45Al8Nb) with the three different nano-coatings; TiAlN+Al_2O_3 (Ti25Al50N) coated Ti45Al8Nb, CrAl2%YN coated Ti45Al8Nb, TiAlYN/CrN+Al_2O_3 coated Ti45Al8Nb exposed to salt mixture 20%NaCl/80%Na_2SO_4 at 1023 K for 150 hours.

The hot corrosion of the samples was induced by spraying salts mixture of 20%NaCl/ 80%Na_2SO_4 with melting point around 700^oC on heated sample surfaces, and subsequently heating the sprayed samples in a furnace at 1023 K for various times. The extent of degradation, assessed by weight changes and examination by SEM (Scanning Electron Microscope), and EDS (Energy Dispersive X-Ray Spectroscopy) indicated that all samples suffered the hot corrosion attack to various degrees.

Ch.VI.Sec.3.2 Kinetics

The hot corrosion behaviour of three different nano-coatings systems: TiAlN+Al_2O_3 coated Ti45Al8Nb, CrAl2%YN coated Ti45Al8Nb, TiAlYN/CrN+Al_2O_3 coated Ti45Al8Nb alloy were studied by exposing these materials to salt mixture 20%NaCl/80%Na_2SO_4 at 1023 K for 150 hours. The hot corrosion was induced by spraying salts mixture of 20%NaCl/80%Na_2SO_4 with melting point around 700^{o}C on heated sample surfaces, and subsequently heating the sprayed samples in a furnace at 1023 K for 150 hours. The kinetic data of exposed samples are presented in **figure 202**.

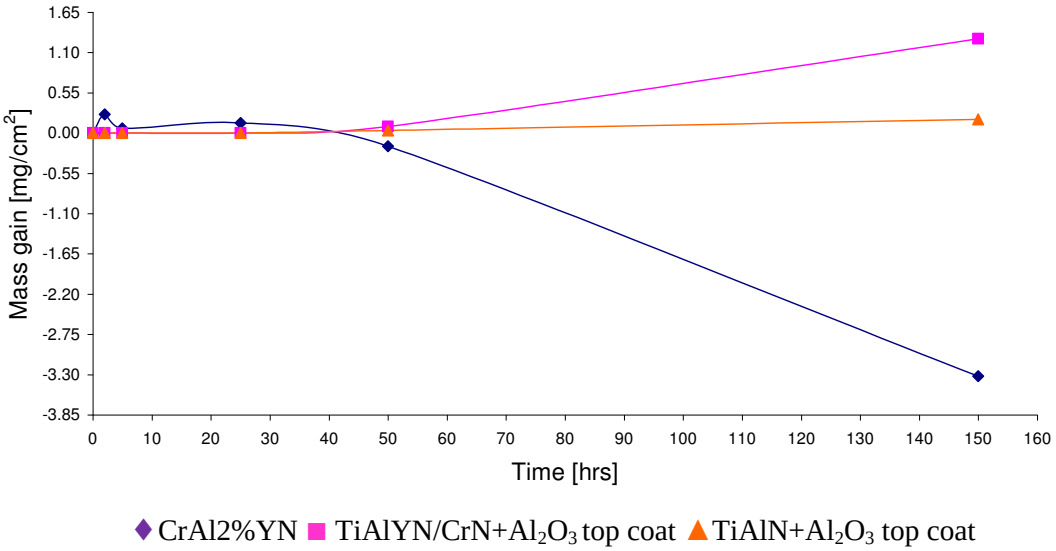

Figure 202 Kinetic data obtained from samples after 150 hours of hot corrosion studies at 1023 K (20%NaCl/80%Na_2SO_4)

Figure 202 illustrates the mass changes per area [mg/cm^2] after 150 hours exposure in salt environment. A significant weight change is visible for CrAl with 2%YN addition where corrosion products developed in significant amounts. The best result was obtained for the TiAlN + Al_2O_3 topcoat where aluminium oxide introduced during preparation of coating played a significant role in diminishing the hot corrosion attack. TiAlYN/CrN produced appreciable mass gain.

Ch.VI.Sec.3.3 TiAlN+Al_2O_3 coated Ti45Al8Nb

The hot corrosion degradation of TiAlN + Al_2O_3 (25Ti25Al50N) top coat coated Ti45Al8Nb is presented in **figure 203**. The SEM images reveal that some parts of the sample were covered by islands of corrosion products (**Figures 203E, 203F**). Other parts of the sample were not covered by any of the corrosion products or were covered by very tinny buttons (**Figure 2B**). The detailed analysis of the corrosion products developed during hot corrosion degradation test is presented in **table 51**.

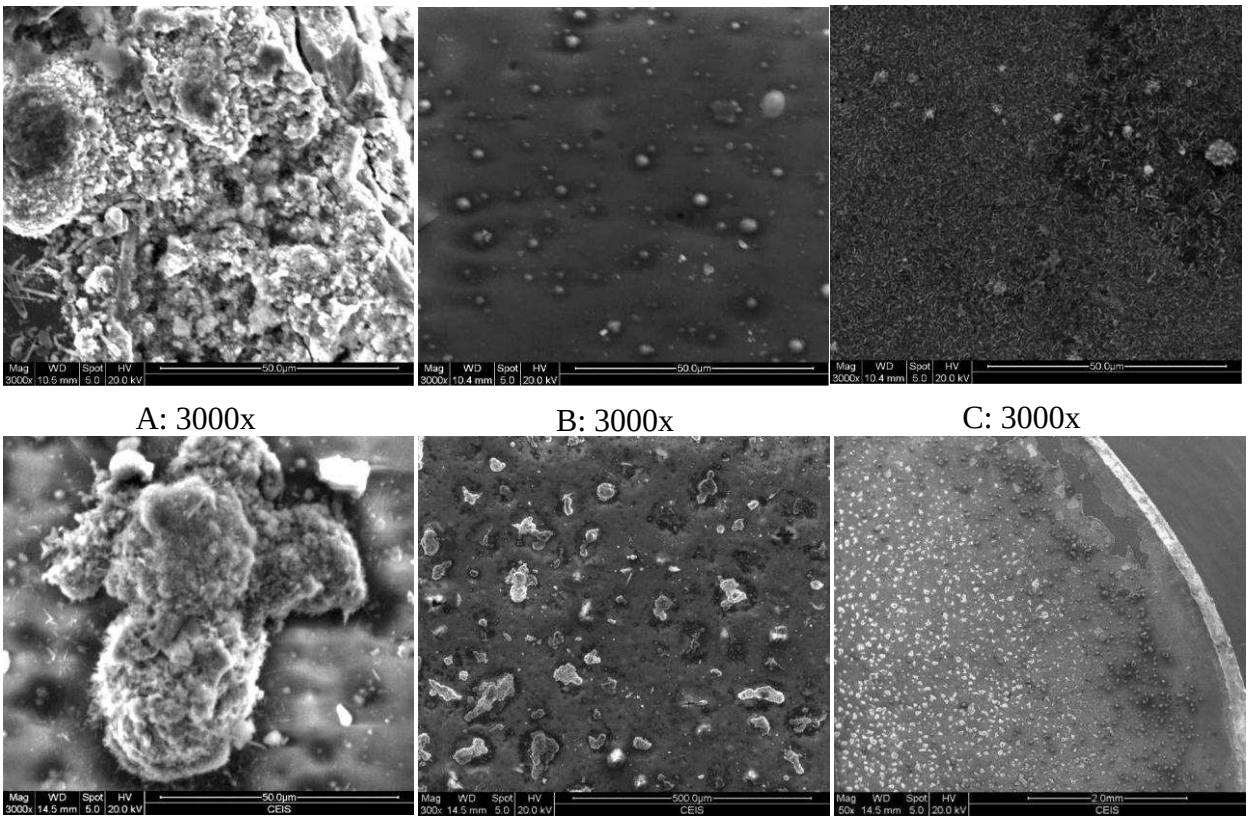

A: 3000x B: 3000x C: 3000x

D: 3000x E: 300x F: 50x

Figure 203 SEM images from surface of TiAlN+Al_2O_3 coated Ti45Al8Nb after 150 hours hot corrosion/oxidation (20%NaCl/80%Na_2SO_4) at 1023 K (magnification under images)

Figure 203 shows the surface SEM images performed on TiAlN+Al_2O_3 coated Ti45Al8Nb after exposure to hot corrosion salt mixture (20%NaCl/80%Na_2SO_4) at 1023 K. The surface of exposed sample was covered by the island of mixed oxides (TiO_2/Al_2O_3 – **Table 51, A, C, and D)**. However the deposited coating Al_2O_3 was also detected **(Table 51, B)**. It was observed that in all investigated places Na was given (up

to 4 at %) and sulphur in trace amounts, additionally Nb was found. The Nb content on the surface was related to crack formation and outward diffusion of Nb, or higher content of Nb was accumulated underneath the deposited Al_2O_3 top coat (the thickness of top coat is equivalent to 3 µm).

Image	at% O	at% Na	at% Al	at% S	at% Cl	at% Ti	at% Nb
A	71.104	0.296	14.461			12.438	1.702
B	63.786	1.014	34.677	0.030	0.041	0.451	
C	62.936	3.987	18.969	0.234	0.018	13.856	
D	63.874	0.547	17.564	0.154	0.058	17.154	0.649

Table 51 Surface analysis of TiAlN+Al_2O_3 coated Ti45Al8Nb after 150 hours hot corrosion/oxidation (20%NaCl80%Na_2SO_4) at 1023 K

The cross – section SEM investigations given in **figure 204**, shows that two regions developed after exposure to hot corrosion regime. The unaffected region **(Fig. 204, upper row)** shows lack of corrosion products; however the outer scale after hot corrosion was very brittle and spalled off from the material. The affected region **(Fig.204, lower row)** displays a thick oxide scale developed, due to the crack formation. Additionally, underneath this developed oxide, structure of the alloy became very porous.

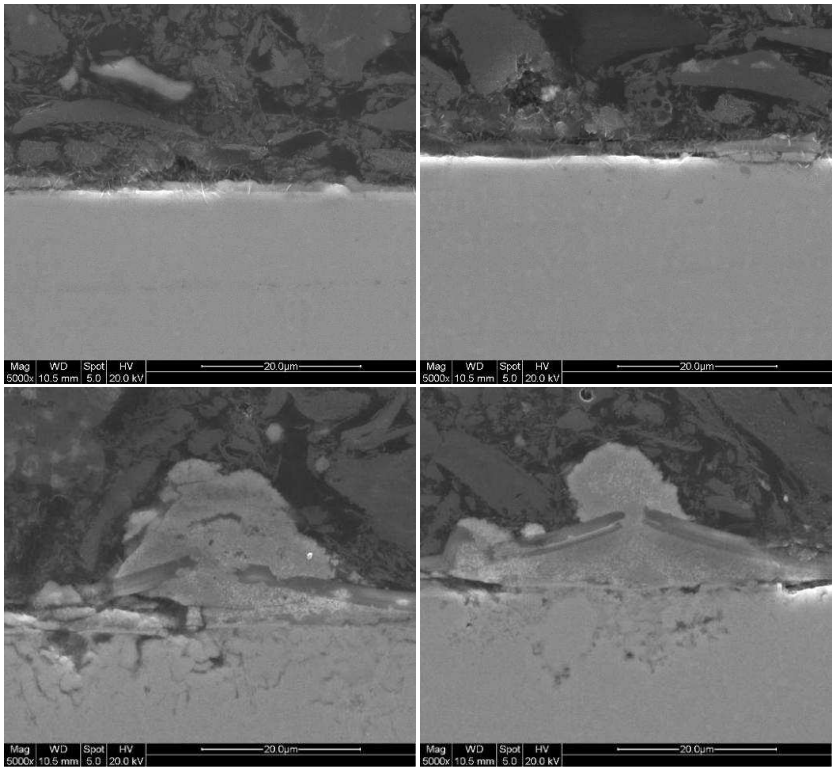

Figure 204 Cross – sectioned images of TiAlN + Al_2O_3 coated Ti45Al8Nb after hot corrosion in salts mixture (20%NaCl/80%Na_2SO_4) at 1023 K

The SEM image in **figure 205** reveals the affected region of TiAlN+Al_2O_3 top coat exposed to hot corrosion environment at 1023 K. The development of a thick TiO_2 oxide scale was due to the crack formation on the Al_2O_3 top coat.

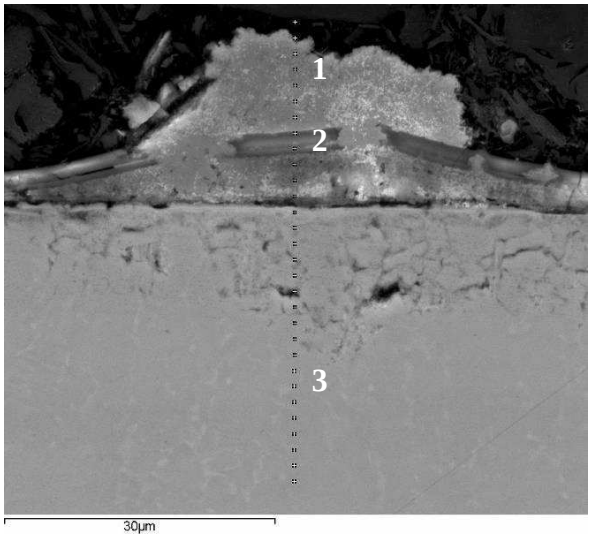

1) TiO_2 top oxide scale

2) Al_2O_3 oxide scale (top coat deposited prior to experiment)

Figure 205 SEM cross section image (mag. 3000x) of TiAlN + Al_2O_3 coated Ti45Al8Nb after hot corrosion in salts mixture (20%NaCl/80%Na_2SO_4) at 1023 K

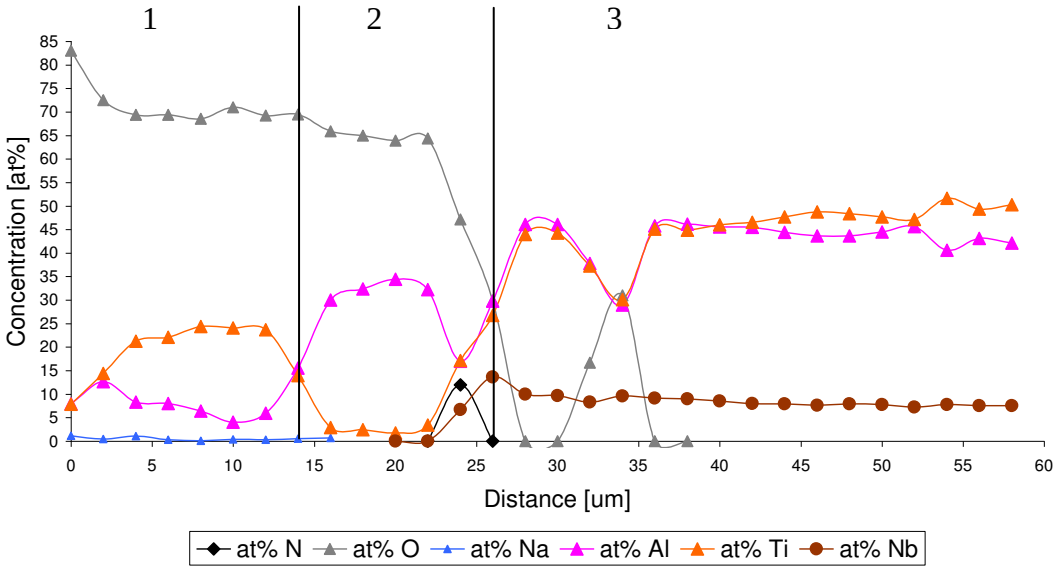

Figure 206 EDS concentration profiles obtained from TiAlN + Al_2O_3 coated Ti45Al8Nb after hot corrosion in salts mixture (20%NaCl/80%Na_2SO_4) at 1023 K

The EDS concentration profiles in **figure 206** shows the following scale structures: 1) TiO_2 top oxide scale, 2) Al_2O_3 oxide scale (part of modified coating), 3) porous structure due to the depletion of Ti ions, 4) Substrate (Ti45Al8Nb). **Figure 207** shows SEM cross – section image from the unaffected part of the sample (TiAlN+Al_2O_3 top coat), the coating was sufficiently resistant to attack, and the scale degradation did

not occur during exposure to salts mixture (20%NaCl/80%Na_2SO_4) at 1023 K for 150 hours. However underneath the deposited coating, the region was fragile and coating showed some small cracks (yellow circles).

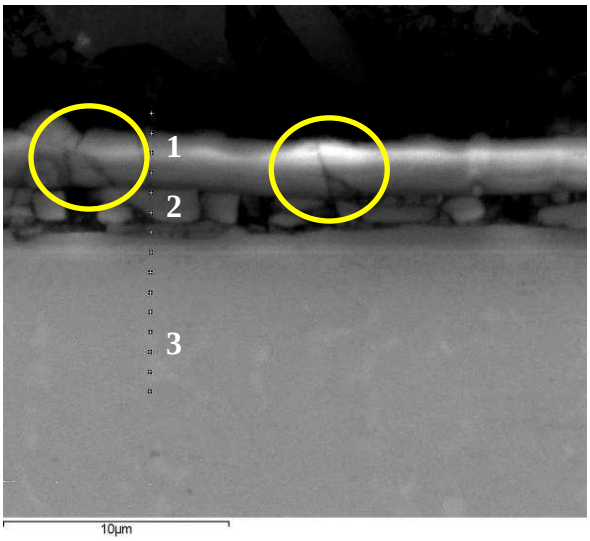

1 Al_2O_3 top oxide scale

2) Modified coating TiAlN + Al_2O_3 and TiO_2 phases (fragile and brittle zone)

Figure 207 SEM cross section image (mag. 10000x) of TiAlN + Al_2O_3 coated Ti45Al8Nb after hot corrosion in salts mixture (20%NaCl/80%Na_2SO_4) at 1023 K

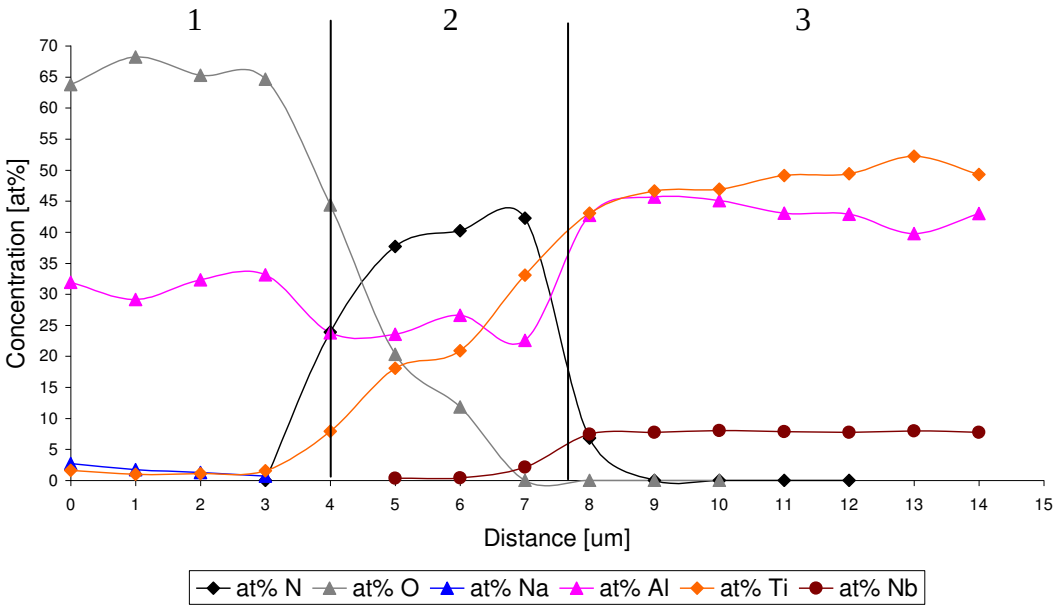

Figure 208 EDS concentration profiles of TiAlN + Al_2O_3 coated Ti45Al8Nb after hot corrosion in salts mixture (20%NaCl/80%Na_2SO_4) at 1023 K

The EDS concentration profiles shown in **figure 208** reveals the following scale structures: 1) Al_2O_3 top oxide scale, 2) Modified coating TiAlN + Al_2O_3 and TiO_2 phases (fragile and brittle zone), 3) Substrate (Ti45Al8Nb alloy). It was observed by the EDS investigation that at the coating/substrate interface TiN layer formed, the formation of TiN layer significantly inhibited the outward diffusion of Ti.

The EDS X-Ray mapping of affected region reveals that the Al_2O_3 cracked, and the Ti diffused outward from the base material. However it is interesting to note that a porous region was captured by Nb ions. The higher concentration of Nb and Al ions **(Fig. 209, Nb, Al map)** suggest the formation of $NbAl_3$ phase underneath cracked coating. This phenomenon was not detected by the EDS investigation **(Fig. 208)**.

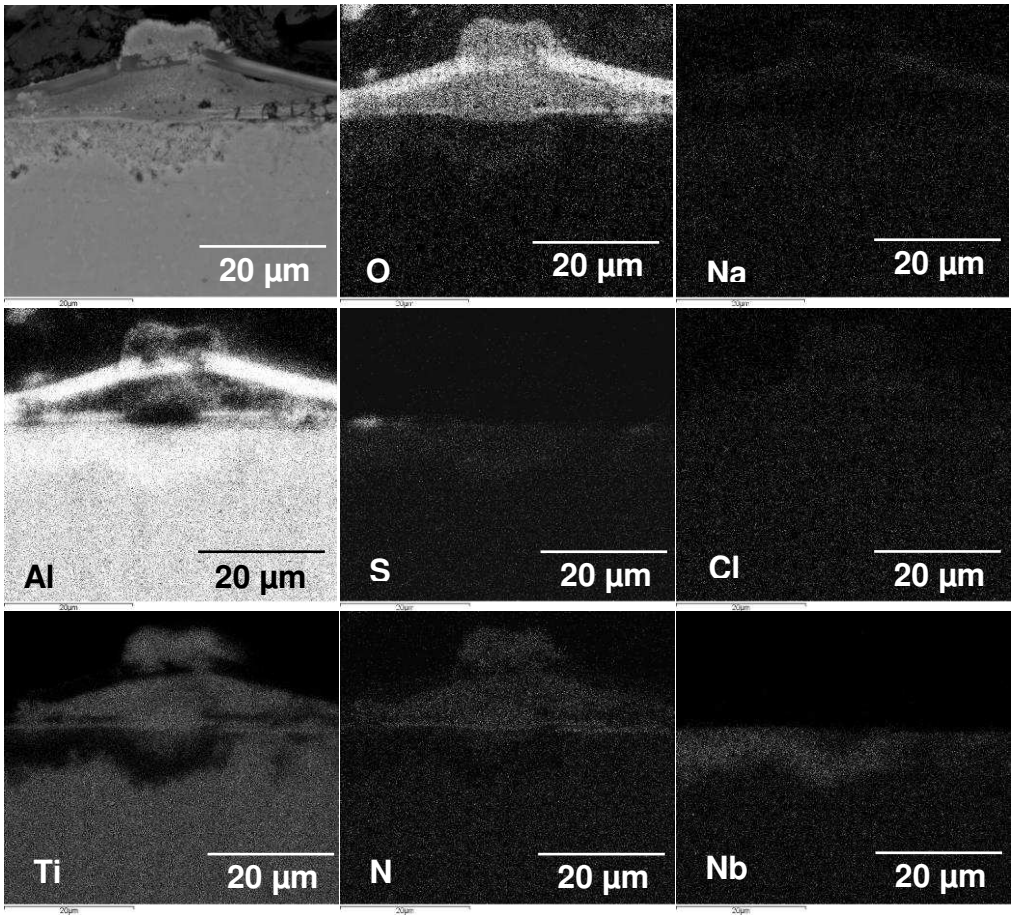

Figure 209 EDS Digimaps of TiAlN + Al_2O_3 top coat coated Ti45Al8Nb after 150 hours hot corrosion exposure at 20%NaCl/80%Na_2SO_4 salts mixture at 1023 K

The unaffected region of TiAlN+Al_2O_3 shown in **figure 210** reveals that the Al_2O_3 oxide deposited prior to experiment survived during hot corrosion test. This protective oxide, improved the hot corrosion resistance of the base material against salt mixture attack at high temperature (T = 1023 K).

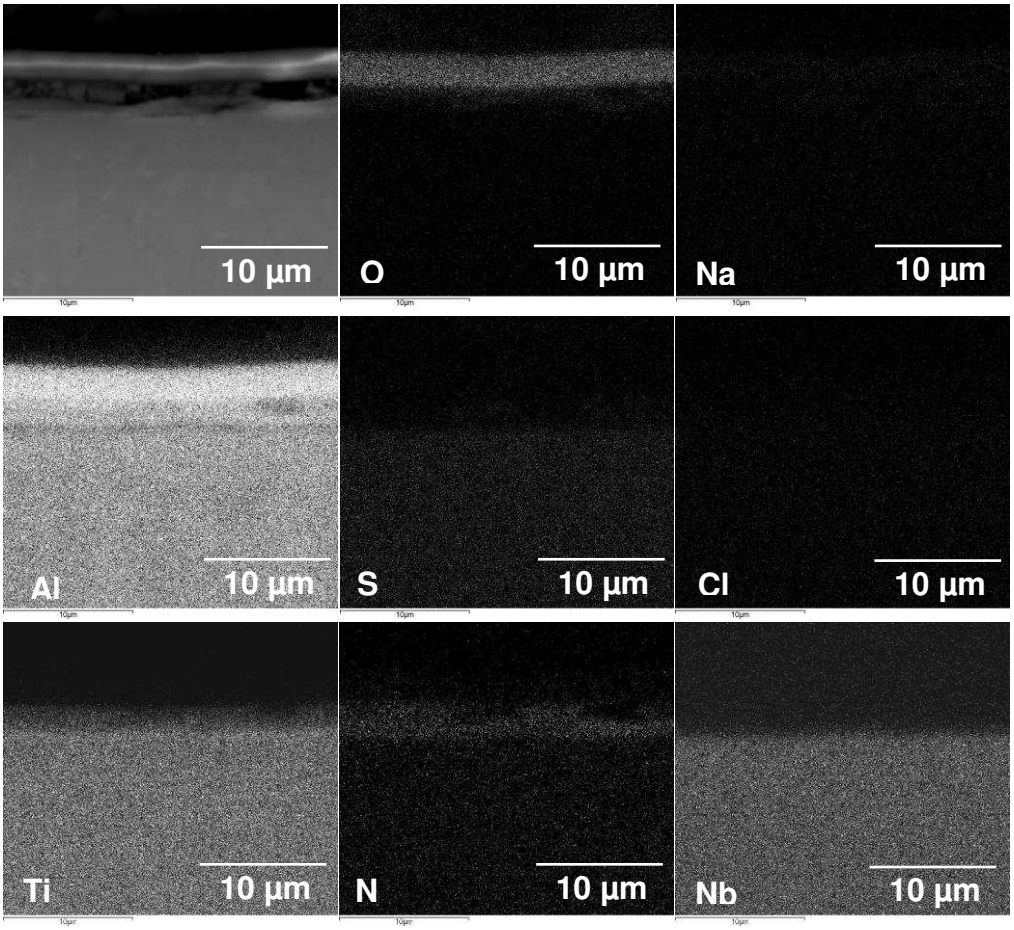

Figure 210 EDS Digimaps of TiAlN + Al_2O_3 top coat coated Ti45Al8Nb after 150 hours hot corrosion exposure at 20%NaCl/80%Na_2SO_4 salts mixture at 1023 K

Ch.VI.Sec.3.4 CrAl2%YN coated Ti45Al8Nb

Figure 211 shows the surface morphologies of the exposed CrAl2%YN coated base alloy to hot corrosion (20%NaCl/80%Na_2SO_4) at 1023 K. Similar to previous the material, here the sample also developed two different regions – the affected region formed on the edges of the sample, the unaffected region in the middle part was free form corrosion products.

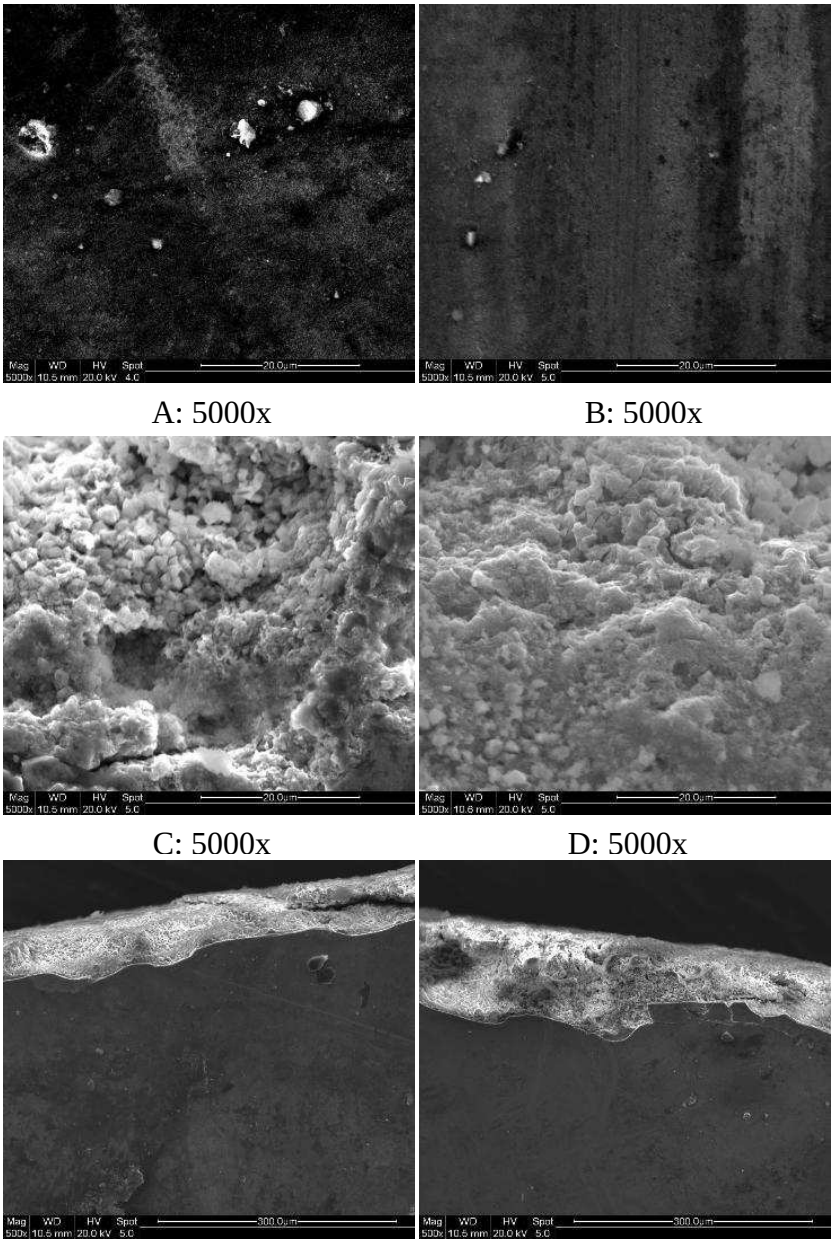

A: 5000x B: 5000x

C: 5000x D: 5000x

E: 500x F: 500x

Figure 211 SEM images from surface of CrAl2%YN+Al_2O_3 coated Ti45Al8Nb after 150 hours hot corrosion/oxidation (20%NaCl/80%Na_2SO_4) at 1023 K (magnification under images)

Table 52 confirms the presence of two regions; some of the areas show a high content of Al Cr, and N; however other places developed a mixed oxide scale consisting of TiO_2 and Al_2O_3, additionally it was observed that in these mixed oxide regions, Nb content was high. High Nb content suggests that the coating spalled off from the

material during the test and the base material was exposed directly to hot corrosion. Cl, Y, and Na were also detected however in trace amounts.

Image	at% N	at% O	at% Na	at% Al	at% Cl	at% Ti	at% Cr	at% Y	at% Nb
A	31.661	20.036		27.227		0.428	20.034	0.614	
B	31.630	17.963		28.372		0.475	20.903	0.657	
C		71.523	0.829	11.522	0.893	8.156	0.463		6.615
D		73.298	1.470	9.204	0.690	4.614			10.723

Table 52 Surface analysis of CrAl2%YN coated Ti45Al8Nb after 150 hours of hot corrosion/oxidation (20%NaCl/80%Na_2SO_4) at 1023 K

The cross – sectional image in **figure 212** reveals the different regions of the exposed sample (CrAl2%YN coated base alloy). The upper row in **figure 212** shows the edges of the material; the porous structure with a large grains appeared. The bottom rows in **figure 212**, reveals that the formed scale was very brittle, and spalled off during test.

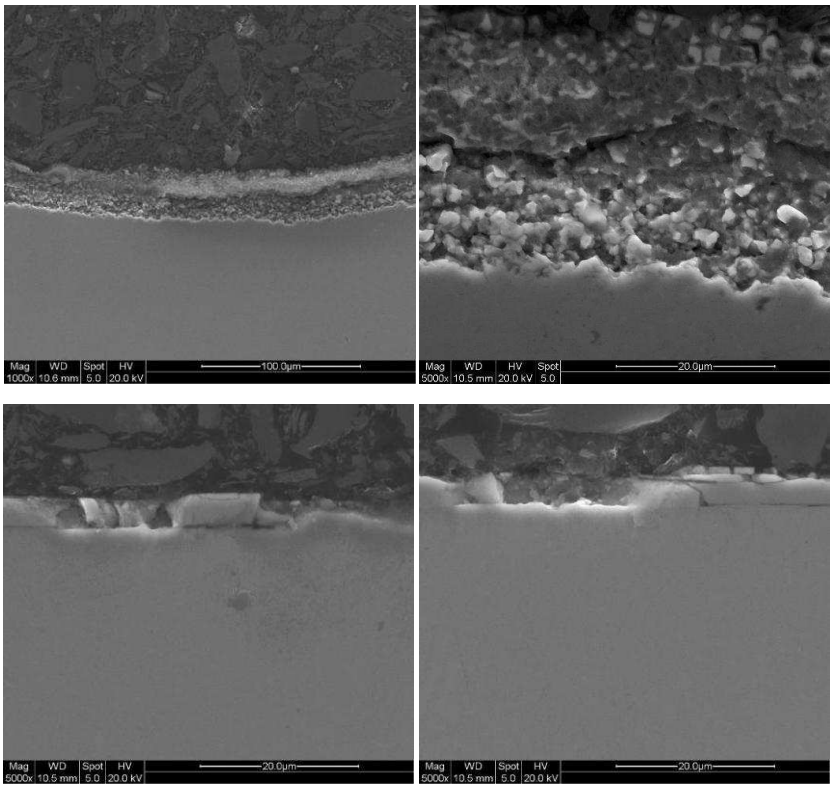

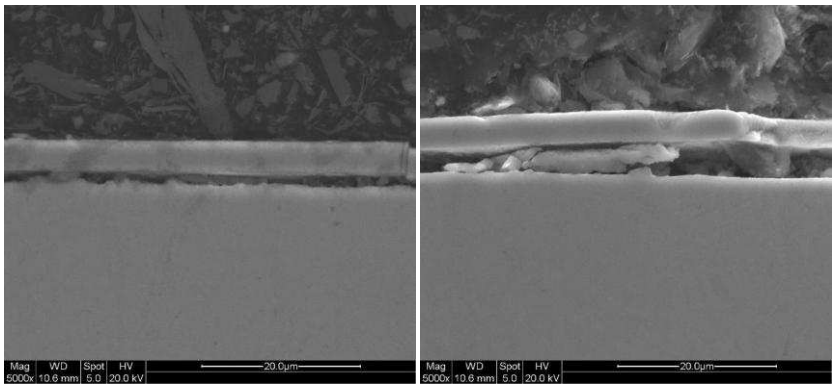

Figure 212 Cross – sectioned images of CrAl2%YN coated Ti45Al8Nb after hot corrosion in salts mixture (20%NaCl/80%Na_2SO_4) at 1023 K

Figure 213 shows the same sample (CrAl2%YN coated Ti45Al8Nb) where the scale remained unaffected after exposure to salts mixture (20%NaCl/80%Na_2SO_4) at 1023 K for 150 hours. Similar to TiAlN + Al_2O_3 coated Ti45Al8Nb alloy, this coating showed good hot corrosion resistance. However between coating and the substrate, gaps appeared suggesting that the phases developed during exposure were very fragile, the fragile phases were removed during polishing and grinding processes performed to facilitate the structural analyses.

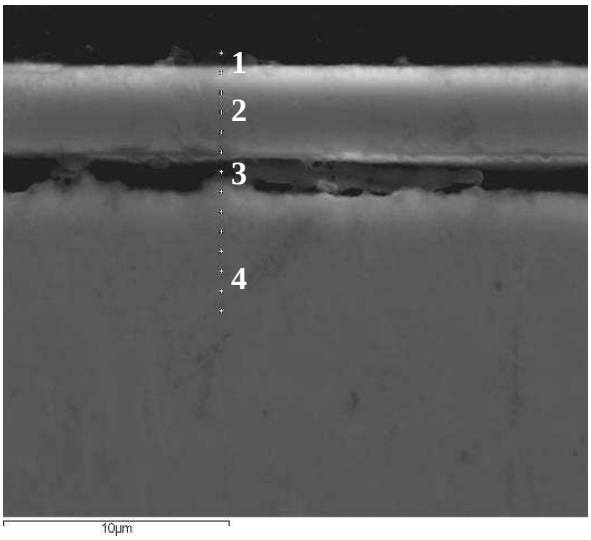

1) Chromium and aluminium oxide layer

2) Modified coating (CrAl2%YN)

3) Chromium rich region

Figure 213 SEM cross section image (mag. 10000x) of CrAl2%YN coated Ti45Al8Nb after hot corrosion in salts mixture (20%NaCl/80%Na_2SO_4) at 1023 K

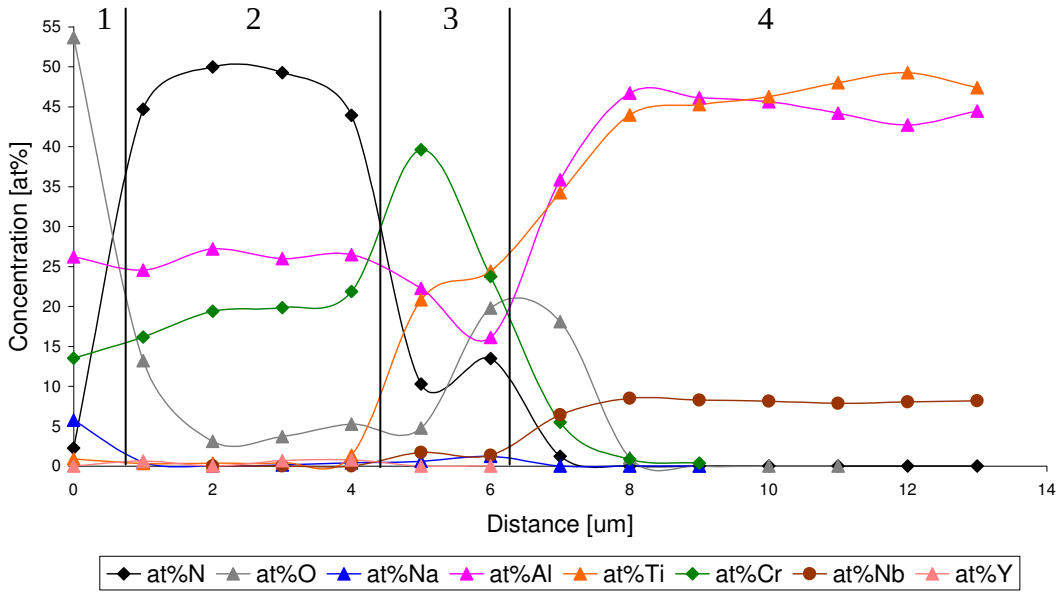

Figure 214 EDS concentration profiles obtained from CrAl2%YN coated Ti45Al8Nb after hot corrosion in salts mixture (20%NaCl/80%Na_2SO_4) at 1023 K – unaffected region

Figure 214 shows the concentration profiles where Cr_2O_3 and Al_2O_3 are developed on the outer layer with a small residual amount of Na. The EDS concentration profiles summarises the region observed: 1) Chromium and aluminium oxide layer, 2) Modified coating (CrAl2%YN), 3) Chromium rich region, 4) Substrate (Ti45Al8Nb alloy).

Figure 215 reveals, that adherence of the scale formed on the exposed sample (CrAl2%YN coated Ti45Al8Nb) was poor. Some of the parts of the coating spalled off and the material was exposed to highly corrosive environment, resulting in the development of a thick scale.

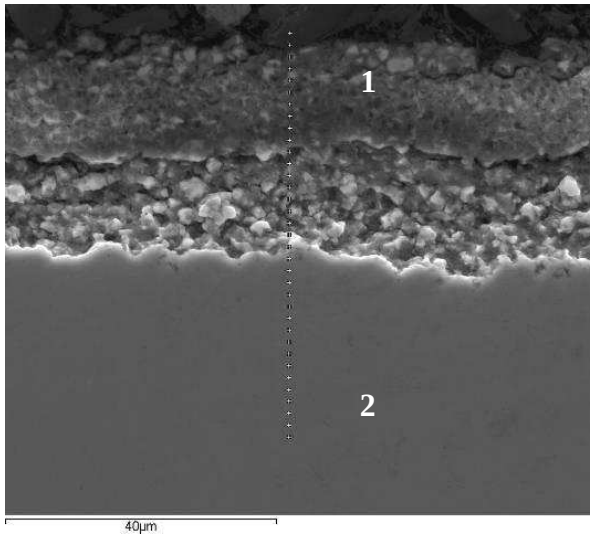

1) Porous and thick scale built from Ti, Al, and Nb elements mixed with Na, S, and Cl from salt deposit

2) Substrate (Ti45Al8Nb)

Figure 215 SEM cross section image (mag. 3000x) of CrAl2%YN coated Ti45Al8Nb after hot corrosion in salts mixture (20%NaCl/80%Na_2SO_4) at 1023 K– affected region (edge of the sample)

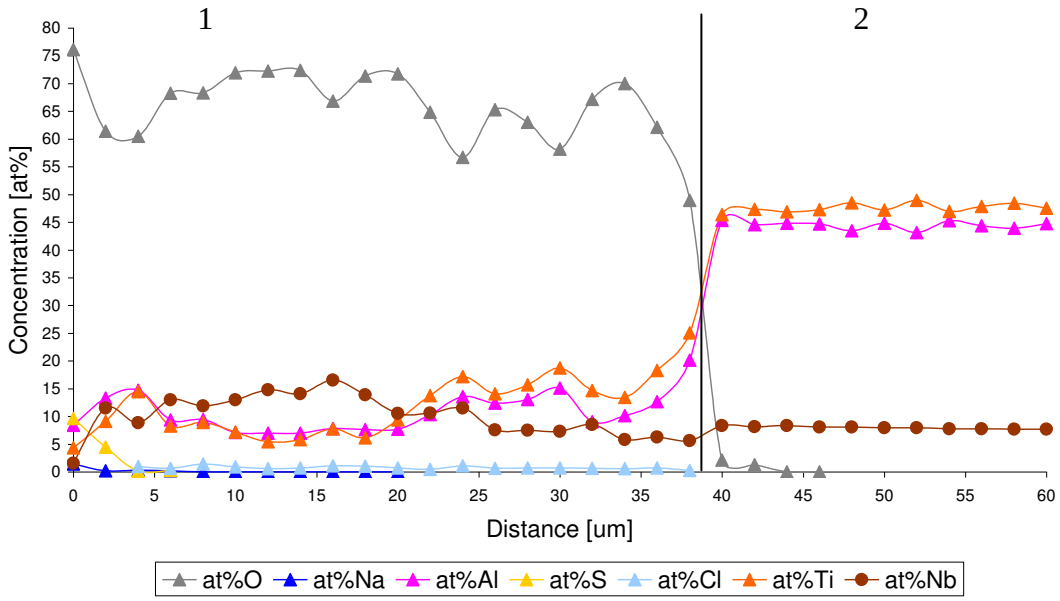

Figure 216 EDS concentration profiles obtained from CrAl2%YN coated Ti45Al8Nb after hot corrosion in salts mixture (20%NaCl/80%Na_2SO_4) at 1023 K – affected region (edge of the sample)

The EDS concentration profiles in **figure 216** shows following regions:

1) Porous and thick scale built from Ti, Al, and Nb elements mixed with Na, S, and Cl from salt deposit, 2) Substrate (Ti45Al8Nb alloy). The EDS X-Ray mapping from the unaffected region shown in **figure 217** reveals good agreement between EDS concentration profiles (**Fig. 214**). The EDS X-Ray mapping confirms the development in the unaffected region the presence of Cr_2O_3 and Al_2O_3 protective oxides. Furthermore it was observed that Cr and N remained in the coating.

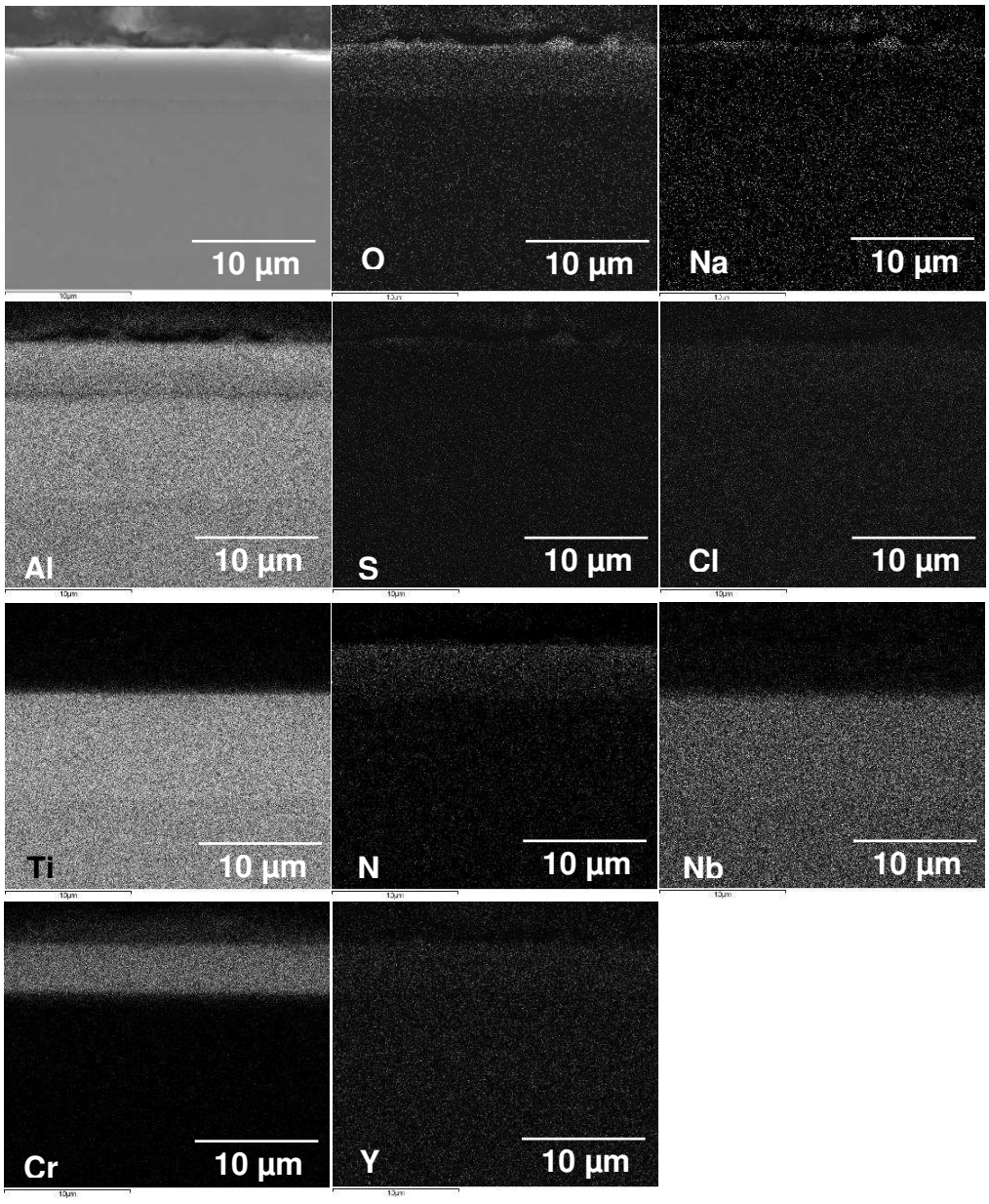

Figure 217 EDS Digimaps of CrAl2%YN coated Ti45Al8Nb after 150 hours hot corrosion exposure at 20%NaCl/80%Na_2SO_4 salts mixture at 1023 K

The EDS X-Ray mapping of affected region of exposed CrAl2%YN coated base alloy given in **figure 218** displays that mainly in affected region Nb, Al, O_2 and S_2 were detected. The lack of chromium and small concentration of Al, suggests that the coating spalled off during exposure to hot corrosion environment, this suggestion is confirmed by kinetic data in **figure 202**.

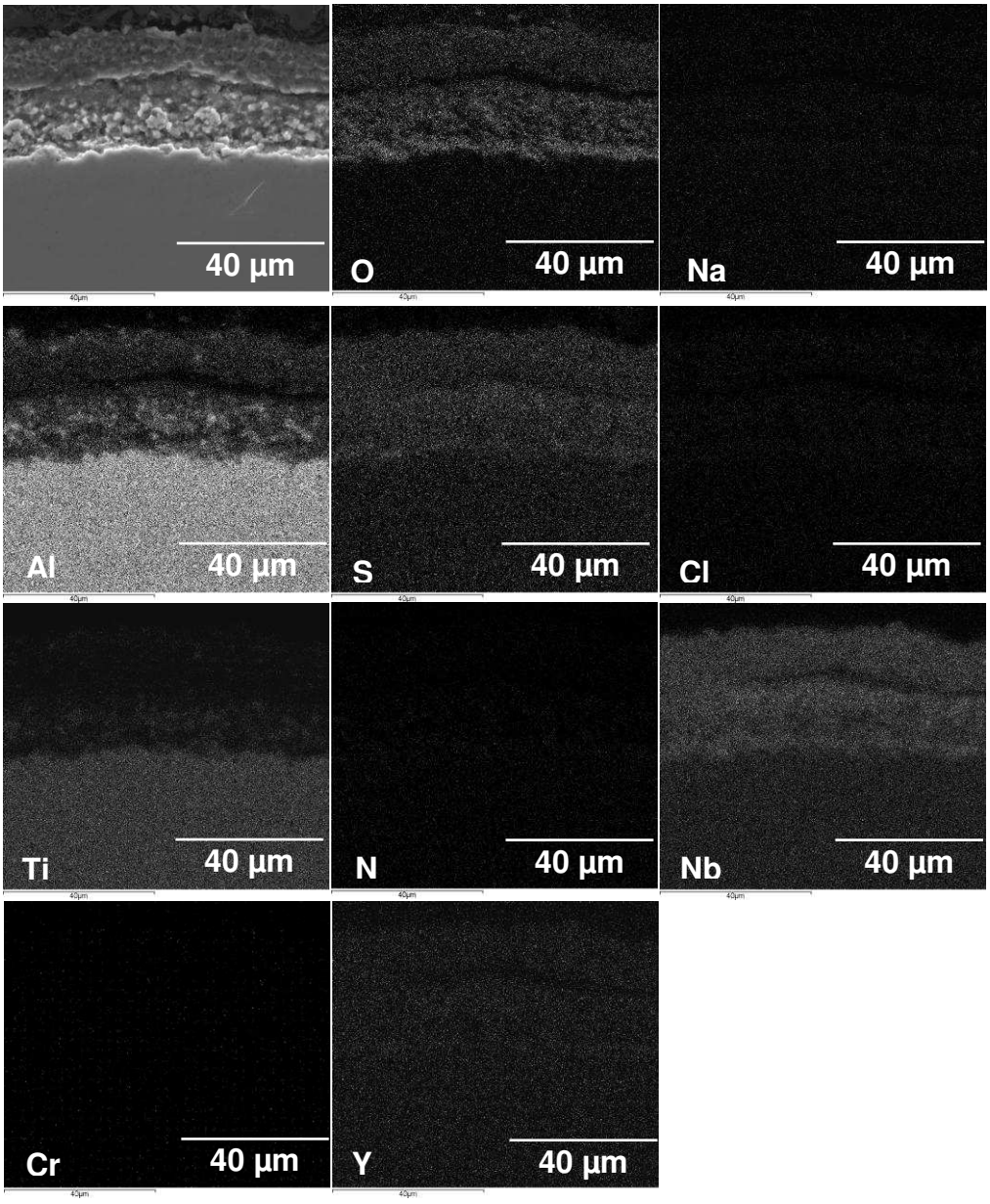

Figure 218 EDS Digimaps of CrAl2%YN coated Ti45Al8Nb after 150 hours hot corrosion exposure at 20%NaCl/80%Na_2SO_4 salts mixture at 1023 K – near to the edge of the sample

Ch.VI.Sec.3.5 TiAlYN/CrN+Al_2O_3 coated Ti45Al8Nb

The SEM images in **figure 219** shows the surface morphology of the exposed material (TiAlYN/CrN+Al_2O_3 coated base alloy) in different regions. The detailed analysis is given in **table 53**.

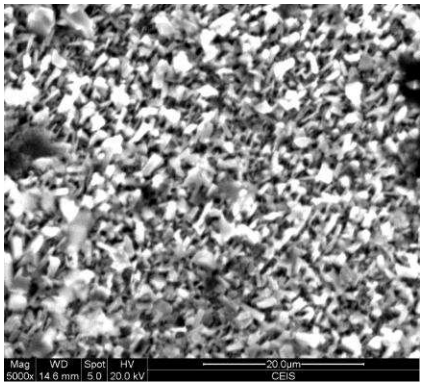

A: 5000x

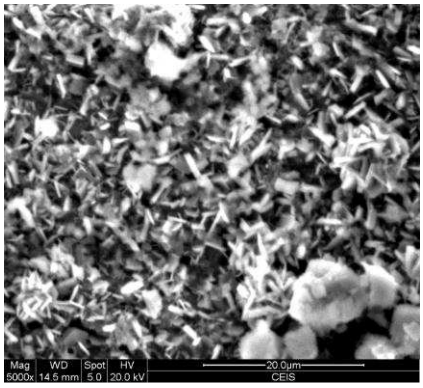

B: 5000x

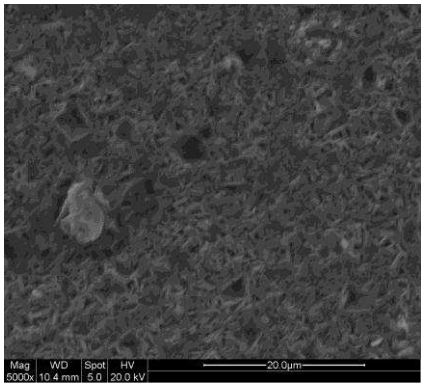

C: 5000x

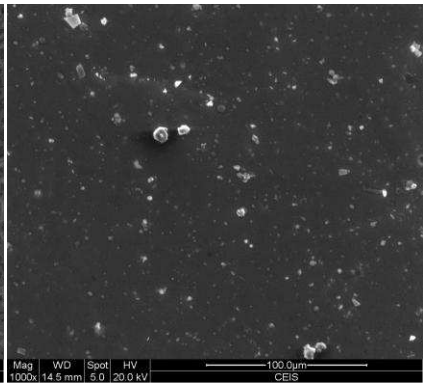

D: 5000x

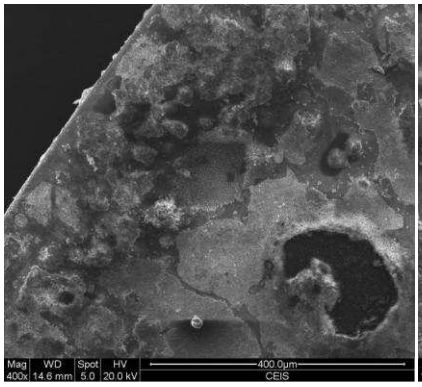

E: 400x

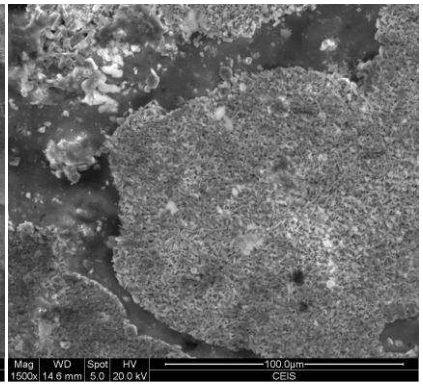

F: 1500x

Figure 219 SEM images from surface of TiAlYN/CrN+Al_2O_3 coated Ti45Al8Nb after 150 hours hot corrosion/oxidation (20%NaCl/80%Na_2SO_4) at 1023 K (magnification under images)

Image	at% O	at% Na	at% Al	at% S	at% Cl	at% Ti	at% Cr	at% Nb
A	55.185	2.332	6.066	0.214	0.285	35.282	0.637	
B	56.202	1.274	16.973	0.176	0.238	22.576	1.424	1.138
C	66.394	3.506	7.782			19.960	2.356	
D	52.828	0.250	33.516	0.030		5.239	8.138	

Table 53 Surface analysis of TiAlYN/CrN+Al_2O_3 coated Ti45Al8Nb after 150 hours hot corrosion/oxidation (20%NaCl/80%Na_2SO_4) at 1023 K

The SEM cross sectioned images in **figure 220** shows that the coating suffered uneven attacks – some areas remaining unaffected and other areas being affected. The unaffected regions were protected by Al_2O_3 deposited before the exposure. The affected regions were where the coating and the top coat cracked during exposure at 1023 K for 150 hours creating a duplex TiO_2/Al_2O_3 scale. Such behaviour of the exposed material suggests that the deposited coating was not uniform (different areas of the deposited coating content different concentration of the elements), or deposited salt in the material had a different thickness before exposure.

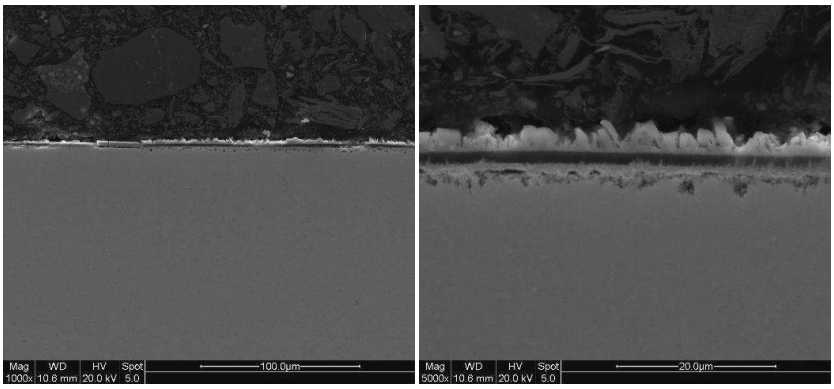

Affected region of TiAlYN/CrN+Al_2O_3 coated Ti45Al8Nb after hot corrosion in salts mixture (20%NaCl/80%Na_2SO_4) at 1023 K. Mag. 1000x (right), 5000x (left)

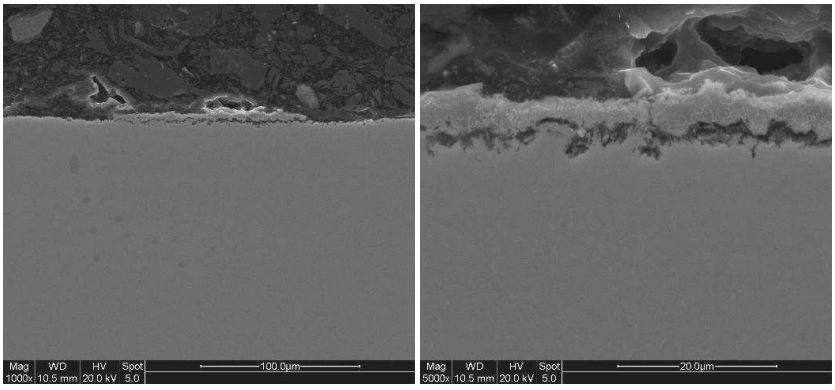

Middle part of TiAlYN/CrN+Al_2O_3 coated Ti45Al8Nb after hot corrosion in salts mixture (20%NaCl/80%Na_2SO_4) at 1023 K. Mag. 1000x (right), 5000x (left)

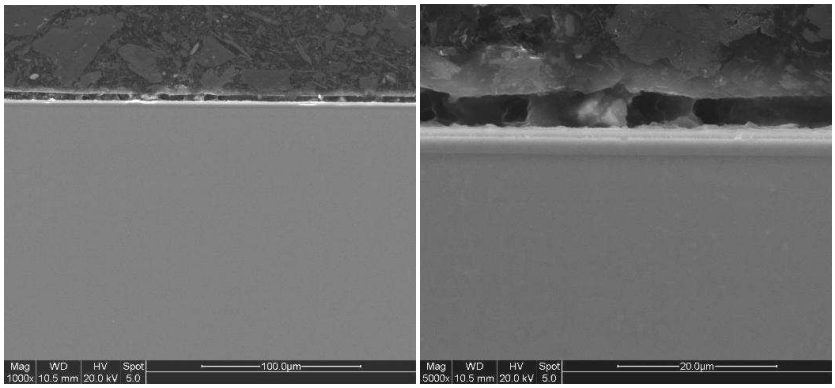

Unaffected region of TiAlYN/CrN+Al_2O_3 coated Ti45Al8Nb after hot corrosion in salts mixture (20%NaCl/80%Na_2SO_4) at 1023 K. Mag. 1000x (right), 5000x (left)

Figure 220 Cross – sectioned images of TiAlYN/CrN coated Ti45Al8Nb after hot corrosion in salts mixture (20%NaCl/80%Na_2SO_4) at 1023 K

Figure 221 shows a SEM image from TiAlYN/CrN+Al_2O_3 coated Ti45Al8Nb alloy after exposure to the salts mixture 20%$Na_2SO_4$80%NaCl at 1023 K for 150 hours.

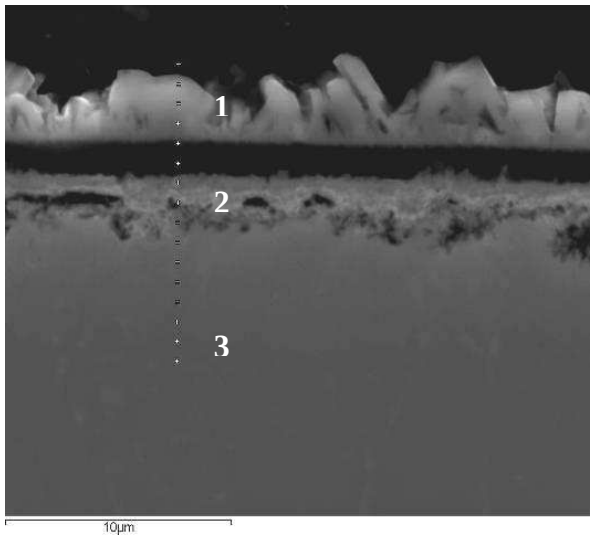

1) TiO_2 oxide top layer

2) Mixed Al_2O_3 and TiO_2 oxides layer

3) Substrate (Ti45Al8Nb)

Figure 221 SEM cross section image (mag. 10000x) of TiAlYN/CrN+Al_2O_3 coated Ti45Al8Nb after hot corrosion in salts mixture (20%NaCl/80%Na_2SO_4) at 1023 K – affected region

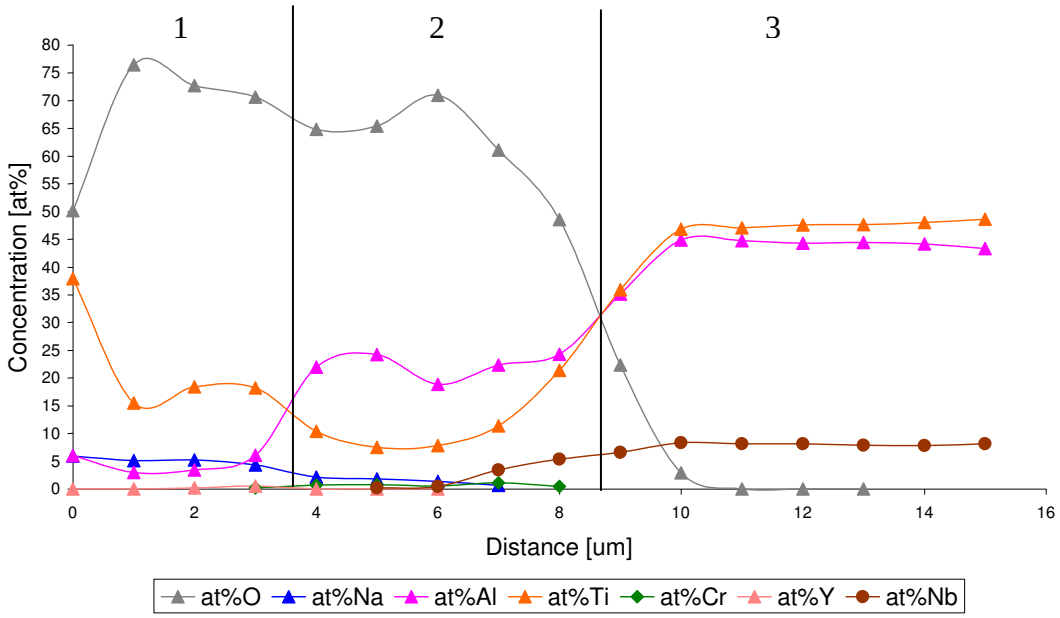

Figure 222 EDS concentration profiles obtained from TiAlYN/CrN+Al_2O_3 coated Ti45Al8Nb after hot corrosion in salts mixture (20%NaCl/80%Na_2SO_4) at 1023 K – affected region

The outer scale (TiO_2) is well confirmed by the EDS concentration profiles shown in **figure 222.** The EDS profiles of exposed sample reveal the following regions: 1) TiO_2 oxide top layer, 2) Mixed Al_2O_3 and TiO_2 oxides layer, 3) Substrate (Ti45Al8Nb alloy)

It was observed that in the affected region nitride phases (TiN, AlN, or CrN) were not detected. This observation leads to conclusion that during exposure at 1023 K, the nitrides become unstable and decomposed.

The affected shown in **figure 223**, displays a poor resistance to hot corrosion. The cracks in the outer scale supported ingress of oxygen ions and other aggressive agents (S, Cl) into the material. The exposed material suffered hot corrosion attack and formed non protective TiO_2/Al_2O_3 scale with inclusions of Na.

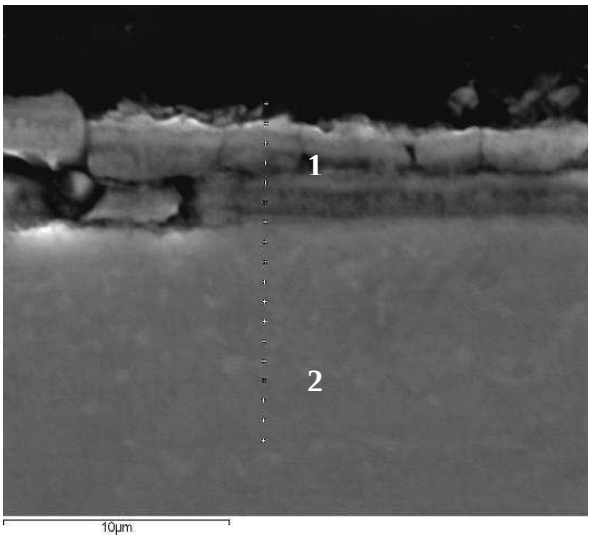

1) Porous mixed oxide scale TiO_2 and Al_2O_3 with trace amount of Na

2) Substrate (Ti45Al8Nb)

Figure 223 SEM cross section image (mag. 10000x) of TiAlYN/CrN+Al_2O_3 coated Ti45Al8Nb after hot corrosion in salts mixture (20%NaCl/80%Na_2SO_4) at 1023 K – affected region

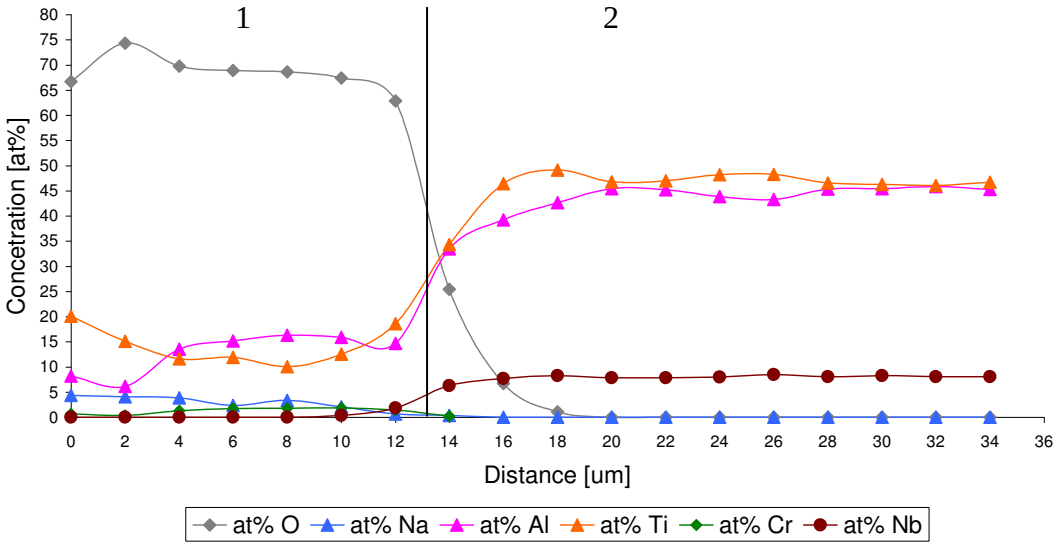

Figure 224 EDS concentration profiles obtained from TiAlYN/CrN+Al_2O_3 coated Ti45Al8Nb after hot corrosion in salts mixture (20%NaCl/80%Na_2SO_4) at 1023 K – affected region

Figure 224 reveals that scale in affected region was very porous as indicated by the high concentration of oxygen. The formed scale did not protect material against hot corrosion attack. The unaffected region of TiAlYN/CrN+Al_2O_3 coated Ti45Al8Nb alloy is given **figure 225**, exposed to the salts mixture (20%NaCl80%Na_2SO_4) at 1023 K for

150 hours. This sample suffered the lowest degradation rate in the hot corrosion environment. Superior corrosion resistance was achieved due to the Al_2O_3 layer deposited prior experiment.

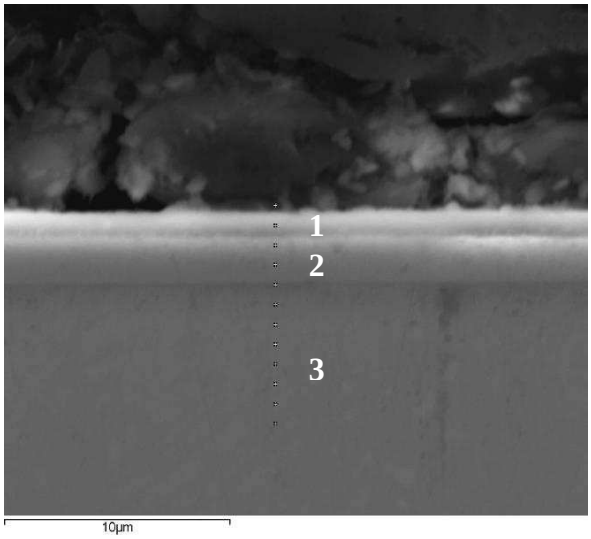

1) Al_2O_3 top oxide layer

2) Modified coating (TiAlYN/CrN)

3) Substrate (Ti45Al8Nb)

Figure 225 SEM cross section image of TiAlYN/CrN+Al_2O_3 coated alloy in 20%NaCl/80%Na_2SO_4 mixture after 150 hrs at 1023 K - unaffected region

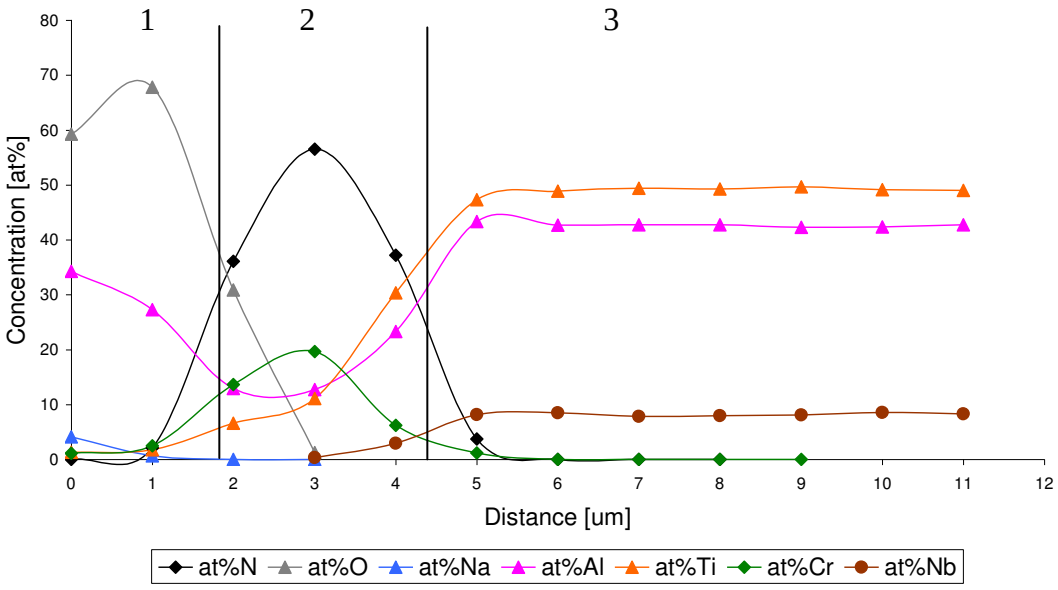

Figure 226 EDS concentration profiles obtained from TiAlYN/CrN+Al_2O_3 coated Ti45Al8Nb after hot corrosion in salts mixture (20%NaCl/80%Na_2SO_4) at 1023 K – unaffected region

The EDS concentration profiles are presented in **figure 226** showing following regions: 1) Al_2O_3 top oxide layer, 2) Modified coating (TiAlYN/CrN), 3) Substrate (Ti45Al8Nb alloy). The Al_2O_3 was introduced during preparation of the material, to improve the corrosion resistance, however, this Al_2O_3 top coat cracked and material suffered hot corrosion degradation. The affected part of the sample was investigated by the EDS X-Ray mapping, the performed investigation is shown in **figure 227**. The outer scale mainly was occupied by TiO_2 and Al_2O_3 phases. Nb remained in the material and did not diffused outwards; additionally Cr and N were not detected. This can suggest that CrN phase decomposed during exposure to hot corrosion regime.

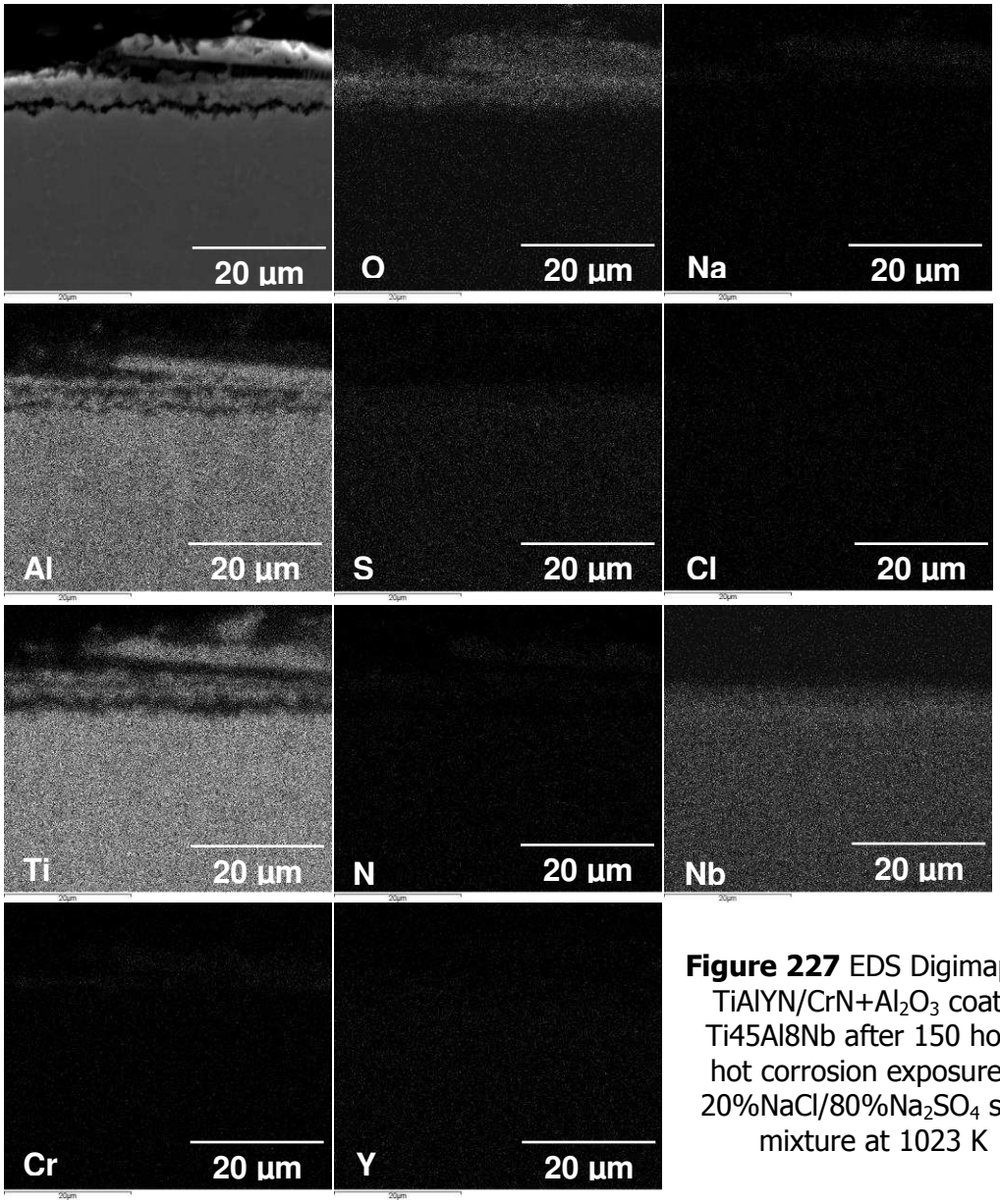

Figure 227 EDS Digimaps of TiAlYN/CrN+Al_2O_3 coated Ti45Al8Nb after 150 hours hot corrosion exposure at 20%NaCl/80%Na_2SO_4 salts mixture at 1023 K

Figure 228 shows the EDS X-Ray mapping of another affected part of exposed material TiAlYN/CrN+Al_2O_3. Similar oxides; TiO_2 and Al_2O_3 developed on the outer part of the scale. Additionally in this region Na was detected.

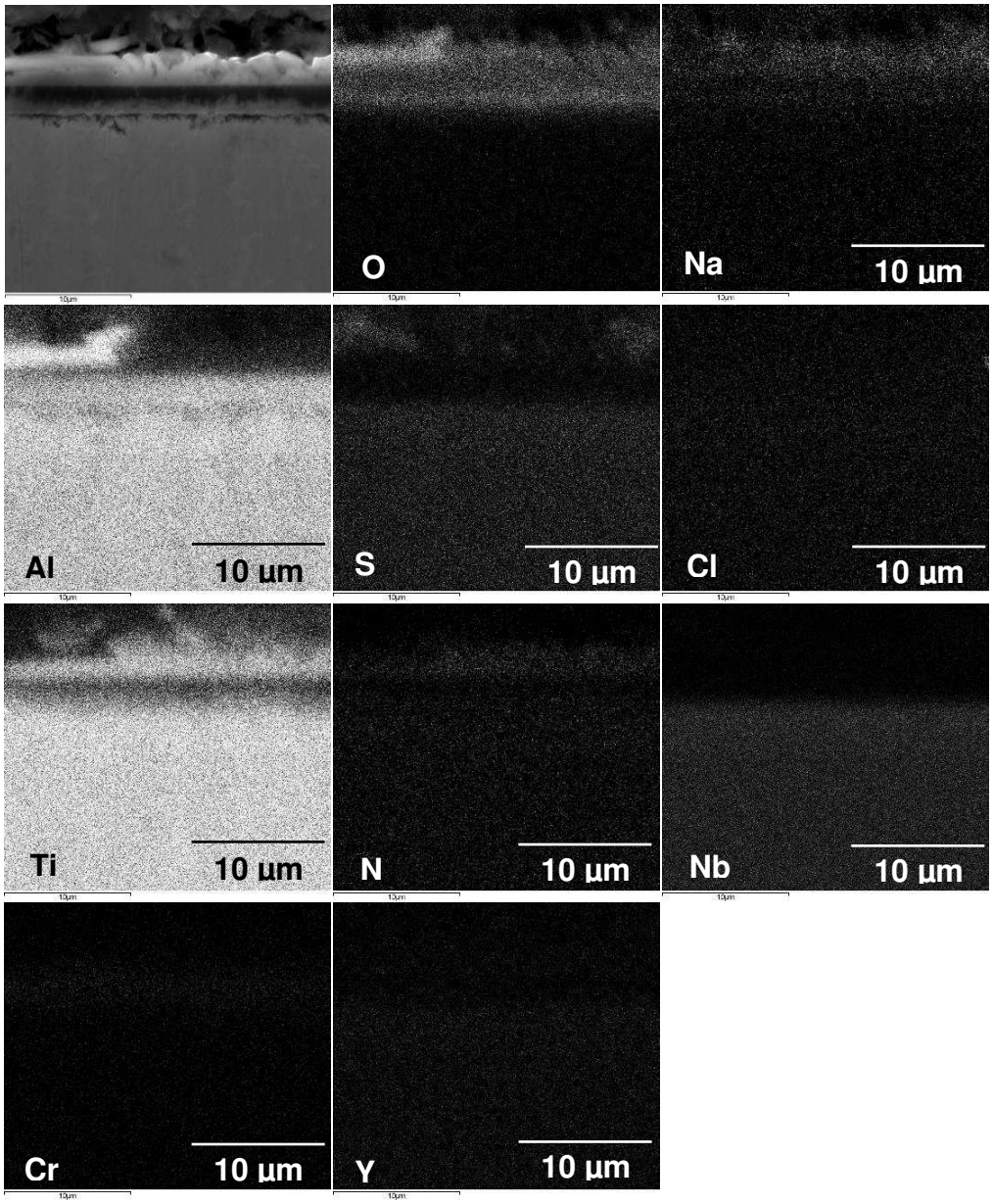

Figure 228 EDS Digimaps of TiAlYN/CrN+Al_2O_3 coated Ti45Al8Nb after 150 hours hot corrosion exposure at 20%NaCl/80%Na_2SO_4 salts mixture at 1023 K

Chapter VI – Section 4 – Interdiffusion Modelling – Results

Ch.VI.Sec.4.1 Introduction

In this section, the results of interdiffusion modelling performed by Generalized Darken Method (GDM) are presented. Interdiffusion has been modelled in TiAlCrY coated Ti45Al8Nb alloy after oxidation at 1023 K for 500 hours in order to predict the simulated concentration profiles of Al, Cr, Ti, and Nb.

Ch.VI.Sec.4.2 Procedure in GDM

1) Measure the initial concentration profiles (e.g., EDS)

2) Perform diffusion annealing in argon atmosphere (close system)

3) Measure the concentration profiles after annealing or oxidation experiments (e.g., EDS)

4) Use Inverse Method to calculate D values, D_o values and diffusional activation energies

5) Use the calculated diffusivities (obtained by Inverse Method) to compute the concentration profiles for the opened system using Darken's Method **(ChII.Sec.4)**

6) The total molar concentration of the for example: Ti45Al8Nb – TiAlCrY alloy $C_{alloy} = 0.10$ mol/cm^3 calculated from equation:

$$c_{alloy} = c_{Al} * x_{Al} + c_{Cr} * x_{Cr} + c_{Ti} * x_{Ti} + c_{Nb} * x_{Nb}$$

Where: C_{alloy} – is a concentration of alloy [mol/cm^3], C_i – elements concentration, X_i – molar fraction of element. To simulate interdiffusion process in opened or closed system, it needs to be formulated following factors:

1) Thickness of the diffusion couple $2\Lambda = 0.01$ cm = 100 μm
2) Time of the process duration t = 1800000 sec (500 hours)
3) Main atomic masses of the elements involved in interdiffusion modelling (TiAlCrY coated Ti45Al8Nb) are shown in **Table 54**.

Element	Atomic mass [g/mol]
Al	26.981
Cr	51.996
Nb	92.606
Ti	47.880

Table 54 The atomic masses of the elements taken into account during interdiffusion modelling performed by GDM

Ch.VI.Sec.4.3 Calculations

Interdiffusion process in open system and when component intrinsic diffusivities constant with composition, has been used for the interdiffusion modelling in a TiAlCrY coated Ti45Al8Nb at the temperature range 1023 – 1223 K. The average intrinsic diffusivities of Al, Cr, Nb, and Ti for open system at different temperature have been calculated using inverse method (**Tables 55 – 57)**.

	Element	D [cm^2/s]	T [K]
		$3.94E^{-10}$	1223
Coating	Al	$4.36E^{-11}$	1123
		$4.71E^{-12}$	1023
	Element	D [cm^2/s]	T [K]
		$3.49E^{-09}$	1223
Alloy	Al	$6.62E^{-10}$	1123
		$5.24E^{-11}$	1023

Table 55 Diffusion coefficients of Al at temperature range 1023 – 1223 K in TiAlCrY coated Ti45Al8Nb alloy

	Element	D [cm^2/s]	T [K]
		$1.65E^{-09}$	1223
Coating	Ti	$2.61E^{-10}$	1123
		$5.10E^{-11}$	1023
	Element	D [cm^2/s]	T [K]
		$4.42E^{-09}$	1223
Alloy	Ti	$3.79E^{-10}$	1123
		$2.26E^{-11}$	1023

Table 56 Diffusion coefficients of Ti at temperature range 1023 – 1223 K in TiAlCrY coated Ti45Al8Nb alloy

	Element	D [cm^2/s]	T [K]
		none	1223
Coating	Cr	$1.36E^{-13}$	1123
		$2.26E^{-14}$	1023

Table 57 Diffusion coefficients of Cr at temperature range 1023 – 1223 K in TiAlCrY coated Ti45Al8Nb alloy

Tables 58 and 61 show the calculated values of E_a (activation energies) and D_o (pre-exponential factor) for TiAlCrY coated Ti45Al8Nb alloy using the D values calculated as above.

Aluminium in Coating	D_o =	0.86	**Aluminium in Alloy**	D_o =	2.17	[cm^2/s]
	R =	8.314		R =	8.314	[J/mol*K]
	Ea =	**229.66**		**Ea =**	**219.15**	**[kJ/mol*K]**

Table 58 D_o and E_a for Al the TiAlCrY coated Ti45Al8Nb system at 1023, 1123 and 1223K in oxidation rig

Titanium in Coating	D_o =	2.54	**Titanium in Alloy**	D_o =	7.71	[cm^2/s]
	R =	8.314		R =	8.314	[J/mol*K]
	Ea =	**180.36**		**Ea =**	**206.98**	**[kJ/mol*K]**

Table 59 D_o and E_a for Ti the TiAlCrY coated Ti45Al8Nb system at 1023, 1123 and 1223 K in oxidation rig

Chromium in Coating	D_o =	0.06	[cm^2/s]
	R =	8.314	[J/mol*K]
	Ea =	237.25	**[kJ/mol*K]**

Table 60 D_o and E_a for Cr the TiAlCrY coated Ti45Al8Nb system at 1023, 1123 and 1223 K in oxidation rig

Niobium in Alloy	D_o =	1.54	[cm^2/s]
	R =	8.314	[J/mol*K]
	Ea =	**266.70**	**[kJ/mol*K]**

Table 61 D_o and E_a for Nb the TiAlCrY coated Ti45Al8Nb system at 1023, 1123 and 1223 K in oxidation rig

Ch.VI.Sec.4.4 Modelling Results for TiAlCrY coated Ti45Al8Nb alloy at 1023 K

Figures 229 – 232 give the calculated concentration profiles for Al, Cr, Nb, and Ti after the coated material was subjected to oxidation at 1023 K for 500 hours (open system).

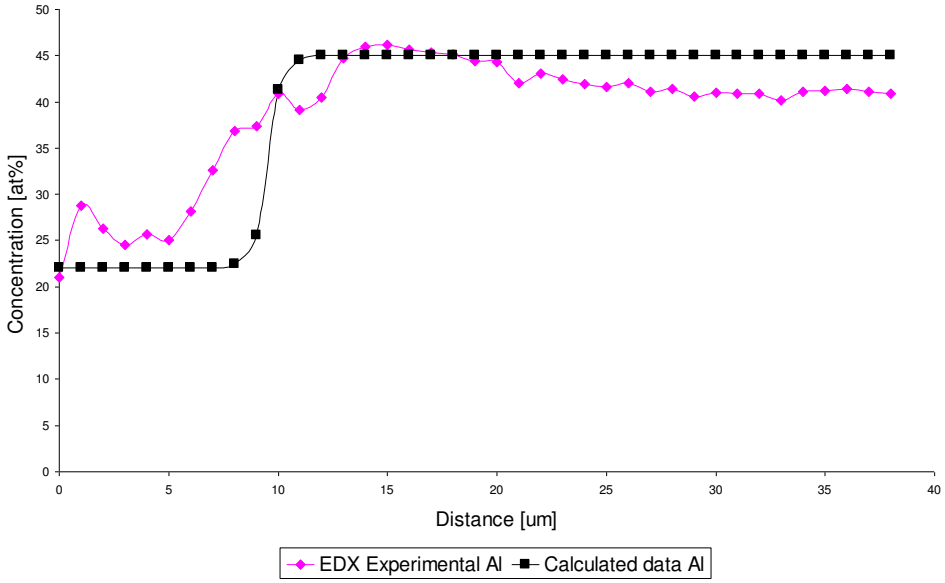

Figure 229 Interdiffusion studies in of TiAlCrY coated Ti45Al8Nb after 500 hours (Al concentration) at 1023 K in open system (oxidation)

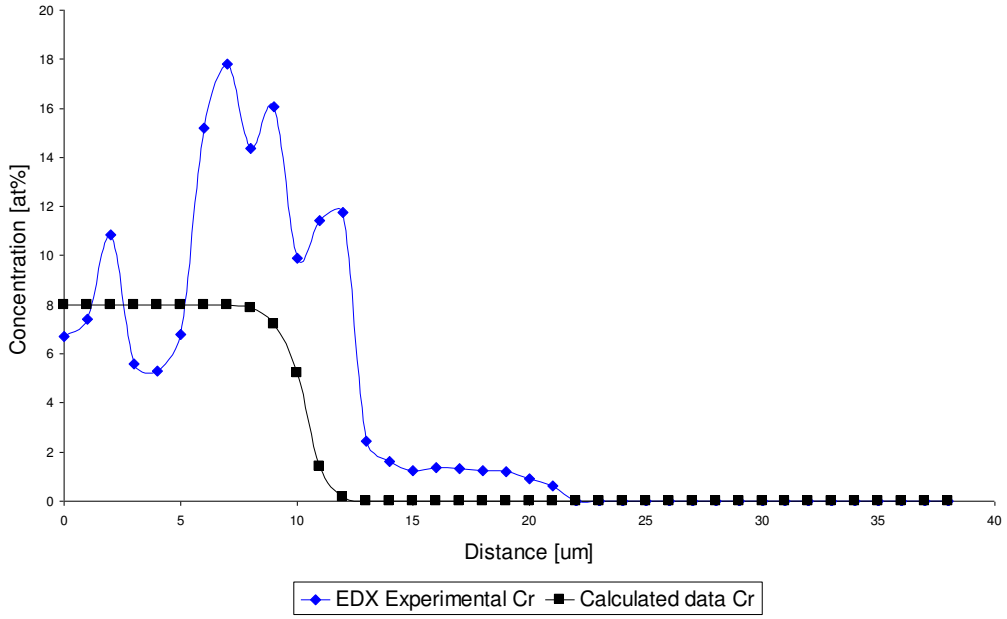

Figure 230 Interdiffusion studies in of TiAlCrY coated Ti45Al8Nb after 500 hours (Cr concentration) at 1023 K in open system (oxidation)

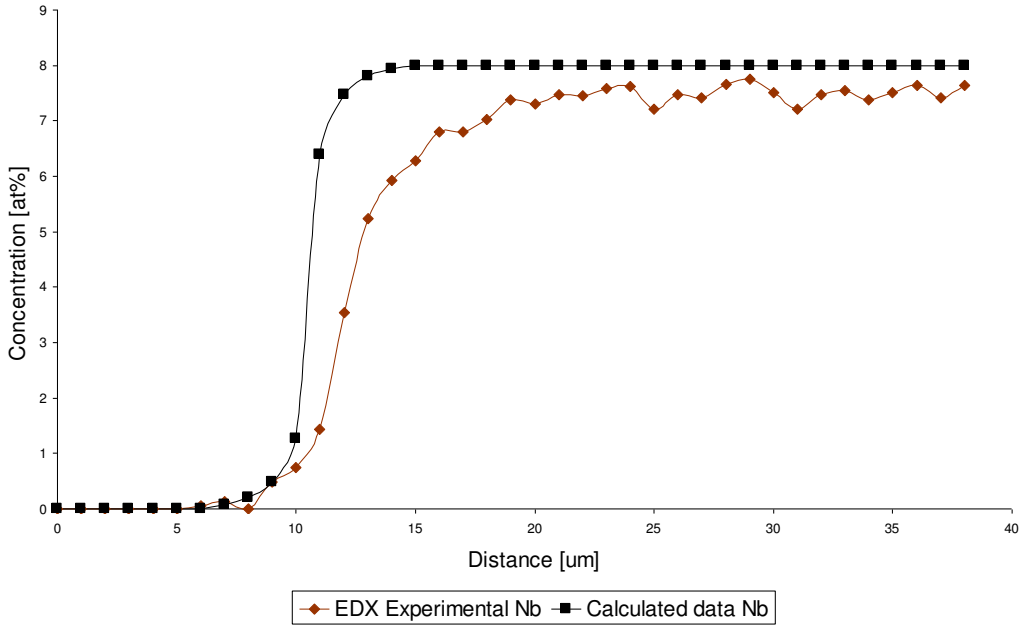

Figure 231 Interdiffusion studies in of TiAlCrY coated Ti45Al8Nb after 500 hours (Nb concentration) at 1023 K in open system (oxidation)

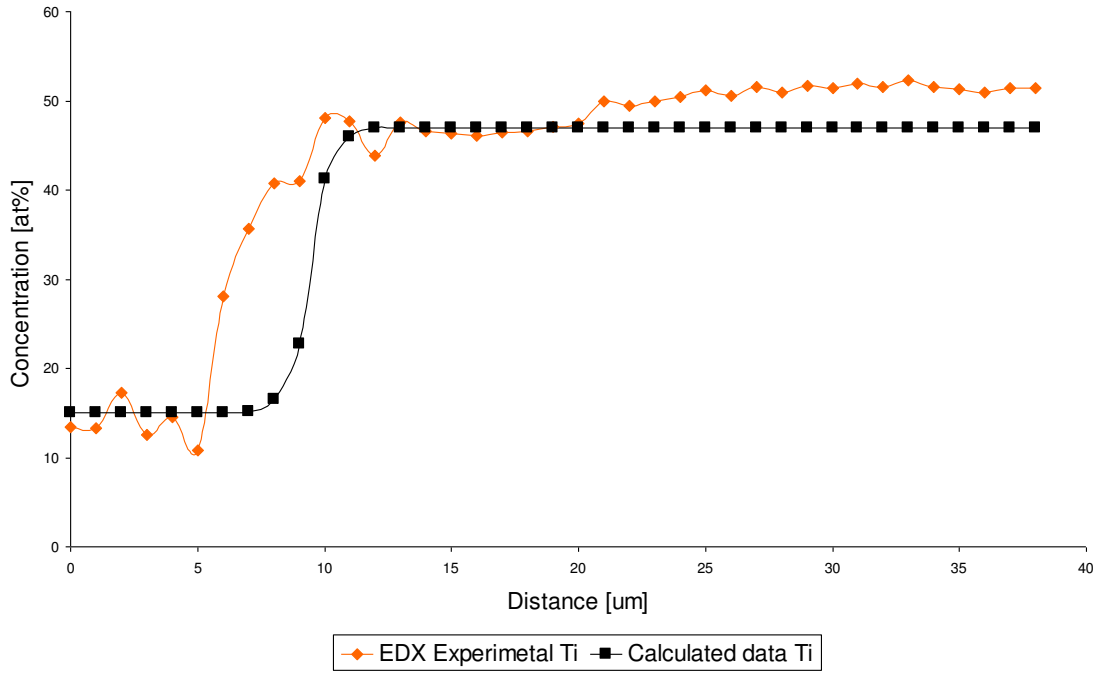

Figure 232 Interdiffusion studies in of TiAlCrY coated Ti45Al8Nb after 500 hours (Ti concentration) at 1023 K in open system (oxidation)

Ch.VI.Sec.4.5 Modelling Results for TiAlCrY coated Ti45Al8Nb alloy at 1023 K

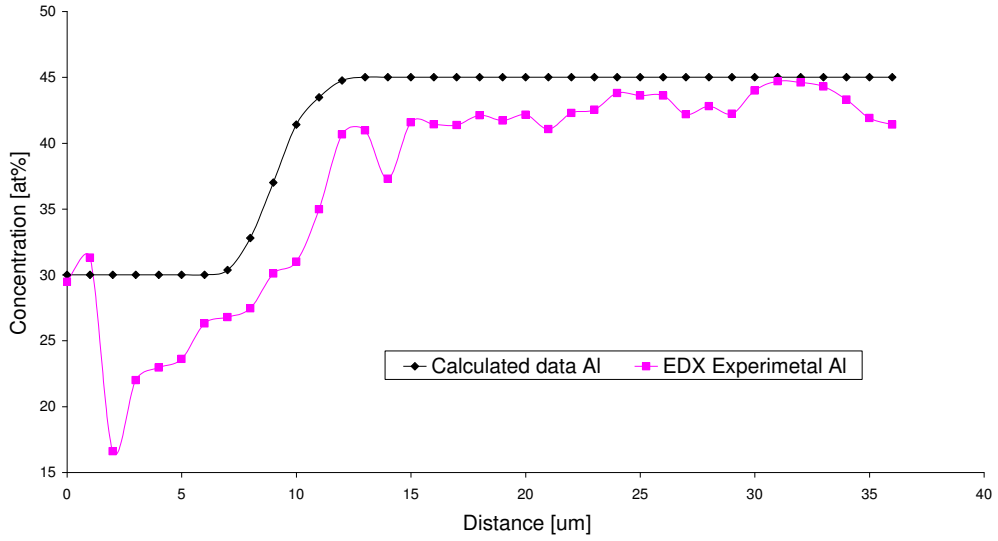

Figure 233 Calculated and experimental concentration profiles for Al in TiAlCrY coated Ti45Al8Nb after 500 hours at 1123 K in open system (oxidation)

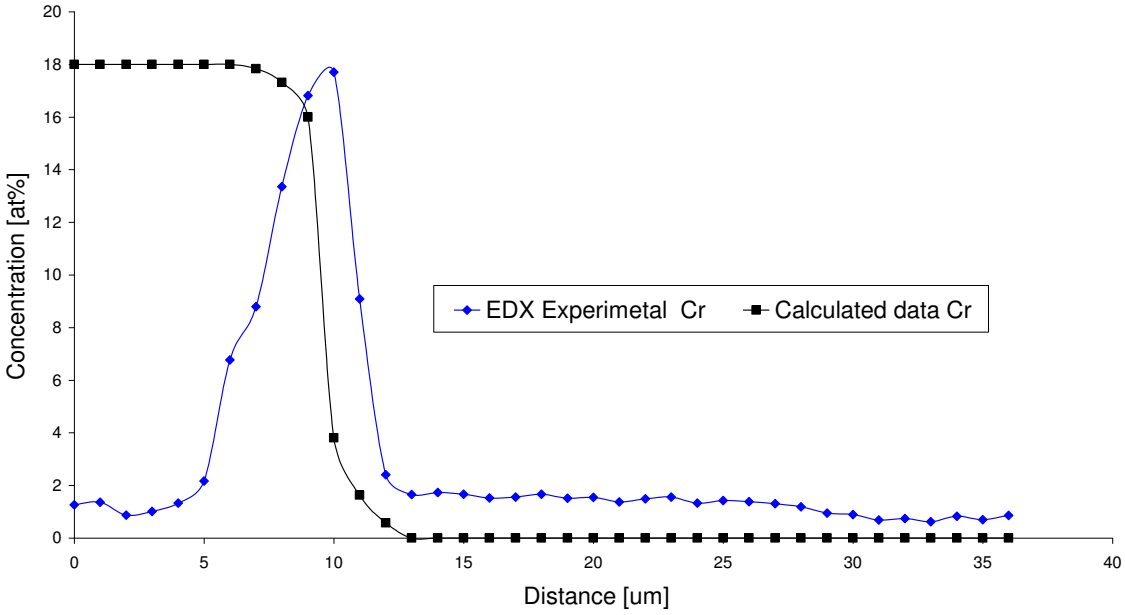

Figure 234 Calculated and experimental concentration profiles for Cr in TiAlCrY coated Ti45Al8Nb after 500 hours at 1123 K in open system (oxidation)

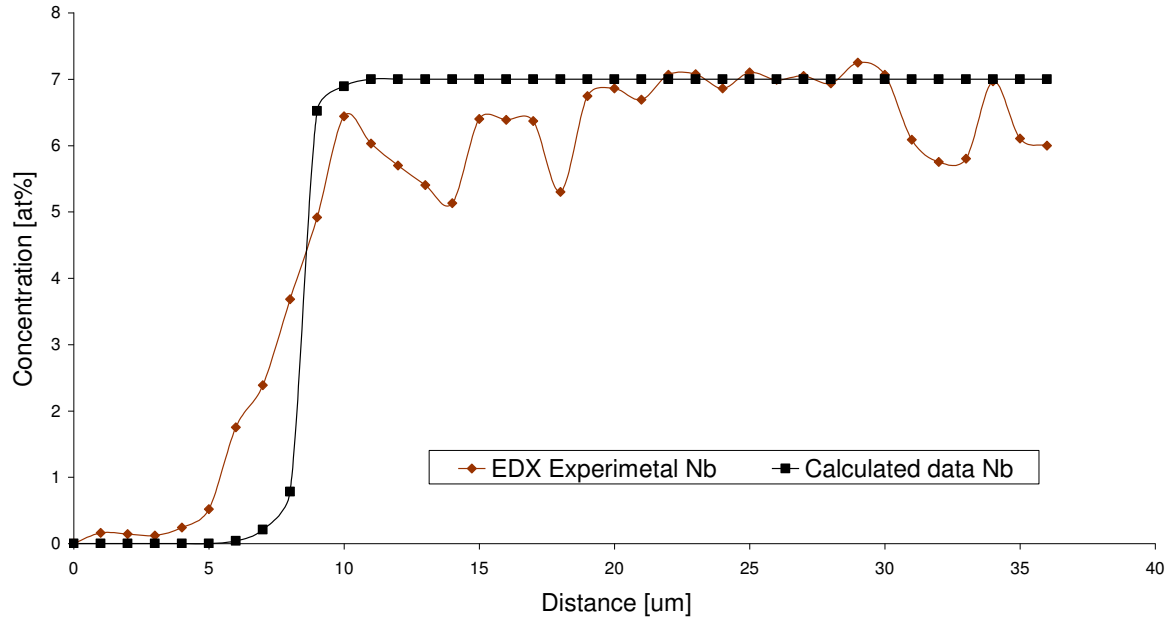

Figure 235 Calculated and experimental concentration profiles for Nb in TiAlCrY coated Ti45Al8Nb after 500 hours at 1123 K in open system (oxidation)

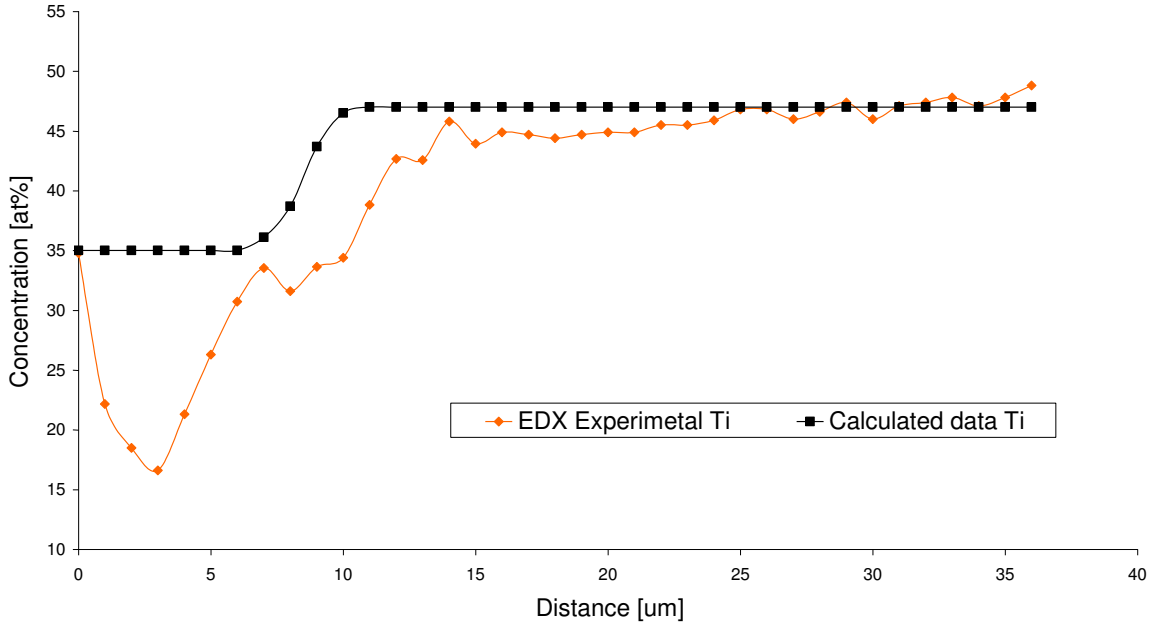

Figure 236 Calculated and experimental concentration profiles for Nb in TiAlCrY coated Ti45Al8Nb after 500 hours at 1123 K in open system (oxidation)

Figures 229 – 232 show the results of interdiffusion modelling performed by GDM after 500 hours oxidation at 1023 K. **Figures 233 – 236** show the experimental and modelled concentration profiles performed by GDM at 1123 K after 500 hours oxidation.

Agreements between the experimental and the calculated concentration profiles can be considered reasonable; some profiles show good agreement, some profiles not.

The observed disagreement between the experimental and calculated experimental and simulated concentration profiles appeared in Al, Ti, and Cr at both temperatures. A good agreement has been achieved for Nb between experimental and modelled concentration profiles at both temperatures.

Chapter VII – Discussion of the Results

ChVII.1 Introduction

Chapter VII presents a discussion of the results obtained from oxidation, sulphidation, and hot corrosion at high temperature of coated intermetallic alloy (Ti45Al8Nb). The chapter consists of the following sections:

- Section one – Oxidation for 500 hours in temperature range 1023 – 1223 K
- Section two – Oxidation for 5000 hours at 1023 K
- Section three – Sulphidation at 1023 and 1123 K for 1000 and 675 hours respectively
- Section four – Hot corrosion in 20%NaCl/80%Na_2SO_4 for 150 hours at 1023 K

Ch.VII.2 Section one – Oxidation for 500 hours at 1023 – 1223 K

Ch.VII.2.1 TiAlCrY coated alloy at 1023 K

The morphology of TiAlCrY (Ti55Al14Cr0.3Y) coating exposed to oxidation environment at 1023 K for 500 hours indicated that the coating was stable and did not suffer much attack **(Ch.VI.Sec.1.Figs.93, 94, 95)**; small cracks, and the observed absence of the scale in some parts of the sample were caused by the cutting processes employed during specimen preparation (no spallation occurred according to the kinetic data **(Ch.VI.Sec.1.Fig 90 Table 30)**). The oxidation of TiAlCrY coated Ti45Al8Nb alloy during high temperature oxidation at 1023 K after 500 hours oxidation was associated with the formation of a mixed oxides of: Al, Ti, and Cr top scale **(Ch.VI.Sec.1.Figs. 94, 95, 96, 97)**. The formation of the top scale is suggested to be caused by the outward diffusion of Al, Ti, and Cr from the coating **(Ch.VI.Sec.1.Figs. 96, 97).**

The oxidation of TiAlCrY coated alloy at 1023 K in the initial stage was related to the formation of a TiO_2 **(Fig. 90)**. The formation of TiO_2 occurred because of the presence of the high partial pressure of oxygen (pO_2 = 21278.25 Pa) in oxidising atmosphere and due to affinity Ti to oxygen [179]. However it needs to be pointed out that the high value of diffusion coefficient of Ti ions played an important role in the scale formation, the calculated diffusion coefficient for Al, Ti, Cr, and Nb are listed in **tables 62, 63, 64, and 65**.

	Element	D [cm^2/s]	T [K]
		$3.94E^{-10}$	1223
Coating	Al	$4.36E^{-11}$	1123
		$4.71E^{-12}$	1023
	Element	D [cm^2/s]	T [K]
		$3.49E^{-09}$	1223
Alloy	Al	$6.62E^{-10}$	1123
		$5.24E^{-11}$	1023

Table 62 Diffusion coefficients of Al at temperature range 1023 – 1223 K in TiAlCrY coated Ti45Al8Nb alloy

	Element	D [cm^2/s]	T [K]
		$1.65E^{-09}$	1223
Coating	Ti	$2.61E^{-10}$	1123
		$5.10E^{-11}$	1023
	Element	D [cm^2/s]	T [K]
		$4.42E^{-09}$	1223
Alloy	Ti	$3.79E^{-10}$	1123
		$2.26E^{-11}$	1023

Table 63 Diffusion coefficients of Ti at temperature range 1023 – 1223 K in TiAlCrY coated Ti45Al8Nb alloy

	Element	D [cm^2/s]	T [K]
		none	1223
Coating	Cr	$1.36E^{-13}$	1123
		$2.26E^{-14}$	1023

Table 64 Diffusion coefficients of Cr at temperature range 1023 – 1223 K in TiAlCrY coated Ti45Al8Nb alloy

	Element	D [cm^2/s]	T [K]
		$9.44E^{-11}$	1223
Alloy	Nb	$7.96E^{-11}$	1123
		$9.97E^{-13}$	1023

Table 65 Diffusion coefficients of Nb at temperature range 1023 – 1223 K in TiAlCrY coated Ti45Al8Nb alloy

The thermodynamic calculations **(Table 66)** of Gibbs Free Energy Formation (ΔG_T^o) indicates that the formation of TiO_2 is less favourable than the formation of more protective Al_2O_3 or Cr_2O_3 oxides. However the diffusion coefficient of Ti^{4+} ions diffuses faster than that of Al^{3+} and Cr^{3+} additionally titanium possesses much higher affinity to oxygen than aluminium or chromium. The free energies of formation of Al_2O_3, Cr_2O_3, and TiO_2 [J/mole] (ΔG_T^o) are given by:

Equation LXXIII $$\Delta G^o_{TiO2,T} = -910.000 + 173T$$

Equation LXXIV $$\Delta G^o_{Al2O3,T} = -1676.000 + 320T$$

Equation LXXV $$\Delta G^o_{Cr2O3,T} = -1121015.7 + 383.72T$$

These equations are valid for TiAlCrY coated Ti45Al8Nb alloy at 1023 and 1123 K; however at 1223 K Cr_2O_3 was not formed on TiAlCrY coating. The calculated values of ΔG_T^o [J/mole] for these equations are given in **table 66**:

ΔG_T^o [J/mole]	T = 1023 K	T = 1123 K	T = 1223 K
TiO_2	-733021	-715721	-698421
Al_2O_3	-1348640	-1316640	-1284640
Cr_2O_3	-728470	-690097	-651725

Table 66 Calculated free energies of formation (ΔG_T^o) of developed oxides at temperature range 1023 – 1223 K

The development of TiO_2 outer scale is given by **reaction 135**:

Reaction 135 $$Ti(s) + O_2(g) \rightarrow TiO_2(s)$$

A schematic model of the scale development on exposed TiAlCrY coated alloy is given in **figure 237**:

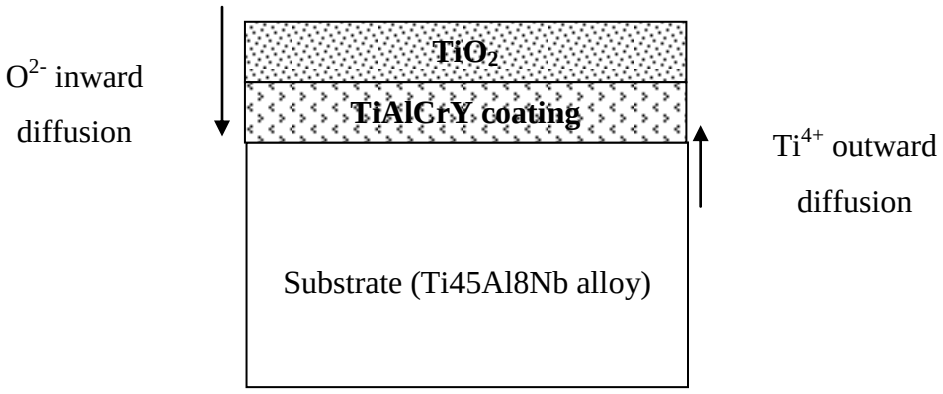

Figure 237 The scale formation at 1023 K on TiAlCrY coated Ti45Al8Nb alloy (initial stage)

Following the formation of TiO_2, the formation of Al and Cr oxides took place, in the TiO_2 outer scale. The formation of TiO_2 oxide as a top scale changed the balance in between Ti, Al, and Cr activity, and also oxygen partial pressure between TiO_2 and substrate. The reduction of Ti activity **(table 67)** led to the formation of Al_2O_3 and Cr_2O_3 according to the **reactions 136** and **137** and **figure 238**:

Reaction 136 $$2\,Al(l) + \frac{3}{2}O_2(g) \rightarrow Al_2O_3(s)$$

Reaction 137 $$2Cr(s) + \frac{3}{2}O_2(g) \rightarrow Cr_2O_3(s)$$

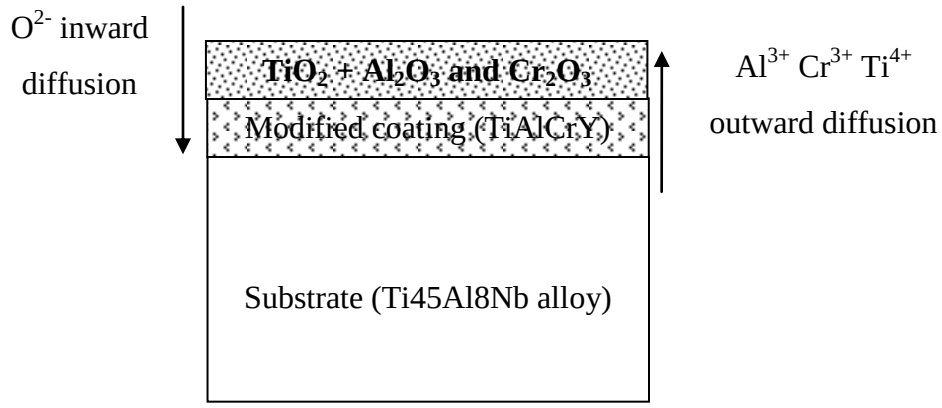

Figure 238 The scale formation at 1023 K on TiAlCrY coated Ti45Al8Nb alloy (formation of the final scale) after 500 hours of oxidation

Table 67 shows the calculated minimum activity of Ti^{4+}, Al^{3+}, and Cr^{3+} at 1023, 1123, and 1223 K respectively [179].

Activity	T = 1023 K	T = 1123 K	T = 1223 K
a_{Al}	$1.2x10^{-35}$	$7.7x10^{-31}$	$1.2x10^{-27}$
a_{Ti}	$3.8x10^{-37}$	$2.4x10^{-33}$	$7.0x10^{-30}$

Table 67 The minimum activities of Ti and Al to form TiO_2 and Al_2O_3 in 0.21 atmosphere of oxygen partial pressure at 1023 – 1223 K

The minimum activities of Al and Ti required for the formation of Al_2O_3 and TiO_2 oxides in **table 67** were calculated based on following equations:

Equation LXXVI
$$\Delta G^{O}_{TiO_2} = -RT\ln K = -RT\ln\frac{aTiO_2}{aTi * pO_2}$$

Equation LXXVII
$$\Delta G^{O}_{Al_2O_3} = -RT\ln K = -RT\ln\frac{aAl_2O_3}{aAl * (pO_2)^{3/2}}$$

The equilibrium constants for **reactions 135** and **136** of the formation TiO_2 and Al_2O_3 oxides can be transformed into another form:

Equation LXXVIII
$$\Delta G^{O}_{TiO_2} = -RT\ln(a_{Ti})^{-1} = 2RT\ln a_{Ti}$$

Equation LXXIX
$$\Delta G^{O}_{Al_2O_3} = -RT\ln(a_{Al})^{-2} = 2RT\ln a_{Al}$$

The observed scale structure **(Ch.II.Sec.1.Figs. 94, 95, 96, 97)** can be rationalised on the consideration of thermodynamics and kinetic factors. Additionally it is important to note that TiN phase was not observed after 500 hours oxidation at 1023 K, where pN_2 = 79033.50 Pa, and high concentration of Ti in the coating were present.

Ch.VII.2.2 TiAlCrY coated alloy at 1123 K

The morphologies following oxidation of TiAlCrY (Ti55Al14Cr0.3Y) at 1123 K) indicated the development of a porous and brittle scale, with voids and cracks

(Ch.VI.Sec.1.Figs. 106, 107, 109). It is suggested that these voids appeared due to the formation of metastable oxide CrO and/or unstable oxides CrO_2, and CrO_3 (these oxides formed at low temperature (initial stage, heating up process) and are only stable at low temperature [185], under oxidation at high temperatures undergo evaporation, and become unstable.

The observed formation of TiO_2 and Al_2O_3 top scale **(Ch.VI.Sec.1.Figs.106, 107, 108, 109)** was associated with the outward diffusion of Ti and Al form the coating, Cr did not form any corrosion products in the top part of the oxide scale, some amounts of Cr_2O_3 phase was detected in deeper region of oxide scale (oxide scale/coating interface) - **(Ch.VI.Sec.1.Fig.107)**. At higher temperature (1123 K) the scale consisted of TiO_2 and Al_2O_3 oxides, whereas Cr_2O_3 remained in the coating **(Ch.VI.Sec.1.Figs.107, 108).** In the initial stage of oxidation TiO_2 formed as a first phase, according to the thermodynamic calculations presented in **tables 62 – 67** and **reactions 135 – 137**. A schematic model of the scale development in TiAlCrY coated alloy is given in **figure 239**:

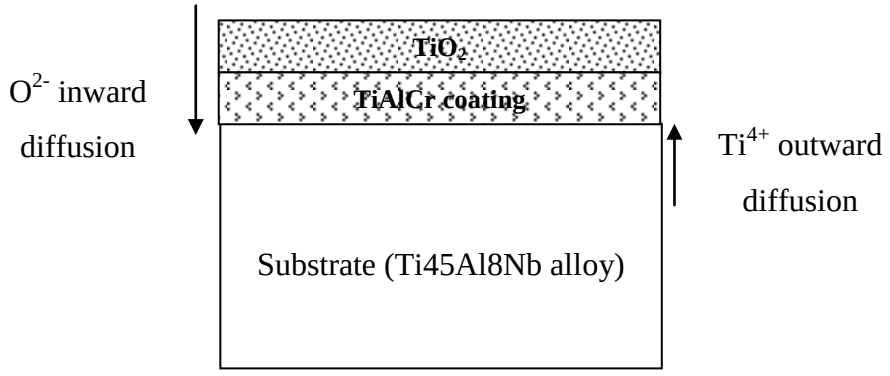

Figure 239 The scale formation at 1123 K on TiAlCrY coating (initial stage)

The formation of TiO_2 oxide similarly as in the case of lower temperature (1023 K) oxidation changed the balance between the Ti and the Al activity and also the oxygen partial pressure between TiO_2 and the substrate. The reduction of Ti activity **(table 6)** led to the formation of Al_2O_3. The formation of Cr_2O_3 was inhibited in the top part of the oxide scale where Al_2O_3 and TiO_2 developed were probably due to the slower diffusion coefficient of Cr^{3+} than Al^{3+} or Ti^{4+} **(table 64)**. Some Cr_2O_3 was formed below the top scale **(Ch.VI.Sec.1.Fig.108, 109)**. This oxide (Cr_2O_3) formed by the ingress of O^{2-} ions through porous scale and relatively high content of Cr^{3+} ions in remainder of the thin

coating (TiAlCrY). Thus at 1123 K Al_2O_3 and TiO_2 oxides formed. The above explanation for the observed scale structure **(Ch.VI.Sec.1.Fig.107)** is presented in **figure 240.**

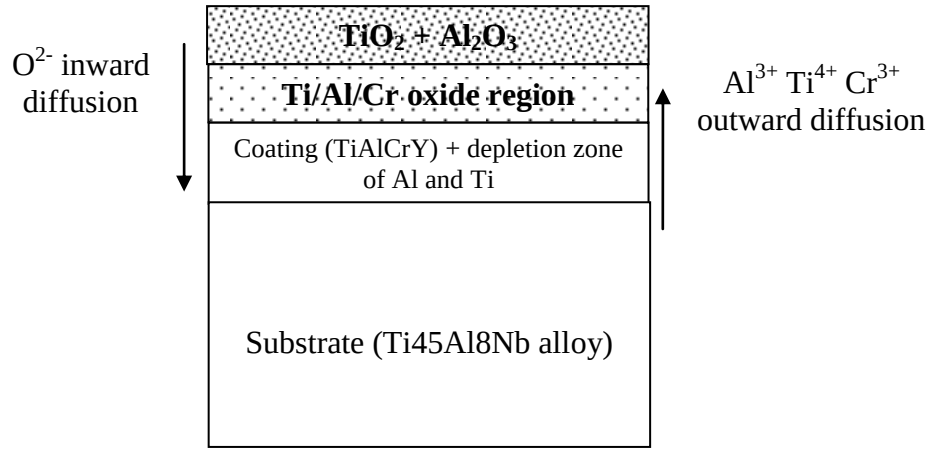

Figure 240 Scale formed in TiAlCrY coated Ti45Al8Nb alloy after 500 hours oxidation at 1123 K

During exposure at 1123 K at the environment (pO_2 = 21278.25 Pa)/ coating (TiAlCrY) interface the following reactions took place:

Reaction 138 $$Ti(s) + O_2(g) \rightarrow TiO_2(s)$$

Reaction 139 $$2Al(l) + \frac{3}{2}O_2(g) \rightarrow Al_2O_3(s)$$

The values of ΔG_T^o [J/mole] are given in **table 68**:

ΔG_T^o [J/mole]	T = 1023 K	T = 1123 K	T = 1223 K
TiO_2	-733021	-715721	-698421
Al_2O_3	-1348640	-1316640	-1284640

Table 68 The standard free energies of formation for TiO_2 and Al_2O_3 in 0.21 atmosphere of oxygen partial pressure at 1023 – 1223 K

Thus the thermodynamic, kinetic factors allow an understanding of the scale development at 1123 K. Similarly as at 1023 K at 1123 K TiN phase was not observed.

Ch.VII.2.3 TiAlCrY coated alloy at 1223 K

The high degradation rate observed for TiAlCrY (Ti55Al14Cr0.3Y) coated alloy material at 1223 K was associated with the formation of non protective TiO_2/Al_2O_3 outer scale, additionally Cr_2O_3 was not observed in the coating **(Ch.VI.Sec.1.Figs. 117, 118)**. The formation of Ti/Al oxides was due to the outward diffusion of Ti and Al ions and inward diffusion of O_2 from ambient atmosphere. At 1223 K the scale formed in TiAlCrY coated Ti45Al8Nb alloy was similar to those at 1123 K.

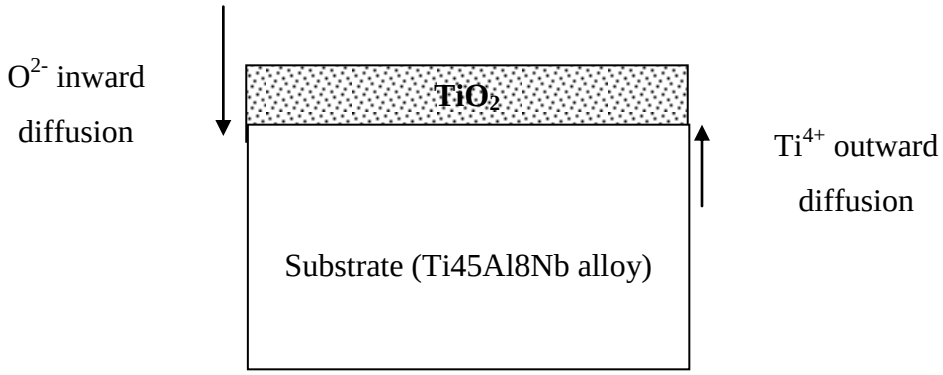

Figure 241 Scale formation in initial period of oxidation at 1223 K on TiAlCrY coated alloy

At the initial stage of oxidation the formation of TiO_2 was favoured because the minimum activity required for TiO_2 development was lower than that of Al **(Table 67).** Also kinetically TiO_2 was likely to be developed, because the diffusion coefficient of Ti is faster than that of Al **(Table 62 and 63).** When the activity of Ti decreased due to the formation of TiO_2 oxide scale, the activity of Al increased to required level, and then Al_2O_3 formed under the TiO_2 scale. **Figure 242** shows the scale formation at 1223 K after 500 hours oxidation.

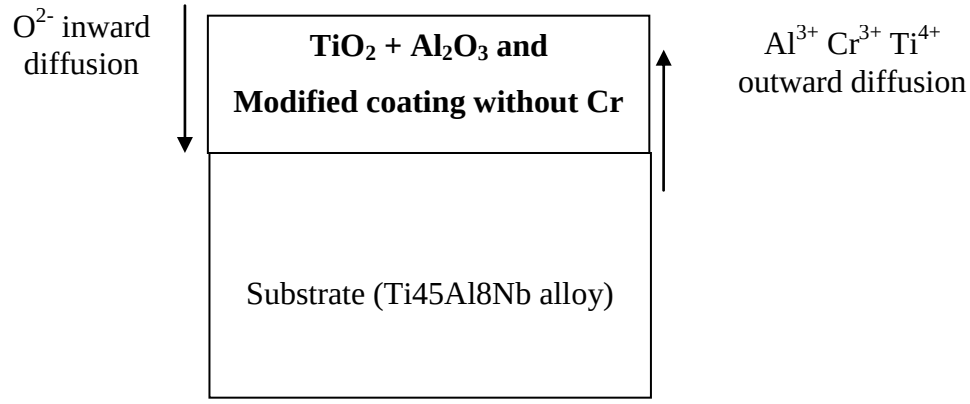

Figure 242 Scale formation after 500 hours oxidation at 1223 K of TiAlCrY coated alloy

It was observed that Cr diffused inward and outward, and did not form any oxide **(Ch.VI.Sec.1.Fig. 117, 118)**, moreover the coating was transformed into the oxide scale, and increased the thickness of the oxide scale. Even in Cr_2O_3 did form it did not survive at this temperature (1223 K).

Ch.VII.2.4 CrAl2%YN coated alloy at 1023 K

The good corrosion resistance of this coating at 1023 K was indicated by the kinetic data **(Ch.VI.Sec.1.Fig. 90, Table 30)** and by the degree of higher integrity of the scale in the middle part of the material **(Ch.VI.Sec.1.Fig. 100).** However the edges of the material showed less integrity and some spallation occurred **(Ch.VI.Sec.1.Fig. 100).** This good corrosion resistance of the material (CrAl2%YN coated Ti45Al8Nb) at 1023 K is suggested to be related to the following processes: the formation of TiN layer at the coating/substrate interface, the formation of highly protective Al_2O_3/Cr_2O_3 mixed outer scale; the outer scale formed by the outward diffusion of Cr^{3+} and Al^{3+} ions from the coating, and inward diffusion of O^{2-} ions from ambient atmosphere. In the initial stage of oxidation at 1023 K the high Al and Cr content (23 and 30 at % respectively) in CrAl2%YN coating supported the development of Cr_2O_3 and Al_2O_3 oxides, scale **(Ch.VI.Sec.1.Figs. 101, 102)**.

In **tables 69, 70, 71**, and **72** are given the calculated diffusion coefficients for Al, Ti, Cr, and Nb, these calculations are critical in order to explain from the thermodynamical point of view the scale development mechanism.

	Element	D [cm^2/s]	T [K]
		$7.01E^{-10}$	1223
Coating	Al	$5.93E^{-11}$	1123
		$7.82E^{-12}$	1023
	Element	D [cm^2/s]	T [K]
		$1.29E^{-10}$	1223
Alloy	Al	$2.66E^{-11}$	1123
		$1.14E^{-12}$	1023

Table 69 Diffusion coefficients of Al at temperature range 1023 – 1223 K in CrAl2%YN coated Ti45Al8Nb alloy

	Element	D [cm^2/s]	T [K]
		$1.24E^{-09}$	1223
Alloy	Ti	$3.37E^{-10}$	1123
		$4.01E^{-11}$	1023

Table 70 Diffusion coefficients of Ti at temperature range 1023 – 1223 K in CrAl2%YN coated Ti45Al8Nb alloy

	Element	D [cm^2/s]	T [K]
		$3.14E^{-12}$	1223
Coating	Cr	$8.21E^{-13}$	1123
		$2.47E^{-14}$	1023

Table 71 Diffusion coefficients of Ti at temperature range 1023 – 1223 K in CrAl2%YN coated Ti45Al8Nb alloy

	Element	D [cm^2/s]	T [K]
		$7.69E^{-10}$	1223
Alloy	Nb	$2.68E^{-11}$	1123
		$2.08E^{-12}$	1023

Table 72 Diffusion coefficients of Ti at temperature range 1023 – 1223 K in CrAl2%YN coated Ti45Al8Nb alloy

A schematic diagram of the scale development is shown in **figure 243:**

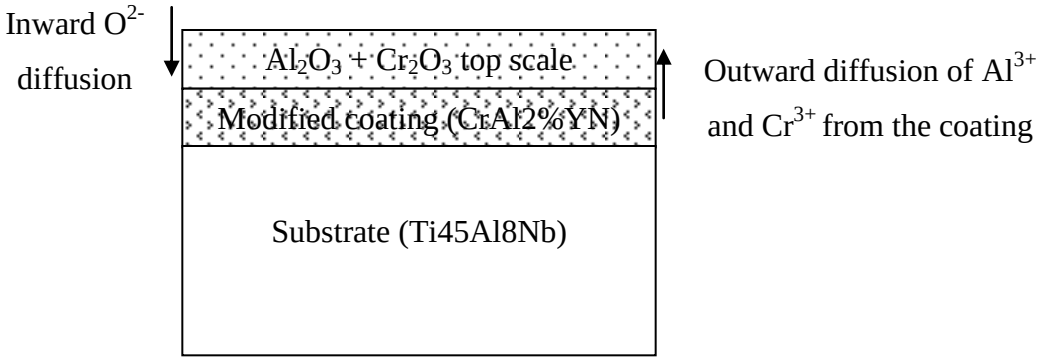

Figure 243 The initial stage of oxidation of CrAl2%YN coated Ti45Al8Nb alloy at 1023 K

During the exposure at 1023 K the following reactions were expected to take place in the oxidation environment:

Reaction 140 $$2\,Al(l) + \frac{3}{2}O_2(g) \rightarrow Al_2O_3(s)$$

Reaction 141 $$2Cr(s) + \frac{3}{2}O_2(g) \rightarrow Cr_2O_3(s)$$

Where ΔG_T^o at [K] is given in **table 73**:

ΔG_T^o [J/mole]	T = 1023 K	T = 1123 K	T = 1223 K
Al_2O_3	-1348640	-1316640	-1284640
TiO_2	-733021	-715721	-698421

Table 73 The Al_2O_3 and Cr_2O_3 ΔG_T^o formation values at temperature range 1023 – 1223 K

In meantime, the titanium diffused outward from the substrate was captured in the interface where a high concentration of N_2 (from deposited coating (around 50 at %) produced a TiN compound according to the reaction below:

Reaction 142 $$2Ti(s) + N_2(g) \rightarrow 2TiN(s)$$

The ΔG_T^o values for the formation of TiN are calculated from **equation LXXX** [180].

Equation LXXX $$\Delta G_T^O = A + BT\log T + CT$$

The ΔG_T^o of TiN formation is estimated from:

Equation LXXXI

$$\Delta G_{TiN}^{O} = -80.250 + 22,2T$$

Where T is temperature [K]

The equilibrium constant can be deduced from equation below:

Equation LXXXII

$$\Delta G_{TiN}^{O} = -RT \ln K = -RT \ln \frac{a\,TiN}{a\,Ti * (pN)^{1/2}}$$

Where K is equilibrium constant, R – gaseous constant (8,314 J/mol*K), T is temperature (K), a – activity.

However during the oxidation process oxygen diffuses inward and TiN allowed a build up the pO_2 partial pressure. When pO_2 partial pressure reached the critical level, the TiN became unstable according to the following reaction:

Reaction 143

$$TiN_{(s)} + O_{2(g)} \rightarrow TiO_2 + 1/2N_2$$

The released nitrogen from **reaction 143** moved inwards via TiN layer and pN_2 gradually increased at the TiN/substrate interface and the nitrogen species encountering Ti from the substrate allowing TiN to form again. The TiN formation inhibited the outward diffusion of Ti to the outer scale, where Cr_2O_3 and Al_2O_3 developed. The final morphology is presented in **figure 244**:

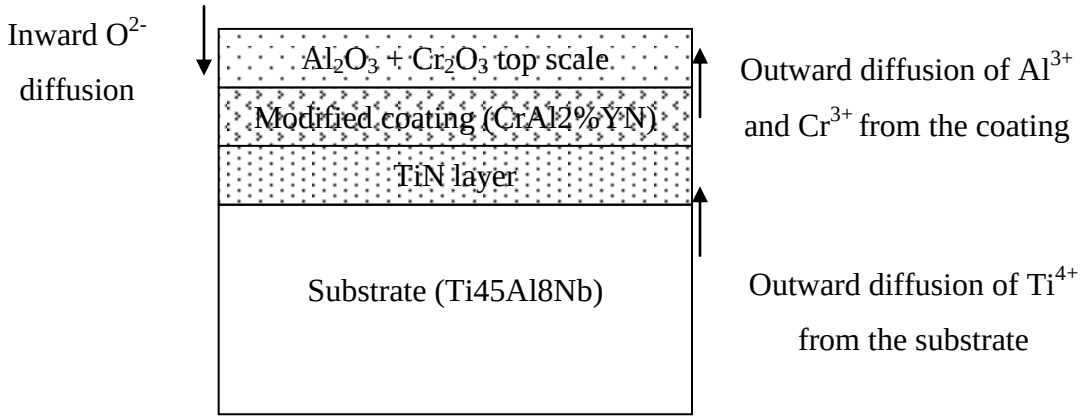

Figure 244 Scale formation after 500 hours oxidation at 1023 K of CrAl2%YN coating

Ch.VII.2.5 CrAl2%YN coated alloy at 1123 K

Similarly good corrosion resistance **(Ch.VI.Sec.1.Fig. 31)** was achieved at 1123 K. A similar morphology with higher degree of scaling integrity was observed **(Ch.VI.Sec.1.Fig. 111).** During oxidation at 1123 K the following processes occurred: the formation of TiN layer at the coating/substrate interface, the outward diffusion of Al^{3+} and Cr^{3+} ions from the coating, the inward diffusion of O^{2-} ions from ambient atmosphere.

At 1123 K the scale morphology formed the same structure as that was observed at 1023 K, except that here both layers: outer scale (Cr_2O_3 and Al_2O_3) and TiN layer were much thicker than at 1023 K **(Ch.VI.Sec.1.Figs. 112, 113, 114)**. The same thermodynamic and kinetic considerations as at 1023 K do apply at 1123 K. The final scale structure is presented below:

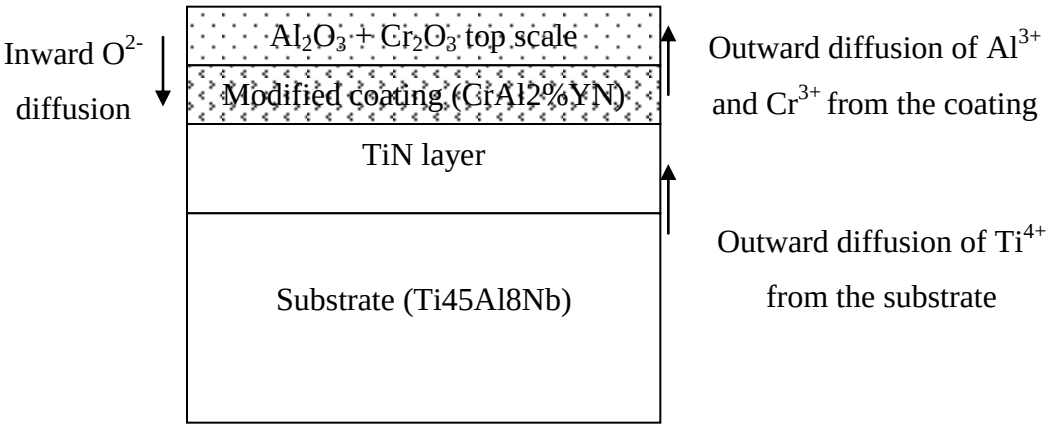

Figure 245 The final scale formed after 500 hours oxidation at 1123 K of CrAl2%YN coated alloy

Ch.VII.2.6 CrAl2%YN coated alloy at 1223 K

The corrosion degradation of CrAl2%YN coated Ti45Al8Nb alloys was observed after 500 hours oxidation at 1223 K, the porous scale, with poor adhesion developed **(Ch.VI.Sec.1.Fig.121).**

The poor corrosion resistance at 1223 K was indicated by high kp value (kp = 4.64201E^{-07} [mg^2/cm^4/s] and the development of a non protective thick (90 µm) scale (subsequently replaced by the alternative formation of layers TiO_2/Al_2O_3) aided by the crack formation on formed scale. These cracks allowed significant diffusion of Ti^{4+} ions from the bulk material. Additionally the lack of TiN, which inhibited the outward diffusion of Ti ions form material at lower temperatures (1023, 1123 K) was observed. The absence of TiN and the formation of cracks, initiated by the thermal mismatch of thermal coefficients between coating and substrate in the initial stage of oxidation produced a sandwich like structure of TiO_2 and Al_2O_3 with alternative layers. When cracks appeared in the outer part of the scale, then Ti ions diffused outward and produced in the initial stage of oxidation a TiO_2 oxide layer.

The higher ΔG_T^o for Ti oxidation **(Table 73)** would not promote the formation of TiO_2 however the faster diffusion coefficient of Ti^{4+} ions **(Table 69)** support early formation of TiO_2 according to the following reaction:

Reaction 144 $$Ti(s) + O_2(g) \rightarrow TiO_2(s)$$

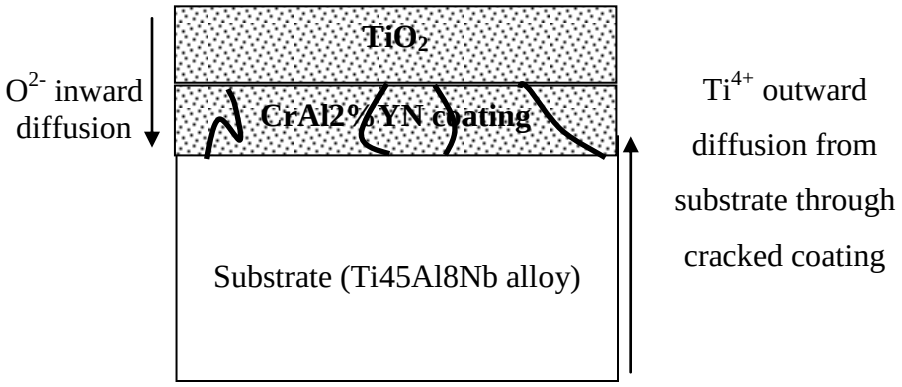

Figure 246 The initial scale development at 1223 K on CrAl2%YN coating

The formation of TiO_2 reduced the Ti concentration and decreased the activity of Ti^{4+} ions. When Ti activities decreased then Al activities increased. Thus Al_2O_3 started to develop according to the reaction:

Reaction 145 $$2Al(l) + \frac{3}{2}O_2(g) \rightarrow Al_2O_3(s)$$

It needs to be pointed out that Cr diffused outward however; Cr did not produce any oxide probably because the partial pressure was too low due to the consumption of O^{2-} in producing TiO_2 and Al_2O_3 oxides, or concentration of Cr ions was also very low. The scale development during oxidation at 1223 K of CrAl2%YN coated alloy is shown in **figure 247**:

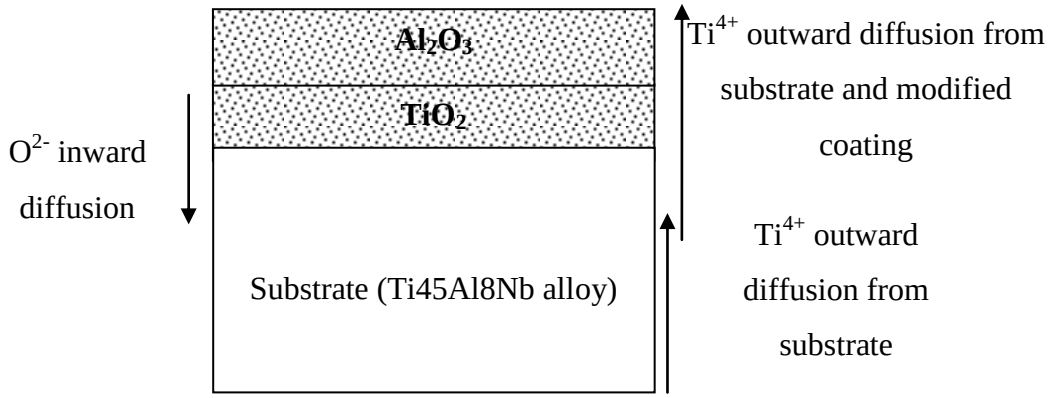

Figure 247 Formation of Al_2O_3/TiO_2 oxide scale at 1223 K on CrAl2%YN coating

Again the activity and the concentration of Al decreased due to the formation of Al_2O_3 phase (**reaction 145**), and Ti^{4+} activity increased leading to TiO_2 formation. This phase formation cycle was observed until the total oxide scale reached the critical thickness value, where spallation of the scale started to occur.

The thermodynamical calculations for the formation of TiO_2 and Al_2O_3 phases are given in **table 73**. The oxidation of CrAl2%YN coated Ti45Al8Nb alloy at 1223 K developed a multilayered – sandwich like structure consisting of alternate layers of TiO_2/Al_2O_3. A schematic diagram of the final scale developed on CrAl2%YN is presented in **figure 248** below:

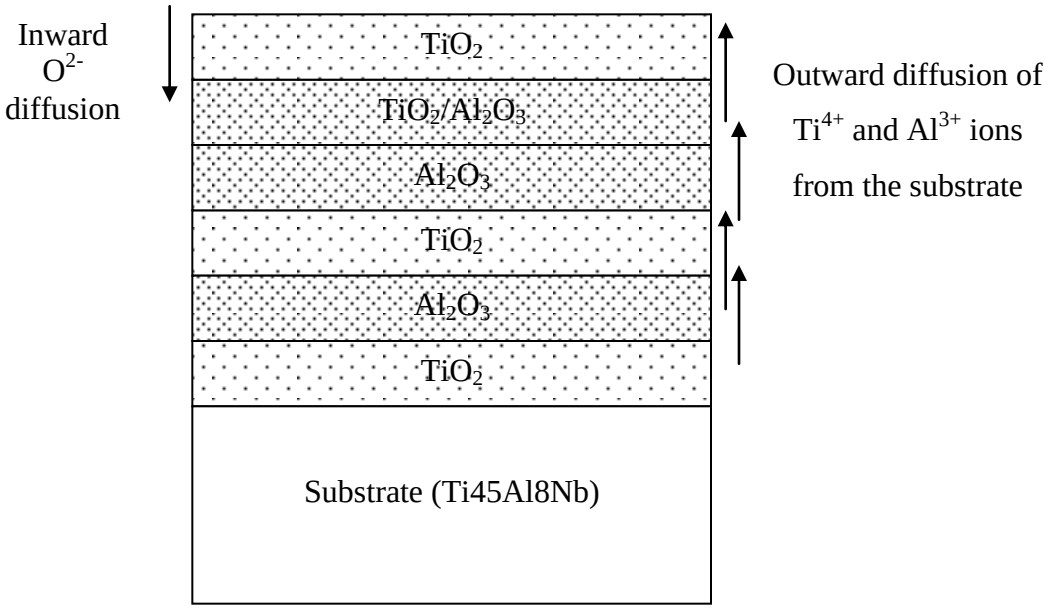

Figure 248 The scale formation after 500 hours oxidation at 1223 K of CrAl2%YN coating

Additionally, the absence of TiN layer during oxidation at 1223 K allowed the fast outward diffusion of Ti from the bulk material and the formation of a thick scale; (at lower temperatures 1023 and 1123 K Ti ions were captured for the formation of TiN layer).

It is important to note that the number of layers (TiO_2/Al_2O_3) dependent on the time of exposure and the temperature **(Ch.VI.Sec.1 Fig.122, 124)**. Thus longer exposure time promoted a higher number of layers (TiO_2/Al_2O_3) **(Ch.VI.Sec.1 Fig.122, 124).**

Ch.VII.3 Section Two – Oxidation for 5000 hours at 1023 K

Ch.VII.3.1 TiAlCr coated alloy

The degradation of TiAlCr (Ti42Al15Cr) coating was characterised by the following processes: the outward diffusion of Ti, and Al from the coating, the lack of Cr_2O_3 formation on the outer part of the scale, the formation of a small amounts of Cr_2O_3 within the scale, the development of a multilayered thick scale, and the scale spallation (when the scale reached the critical thickness) of the scales.

The oxidation behaviour of TiAlCr coated alloy at 1023 K for 5000 hours exposure, was investigated in static air (pO_2 = 21278.25 Pa). The scale formed in the exposed material had a multilayered structure where alternative layers of TiO_2 and Al_2O_3 oxide developed. The scale formed mainly via the outward diffusion of elements (Ti, Al) from the deposited coating (TiAlCr), Cr ions also diffused however did not produced Cr_2O_3 oxide on the top of outer scale, some small amounts of Cr_2O_3 were detected by within the oxide scale **(Ch.VI.Sec.1.Figs. 129, 132).**

The formation of the oxide scale based on thermodynamical calculation (**Tables 62, 63** and **66**, **67**) and **reactions 140, 141** associated with **equations LXXIII, LXXIV, LXXVI, and LXXIX** can be described as follows.

When TiAlCr coated Ti45Al8Nb material was exposed to the oxidation environment, then the oxygen partial pressure (pO_2 = 21278.25 Pa) promoted the formation of TiO_2 oxide and the oxide formed according to the following reaction:

Reaction 146 $$Ti(s) + O_2(g) \rightarrow TiO_2(s)$$

The TiO_2 film formed on the surface of the exposed material separated the material from external environment. The pO_2 at the interface of TiO_2 and the coating, decreased to the dissociation partial pressure of TiO_2 (dissociation partial pressure of TiO_2 is equivalent to a_{minTi} value **(Table 67)**.

When Ti ions formed the TiO_2 oxide scale, then the activity of Ti decreased, here the activity of Al increased causing the development of Al_2O_3. The development of Al_2O_3 phase can be presented by the following reaction:

Reaction 147 $$2\,Al(l) + \frac{3}{2}O_2(g) \rightarrow Al_2O_3(s)$$

A relatively pure Al_2O_3 layer formed underneath the mixed layer of TiO_2 and Al_2O_3 **(Ch.VI.Sec.1.Figs.129, 132),** the Al_2O_3 formed due to the ingress of oxygen from the ambient atmosphere and decreased in Ti activity in the oxide scale. The TiAlCr coated alloy material developed several alternative layers of TiO_2/Al_2O_3 and the scale structure of exposed material can be described as follows: TiO_2/TiO_2-$Al_2O_3/Al_2O_3/TiO_2/Al_2O_3/TiO_2$/Alloy (Ti45Al8Nb)

It needs to be pointed out, that after 5000 oxidation Cr_2O_3 formed within the oxide scale and the lack of formation Cr_2O_3 was observed on the top part of the oxide scale. This behaviour was associated with fact, that the partial pressure of oxygen was reduced due to the formation of Al_2O_3 and TiO_2 oxides; additionally the diffusion coefficient of Cr is much slower than that of Al, and Ti **(Tables 62, 63, 64).**

During the exposure, the thickness of the inner and the outer layers in the formed oxide scale on the TiAlCr coated material increased, the plasticity of the scale is lower when experiment was longer and the thickness of the scale was higher. Thus when the oxide scale exceeded the critical value, the crack formation was initiated. The different thermal coefficients between the substrate and the oxide scale played an important role in the corrosion resistance of TiAlCr coated alloy material. The formation of crack/s caused the detachment between the formed oxide scale and the substrate (Ti45Al8Nb), thus the mass transport from the substrate was more difficult. A schematic diagram of scale development of TiAlCr coated Ti45Al8Nb alloy is presented below **(Fig. 249)**:

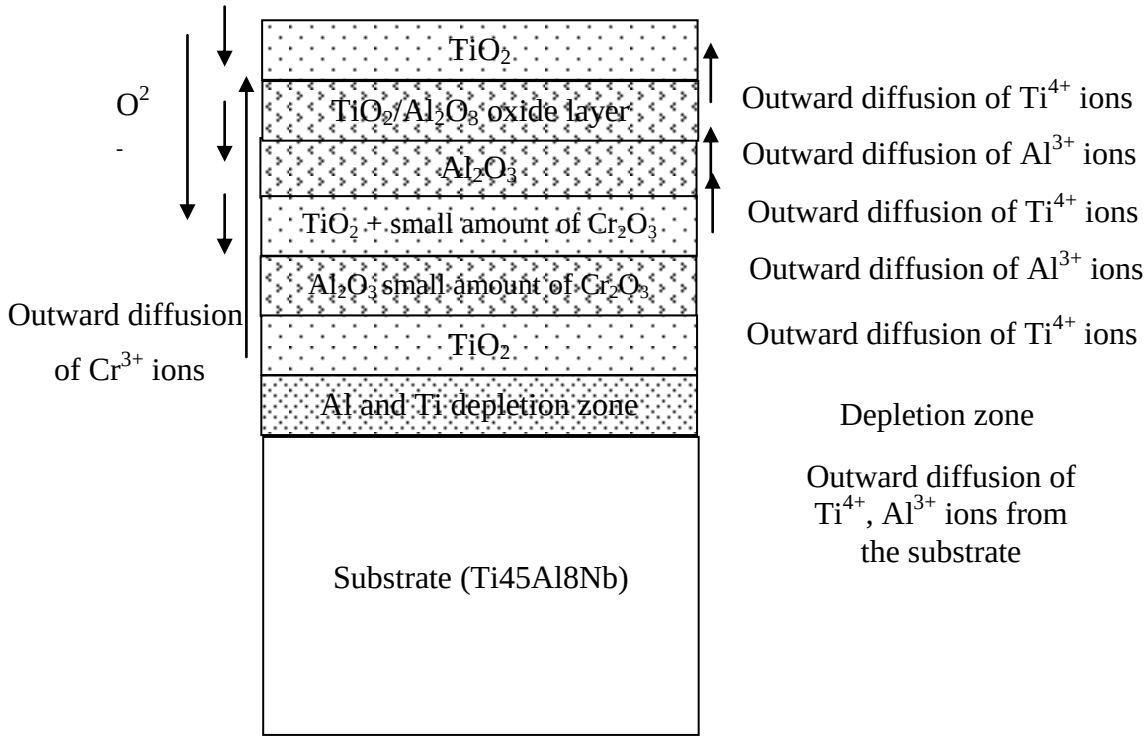

Figure 249 Schematic diagram of the oxidation mechanism and scale development on TiAlCr coated Ti45Al8Nb after 5000 hours oxidation at 1023 K

It was observed that after oxidation at 1023 K for 5000 hours, the TiN layer was not formed due to the high value of Gibbs free energy. **(ChVI.Sec.1.Fig.129)**. However, the partial pressure of N_2 (pN_2 = 79033.5 Pa) was higher than that of O_2 (pO_2 = 21278.25 Pa). This showed that the Ti has a higher affinity to oxygen that than to nitrogen the formation TiO_2 (or other Ti oxides) was likely to occur. The thermodynamical calculations **(Table 74)** confirmed scale structure described in **figure 249**.

ΔG_T^o [J/mole]	T = 1023 K
Al_2O_3	-1348640
TiO_2	-733021
TiN	-240906

Table 74 Free energies of the formation of Al, and Ti oxides and TiN at 1023 K

The long term oxidation for 5000 hours at 1023 K showed also, that the middle part of the sample formed a different scale morphology; the scale was thinner than that in the edges **(ChVI.Sec.1.Figs. 128, 130)**. However the phase composition was very similar. The formed scale consisted of TiO_2 and Al_2O_3 alternative layers. The presence

of a thinner scale in the middle of the sample indicates that: the outer scale spalled off from the material after exceeded a critical level of thickness and lost plasticity, or the coating developed a thin Al_2O_3 protective layer with some amount of TiO_2 oxide. It also was observed that in the coating the Cr content was high (around 15 at%).

Thus the middle part of the scale contained Al_2O_3 with some TiO_2 and also Cr_2O_3 phases **(ChVI.Sec.1.Figs.130, 131, 133)**. The formation of Cr_2O_3 was related to the following reaction:

Reaction 148 $$2Cr(s) + \frac{3}{2}O_2(g) \rightarrow Cr_2O_3(s)$$

ΔG_T^o of this reaction can be described as follows:

Equation LXXXIII $$\Delta G^o_{Cr2O3,T} = -1121015.7 + 383.72T$$

The equilibrium constant

Equation LXXXIV $$\Delta G^O_{Cr2O3} = -RT \ln K = -RT \ln \frac{aCr_2O_3}{aCr * (pO_2)^{3/2}}$$

The calculated ΔG_T^o values are given in **table 75**:

ΔG_T^o [J/mole]	T = 1023 K	T = 1123 K	T = 1223 K
TiO_2	-733021	-715721	-698421
Al_2O_3	-1348640	-1316640	-1284640
Cr_2O_3	-728470	-690097	-651725

Table 75 Calculated free energies of formation (ΔG_T^o) of developed Al_2O_3, TiO_2 and Cr_2O_3 oxide at temperature range 1023 – 1223 K

The calculated free energies formation of Cr_2O_3 indicates that Cr_2O_3 formed after Al_2O_3 and TiO_2 oxides, due to the higher values of ΔG_T^o than that of TiO_2 and Al_2O_3. Also the faster diffusion coefficients of Al, and Ti than that of Cr allowed the development of Al_2O_3/TiO_2 mixed oxide on the top of the oxide scale. The calculated diffusion coefficients for Al, Cr, and Ti are presented in **table 76**:

Diffusion coefficient [cm^2/s]			
Temperature [K]	D_{Al}	D_{Cr}	D_{Ti}
1023	$1.97E^{-12}$	$8.12E^{-13}$	$2.99E^{-11}$
1123	$2.03E^{-11}$	$8.18E^{-12}$	$1.48E^{-10}$
1223	$1.43E^{-10}$	$5.65E^{-11}$	$5.65E^{-10}$

Table 76 Calculated diffusion coefficients for Al, Ti, and Cr at temperature range 1023 – 1223 K

Ch.VII.3.2 TiAlYN/CrN+Al_2O_3 coated alloy

The scale degradation of TiAlYN/CrN+Al_2O_3 coated alloy was due to the crack formation in the deposited Al_2O_3 top coat. The cracks allowed the ingress of oxygen and the outward diffusion of Ti form the bulk material. The development of a non protective scale consisted of mixed oxide scale (Al_2O_3/TiO_2). It was observed that some parts of the exposed sample showed excellent corrosion resistance, due to the deposited Al_2O_3 top coat prior to experiment.

The long term exposure of TiAlYN/CrN+Al_2O_3 coated alloy material after oxidation for 5000 hours at 1023 K showed the best corrosion resistance (**Ch.Vi.Sec.1.Fig. 125).** The lowest kp value ($5.068E^{-09}$ [$mg^2/cm^4/s$]) for this sample was

related to the protective behaviour of Al_2O_3 top coat deposited during manufacture of the coating.

However some places of the exposed sample suffered high temperature oxidation due to the crack formation. The crack formation in the deposited top coat (Al_2O_3) was mainly related to the mismatch in the thermal coefficients between the sub-layers within the coating (Al_2O_3/TiAlYN/CrN) and also between the coating and the substrate material (Ti45Al8Nb alloy). During cooling down period of the exposed material some parts were cooled faster (intermetallic core) and other parts of the exposed material were cooled down slower. The differences between the rates of cooling down process promoted the formation of strains within the material. Such strains formed the cracks; when cracks developed then the thermodynamics played its role. The higher affinity of Al and Ti to oxygen than that of Cr caused the formation of TiO_2/Al_2O_3 mixed outer scale in affected region by the crack formation **(Ch.VI.Sec.1.Figs. 136, 137)**.

In the initial period of exposure when top coat cracked the TiO_2 formed first due to the faster diffusion coefficient of Ti that that of Al, according to the reaction:

Reaction 149 $$Ti(s) + O_2(g) \rightarrow TiO_2(s)$$

The formed TiO_2 changed the partial pressure of oxygen in the ambient atmosphere, and also changed the activity of Ti; activity of Ti decreased and led to the development of Al_2O_3 phase The Al_2O_3 layer developed according to the reaction:

Reaction 150 $$2Al(l) + \frac{3}{2}O_2(g) \rightarrow Al_2O_3(s)$$

The development of Al_2O_3 decreased the activity of Al, and then again TiO_2 formed underneath Al_2O_3.

Figure 250 shows the final stage of the scale developed on the exposed TiAlYN/CrN+Al_2O_3 coated Ti45Al8Nb alloy at 1023 K for 5000 hours in the affected region.

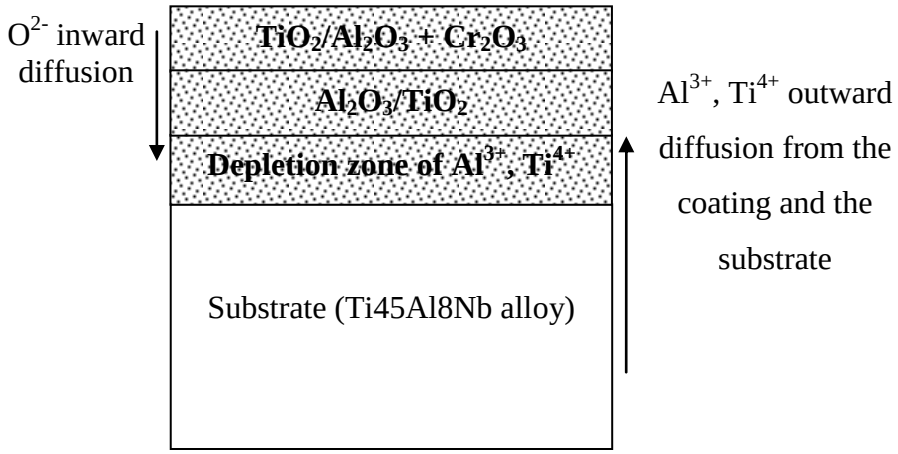

Figure 250 Final scale developed on TiAlYN/CrN+Al_2O_3 coated Ti45Al8Nb alloy in affected region at 1023 K for 5000 hours

It was observed that Cr_2O_3 oxide was presented in the outer scale in very small amounts. The calculated diffusion coefficient of Cr, suggested that the small amounts of Cr_2O_3 oxide was associated with the lowest value of diffusion coefficient of Cr **(Table 76)**.

It was observed that the CrN phase was not detected during the EDS investigation **(Ch.VI.Sec.1.Fig. 137)** in the affected region. The absence of CrN suggests that CrN phase decomposed during 5000 hours oxidation due to the N flux away from the deposited coating. It can be suggested, when the cracks appeared in the deposited coating, then O^{2-} diffused inward. The inward diffusion of O^{2-} led to increase of partial pressure of oxygen in the deposited cracked coating and oxygen reacted with CrN:

Reaction 151

$$2CrN_{(s)} + \frac{3}{2}O_{2(g)} \rightarrow Cr^{3+} + O^{2-} + N_2$$

The formed free Cr^{3+} ions were unable to form oxide (Cr_2O_3) in high amounts because of higher affinity of Al^{3+} and Ti^{4+} to oxygen than Cr^{3+}.

The Al_2O_3 top coat effectively inhibited the formation of a non protective TiO_2, oxide scale, or Al_2O_3/TiO_2 oxide **(Ch.VI.Sec.1.Figs. 138, 139).** The unaffected region on TiAlYN/CrN+Al_2O_3 top coat coated alloy showed the excellent corrosion resistance.

The mass transport from the material (Ti45Al8Nb) was blocked by the adherent Al_2O_3 top coat. The final scale after 5000 hours oxidation in unaffected region is given in **figure 251**.

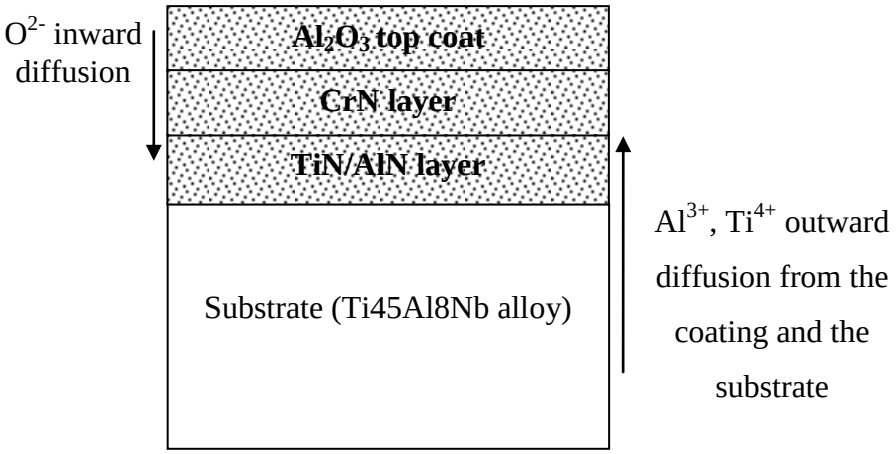

Figure 251 Final scale developed on TiAlYN/CrN+Al_2O_3 coated Ti45Al8Nb alloy in unaffected region at 1023 K for 5000 hours

It was observed that during exposure, the formation of TiN layer occurred, underneath the deposited coating, the formation of TiN additionally inhibited the outward diffusion of Ti from the bulk material, Ti^{3+} ions were captured in order to form TiN phase. It also was suggested that TiN layer formed as a last phase during exposure, (the highest value of ΔG_T^o [J/mole]). The thermodynamic calculation of the formation of TiN (ΔG_T^o [J/mole]) is given in **table 77**.

ΔG_T^o [J/mole]	T = 1023 K
TiO_2	-733021
Al_2O_3	-1348640
Cr_2O_3	-728470
TiN	-240906

Table 77 The TiN ΔG_T^o formation values at 1023 K

Ch.VII.3.3 TiAlN + Al_2O_3 coated alloy

The degradation of the exposed material (TiAlN (Ti25Al50N) + Al_2O_3 top coat) was associated with the formation of the mixed TiO_2/Al_2O_3 scale, the crack formation in the top scale (Al_2O_3) which allowed Ti outward diffusion, the TiN formation occurred in some places in the material, these places showed a better corrosion resistance **(Ch.VI.Sec.1.Figs. 142, 143, 144, 145)**, the kp value was equivalent to $3.079E^{-08}$ [$mg^2/cm^4/s$].

The exposed TiAlN+Al_2O_3 coated alloy material exposed at 1023 K for 5000 hours showed a similar oxidation behaviour as TiAlYN/CrN+Al_2O_3 material. The formation of cracks accelerated the degradation process during the high temperature oxidation. The deposited Al_2O_3 protected the exposed material against high temperature oxidation; however during thermal cycles, when temperature was cooled down, the formation of the cracks occurred. Similar to the TiAlCr coated alloy, TiAlN+Al_2O_3 coated Ti45Al8Nb material developed two regions, in the edges and in the middle of the sample.

Figure 252 shows the scale developed in the middle of the sample in the initial time of exposure.

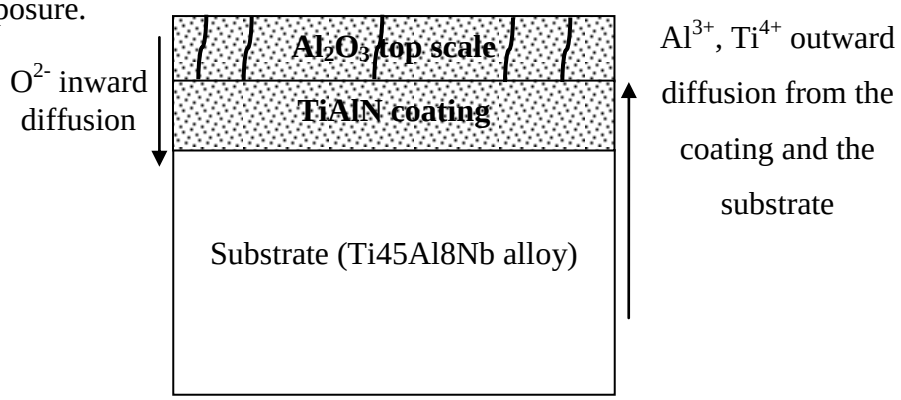

Figure 252 Initial morphology developed during oxidation of TiAlYN/CrN+Al_2O_3 coated alloy at 1023 K – middle of the sample

The cracked top coat allowed the ingress (inward diffusion) of O^{2-} from the ambient atmosphere where pO_2 = 21278.25 Pa **(Fig. 252)**.

During further exposure, the cracks degraded the top coat; the degraded Al_2O_3 top coat increased the oxygen partial pressure upon the coating. The high concentration of O^{2-} decomposed the TiAlN phase (TiN + AlN), the decomposition of TiAlN phase was according to the following reactions:

Reaction 152 $$TiN + O_2 \rightarrow Ti^{4+} + O_2 + \frac{1}{2}N_2$$

Reaction 153 $$AlN + O_2 \rightarrow Al^{3+} + O_2 + \frac{1}{2}N_2$$

And then oxidation of Ti and Al ions occurred:

Reaction 154 $$Ti(s) + O_2(g) \rightarrow TiO_2(s)$$

Reaction 155 $$Al(l) + \frac{3}{2}O_2(g) \rightarrow Al_2O_3(s)$$

The formation of these phases (TiO_2 and Al_2O_3) released free N_2, the free N_2 fluxed from the material **(reactions 152 and 153)**. The mixed oxide scale TiO_2/Al_2O_3 formed according to the thermodynamic calculations, the (ΔG_T^o [J/mole]) for **reactions 20** and **21** was calculated from the **equations LXXXV** and **LXXXVI**:

Equation LXXXV $$\Delta G^o_{TiO2,T} = -910.000 + 173T$$

Equation LXXXVI $$\Delta G^o_{Al2O3,T} = -1676.000 + 320T$$

The calculated values of (ΔG_T^o [J/mole]) formation are given in **table 78**:

ΔG_T^o [J/mole]	T = 1023 K
TiO_2	-733021
Al_2O_3	-1348640

Table 78 The ΔG_T^o formation values at 1023 K for TiO_2 and Al_2O_3 phases

Table 78 shows that the TiO_2 was less favourable in oxidising environment than formation of Al_2O_3; the standard free energy value for TiO_2 is much higher than for Al_2O_3. The SEM and the EDS concentration profiles in **Ch.VI.Sec.1.Figs. 144, 145** confirmed that the Al_2O_3 mainly formed as a top scale. **Figure 253** shows the final stage

of the scale, developed on TiAlN+Al_2O_3 coated alloy after 5000 hours oxidation at 1023 K.

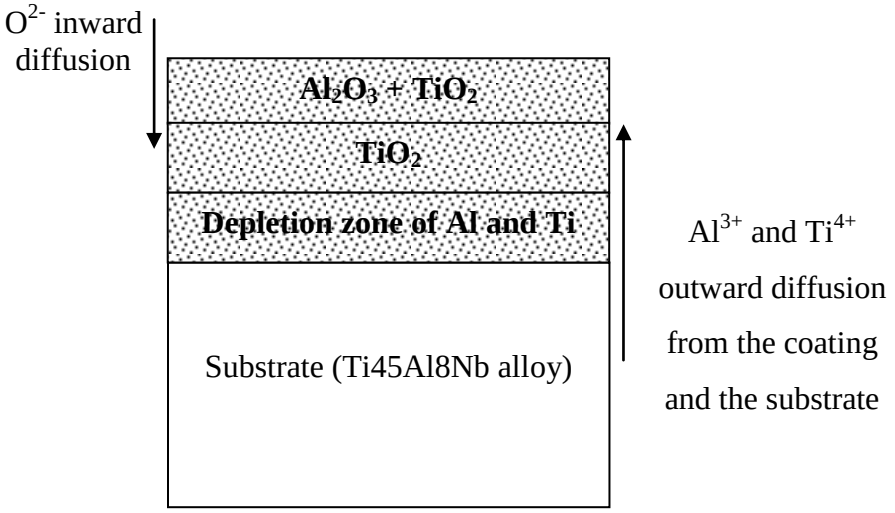

Figure 253 Final scale developed on TiAlYN/CrN+Al_2O_3 coated Ti45Al8Nb alloy in unaffected region at 1023 K for 5000 hours (middle of the sample)

A different situation was observed at the edge of the exposed sample (TiAlN+Al_2O_3 coated alloy) in the SEM micrograph (**Ch.VI.Sec.1.Figs.144, 145).** In the edge of the exposed material the Al_2O_3 phase was also detected as a top layer. The TiN and AlN nitrides also were detected. The lack of decomposition of nitrides on the edges of exposed material can be associated with the higher N_2 pressure in the edges of exposed sample than in the middle part. It can be suggested that in the middle part of the material, the partial pressure of nitrogen was lower. The low partial pressure of N_2 than that of oxygen partial pressure decomposed TiN and AlN layers **(Reactions LXXXV and LXXXVI)**. The nitrogen pressure decreased below the dissociation pressure of TiN, AlN, and TiN and AlN decomposed. The edges of the sample were supported by the higher partial pressure of N_2. The ingress of N_2 (inward diffusion of N_2) sustained the formation of TiN and AlN in the material. The higher partial pressure of N_2 at the edge of the sample, than in the middle part shifted the partial pressure of TiN and AlN above the dissociation partial pressure. When the partial pressure around the edge of exposed sample was enough high (pN_2 = 79033.5 Pa) then TiN and AlN phases are detected in the exposed material, after 5000 hours oxidation at 1023 K.

The final scale developed during 5000 hours oxidation is given in **figure 254**.

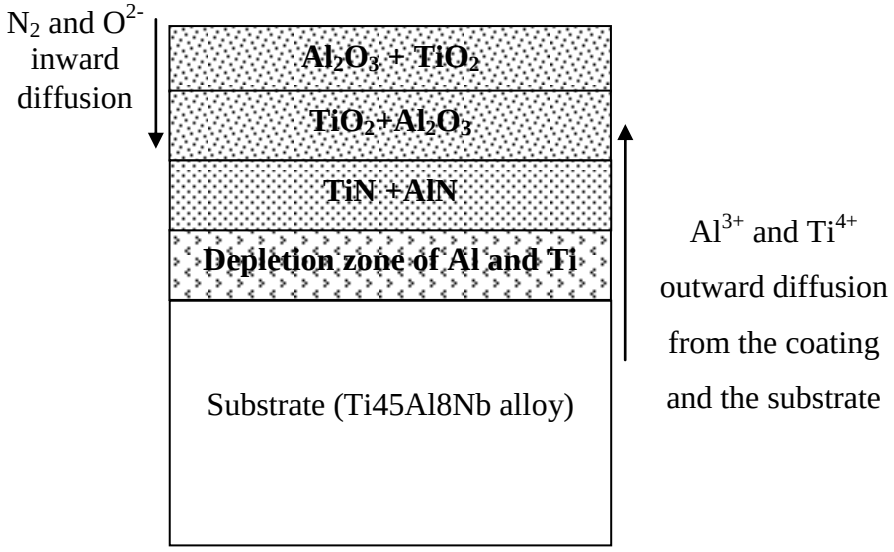

Figure 254 Final scale developed on TiAlYN/CrN+Al_2O_3 coated Ti45Al8Nb alloy in unaffected region at 1023 K for 5000 hours (edge of the sample)

The chemical reactions during exposure of TiAlN+Al_2O_3 coated alloy can be written as follows:

Reaction 156 $\mathrm{Ti(s) + O_2(g) \rightarrow TiO_2(s)}$

Reaction 157 $\mathrm{2Al(l) + \frac{3}{2}O_2(g) \rightarrow Al_2O_3(s)}$

Reaction 158 $\mathrm{Ti + \frac{1}{2}N_2 \rightarrow TiN}$

Reaction 159 $\mathrm{Al + \frac{1}{2}N_2 \rightarrow AlN}$

Based on these reactions the ΔG_T^o [J/mole] for TiO_2, Al_2O_3, TiN, and AlN can be calculated from following equation [180]:

Equation LXXXVII $\Delta G_T^O = A + BT\log T + CT$

The ΔG_T^o of formation for Al_2O_3, TiO_2, TiN, and AlN can be estimated from following equations:

Equation LXXXVIII $$\Delta G^o_{Al2O3,T} = -1676.000 + 320T$$

Equation LXXXIX $$\Delta G^o_{TiO2,T} = -910.000 + 173T$$

Equation XC $$\Delta G^O_{TiN} = -80.250.0 + 22,2T$$

Equation XCI $$\Delta G^O_{AlN} = -77.000 + 22,25T$$

The equilibrium constant of following reactions (**reactions 156 – 159**) can be estimated from the equations below:

Equation XCII $$\Delta G^O_{TiO2} = -RT \ln K = -RT \ln \frac{aTiO_2}{aTi * pO_2}$$

Equation XCIII $$\Delta G^O_{Al2O3} = -RT \ln K = -RT \ln \frac{aAl_2O_3}{aAl * (pO_2)^{3/2}}$$

Equation XCIV $$\Delta G^O_{TiN} = -RT \ln K = -RT \ln \frac{aTiN}{aTi * (pN)^{1/2}}$$

Equation XCV $$\Delta G^O_{AlN} = -RT \ln K = -RT \ln \frac{aAlN}{aAl * (pN)^{1/2}}$$

Where K is equilibrium constant, R – gaseous constant (8,314 J/mol*K), T is temperature (K), a – activity. The calculated ΔG_T^o [J/mole] values from **equation**s **LXXXVIII - XCI** at 1023 K are given in **table 79.**

ΔG_T^o [J/mole]	T = 1023 K
TiO_2	-733021
Al_2O_3	-1348640
TiN	- 240906
AlN	- 227084

Table 79 Calculated free energies of formation (ΔG_T^o [J/mole]) of Al_2O_3, TiO_2, AlN, and TiN at 1023 K

From the calculated ΔG_T^o [J/mole] values, thermodynamics allowed to predict the formation of the phases in the exposed material (TiAlN+Al_2O_3 coated alloy). It was

suggested that the deposited Al_2O_3 top coat inhibited large outward diffusion of Ti form the bulk material. The higher content of N_2 near to the edge of the material sustained TiN, AlN formation. It was observed ((**Ch.VI.Sec.1.Fig. 145)** that the small amounts of TiO_2 formed within the Al_2O_3 oxide. The TiO_2 oxide formed due to the higher diffusion coefficient value at 1023 K (D_{Ti} = 2.99E^{-11} [cm^2/s]) than that for Al **(**D_{Al} = 1.97E^{-12} [cm^2/s]).

Ch.VII.4 Section Three – Sulphidation at 1023 K and 1123 K for 1000 and 675 hours respectively

A brief summary of the materials investigated is given in **table 80** to facilitate interpretation of the results.

Ti42Al15Cr (TiAlCr)	Sulphidation (pO_2 =10^{-18} Pa, pS_2 = 10^{-1} Pa)	T = 1023 K	t = 1000 h
Al_2Au	Sulphidation (pO_2 =10^{-18} Pa, pS_2 = 10^{-1} Pa)	T = 1023 K	t = 1000 h
CrAlYN/CrN+CrAlYON etched by Cr	Sulphidation (pO_2 =10^{-18} Pa, pS_2 = 10^{-1} Pa)	T = 1023 K	t = 1000 h
CrAlYN/CrN+CrAlYON etched by CrAl	Sulphidation (pO_2 =10^{-18} Pa, pS_2 = 10^{-1} Pa)	T = 1023 K	t = 1000 h
CrAlYN/CrN+CrAlYON etched by Y	Sulphidation (pO_2 =10^{-18} Pa, pS_2 = 10^{-1} Pa)	T = 1023 K	t = 1000 h
CrAlYN/CrN coating Y etch, CrAl (thin)	Sulphidation (pO_2 =10^{-18} Pa, pS_2 = 10^{-1} Pa)	T = 1123 K	t = 675 h
CrAlYN/CrN coating, Y etch, CrAlY (thick)	Sulphidation (pO_2 =10^{-18} Pa, pS_2 = 10^{-1} Pa)	T = 1123 K	t = 675 h
CrAlYN/CrN coating Cr etch, CrAl (thin)	Sulphidation (pO_2 =10^{-18} Pa, pS_2 = 10^{-1} Pa)	T = 1123 K	t = 675 h

Table 80 Specimens investigated in sulphidising/oxidising environment

The presented results in **chapter VI section 2** indicate that TiAl based intermetallic alloys produced two types of scales; the structure of formed scales depending on the nature of deposited coating.

The interpretation of these results can be understood in terms of thermodynamic calculations, the thermodynamic discussion needs to be divided into two sub-sections;

subsection one considers discussion on uncoated material and on intermetallic coating while subsection two presents discussion on ceramic coatings.

Ch.VII.4.1 Ti45Al8Nb uncoated material

The degradation of uncoated material in sulphidising environment was associated with following processes: the outward diffusion of Ti, and Al form the bulk material, the formation of a thick TiO_2/Al_2O_3 oxide scale, the ingress of sulphur and sulphides (Al_2S_3, TiS_2, NbS_2) formation in the middle of the scale **(Ch.VI.Sec.2. Fig. 150)**.

The sulphidation of uncoated material (Ti45Al8Nb) in ($H_2/H_2O/H_2S$ with $pO_2 = 10^{-18}$ Pa and $pS_2 = 10^{-1}$ Pa at 1023 K) was associated with the following reactions:

Reaction 160 $$Ti(s) + O_2(g) \rightarrow TiO_2(s)$$

Reaction 161 $$2Al(l) + \frac{3}{2}O_2(g) \rightarrow Al_2O_3(s)$$

Reaction 162 $$2Nb(s) + \frac{5}{2}O_2(g) \rightarrow Nb_2O_5(s)$$

For **reactions 160 – 162** the standard free energy formation (ΔG_T^o [J/mole]) was estimated from following equations:

Equation XCVI $$\Delta G^o_{Al2O3,T} = -1676.000 + 320T$$

Equation XCVII $$\Delta G^o_{TiO2,T} = -910.000 + 173T$$

Equation XCVIII $$\Delta G^o_{Nb2O5,T} = -1920.000 - 120.4T + 800T$$

Also:

Equation XCIX $$\Delta G^O_{TiO2} = -RT \ln K = -RT \ln \frac{aTiO_2}{aTi * pO_2}$$

Equation C $$\Delta G^{O}_{Al2O3} = -RT\ln K = -RT\ln\frac{aAl_2O_3}{aAl*(pO_2)^{3/2}}$$

Equation CI $$\Delta G^{O}_{Nb2O5} = -RT\ln K = -RT\ln\frac{aNb_2O_5}{(aNb)^2*(pO_2)^{5/2}}$$

Where K_{TiO2}, K_{Al2O3}, and K_{Nb2O5} are equilibrium constants for the reactions, under certain pO_2 and pS_2 values the minimum activities for Ti, Al, and Nb to form Al_2O_3, TiO_2, and Nb_2O_5 can be calculated. The calculated values of standard free energy formation (ΔG^{o}_{T} [J/mole]) are given in **table 81** show the preferential formation of oxides $Nb_2O_5 \rightarrow Al_2O_3 \rightarrow TiO_2$. The EDS concentration profiles and EDS X-Ray mapping **(Ch.VI.Sec.2, Figs.150, 151)** showed the formation of Al_2O_3 and TiO_2 on top part of the scale and Nb_2O_5 formation at the scale/substrate interface.

ΔG^{o}_{T} [J/mole]	T = 1023 K
TiO_2	-733021
Al_2O_3	-1348640
Nb_2O_5	-3060031

Table 81 Calculated free energies of formation (ΔG^{o}_{T} [J/mole]) of Al_2O_3, TiO_2, and Nb_2O_5 at 1023 K

It needs to be pointed out that sulphide formation also occurred during sulphidation oxidation exposure **(Ch.VI.Sec.2, Figs.150, 151)**. The chemical reactions of sulphides formation with free energies formation are below:

Reaction 163

$$\Delta G^{o} = -219000\ (J/mole) \qquad 4Al + \frac{3}{2}S_2 \rightarrow 2Al_2S_3 \quad [188]$$

Reaction 164

$$\Delta G^{o} = -293000\ (J/mole)\ Ti + S_2 \rightarrow TiS_2\ [188]$$

Reaction 165

$$\Delta G^{o} = -293076\ (J/mole)\ Nb + S_2 \rightarrow NbS_2\ [188]$$

The equilibrium constants for **reactions 163 - 165** can be written as:

Equation CII
$$\Delta G^{O}_{Al2S3} = -RT \ln K = -RT \ln \frac{(aAl_2S_3)^2}{(aAl)^4 * (pS_2)^{3/2}}$$

Equation CIII
$$\Delta G^{O}_{TiS2} = -RT \ln K = -RT \ln \frac{aTiS_2}{aAl * pS_2}$$

Equation CIV
$$\Delta G^{O}_{NbS2} = -RT \ln K = -RT \ln \frac{aNbS_2}{aNb * pS_2}$$

From equilibrium constant (**equations CII - CIV**) it was possible to calculate activities of Ti and Al which are essential for the formation of Al_2S_3, TiS_2, and NbS_2 sulphides. The calculated values of ΔG^{o}_{T} [J/mole] **(reaction 163 – 165)** for Al_2S_3, TiS_2, and NbS_2 formation indicate that Al, Ti, and Nb sulphides were possible to form.

However during the exposure of uncoated material (Ti45Al8Nb) TiO_2 oxide formed on outer scale, the development of TiO_2, reduced the activity of Ti and increased the activity of Al beneath TiO_2 oxide scale. The increased Al activity led to formation Al_2O_3 underneath the TiO_2 layer. Meanwhile, simultaneously the ingress of oxygen and sulphur through TiO_2, and Al_2O_3 bands occurred. Here the partial pressure of oxygen was much lower than that in ambient sulphidising/oxidising atmosphere ($pO_2 = 10^{-18}$ Pa), thus sulphur from ambient atmosphere diffused inward and is likely reacted with Ti and Al from the substrate (Ti45Al8Nb).

From thermodynamical point of view, the formation of NbS_2 is the most favourable than TiS_2 and Al_2S_3 (the lowest ΔG^{o}_{T} [J/mole] **(reaction 163 – 165)** value for NbS_2 than for Al_2S_3 and TiS_2) this observation via thermodynamic calculations **(reactions 163, 164** and **165)** are also confirmed by the EDS X-Ray mapping (**Ch.VI.Sec.2.Fig. 151)**.

It was observed that $NbAl_3$ did not form within the scale formed on uncoated alloy (Ti45Al8Nb), however, the Nb ions was introduced to alloy in order to decrease the number of defects in TiO_2, Nb also has a beneficial influence for a thermodynamic activity (increases Al activity) of Al, and finally Nb decreases the solubility of oxygen in the subjected alloy.

At 1123 K the uncoated material suffered sulphidation degradation at 1123 K for 675 hours in a similar way (a multilayered scale formed consisted of TiO_2 and Al_2O_3 alternative layers) as at 1023 K for 1000 hours sulphidation. However more alternative layers were formed at 1123 K than at 1023 K, it is suggested that higher temperature (1123 K) mainly supported the development of alternative layers of TiO_2 and Al_2O_3 [181,182,183]. The sulphidation mechanism of degradation of uncoated material (Ti45Al8Nb) was discussed.

Ch.VII.4.2 TiAlCr and Al_2Au coated alloy

The degradation of TiAlCr (Ti42Al15Cr) and Al_2Au materials was accompanied by the following processes: the formation of a thick TiO_2 outer scale, the ingress of sulphur and oxygen to the scale, the formation of sulphides/oxide region, $NbAl_3$ formation within the scale.

The high affinity titanium and aluminium for oxygen led to the formation of an outer layer of TiO_2 beneath which Al_2O_3 layer developed [184]. The development of TiO_2 layer led to the depletion of Ti increasing the aluminium activity beneath the TiO_2 layer which promoted the formation of Al_2O_3 layer by the ingress of oxygen species through the TiO_2. The thermodynamic calculations of the formation TiO_2 and Al_2O_3 have been presented by the **reactions 160** and **161**.

The sulphur and oxygen ions diffused through both oxides (TiO_2 and Al_2O_3) and reached the interface between TiO_2 and the coating. Here the oxygen partial pressure was lower than that on the external environment. This was again favourable the formation of TiO_2 due to reduction of Al activity.

The formation of TiO_2 again reduced the Ti activity beneath this TiO_2 layer. Here the oxygen partial pressure was not high enough to form aluminium oxide, as a

result an Al - enriched layer $NbAl_3$ developed (Al_2Au coated Ti45Al8Nb alloy – **(Ch.VI.Sec.2.Figs.16, 17, 18).** Additionally the formation of $NbAl_3$ band in Al_2Au coated alloy formed was promoted by the Ti depletion near at the scale/coating interface, caused by the outward diffusion of Ti to the outer part of the scale.

Moreover sulphur ions migrated inward through TiO_2, Al_2O_3 phases and reached the interface between the formed scale and the substrate. Thermodynamic calculations for Al, Ti, and Nb sulphides formation have been presented by the **reactions 163** and **165**. Also Cr_2S_3 formation was observed to occur, according to the following reaction:

Reaction 166 $$4Cr + \frac{3}{2}S_2 \rightarrow 2Cr_2S_3$$

$\Delta G^o = -135000(J/mole)$ [188]

The thick scales in both coated materials had a similar structure, in the case of Al_2Au coated Ti45Al8Nb phases were; $TiO_2/Al_2O_3/TiO_2$ (TiS_2) /$NbAl_3$/modified coating/substrate in the case of TiAlCr coated Ti45Al8Nb phases were: $TiO_2/Al_2O_3/TiO_2/TiS_2/Cr_2S_3$/substrate **(ChVI.Sec.2.Fig 161)**. In TiAlCr coated Ti45Al8Nb coating was transformed and consumed during the sulphidation test at 1023 K **(ChVI.Sec.2.Fig 155, 156)**.

The presence of Nb is believed to decrease the concentration of oxygen vacancies in an oxide scale (TiO_2), and slows down the diffusion transport through oxide scale to the substrate. The high concentration on Nb near the modified coating/substrate interface might reduce the outward diffusion transport of Ti and slow down the oxidation process. TiO_2 is semiconductor n-type and contains the interstitials based on Ti^{3+} and Ti^{4+} existing together with doubly ionized oxygen vacancies [185]. Karake et al. indicated that the doubly ionised oxygen vacancies are responsible for kinetic rate of growth TiO_2 scale over Ti, thus, any dopant element in the titanium oxide scale (TiO_2) that is able to minimize the concentration of these vacancies will reduce the oxidation rate [186]. Nb atoms substitute the Ti site in the TiO_2 lattice, reducing the number of interstitial oxygen ion vacancies in the oxide [187]. The reduced number of defects protects is expected to decrease the ingress of aggressive agents (sulphur, hydrogen) to the formed scale, and improves high temperature resistance.

It is also important to note in this instance the number of phases (layers) developed during experiments was strongly dependent on the time of exposure. Increasing exposure time led to an increase in the number and thickness of the layers. It was observed that these layers contained other phases/elements **(Ch.VI.Sec.2.Figs.155, 156, 157, 161, 162, and 163)**.

Ch.VII.4.3 Ceramic coatings at 1023 and 1123 K

Ceramic coatings at 1023 K

1) CrAlYN/CrN+CrAlYON coated Ti45Al8Nb etched by Cr

2) CrAlYN/CrN+CrAlYON coated Ti45Al8Nb etched by CrAl

3) CrAlYN/CrN+CrAlYON coated Ti45Al8Nb etched by Y

Ceramic coating at 1123 K

4) CrAlYN/CrN coating Y etch, CrAl (thin) coated Ti45Al8Nb

5) CrAlYN/CrN coating Cr etch, CrAl (thin) coated Ti45Al8Nb

6) CrAlYN/CrN coating, Y etch, CrAlY (thick) coated Ti45Al8Nb

The degradation of ceramic coatings was mainly associated with the development of two regions; unaffected, affected.

The unaffected regions developed a thin (1 μm) Al_2O_3/Cr_2O_3 scale due to Al, Cr outward diffusion and inward diffusion of O_2 from the ambient atmosphere. Underneath the Cr, Al oxide scale, the deposited coating was observed. Beneath the protective coating, the region with a large amount of oxygen (25 at%) and sulphur (10 at%) with Al, Cr, and Ti ions developed.

The affected regions (**(ChVI.Sec.2.Fig 172, 173)** were associated with crack formation during the cooling periods, the outward diffusion of Ti from the bulk material, the ingress of oxygen and sulphur to the material, the formation of TiO_2 non protective scale at cracked areas, the formation of the sulphides (Al_2S_3, TiS_2) under the deposited coating, the depletion zones of Ti at cracked places and the formation of $NbAl_3$ phase at depletion zones.

The observed formation of the scale structure in affected region **(Ch.VI.Sec.2.Figs. 193, 194, 195)** consisted of: TiO_2/Thin Al_2O_3 layer/TiO_2/Chromium titanium thin layer/Modified coating/less dense Al_2O_3 oxide and sulphides region(TiS_2, Al_2S_3, NbS_2)/$NbAl_3$/Substrate (Ti45Al8Nb) can be explained in following way.

The outward diffusion of Ti through the crack **(yellow circle Ch.VI.Sec.2.Fig.193)** led to the development a TiO_2 outer scale and caused Ti depletion within the substrate under the deposited coating (EDS concentration profiles in **(Ch.VI.Sec.2.Fig.194).** A thin layer of Al_2O_3 developed within a thick (17 μm) TiO_2 outer layer. It can be suggested that the outward diffusion of Al was associated with the diffusion of Ti ions (when activity of Ti became lower than the activity of Al became higher). The depletion zone which was observed under the deposited coating was rich in Al, O, S, and Nb elements (see maps of Al, S_2, and Nb in **(Ch.VI.Sec.2.Fig.195).** The presence of a high concentration region of oxygen due to the inward diffusion of oxygen developed an internal oxidation region under the deposited coating. The presence of internal oxidation region was confirmed by EDS X-Ray mapping given in **Ch.VI.Sec.2.Fig.195.** Mapping was performed in affected region where coating failed).

The deposited multilayered nano-coatings showed a reasonably good sulphidation/oxidation resistance at 1023 K and 1123 K. However, the degradation of these coatings was mainly related to the mechanical properties or to thermal resistance of these coatings. All exposed coatings showed a lack of resistance to thermal cycles; cracks formed in all exposed samples at 1023 and 1123 K in sulphidation/oxidation atmosphere. The cracks formation was the key point influencing the sulphidation/oxidation resistance of these materials. The sulphidation/oxidation behaviour of the ceramic coatings exposed at 1023 K and 1123 K can be interpreted also in terms of thermodynamic.

The thermodynamic interpretation of the scale degradation in the affected region was related to the formation of non – protective and porous TiO_2 oxide in the places where coating cracked. The high affinity of Ti to oxygen, even in low pO_2 ($pO_2 = 10^{-18}$ Pa) led to the formation of TiO_2 oxide, however, when TiO_2 oxide is forming, the Ti activity decreased, and the activity of Al increased leading to the formation of Al_2O_3

within the porous TiO_2 oxide scale. The r**eactions 167** and **177** show the formation of the porous and non-protective scale:

Reaction 167 $$Ti(s) + O_2(g) \rightarrow TiO_2(s)$$

Reaction 168 $$2\,Al(l) + \frac{3}{2}O_2(g) \rightarrow Al_2O_3(s)$$

Equation CV $$\Delta G^{o}_{TiO2,T} = -910.000 + 173T$$

Equation CVI $$\Delta G^{o}_{Al2O3,T} = -1676.000 + 320T$$

Also:

Equation CVII $$\Delta G^{O}_{TiO\,2} = -RT \ln K = -RT \ln \frac{aTiO_2}{aTi * pO_2}$$

Equation CVIII $$\Delta G^{O}_{Al2O3} = -RT \ln K = -RT \ln \frac{aAl_2O_3}{aAl * (pO_2)^{3/2}}$$

The values of ΔG^{o}_{T} [J/mole] are given in **table 82**:

ΔG^{o}_{T} [J/mole]	T = 1023 K	T = 1123 K
TiO_2	-733021	-715721
Al_2O_3	-1348640	-1316640

Table 82 The standard free energies of TiO_2 and Al_2O_3 in sulphidation/oxidation environment at 1023 – 1123 K

Further exposure to sulphidation/oxidation atmosphere led to the depletion of Ti form the bulk material (Ti45Al8Nb) due to the outward diffusion of Ti. However it was observed that the depletion zone of Ti was filled by the oxygen and sulphur diffused inward, the inward diffusion of oxygen and sulphur formed the internal oxidation and sulphidation region, where mainly Al_2O_3 and NbS_2 formed (**Ch.VI.Sec.2.Fig.195).**

ΔG_T^o [J/mole]	T = 1023 K	T = 1123 K
NbS_2	-314010 [188]	-293076[188]
Al_2O_3	-1348640 [188]	-1316640 [188]

Table 83 The standard free energies of NbS_2 and Al_2O_3 in sulphidation/oxidation environment at 1023 – 1123 K

It also was observed that beside Nb_2S and Al_2O_3 in the internal oxidation/sulphidation region Al_2S_3 was detected. The formation of Al_2S_3 is related to the high amount of sulphur in the internal part of the formed scale and high affinity of sulphur to aluminium. Thus when Ti diffused outward then high concentration of S_2 in the depletion zone of Ti which diffused inward, formed Al_2S_3, the formation of Al_2S_3 can be described by the following **reaction 169**:

Reaction 169 $$4\,Al + \frac{3}{2}S_2 \rightarrow 2\,Al_2S_3$$

The final structure of the scale developed during sulphidation/oxidation test of ceramic coated TiAl intermetallic alloy is shown in **figure 255:**

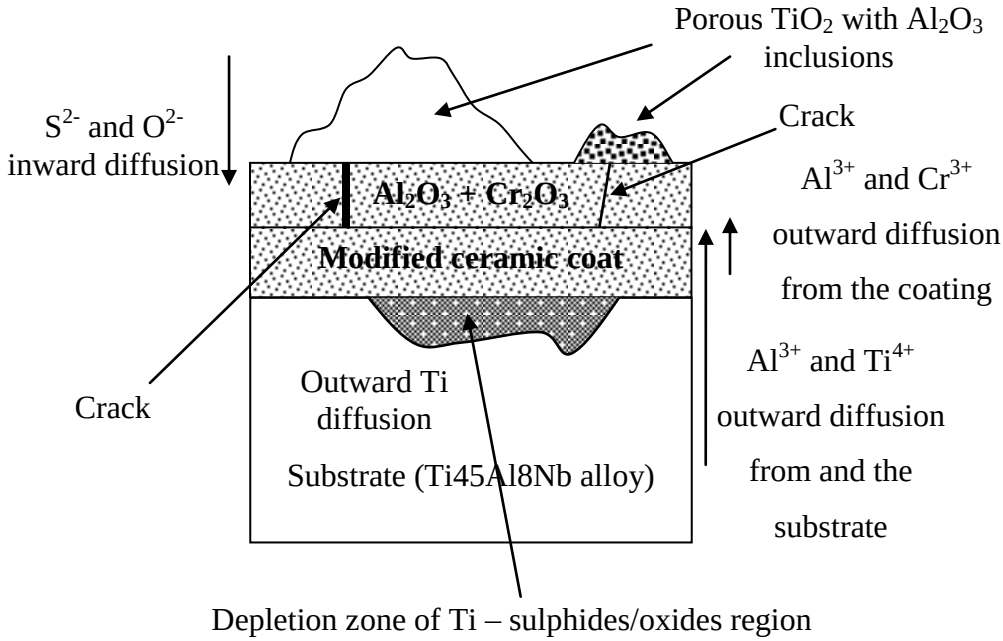

Figure 255 The final stage of sulphidation/oxidation of ceramic coated alloy at 1023 and 1123 K – affected region by crack formation

The thermodynamical interpretation of the results from unaffected region was related to the formation of Al_2O_3 and Cr_2O_3 phases, these phases formed according to the following reactions:

Reaction 170 $$2\,Al(l) + \frac{3}{2}O_2(g) \rightarrow Al_2O_3(s)$$

Reaction 171 $$2Cr(s) + \frac{3}{2}O_2(g) \rightarrow Cr_2O_3(s)$$

For both reactions (**reactions 170, 171**) it is possible to calculate standard free energy of formation, according to equations below:

Equation CIX $$\Delta G^{o}_{Al2O3,T} = -1676.000 + 320T$$

Equation CX $$\Delta G^{o}_{Cr2O3,T} = -1121015.7 + 383.72T$$

Table 84 shows the calculated values form **equations CIX** and **CX**

ΔG^{o}_{T} [J/mole]	T = 1023 K)	T = 1123 K
Al_2O_3	-1348640	-1316640
Cr_2O_3	-728470	-690097

Table 84 The standard free energies of formation for Cr_2O_3 and Al_2O_3 in sulphidation/oxidation atmosphere at 1023 – 1123 K

It is suggested based on above calculations that the Al_2O_3 should formed first, because Cr_2O_3 free energy formation has a higher value than that for Al_2O_3, additionally the lower value of diffusion coefficient for Al favourable Al_2O_3 formation, than Cr_2O_3 formation. Diffusion coefficients for Al and Cr are presented in **table 85**.

Diffusion coefficient [cm^2/s]		
Temperature [K]	D_{Al}	D_{Cr}
1023	$1.97E^{-12}$	$8.12E^{-13}$
1123	$2.03E^{-11}$	$8.18E^{-12}$

Table 85 Diffusion coefficients of Al and Cr at temperature range 1023 – 1123 K

The formation of Al decreased the activity of Al in the deposited coating; this decrease led to the formation of Cr_2O_3 oxide. The initial structure of scale development in unaffected ceramic coating is shown by a schematic diagram in **figure 256**.

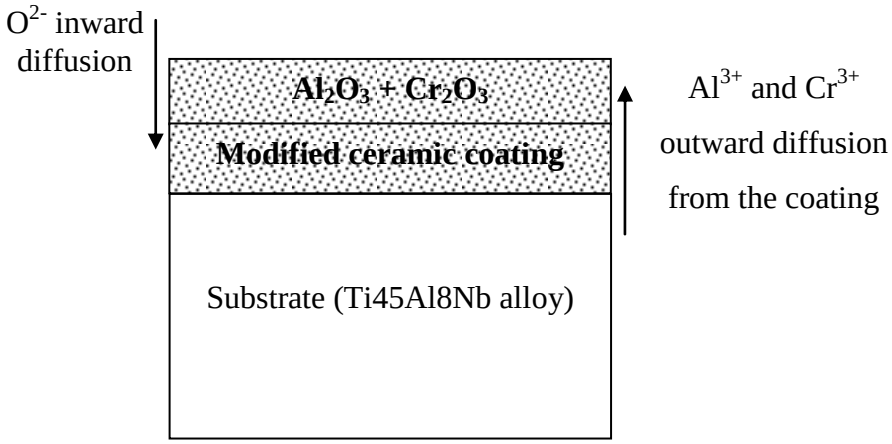

Figure 256 The initial stage of sulphidation/oxidation of ceramic coated alloy at 1023 and 1123 K – unaffected region

It was also observed that despite of the formation Al_2O_3 and Cr_2O_3 in the unaffected region, sulphur and oxygen diffused inward underneath the deposited coating **(Ch.VI.Sec.2.Figs.196, 197)** probably through the micro-cracks. The inward diffusion of sulphur and oxygen formed the observed oxide/sulphides zone underneath the coating **(Ch.VI.Sec.2.Figs.196, 197)**. The oxide/sulphide formation can be expressed by following observations.

Within this zone, oxide would form first due to the higher affinity Al and Ti and Cr to oxygen than to sulphur. When the activities of Ti, Al, and Cr decreased then sulphides of Cr and Al and Ti would form in order $TiS_2 \rightarrow Al_2S_3 \rightarrow Cr_2S_3$. The calculated values of ΔG_T^o [J/mole] are presented in **table 86**.

ΔG_T^o [J/mole]	T = 1023 K	T = 1123 K
Al_2O_3	-1348640	-1316640
Cr_2O_3	-728470	-690097
TiO_2	-733021	-715721
TiS_2	-293000 [188]	-268000 [188]
Cr_2S_3	-135000 [40]	-101000 [188]
Al_2S_3	-219000 [40]	-191000 [188]

Table 86 The standard free energies for oxides and sulphides in sulphidation/oxidation atmosphere at 1023 – 1123 K

The micro-cracks can be also formed due to the formation of sulphide/oxide formation. During formation of oxides and sulphides, formed compounds enlarge own size due to the chemical reactions between metallic ions and gaseous spices:

Reaction 172 $4\,Al + \frac{3}{2}S_2 \rightarrow 2\,Al_2S_3$

Reaction 173 $4Cr + \frac{3}{2}S_2 \rightarrow 2Cr_2S_3$

Reaction 174 $Ti(s) + S_2(g) \rightarrow TiO_2(s)$

Reaction 175 $Ti(s) + O_2(g) \rightarrow TiO_2(s)$

Reaction 176 $2\,Al(l) + \frac{3}{2}O_2(g) \rightarrow Al_2O_3(s)$

Reaction 177 $2Cr(s) + \frac{3}{2}O_2(g) \rightarrow Cr_2O_3(s)$

The formation of the final scale of unaffected region is presented in **figure 257**:

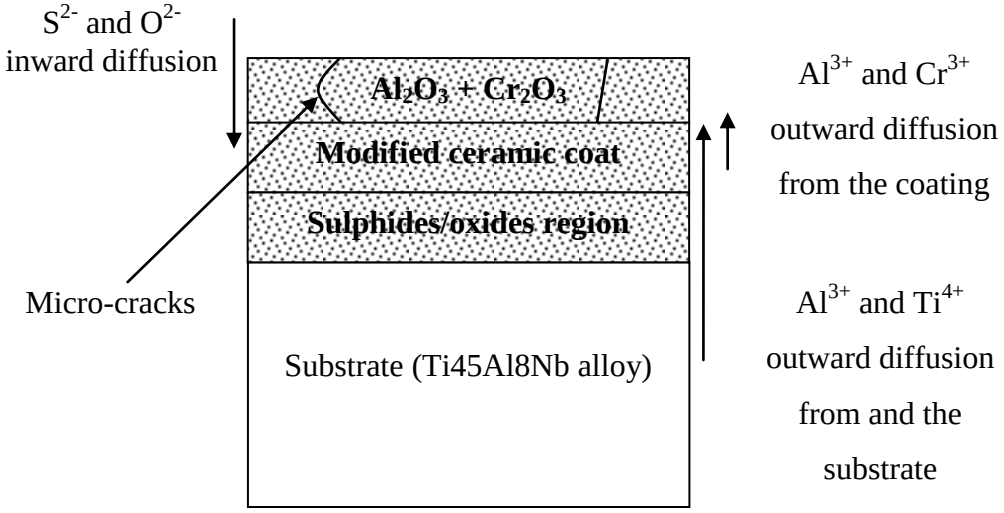

Figure 257 The final stage of sulphidation/oxidation of ceramic coated alloy at 1023 and 1123 K – unaffected region

Ch.VII.5 Section Four – Hot corrosion in 20%NaCl/80%Na_2SO_4 for 150 hours at 1023 K

Ch.VII.5.1 TiAlN+Al_2O_3 coated Ti45Al8Nb alloy

The degradation of TiAlN+Al_2O_3 (Ti25Al50N) top coated Ti45Al8Nb in hot corrosion atmosphere was associated with the formation of two regions: affected contained: TiO_2 top oxide scale, Al_2O_3 oxide scale (top coat deposited prior to experiment), the substrate (Ti45Al8Nb alloy **(Ch.VI.Sec.3.Figs.205, 206, and 209)**. and unaffected region consisted of: Al_2O_3 top oxide scale, the modified coating (TiAlN + Al_2O_3), the substrate (Ti45Al8Nb) **(Ch.VI.Sec.3.Figs.207, 208, and 210)**.

The affected region by the crack formation allowed the ingress of oxygen and sulphur by the inward diffusion, and the development of a thick and non protective oxide scale (TiO_2).

The thermodynamic interpretation of the scale degradation on TiAlN+Al_2O_3 top coat was related mainly to the formation of non – protective and porous TiO_2 oxide in the places where coating cracked.

It was also suggested that melted slats 20%NaCl and 80%Na_2SO_4 (the melting point of these salts is around 973 K) accelerated the degradation and cracking processes (formation of volatile chlorides, formation of defected sulphides). The released Na^+ Cl^-, S^{2-}, and O^{2-} ions from the reactions below:

Reaction 178 $Na_2SO_4 \rightarrow 2Na^+ + SO_4^{2-}$

Reaction 179 $SO_4^{2-} \rightarrow S^{2-} + 4O^{2-}$

Reaction 180 $NaCl \rightarrow Na^+ + Cl^-$

The released ions diffused inward (Na^+ Cl^-, S^{2-}, and O^{2-}) and reacted with the oxide scale (TiO_2, Al_2O_3) developed in the initial stage of exposure, (when temperature was rising), The Al_2O_3, and TiO_2 oxide formed according to the following reactions:

Reaction 181 $2\,Al(l) + \frac{3}{2}O_2(g) \rightarrow Al_2O_3(s)$

Reaction 182 $Ti(s) + O_2(g) \rightarrow TiO_2(s)$

The high affinity of Ti to oxygen and lower diffusion coefficient than that of Al **(Table 87)** produced the TiO_2 oxide.

Diffusion coefficient [cm^2/s]		
Temperature [K]	D_{Al}	D_{Ti}
1023	$1.97E^{-12}$	$2.99E^{-11}$

Table 87 Diffusion coefficients for Ti and Al at 1023 K

The formation of TiO_2 oxide caused decrease in the Ti activity, here Al activity increased and leading to the formation of Al_2O_3 oxide. The initial stage of degradation of $TiAlN+Al_2O_3$ top coat material is shown in figure below:

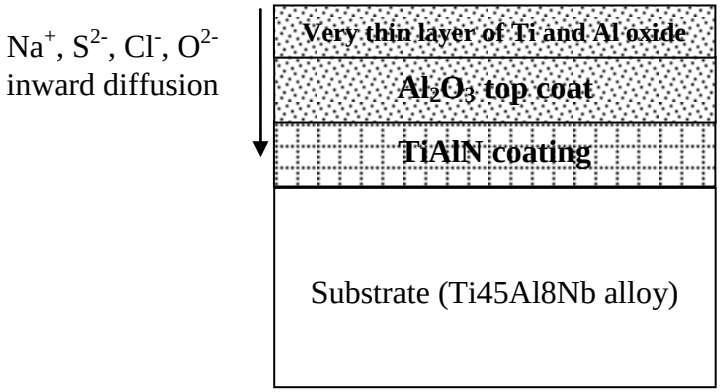

Figure 258 Initial stage of hot corrosion/oxidation degradation of $TiAlN+Al_2O_3$ top coat material at 1023 K

The formed Al_2O_3 and TiO_2 phases undergo further reactions with released ions (Na^+) according to the reactions below:

Reaction 183 $4TiO_2 + 2Na_2O + O_2(gas) \rightarrow 4NaTiO_4$

Reaction 184 $2Al_2O_3 + 2Na_2O + O_2(gas) \rightarrow 4NaAlO_2$

Additionally the released chlorine ions (Cl^-) from decomposition of NaCl salt **(reaction 180)** reacted with the products of **reactions 186 and 187**.

Reaction 185 $$2NaTiO_4 + 2Cl_2 \rightarrow 2TiCl_4 + 2TiCl_2 + Na_2O + \frac{1}{2}O_2 + 3O_2$$

Reaction 186 $$2NaAlO_2 + 3Cl_2 \rightarrow 2AlCl_3 + Na_2O + \frac{3}{2}O_2$$

The highly volatile chlorides formed during **reactions 185** and **186**, decomposed and again Ti and Al reacted with oxygen (pO_2 = 21278.25 Pa) to produced oxides (as on **reactions 181** and **182**).

In the same time S^{2-} from **reaction 179** reacted with Ti, and Al, in order to form sulphides:

Reaction 187 $$2Al + 3S^{2-} \rightarrow Al_2S_3$$

Reaction 188 $$Ti + S^{2-} \rightarrow TiS_2$$

The **reactions 183 – 188** associated with cooling down periods generated strains, the generated strains caused that the top coat (Al_2O_3) cracked. In this moment the outward diffusion of Ti (lower diffusion coefficient than that for Al **(Tables 69, 70)** developed a thick non protective scale **(Ch.VI.Sec.3.Figs.204, 205)**. **Equations CXI and CXII** show the thermodynamic calculations of ΔG_T^o [J/mole] for the **reactions 181 and 182**.

Equation CXI $$\Delta G^o_{TiO2,T} = -910.000 + 173T$$

Equation CXII $$\Delta G^o_{Al2O3,T} = -1676.000 + 320T$$

The values of ΔG_T^o [J/mole] are given in **table 88**:

ΔG_T^o [J/mole]	T = 1023 K
TiO_2	-733021
Al_2O_3	-1348640

Table 88 The standard free energies of TiO_2 and Al_2O_3 in hot corrosion/oxidation environment at 1023 K

The minimum activity of Ti and Al to form TiO_2 and Al_2O_3 can be calculated from equations below:

Equation CXIII $$\Delta G^{O}_{TiO_2} = -RT \ln K = -RT \ln \frac{aTiO_2}{aTi * pO_2}$$

Equation CXIV $$\Delta G^{O}_{Al_2O_3} = -RT \ln K = -RT \ln \frac{aAl_2O_3}{aAl * (pO_2)^{3/2}}$$

Table 89 shows the calculated minimum activity of $Ti^{4+}$and Al^{3+} ions at 1023 K [179].

Activity	T = 1023 K
a_{Al}	$1.2x10^{-35}$
a_{Ti}	$3.8x10^{-37}$

Table 89 The minimum activities of Ti and Al to form TiO_2 and Al_2O_3 in 0.21 atmosphere of oxygen partial pressure at 1023 K

Thus the outward diffusion of Ti decreased the activity of Ti, here Al activity increased and Al_2O_3 formed. Additionally the depletion zone formed underneath the deposited coating (**(Ch.VI.Sec.3.Figs.204, 205)** allowed the ingress of O^{2-} ions. The final stage of the exposed TiAlN+Al_2O_3 top coat coated Ti45Al8Nb alloy is given in **figure 259**.

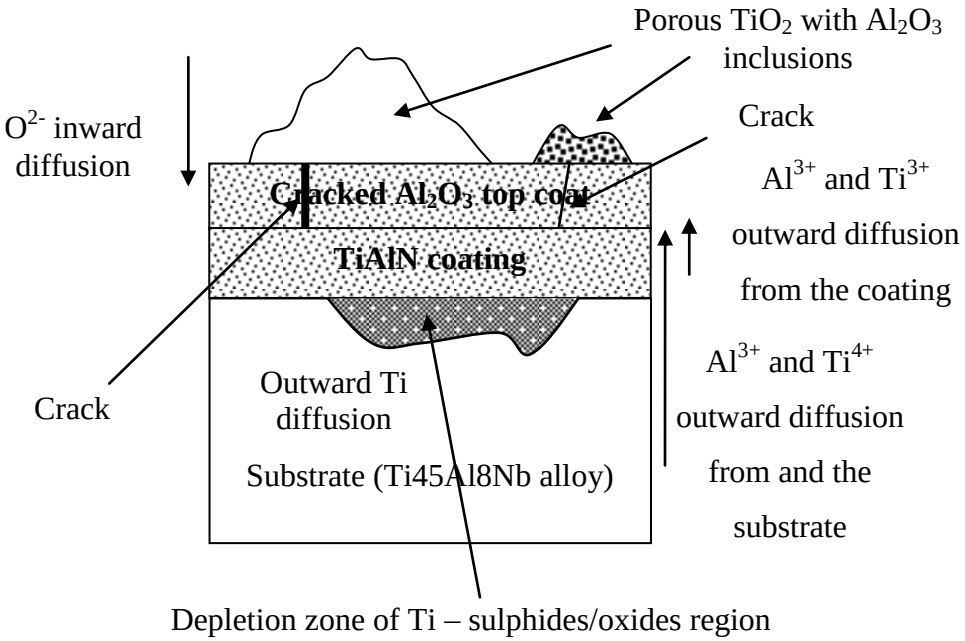

Figure 259 Final stage of exposure of TiAlN+Al_2O_3 coated Ti45Al8Nb alloy during hot corrosion test at 1023 K – affected region by crack formation

The unaffected region of exposed TiAlN+Al_2O_3 top coat coated Ti45Al8Nb material **(Ch.VI.Sec.3.Figs. 207, 208, 210)** presented excellent resistance for hot corrosion degradation in salt mixture (20%NaCl/80%Na_2SO_4) at 1023 K after 150 hours of exposure. However it was observed that some places in intact deposited coat presented micro-crack formation **(yellow circle Ch.VI.Sec.3.Fig.207).** Is suggested here, that these micro-cracks are responsible for the crack formation, cased the degradation of the exposed material. The presence of micro-cracks is related mainly to the mismatch in thermal expansion coefficient between Al_2O_3 top coat and TiAlN deposited coating; however these micro-cracks did not influence the resistance against hot corrosion at 1023 K. The cross – section concentration profiles and the EDS X-Ray profiles presented in **Ch.VI.Sec.3.Fig.208, 210** respectively, revealed that lack of inward diffusion of Na, S_2, and Cl_2 was observed, only oxygen diffused inward and reached the TiAlN coating.

However despite of excellent high temperature corrosion resistance in unaffected places, the exposed material showed relatively poor mechanical properties. Underneath the Al_2O_3 top coat a very fragile structure of TiAlN + Al_2O_3 and TiO_2 phases was observed **Ch.VI.Sec.3.Fig.207, 208, 210**. The fragile structure, underneath the deposited top coat was associated with SEM cross – section sample preparation. The kinetic data did not show any spallation **(Ch.VI.Sec.3.Fig.202).** A schematic diagram of unaffected region is given in **figure 260**:

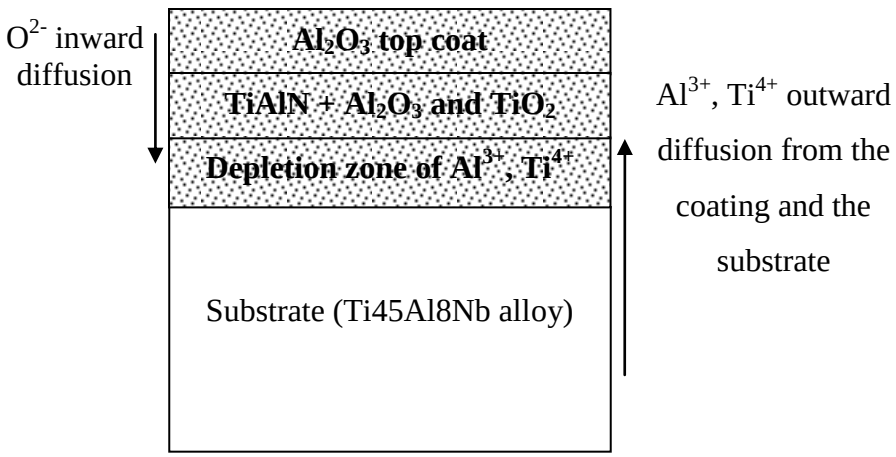

Figure 260 Final stage of exposure of TiAlN+Al_2O_3 coated Ti45Al8Nb alloy during hot corrosion test at 1023 K – unaffected region by crack formation

Ch.VII.5.2 CrAl2%YN coated Ti45Al8Nb alloy

The hot corrosion environment caused the degradation of exposed material (CrAl2%YN coated Ti45Al8Nb alloy) in two different ways; 1) the lack of protection, and scale spallation form the edges of the material **(Ch.VI.Sec.3.Figs.211E, 211F, Table 52),** this spallation allowed the ingress of sulphur, chlorine, and sodium under the coating (**(Ch.VI.Sec.3.Figs.215, 216).**

It is suggested here that mismatch of thermal coefficients between alloy and coating promoted the crack formation and scale spallation and caused the inferior corrosion. Also it is suggested here that the suspended sample during hot corrosion test suffered corrosion attack on the edges due to the large amount of salt which accommodated on the edges whereas temperature was raised. The large amounts of salt on the edge of the sample significantly accelerated the degradation of the material.

The development of protective Al_2O_3/Cr_2O_3 scale in the middle part of the material which protects material against aggressive environment at 1023 K **(Ch.VI.Sec.3.Figs.211A, 211B, Table 52)**

The mechanism of the scale degradation on CrAl2%YN coated alloy can be presented in following way; **figures 261** shows the initial stage of scale development on the edges of the material exposed to hot corrosion (20%NaCl80%Na_2SO_4) environment at 1023 K for 150 hours.

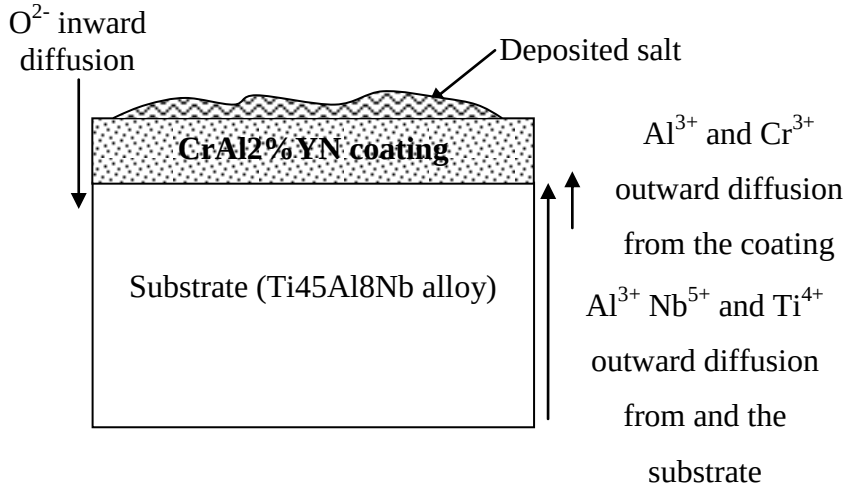

Figure 261 Initial stage of exposure of CrAl2%YN coated Ti45Al8Nb alloy during hot corrosion test at 1023 K

When the sample was exposed the melted salt released the Na^+ Cl^-, S^{2-}, and O^{2-} ions, according to the following reactions:

Reaction 189 $Na_2SO_4 \rightarrow 2Na^+ + SO_4^{2-}$

Reaction 190 $SO_4^{2-} \rightarrow \frac{1}{2}S_2 + 4O^{2-}$

Reaction 191 $NaCl \rightarrow Na^+ + Cl^-$

These ions diffused inward through the liquid salt and reacted with the oxide scale developed in the initial stage of exposure, when temperature was rising, Al_2O_3, and Cr_2O_3 oxide formed, according to the following reactions:

Reaction 192 $2Al(l) + \frac{3}{2}O_2(g) \rightarrow Al_2O_3(s)$

Reaction 193 $2Cr(s) + \frac{3}{2}O_2(g) \rightarrow Cr_2O_3(s)$

The Al_2O_3 formed first then Cr_2O_3 phase because ΔG_T^o [J/mole] value of the formation of Al_2O_3 is much lower than that for Cr_2O_3.

ΔG_T^o [J/mole]	T = 1023 K
Al_2O_3	-1348640
Cr_2O_3	-728470

Table 90 Value of ΔG_T^o [J/mole] formation for Al_2O_3 and Cr_2O_3 at 1023 K

Additionally the diffusion coefficient of Al is one order of magnitude higher than that for Cr **(Tables 69 and 71)**. The released ions (Na^+ and O^{2-}) reacted with Al and Cr oxides according to the following reactions:

Reaction 194 $2Cr_2O_3 + 2Na_2O + O_2(gas) \rightarrow 4NaCrO_2 + O_2$

Reaction 195 $2Al_2O_3 + 2Na_2O + O_2(gas) \rightarrow 4NaAlO_2 + O_2$

Additionally the released chlorine during decomposition of NaCl salt **(reaction 191)** also reacted with reaction products (chromate, aluminate – **reactions 196, 197**).

Reaction 196 $$2NaAlO_2 + \frac{3}{2}Cl_2 \rightarrow AlCl_3 + Na_2O + \frac{3}{2}O_2$$

Reaction 197 $$2NaCrO_2 + \frac{3}{2}Cl_2 \rightarrow 2CrCl_3 + Na_2O + \frac{3}{2}O_2$$

The highly volatile chlorides formed during **reactions 196 and 197** decomposed and released Cr and Al ions and again these ions (Cr and Al) reacted with oxygen (pO_2 = 21278.25 Pa) to produce oxides **(as on reactions 192 and 193).**

At the same time, S_2 released from decomposed SO_2 or SO_3 **(reaction198)** reacted with Cr, and Al to form sulphides in the outer part of the scale, where partial pressure of sulphur was high enough:

Reaction 198 $$4Al + \frac{3}{2}S_2 \rightarrow 2Al_2S_3$$

$$\Delta G^o = -219000\ (J/mole)$$

Reaction 199 $$2Cr + \frac{2}{3}S_2 \rightarrow Cr_2S_3$$

$$\Delta G^o = -135000\ (J/mole)$$

The higher value ΔG_T^o [J/mole] formation for Al than that of Cr sulphide (**reaction 198 and 199)** suggest that the Al_2S_3 formed first (lower value of ΔG_T^o than that for Cr sulphide (Cr_2S_3)). It was observed that the development of sulphides supported the degradation of the material which produced brittle scale, which easily spalled off from the material (**Ch.VI.Sec.3.Fig.215).**

The final stage of the CrAl2%YN material exposed to hot corrosion (20%NaCl/80%Na_2SO_4) from two different places are shown in a schematic models in **figures 262** and **263**.

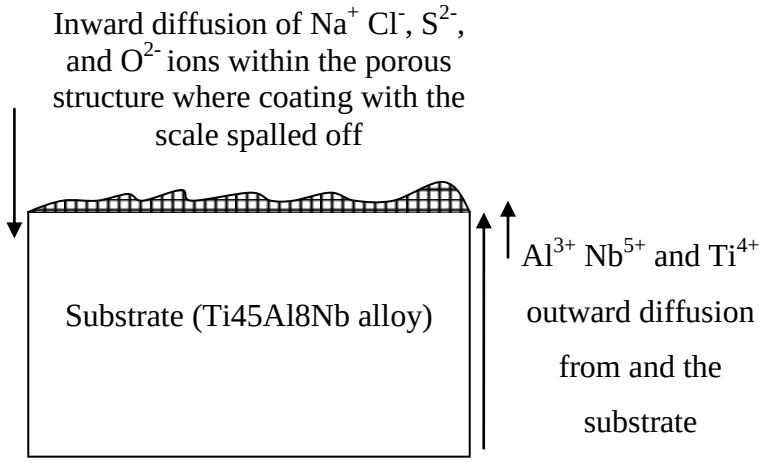

Figure 262 Final stage of exposed CrAl2%YN coated Ti45Al8Nb alloy during hot corrosion test at 1023 K – edge of the material

The middle part of the sample developed highly protective scale consisted of Al_2O_3 and Cr_2O_3. The formation of Al_2O_3, and Cr_2O_3 oxide was related to the following reactions:

Reaction 200 $$2\,Al(l) + \frac{3}{2}O_2(g) \rightarrow Al_2O_3(s)$$

Reaction 201 $$2Cr(s) + \frac{3}{2}O_2(g) \rightarrow Cr_2O_3(s)$$

The Al_2O_3 formed first then Cr_2O_3 phase because ΔG_T^o [J/mole] value of the formation of Al_2O_3 is much lower than that for Cr_2O_3.

ΔG_T^o [J/mole]	T = 1023 K
Al_2O_3	-1348640
Cr_2O_3	-728470

Table 91 Value of ΔG_T^o [J/mole] formation for Al_2O_3 and Cr_2O_3 at 1023 K

Additionally the diffusion coefficient of Al is one order of magnitude higher than that for Cr **(Tables 69 and 71)**. The regions where protective scale formed did not underwent further reactions. The final scale of exposed CrAl2%YN coated Ti45Al8Nb

material is given in **figure 228**. However between the coating and the substrate the region with poor adhesion developed **(Ch.VI.Sec3.Fig.213).** The slope of the mass gain which has been observed **(Ch.VI.Sec3.Fig.202)** for this material was mainly related to the spallation occurred from the edges of the exposed material.

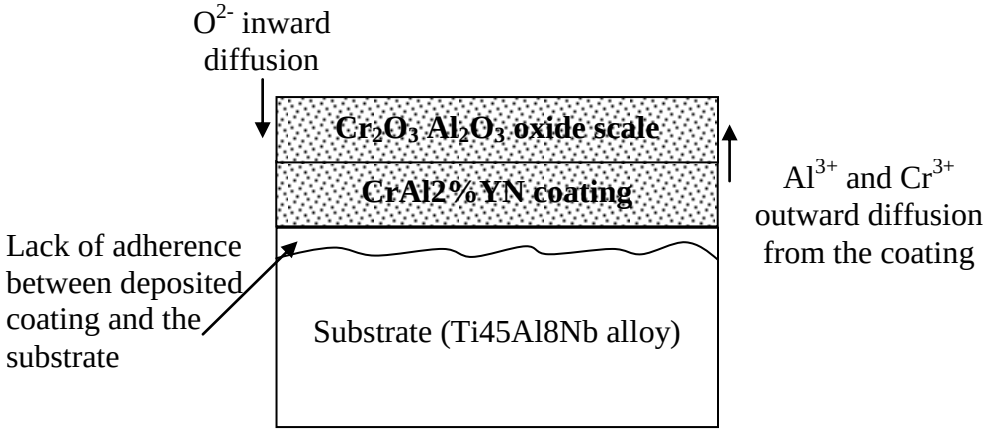

Figure 263 Final stage of exposure of CrAl2%YN coated Ti45Al8Nb alloy during hot corrosion test at 1023 K – middle of the material

Ch.VII.5.3 TiAlYN/CrN+Al_2O_3 coated Ti45Al8Nb

The degradation of the material TiAlYN/CrN+Al_2O_3 coated Ti45Al8Nb was associated with: crack formation in different areas of the material, the cracks allowing for the ingress of S^{2-}, Cl^-, and O^{2-} ions, volatile chlorides, caused the crack formation, the outward diffusion of Ti produced TiO_2 scale in affected regions.

Similar to pervious coatings the TiAlN+Al_2O_3 top coat and the CrAl2%YN coated Ti45Al8Nb developed two regions, affected and unaffected.

The unaffected region was protected by Al_2O_3 deposited during manufacture of the material **(Ch.VI.Sec.3.Figs. 225)**. However other parts of the exposed material showed the development of non protective TiO_2 oxide scale. The scale formed due to the outward diffusion of Ti from the bulk material. The crack formation in the top coat (Al_2O_3) allowed the mass transport; the inward diffusion of O_2 form the atmosphere, and the outward diffusion if Ti from bulk material **(Ch.VI.Sec.3.Figs. 221, 223).** Additionally the presence of highly volatile chlorine caused scale spallation.

The formation of TiO_2 in affected regions of the exposed material can be explained from thermodynamic point of view. The formation of TiO_2 phase was less favourable than formation of Al_2O_3 scale **(table 92** shows the ΔG_T^o [J/mole] values**)**, however the diffusion coefficient for Ti promotes oxidation of Ti **(table 93)**. When the TiO_2 formed, the activity of Ti decreased, here Al activity increased and Al_2O_3 formed. It was observed additionally that porous scale (TiO_2) accommodated large amounts of Na **(Ch.VI.Sec.3.Fig. 222).**

ΔG_T^o [J/mole]	T = 1023 K
TiO_2	-733021
Al_2O_3	-1348640

Table 92 The standard free energies of TiO_2 and Al_2O_3 in sulphidation/oxidation environment at 1023 K

Diffusion coefficient [cm^2/s]		
Temperature [K]	D_{Al}	D_{Ti}
1023	$1.97E^{-12}$	$2.99E^{-11}$

Table 93 Diffusion coefficients for Ti and Al at 1023 K

Figures 264 and **265** show the final stage of the exposed material TiAlYN /CrN+Al_2O_3 coated Ti45Al8Nb after hot corrosion test at 1023 K in the affected and in the unaffected regions respectively.

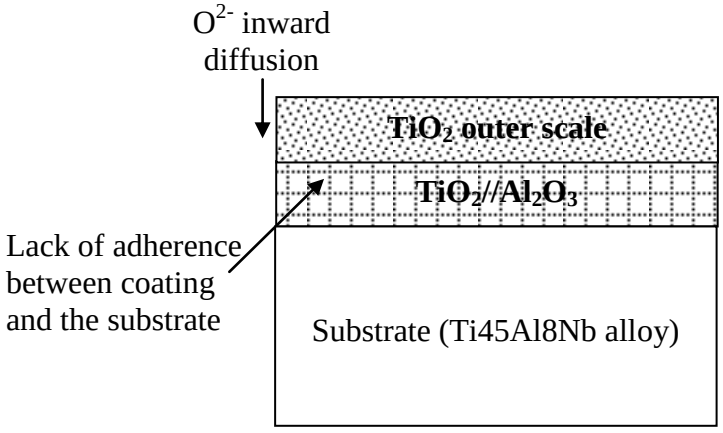

Figure 264 Final stage of exposure of TiAlYN/CrN+Al_2O_3 coated Ti45Al8Nb alloy during hot corrosion test at 1023 K – affected region

It needs to be pointed out, that the crack formation in affected regions caused by the aggressive atmosphere (salt mixture 20%NaCl/80%Na_2SO_4) and the reaction which took place during exposure supported with cooling down cycles decomposed TiN and CrN layers. These layers were not detected during micro-structural investigations (EDS, EDS X-Ray mapping) **(Ch.VI.Sec.3.Fig.227, 228).**

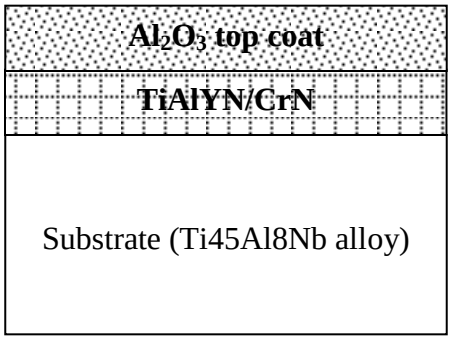

Figure 265 Final stage of exposure of TiAlYN/CrN+Al_2O_3 coated Ti45Al8Nb alloy during hot corrosion test at 1023 K – unaffected region

The unaffected region was characterized with the coating protecting the material (Al_2O_3 top coat) and inhibiting the mass transport between ambient atmosphere, salt mixture and the substrate **(Ch.VI.Sec.3.Fig.225, 226).**

Chapter VIII - Conclusions and Future Work

Ch.VIII.1 Oxidation (static air) at 1023 - 1223 K for 500 hours

Ch.VIII.1.1 TiAlCrY coated Ti45Al8Nb alloy – oxidation at 1023 K for 500 hours

TiAlCrY (Ti55Al14Cr0.3Y) coated Ti45Al8Nb after 500 hours oxidation at temperature 1023 K developed an oxide scale consisting of TiO_2, Al_2O_3, and Cr_2O_3 consistent with thermodynamic and kinetic factors **(Ch.VI.Sec.1.3. Fig.90, Ch.VII.2, Table 66)**. The developed scale showing good adhesion between oxide scale/coating and coating/substrate prevented spallation. The scale structure consisted of: 1) Al/Ti/Cr oxide scale, 2) Modified coating (TiAlCrY) and depletion zone of Ti and Al, 3) Pre-depletion zone of Ti and Al 4) Substrate (Ti45Al8Nb alloy). The kinetic data (kp = $3.51304E^{-10}$ [$mg^2/cm^4/s$], and the morphology indicate good corrosion behaviour.

Ch.VIII.1.2 TiAlCrY coated Ti45Al8Nb alloy – oxidation at 1123 K for 500 hours

At higher temperature (1123 K) after 500 hours oxidation TiAlCrY (Ti55Al14Cr0.3Y) material shows similar behaviour as that at 1023 K; however only two oxides developed: TiO_2, Al_2O_3. The Cr_2O_3 oxide did not form in the outer part of the scale but in the deeper region some presence of Cr_2O_3 oxide was observed. Thus the formed scale consisted of: 1) TiO_2 and Al_2O_3 oxide top scale, 2) Ti/Al/Cr oxide region, 3) Coating (TiAlCrY) and depletion zone of Ti and Al, 4) Substrate (Ti45Al8Nb) **(Ch.VI.Sec.1.5. Fig.108)**.The kinetic data is equivalent to kp = $1.08145E^{-09}$ [$mg^2/cm^4/s$]. Additionally voids and cracks appeared in the oxide scale showed poor oxidation resistance.

Ch.VIII.1.3 TiAlCrY (Ti55Al14Cr0.3Y) coated Ti45Al8Nb alloy – oxidation at 1223 K for 500 hours

Oxidation tests at 1223 K for 500 hours showed, that only TiO_2, Al_2O_3 phases developed **(Ch.VI.Sec.1.7. Fig.118)**. The absence of Cr_2O_3 was probably caused by the instability of Cr_2O_3 at this temperature. The formation of a large amount of TiO_2 was due to the oxidation of Ti form the coating and from the substrate with the cracks formed. The kinetic data (kp = 1.18304E^{-08} [mg^2/cm^4/s].

Ch.VIII.1.4 CrAl2%YN coated Ti45Al8Nb alloy at 1023 K

CrAl2%YN coatings exposed to oxidising environment at 1023 K for 500 hours developed a protective Al_2O_3 and Cr_2O_3 scale consistent with thermodynamic predictions **(Ch.VII.2.4, Table 73)**. A TiN phase formed at the coating/substrate interface played a role in improving the oxidation resistance, by inhibiting the outward diffusion of Ti form the substrate. The structure of the scale developed consisted of: 1) Al and Cr oxide scale, 2) Modified coating (CrAl2%YN), 3) Ceramic layers (TiN, AlN) and depletion zone of Ti and Al, 4) Substrate (Ti45Al8Nb alloy) **(Ch.VI.Sec.1.4. Figs. 101, 102, 103)**. The kinetic data was equivalent to: kp = 9.71493E^{-12} [mg^2/cm^4/s].

Ch.VIII.1.5 CrAl2%YN coated Ti45Al8Nb alloy – oxidation at 1123 K for 500 hours

Oxidation at higher temperature (1123 K) for 500 hours revealed that CrAl2%YN coating also developed protective phases: Al_2O_3 and Cr_2O_3. The thickness of the developed oxide scale was larger than that at lower temperature (1023 K) – 1µm at 1023 K, and 2,5 µm at 1123 K **(Ch.VI.Sec.1.4. Fig. 102, Ch.VI.Sec.1.6. Fig. 113 respectively)**. Additionally TiN layer formed at the coating/substrate interface also was thicker than that at 1023 K – 2,5 µm at 1023 K, and 5 µm at 1123 K **(Ch.VI.Sec.1.4.**

Fig. 102, Ch.VI.Sec.1.6. Fig. 113 respectively). The scale formed contained: 1) Cr_2O_3 and Al_2O_3 oxides scale

2) Modified coating (CrAl2%YN, 3) TiN layer, 4) Substrate (Ti45Al8Nb alloy), kp = $5.88475E^{-10}$ [$mg^2/cm^4/s$].

Ch.VIII.1.6 CrAl2%YN coated Ti45Al8Nb alloy – oxidation at 1223 K

Oxidation at 1223 K showed, that CrAl2%YN coating was unable to protect effectively the material against oxidation at this temperature. A thick non protective scale formed consisted alternate layers consisted of TiO_2 and Al_2O_3. The total thickness of the oxide scale formed at 1223 K was equivalent to around 95 µm – 1µm at 1023 K), and 2,5 µm at 1123 K **(Ch.VI.Sec.1.8. Fig. 123)** Additionally in the oxide scale Cr_2O_3 was not detected as well as TiN layer was absent at the coating/substrate interface, kp = $4.64201E^{-07}$ [$mg^2/cm^4/s$].

Ch.VIII.2 Oxidation (static air) at 1023 K for 5000 hours

Ch.VIII.2.1 TiAlCr coated Ti45Al8Nb alloy – oxidation for 5000 hours at 1023 K

Oxidation of TiAlCr (Ti42Al15Cr) coated alloy at 1023 K for 5000 hours led to the formation a multilayered scale (– 1µm at 1023 K), and 2,5 µm at 1123 K **(Ch.VI.Sec.1.10. Fig. 127)**. The oxide scale formed consisted of: TiO_2//TiO_2/Al_2O_3 //Al_2O_3// TiO_2// Al_2O_3//TiO_2 /diffusion zone of Al and Ti//substrate (Ti45Al8Nb alloy) with trace amounts of Cr **(Ch.VI.Sec.1.10. Fig. 129)**. Additionally some parts of the exposed sample lost part or parts of the outer scale indicating weakness in these parts in terms of brittleness and lack of adhesion. This behaviour indicates that the oxide scale formed had a tendency to spallation and revealing its poor mechanical properties

Ch.VIII.2.2 TiAlYN/CrN+Al_2O_3 coated Ti45Al8Nb alloy – oxidation for 5000 hours at 1023 K

The long term oxidation experiment (5000 hours) performed at 1023 K indicates that the material corroded in two different ways; some part of the exposed material formed a multilayered oxide scale, consisting of: Al_2O_3 layer with TiO_2 oxide inclusions/TiO_2 layer with Al_2O_3 oxide inclusions//TiO_2/Al_2O_3 oxide layer/diffusion zone/TiAl layer/Ti_2Al layer/substrate (Ti45Al8Nb alloy) - **(Ch.VI.Sec.1.11. Fig. 136, 137)**. These structures were formed due to the crack formation in the Al_2O_3 deposited prior to oxidation experiment. These areas of the sample easily spalled off from the material during cutting process and showed brittle structure. Excellent high temperature oxidation behaviour was achieved where Al_2O_3 phase was not cracked. In these places Al_2O_3 protected the material and no corrosion products were detected **(Ch.VI.Sec.1.11. Fig. 138, 139)**. Additionally due to the protectivity of Al_2O_3 deposited layer, the outward diffusion of Ti ions were inhibited, and because of this, TiN layer formed in the coating/substrate interface.

Ch.VIII.2.3 TiAlN + Al_2O_3 coated Ti45Al8Nb alloy – oxidation for 5000 hours at 1023 K

The high temperature oxidation of TiAlN (Ti25Al50N)+Al_2O_3 coated Ti45Al8Nb alloy, shows that after 5000 hours at 1023 K, good oxidation resistance was achieved due to the Al_2O_3 top coat deposited prior to experiment (kp = 5.068E^{-09} [mg^2/cm^4/s]). However the exposed material showed the development of a multilayered structure in some places consisting of Al_2O_3 oxide layer//Al_2O_3/TiO_2 oxide layer/modified coating (TiAlN)/diffusion zone of Al and Ti/substrate (Ti45Al8Nb alloy) **(Ch.VI.Sec.1.12. Fig. 141, 142, 143)**. In other areas of the exposed material, some parts of the outer part of the oxide scale spalled off indicating that the coating was very brittle and adherence between layers within the coating was poor. **(Ch.VI.Sec.1.12. Fig. 144, 145).**

Ch.VIII.3 Sulphidation ($pO_2 = 10^{-18}$ Pa, $pS_2 = 10^{-1}$ Pa) at 1023 K for 1000 hours

Ch.VIII.3.1 Ti45Al8Nb uncoated alloy

The uncoated material exposed to sulphidation atmosphere, showed the development of a thick and multilayered scale consisting of: 1) Titanium oxide (TiO_2), 2) Titanium /aluminium oxide layer with sulphur inclusions 3) diffusion zone of Al and Ti, 4) Substrate (Ti45Al8Nb - **(Ch.VI.Sec.2.4 Fig. 149, 150)**.

The formed scale showed lack of adherence, and porous structure with tendency to the crack formation **(Ch.VI.Sec.2.4 Fig. 148, 149)**. Thus sulphidation resistance of the uncoated material was poor (kp = $1.48E^{-07}$ [$mg^2/cm^4/s$].

Ch.VIII.3.2 TiAlCr coated Ti45Al8Nb alloy

TiAlCr (Ti42Al15Cr) coated Ti45Al8Nb after 1000 hours sulphidation test in sulphidized atmosphere showed the formation of a scale with a multilayer structure: $TiO_2/Al_2O_3/TiO_2/TiS/NbAl_3$ layer/diffusion zone of Al and Ti/substrate (Ti45Al8Nb). The formed thick scale developed cracks; additionally the lack of adherence appeared between the substrate and the formed scale, which iondicated poor sulphidation resistance **(Ch.VI.Sec.2.5 Fig. 154, 155, 156)**, kp = $2.11E^{-07}$ [$mg^2/cm^4/s$].

Ch.VIII.3.3 Al_2Au coated Ti45Al8Nb

Al_2Au coating on Ti45Al8Nb alloy exposed to highly sulphidized atmosphere revealed that the scale formed, consisted of TiO_2 crystals. Similar to that formed in TiAlCr material a porous scale with poor adhesion developed with a multilayered structure: $TiO_2/Al_2O_3/$ $TiS/TiO_2/NbAl_3$ /modified coating (Al_2Au)/diffusion zone of Ti/substrate (Ti45Al8Nb) **(Ch.VI.Sec.2.6 Fig. 161, 162)**. The poor sulphidation resistance of this coating was due to the formation of a thick scale, where kp value is equivalent to: kp = $1.68E^{-07}$ [$mg^2/cm^4/s$].

Ch.VIII.3.4 CrAlYN/CrN+CrAlYON coated Ti45Al8Nb alloy etched by Cr

The coating exposed to sulphidation atmosphere ($pO_2 = 10^{-18}$ Pa, $pS_2 = 10^{-1}$ Pa) at 1023 K for 1000 hours showed the development of different regions undergoing various degrees of attack **(Ch.VI.Sec.2.7 Fig. 167, Table 45)**. In the unaffected regions the coating remained intact. The affected regions showed the formation of cracks where TiO_2 formed due to the outward diffusion of Ti^{4+} ions from the bulk material. The kinetic data shows that the kp value of exposed sample was much lower than that in Al_2Au (kp = $1.68E^{-07}$ [$mg^2/cm^4/s$]) and in TiAlCr coated material (kp = $2.11E^{-07}$ [$mg^2/cm^4/s$].). kp = $5.21E^{-09}$ [$mg^2/cm^4/s$]

Ch.VIII.3.5 CrAlYN/CrN+CrAlYON coated Ti45Al8Nb alloy etched by CrAl

A similar morphology, and scale structure was observed in CrAlYN/CrN+CrAlYON coated Ti45Al8Nb alloy etched by CrAl after 1000 hours sulphidation where corrosion pattern was uneven **(Ch.VI.Sec.2.8 Fig. 171, Table 46)**. The exposed sample showed the presence of both unaffected (not corroded) and affected (corroded) areas. The corroded places formed a multilayered scale consisted of: TiO_2/Cr_2S_3+ Cr_2O_3 with Ti inclusions/modified coating/ceramic bond (TiAlN)/substrate (Ti45Al8Nb). The crack formation in the coating allowed outward diffusion of Ti from the substrate leading to the formation of the observed TiO_2 phase. The kinetic data shows that kp value for CrAl etched sample was similar to that of the previous sample (Cr etched) and was equivalent to: kp = $1.90E^{-09}$ [$mg^2/cm^4/s$]

Ch.VIII.3.6 CrAlYN/CrN+CrAlYON coated Ti45Al8Nb alloy etched by Y

Sulphidation of CrAlYN/CrN+CrAlYON coated Ti45Al8Nb alloy etched by Y in high partial pressure of sulphur ($pS_2 = 10^{-1}$ Pa) and low partial pressure of oxygen ($pO_2 = 10^{-18}$ Pa) showed similar structure and similar behaviour as those observed in the above samples. The exposed material displayed an excellent sulphidation resistance (no corrosion products) where coating was not cracked **(Ch.VI.Sec.2.9 Fig. 178)**. However in other places, where coating cracked (mismatch in thermal coefficients between the coating and the substrate), a multilayered structure developed, consisting of: TiO_2 with sublayer of chromium sulphide (Cr_2S_3) and chromium oxide (Cr_2O_3)/modified coating/aluminium rich region/substrate (Ti45Al8Nb), kp = $6.09E^{-09}$ [$mg^2/cm^4/s$]

Ch.VIII.4 Sulphidation ($pO_2 = 10^{-18}$ Pa, $pS_2 = 10^{-1}$ Pa) at 1123 K for 675 hours

Ch.VIII.4.1 Ti45Al8Nb uncoated

The uncoated material (Ti45Al8Nb alloy) exposed to the higher temperature in the same sulphidation conditions, showed the development of a porous and multilayered scale which consisted of: $TiO_2/Al_2O_3/TiO_2/Al_2O_3$/substrate (Ti45Al8Nb) with poor sulphidation resistance **(Ch.VI.Sec.2.12 Fig. 187, 188, 189)**, kp = $1.4x10^{-07}$ [mg^2/cm^4s^{-1}].

Ch.VIII.4.2 CrAlYN/CrN coating Y etch, CrAl (thin) coated Ti45Al8Nb, CrAlYN/CrN coating, Y etch, CrAlY (thick), CrAlYN/CrN coating Cr etch, CrAl (thin)

All three materials subjected to sulphidation atmosphere (T = 1123 K) t = 675 hours) corroded in the same way (**(Ch.VI.Sec.2.13, Table 49).** The crack formation significantly increased the corrosion processes and a thick non protective TiO_2 outer scale formed. However some parts of the sample showed superior corrosion resistance, due to the development a highly protective Al_2O_3 and Cr_2O_3 scale. The kp values for exposed material were:

1) CrAlYN/CrN coating Y etch, CrAl (thin) coated Ti45Al8Nb (2ah22), kp = $3.6x10^{-09}$ [mg^2/cm^4s^{-1}]
2) CrAlYN/CrN coating Cr etch, CrAl (thin) coated Ti45Al8Nb (2ah23), kp = $2.6x10^{-09}$ [mg^2/cm^4s^{-1}]
3) CrAlYN/CrN coating, Y etch, CrAlY (thick) coated Ti45Al8Nb (2ah24), kp = $5.6x10^{-10}$ [mg^2/cm^4s^{-1}]

Ch.VIII.5 Hot corrosion (20%NaCl/80%Na_2SO_4) at 1023 K for 150 hours

Ch.VIII.5.1 TiAlN + Al_2O_3 coated Ti45Al8Nb

Hot corrosion investigation on TiAlN (Ti25Al50N) + Al_2O_3 coated Ti45Al8Nb showed that the material after exposure developed two different regions; unaffected and affected **(Ch.VI.Sec.3.3 Figs. 203, 204)**. The unaffected region was covered by the Al_2O_3 (deposited prior experiment) scale **(Ch.VI.Sec.3.3 Figs. 207, 208)**. However the sample also developed regions where cracks developed. The cracked Al_2O_3 top coated support the development of a non protective TiO_2 oxide scale (outward diffusion Ti form the bulk material) **(Ch.VI.Sec.3.3 Figs. 205 206).**

Ch.VIII.5.2 CrAl2%YN coated Ti45Al8Nb

The high rate of the corrosion degradation was observed in CrAl2%YN coated intermetallic alloy in hot corrosion environment. Especially the edges of the sample lost adherence and spalled off from the base material. The middle parts of the exposed material showed relatively good corrosion resistance and developed a Al_2O_3 and Cr_2O_3 mixed scale **(Ch.VI.Sec.3.4 Figs. 213, 214,).**

Ch.VIII.5.3 TiAlYN/CrN+Al_2O_3 coated Ti45Al8Nb

The exposure of TiAlYN/CrN+Al_2O_3 coated Ti45Al8Nb material to hot corrosion atmosphere showed various regions which developed. Some regions exhibited excellent corrosion behaviour (Al_2O_3 deposited prior experiment prevented corrosion degradation), some parts of the sample indicated, that the outer scale (Al_2O_3) was vanished from the material, a non protective TiO_2 scale was formed. Additionally the exposed sample showed lack or poor adherence between the deposited coating and the substrate in places where Al_2O_3 top coat was destroyed **(Ch.VI.Sec.3.5 Figs. 220)**.

Ch.VIII.6 Interdiffusion modelling by Generalized Darken's Method (GDM)

This represented a novel aspect of the thesis. This is the first time when interdiffusion modelling by GDM has been applied to multicomponent TiAl intermetallic systems.

The exposed material TiAlCrY (Ti55Al14Cr0.3Y) coated Ti45Al8Nb alloy after 500 hours oxidation (static air)) at 1023 and 1123 K was modeled in order to predict the interdiffusion between the coating and the substrate **(Ch.II.Sec.4.2).**

Agreements between the experimental and the calculated concentration profiles were generally reasonable; some profiles show good agreement, some profiles not.

The observed reasonable agreement between the experimental and calculated experimental and simulated concentration profiles appeared in Al, Ti, and Cr at both

temperatures. A very good agreement has been achieved for Nb between the experimental and modelled concentration profiles at temperatures.

Ch.VIII.7 Suggestions of the future work

Much success has been archived in understanding the properties and behaviour of TiAl based intermetallics. Improved understanding has been achieved on the corrosion behaviour of coated TiAl based intermetallics. New methods of producing new generation of coatings to protect these materials against high temperature degradation have been devised.

This research has allowed to identify certain areas for future investigations. Suggestions for future work are categorised under following headings:

Ch.VIII.7.1 Deposition of Coatings and Compositions

Further improvements in deposition techniques are recommended. Interplay between various processing parameters (bias voltage, pN_2, pAr, current density, temperature, deposition time) needs to be further researched. Here plasma modelling is expected to play a critical role. Regarding the coating composition, several issues needs to be further considered. Based on the present results, it can be said that the amount of protective elements (Al, Cr) needs to be increased in such a way, that their participation in protective scale formation is increased.

Consideration can be given to the incorporation of Si in the coating as SiO_2 is a protective oxide against high temperature corrosion. Consideration should be also given to incorporate rare earth elements (Y, Hf, and Ce) in the coating composition to enhance the scale/coating adhesion (integrity of the coating, crack inhibition). The use of diffusional barrier to minimize coating/substrate interdiffusion needs further investigations. To extend the use of these coatings for blades protection in aerospace, new coatings, with thermal barrier needs to be considered.

Ch.VIII.7.2 High Temperature Corrosion Studies

High temperature corrosion studies need to be extended to include, different environments, with different pO_2, pS_2 ratio and gas mixtures (sulphidation processes), water vapor, pure oxygen (oxidation processes), different salt mixture (hot corrosion processes) and a wider range of temperatures.

Ch.VIII.7.3 Structural Analyses

Analyses need to be carried out at the nanoscale using Scanning Tunnelling Microscope (STM), Scanning Tunnelling Spectroscopy (STS) which will provide detailed information on the initial stage of scale formation and scale growth. Additionally XPS (X-Ray Photoelectron Spectroscopy) is essential to investigate the kinetic energy distribution of the emitted photoelectrons, and to study the composition and electronic state of the surface region of a sample.

Ch.VIII.7.4 Modelling

In the area of modelling, new modelling techniques need to be considered; Genetic Algorithm with Numerical Techniques using the 3x3 diffusion coefficient matrix $\begin{bmatrix} D_{11} & D_{12} & D_{13} \\ D_{21} & D_{22} & D_{23} \\ D_{31} & D_{32} & D_{33} \end{bmatrix}$ under three different conditions:

a) Constant diagonal terms

b) Constant diagonal and cross – terms

c) Variable diagonal and cross – terms (where the terms were considered composition dependent)

Ch.VIII.7.5 General Summary of the results achieved

The aim of this project was to investigate the TiAl alloy (Ti45Al8Nb) coated with intermetallic and ceramic bond coatings. The high temperature corrosion tests were carried out at a temperature above 923 K for various periods of time. In general coated Ti45Al8Nb material showed poor behaviour at a high temperature (1023 K) and long exposure time (5000 hours). Oxidation for a shorter period of time (500 hours) showed that at 1023 K and 1123 K, coated material (Ti45Al8Nb coated CrAl2%YN) revealed good oxidation behaviour (due to the formation of highly protective Cr_2O_3 and Al_2O_3 oxides). However at 1223 K coated material (Ti45Al8Nb coated CrAl2%YN), showed very poor resistance, due to the development of a thick and non-protective scale (TiO_2 – Al_2O_3 alternative layers). Intermetallic coating (TiAlCrY) showed good high temperature behaviour only at 1023 K.

The sulphidation experiments were carried out only on the ceramic, multilayer nano-coatings (uncoated material (Ti45Al8Nb alloys has been used as a reference sample only). The test showed that all ceramic samples developed a thin Al_2O_3 – Cr_2O_3 oxide layer. This layer protected the material against the sulphidation environment. The bottleneck of these coatings was their brittleness, where the coating cracked during cooling periods. Some benefits were achieved, when the coating contained Y ions, the crack formation was inhibited but not eliminated.

In hot corrosion environment at 1023 K, all coated materials showed poor corrosion behaviour due to the spallation and formation of non protective oxides.

Thus the TiAl alloys possess small density and other advantages, however the high temperature corrosion is the weak side of these alloys and they can be used only at lower temperatures (<1023 K).

References – PhD Thesis Tomasz Dudziak

1 Per Kofstad, High Temperature Corrosion, Springer; 1 edition, (1988)

2 http://www.doitpoms.ac.uk/tlplib/recycling-metals/ellingham.php?printable=1

3 S.Mrowec, T.Weber, Korozja Gazowa Metali, wydawnictwo Slask, (1967)

4 G. Tamman, anorg. allg. Chem. 111, (1920), 78

5 L. Czerski, S. Mrowec, T.Weber, Rocznik Chemiczny. 33, 763

6 P.K Datta, H.L. Du, J.S Burnell Gray, ASM Handbook, Corrosion Materials, Vol. 13B ASM International, (2002), pp.490 – 510,

7 ASM Handbook, Corrosion Materials, Vol. 13B ASM International, (2002)

8 J.R. Davis, Stainless Steels, ASM Speciality Handbook, ASM Materials Park, OH, (1994)

9 G.Granaud, R.A. Rapp, Oxidation of Metals, Vol. 11, (1977), 193

10 L.Himmel, R.T. Mehel, C.E. Birchenall, Journal of Metals, 5, (1953), 827,

11 S.MAtsunaga, T.Homma, Oxidation of Metals, Vol. 10, (1976), 193

12 W.Wegener, G.Borchardt, Oxidation of Metals, Vol. 36, (1991), 339

13 R.C.Lobb, H.E.Evans, Metal Science, (1981), 267

14 D.R.Baer, M.D.Merz, Metalurgicall Transactions A, (1980) 11A, (1973)

15 F.J.Perez, F.Pedraza, C.Sanz, M.P.Hierro, C.Gomez, Materials and Corrosion, 53, (2002), 231,

16 R.J.Hussey, M.Cohen, Corrosion Science, 11, (1971), 713

17 Gerald E. Wasielewski and Robert A. Rapp, "*High Temperature Oxidation," in "The Superalloys*", edited by C.S. Sims and W. Hagel, John Wiley & Sons, Inc. (1972), pp. 287-317

18 G.S. Giggins and F.S. Pettit, Trans. Met. Soc. AIME, 245, (1969), pp.2495-2514

19 N. Birks and H. Rickert, J. Inst. Met., 91, (1961), 308

20 C.T. Sims, P.A. Bergman, and A.M. Beltran, ASME Preprint 69-GT-16, March, (1969)

21 G.Wood, T.Hodgkiess, D.Whittle, Corrosion Sci. 6, (1966), 129

22 D. Ignatow, R. Szamugunowa, O mechanizmie okreslenia spawow na osnowie Ni and Cr, USSR, Moscow, 1960

23 V.B. Trindade, U. Krupp, Oxidation mechanisms of Cr – containing steles and N- base alloys at high temperatures – Part 1: The different role of alloy grain boundaries, Materials and Corrosion, Vol. 56, (2005), No 11

24 A.I.Kahveci, G.Welsch, High temperature oxidation of Fe-3wt%Cr alloy, Scripta Metallurgica, Vol.17, (1983), pp. 121 – 126

25 A. Atkinson, R.I. Taylor, A.E. Hughes, Phil. Mag. A 45, 45, (1982), 823

26 Shen Jianian, Zhou Lonhjiang, Li Tiefan, High Temperature Oxidation of Fe-Cr Alloys in Wet Oxygen, Oxidation of Metals, Vol.48, (1997), Nos.3/4

27 I.Kvernes, M.Oliviera, P. Kofstad, Corrosion Science, 17, (1977), 273

28 R.A.Rapp, Metall. Trans. A15, (1984), 765

29 J.R.Nicholls, P.Hancock, The Reactive Element Effect, E. Lang, ed (Amsterdam, Elsevier, (1989)), pp. 195

30 S.J. Hong, G.H.Hwang, W.K. Han, S.G. Kang, Cyclic oxidation of Pt/Pd modified aluminide coating on a nickel base superalloy at 1150oC, Intermetallics, Vol.17, (2009), pp.381 – 386

31 R.A Perkins and G.H Meier, Proc. Industry - University Advanced Materials Conference, FW Smith, Ed., Denver, (1991), pp. 92

32 J.L Smialek and D.L Humphrey, Scr Metall. Mater., Vol. 26 (No.11), (1992), pp. 1763-1768

33 G.Welsh and A.I Kaveci, Oxidation of High Temperature Intermetallic, T.Grobstein and J.Doychak, Ed., The Minerals, Metals and Materials Society, (1989)

34 G.Welsh, S.Friedman and A.Kahveci, Microscopy of Oxidation, M.J.Benett and G.W.Lorimer, Ed., Institute of Materials, London, (1991)

35 H.L.Du, P.K. Datta, D.B.Lewis and J.S. Burnell-Gray, Corrosion Science, Vol. 36 No.4, (1994), pp. 631-642

36 G.Fisher, P.K. Datta and J.S Burnell-Gray, Surface .Coating Technology, Vol. 113, No.3, (1999), pp. 259-267

37 P.K. Datta, H.L.Du, J.S Burnell-Gray,; Corrosion of Intermetallics, ASM Handbook Vol. 13B, Corrosion: Materials, (2005), pp. 490-512

38 D. Legzdina, I.M. Robertson, H.K. Birnbaum, Oxidation behaviour of single phase γ-TiAl alloy in low-preasure oxygen and hydrogen, Acta Materiala 53 (2005), pp. 601-608

39 M. Yoshihara, K. Miura, Effects of Nb addition on oxidation behaviour of TiAl, Intermetallics 3 (1995), pp. 357-363

40 P.Kofstad, J.Less-Common Metals, , 13, (1967), pp. 635

41 H. Jiang, M. Hirohasi, Y.Lu, H.Imanari, Effect of Nb on the high temperature oxidation of Ti(0-50 at%)Al, Scripta Materiala 46, (2002), pp. 639 – 643

42 Y.G.Zhang, X.YLi, C.Q.Chen, W.Wang, Vincent Ji, The influence of Nb ion implantation upon oxidation behaviour and hardness of Ti48Al alloy, Surface and Coating Technology, 100 – 101, (1998), pp. 214 – 218

43 X.YLi, S.Taniguchi, Y.C.Zhu, K.Fujita, N.Iwamoto, Y.Matsunga, K.Nakagawa, Oxidation behaviour of TiAl protected by Al and Nb combined ion implantation at high temperature, Nuclear Instruments and Methods in Physics Research, B, 127, (2002), pp. 207 – 214

44 H.J.Schumtzler, N.Zheng, W.J.Quadkkers, M.F. Stroosnijder, The influence of niobium implantation on the high temperature oxidation behaviour of Ti48Al2Cr , Surface and Coatings Technology, 83, (1996), pp. 212 – 217

45 M. Schmitz-Niederau and M. Schutze, The Oxidation Behavior of Several TiAl Alloys at 900oC in Air, Oxidation of Metals, Vol. 52, (1999), Nos. 3/4,

46 H.L.Du, P.K.Datta, D.B Lewis, and J.S Burnell – Gray, High temperature Corrosion of Ti and Ti6Al4V Alloy, Oxidation of Metals, Vol.45, (1996), Nos. 5/6

47 D. W. Mckee and S-C. Huang, "Oxidation Behaviour of Gamma-Titanium Aluminide Alloys," High Temperature Ordered Intermetallic Alloys IV, EDS: L. A. Johnson, D. P. Pope and J. O. Stiegler, MRS Symp. Proc., Vol. 213, (1991), pp. 939−943

48 G. Welsch and A. I. Kahveci, "Oxidation Behaviour of Titanium Aluminide Alloys," Oxidation of High-Temperature Intermetallics, eds: T. Grobstein and J. Doychak, TMS Warendale, (1989), pp. 207−212

49 V.A.C Haanappel, J.D.Sunderkotter, M.F Stroosnijder, The isothermal and cyclic high temperature oxidation behaviour of Ti48Al2Mn2Nb compared with Ti48Al2Cr2Nb and Ti482Cr, Intermetallics 7, (1999), pp. 529 – 541

50 JM. Herbelin, M. Mantel, Journal de Physique IV, Colloque C7, supplement au Journal de Physique III, (1995), pp. 5 – 365,

51 Fuhui Wang, Zhaolin Tang, and Weitao Wu, Effect of Chromium on the Oxidation Resistance of TiAl intermetallics, Oxidation of Metals, Vol. 48, (1997), Nos. 5/6,

52 J.D. Sunderkotter, H.J.Schmutzler, V.A.C.Haanappel, R.Hofman, W.Glatz, H.Clemens, M.F.Stroosnijder, The High Temperature Oxidation Behaviour of Ti47Al2Cr0.2Si and Ti48Al2Cr2Nb compared with Ti48Al2Cr, Intermetallics 5, (1997), pp 525 – 534

53 C. Lang, M. Schutze, Microscopy of Oxidation 3.ed. S.B. Newcomb, Institute of Materials, London and Cambridge, UK, in press

54 H.L.D, P.K.Datta, D.B.Lewis and J.S. Burnell-Gray, Air Oxidation Behaviour of Ti6Al4V alloy between 650oC and 850^{o}C, Corrosion Science, Vol. 36, No.4, (1994), pp. 631 – 642

55 H.L.Du, A.Aljarany, K.Klusek, P.K.Datta, J.S. Burnell – Gray, Effects of Oxygen Partial Pressures on the Oxidation Behaviour of Ti46.71.9W0.5Si between 750 – 950^{o}C, Corrosion Science, Vol. 47, (No.7), (2005), pp. 1706 – 1723

56 U.Figge, A.Elschner, N.Zheng, H.Schuster, W.J.Quadakkers: Fesenius, J. Anal. Chemistry, 346, (1993), pp. 75 – 78

57 Ch.Lang, M.Schutze: to be published

58 G.H.Meier, F.S.Petit, S.Hu: J.Physique IV, Vol.3, (1993), p. 395

59 S.Mrowec, Korozja gazowa Metali, Wyd. Slask, (1975)

60 U.Kamachi, Mudali Baldev Raj, Corrosion Science and Technology, (2008), pp. 50 – 90

61 S.Mrowec, K.Przybylski, High Temperature Mater. Proc, Vol. 6 (1984)

62 Per Kostad, High Temperature Corrosion, (1989), pp. 428 – 440

63 B.Gleeson, Alloy Degradation Under Oxidising – Sulphidising Conditions at Elevated Temperatures, Mat.Research, Vol.7, No.1 (2004), pp. 61 – 69

64 G.Romeo, W.W. Smeltzer, J.Electrochem, Soc., 119, (1972), pp. 1267,

65 E.J Vineberg, D.L. Douglass, Effect of Yttrium on the Sulphidation Behaviour of Ni-Cr-Al Alloys at 700^{o}C, Oxidation of Metals, Volume 25, Numbers 1-2 / February), (1986), pp. 1 – 27

66 Z.Zurek, J.Jedlinski, K.Kowalski, V.Koralik, W.Engel, J.Musil, Suplhidation and oxidation of the Ni22Cr10al-1Y alloy in H2/H2S and SO2 atmospheres at high temperatures, Journal Materials Science, Vol. 35, No 3, (2000), pp. 685 – 692

67 T.B.Massalski, Binary Alloy Phase Diagrams, American Society of Metals, Metals Park Ohio (1986)

68 Douglass and Wu, Sulphidation Behaviour of NiCrMo Alloys at 700oC, Oxidation of Metals, Vol. 22, (1984), No 1 – 2,

69 D.J Young, W.W. Smeltzer, J.S. Kirkaldy, Oxid. Met. 7, 149

70 J.S.Kirkaldy, G.M.Bolze, D.McCutcheon and D.J.Young, Met.Trans. 6A 1205 (1975)

71 G.Southwell, D.J Young, High Temperature Sulphidation of Fe-Mn-Cr Alloys, Oxidation of Metals, Vol. 30, (1991), Nos. ¾

72 T. Narita, W.W Smeltzer, K.Nishida, Oxidation of Metals. Vol.17, (1982), pp.299,

73 P. Papaiacovou, H.J. Grabke and P.Schmidt, Werkst. Korrosion. 36, (1985), 320,

74 H.L.Du, P.K.Datta, J.S Gray and K.N Strafford, Oxidation of Metals, 39, 107, (1993), pp. 107 – 135

75 H.L.Du, P.K.Datta, J.S Gray and K.N Strafford, Corrosion Science, 36, (1994), pp. 99 – 112,

76 S.Mrowec, Corrosion Science, 7, (1976), pp.563

77 H.L.Du, P.K.Datta, D.Griffin, A.Aljarany and J.S Burnell – Gray, Oxidation and Sulphidation Behaviour of AlTiN – Coated Ti46.7Al1.9W0.5Si Intermetallic with CrN and NbN Diffusion Barriers, Oxidation of Metals Vol.60, (2003), Nos. ½

78 H.L.Du, P.K. Datta, D.Hu, X.Wu, High Temperature corrosion mechanisms of certain new TiAl-based intermetallic alloy in an aggressive $H_2/H_2O/H_2S$ environment at 850^{o}C, Corrosion Science 49, (2007), pp. 2406 – 2420

79 O.Kubaschewski, E.L.L, Evans, C.B Alcock, Metallurgical Thermochemistry, Pergamon Press, (1967)

80 P.K Datta, H.L.Du, J.S Burnell-Gray, ASM Handbook 13B, Corrosion of Nonferrous Metals and Speciality Products, (2005), pp. 490 – 512

81 P. Kofstad, P.B Anderson, O.JKrudtaa, J.Less Common Metals, (1961), pp. 89

82 S.A Karake, P.B. Aswath, J.Mater.Sci, 32 (1997), pp. 2845

83 Y.G Zhang, X.Y.Li, C.Q.Chen, W.Wang, Vincent.Ji, Surface and Coatings Technology 100-1-1 (1998), pp. 214 – 218

84 M. Yoshihara, K. Miura, Effects of Nb addition on oxidation behaviour of TiAl, Intermetallics 3, (1995) pp. 357-363

85 H.L.Du, P.K Datta, S.K Hwang, High Temperature Corrosion Behaviour of Ti46.6Al1.4Mn2Mo in Environments of Low Oxygen and High Sulphur Potentials at 750^{o}C and 900^{o}C, Materials Science Forum, Vols. 251 – 254, (1997), pp. 219 – 226

86 H.L. Du, P.K.Datta, S.K.Hwang, Scaling Behaviour of Ti46,6Al1,4Mn2Nb in air between 700 and 900^{o}C, to be published

87 A.Gil, Z,Zurek, A.Stawiarski, JU.Zurek, B.Sulikowski, W.J Quadakkers, A.Kuc, Phase Transformation Caused By Corrosion of Ternary and Quaternary γ-TiAl Based Alloys in SO2 Atmosphere

88 Journal of Phase Equilibria and Diffusion Vol.29. No.1, (2008), pp.112 – 113

89 Takeshi Izumi, Takayuki Yoshioka, Shigenari Hayasshi, Toshio Nitra, Sulphidation properties of TiAl-2at%X (X= V, Fe, Co, Cu, Nb, Mo, Ag, and W) alloys at 1173 K and 1,3 Pa sulphur pressure in H2S-H2 gas mixture, Intermetallics 8, (2000), pp.891 – 901

90 P.Vilars, A.Prince, H.Okamoto, Handbook of ternary alloy phase diagrams. ASM International (1995), pp.3371

91 H.L.Du, P.K.Datta, D.B Lewis, and J.S Burnell – Gray, High temperature Corrosion of Ti and Ti6Al4V Alloy, Oxidation of Metals, Vol.45, (1996), Nos. 5/6

92 N.Eliaz, G.Shemesh, R.M.Latanision, Hot corrosion in gas turbine components, Engineering, Failure Analysis 9, (2002), pp. 31-43

93 ASM Handbook Vol.13B. (2005), pp. 165 – 168

94 I.G Wright, High temperature corrosion. In. Metals Handbook, Vol.13.9th ed. Metals Park: ASM, (1987), pp. 97-103

95 GH Meier. A review of advances in high temperature corrosion. Mater Sci Eng A; (1989), 120:1-11

96 Goward GW. Progress in coatings for gas turbine airfoils, Surface Coat. Technology Vol.7,(1998), pp. 536-544

97 P.Hanccok, Vanadic and chlorine attack of superalloys. Mater.Sci.Technol. Vol.7. 536-44 (1987)

98 Linke, W.F.; A. Seidell, Solubilities of Inorganic and Metal Organic Compounds, 4th edition ed. Van Nostrand, (1965)

99 B.C. Markham, Marine Proteus Engines for the Brave Class Petrol Boats, Trans Institute of Marine Engineering Vol. 71, (1959)

100 E.L Simons G.T Browning and H.A Liebhafsky, Corrosion. Vol. P 279, (1955)

101 N.S Bronstein, M.A Decresente, Transactions of the Metallurgical Society of AIME Vol.245. (1969), pp. 1947

102 R.A.Rapp and K.Goto, Proceedings of the fused salt symposium II (Ed) J.Bronstein. The Electrochemical Society, Princeton, (1979)

103 J.A. Goebel and F.S.Petit. The Na2SO4 Induced Accelerated Oxidation (Hot Corrosion) of Ni base alloys, Metallurgical Transaction Vol.1. (1970), pp.1943

104 A. S. Khanna, Introduction to High Temperature Oxidation and Corrosion, ASM International, (2002)

105 K.L.Luthra, Low Temperature corrosion of Cobalt – Base Alloys: Part 1 Morphology of the Reaction Product, Metall. Trans Vol. 13A, (1982)

106 Dilip. K. Gupta, R.Rapp, The Solubilities of NiO, Co_3O_4 and Ternary Oxides in Fused Na2SO4 at 1200 K, The Ohio state University

107 J.A. Goebel, F.S Petit, G.W.Goward, Mechanisms for the Hot corrosion of Ni- base alloys, Metall. Trans. Vol.4, (1973)

108 Zhaolin Tang, Fuhui Wang, Weitao Wu, Hot Corrosion of TiAl base Intermetallics in molten salts, Oxidation of Metals, Vol. 51, (1999), Nos. 314

109 Kai Zhang, Zhengwei Li, Wei Gao, Hot corrosion behaviour of TiAl based intermetallics, Materilas Letters 57, (2002), pp. 834 – 843

110 Zhaolin Tang, Fuhui Wang, Weitao Wu, Effect of a sputtered TiAlCr coating on hot corrosion resistance of γ-TiAl, Intermetallic 7, (1999), pp. 1271 – 1274

111 Fuhui Wang, Zhaolin Tang, Weitao Wu, Effect of Cr on the oxidation resistance of TiAl intermetallics, Oxidation of metals, Vol. 48, (1997), Nos. 5/6,

112 Tai-Kang Liu and Renato G. Bautista, Prediction of the chromium oxide oxidation rate from the equilibrium constants and the mass transfer coefficients at high temperatures, Oxidation of Metals, (1975), pp. 277-286

113 Zhaolin Tang, Fuhui Wang, Weitao Wu, Effect of Al_2O_3 and enamel coatings at 900oC oxidation and hot corrosion behaviour of gamma TiAl, Materials Science and Engineering, A276, (2000), pp. 70 – 75

114 Kai Zhang, Wei Gao, Jing Liang, Molten salt vapour corrosion of TiAlAg intermetallics, Intermetallics 12, (2004), pp. 539 – 544

115 E.H.Copland, B.Gleeson, D.J Young, Formation of Z-Ti50Al30O20 in the sub-oxide zones of γ-TiAl based alloys during oxidation at 1000oC, Acta. Mater. Vol. 47, No.10, (1999), pp. 2937-2949

116 I.Gurrappa, Mechanism of degradation Titanium alloy IMI 834 and its protection under hot corrosion conditions, Oxidation of Metals, Vol. 59, (2003), Nos. 3/4

117 Mu Rong Yang, Shyi Kaon Wu, Oxidation resistance Improvement of TiAl intermetallics using surface modification, N.T.U, No 89, (2003), pp. 3 – 19

118 R.Samuel, N Lockington, Metall. Treat (1951), 18, 354, 407, 440, 495

119 N. Linblad, J.Oxidation of Metals, (1969), 143,

120 R.Reidler, S.Powell, J.Cambel, L.Yntema, J. Electrochemistry Society, 17, (1964), 94

121 R.Bartlett, P.Gage, P.Larsen, Trans. AIME 230, (1964), 1528

122 Nianqiang Wu, Zheng Chen, Scot X. Mao, Hot corrosion Mechanism of composite Alumina/Yttria – Stabilized Zircona Coating in Molten sulphate – Vanadate Salt, J.Am.Soc. 88. [3] (2005), pp. 675 – 682

123 E.A Ushe, L.A Klinkova, Solution of Corundum in Fused Vanadates, Russ, J.Inorg, Chemistry 20 [2] (1975), pp. 799 – 803

124 J.G Gonzalez – Rodriguez, S.Haro, A.Martinez – Villafene, V.M Salinas – Bravo, J.P Calderon, Corrosion performance of heat resistant alloys in Na2SO4 – V2O5 molten salts, Materials Science and Engineering A 435 – 436, (2006), pp. 258 – 265

125 L.S. Darken, Trans. AIME, 180, (1948), 430

126 A.C. Smigelskas and E.O. Kirkendall, Trans. AIME, 171, (1947), 2071,

127 L. Onsager, Phys. Rev. 37, (1931), 405

128 S.R. de Groot and P. Mazur, Non-Equilibrium Thermodynamics, Dover Publications, Inc., New York, (1984)

129 M. Planck, Ann. Phys. Chem. (Wiedemann) 39, (1890), 161,

130 S. Datta, R.Filipek, M. Danielewski, Interdiffusion Issues in Pt-Modified NiAl coatings, Defects and Diffusion Forum, Vols. 203 – 205, (2002), pp. 47-60

131 P.K. Datta, J.S. Burnell-Gray, K. Natesan, Intermetallic Compounds, Principles and Practice, Vol. 3 - Progress, Chapter 27, (2002), pp. 561 – 586

132 Bachorczyk, M. Danielewski, P. K. Datta, Robert Filipek, G. Fisher, Computer simulations of heterogeneous reactions controlled by diffusion in modified aluminide coatings on a nickel-based superalloy, Solid State Phenomena. Vol. 72, (1999), pp. 53–58

133 R. Bachorczyk, M. Danielewski, S. Datta, R. Filipek, A. Rakowska, Intrinsic diffusivities and thermal stability of multicomponent coatings, Schriften des Forschungszentrum Jülich : Reihe Energietechnik, Vol. 10, (2000), pp. 182

134 R. Bachorczyk, M. Danielewski, P. K. Datta, R. Filipek, Model of heterogeneous reactions controlled by diffusion, Journal of Molecular Liquid, vol. 86 issue 1–3, (2000), pp. 61–67

135 R. Filipek, M. Danielewski, R. Bachorczyk, Interdiffusion Studies in Co-Fe-Ni Alloys, Polish State Committee for Scientific Research Grant No. 4T08A 001 25 during the period (2003-2005)

136 Kenichi Hirano, R.P Agarwala, B.L.Averbach, Morris Cohen, J. Appl. Phys. Vol. 33 (10), (1962), pp. 3049

137 T.Ustad, H. Sorum, phys. stat. sol. (a) Vol. 20, (1973), pp. 285

138 R. J. Goldston and P. H. Rutherford, Introduction to Plasma Physics. IOP Publ., Bristol, UK, (1995)

139 S. M. Rossnagel, and K. L. Saenger. Optical Emission in Magnetrons: Nonlinear Aspects. J. Vac. Sci. Technol. A, (1989), 7(3):968

140 A. Matthews, K. S. Fancey, A. S. James, and A. Leyland. Ionization in Plasma-

Assisted Physical Vapour Deposition Systems. Surface and Coaing. Technology, (1993), 61(1-3):121

141 N. Savvides and B. Window, Unbalanced Magnetron Ion-Assisted Deposition and Property Modification of Thin Films, J. Vac. Sci. Technol. A, (1986), 4(3):504,

142 I. V. Svadkovski, D. A. Golosov, and S. M. Zavatskiy, Characterization parameters for unbalanced magnetron sputtering systems, Vacuum, (2002), 68(4):283

143 F.Rovere, P.H.Mayrhofer, J.Vac.Sci.Technol. (2007), A 25, 1336,

144 F.Rovere, P.H.Mayrhofer, J.Vac.Sci.Technol. (2008), A 26, 29,

145 A.Gil, B.Rajchel, N.Zheng, W.J. Quadakkers, H.Nickel, The influence of implanted chromium and yttrium on the oxidation behaviour of TiAl based intermetallics

146 RA. Perkins, KT Chiag, GH Meier, Scripta Metal. (1987), pp. 21:1505

147 Zhaolin Tang, Fuhui Wang, Weitao Wu, Effect of a sputtered TiAlCr coating on hot corrosion resistance of γ-TiAl, Intermetallics 7, (1999), pp. 1271-1274,

148 Christian Mitterer, Helmut Lenhart, Paul H. Mayrhofer, Martin Kathrein, Sputtered Coatings Based on the Al2Au Phase, Materials Research Society, Vol. 842, (2005), pp. S5.38.1

149 T.B.Masalski, (Ed), Binary Alloy Phase Diagrams 2nd Ed. Vol. 3, p. 2924

150 A. Rahmel, P.J. Spencer, Oxidation of Metals, Vol. 35, (1991), 53

151 K.L. Luthra, Oxidation of Metals, Vol. 36, (1991), 475

152 S. Becker, A. Rahmel, M. Schorr, M. Schutze, Oxidation of Metals Vol. 38, (1992), 425

153 M.X. Zhang, K.C. Hsieh, J. DeKock, Y.A. Chang, Scripta Metallurguica et Metarialia, 27, (1992), 1361

154 A.Gil, H.Hoven, E.Wellura, W.J. Quadakkers, Corrosion Science, Vol. 34, (1993), 6154

155 L.Gauer, S.Alperine, P.Steinmetz, A.Vassel, Oxidation of Metals, Vol. 42, (1994), 49

156 N.Zheng, W.J.Quadakkers, Research Centre Julich, FRG, To be published

157 D. Banerjee, A.K. Gogia, T.K. Nandy, K.Muraleedharan and R.S.Mishra, The physical Metallurgy of Ti3Al Based Alloys, Structural Intermetallics eds: R. Darolia, J.J. Lewandowski, C.TLiu, P.L. Martin, D.B Miracle and M.V Nathal, TMS, Warendale Pa, (1993), pp. 19 – 33

158 T.Tetsui, S.Ono, Endurance on Composition And Microstructure Effects on Endurance TiAl Used in Turbochargers, Intermetallics, Vol. 7, (1999), pp. 1984 – 1989

159 J.D. Sunderkotter, H.J. Schmultzer, V.A.CHannappel, R.Hofman, W.Glatz, H.Clemens, M.F.Stroosnijder, The High Temperature Oxidation Behaviour of Ti-47Al2Cr-0.2Si and Ti-48Al2Cr2Nb compared with Ti48Al2Cr, Intermetallics, Vol. 5, (1997), pp. 525 – 534

160 B.G.Kim, G.M.Kim and C.J.Kim, Oxidation Behaviour of TiAl-X (X = Cr, V, Si, Mo, Nb), Intermetallics at Elevated Temperature, Scripta Metall. Mater., Vol. 33, (1995), pp 1117 – 1125

161 M.Yoshihara, K.Miura, Effect of Nb addition on Oxidation Behaviour of TiAl, Intermetallics, Vol. 3, pp. (1995), 357 – 363

162 H.L.D, P.K.Datta, D.B.Lewis and J.S.Burnell-Gray, Air Oxidation Behaviour of Ti6Al4V alloy between 650oC and 850^{o}C, Corrosion Science, Vol. 36, No.4, (1994), pp. 631 – 642

163 V.A.C Haanappel, J.D.Sunderkotter, M.F Stroosnijder, The isothermal and cyclic high temperature oxidation behaviour of Ti48Al2Mn2Nb compared with Ti48Al2Cr2Nb and Ti482Cr, Intermetallics 7, (1999), pp. 529 – 541

164 G. Welsch and A. I. Kahveci, "Oxidation Behaviour of Titanium Aluminide Alloys," Oxidation of High-Temperature Intermetallics, eds: T. Grobstein and J. Doychak, TMS Warendale, (1989), pp. 207−212

165 H.J.Schumtzler, N.Zheng, W.J.Quadkkers, M.F. Stroosnijder, The influence of niobium implantation on the high temperature oxidation behaviour of Ti48Al2Cr , Surface and Coatings Technology, 83, (1996), pp. 212 – 217

166 S. Datta, R.Filipek, M. Danielewski, Interdiffusion Issues in Pt-Modified NiAl coatings, Defects and Diffusion Forum, Vols. 203 – 205, (2002), pp. 47-60

167 P.K. Datta, J.S. Burnell-Gray, K. Natesan, Intermetallic Compounds, Principles and Practice, Vol. 3 - Progress, Chapter 27, (2002), pp. 561 – 586

168 Bachorczyk, M. Danielewski, P. K. Datta, Robert Filipek, G. Fisher, Computer simulations of heterogeneous reactions controlled by diffusion in modified aluminide coatings on a nickel-based superalloy, Solid State Phenomena. Vol. 72, (1999), pp. 53–58

169 R. Bachorczyk, M. Danielewski, S. Datta, R. Filipek, A. Rakowska, Intrinsic diffusivities and thermal stability of multicomponent coatings, Schriften des Forschungszentrum Jülich : Reihe Energietechnik, Vol. 10, (2000), pp. 182

170 R. Bachorczyk, M. Danielewski, P. K. Datta, R. Filipek, Model of heterogeneous reactions controlled by diffusion, Journal of Molecular Liquid, vol. 86 issue 1–3, (2000), pp. 61–67

171 R. Filipek, M. Danielewski, R. Bachorczyk, Interdiffusion Studies in Co-Fe-Ni Alloys, Polish State Committee for Scientific Research Grant No. 4T08A 001 25 during the period (2003-2005)

172 P.K. Datta, J.S. Burnell-Gray, K.Natesan, Intermetallic Compounds, Principles and Practice, Vol. 3 - Progress, Chapter 27, (2002), pp. 561 – 586

173 J. M. Rakowski, F. S. Pettit, and G. H. Meier, The effect of nitrogen on the oxidation of γ-TiAl, Scripta Mallurgica et Materialia , Vol. 33. No. 6, (1995), pp. 997-1003

174 P.K Datta, H.L. Du, J.S Burnell Gray ASM Handbook, Corrosion Materials, Vol. 13B ASM International, (2002), pp.490 – 510

175 P.K Datta, H.L. Du, J.S Burnell Gray, Corrosion Science and Technology, Chapter 2, (2009), pp. 50 – 94

176 G. Welsch and A. I. Kahveci, "Oxidation Behaviour of Titanium Aluminide Alloys," Oxidation of High-Temperature Intermetallics, eds: T. Grobstein and J. Doychak, TMS Warendale, (1989), pp. 207−212

177 H.L.Du, P.K.Datta, D.B Lewis, and J.S Burnell – Gray, High temperature Corrosion of Ti and Ti6Al4V Alloy, Oxidation of Metals, Vol.45, (1996), Nos. 5/6

178 S. Datta, R.Filipek, M. Danielewski, Interdiffusion Issues in Pt-Modified NiAl coatings, Defects and Diffusion Forum, Vols. 203 – 205, (2002), pp. 47-60

179 ASM Handbook, Corrosion Materials, Vol. 13B, (2005), pp. 490 – 510

180 O.Kubashewski, E.Li.Evans, C.B.Alcock, Metallurgical Thermochemistry, Vol. 1, (1967)

181 H.L.Du, P.K.Datta, D.B Lewis, and J.S Burnell – Gray, High temperature Corrosion of Ti and Ti6Al4V Alloy, Oxidation of Metals, Vol.45, Nos. 5/6, (1996)

182 P.K Datta, H.L.Du, J.S Burnell-Gray, ASM Handbook 13B, Corrosion of Nonferrous Metals and Speciality Products, (2005), pp. 490 – 512

183 H.L.Du, P.K. Datta, D.Hu, X.Wu, High Temperature corrosion mechanisms of certain new TiAl-based intermetallic alloy in an aggressive H2/H2O/H2S environment at 850^{o}C, Corrosion Science 49, (2007), pp. 2406 – 2420

184 P.K Datta, H.L.Du, J.S Burnell-Gray, ASM Handbook 13B, Corrosion of Nonferrous Metals and Speciality Products (2005), pp. 490 – 512

185 P. Kofstad, P.B Anderson, O.JKrudtaa, J.Less Common Metals,Ch.12, (1961), pp. 389

186 S.A Karake, P.B. Aswath, J.Mater.Sci, 32 (1997), 2845

187 Y.G Zhang, X.Y.Li, C.Q.Chen, W.Wang, Vincent.Ji, Surface and Coatings Technology 100-1-1 (1998), pp. 214 – 218

188 U.Kamachi Mudali, Baldev Raj. Corrosion Science and Technology – Mechanism, Migration and Monitoring, (2009), pp. 51 – 94